

## Durham E-Theses

---

### *In Vitro Investigation into the use of Dual Mobility for Partial Revision of a Failed Metal Hip Resurfacing*

LOVELADY, ELAINE

#### How to cite:

---

LOVELADY, ELAINE (2014) *In Vitro Investigation into the use of Dual Mobility for Partial Revision of a Failed Metal Hip Resurfacing*, Durham theses, Durham University. Available at Durham E-Theses Online: <http://etheses.dur.ac.uk/10646/>

#### Use policy

---

The full-text may be used and/or reproduced, and given to third parties in any format or medium, without prior permission or charge, for personal research or study, educational, or not-for-profit purposes provided that:

- a full bibliographic reference is made to the original source
- a [link](#) is made to the metadata record in Durham E-Theses
- the full-text is not changed in any way

The full-text must not be sold in any format or medium without the formal permission of the copyright holders.

Please consult the [full Durham E-Theses policy](#) for further details.

# ***In Vitro* Investigation into the use of Dual Mobility for Partial Revision of a Failed Metal Hip Resurfacing**

**Elaine Lovelady**

Thesis presented for the degree of  
Doctor of Philosophy



School of Engineering and Computing Sciences

Durham University

December 2013

---

## Abstract

The aim of this work is to investigate whether a failed MOM total hip resurfacing arthroplasty (THRA) can be converted to a successful total hip arthroplasty (THA) during partial revision surgery using an alternative bearing surface for the femoral bearing surface only. It is estimated that around 10% of primary hip replacements will fail each year and with a large number of patients receiving hip replacements at a younger age, as well as living longer, it is essential that the quality of options for revision surgery is as high as possible.

The alternative femoral component used in this study was the Biomet Dual Mobility (DM) femoral bearing, comprising of a small head and a mobile bearing Vitamin-E infused UHMWPE liner which is completely free to move between the head and cup.

DM bearings are suggested in this project for use during partial revision procedures because one of the main reasons for implant failure after revision surgery is joint instability and DM bearings are reported to improve joint stability and prevent component dislocation.

This thesis is structured with four main results sections:

Firstly, retrieved CoCrMo components from failed THA were analysed and the surface features were characterised using zygo non-contacting profilometry, optical microscopy and scanning electron microscopy. The average surface roughness across the explanted CoCrMo cups was  $0.031 \pm 0.03 \mu\text{m}$  with a corresponding surface skewness of  $-5.04 \pm 4.68$ . Microscopy images showed a wide range of surface features including multidirectional scratching and carbide removal.

Secondly, MOM biotribological studies using the Durham hip simulator were undertaken in order to generate physiologically scratched CoCrMo acetabular cups *in vitro* that were similar to the retrievals. This was done through two methods; one simulation used ISO-standard wear conditions whilst another simulation investigated the effect of clinically relevant third-body particles on the MOM articulation. The aim was to produce CoCrMo cups with the desired surface roughness from multidirectional abrasive scratching combined with negative surface skewness.

---

Thirdly, DM biotribological studies using the ProSim hip simulator were then carried out using the previously scratched CoCrMo cups under aggressive testing conditions in order to fully assess the performance of the DM joint and its suitability for use in partial revision procedures. This project has tested a wide variety of CoCrMo cups with worn features similar to that seen *in vivo* from failed MOM bearings against DM heads and all vitamin-E infused UHMWPE liners have experienced very low wear rates in comparison to UHMWPE, from 0.23 – 5.15 mm<sup>3</sup>/MC depending on the test conditions.

Finally, test serum from the MOM ISO-standard simulation was analysed and compared to digested test serum from the DM simulations. Problems encountered with isolating CoCr particles from the DM test serum raised important concerns about the initial test set up which would have to be modified in order for future work to produce clinically relevant wear debris.

Overall this research has successfully increased the understanding of DM bearings for application in partial revision procedures and the results indicate that DM heads are indeed a viable solution for the conversion of a failed MOM THRA into a successful THA.

---

## **Declaration**

The work in this thesis is based on research carried out in the School of Engineering at Durham University. No part of this thesis has been submitted elsewhere for any other degree or qualification and it is all my own work unless referenced to the contrary in the text.

### **Copyright © 2013 by Elaine Lovelady**

“The copyright of this thesis rests with the author. No quotations from it should be published without the author’s prior written consent and information derived from it should be acknowledged.”

---

## Acknowledgements

Firstly I would like to warmly thank my principal supervisor Dr Jun Jie Wu for giving me the opportunity to undertake this work and for helping and supporting me throughout the project. Great thanks also go to Biomet and EPSRC for funding the project; with thanks in particular to my industrial supervisor Dr. Imran Khan as well as Dr Sui Yan Mak, Dr Tim Marriot, Tony Lane and Hannah Wilson from Biomet for the material provision and for your help. Thank you also to my secondary supervisor Professor Neil Cameron.

There are many people who have been invaluable in terms of technical knowledge and assistance during this PhD. Namely Dr Budhika Mendis, Dr Chris Ottley, Helen Riggs, Colin Wintrip and of course Arthur Newman. Arthur - thank you so much for making all the test components and for all your help when things in the lab went wrong.

To my friends from the Bioengineering group Dr QianQian Wang, Dr Martin Stanley, Daniel Giddings and Saurabh Lal - thank you for all the training, help and good times. Thank you also to Geri Rosser and the tea breaks that have kept me going. I'll miss working with you all.

I would also especially like to thank the Loveladies (yes that's you Mum and Dad!) and the Partons (Helena, Neil and Zach) for all their help and encouragement throughout this PhD including all the trips they have made up to the North East to see me.

My final words of thanks go to my wonderful Barry who has allowed me to talk incessantly about hips for three years and accompanied me on countless weekend simulator checks without complaint. I couldn't have done it without you.

Thank you so much.

---

## Contents

1. Introduction.....	1
1.1 Motivation and aim.....	1
1.2 Organisation of thesis.....	3
1.3 References.....	4
2. Literature review.....	5
2.1 Osteoarthritis and the need for total hip arthroplasty.....	5
2.2 Historical Overview.....	5
2.2.1 Total hip arthroplasty.....	5
2.2.2 Total hip resurfacing arthroplasty.....	15
2.2.3 Dual mobility THA.....	18
2.3 In vitro testing of orthopaedic biomaterials used in THA and THRA.....	20
2.3.1 Wear screening.....	20
2.3.2 The human gait cycle and hip simulators.....	22
2.3.3 Lubricant used for biotribological testing.....	29
2.3.4 The need for aggressive testing conditions.....	31
2.4 Wear and lubrication theory.....	38
2.4.1 Wear mechanisms.....	38
2.4.2 Lubrication.....	40
2.5 Wear debris from THA and THRA.....	42
2.5.1 <i>In vivo</i> reaction to wear debris.....	42
2.5.2 <i>In vitro</i> isolation and characterisation of wear debris.....	47
2.6 Revision THA.....	52
2.7 Clinical relevance of project.....	58
2.8 References.....	59

---

3. Analysis of retrieved CoCrMo components.....	71
3.1 Introduction.....	71
3.2 Surface characterisation techniques.....	73
3.3 Surface characterisation results.....	75
3.4 Limitations.....	85
3.5 Discussion.....	86
3.6 Conclusion.....	92
3.7 References.....	93
4.1 Generation of physiologically scratched CoCrMo cups.....	95
4.1 Introduction.....	95
4.2 Durham hip simulator.....	96
4.3 Pin-on-plate machine.....	97
4.4 Lubricant.....	98
4.4.1 ISO-standard lubricant.....	98
4.4.2 Lubricant with Third-Body Particles.....	99
4.5 Wear characterisation.....	103
4.5.1 Gravimetric method.....	103
4.5.2 Surface characterisation techniques.....	103
4.6 MOM Test 1: ISO-standard biotribological study.....	104
4.6.1 Joint replacement clearance.....	104
4.6.2 Wear results.....	105
4.6.3 Surface characterisation.....	110
4.6.4 Limitations.....	118
4.6.5 Discussion.....	118
4.6.6 Conclusion.....	124
4.7 MOM pin-on-plate wear screening for MOM Test 2: third-body aggressive wear.....	124
4.7.1 Wear results.....	125
4.7.2 Surface characterisation.....	128

---

---

4.7.3	Limitations.....	132
4.7.4	Discussion.....	133
4.7.5	Conclusion.....	133
4.8	MOM Test 2: aggressive third-body biotribological study.....	134
4.8.1	Joint replacement clearance.....	135
4.8.2	Wear results.....	136
4.8.3	Surface characterisation.....	138
4.8.4	Limitations.....	148
4.8.5	Discussion.....	149
4.8.6	Conclusion.....	154
4.9	References.....	155
5.	DM biotribological studies including two in vitro partial revision simulations.....	156
5.1	Introduction.....	156
5.2	Prosim hip simulator.....	158
5.3	DM Test 1: aggressive biotribological study with worn CoCrMo cups from MOM Test 1.....	159
5.3.1	Joint replacement clearance.....	159
5.3.2	Soaking data.....	160
5.3.3	Wear results.....	161
5.3.4	Surface characterisation.....	166
5.3.5	Limitations.....	182
5.3.6	Discussion.....	183
5.3.7	Conclusion.....	187
5.4	DM Test 2: aggressive biotribological study with unworn CoCrMo cups.....	188
5.4.1	Joint replacement clearance.....	188
5.4.2	Soaking data.....	189
5.4.3	Wear results.....	190

---

---

5.4.4 Surface characterisation.....	193
5.4.5 Limitations.....	210
5.4.6 Discussion.....	211
5.4.7 Conclusion.....	213
5.5 DM Test 3: aggressive biotribological study with worn CoCrMo cups from MOM Test 2.....	214
5.5.1 Joint replacement clearance.....	214
5.5.2 Soaking data.....	215
5.5.3 Wear results.....	216
5.5.4 Surface characterisation.....	219
5.5.5 Limitations.....	236
5.5.6 Discussion.....	237
5.5.7 Conclusion.....	240
5.6 References.....	241
6. Metal particle analysis.....	242
6.1 Introduction.....	242
6.2 Serum digestion.....	242
6.3 Transmission electron microscopy.....	244
6.4 Inductively coupled plasma mass spectrometry.....	245
6.5 Results from COM study.....	246
6.6 Results from MOM Test 1.....	250
6.7 Results from Dual Mobility Tests 1-3.....	253
6.8 Limitations.....	258
6.9 Discussion.....	261
6.10 Conclusion.....	265
6.11 References.....	266

---

7. Discussion and conclusion.....	267
7.1 Discussion.....	267
7.1.1 Comparison of retrieved CoCrMo cups with physiologically scratched CoCrMo cups from MOM Test 1 and 2.....	267
7.1.2 Comparison of results from DM Tests 1-3.....	273
7.1.3 Particle analysis.....	285
7.1.4 Options available for partial revision of failed MOM THRA.....	289
7.2 Conclusion.....	292
7.3 Suggestions for further work.....	296
7.4 References.....	297
Appendix A: ISO 14242-1.....	300
Appendix B: Cleaning, weighing and drying protocol.....	309
Appendix C: ICPMS protocol.....	310

---

## List of Figures

Figure 1.1: Overview of results chapters 3-6. Relevant chapter sections are shown in bold square brackets.....	3
Figure 2.1: Total hip arthroplasty, schematic modified from Quigley <i>et al.</i> 2010 [2].....	6
Figure 2.2: McKee-Farrar prosthesis, McKee <i>et al.</i> 1966 [4].....	7
Figure 2.3: Chemical structures of polytetrafluoroethylene and polyethylene.....	8
Figure 2.4: Production of UHMWPE acetabular cups. A: UHMWPE resin powder. B: Semi-finished UHMWPE rods that have been consolidated from the resin powder. C: Machining of the UHMWPE rods on a lathe. D: UHMWPE acetabular cups after machining. Images from Kurtz <i>et al.</i> 2009 [30].....	11
Figure 2.5: UHMWPE undergoing gamma radiation, from Campbell <i>et al.</i> 2004 [36].....	12
Figure 2.6: Structure of hydroperoxides.....	13
Figure 2.7: $\alpha$ -tocopherol free radical.....	14
Figure 2.8: Biomet E1 production process.....	15
Figure 2.9: Comparison of A: THA and B: THRA in terms of femoral bone conservation [Image modified from <a href="http://www.mcminncentre.co.uk/birmingham-hip-resurfacing.html">http://www.mcminncentre.co.uk/birmingham-hip-resurfacing.html</a> ].....	16
Figure 2.10: Commonly used resurfacing systems in the UK, as described in Table 2.2..	17
Figure 2.11: Labelled diagram of a dual mobility total hip arthroplasty, modified from video supplied by Biomet.....	19
Figure 2.12: Diagram showing the inner and outer articulation for dual mobility total hip arthroplasty.....	19
Figure 2.13: Examples of wear screening devices, Affatato <i>et al.</i> 2008 [84].....	21
Figure 2.14: The human gait cycle, Zajac <i>et al.</i> 2003 [89].....	22
Figure 2.15: Transverse, sagittal and coronal planes of the body, Applegate <i>et al.</i> 2010 [91].....	23
Figure 2.16: Images of simulators used for <i>in vitro</i> mechanical testing of orthopaedic implants. A: MTS-Bionix Hip Simulator, B: Endolab Hip Simulator, C: Leeds Mark II Hip Simulator, D: Shore Western Hip Simulator.....	27
Figure 2.17: Variation with time of angular movement to be applied to the femoral test specimen, ISO 14242-1.....	28

---

Figure 2.18: Radiograph showing method of determining inclination angle, labelled ‘ $\alpha$ ’ [122].....	31
Figure 2.19: Subject undergoing a fluoroscopic evaluation whilst walking on a treadmill, Lombardi <i>et al.</i> 2000 [135].....	32
Figure 2.20: Common wear mechanisms, Wright <i>et al.</i> 2001 [159].....	40
Figure 2.21: Length of particles isolated from tissue samples collected from different periprosthetic capsular sites, measured by image analysis of TEM micrographs, Catelas <i>et al.</i> 2004 [183].....	44
Figure 2.22: MRI scan showing a pseudotumor arising from the posterior joint space (arrow), Pandit <i>et al.</i> 2008 [184].....	45
Figure 2.23: TEM micrographs showing the presence of metal wear nanoparticles in living macrophages and in tissue taken at biopsy from a pseudotumor, Xia <i>et al.</i> 2011 [188].....	46
Figure 2.24: A: Schematic diagram showing the SWD Protocol, B: polyethylene wear debris displayed on silicon wafer, C: magnified polyethylene wear debris, Billi <i>et al.</i> 2012 [194].....	49
Figure 2.25: Images of isolated metal wear particles from A: Catelas <i>et al.</i> 2001 [201] (TEM image). B: Billi <i>et al.</i> 2011 [203] (TEM image) The darker particles indicate presence of cobalt. C: Tipper <i>et al.</i> 1999 [23] (SEM image). D. Brown <i>et al.</i> 2007 [144] (SEM image) .....	51
Figure 2.26: Risk of revision by bearing surface (cumulative hazard with 95% confidence intervals), UK National Joint Registry [66].....	53
Figure 2.27: Cup-stem brand combination that accounted for the highest percentage of total primary hip procedures in 2012 according to the UK National Joint Registry.....	55
Figure 2.28: Cup-stem brand combination that accounted for the highest percentage of total revision hip procedures in 2012 according to the UK National Joint Registry.....	56
Figure 3.1: Retrieved femoral components, A: FAR 4, B: FAR 33, C: FAR 72, D: FAR 77, E: FAR 149, F: FAR 164.....	72
Figure 2: Retrieved acetabular components, A: FAR 4, B: FAR 33, C: FAR 77, D: FAR 80, E: FAR 86, F: FAR 101, G: FAR 149, H: FAR 164.....	73
Figure 3.3: Surface roughness (Ra) of retrieved CoCrMo heads.....	76

---

---

Figure 3.4: Skewness (Rskw) of retrieved CoCrMo heads.....	77
Figure 3.5: Selection of surface profiles taken from retrieved femoral heads.....	78
Figure 3.6: Surface roughness (Ra) of retrieved CoCrMo cups.....	79
Figure 3.7: Skewness (Rskw) of retrieved CoCrMo cups.....	79
Figure 3.8: Selection of surface profiles taken from retrieved CoCrMo cups.....	81
Figure 3.9: Selection of optical images taken from retrieved femoral heads.....	82
Figure 3.10: Selection of optical images taken from retrieved acetabular cups.....	83
Figure 3.11: Selection of SEM images. A: scratching and metal removal from FAR 86, B: FAR 86 positioned in SEM chamber, C: scratching from FAR 72, D: scratching from FAR 101.....	84
Figure 3.12: SEM images of carbides from FAR 72, A: Carbides among scratching, B: Magnified image of carbide.....	85
Figure 3.13: Zygo roughness data from the current study compared to (*) data from Joyce <i>et al.</i> 2009 [17].....	87
Figure 3.14: Zygo image of explanted femoral head from patient 1 in Joyce <i>et al.</i> 2009 [17].....	88
Figure 3.15: Scratched acetabular cup from Loving <i>et al.</i> 2013 [22].....	88
Figure 3.16: Scratched femoral CoCrMo head taken from Lee <i>et al.</i> 2009 [23].....	89
Figure 4.1: Durham hip simulator.....	96
Figure 4.2: Pin-on-plate machine, front view.....	97
Figure 4.3: Pin-on-plate machine, side view.....	98
Figure 4.4: Porous titanium coating on the back of CoCrMo acetabular cup.....	99
Figure 4.5: SEM image of HA particles.....	100
Figure 4.6: Size distribution of HA particles from SEM images.....	101
Figure 4.7: SEM image of Ti particles.....	101
Figure 4.8: Size distribution of Ti particles from SEM images.....	102
Figure 4.9: HA stirring in test lubricant for 4 hours prior to pin-on-plate simulation..	102
Figure 4.10: 60mm ReCap CoCrMo Resurfacing Head and Cup.....	104
Figure 4.11: Summary of complications with gaiters throughout 5 MC.....	106
Figure 4.12: Cumulative weight loss of 60mm resurfacing CoCrMo heads from Stn 1b and Stn 4, accounting for the load soak.....	107

---

---

Figure 4.13: Cumulative weight loss of 60mm acetabular CoCrMo cups from Stn 1b and Stn 4, accounting for the load soak.....	107
Figure 4.14: Cumulative weight loss of 60mm resurfacing CoCrMo heads from Stns 2,3 and 5, accounting for the load soak.....	108
Figure 4.15: Cumulative weight loss of 60mm acetabular CoCrMo cups from Stns 2,3 and 5, accounting for the load soak.....	108
Figure 4.16: Surface roughness of 60mm resurfacing CoCrMo heads during testing.....	110
Figure 4.17: Surface roughness of 60mm acetabular CoCrMo cups during testing.....	111
Figure 4.18: Skewness of 60mm resurfacing CoCrMo heads during testing.....	111
Figure 4.19: Skewness of 60mm acetabular CoCrMo cups during testing.....	112
Figure 4.20: Surface profiles of femoral resurfacing heads imaged throughout this test. A: OMC from Station 1b, B: 5 MC from Station 1b, C: 5 MC from Station 2, D: 5 MC from Station 3, E: 5 MC from Station 4, F: 5 MC from Station 5.....	113
Figure 4.21: Surface profiles of acetabular cups imaged throughout this test. A: OMC from Station 1b, B: 5 MC from Station 1b, C: 5 MC from Station 2, D: 5 MC from Station 3, E: 5 MC from Station 4, F: 5 MC from Station 5.....	114
Figure 4.22: Surface images taken throughout this test. A: OMC from Station 1b, B: 0.5 MC from Station 1b, C: 0.5 MC from Station 2, D: 0.5 MC from Station 3, E: 0.5 MC from Station 4, F: 0.5 MC from Station 5.....	115
Figure 4.23: Surface images taken after 2.5 MC of this test. A: Station 1b, B: Station 2, C: Station 3, D: Station 4, E: Station 5, F: the load control station.....	116
Figure 4.24: Surface images taken after 5 MC of this test. A: Station 1b, B: Station 2, C: Station 3, D: Station 4, E: Station 5, F: the load control station.....	117
Figure 4.25: Alternative available gaiter with concertinaed edges (pulled over cup holder and base plate).....	118
Figure 4.26: Comparison of the run-in wear data from Stns 1b and 4 with previously published simulator studies.....	119
Figure 4.27: Comparison of the steady state wear data from Stns 1b and 4 with previously published simulator studies.....	119
Figure 4.28: Comparison of the wear data from Stns 2, 3 and 5 with retrieval data published by Lord <i>et al.</i> [10].....	121

---

---

Figure 4.29: Zygo data showing average surface roughness (Ra) and skewness (Rskw) values across all test components in comparison to retrieved acetabular components.....	122
Figure 4.30: Optical images taken from the surfaces of A: Cup 1b after 5 MC, B: retrieved component FAR 77, C: Cup 4 after 5 MC, D: retrieved component FAR 164.....	123
Figure 4.31: Optical images taken from A: retrieved component FAR 4 (a lot of multidirectional scratches), B: Cup 2 after 5 MC (a lot of deep, unidirectional scratches).....	123
Figure 4.32: Cumulative weight loss of CoCrMo pins, accounting for the soak control.....	125
Figure 4.33: Cumulative weight loss from an average of the four active pins, noting the different test conditions.....	126
Figure 4.34: Cumulative weight loss of CoCrMo plates, accounting for the soak control.....	127
Figure 4.35: Cumulative weight loss from an average of the four active plates, noting the different test conditions.....	127
Figure 4.36: Average volume loss from the pins and plates over 2 MC, noting the test conditions.....	128
Figure 4.37: Surface roughness of CoCrMo plates during 2.0 MC.....	128
Figure 4.38: The edge of wear track on plate 2 throughout test in comparison to the soak control.....	130
Figure 4.39: The centre of the wear track on plate 1 throughout test in comparison to the soak control.....	131
Figure 4.40: Centre of all active pins at 2 MC.....	132
Figure 4.41: A: 60 mm ReCap CoCrMo resurfacing head and cup, B: HA particles, C: Ti particles.....	135
Figure 4.42: Cumulative weight loss of 60 mm resurfacing CoCrMo heads during third-body particle test, accounting for the load soak.....	136
Figure 4.43: Cumulative weight loss of 60 mm acetabular CoCrMo cups during third-body particle test, accounting for the load soak.....	137
Figure 4.44: Surface roughness of 60 mm CoCrMo resurfacing heads during 2.0 MC third-body test.....	139

---

---

Figure 4.45: Skewness of 60 mm CoCrMo resurfacing heads during 2.0 MC third-body test.....	139
Figure 4.46: Surface profiles of CoCrMo heads after 2 MC of third-body particle test...	140
Figure 4.47: Surface roughness of 60 mm CoCrMo acetabular cups during 2.0 MC third-body test.....	141
Figure 4.48: Skewness of 60 mm CoCrMo acetabular cups during 2.0 MC third-body test.....	141
Figure 4.49: Zygo data from Cup 1 after 0.5 MC showing the 2D plot and the corresponding line profile of the surface.....	142
Figure 4.50: Comparison of surface profiles of the CoCrMo cups at the end of the dual mobility test with the resulting surface at the end of the third-body particle test.....	143
Figure 4.51: Zygo data from Cup 5 after 1.5 MC showing the 2D plot and the corresponding line profile of the surface.....	144
Figure 4.52: Optical images taken within the wear patch of 60 mm CoCrMo cups after 0.5 MC (serum with HA).....	145
Figure 4.53: Optical images taken within the wear patch of 60 mm CoCrMo cups after 1.0 MC (serum).....	146
Figure 4.54: Optical images taken within the wear patch of 60 mm CoCrMo cups after 1.5 MC (serum with Ti).....	147
Figure 4.55: Optical images taken within the wear patch of 60 mm CoCrMo cups after 2.0 MC (serum).....	148
Figure 4.56: Settled Ti particles on base of platform 3 after 1.5 MC.....	149
Figure 4.57: Comparison of the average cumulative weight loss of 60 mm resurfacing CoCrMo heads during the third-body particle test (MOM T2) with an average of cumulative weight loss of 60 mm resurfacing CoCrMo heads in MOM test 1 which did not experience dry wear.....	150
Figure 4.58: Comparison of the average cumulative weight loss of 60 mm acetabular CoCrMo cups during the third-body particle test (MOM T2) with an average of cumulative weight loss of 60 mm acetabular CoCrMo cups in MOM test 1 which did not experience dry wear.....	151
Figure 4.59: Optical images taken from CoCrMo cups in MOM T1 and MOM T2.....	152
Figure 4.60: Optical images taken from retrieved CoCrMo cups in comparison to cups from MOM T2.....	153

---

---

Figure 4.61: Comparison of zygo Ra data from retrieved cups (yellow) to MOM T2 cups (green).....	154
Figure 5.1: Selection of dummy 28 mm heads with sectioned cuts at four different angles: 0°, 15°, 20°, 25° .....	156
Figure 5.2: Left, PMMA coated stainless steel taper. Right, dual mobility head arrangement held in place with locking nut.....	157
Figure 5.3: ProSim Hip Simulator.....	158
Figure 5.4: 28 mm CoCrMo head, E1 liner, 60 mm CoCrMo cup.....	159
Figure 5.5: Cumulative weight change of E1 liners during soaking over 5 weeks prior to the wear simulation.....	161
Figure 5.6: Surface roughness of E1 liners prior to test, before and after soaking.....	161
Figure 5.7: Cumulative weight loss of 28 mm CoCrMo heads under standard conditions, accounting for the load soak.....	162
Figure 5.8: Cumulative weight loss of 28 mm CoCrMo heads under microseparation conditions, accounting for the load soak and a comparison with the mean of the corresponding data for standard conditions.....	163
Figure 5.9: Cumulative weight loss from E1 liners under standard conditions, accounting for the load soak. Note that station 1 was affected by serum loss during the first 0.5 MC.....	163
Figure 5.10: Cumulative weight loss from E1 liners under microseparation conditions, accounting for the load soak.....	164
Figure 5.11: Cumulative weight loss of 60 mm CoCrMo cups under standard conditions, accounting for the load soak.....	164
Figure 5.12: Cumulative weight loss of 60 mm CoCrMo cups under microseparation conditions, accounting for the load soak.....	165
Figure 5.13: Surface roughness of 60 mm CoCrMo cups during 5.0 MC.....	167
Figure 5.14: Skewness of 60 mm CoCrMo cups during 5.0 MC.....	167
Figure 5.15: Surface roughness of 28 mm CoCrMo heads during 5.0 MC.....	168
Figure 5.16: Skewness of 28 mm CoCrMo heads during 5.0 MC.....	168
Figure 5.17: Surface roughness of E1 liners during 5.0 MC.....	169
Figure 5.18: Skewness of E1 liners during 5.0 MC.....	169

---

---

Figure 5.19: Zygo set up at 45° with E1 liner.....	170
Figure 5.20: Additional data for surface roughness and skewness at 45° around E1 liners.....	170
Figure 5.21: Surface profiles of E1 liners imaged after 5 MC at 45 ° ..	171
Figure 5.22: Inner pole of E1 liners after 0.5 MC.....	172
Figure 5.23: Outer pole of E1 liners after 0.5 MC.....	173
Figure 5.24: Inner pole of E1 liners after 2.5 MC.....	174
Figure 5.25: Outer pole of E1 liners after 2.5 MC.....	175
Figure 5.26: Inner pole of E1 liners after 5.0 MC.....	176
Figure 5.27: Outer pole of E1 liners after 5.0 MC.....	177
Figure 5.28: Pole of 28 mm CoCrMo heads after 1.0 MC.....	178
Figure 5.29: Pole of 28 mm CoCrMo heads after 5.0 MC.....	179
Figure 5.30: Optical images taken from 60 mm CoCrMo cups from Stations 1, 3 and 5 before and after the dual mobility test.....	180
Figure 5.31: Photographs of the E1 liners at 5 MC.....	181
Figure 5.32: ESEM images around the liner rim after 5 MC.....	182
Figure 5.33: Left: 'New' gaiter, Right: 'Old' gaiter.....	183
Figure 5.34: Cumulative weight loss of 60 mm CoCrMo cups throughout both tests, accounting for the load soak.....	184
Figure 5.35: Cumulative weight loss of 60 mm CoCrMo cups throughout both tests, accounting for the load soak.....	184
Figure 5.36: Photo taken from [7] showing homogenous and symmetrical wear around the rim of a retrieved DM liner.....	186
Figure 5.37: 28 mm CoCrMo head, E1 liner, 60 mm CoCrMo cup.....	188
Figure 5.38: Cumulative weight change of E1 liners during soaking over 5 weeks prior to the wear simulation.....	190
Figure 5.39: Surface roughness of E1 liners prior to test, before and after soaking.....	190
Figure 5.40: Cumulative weight loss of 28 mm CoCrMo heads under standard and microseparation conditions, accounting for the load soak.....	191
Figure 5.41: Cumulative weight loss from E1 liners under standard and microseparation conditions, accounting for the load soak.....	191
Figure 5.42: Cumulative weight loss of 60 mm CoCrMo cups under standard and microseparation conditions, accounting for the load soak.....	192

---

---

Figure 5.43: Surface roughness of 60 mm CoCrMo cups during 5.0 MC.....	193
Figure 5.44: Skewness of 60 mm CoCrMo cups during 5.0 MC.....	194
Figure 5.45: Surface roughness of 28 mm CoCrMo heads during 5.0 MC.....	194
Figure 5.46: Skewness of 28 mm CoCrMo heads during 5.0 MC.....	195
Figure 5.47: Surface roughness of E1 liners during 5.0 MC.....	195
Figure 5.48: Skewness of E1 liners during 5.0 MC.....	196
Figure 5.49: Additional data for surface roughness and skewness at 45° around E1 liners.....	197
Figure 5.50: Surface profiles of E1 liners imaged after 5 MC at 45 °.....	197
Figure 5.51: Inner pole of E1 liners after 0.5 MC.....	199
Figure 5.52: Outer pole of E1 liners after 0.5 MC.....	200
Figure 5.53: Inner pole of E1 liners after 2.5 MC.....	201
Figure 5.54: Outer pole of E1 liners after 2.5 MC.....	202
Figure 5.55: Inner pole of E1 liners after 5.0 MC.....	203
Figure 5.56: Outer pole of E1 liners after 5.0 MC.....	204
Figure 5.57: Pole of 28 mm CoCrMo heads after 1.0 MC.....	205
Figure 5.58: Pole of 28 mm CoCrMo heads after 5.0 MC.....	206
Figure 5.59: Optical images taken within the wear patch of 60mm CoCrMo cups after 1.0 MC.....	207
Figure 5.60: Optical images taken within the wear patch of 60mm CoCrMo cups after 5.0 MC.....	208
Figure 5.61: ESEM images taken around the E1 liner rim at 1.0 MC.....	209
Figure 5.62: ESEM images taken around the E1 liner rim at 5.0 MC.....	210
Figure 5.63: Zygo data from Cup 1 at 0 MC showing the 2D plot and the corresponding line profile of the surface.....	212
Figure 5.64: Zygo data from Cup 1 after 5 MC showing the 2D plot and corresponding line profile of the surface.....	212
Figure 5.65: 28 mm CoCrMo head, E1 liner, 60 mm CoCrMo cup.....	214
Figure 5.66: Cumulative weight change of E1 liners during soaking over 5 weeks prior to the wear simulation.....	216
Figure 5.67: Surface roughness of E1 liners prior to test, before and after soaking.....	216
Figure 5.68: Cumulative weight loss of 28 mm CoCrMo heads under standard and microseparation conditions, accounting for the load soak.....	217

---

---

Figure 5.69: Cumulative weight loss from E1 liners under standard and microseparation conditions, accounting for the load soak.....	217
Figure 5.70: Cumulative weight loss of 60 mm CoCrMo cups under standard and microseparation conditions, accounting for the load soak.....	218
Figure 5.71: Surface roughness of 60 mm CoCrMo cups during 5.0 MC.....	219
Figure 5.72: Skewness of 60 mm CoCrMo cups during 5.0 MC.....	219
Figure 5.73: Surface roughness of 28 mm CoCrMo heads during 5.0 MC.....	220
Figure 5.74: Skewness of 28 mm CoCrMo heads during 5.0 MC.....	220
Figure 5.75: Surface roughness of E1 liners during 5.0 MC.....	221
Figure 5.76: Skewness of E1 liners during 5.0 MC.....	221
Figure 5.77: Additional data for surface roughness and skewness at 45° around E1 liners.....	222
Figure 5.78: Surface profiles of E1 liners imaged after 5 MC at 45 °.....	223
Figure 5.79: Inner pole of E1 liners after 0.5 MC.....	224
Figure 5.80: Outer pole of E1 liners after 0.5 MC.....	225
Figure 5.81: Inner pole of E1 liners after 2.5 MC.....	226
Figure 5.82: Outer pole of E1 liners after 2.5 MC.....	227
Figure 5.83: Inner pole of E1 liners after 5.0 MC.....	228
Figure 5.84: Outer pole of E1 liners after 5.0 MC.....	229
Figure 5.85: Pole of 28 mm CoCrMo heads after 1.0 MC.....	231
Figure 5.86: Pole of 28 mm CoCrMo heads after 5.0 MC.....	232
Figure 5.87: Optical images taken within the wear patch of 60mm CoCrMo cups after 1.0 MC.....	233
Figure 5.88: Optical images taken within the wear patch of 60mm CoCrMo cups after 5.0 MC.....	234
Figure 5.89: ESEM images taken around the E1 liner rim at 1.0 MC.....	235
Figure 5.90: ESEM images taken around the E1 liner rim at 5.0 MC.....	236
Figure 5.91: Cumulative weight loss of 60 mm CoCrMo cups throughout MOM Test 2 and DM Test 3, accounting for the load soak.....	237
Figure 5.92: Zygo data from Cup 1 at 0 MC (left) and 0.5 MC (right) showing the 2D plot and corresponding image taken at the surface.....	238
Figure 5.93: Zygo data from Cup 3 at 0 MC (left) and 0.5 MC (right) showing the 2D plot and corresponding image taken at the surface.....	239

---

---

Figure 6.1: Particle pellet from dual mobility test serum after centrifugation at 16,000 x g.....	243
Figure 6.2: Overview of the digestion protocol.....	244
Figure 6.3: JEOL 2100F FEG TEM used in the Physics Dept. of Durham University.....	245
Figure 6.4: ICPMS overview.....	245
Figure 6.5: 60mm ZTA ceramic modular head and 60 mm CoCrMo acetabular cup.....	246
Figure 6.6: TEM image: Cr particles after 3.8 MC from Wear Condition 1 including EDX spectra.....	247
Figure 6.7: Particle distribution after 3.8 MC from Wear Condition 1.....	248
Figure 6.8: Particle distribution after 5 MC from Wear Condition 1.....	248
Figure 6.9: TEM image: Cr particles after 0.5 MC from Wear Condition 2 including EDX spectra.....	249
Figure 6.10: Particle distribution after 0.5 MC from Wear Condition 2.....	249
Figure 6.11: Particle distribution after 1 MC from Wear Condition 2.....	250
Figure 6.12: TEM images of CoCr particles seen from Station 2 after A: 0.5 MC, B: 1.0MC. E showing particles to be CoCr at the bottom right.....	252
Figure 6.13: TEM images of CoCr particles seen from Station 4 after A: 1.0 MC, B: 2.5 MC, C: 5.0 MC, D: EDX analysis showing particles confirming CoCr present.....	252
Figure 6.14: Selection of TEM images taken of stainless steel wear particles present in DM Test samples. A: DM Test 1 (standard), B: DM Test 1 (Microseparation), C: DM Test 2 (standard), D: DM Test 3 (standard), E: EDX spectra confirming presence of Chromium, Iron and Nickel.....	253
Figure 6.15: Photograph showing the dry set up of the dual mobility joint.....	254
Figure 6.16: Zygo data taken from around the head stems at the end of dual mobility testing.....	255
Figure 6.17: A and B: TEM images of CoCr particles found in serum from DM Test 2 (microseparation) C: EDX spectra confirming presence of CoCr.....	256
Figure 6.18: A: TEM image showing agglomeration of CoCr/stainless steel wear debris, B: EDX spectra confirming presence of Co, Cr, Fe.....	256
Figure 6.19: A: TEM image from DM Test 2 (microseparation), B: TEM image from DM Test 3 (microseparation) C: EDX spectra confirming presence of Cr.....	257

---

---

Figure 6.20: Timeline showing the number of metal wear particles sized in previous studies.....	259
Figure 6.21: Ratio of rod-like particles to spherical particles in all digested samples from the COM studies and MOM Test 1.....	261
Figure 6.22: Optical images taken at the surface of a CoCrMo acetabular component from Simulation 3.....	262
Figure 6.23: Photograph of the Echo FX Stem taken from the Biomet Echo Hip System product brochure.....	264
Figure 7.1: Comparison of zygo Ra data from retrieved CoCrMo cups (blue) with CoCrMo cups from MOM T1 and T2 (green).....	268
Figure 7.2: Comparison of zygo Rskw data from retrieved CoCrMo cups (blue) with CoCrMo cups from MOM T1 and T2 (green).....	269
Figure 7.3: Comparison of surface profiles from retrieved CoCrMo cups with the CoCrMo cups at the end of MOM T1 and T2.....	271
Figure 7.4: Optical images taken within the wear patch of retrieved CoCrMo cups in comparison to the CoCrMo cups at the end of MOM T1 and T2.....	272
Figure 7.5: Cumulative volume loss of 28 mm CoCrMo heads in all dual mobility tests under standard conditions, accounting for the load soak.....	274
Figure 7.6: Cumulative volume loss of 28 mm CoCrMo heads in all dual mobility tests under microseparation conditions, accounting for the load soak.....	274
Figure 7.7: Cumulative volume loss from E1 liners in all dual mobility tests under standard conditions, accounting for the load soak.....	275
Figure 7.8: Cumulative volume loss from E1 liners in all dual mobility tests under microseparation conditions, accounting for the load soak.....	276
Figure 7.9: Cumulative volume loss of 60 mm CoCrMo cups in all dual mobility tests under standard conditions, accounting for the load soak.....	277
Figure 7.10: Cumulative volume loss of 60 mm CoCrMo cups in all dual mobility tests under microseparation conditions, accounting for the load soak.....	277
Figure 7.11: Optical images taken from around the pole of the E1 liners in Dual Mobility Test 1: Worn cups from MOM Test 1 vs. dual mobility heads.....	281

---

---

Figure 7.12: Optical images taken from around the pole of the E1 liners in Dual Mobility Test 2: Unworn cups vs. dual mobility heads.....	282
Figure 7.13: Optical images taken from around the pole of the E1 liners in Dual Mobility Test 3: Worn cups from MOM Test 2 vs. dual mobility heads.....	283
Figure 7.14: Comparison of wear rate ( $\text{mm}^3/\text{MC}$ ) from the three different materials studied by Traynor <i>et al.</i> [8] (after 5 MC for HXLPE and ECiMa, 3 MC for UHMWPE)...	286
Figure 7.15: Comparison of previous <i>in vitro</i> testing of 28 mm CoCrMo heads against single articulation UHMWPE bearings with the current DM study.....	288
Figure 7.16: Metallosis 1.5 years after treatment with a MOP bearing in the case of a ceramic fracture. [27].....	290

---

## List of Tables

Table 2.1: Chemical composition for ASTM F75 CoCrMo alloy.....	9
Table 2.2: Revision rates (all-cause) for main hip resurfacing brands (95% confidence intervals) as published by the UK Joint Registry 2012 [66].....	17
Table 2.3: Description of different hip simulators available. A/A: Abduction/Adduction, F/E: Flexion/Extension, I/E: Internal/External rotation.....	25
Table 2.4: Commonly used lubricants for in vitro testing and their advantages/disadvantages [121].....	30
Table 2.5: Previous work using hip simulators that have been modified to achieve microseparation.....	34
Table 2.6: Comparison of previous simulator studies with the addition of third body particles.....	36
Table 2.7: Sources of third body wear, Brown <i>et al.</i> 2009 [155].....	37
Table 2.8: Overview of techniques used to isolate polyethylene wear debris from <i>in vitro</i> test serum.....	48
Table 2.9: Overview of techniques used to isolate metal wear debris from in vitro test serum.....	50
Table 2.10: Summary of biological studies using CoCr particles.....	52
Table 2.11: Top five cup-stem brand combinations for primary hip procedures performed during 2012 [66] . Cemented prostheses are shown in italics.....	55
Table 2.12: Top five cup-stem brand combinations for revision hip procedures performed during 2012 [66] . Cemented prostheses are shown in italics.....	56
Table 2.13: Frequency of femoral head sizes for hip procedures performed in 2012 [66].....	57
Table 3.1: Available information from all received retrievals.....	72
Table 3.2: Experimental results from explanted resurfacing implants, published by Joyce <i>et al.</i> 2009 [17].....	87
Table 3.3: Methods previously employed to scratch femoral heads <i>in vitro</i> .....	91
Table 4.1: Summary of morphology and size of third-body particles.....	100
Table 4.2: Radial clearance of 60mm CoCrMo components.....	105

---

Table 4.3: Wear rates for 60mm resurfacing CoCrMo heads, mm <sup>3</sup> /MC.....	109
Table 4.4: Wear rates for 60mm acetabular CoCrMo cups, mm <sup>3</sup> /MC.....	109
Table 4.5: Total wear rate at different stages during pin-on-plate test, mm <sup>3</sup> /MC.....	128
Table 4.6: Radial clearance of 60 mm CoCrMo components.....	135
Table 4.7: Wear rates for each stage of third-body particle test, mm <sup>3</sup> /MC.....	138
Table 4.8: Comparison of wear rates for the heads in MOM T1 with MOM T2, mm <sup>3</sup> /MC.....	150
Table 4.9: Comparison of wear rates for the cups in MOM T1 with MOM T2, mm <sup>3</sup> /MC.....	151
Table 5.1: Radial clearance of dual mobility components.....	160
Table 5.2: Cup combinations for the dual mobility test.....	160
Table 5.3: Wear rates based on overall test, mm <sup>3</sup> /MC. * Wear rate calculated between 1- 5 MC.....	166
Table 5.4: Volume loss from each cup 2.5 MC prior to the replacement of the femoral head with the dual mobility head compared with the corresponding data after the replacement. 'm' indicates that the cup was subject to microseparation.....	185
Table 5.5: Inner clearance of dual mobility components.....	189
Table 5.6: Outer clearance of dual mobility components.....	189
Table 5.7: Wear rates based on overall test, mm <sup>3</sup> /MC.....	192
Table 5.8: Inner clearance of dual mobility components.....	214
Table 5.9: Outer clearance of dual mobility components.....	215
Table 5.10: Wear rates based on overall test, mm <sup>3</sup> /MC.....	218
Table 5.11: R <sub>a</sub> data taken from the E1 liners at 0 and 0.5 MC during the three DM tests.....	238
Table 6.1: Average particle size of CoCr particles isolated from MOM serum samples, shown with 95% confidence intervals.....	251
Table 6.2: ICPMS carried out on digested serum after 1.0 MC from Wear Condition 2. The corrected total weight loss was determined by ICPMS on serum taken from the load control.....	259

---

---

Table 7.1: Wear rates from each component in each of the three dual mobility tests, mm <sup>3</sup> /MC.....	278
Table 7.2: Comparison of previous <i>in vitro</i> testing of 28 mm CoCrMo heads against single articulation UHMWPE bearings with the current DM study.....	287

---

## List of Abbreviations

A/A	Abduction/Adduction
ALVAL	Aseptic Lymphocytic Vasculitis-Associated Lesions
ASTM	American Society for Testing and Materials
Co	Cobalt
COC	Ceramic-on-Ceramic
COP	Ceramic-on-Polyethylene
Cr	Chromium
DM	Dual Mobility
EDTA	Ethylenediaminetetraacetic acid
EDXA	Energy Dispersive X-Ray Analysis
F/E	Flexion/Extension
HA	Hydroxyapatite
I/E	Internal/External rotation
ICPMS	Inductively Coupled Plasma Mass Spectrometry
ISO	International Organisation for Standardisation
MC	Million Cycles
Mo	Molybdenum
MOM	Metal-on-Metal
MOP	Metal-on-Polyethylene
NaOH	Sodium hydroxide
PE	Polyethylene
PMMA	Polymethylmethacrylate
PTFE	Polytetrafluoroethylene
R <sub>a</sub>	Average surface roughness
R <sub>skw</sub>	Average surface skewness
SEM	Scanning Electron Microscope
SWD	Silicon Wafer Display
TEM	Transmission Electron Microscope
THA	Total Hip Arthroplasty
THRA	Total Hip Resurfacing Arthroplasty
Ti	Titanium
UHMWPE	Ultra High Molecular Weight Polyethylene

# 1. Introduction

---

## 1.1 Motivation and aim

The problems associated with Metal-on-Metal (MOM) hip implants have been well publicised in the media. Most notably DePuy issued a product recall in August 2010 after numerous medical studies confirmed two of their metal systems failed early following implantation, many due to the growth of pseudotumors. With hundreds of thousands of hip replacement operations being carried out each year around the world it is imperative that the problems associated with metal implants are addressed. Although the wear rates are low when the implants are surgically well positioned, the metal wear debris being produced can cause a foreign body response resulting in implant failure and the need for revision surgery. The reason why the debris induces this response is unknown. It may be due to the size of the particles, the form of the metal or the quantity being produced.

The aim of this project is to investigate whether a failed MOM resurfacing arthroplasty can be converted to a successful Total Hip Arthroplasty (THA) during partial revision surgery using an alternative bearing surface for the femoral bearing surface only.

This is especially important because a larger number of patients are receiving hip replacements at a younger age, and also living longer, so the quality of options for revision surgery must be as high as possible. According to Kurtz *et al.* [1] if the historical growth trajectory of joint replacement surgeries continues then demand for primary THA among patients below sixty-five years old will account for 52% of all THAs in 2030. Therefore it is essential that THAs provide long-term durability, stability, function and relieve any pain experienced by the patient. The wear debris produced by the implant must also be kept to a minimum in order to reduce any foreign body reactions that could result in discomfort and the need for further revision surgery.

This project tested new alternative femoral components against worn acetabular cups. This was in order to fully mimic the situation whereby a patient undergoing revision surgery receives a new femoral component, which would then articulate against the metal cup left in the body from their original hip replacement operation. It was hoped

that the alternative femoral component to be tested in this project would be proven to be a better option than the current metal resurfacing heads.

The alternative femoral component used in this study was the Biomet Dual Mobility femoral bearing, comprising of a small CoCrMo head and a mobile bearing liner which is completely free to move between the CoCrMo head and CoCrMo cup. The liner was made from Vitamin-E infused UHMWPE. The infusion of Vitamin E has been shown to dramatically improve the wear properties of UHMWPE *in vitro*.

The concept of dual mobility was introduced in the 1970s in an attempt to prevent component dislocation and provide patients with a large range of motion. It is suggested for employment during partial revision in this project due to joint instability being one of the main concerns with implant failure post-revision surgery.

Aggressive testing conditions were employed in order to engage the outer articulation of the dual mobility bearing and assess the worst case wear scenario for the new femoral component.

Leslie *et al.* [2] stated that “the combination of high inclination angle and microseparation resulted in greater increases in wear rate than when tested with increased cup angle alone, thus bringing the experimental model closer to replicating the higher wear rates reported clinically when edge loading occurs”.

Therefore it is hoped that the combination of high inclination and microseparation used in this project will provide an adequate insight into how the dual mobility heads will perform clinically in two scenarios; firstly in a partial revision surgery using scratched CoCrMo cups and also in THA using unworn CoCrMo cups.

To the author’s best knowledge, it is the first time that investigations into the dual mobility articulation under both high inclination and microseparation have been undertaken.

There are concerns that the use of dual mobility joints, which have three contact areas that can produce wear debris, will experience increased wear over a traditional MOP THA. As well as this, there is very limited information on the effect of using worn cups with dual mobility heads. This project aims to address these concerns and increase the understanding of dual mobility bearings for application in partial revision procedures.

## 1.2 Organisation of thesis

Following on from this introduction will be the literature review (Chapter 2) which provides a more in-depth discussion of the work that has led to this project. The results from this work are detailed in Chapters 3-6 and the materials and methods used in each section are reviewed at the start of each chapter.

A schematic diagram showing the structure of the results chapters is provided for the reader in Figure 1.1.

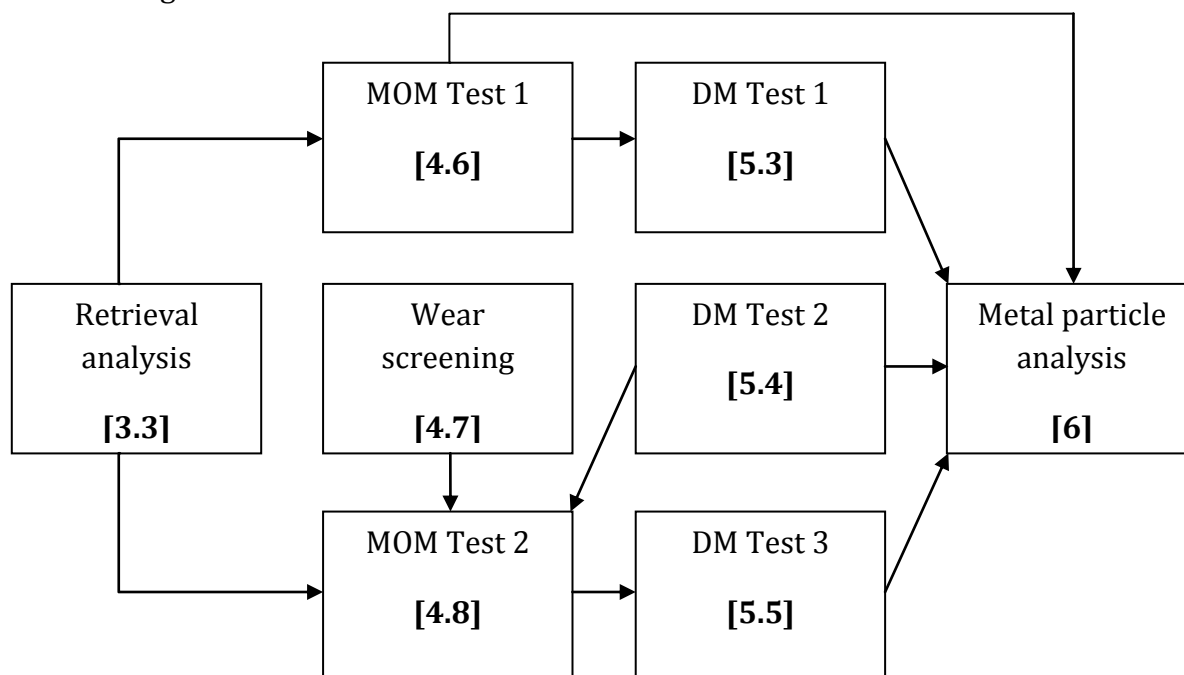


**Figure 1.1: Overview of results chapters 3-6. Relevant chapter sections are shown in bold square brackets.**

Chapter 3 shows the analysis of retrieved CoCrMo components. It is essential during this project to ensure that the worn acetabular cups have a wear pattern similar to those seen *in vivo*, hence in this report surface analysis of retrieved acetabular cups has been performed and the surface features have been characterised.

Chapter 4 details the methods used in order to generate physiologically scratched CoCrMo cups with wear patterns similar to those seen in the retrievals from chapter 3. Firstly in MOM Test 1 the MOM articulation using new CoCrMo resurfacing heads and cups was studied *in vitro*. Secondly, wear screening with the use of a multidirectional pin-on-plate machine was carried out prior to MOM Test 2 in order to trial the effect of clinically relevant third body particle concentration on the MOM articulation. The

particles investigated were hydroxyapatite and titanium. Thirdly, in MOM Test 2, the effects of the clinically relevant third body particles on the MOM articulation using new CoCrMo resurfacing heads and the CoCrMo cups from DM Test 2 were investigated. The worn cups from both simulations were assessed in comparison to the retrieved cups.

To the author's best knowledge, it is the first time that the effect of hydroxyapatite and titanium particles on the MOM interface using resurfacing joints has been examined.

Chapter 5 shows the results from the three aggressive dual mobility (DM) simulations carried out using the ProSim hip simulator. DM Test 1 uses the worn cups from MOM Test 1 against DM heads. DM Test 2 uses previously unworn CoCrMo cups against DM heads. This test not only provides the cups for MOM Test 2 but also acts as a baseline for comparison against the two other DM studies. DM Test 3 then uses the worn cups from MOM Test 2 against DM heads. Both DM Test 1 and DM Test 3 simulate *in vitro* partial revision of a failed MOM resurfacing arthroplasty with DM femoral bearings.

Chapter 6 shows the results of digesting test serum from MOM Test 1 and DM Test 1, 2 and 3 in order to isolate and characterise metal wear particles.

Finally, the data is discussed and concluded in Chapter 7.

This work includes a large number of references therefore the relevant references are listed at the end of each chapter for the convenience of the reader.

### **1.3 References**

- [1] S.M. Kurtz, E. Lau, K. Ong, K. Zhao, M. Kelly, K.J. Bozic, *Clinical Orthopaedics and Related Research* 467 (2009) 2606-2612.
- [2] I.J. Leslie, S. Williams, G. Isaac, E. Ingham, J. Fisher, *Clinical Orthopaedics and Related Research* 467 (2009) 2259-2265.

## 2. Literature review

---

### **2.1 Osteoarthritis and the need for total hip arthroplasty**

Total Hip Arthroplasty (THA) is the surgical replacement of the natural hip joint with a prosthetic hip joint and is the ultimate solution for patients suffering from osteoarthritis. Osteoarthritis currently affects over 27 million people in the world and this figure is increasing [1]. It is a painful, degenerative joint disease that can affect any joint in the body, with the hip joint being the most commonly affected. The cause of osteoarthritis is unknown and many factors can play a part in its development including age, sex, weight or genetic predisposition. During osteoarthritis the cartilage present at the ends of bones deteriorates allowing the bones under the cartilage to rub together. This can result in distress due to pain, uncomfortable swelling and loss of motion. Walking aids can reduce the stress put on the hip but when pain is severe and movement is limited THA is recommended to restore normality to a patient's everyday life. It is estimated that more than 600,000 hip arthroplasties are performed each year worldwide. THA involves the surgical resection of the head and proximal neck of the femur along with the removal of the acetabular cartilage and subchondral bone. An artificial canal is created in the proximal medullary region of the femur and a metal femoral prosthesis is inserted into the femoral medullary canal. An acetabular component is then inserted proximally into the enlarged acetabular space.

### **2.2 Historical Overview**

#### **2.2.1 Total hip arthroplasty**

There are a range of artificial hip implants on offer today. A THA consists of three parts: the femoral prosthetic stem, which fits into the femur; the femoral prosthetic head, which replaces the head of the femur; and the acetabular prosthesis, which is the new hip socket (see Figure 2.1). Each part can be made from a range of materials, in a range of sizes, based specifically on the patient's requirements.

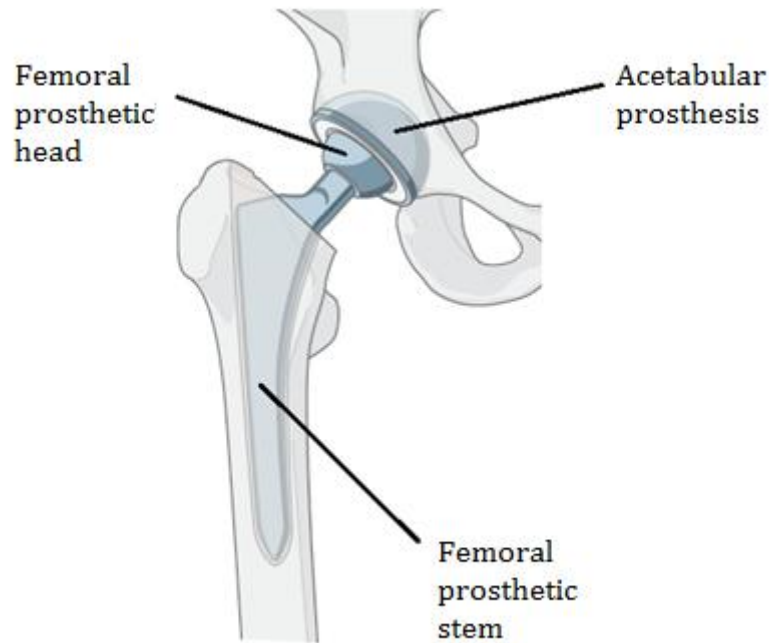


**Figure 2.1: Total hip arthroplasty, schematic modified from Quigley *et al.* 2010 [2].**

The most commonly used THA implants are Metal-on-Polyethylene (MOP). This means that the prosthetic stem and prosthetic femoral head are made from metals such as titanium and cobalt chrome. The acetabular component is made from polyethylene (PE). Metal-on-Metal (MOM) implants are available, where each of the three components is manufactured from the metals listed above. This has the advantage of a volumetric rate of wear 60 times lower than that of PE implants [3]. However, there is controversy about the effects of metal debris build up in the body. This will be discussed later in greater detail.

Ceramic-on-Ceramic (COC) implants are also available, with wear rates lower than MOM, but there is no long-term data obtainable on the success of these implants over time.

Philip Wiles was reported to have performed the first THA in 1938. It was a MOM prosthesis made from stainless steel that was attached to the bone by “carpentry” with screws. In 1960, John Charnley pioneered the use of polymethylmethacrylate (PMMA) in joint replacement by using it as cement with which to hold arthroplasty components in place.



**Figure 2.2: McKee-Farrar prosthesis, McKee *et al.* 1966 [4].**

Early stainless steel prosthetics would loosen or fracture within a year of implantation. This led to the introduction of the McKee-Farrar prosthesis in the 1960s [4], see Figure 2.2. The whole prosthesis was made of cobalt chrome alloy and employed cement fixation. This design was popular up until the 1970s when the Charnley MOP articulation gained favour due to increasing concern about the effect of long-term exposure to metal debris. However a follow-up study carried out by Zahiri *et al.* [5] argued that failure of the implants due to aseptic loosening were a result of the femoral stem design, biomechanics and surgical implantation technique.

The Charnley MOP articulation continued to gain popularity with the acetabular component made from Ultra High Molecular Weight Polyethylene (UHMWPE).

Charnley's initial designs were made from Polytetrafluoroethylene (PTFE). Although the follow up after ten months *in vivo* was encouraging [6], over 99% had to be revised within two to three years due to severe wear and inflammatory response [7]. The replacement of PTFE with UHMWPE is described in Charnley's biography [8]:

*“After running day and night for three weeks, this new material, which very few people in engineering circles had heard about at that time, had not worn as much as PTFE would have worn in 24 hours under the same conditions. There was no doubt about it, ‘we were on’.”*

The chemical structures for both PTFE and polyethylene are shown in Figure 2.3.

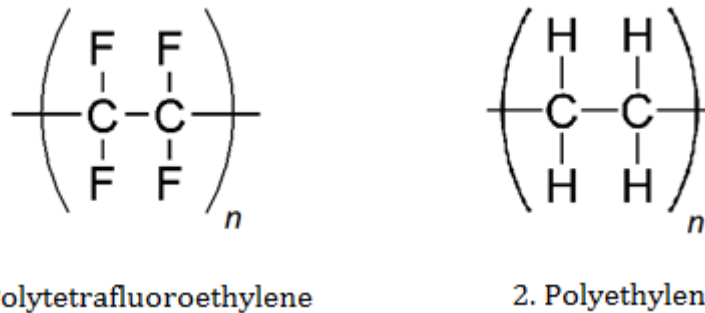


Figure 2.3: Chemical structures of polytetrafluoroethylene and polyethylene.

After the promising wear results from UHMWPE, Charnley then went on to carry out personal biocompatibility tests by implanting both UHMWPE and PTFE into his own thigh [9]. He was convinced that UHMWPE wear debris was biocompatible hence he began to implant UHMWPE into patients in 1962 but withheld from publishing his experience with UHMWPE until the 1970s [7].

Publications throughout the 1980s [10; 11] reported that the clinical performance of the MOM McKee-Farrar prosthesis was in fact comparable to that of the newly popular MOP Charnley design. This led to the development of a second generation of MOM implants to address the design problems associated with that of the earlier articulation.

CoCrMo alloys are currently the most commonly used MOM bearings in orthopaedic applications due to their high wear resistance as well as their high resistance to corrosion [12]. The chemical composition for such alloys is defined by the American Society for Testing and Materials (ASTM) standards and this project will focus on the use of ASTM F75, as shown in Table 2.1.

**Table 2.1: Chemical composition for ASTM F75 CoCrMo alloy.**

<b>Element</b>	<b>Weight %</b>
Chromium, Cr	27-30
Molybdenum, Mo	5-7
Nickel, Ni	<0.5
Iron, Fe	<0.75
Carbon, C	<0.35
Silicone, Si	<1
Manganese, Mn	<1
Tungsten, W	<0.2
Phosphorus, P	<0.02
Sulphur, S	<0.01
Nitrogen, N	<0.25
Aluminium, Al	<0.1
Titanium, Ti	<0.1
Boron, B	<0.01
Cobalt, Co	Balance

It is the presence of chromium in the alloy that allows a chromium-rich passive oxide layer, typically 1-4 nm thick, to spontaneously form on the surface of the metal bearing which provides good corrosion resistance [12-15]. It is this passive oxide layer that is the main reason for the alloy being biocompatible [12]. Molybdenum also helps to improve the mechanical properties of the alloy by providing good localised corrosion resistance [13].

CoCrMo alloys can be either 'high carbon' or 'low carbon' depending on the amount of carbon added during the casting process. High carbon alloys typically contain 0.15-0.25 wt% carbon whereas low carbon alloys usually have <0.06 wt% carbon [13].

High carbon CoCrMo alloys have been proven to have lower wear rates and superior corrosion resistance in comparison to low carbon alloys [13; 16]. The increase in wt% of carbon has been shown to favour the formation of carbides [17; 18].

The carbide microstructure and therefore the mechanical and tribological properties of CoCrMo alloys can not only differ with variation in the carbon content of the alloy but also with variation in the conditions of manufacture and any subsequent thermal treatments [18-23].

This project utilizes as-cast high carbon CoCrMo bearings. As-cast CoCrMo has a dendritic structure with  $M_{23}C_6$  carbides present in the matrix [24]. Carbides are rich in chromium and molybdenum and have a large, irregular and blocky morphology within the grains and at the grain boundaries [21]. These carbides have the same hardness as alumina ceramic and confer wear resistance on the metal bearing surface [25].

During *in vitro* mechanical wear testing, CoCrMo bearings are reported to exhibit low wear rates typically below  $1 \text{ mm}^3/\text{MC}$  [26; 27]. However under adverse loading of the femoral head onto the rim of the cup, the wear rate of MOM bearings has been seen to increase dramatically by between 10 and 100 fold [27-29]. This is a huge concern affecting the consideration of metal bearings for continued use in orthopaedic applications as it can lead to adverse tissue reactions and joint failure. This is discussed further in chapter section 2.5.1.

Today, CoCrMo femoral heads articulating against UHMWPE cups are considered to be the 'gold standard' in THA with a clinical track record for MOP bearings spanning the last fifty years. However, as with metal bearings, UHMWPE has also been developed and the wear properties have been improved over the last five decades.

In order to produce UHMWPE acetabular cups, ethylene gas must be polymerised to form UHMWPE in the form of a resin powder which is then consolidated into sheets or rods and machined into its final shape, as shown in [30].



**Figure 2.4: Production of UHMWPE acetabular cups. A: UHMWPE resin powder. B: Semi-finished UHMWPE rods that have been consolidated from the resin powder. C: Machining of the UHMWPE rods on a lathe. D: UHMWPE acetabular cups after machining. Images from Kurtz *et al.* 2009 [30].**

Once the UHMWPE acetabular components are complete they must be packaged and sterilised prior to distribution. Historically, Charnley acetabular cups were commercially provided by Thackray from 1968 and were gamma irradiated with 25 kGy of gamma radiation in the presence of air [31].

Gamma radiation has been proven to induce cross-linking in UHMWPE. Ionising radiation induces radiolytic cleavage of the polymer chains in UHMWPE, forming carbon and hydrogen free radicals. Recombination reactions along the backbone are favoured which limits the polymer chains breaking apart. The remaining free radicals then recombine with free radicals on different chains to form cross-links [32].

By the 1990s the dose of gamma radiation had increased by many manufacturers to between 50 and 100 kGy in a reduced oxygen environment [33] and highly cross-linked

UHMWPE was developed. UHMWPE that has been irradiated with the historical sterilization dose of 25 to 40 kGy is referred to as 'conventional' UHMWPE whereas UHMWPE that has been irradiated with a dose greater than 40 kGy is referred to as 'highly cross-linked'.

Gamma radiation is now carried out in a reduced oxygen environment because radiation in the presence of air was shown to cause oxidative degradation of the polymer, both *in vitro* prior to implantation as well as *in vivo* after implantation. This has been shown to increase the wear rate [34]. Delamination, cracking or rim fracture may also occur as oxidation is concentrated in the subsurface areas [35]. A diagram explaining how gamma radiation can break carbon-carbon or carbon-hydrogen bonds, leading to chain scission or immediate oxidation in the presence of oxygen is shown in Figure 2.5 [36]. As a result of this, alternative sterilisation techniques using ethylene oxide or gas plasma are preferred by some manufacturers [37]. However these techniques do not induce cross-linking within UHMWPE and this affect has been shown to substantially lower wear rates *in vitro* when articulating against smooth femoral heads [38-40].

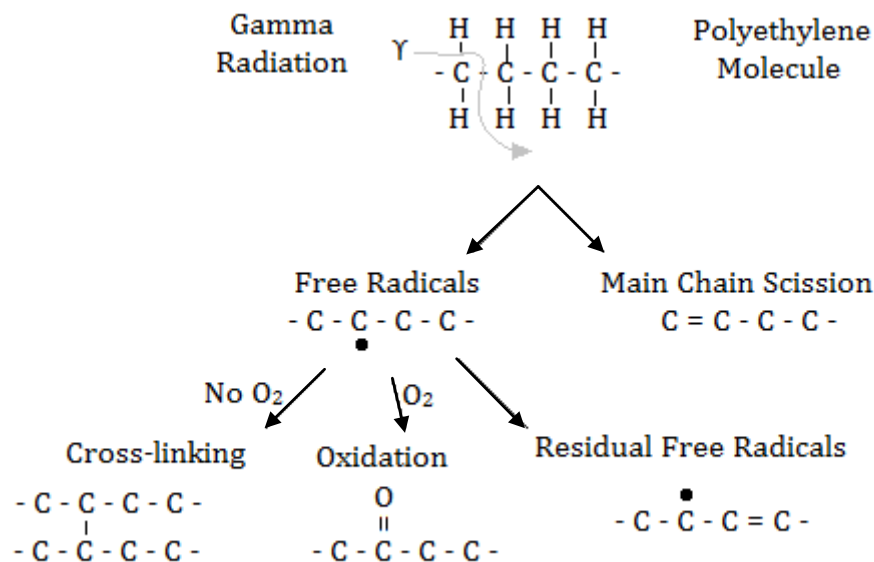


Figure 2.5: UHMWPE undergoing gamma radiation, from Campbell *et al.* 2004 [36].

During *in vitro* mechanical testing of MOP bearings under standard walking conditions, the wear rate of 28 mm acetabular cups is reported to range between 30-40 mm<sup>3</sup>/MC [41; 42]. This means that these bearings can reach the cumulative threshold for

osteolysis of 500 mm<sup>3</sup> [43] in 10-15 years. Wear particle induced osteolysis has been the number one failure mode in MOP bearings and is the biggest problem affecting the long-term survivorship of polyethylene [44]. The *in vivo* effect of polyethylene wear debris is discussed further in chapter section 2.5.1. Metal wear from the femoral head in MOP bearings is often assumed to be negligible in comparison to polyethylene wear [45].

With highly cross-linked MOP bearings the wear rate is reported to lie between 5 and 10 mm<sup>3</sup>/MC for 28 mm and 36 mm acetabular cups respectively [46]. This is a substantial reduction in comparison to conventional UHMWPE.

However, in any form of irradiated UHMWPE, breaking of the C-H bonds results in carbon free radicals [47]. In the presence of oxygen, O<sub>2</sub> will react with the carbon free radicals to form peroxy free radicals which can then abstract a hydrogen atom from other polyethylene chains [48; 49]. This then creates more carbon free radicals which spur on the reaction with oxygen. Peroxy free radicals can also react with hydrogen to form hydroperoxides, Figure 2.6, which are unstable and degrade into oxidation products like ketones, esters and acids [50-52].

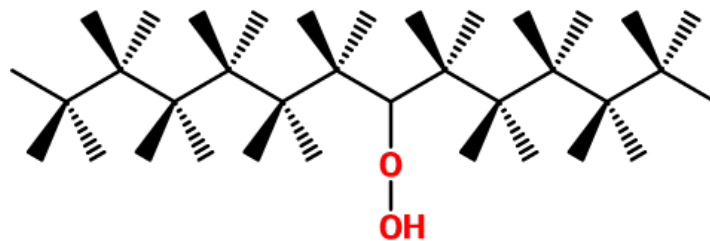
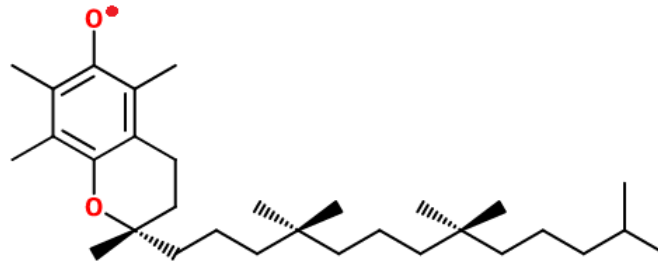


Figure 2.6: Structure of hydroperoxides.

Their formation causes shortening of the overall chain length and hence the molecular weight of polyethylene is reduced. Any reduction in molecular weight means a reduction in mechanical properties of the polyethylene and hence an increase in wear rate [53; 54]. This problem with oxidative degradation has initiated the addition of antioxidants to UHMWPE.

Vitamin E is the most abundant and effective chain-breaking antioxidant present in the human body [55].  $\alpha$ -tocopherol is the most relevant form for human physiology since it accounts for the majority of vitamin E present in human tissues [56].

In the presence of the powerful antioxidant vitamin E, the peroxy free radicals abstract a hydrogen atom from vitamin E instead, Figure 2.7, without the production of any new carbon free radicals. Hence the oxidation process which weakens the polyethylene is hindered and the wear is reduced [57].



**Figure 2.7:  $\alpha$ -tocopherol free radical.**

This project utilizes Biomet 'E1' polymer bearings. E1 is made from the same isostatically compressed moulded polyethylene barstock as Biomet's ArCom. The bars are then gamma ray irradiated to induce a high level of cross-linking. Vitamin E is subsequently infused into the highly crosslinked polyethylene to neutralise residual free radicals present after irradiation. The production process is summarised in Figure 2.8.

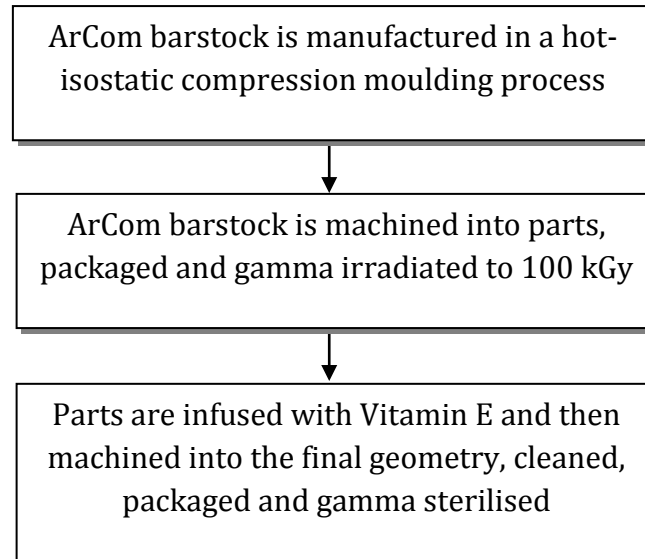


**Figure 2.8: Biomet E1 production process.**

ArCom was the first polyethylene to be packaged in **Argon** and undergo **Compression** moulding manufacturing techniques, hence the name. The infusion of vitamin E into ArCom is reported to provide outstanding oxidation resistance whilst offering similar mechanical strength and very low wear rates below  $1 \text{ mm}^3/\text{MC}$  [58].

E1 was introduced to the orthopaedic market in 2010 and long term clinical studies over the next twenty years will be needed in order to determine any differences in survivorship for these bearings in comparison to conventional and highly cross-linked UHMWPE under normal walking conditions.

### **2.2.2 Total hip resurfacing arthroplasty**

Total Hip Resurfacing Arthroplasty (THRA) is a bone conserving alternative to THA. THA involves the complete removal of the head of the femur and insertion of a prosthetic stem into the femoral medullary canal whereas THRA involves reshaping of the femoral head and placing a metal shell over the top of the femur instead. This saves both the femoral head and neck without any need to enter the medullary canal.

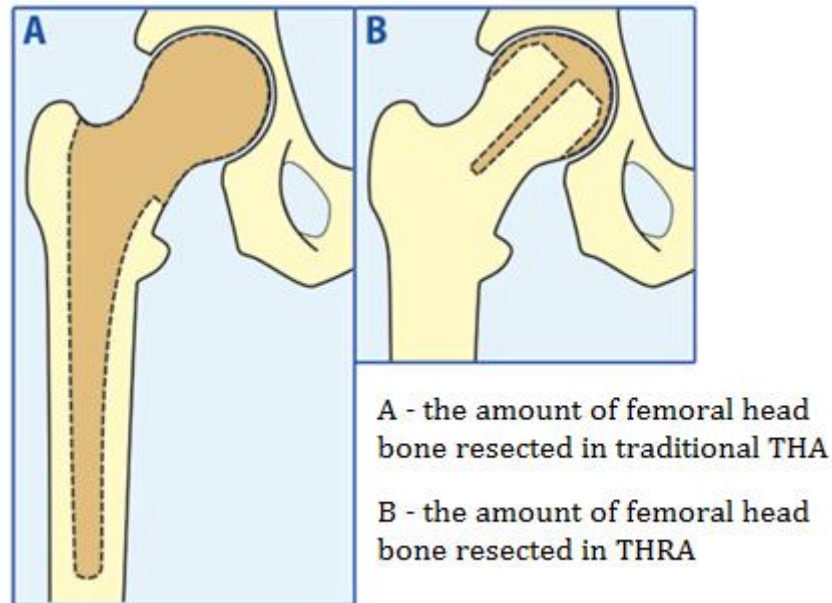


**Figure 2.9: Comparison of A: THA and B: THRA in terms of femoral bone conservation [Image modified from <http://www.mcminncentre.co.uk/birmingham-hip-resurfacing.html>].**

As well as preserving bone stock, the procedure is reported to provide the patient with greater stability and decreased risk of dislocation due to the larger femoral head size [59-61]. It has been introduced as a solution for younger patients with end-stage hip arthritis due to the ease of revision if necessary later in life.

Currently only metallic bearings can be manufactured with sufficient strength to provide THRAs capable of long-term clinical success. Early attempts at hip resurfacing using polyethylene cups were criticised because the procedure had to accommodate a thick UHMWPE cup articulating against a large diameter femoral head and hence was not bone conserving on the acetabular side [62].

Although attempts to treat osteoarthritic hips without resecting the femoral head and neck have been made since the late 1940s [63], it is only since new generation MOM THRA were developed in 1990s that their popularity has increased [64].

THRA became widely criticised by the media after data published from the UK Joint Registry indicated that the revision rates for the DePuy ASR resurfacing system within 5 years were approximately 13%. This led DePuy to issue a product recall on 24 August 2010 affecting over 93,000 patients [65]. The revision rates for the main hip resurfacing brands, as published by the UK Joint Registry 2012 [66], are given in Table 2.2 with images of the corresponding resurfacing systems provided in Figure 2.10.

**Table 2.2: Revision rates (all-cause) for main hip resurfacing brands (95% confidence intervals) as published by the UK Joint Registry 2012 [66].**

Resurfacing brand	Number of patients	Year 1	Year 3	Year 5	Year 7
Adept Resurfacing	3,137	1.22% (0.88-1.68)	2.48% (1.95-3.17)	4.41% (3.39-5.73)	-
ASR Resurfacing	2,982	1.53% (1.15-2.05)	5.97% (5.14-6.94)	13.77% (12.29-15.42)	24.22% (21.31-27.52)
BHR Resurfacing	17,519	1.07% (0.93-1.24)	2.41% (2.18-2.67)	3.67% (3.36-4.01)	5.09% (4.64-5.57)
Conserve Plus	1,275	2.00% (1.35-2.97)	5.16% (3.99-6.67)	8.52% (6.76-10.73)	-
Cormet 2000	3,532	1.35% (1.01-1.79)	3.61% (3.02-4.32)	7.13% (6.15-8.25)	10.38% (8.86-12.15)
Durom Resurfacing	1,608	1.46% (0.97-2.20)	3.77% (2.90-4.90)	5.99% (4.74-7.58)	-
Recap Resurfacing	1,618	1.82% (1.26-2.61)	3.63% (2.75-4.79)	5.96% (4.35-8.16)	-

Note: Revision rates are only shown where at least 100 patients have been observed for at least that period of time.



**Figure 2.10: Commonly used resurfacing systems in the UK, as described in Table 2.2.**

The reasons why the DePuy ASR failure rate has been so high have been widely investigated [67-70]. Penny *et al.* [68] concluded that the ASR femoral component achieves initial stability and that early migration is not the mode of failure. Langton *et al.* [70] suggested that wear at the trunion-taper interface is an important factor in the development of adverse tissue reactions and subsequent joint failure.

Underwood *et al.* [67] compared sixty-six ASR components with sixty-four BHR components. As can be seen in Table 2.2, the BHR has a much lower rate of revision

after seven years in comparison to the ASR joint. Underwood found a significantly increased occurrence of edge loading ( $p < 0.005$ ) for the ASR components which implied that the ASR design is more sensitive to suboptimal positioning than the BHR design. Suboptimal positioning leads to increased wear rates and increased metal wear debris release into the joint cavity. The *in vivo* reaction to metal wear debris is discussed in chapter section 2.5.1.

### **2.2.3 Dual mobility THA**

The concept of dual mobility was introduced by Professor G. Bousquet in 1976 in an attempt to prevent component dislocation [71].

The concept combines the fundamental principle established by Sir J. Charnley, stating how a small 22 mm head articulating against a polyethylene liner has a low risk of failure due to wear [72], with that of McKee stating how the use of large diameter bearings minimises the risk of subluxation.

The small metal head is designed to press-fit in to the polyethylene liner and cannot be removed unless it is levered out. The larger diameter liner then requires the head to travel more distance before it can 'jump' out of the metal cup and hence the design offers a greater stability, resistance to subluxation and intra-prosthetic dislocation [73]. A screenshot taken from a video produced by Biomet to demonstrate the dual mobility concept is shown in Figure 2.11 and has been labelled to highlight the three bearings which together form a dual mobility THA.



**Figure 2.11: Labelled diagram of a dual mobility total hip arthroplasty, modified from video supplied by Biomet.**

The dual mobility concept also has the benefit of giving a large range of motion. The first motion occurs between the small metal head and the concave surface of the polyethylene liner until the neck of the femoral stem comes into contact with the liner. This is also known as the ‘inner articulation’.

The neck of the femoral stem will only contact the polyethylene liner when a larger range of motion is required and a secondary motion then occurs between the polyethylene liner and the metal shell [74]. This is known as the ‘outer articulation’.

The difference between the inner and outer articulation is summarised in Figure 2.12.

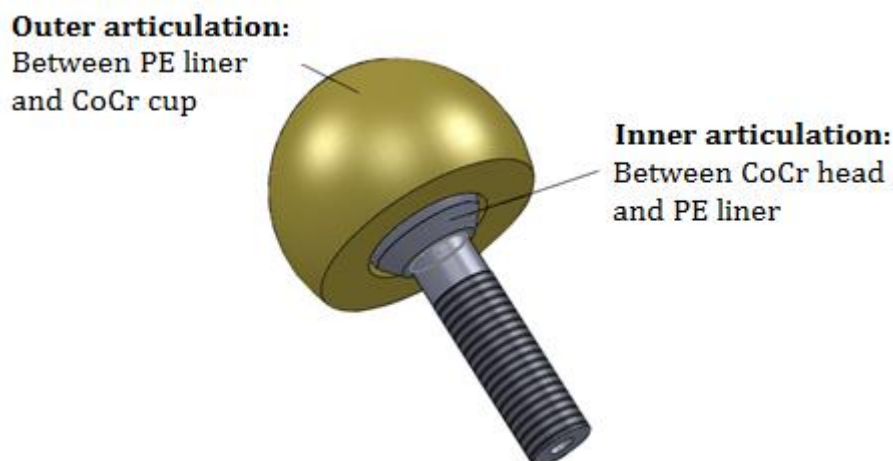


**Figure 2.12: Diagram showing the inner and outer articulation for dual mobility total hip arthroplasty.**

Interest in dual mobility bearings is currently increasing due to the failure of new-generation MOM THRA's which has led to the need for revision surgery.

Springer *et al.* [75] found that the most common cause of failure after revision surgery is joint instability and this accounts for 35% of all failed revision THAs. It is estimated that between 7-20% of revision THAs will dislocate [76; 77].

Dual mobility heads were designed in order to prevent component dislocation and have been proven to reduce the risk of dislocation in THA [78; 79]. It has also been shown that they prevent dislocation following revision THA [80-83]. Hence dual mobility bearings are investigated in this project as a solution for partial revision THA.

### **2.3 *In vitro* testing of orthopaedic biomaterials used in THA and THRA**

There are a large range of different testing methods available which can be utilised in order to study the tribology of different orthopaedic biomaterials. Initially a relatively simple and inexpensive wear screening such as a pin-on-plate test is carried out in order to assess the wear properties of the materials under investigation. If the results are promising then hip simulator studies are carried out in order to further assess the implants with testing conditions more similar to that seen *in vivo*.

Test results from different laboratories do not always agree with each other because the test conditions used in each can vary in terms of lubricant, load profile, inclination angle, bearing diameter, clearance, microseparation and test duration.

#### **2.3.1 Wear screening**

Biomaterials are initially assessed for use in orthopaedic applications using wear screening devices. Different laboratories have slight variations in the devices they use for wear screening, see Figure 2.13. All tests involve simplified components, rather than actual prosthetic joints and provide information exclusively on the intrinsic features of the materials under investigation [84].

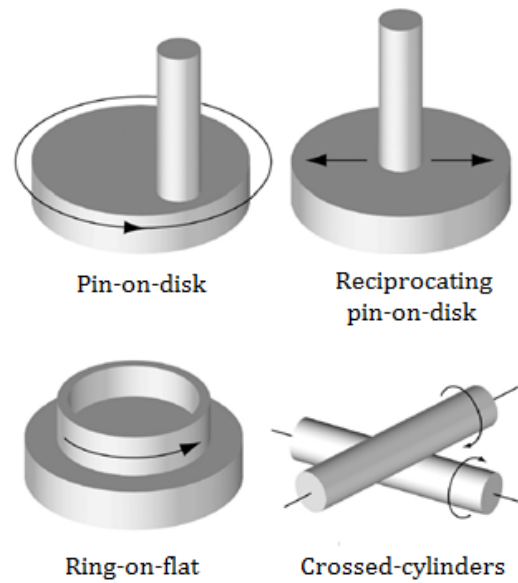


Figure 2.13: Examples of wear screening devices, Affatato *et al.* 2008 [84].

Within Durham University the bioengineering group use pin-on-plate machines for wear screening which provide both reciprocation and rotational motion. The machine used during this project is described in detail in section 3.3. Similar machines are also in use in other institutions [23; 85].

Pin-on-plate machines do not aim to recreate the exact loading and motions experienced in the body. However, the reciprocating and rotational motion that the materials incur during the tests are comparable contact speeds and stresses to those found *in vivo*. Hence they are a relatively fast and inexpensive method for ranking different materials [86; 87].

Wear screening is an important first step in evaluating biomaterials. After wear screening has been carried out, further testing is then required in order to determine the likely clinical performance of the bearing combination. This is achieved through the use of hip simulators and biocompatibility studies in order to determine the effects that the wear debris may have *in vivo*.

Hip simulators and the effect of wear debris from THA are discussed in greater detail in sections 2.3.2 and 2.5 respectively.

### 2.3.2 The human gait cycle and hip simulators

A hip simulator is defined to be:

*“any device which, under appropriate test conditions, causes a prosthesis to wear in a manner substantially equivalent to that which it would experience in typical clinical use in a patient. In order to accomplish this, a hip joint wear simulator will typically apply a set of motions and loads and a lubricant that, in combination, create tribological conditions comparable, but not necessarily identical, to those occurring in vivo” [88].*

To understand hip simulator motion it is first important to consider the human gait cycle as seen in Figure 2.14 [89].

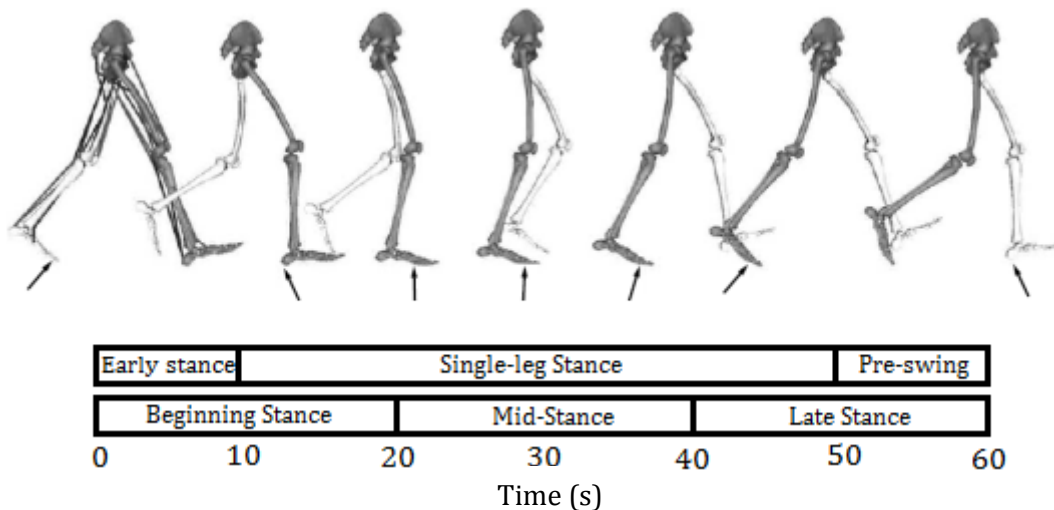
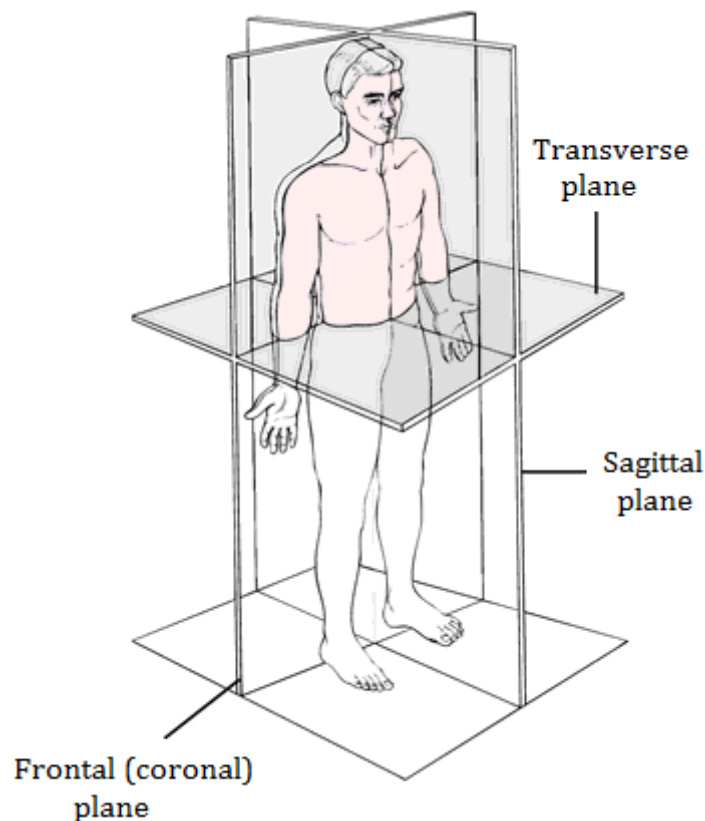


Figure 2.14: The human gait cycle, Zajac *et al.* 2003 [89].

Each cycle involves a period of ‘stance’ when the foot is in contact with the ground. This is followed by a ‘swing phase’ where the foot is in contact with the air and the limbs exchange their weight-bearing roles. The cycle ends when the swing foot contacts the floor, this is known as ‘heel strike’. From 30° flexion at initial contact, the hip progressively extends. The maximum extension is accomplished at the end of the terminal stance [90].

The hip joint allows motion in three planes: the sagittal plane, the coronal plane and the transverse plane, see Figure 2.15 [91]. Abduction is the movement of the limb away from the sagittal plane while adduction is the movement towards the sagittal plane. Internal rotation is the rotation towards the centre of the body (medial) while external

rotation is the rotation away from the centre of the body (lateral). In the body, the lower gluteus maximus and adductor magnus serve as the primary extensor muscles. The hamstrings also have a role in extension. Abductor support of the hip is through three muscles: gluteus medius-minimus complex; upper gluteus maximus and tensor fascia lata. Flexion of the hip is provided by the iliacus, adductor longus, rectus femoris, sartorius and gracilis. The adductor magnus, adductor longus and gracilis are the three hip adductors.



**Figure 2.15: Transverse, sagittal and coronal planes of the body, Applegate *et al.* 2010 [91].**

In order to determine the loading profile during normal gait, Paul [92] measured the muscle activity during walking from sixteen young and healthy adults. Markers placed on the skin of each person were used to measure movement with cinematic film whilst a force plate on the floor measured the ground to foot forces. The loading profile established in this work is now the most commonly used loading profile for hip simulator testing.

There are a wide variety of hip simulators employed worldwide which differ from each other in many parameters.

Table 2.3 gives a summary of different hip simulators available for use today. Only multi-station simulators are described because they are able to perform multivariate analyses with greater confidence within a single test [93].

## 2. Literature review

Table 2.3: Description of different hip simulators available. A/A: Abduction/Adduction, F/E: Flexion/Extension, I/E: Internal/External rotation.

Hip Simulator	Degrees of Freedom	Load Data	Test Lubricant	No. of Test Stations	Reference
<b>Durham Mark II</b> (custom-made)	F/E: + 30° to - 10° I/E: ± 10°	Type: pneumatic Profile: square wave L <sub>max</sub> : 2500 N, L <sub>min</sub> : 100 N Frequency: 1Hz	25 % newborn calf serum	Five	[94; 95]
<b>Endolab</b> (commercial)	A/A: + 7° to - 4° F/E: + 25° to - 4° I/E: +2° to - 11°	Type: hydraulic Profile: Paul L <sub>max</sub> : 3000 N, L <sub>min</sub> : 300 N Frequency: 1Hz	25 % newborn calf/bovine serum	Six	[96-98]
<b>HUT-4</b> (Helsinki University of Technology, custom-made)	A/A: ± 6° F/E: ± 23°	Type: pneumatic Profile: Paul L <sub>max</sub> : 2000 N, L <sub>min</sub> : 400 N Frequency: 1 Hz	50 % calf serum	Twelve	[99]
<b>Leeds Mark II</b> (custom-made)	F/E: +30° to - 15° I/E: ± 10°	Type: pneumatic Profile: Paul L <sub>max</sub> : 3000 N, L <sub>min</sub> : 0 N Frequency: 1 Hz	25 % bovine serum	Six	[100-102]

Table 2.3 (cont.)

Hip Simulator	Degrees of Freedom	Load Data	Test Lubricant	No. of Test Stations	Reference
<b>MTS-Bionix</b> (commercial)	Bi-axial Rocking Motion, $\pm 22.5^\circ$	Type: Hydraulic Profile: Paul $L_{\max}$ : 2450 N, $L_{\min}$ : 50 N Frequency: 1Hz	50 % calf serum	Twelve	[103; 104]
<b>ProSim</b> (commercial)	F/E: $+30^\circ$ to $-15^\circ$ I/E: $\pm 10^\circ$	Type: pneumatic Profile: Paul $L_{\max}$ : 3000 N, $L_{\min}$ : 100N Frequency: 1Hz	25 % newborn calf serum	Ten	[28; 41]
<b>Shore Western</b> (commercial)	Bi-axial Rocking Motion, $\pm 22.5^\circ$	Type: Hydraulic Profile: Sinusoidal $L_{\max}$ : 2450 N, $L_{\min}$ : 150 N Frequency: 1.1 Hz	Bovine calf serum	Twelve	[105-108]

Images from four of the simulators described in Table 2.3 can be seen in Figure 2.16. The *in vitro* mechanical testing of orthopaedic implants carried out during this project utilised the Durham Mark II hip simulator and the ProSim hip simulator. Calonijs *et al.* [109] showed both of these simulators to produce wear vectors comparable to ISO-14242-1. Images of the aforementioned simulators are provided later in Chapter 4. ISO 14242-1 is provided in the Appendix. The standard specifies the relative angular movement between articulating components, the pattern of the applied force, speed and duration of testing for wear testing of hip joint prosthesis. Figure 2.17 shows the variation with time of angular movement to be applied to the femoral test specimen in accordance with ISO 14242-1.



**Figure 2.16: Images of simulators used for *in vitro* mechanical testing of orthopaedic implants. A: MTS-Bionix Hip Simulator, B: Endolab Hip Simulator, C: Leeds Mark II Hip Simulator, D: Shore Western Hip Simulator.**

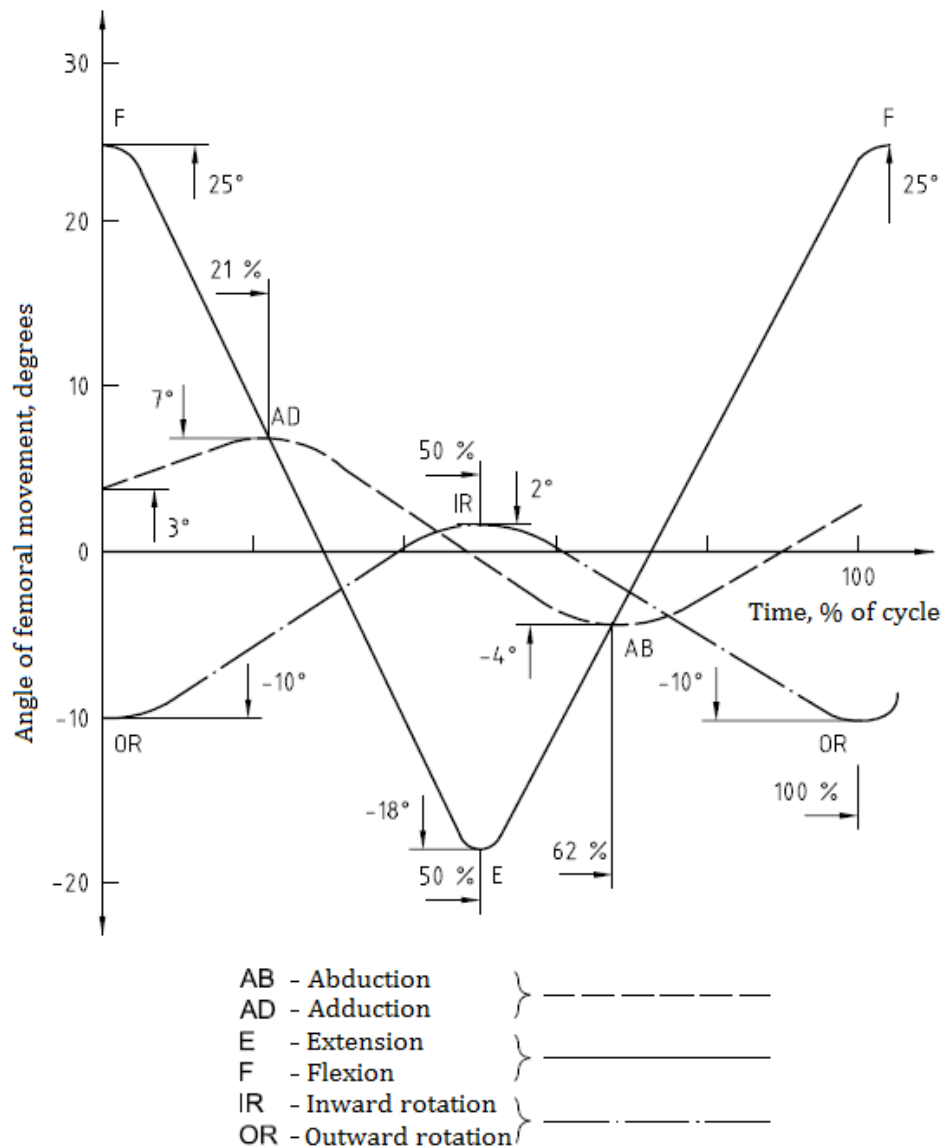


Figure 2.17: Variation with time of angular movement to be applied to the femoral test specimen, ISO 14242-1.

The MTS-Bionix and Shore Western hip simulators both have a bi-axial rocking motion as mentioned in Table 2.3. The acetabular cup is fixed in the anatomical position above the head which is mounted on a rotating shaft set at an angle to a rotating block. A single vertical load is applied and as the block rotates the head rotates about two axes to generate biaxial motion at the articulating interface.

The remainder of the hip simulators described in Table 2.3 have either two or three degrees of freedom. Whilst a hip simulator with A/A, F/E and I/E will provide the most accurate wear conditions in comparison to those seen physiologically, the resulting simulators are complex and costly. Barbour *et al.* [100] established that simplified hip

simulators with one axis of load and two axes of rotation (F/E and I/E) provided similar wear rates so long as the two axes of rotation were modified to be 90° out of phase.

Smith *et al.* [110] verified that the simplified square loading profile utilised by the Durham Mark II hip simulator provided similar wear data to that produced by a simulator following a Paul loading profile and was also more cost effective.

### **2.3.3 Lubricant used for biotribological testing**

One of the most important things to consider when testing biomaterial combinations for use in orthopaedic applications is the choice of lubricant.

Synovial fluid is the body's natural lubricant. It is found within the cavities of synovial joints.

The protein concentration of synovial fluid in healthy adults has been reported between 15 g/l and 35 g/l [111-113]. For patients with osteoarthritis and rheumatoid arthritis the concentration has been reported as 30 g/l [114] and 45 g/l [113] respectively. Albumin is the most abundant protein in synovial fluid, accounting for 56% of the protein content [115].

Hyaluronic acid is the largest molecule in synovial fluid [116] and is reported to determine the efficiency of hydrodynamic lubrication by synovial fluid in the natural hip joint [117].

Synovial fluid is non-Newtonian in nature and so the viscosity decreases greatly when the shear rate increases [118]. For patients with osteoarthritis or rheumatoid arthritis, the viscosity and elasticity of the synovial fluid decreases [115].

The natural hip joint is lubricated by 0.2-0.4 ml synovial fluid [113; 119]. The volume of lubricant required during *in vitro* mechanical testing can range between 40 and 600 ml [120]. This means that for a 5 MC simulator study the volume of lubricant required can be around 40 L. Needless to say, it would not be possible to obtain such a large quantity of human synovial fluid for these tests.

A range of alternative lubricants for *in vitro* biomaterial testing have been used in the literature and their effectiveness has been analysed based on comparison of the wear rates and wear debris with that seen *in vivo*. Water, Ringer's solution, bovine or calf

serum and gelatine-based protein solutions are among the lubricants which have been trialled. The advantages and disadvantages of each have been summarised by Harsha *et al.* [121] and the results are shown in Table 2.4.

**Table 2.4: Commonly used lubricants for in vitro testing and their advantages/disadvantages [121].**

<b>Lubricant</b>	<b>Advantages</b>	<b>Disadvantages</b>
<b>Water</b>	Inexpensive and safe, minimal degradation or contamination by bacteria	Wear rates are inconsistent due to transfer film. Wear debris size and shape are not representative of clinical wear debris
<b>Ringer's solution</b>	Inexpensive and safe, minimal degradation or contamination by bacteria	Wear rates are inconsistent due to transfer film. Wear debris size and shape are not representative of clinical wear debris
<b>Dilute bovine serum</b>	Wear rates generally of the same order of magnitude as those seen clinically	Relatively expensive, degrades fairly quickly and may be contaminated by bacteria
<b>Gelatin-based protein solution (Gelofusine)</b>	Wear rates are similar to bovine serum	Expensive and may be contaminated by bacteria. Wear debris size is similar to that produced when water is the lubricant
<b>Gelatin-based protein solution (Plasmion)</b>	Synthetic serum with protein content of 30 g/l	Expensive, wear rates are similar to that observed when water is used as the lubricant. Wear debris produced is not representative of clinical wear debris

The lubricant chosen for use in this project was bovine serum. This was in accordance with the recommendation by the International Organisation for Standardisation (ISO) standard 14242-1. This standard is provided in the Appendix and states that the test lubricant must not have a protein mass concentration less than 17 g/l.

The test lubricant was replaced every 0.5 MC and the anti-microbial reagent sodium azide was added in order to overcome the problems of degradation and potential microbial contamination. EDTA was also added in order to prevent calcium deposition.

Bovine serum can vary from batch to batch and hence there may be variation in wear data between different investigators using different batches of serum.

### 2.3.4 The need for aggressive testing conditions

#### 1) Increased inclination angle

The inclination angle of the acetabular component can be determined clinically by measuring the angle between a line drawn along the opening of the acetabular cup and one joining the ischial tuberosities, as shown in Figure 2.18 [122].

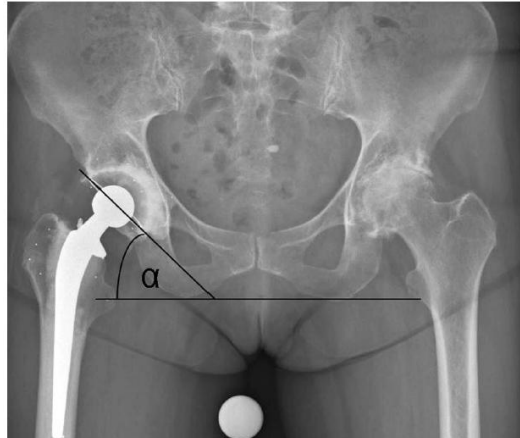


**Figure 2.18: Radiograph showing method of determining inclination angle, labelled 'α' [122].**

Analysis of retrieved THAs of various designs has shown a large variation in wear with wear rates exceeding that anticipated from simulator studies. Often the retrievals with high wear rates have inclination angles above 55° and surface wear features which suggest an edge-loading mechanism.

Standard simulation conditions currently assume that:

1. The prosthesis is correctly positioned within the patient, at approximately 45°.
2. The patient has a standard walking cycle.
3. The patient has a standard weight and physiology.

In reality however:

1. Both rotational and translational mal-positioning of the prosthesis can occur *in vivo* based on the surgical technique. Rotational mal-positioning occurs when the acetabular cup is inclined at a steep angle which moves the wear patch towards the cup rim and can result in edge loading. Translational mal-positioning occurs when the centre of rotation of the femoral head is not in-line with the centre of rotation of the acetabular cup. This can also result in edge-loading. [28; 29; 123-128]

2. The patient may also undergo activities such as jogging or walking up stairs which can place additional strain on the prosthesis.
3. Patients can vary greatly in terms of weight, height, synovial fluid and adverse reaction to the prosthesis.

The contradictions between data from simulator studies and clinical data confirm the need for more aggressive testing conditions in order to fully anticipate the clinical performance of any replacement hip joint.

Clinically, cup inclination angles over 50° have been shown to increase the whole blood level concentrations of metal ions after MOM THRA [129; 130]. *In vitro*, MOM simulator studies with cups positioned at 55° and 60° have been shown to cause an increase in wear rate [29; 131]. Increased wear rate has also been reported clinically for COC and MOP bearings with increased cup inclination angles [132-134].

### 2) Microseparation

Since the early 2000's, video fluoroscopy has been used to determine the *in vivo* kinematics of the hip joint [135-138]. Lombardi *et al.* [135] investigated the extent to which hip joints separate during normal gait, known as microseparation. Eight patients with a total of ten THA's performed successive gait motions on a treadmill whilst under fluoroscopy, see Figure 2.19.



**Figure 2.19: Subject undergoing a fluoroscopic evaluation whilst walking on a treadmill, Lombardi *et al.* 2000 [135].**

X-rays and a fluorescent screen coupled to a camera allowed two-dimensional images of the internal hip bearings to be recorded. The images were then analysed using a three-dimensional model-fitting technique that converts two-dimensional fluoroscopic images into three-dimensional real time images. Hip joint separation was determined to be present if the amount of separation was greater than 0.75 mm, which was the calculated linear error. The results confirmed that all ten joints experienced separation between the head and the cup although contact was maintained at the superior most tip of the cup. The magnitude of separation ranged from 0.8 to 2.8 mm with an average separation of 1.2 mm.

In a separate investigation by Komistek *et al.* [137], ten patients with MOM THAs were compared to ten patients with MOP THAs whilst performing normal gait on a treadmill under fluoroscopy. No separation of the hip joint was observed in patients with MOM THAs over the threshold value of 0.75 mm whilst all of the patients with MOP THAs experienced separation. The magnitude of separation ranged from 0.8 to 3.1 mm with an average of 2 mm.

However the accuracy of fluoroscopic measurements for the investigation of *in vivo* kinematics has been criticised [139]. More recently a study by Glaser *et al.* [138] claimed higher accuracy and hip joint separation could be determined if the amount of separation was greater than 0.5 mm. The investigation showed that separation occurred in all bearings and also suggested that the timing and separation could vary between patients and bearings.

Despite the controversy surrounding fluoroscopic measurements, the addition of 'microseparation' testing conditions to hip simulators has been applied successfully in order to produce wear patterns found in retrieval studies such as stripe wear seen in ceramic joints [140; 141].

Researchers have modified hip simulators using a number of different techniques in order to incorporate microseparation into their simulator studies, see Table 2.5. It is suggested that high inclination angle as well as microseparation testing conditions are employed in order to sufficiently and aggressively test new implants and to provide clinically relevant wear data [28].

## 2. Literature review

**Table 2.5: Previous work using hip simulators that have been modified to achieve microseparation.**

<b>Author</b>	<b>Year</b>	<b>Bearing Combination</b>	<b>Test Simulator</b>	<b>Modification made in order to achieve microseparation</b>	<b>Microseparation (mm)</b>
Nevelos [142]	2000	COC	Not stated	Achieved by applying a force of approx. 400 N in the lateral direction using a spring. This force, combined with a low swing phase load of less than 200 N allowed the joint to separate	0.2-0.8
Stewart [143]	2003	COC	Leeds Mark II	A small lateral to medial load was applied with a spring which during swing phase produced medial and superior translation of the insert relative to the head	0.2-0.5
Williams [127]	2003	COP	ProSim	A small negative load (less than 100 N) was applied to separate the components during swing phase	0.7
Manaka [140]	2004	COC	Shore Western	Horizontal displacement applied by spring, vertical displacement provided by applying a negative load	0.5-1.0
Brown [144]	2007	MOM	Leeds Mark II	A small lateral load applied to the cup relative to the head during swing phase	0.5
Bowsher [145]	2008	MOP	Shore Western	Preloading spring provided separation during each swing phase, set using a dial gauge-indicator	1.0-1.5
Williams [95]	2011	COM	Durham Mark II	A displacement block together with a modified loading cycle (0 to 2500 N) allowed the head to displace inferiorly and laterally during the low load swing phase	1.0 ± 0.2
Williams [146]	2013	COM, MOM	Leeds Mark II	Lateral to medial load was applied to the acetabular cup using a spring which during swing phase produced medial and superior translation of the cup relative to the head	0.4-0.5

### **3) Addition of third body particles**

There have also been incidences with increased wear in retrievals due to the presence of third body particles. Third body wear occurs when external wear particles are trapped in-between the bearing surfaces and act like an abrasive asperity removing material from the articulating surfaces [147].

Third body particle wear analysis has been used extensively in literature to analyse the affect of PMMA concentration on UHMWPE bearings and to assess the potential for causing osteolysis due to increased implant wear, see Table 2.6. Third body wear has a greater effect on hard-on-soft articulations as opposed to hard-on-hard articulations as is the case in MOM joint combinations. This thesis focuses specifically on the effect of third body particles on the MOM articulation in order to produce worn cups with features similar to that seen in retrievals; hence the data in Table 2.6 only presents the effect of the PMMA particles on the metal bearing surface. The addition of third body particles to test lubricant during hip simulations was shown to generally produce mild multidirectional scratches on the CoCrMo surface.

The concentration of PMMA particles added to the test lubricant in the studies shown in Table 2.6 varied between 0.15 mg/ml and 10 mg/ml but it is difficult to know the exact concentration of particles which will have entered the tribocontact. Clinically, it is also extremely difficult to know the concentration of debris that may actually migrate to the articulating surface because some wear particles will be removed from the joint space by the surrounding tissues, digestion and via the lymphatic system.

## 2. Literature review

Table 2.6: Comparison of previous simulator studies with the addition of third body particles.

Author	Year	Bearing Combination	Test lubricant	Third body particle	Particle size and concentration	Test duration	Effect on CoCr
Wang [148]	2001	CoCr vs. UHMWPE (32 mm)	50 % bovine serum	PMMA	160 $\mu\text{m}$ , 10 mg/ml	1 MC	Mild scratching
Affatato [149]	2002	CoCr vs. UHMWPE (28 mm)	-	Radiopaque PMMA (90% PMMA, 10% BaSO <sub>4</sub> )	170 $\mu\text{m}$ , 1 mg/ml	2.5 MC	Evidence of macroscopic damage, looping scratches observed
Wang [150]	2003	CoCr, alumina and zirconia vs. CXPE (32 mm)	50 % bovine serum (20 g/l)	PMMA	150 $\mu\text{m}$ , 5 mg/ml	1.5 MC standard, 2 MC PMMA, 1 MC standard	Multiple scratches
Bragdon [151]	2003	CoCr vs. CXPE (28 mm)	-	Aluminium oxide (severe wear) and PMMA (mild wear)	1 $\mu\text{m}$ and 30 $\mu\text{m}$ respectively, 0.15 mg/ml	1 MC standard, 5 MC aluminium oxide, 2 MC standard, 5 MC PMMA	Highly scratched with aluminium oxide Fine scratches with PMMA
Bragdon [152]	2005	CoCr vs. UHMWPE (28, 38, 46 mm)	-	PMMA containing BaSO <sub>4</sub>	< 30 $\mu\text{m}$ , 0.15 mg/ml	5 MC	Multidirectional scratches
Kubo [153]	2009	CoCr vs. CXPE (32 mm) CoCr vs. HXPE (44 mm)	Bovine serum (20 g/l)	PMMA	40 $\mu\text{m}$ , 5 mg/ml	1.5 MC standard, 1.5 MC PMMA	Mild multidirectional scratches
Sorimachi [154]	2009	CoCr vs. CXPE (32 mm) CoCr vs. HXPE (44 mm)	50 % bovine serum (20 g/l)	PMMA	40 $\mu\text{m}$ , 10 mg/ml	1.5 MC standard, 2 MC PMMA, 2 MC standard	Surface roughness unaffected

PMMA is a third body particle which can be commonly found in the joint cavity from the bone cement which was used to fix the joint in place but it is not the only third body particle which may be present. There are many sources of third body wear, see Table 2.7 [155].

**Table 2.7: Sources of third body wear, Brown *et al.* 2009 [155].**

<b>Source</b>
Bone cement
Radiopacifier particles
Bone particles
Trochanteric reattachment wires
Burnishing from loose stems
Hydroxyapatite particles
Fixation screw fretting
Neck impingement
Matt/precoat stem abrasion
Instrument scratching
Modular connection fretting
Cutting guide abrasion
Porous coating particles
Locking mechanism breakage
Microseparation impact
Assembly/impaction chipping

If a THA or THRA fails due to implant loosening then it is possible that particulate debris from the porous coating on the back of the acetabular cup or the femoral head stem may disintegrate and enter the joint cavity which could then have the ability to accelerate wear as well as cortical bone debris [156; 157].

Hydroxyapatite and titanium are common coatings which are used in order to aid fixation and prevent components from loosening. Morscher *et al.* [156] have seen clinically that hydroxyapatite wear particles have scratched CoCrMo femoral heads when articulating against UHMWPE *in vivo*. Davidson *et al.* [157] have reported that

titanium particles can cause light abrasive wear to CoCrMo when using a reciprocating, linear wear tester in a deionized water bath.

This project will investigate the effect of both of these wear particles, hydroxyapatite and titanium, on the MOM articulation.

Further to this, the performance of dual mobility bearings under aggressive testing conditions will be investigated. The aggressive conditions employed in the project include the use of scratched CoCrMo cups, testing at a high inclination angle as well as under microseparation conditions.

## **2.4 Wear and lubrication theory**

### **2.4.1 Wear mechanisms**

A wear mechanism is the fundamental microscopic process by which material is removed from a surface [158]. The most common wear mechanisms are shown in Figure 2.20 and include [84; 158-160]:

#### **1) Adhesive wear**

During adhesive wear, adhesion (or bonding) occurs at the asperity contacts on the interface. Fragments from one surface are pulled off and adhere to the alternate surface. In MOM bearings, adhesion is often prevented by an oxide layer but adhesion can occur readily in hard-on-soft bearings, such as MOP, where small fragments of the polyethylene surface adhere to the opposing metal bearing surface. It is believed that the material transferred by adhesion will finally be detached from the alternate surface through fatigue wear.

#### **2) Fatigue wear**

Fatigue wear occurs when the surface and subsurface are subject to repeating loading and unloading cycles which result in subsurface delamination and cracking. Large fragments break off resulting in pitting on the surface. In MOP bearings, where polyethylene is the weaker of the two materials, fatigue wear damage to the polyethylene component is dominant. The wear particles formed through fatigue wear are typically larger than those formed through abrasive wear.

### **3) Abrasive wear**

Abrasive wear occurs when micro-roughened regions and small asperities on a hard bearing surface locally plough through the softer bearing surface. The softer material is progressively lost from the track traced by the asperity during motion of the harder surface. Abrasive wear is also called ploughing, scratching, scoring, gouging or cutting depending on the degree of severity.

### **4) Third-body wear**

Third-body wear is a form of abrasive wear that occurs when hard third-body particles from sources such as those listed in Table 2.7 become embedded in a soft surface. In MOM bearings, which form a passivation layer with the surrounding medium, third-body particles may be in the form of corrosion products. These particles are usually oxides which have different shear strengths than those of the metal bearing surfaces from which they were derived.

Third-body particles act in the same way as an asperity of a harder material in abrasive wear by removing material from its path.

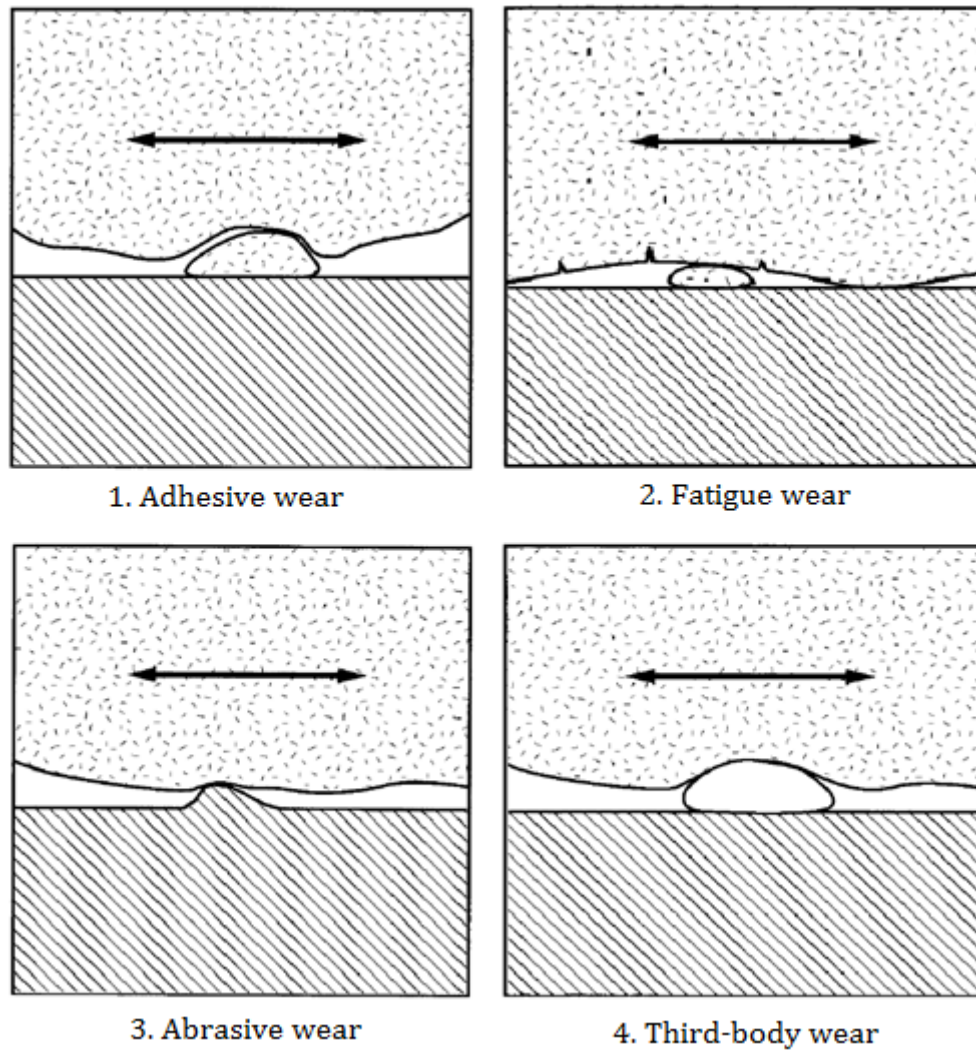


Figure 2.20: Common wear mechanisms, Wright *et al.* 2001 [159].

### 2.4.2 Lubrication

As discussed in section 2.3.3, synovial fluid is the body's natural lubricant. A lubricant is any substance which, when applied to the interface between two solids, will reduce friction and wear between the two surfaces. There are four principal lubrication regimes and they are defined below [161].

#### 1) Hydrodynamic lubrication (also known as **fluid-film lubrication**)

This occurs when a lubricant film is sufficiently thick enough to prevent opposing bearing surfaces from coming into contact with each other. The two surfaces are completely separate and friction is only generated through shearing of the lubricant.

This is considered to be the ideal lubrication regime and results in low friction and low wear.

### **2) Elastohydrodynamic lubrication**

This is a form of hydrodynamic lubrication whereby the fluid-film thickness is smaller and the pressure in the film causes elastic deformation of the bearing surfaces. However the articulating surfaces are still protected and no gross asperity contact occurs between the surfaces.

### **3) Boundary lubrication**

This occurs when the lubricant films adsorb to the surface and wear occurs through contact between asperities which have broken through the fluid film. The friction behaviour can be similar to that seen in dry contact.

### **4) Mixed Lubrication**

This occurs when boundary and hydrodynamic lubrication regimes are operating simultaneously. Partial fluid-film lubrication operates in the bulk of the space between two articulating surfaces, but asperity contact may also occur. Generally, this regime results in less wear than boundary lubrication but more wear than during hydrodynamic lubrication.

Fluid-film lubrication is the predominant lubrication mechanism in natural synovial hip joints under physiological walking conditions [162]. It has been shown that fluid-film lubrication may be achieved in hard-on-hard bearings such as MOM and COC provided that the bearing surface is manufactured within certain tolerances and that the radial clearance is chosen correctly and can be maintained [163].

It is not possible to achieve full fluid-film lubrication for MOP bearings which experience mixed lubrication of boundary lubrication regimes instead [164]. This is because the roughness of the UHMWPE bearing is much larger than the generated lubricating film thickness.

## 2.5 Wear debris from THA and THRA

Wear is the removal of material from one or both of two solid surfaces in a solid-state contact and will occur when the surfaces are in a sliding, rolling or impact motion relative to one another [160]. The wear particles released from the articulating bearing surfaces in THA and THRA are discussed in the following sections 2.5.1-2.5.2 with the focus being on the *in vivo* effect, isolation and characterisation of both polymeric and metallic wear debris.

### 2.5.1 *In vivo* reaction to wear debris

The majority of available clinical data regarding the *in vivo* reaction to wear debris from THA concerns polyethylene and metal debris.

#### 1) *In vivo* reaction to polymeric wear debris

The biological response to polyethylene wear debris, either alone or in combination with other factors, can cause aseptic loosening of the components which is ultimately responsible for the failure of MOP THA.

The polyethylene wear debris generated at the articulating surfaces enters the periprosthetic tissue where it is phagocytised by macrophages. This occurs when the concentration of the wear volume is within 0.2 – 0.8  $\mu\text{m}$  which is the critical size for macrophage activation. Cytokines and proinflammatory mediators are then released which stimulates osteo-clastic bone resorption causing the bone surrounding the implant to break down and the prosthesis to become loose [165].

Initially in the early 1980s PMMA was believed to be the problem causing the bone resorption [166-168] but by the late 1980s retrieval analyses and animal studies were showing polyethylene wear debris to be responsible [169-173].

By the mid 1990s it was established that retrieved UHMWPE particles are generally globular spheroids and on average 0.5  $\mu\text{m}$  in diameter with range from 0.1 to 2.0  $\mu\text{m}$  [174]. It has been reported that ninety per cent of particles are less than 1  $\mu\text{m}$  in diameter [175; 176]. These studies imply that most polyethylene particles generated from the bearing surface are within the critical size range to initiate an inflammatory response.

As research into improving the wear properties of conventional UHMWPE progressed and highly cross-linked UHMWPE developed it was hoped that the occurrence of wear particle induced osteolysis would reduce as the wear rate reduced. Baxter *et al.* [177] collected tissue samples taken at revision surgery from nine conventional UHMWPE as well as nine highly cross-linked UHMWPE cups. For both sets of UHMWPE cups correlations were observed between the wear debris present and the magnitude of individual patient macrophage responses. Numbers of both wear debris and macrophages were lower in highly cross-linked UHMWPE however this may have been a consequence of shorter implantation times. The highly cross-linked UHMWPE cups had an average implantation time of only 3.3 years whereas the conventional UHMWPE cups had been implanted for on average 13.3 years. Baxter concluded that the short-term clinical data does suggest that wear debris from highly cross-linked UHMWPE may still contribute to early implant loosening. Despite this, several clinical studies in the mid 2000s have reported no incidence of osteolysis at mid-term follow up for highly cross-linked UHMWPE [178-181].

It was this failure due to implant loosening in MOP THA that has led to a resurgence of interest in hard-on-hard bearings such as MOM.

### **2) *In vivo* reaction to metallic wear debris**

Metal wear particles released from artificial hip implants are also phagocytised by macrophages that accumulate around the implant, in the periprosthetic tissues and local bone marrow [182]. Metal wear debris are typically much smaller than polyethylene wear particles and are nanometre in size, see Figure 2.21 [183].

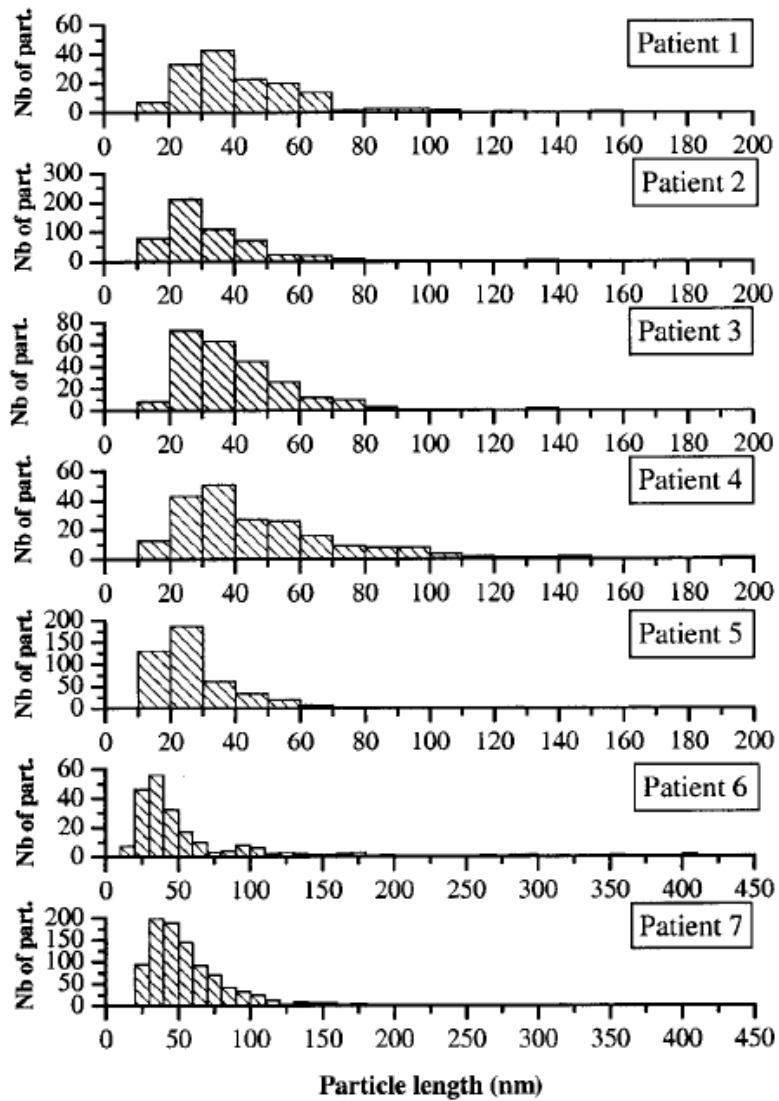
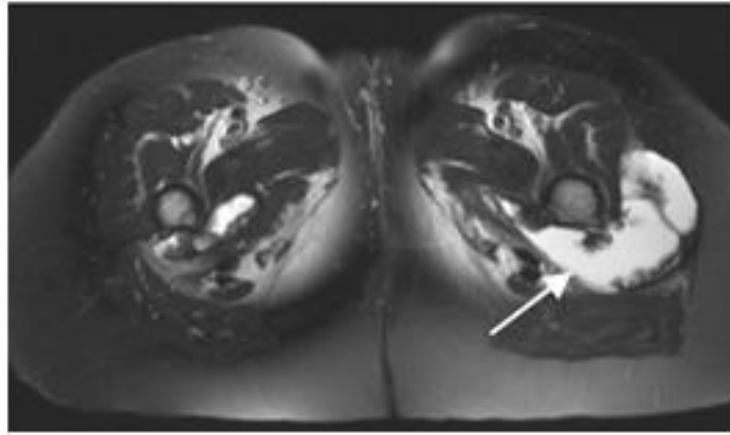


Figure 2.21: Length of particles isolated from tissue samples collected from different periprosthetic capsular sites, measured by image analysis of TEM micrographs, Catelas *et al.* 2004 [183].

The nanometre-sized particles can also be bound into proteins and so are transported within lymphatic channels and can reach distant lymph nodes, the liver, and the spleen. This process can lead to the production of pseudotumors, see Figure 2.22 [184].



**Figure 2.22: MRI scan showing a pseudotumor arising from the posterior joint space (arrow), Pandit *et al.* 2008 [184].**

A pseudotumor is a large focal solid or semiliquid mass, normally occurring on the medial aspect of the femoral component just below the midpoint of the prosthesis [185]. It is not infective but can be locally destructive and often requires revision surgery [186]. Hart *et al.* [187] looked at tissue from a range of failed MOM prostheses and established a clear correlation between the dark macrophages and the presence of chromium. Xia *et al.* [188] analysed biopsies from a typical case of pseudotumor following MOM THRA using light microscopy, transmission electron microscopy, backscatter electron microscopy and energy dispersive x-ray spectrometry. Chromium nanoparticles were predominant in the tissue and the study suggested that it was actually the corrosion of cobalt in the macrophages and the resultant cobalt ion release that led to tissue necrosis and adverse reactions. The exact cause of pseudotumors remains unclear.

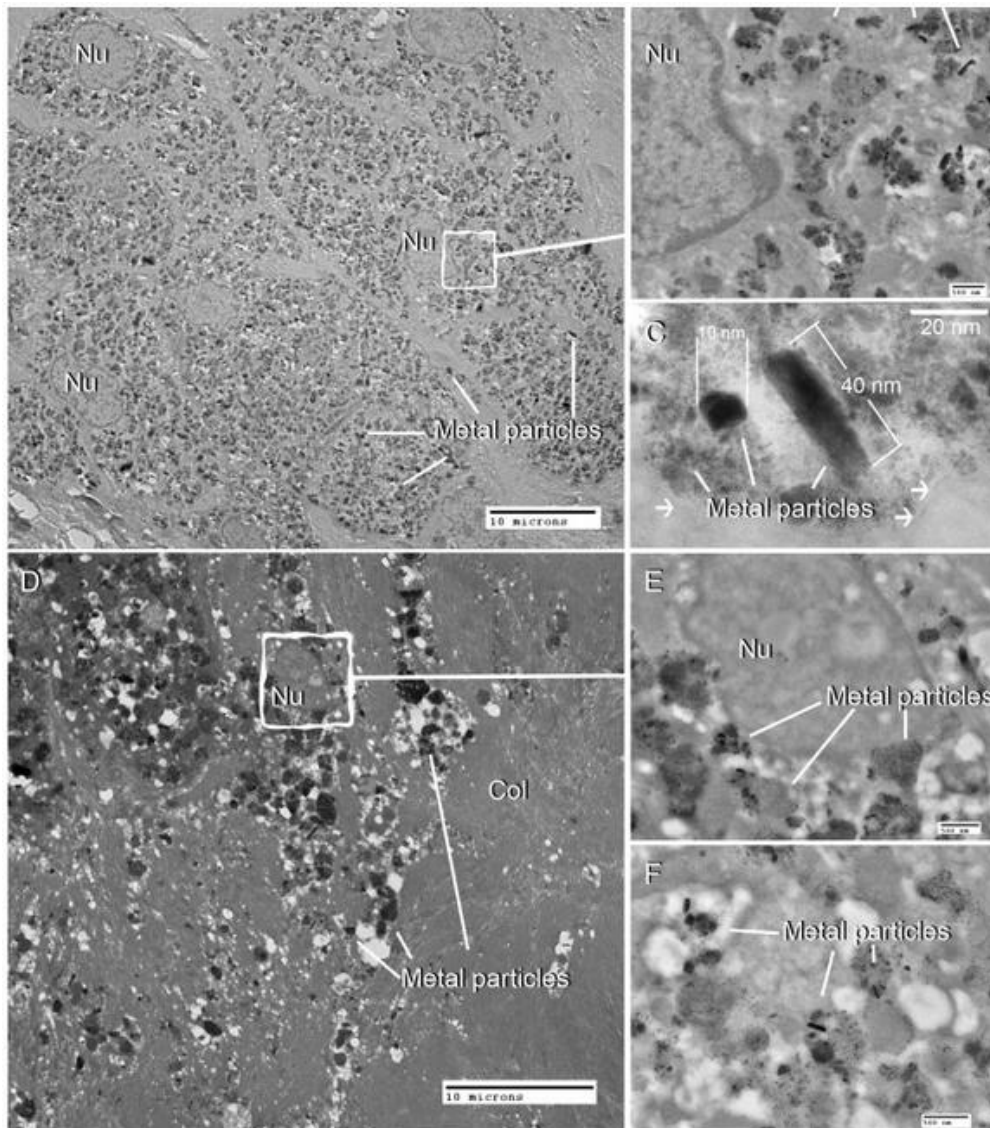


**Figure 2.23: TEM micrographs showing the presence of metal wear nanoparticles in living macrophages and in tissue taken at biopsy from a pseudotumor, Xia *et al.* 2011 [188].**

Incidences of MOM hypersensitivity have been reported in less than 1% of cases and the mechanism is still not completely understood. Skin patch testing has documented an overall increase in the prevalence of metal allergy in people with metal implants [189; 190] but it is still unclear whether metal sensitivity is a contributing factor to implant failure.

Delayed hypersensitivity-like reactions, including metal hypersensitivity and pseudotumors, have been termed aseptic lymphocytic vasculitis-associated lesions (ALVAL).

Whilst histopathologic descriptions of ALVAL are similar to general samples of soft tissue taken from around failed THAs and feature an increase in macrophages, the

single unique feature of ALVAL is the presence of a dense perivascular infiltrate [191]. Hence the term “vasculitis-associated lesion”.

Recently the numerous reports of adverse tissue reactions to MOM bearings for THA and even more so for THRA have raised doubts in the orthopaedic community over the benefits of metal bearing surfaces for orthopaedic applications. Whilst some think it is worth pursuing and improving the design and surgical technique, the media coverage has caused anxiety among patients and surgeons alike [192].

### **2.5.2 *In vitro* isolation and characterisation of wear debris**

As concern surrounding the *in vivo* reaction to wear debris from THA grew, increasing importance was placed on determining not only the wear rates of potential bearing combinations for orthopaedic applications but also the size and shape of the wear debris produced during wear testing.

In order to isolate wear particles from the bovine serum used as lubricant in wear simulations the protein in the serum must first be digested. This then releases any particles bound within it. Great care must be taken so as not to damage the particles or change their size and shape during the digestion process.

#### **1) *In vitro* isolation and characterisation of polymeric wear debris**

Polyethylene wear particles have been isolated using a number of methods. A brief overview of previously employed techniques is provided in Table 2.8 which comprises strong base, acid and enzymatic digestion processes. The ‘Silicon Wafer Display (SWD) protocol’ mentioned in Table 2.8 was awarded the John Charnley Award and is shown fully in Figure 2.24 alongside images of isolated polyethylene particles obtained through the procedure.

Highly cross-linked polyethylene particles are reported to be smaller than conventional UHMWPE particles [42; 193; 194] and size is expected to vary between implants depending on irradiation procedure and machining [195].

## 2. Literature review

**Table 2.8: Overview of techniques used to isolate polyethylene wear debris from *in vitro* test serum.**

<b>Author</b>	<b>Year</b>	<b>Digestion process</b>	<b>Particle size</b>
Hailey <b>[196]</b>	1996	Serum added to 12 M KOH at 60° followed by centrifugation and filtration.	Aggregates of particles, generally ranging from 10-100 µm. Some mm in size.
Wang <b>[197]</b>	1996	5 N KOH added to serum in ratio 2:1 at 65° followed by density gradient centrifugation and filtration.	Spherical particles generally less than 0.3 µm diameter. Fibrous particles generally 1-2 µm long and less than 0.5 µm wide.
Affatato <b>[198]</b>	2001	Serum added to 12 M KOH at 60° followed addition of ethanol with continuous stirring and filtration.	Generally 10-15 µm in diameter and flakes up to 100µm also seen.
Niedzwiecki <b>[199]</b>	2001	37 vol % HCl added to serum in ratio 5:1 at 60°, 1 ml extracted and added to methanol for filtration.	Majority of particles were less than 0.1 µm <sup>2</sup> .
Niedzwiecki <b>[199]</b>	2001	30 mg of Proteinase K added to diluted serum in ratio 1:1 with distilled water at 37°, 1 ml extracted and added to 10 ml distilled water for filtration.	Majority of particles were less than 0.1 µm <sup>2</sup> .
Endo <b>[42]</b>	2002	Serum added to 12 M KOH at 60° followed by chloroform/methanol extraction of lipids, centrifugation and filtration.	Generally 0.1-1 µm for non cross-linked UHMWPE and 0.1-0.5 µm for moderately cross-linked UHMWPE.
Billi <b>[194]</b>	2012	SWD protocol, as detailed in Figure 2.24.	Separated into round, oval, rod, irregular and fibril shapes with average size ranging from 0.1-48 µm depending on particle shape and degree of UHMWPE cross-linking.

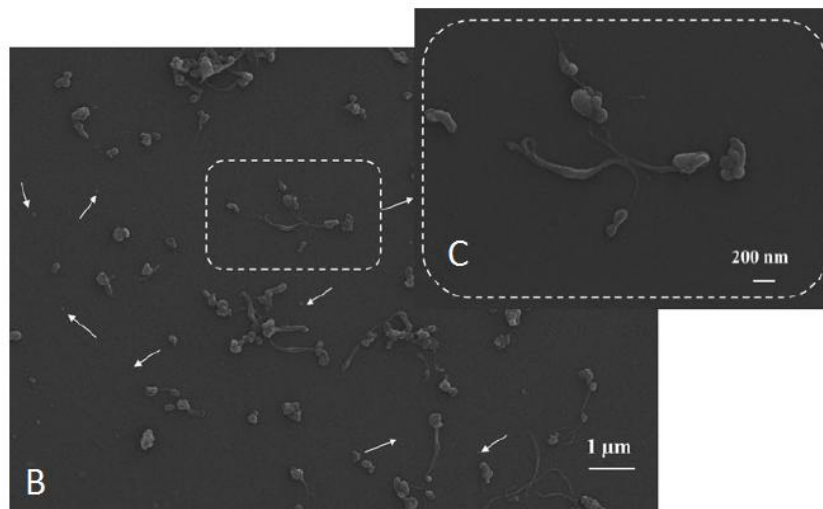
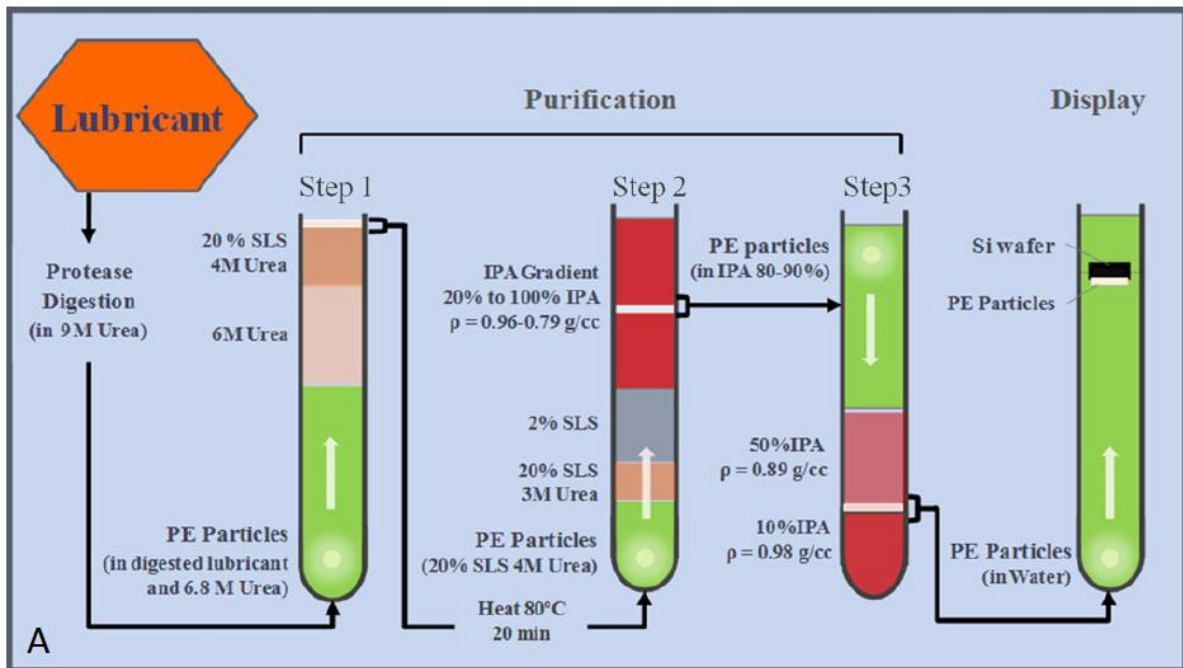


Figure 2.24: A: Schematic diagram showing the SWD Protocol, B: polyethylene wear debris displayed on silicon wafer, C: magnified polyethylene wear debris, Billi *et al.* 2012 [194].

Whilst smaller polyethylene particles have been reported to be more biologically active in stimulating cytokine release and bone resorbing activity [200] it has to be remembered that this potential increase in biological activity, in comparison to wear particles produced from conventional UHMWPE bearings, will be counterbalanced *in vivo* by lower wear rates due to cross-linking and hence a smaller volume of polyethylene particles being generated [102].

## 2) *In vitro* isolation and characterisation of metallic wear debris

Isolation of metal debris from test serum is more challenging due to the nature of the particles which tend to be nanometre in size, reactive in nature and can form agglomerations. Catelas *et al.* [201; 202] showed that digestion protocols using strong base could potentially damage metal particles, reduce their size and affect their shape. Chromium oxide particles were found to disappear increasingly after treatment with base digestion as the time and base concentration increased. Instead, enzymatic digestion is preferred for metal debris isolation because damage to particles is low and no hazardous waste is produced.

Table 2.9 gives a brief overview of previously used techniques to isolate metal particles from *in vitro* test serum generated from simulations using CoCrMo bearings. The particles isolated are typically CoCr or Cr-rich in composition. Cr-rich particles are indicative of mild wear removing the protective passivation layer at the bearing surface and the production of chromium oxide particles [203]. Figure 2.25 shows TEM images of previously isolated metal wear particles.

**Table 2.9: Overview of techniques used to isolate metal wear debris from *in vitro* test serum.**

<b>Author</b>	<b>Year</b>	<b>Digestion process</b>	<b>Particle size and composition</b>
Tipper [23]	1999	Digestion with KOH at 60° followed by extraction with chloroform/methanol extraction and repeated washes with 50% acetone	60-90 nm CoCr particles. (pin-on-plate test)
Catelas [201]	2001	Comparison of four techniques: three with base digestion (2N KOH, 12N KOH and 5N NaOH for either 2 or 48 hours) and enzymatic digestion using papain, proteinase K and six purification steps	12-250 nm with mean 80±40 nm. Either CoCr or Cr-rich particles.
Brown [144]	2007	Digestion with papain, proteinase K, yeast lytic enzyme, zymolase and twelve step purification process	6-156 nm with mean typically 30-40 nm. CoCr particles.
Billi [203]	2011	Digestion with proteinase K and one step purification process using density gradient centrifugation	Cr-rich particles 100±80 nm. CoCr particles 300±200 nm.

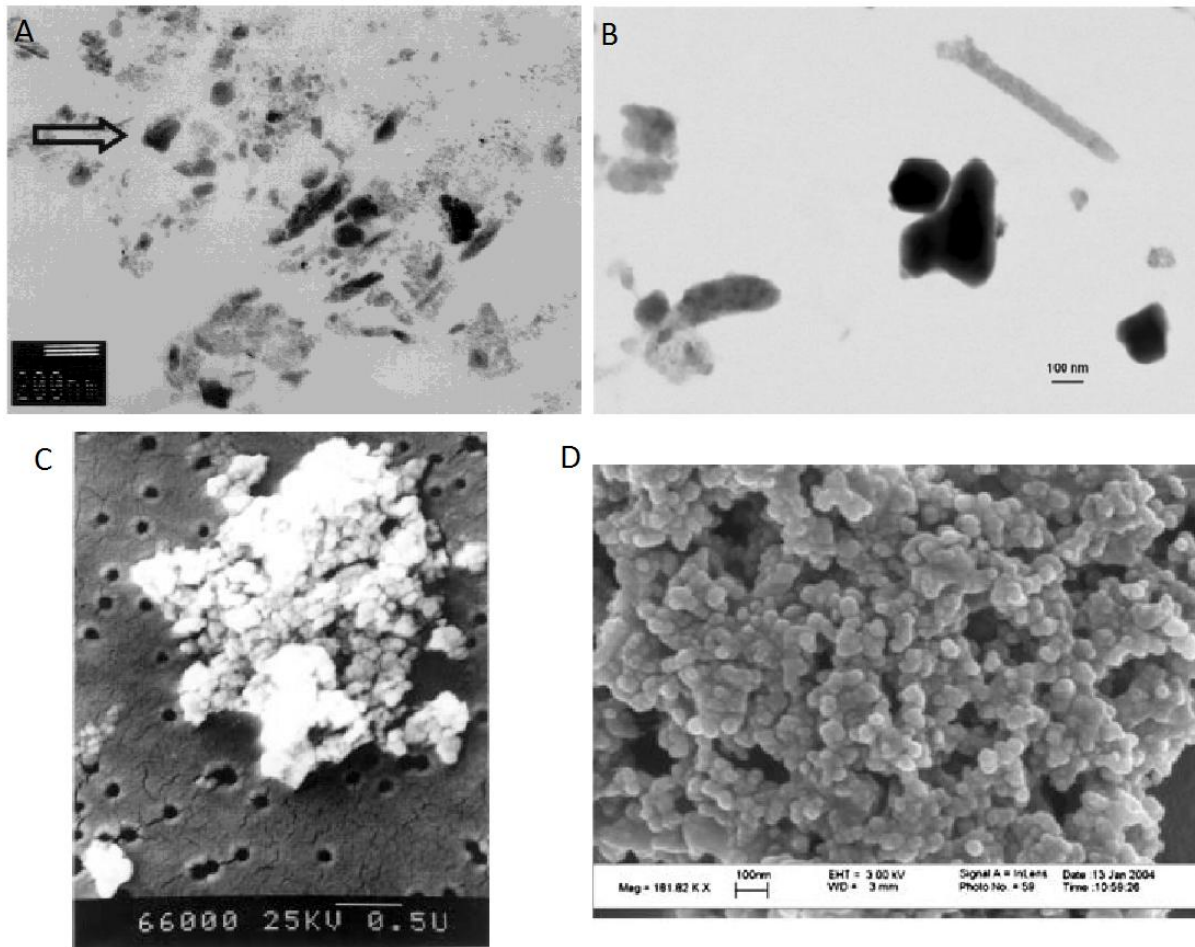


**Figure 2.25:** Images of isolated metal wear particles from A: Catelas *et al.* 2001 [201] (TEM image). B: Billi *et al.* 2011 [203] (TEM image) The darker particles indicate presence of cobalt. C: Tipper *et al.* 1999 [23] (SEM image). D. Brown *et al.* 2007 [144] (SEM image).

Wear debris isolation is challenging but crucial since it is only once wear particles have been successfully isolated and characterised that the *in vivo* reaction, in terms of cell and macrophage/cytokine response, can be assessed.

It is very difficult to produce samples of isolated metal wear particles from *in vitro* hip simulator studies that are free from impurities and of sufficient concentration for biological studies. Often pin-on-plate tests are run in water in order to provide a large quantity of CoCr particles, or commercially available CoCr is used. Table 2.10 provides a summary of studies applying metal wear particles to cells. Questions remain whether the particles used in these studies are sufficiently similar to particles produced *in vivo* in order to provide clinically relevant results and research in this area is ongoing.

Table 2.10: Summary of biological studies using CoCr particles.

Author	Year	Wear particles	Particle source	Cell-line used
Doran [204]	1998	Co, Cr, Ni, Fe, Mo, Al, V and Ti	Co-Cr alloy particles (< 104 µm) from Howmedica Inc.	C3H10T½ mouse fibroblast
Germain [205]	2003	CoCr	Generated using pin-on-plate test run in water	U937 macrophages and L929 fibroblasts
Williams [206]	2004	CoCr and CrN	Generated using pin-on-plate test run in water	U937 macrophages and L929 fibroblasts
Papageorgiou [182]	2008	CoCr	From Osprey Ltd with composition similar to that used in orthopaedic joints	THP-1 monocytes
Andrews [207]	2011	Co <sup>2+</sup> , Cr <sup>3+</sup> , Cr <sup>6+</sup>	Cobalt (II) chloridehexahydrate, chromium (III) chloride hexahydrate from Sigma, and chromium (VI) oxide from BDH	SaOS-2 osteoblast-like cells
Zijlstra [208]	2011	Co <sup>2+</sup> , Cr <sup>3+</sup> , Co <sup>2+</sup> , and Cr <sup>3+</sup> in ratio 1:2	CoCl <sub>2</sub> .6H <sub>2</sub> O and CrCl <sub>3</sub> .6H <sub>2</sub> O	SaOS-2 osteoblast-like cells

## 2.6 Revision THA

The failure of a THA or THRA leads to the need for revision surgery. Potential reasons for hip revisions can be summarised into three categories [209]:

- Patient-related factors including sickle cell anaemia, poor bone quality and possibly high body mass index.
- Implant-related factors including osteolysis, aseptic loosening, metallosis, periprosthetic fractures and delamination of the porous coating.

- Failures related to inadequate surgical technique through malpositioning of the components.

About 40,000 primary THAs are performed in NHS hospitals in England with about 4,000 revision procedures being performed each year [210]. Figure 2.26 is taken from the UK Joint Registry 2012 [66] and shows the risk of revision according to the primary bearing surface. A large number of patients are receiving THAs at a younger age, and also living longer, so it is important that the initial implant allows for revision. Revision surgery can involve either the revision of the acetabular component, with restoration of bone stock, or revision of the femoral component.

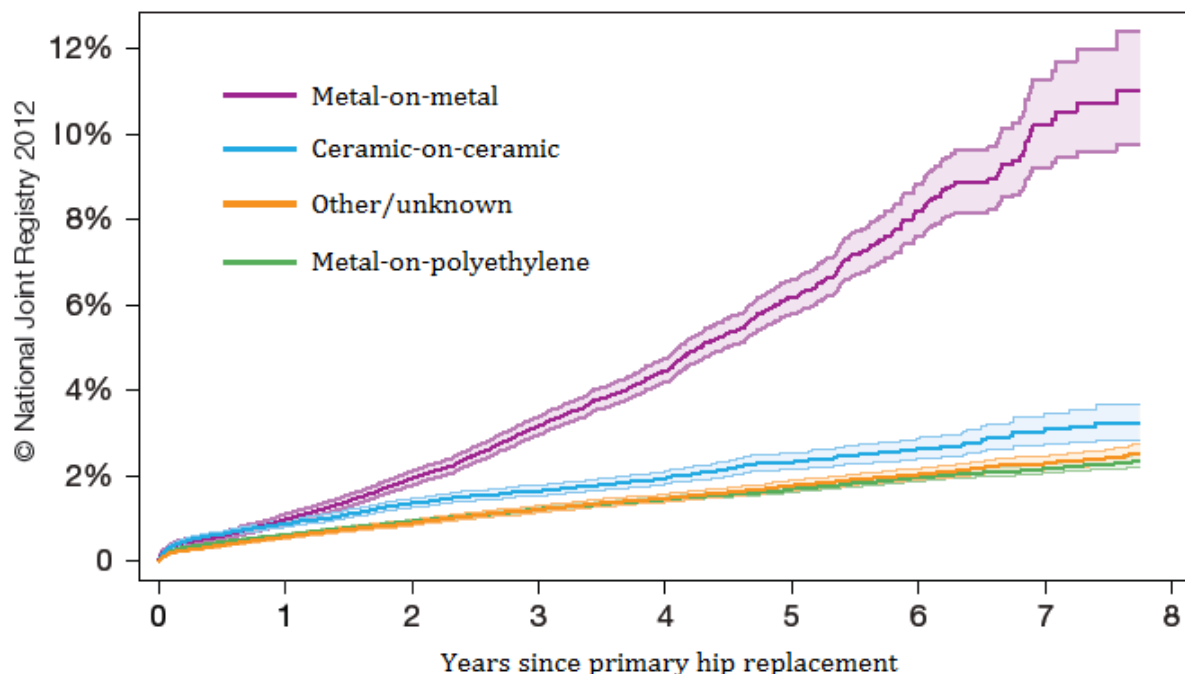


Figure 2.26: Risk of revision by bearing surface (cumulative hazard with 95% confidence intervals), UK National Joint Registry [66].

The key points for treatment in case of failure that must be considered are [211]:

- To identify the origin of the problem in order to avoid repeating the failure
- To verify implant stability
- To evaluate if components are malpositioned
- To optimize the new coupling in order to reduce further wear
- To restore the centre of rotation and bone stock where possible
- To treat any soft tissue damage

- To treat and avoid any impingement

The aim of revision surgery is to provide the patient with a low wearing THA through a surgical procedure that is as minimally invasive as possible.

There are two main types of revision implants available; cemented or cementless. A cemented prosthesis requires cement to attach the metal components to the bone whereas a cementless prosthesis has a porous backing which allows for bone ingrowth and hence biological fixation.

The top five cup-stem brand combinations for both primary and revision hip procedures performed during 2012 are compared in Table 2.11 and Table 2.12 respectively from data published by the UK National Joint Registry [66]. The cup and stem brands shown in italics are cemented prostheses. The remaining brands are cementless prostheses.

Note that the top five cup-stem brand combinations in Table 2.11 account for 45% of all primary hip procedures performed in 2012 whereas the corresponding top five cup-stem brand combinations in Table 2.12 account for only 21% of all revision hip procedures performed in the same year. This indicates that there are less 'common choices' for cup-stem brand combinations at revision surgery since the combination selection is dependent on the reason for primary hip failure.

The cup-stem brand combinations which account for the highest percentage of both primary and revision hip procedures during 2012 are shown in Figure 2.27 and Figure 2.28 respectively.

The femoral-acetabular prosthesis combinations used with these fixation devices, in terms of both material choice and head size, are shown in Table 2.13 from the UK National Joint Registry [66]. This data shows that the most commonly used femoral-acetabular prosthesis combination during 2012 was MOP with femoral head size 28 mm and also indicates that 56% of the components used in MOM articulations were over 50 mm in diameter.

**Table 2.11: Top five cup-stem brand combinations for primary hip procedures performed during 2012 [66]. Cemented prostheses are shown in italics.**

<b>Cup manufacturer</b>	<b>Cup brand</b>	<b>Stem manufacturer</b>	<b>Stem brand</b>	<b>Number of procedures</b>	<b>% of total procedures</b>
DePuy	Pinnacle	DePuy	<i>Corail</i>	13,032	18
Stryker	<i>Contemporary</i>	Stryker	<i>Exeter V40</i>	8,656	12
Stryker	Trident	Stryker	<i>Exeter V40</i>	5,094	7
Stryker	Trident	Stryker	Accolade	3,176	4
Biomet	Exceed ABT	Biomet	Taperloc cementless stem	2,936	4



DePuy Pinnacle



DePuy Corail

**Figure 2.27: Cup-stem brand combination that accounted for the highest percentage of total primary hip procedures in 2012 according to the UK National Joint Registry**

**Table 2.12: Top five cup-stem brand combinations for revision hip procedures performed during 2012 [66]. Cemented prostheses are shown in italics.**

<b>Cup manufacturer</b>	<b>Cup brand</b>	<b>Stem manufacturer</b>	<b>Stem brand</b>	<b>Number of procedures</b>	<b>% of total procedures</b>
Zimmer	Trabecular Metal Cementless Cup	Stryker	<i>Exeter V40</i>	226	5
Stryker	<i>Exeter Rimfit</i>	Stryker	<i>Exeter V40</i>	196	4
Stryker	<i>Contemporary</i>	Stryker	<i>Exeter V40</i>	193	4
DePuy	Pinnacle	DePuy	<i>Corail</i>	178	4
Stryker	Tritanium	Stryker	<i>Exeter V40</i>	170	4



Zimmer Trabecular Metal  
Cementless Cup



Stryker Exeter V40

**Figure 2.28: Cup-stem brand combination that accounted for the highest percentage of total revision hip procedures in 2012 according to the UK National Joint Registry**

2. Literature review

Table 2.13: Frequency of femoral head sizes for hip procedures performed in 2012 [66].

	Ceramic acetabulum articulation	Ceramic acetabulum articulation	Metal acetabulum articulation	Metal acetabulum articulation	Polyethylene acetabulum articulation	Polyethylene acetabulum articulation	Number of procedures with complete articulation	% of Procedures
Head Size (mm)	Ceramic Head	Metal Head	Ceramic Head	Metal Head	Ceramic Head	Metal Head		
	18,284	77	69	1,369	13,630	48,933	82,362	
22.25	<1%	0%	0%	1%	2%	2%	1,230	1%
26	0%	0%	0%	0%	<1%	2%	945	1%
28	7%	68%	19%	10%	34%	47%	28,970	35%
30	0%	0%	0%	0%	0%	<1%	41	<1%
32	28%	6%	0%	1%	35%	32%	25,417	31%
34	0%	0%	0%	0%	0%	<1%	1	<1%
36	58%	26%	78%	7%	28%	16%	22,610	27%
38	0%	0%	0%	<1%	0%	<1%	11	<1%
40	6%	0%	3%	<1%	<1%	1%	1,709	2%
42	0%	0%	0%	1%	0%	<1%	41	<1%
44	<1%	0%	0%	2%	<1%	<1%	289	<1%
46	0%	0%	0%	7%	0%	<1%	109	<1%
48	<1%	0%	0%	13%	0%	<1%	214	<1%
50	0%	0%	0%	24%	0%	0%	332	<1%
52	0%	0%	0%	17%	0%	0%	234	<1%
54+	0%	0%	0%	15%	0%	0%	209	<1%
<b>Total</b>	100%	100%	100%	100%	100%	100%		100%

© National Joint Registry 2013

## 2.7 Clinical relevance of project

The aim of this project is to simulate and explore the viability of partial revision surgery (where only the femoral component is revised) using a dual mobility head for a patient who has suffered a failed MOM THRA.

The project aims to investigate:

1. How to recreate surface features seen *in vivo* in CoCrMo acetabular cups from failed MOM THRA.
2. How the wear rate of a dual mobility head is affected by the initial surface roughness of the mating CoCrMo acetabular cup.
3. How the wear rate of dual mobility THA is affected by high inclination and microseparation testing conditions.
4. Whether dual mobility THA produces comparable wear rates to traditional MOP THA.
5. Whether the form, size and shape of metallic debris released from MOM THRA vary in comparison to that from dual mobility THA.
6. Whether a failed MOM THRA can be converted into a successful THA using a dual mobility head.

The literature review in this chapter has provided a historical overview of THA and the problems encountered with MOM bearings with special focus on the failure of MOM THRA. Whilst further research is still needed in order to understand the cause of adverse reaction to metal debris, it is hoped that by providing patients with high quality options at revision surgery that their pain and discomfort will be improved and the need for any further revision surgery will be avoided.

This is especially important today when MOM THRA failure rates are high and media attention has heightened the concern surrounding metal prostheses.

## 2.8 References

- [1] F. Oliviero, R. Ramonda, L. Punzi, *Swiss Medical Weekly* 140 (2010) 1-13.
- [2] L. Quigley, S. Sprague, M. Bhandari, *Joint Evidence* 4 (2010) 1-33.
- [3] W.-C. Witzleb, U. Hanisch, J. Ziegler, K.-P. Guenther, *The Journal of arthroplasty* 24 (2009) 951-6.
- [4] G.K. McKee, J. Farrar, *Journal of Bone and Joint Surgery* 48 (1966) 245-59.
- [5] C.a. Zahiri, T.P. Schmalzried, E. Ebramzadeh, E.S. Szuszczewicz, D. Salib, C. Kim, H.C. Amstutz, *The Journal of arthroplasty* 14 (1999) 326-32.
- [6] J. Charnley, *Lancet* 1 (1961) 1129-32.
- [7] S.M. Kurtz, Chapter 4-The Origins of UHMWPE in Total Hip Arthroplasty, 2009, 31-41.
- [8] W. Waugh, *John Charnley: The Man and the Hip*, Springer-Verlag (April 1990), 1990.
- [9] J. Charnley, *The Lancet* 282 (1963) 1379.
- [10] K. Djerf, O. Wahlstrom, *Arch Orthop Trauma Surg* 105 (1986) 158-62.
- [11] A.C. August, C.H. Aldam, P.B. Pynsent, *J Bone Joint Surg Br* 68 (1986) 520-7.
- [12] Y. Yan, A. Neville, D. Dowson, *Journal of Physics D-Applied Physics* 39 (2006) 3206-3212.
- [13] Y. Yan, A. Neville, D. Dowson, *Wear* 263 (2007) 1105-1111.
- [14] E.N. Codaro, P. Melnikov, I. Ramires, A.C. Guastaldi, *Russian Journal of Electrochemistry* 36 (2000) 1117-1121.
- [15] F. Contu, B. Elsener, H. Bohni, *Journal of the Electrochemical Society* 150 (2003) B419-B424.
- [16] A. Kinbrum, A. Unsworth, *Proceedings of the Institution of Mechanical Engineers Part H Journal of engineering in medicine* 222 (2008) 887-895.
- [17] Y.F. Liao, E. Hoffman, M. Wimmer, A. Fischer, J. Jacobs, L. Marks, *Physical Chemistry Chemical Physics* 15 (2013) 746-756.
- [18] A.J.T. Clemow, B.L. Daniell, *Journal of Biomedical Materials Research* 13 (1979) 265-279.
- [19] R.M. Streicher, M. Semlitsch, R. Schon, H. Weber, C. Rieker, *Proc Inst Mech Eng H* 210 (1996) 223-32.

- [20] H. Mancha, E. Carranza, J.I. Escalante, G. Mendoza, M. Mendez, F. Cepeda, E. Valdes, *Metallurgical and Materials Transactions a-Physical Metallurgy and Materials Science* 32 (2001) 979-984.
- [21] J. Cawley, J.E.P. Metcalf, A.H. Jones, T.J. Band, D.S. Skupien, *Wear* 255 (2003) 999-1006.
- [22] L.Z. Zhuang, E.W. Langer, *Journal of Materials Science* 24 (1989) 381-388.
- [23] J.L. Tipper, P.J. Firkins, E. Ingham, J. Fisher, M.H. Stone, R. Farrar, *Journal of materials science. Materials in medicine* 10 (1999) 353-62.
- [24] J.V. Giacchi, C.N. Morando, O. Fornaro, H.A. Palacio, *Materials Characterization* 62 (2011) 53-61.
- [25] D. McMinn, J. Daniel, *Proceedings of the Institution of Mechanical Engineers Part H-Journal of Engineering in Medicine* 220 (2006) 239-251.
- [26] I. Leslie, S. Williams, C. Brown, G. Isaac, Z. Jin, E. Ingham, J. Fisher, *Journal of biomedical materials research Part B Applied biomaterials* 87 (2008) 163-172.
- [27] S. Williams, D. Jalali-Vahid, C. Brockett, Z. Jin, M.H. Stone, E. Ingham, J. Fisher, *J Biomech* 39 (2006) 2274-81.
- [28] I.J. Leslie, S. Williams, G. Isaac, E. Ingham, J. Fisher, *Clinical Orthopaedics and Related Research* 467 (2009) 2259-2265.
- [29] S. Williams, I. Leslie, G. Isaac, Z. Jin, E. Ingham, J. Fisher, *J Bone Joint Surg Am* 90 Suppl 3 (2008) 111-7.
- [30] S.M. Kurtz, Chapter 2-From Ethylene Gas to UHMWPE Component: The Process of Producing Orthopedic Implants, 2009, 7-19.
- [31] G.H. Isaac, D. Dowson, B.M. Wroblewski, *Proc Inst Mech Eng H* 210 (1996) 209-16.
- [32] E. Oral, O.K. Muratoglu, *Nucl Instrum Methods Phys Res B* 265 (2007) 18-22.
- [33] A. Wang, C. Stark, J.H. Dumbleton, *Proc Inst Mech Eng H* 210 (1996) 141-55.
- [34] J. Fisher, K.L. Chan, J.L. Hailey, D. Shaw, M. Stone, *J Arthroplasty* 10 (1995) 689-92.
- [35] S.M. Kurtz, Chapter 3-Packaging and Sterilization of UHMWPE, 2009, 31-41.
- [36] P. Campbell, F.-W. Shen, H. McKellop, *Clinical Orthopaedics and Related Research* 90007 (2004) 98-111.
- [37] E.A. Reeves, D.C. Barton, D.P. FitzPatrick, J. Fisher, *Proc Inst Mech Eng H* 214 (2000) 249-55.

- [38] O.K. Muratoglu, C.R. Bragdon, D.O. O'Connor, M. Jasty, W.H. Harris, R. Gul, F. McGarry, *Biomaterials* 20 (1999) 1463-70.
- [39] H. Marrs, D.C. Barton, R.A. Jones, I.M. Ward, J. Fisher, C. Doyle, *J Mater Sci Mater Med* 10 (1999) 333-42.
- [40] H. McKellop, F.W. Shen, B. Lu, P. Campbell, R. Salovey, *J Orthop Res* 17 (1999) 157-67.
- [41] P.S. Barbour, M.H. Stone, J. Fisher, *Proceedings of the Institution of Mechanical Engineers Part H Journal of engineering in medicine* 214 (2000) 569-576.
- [42] M. Endo, J.L. Tipper, D.C. Barton, M.H. Stone, E. Ingham, J. Fisher, *Proc Inst Mech Eng H* 216 (2002) 111-22.
- [43] J.H. Dumbleton, M.T. Manley, A.A. Edidin, *The Journal of arthroplasty* 17 (2002) 649-661.
- [44] W.H. Harris, *Clin Orthop Relat Res* (2001) 66-70.
- [45] Weisenburger, J., K. Garvin, H. Haider, *J Bone Joint Surg Br* 94-B (2012) 215.
- [46] A.L. Galvin, J.L. Tipper, L.M. Jennings, M.H. Stone, Z.M. Jin, E. Ingham, I. Fisher, *Proc Inst Mech Eng H* 221 (2007) 1-10.
- [47] D.J. Carlsson, S. Chmela, J. Lacoste, *Macromolecules* 23 (1990) 4934-4938.
- [48] D.J. Carlsson, C.J.B. Dobbin, D.M. Wiles, *Macromolecules* 18 (1985) 2092-2094.
- [49] M. Kuzuya, S.-i. Kondo, M. Sugito, T. Yamashiro, *Macromolecules* 31 (1998) 3230-3234.
- [50] R.A. Assink, M. Celina, T.D. Dunbar, T.M. Alam, R.L. Clough, K.T. Gillen, *Macromolecules* 33 (2000) 4023-4029.
- [51] L. Costa, M.P. Luda, L. Trossarelli, *Polymer Degradation and Stability* 55 (1997) 329-338.
- [52] L. Costa, M.P. Luda, L. Trossarelli, *Polymer Degradation and Stability* 58 (1997) 41-54.
- [53] J.P. Collier, L.C. Sutula, B.H. Currier, J.H. Currier, R.E. Wooding, I.R. Williams, K.B. Farber, M.B. Mayor, *Clin Orthop Relat Res* (1996) 76-86.
- [54] S.M. Kurtz, W. Hozack, M. Marcolongo, J. Turner, C. Rimnac, A. Edidin, *J Arthroplasty* 18 (2003) 68-78.
- [55] L. Packer, *The American Journal of Clinical Nutrition* 53 (1991) 1050S-1055S.
- [56] A. Rigotti, *Molecular Aspects of Medicine* 28 (2007) 423-436.
- [57] E. Oral, O.K. Muratoglu, *International Orthopaedics* 35 (2011) 215-223.

- [58] E. Oral, S.D. Christensen, A.S. Malhi, K.K. Wannomae, O.K. Muratoglu, J Arthroplasty 21 (2006) 580-91.
- [59] B.R. Burroughs, B. Hallstrom, G.J. Golladay, D. Hoeffel, W.H. Harris, J Arthroplasty 20 (2005) 11-9.
- [60] D.W. Howie, O.T. Holubowycz, R. Middleton, G. Large Articulation Study, J Bone Joint Surg Am 94 (2012) 1095-102.
- [61] A. Ebied, S. Journeaux, Current Orthopaedics 16 (2002) 420-425.
- [62] H.C. Amstutz, M.J. Le Duff, Proceedings of the Institution of Mechanical Engineers, Part H: Journal of Engineering in Medicine 220 (2006) 85-94.
- [63] M.N. Smith-Petersen, J Bone Joint Surg Br 30B (1948) 59-75.
- [64] D. McMinn, R. Treacy, K. Lin, P. Pynsent, Clin Orthop Relat Res (1996) S89-98.
- [65] D. Cohen, Bmj 342 (2011) 1-7.
- [66] National Joint Registry for England and Wales, This document is available in PDF format for download from the NJR website at [www.njrcentre.org.uk](http://www.njrcentre.org.uk), 2012, 1-212.
- [67] R. Underwood, A. Matthies, P. Cann, J.A. Skinner, A.J. Hart, J Bone Joint Surg Br 93 (2011) 1169-77.
- [68] J.O. Penny, M. Ding, J.E. Varmarken, O. Ovesen, S. Overgaard, J Bone Joint Surg Br 94 (2012) 1344-50.
- [69] D.J. Langton, S.S. Jameson, T.J. Joyce, N.J. Hallab, S. Natsu, A.V. Nargol, J Bone Joint Surg Br 92 (2010) 38-46.
- [70] D.J. Langton, S.S. Jameson, T.J. Joyce, J.N. Gandhi, R. Sidaginamale, P. Mereddy, J. Lord, A.V. Nargol, J Bone Joint Surg Br 93 (2011) 1011-6.
- [71] G. Bousquet, D. Gazielly, P. Girardin, J. Debieesse, M. Relave, A. Israeli, J Orthop Surg Tech. (1985) 15-28.
- [72] J. Charnley, The Journal of bone and joint surgery British volume 54 (1972) 61-76.
- [73] O. Guyen, Q.S. Chen, J. Bejui-Hugues, D.J. Berry, K.-N. An, Clinical Orthopaedics and Related Research 455 (2007) 202-208.
- [74] R. Philippot, J.P. Camilleri, B. Boyer, P. Adam, F. Farizon, International Orthopaedics 33 (2009) 927-932.
- [75] B.D. Springer, T.K. Fehring, W.L. Griffin, S.M. Odum, J.L. Masonis, Clin Orthop Relat Res 467 (2009) 166-73.

- [76] G.M. Alberton, W.a. High, B.F. Morrey, *The Journal of bone and joint surgery. American volume* 84-A (2002) 1788-92.
- [77] B.F. Morrey, *Orthop Clin North Am* 23 (1992) 237-48.
- [78] S. Tarasevicius, M. Busevicius, O. Robertsson, H. Wingstrand, *Bmc Musculoskeletal Disorders* 11 (2010).
- [79] A. Combes, H. Migaud, J. Girard, A. Duhamel, M.H. Fessy, *Clin Orthop Relat Res* (2013).
- [80] R. Civinini, C. Carulli, F. Matassi, L. Nistri, M. Innocenti, *Clinical Orthopaedics and Related Research* 470 (2012) 3542-3548.
- [81] R. Philippot, P. Adam, M. Reckhaus, F. Delangle, F.X. Verdot, G. Curvale, F. Farizon, *Orthopaedics & Traumatology-Surgery & Research* 95 (2009) 407-413.
- [82] P. Mertl, A. Combes, F. Leiber-Wackenheim, M.H. Fessy, J. Girard, H. Migaud, *HSS J* 8 (2012) 251-6.
- [83] N.P. Hailer, R.J. Weiss, A. Stark, J. Karrholm, *Acta Orthop* 83 (2012) 566-71.
- [84] S. Affatato, M. Spinelli, M. Zavalloni, C. Mazzega-Fabbro, M. Viceconti, *Med Eng Phys* 30 (2008) 1305-17.
- [85] V. Saikko, *J Biomed Mater Res* 41 (1998) 58-64.
- [86] S.C. Scholes, A. Unsworth, *J Mater Sci Mater Med* 12 (2001) 299-303.
- [87] S.C. Scholes, A. Unsworth, *J Mater Sci Mater Med* 20 (2009) 163-70.
- [88] A. International, ASTM-WK451. New method for wear assessment of prosthetic hip designs in simulator devices, West Conshohocken, PA, 2008.
- [89] F.E. Zajac, R.R. Neptune, S.a. Kautz, *Gait & posture* 17 (2003) 1-17.
- [90] V. Wright, E.L. Radin, *Mechanics of Human Joints*, Marcel Dekker, New York, 1993.
- [91] E. Applegate, *The Anatomy and Physiology Learning System*, Saunders, USA, 2010.
- [92] J.P. Paul, *Proc Inst Mech Eng Conf Proc* 181 (1966) 8-15.
- [93] I.C. Clarke, *Critical Reviews in Biomedical Engineering* 8 (1982) 29-91.
- [94] S.L. Smith, A. Unsworth, *Proceedings of the Institution of Mechanical Engineers Part H Journal of engineering in medicine* 215 (2001) 61-64.
- [95] S.R. Williams, J.J. Wu, A. Unsworth, I. Khan, *Proceedings of the Institution of Mechanical Engineers Part H-Journal of Engineering in Medicine* 225 (2011) 783-796.
- [96] C. Kaddick, M.A. Wimmer, *Proc Inst Mech Eng H* 215 (2001) 429-42.

- [97] T. Oberbach, S. Begand, W. Glien, C. Kaddick, *Bioceramics*, Vol 20, Pts 1 and 2 361-363 (2008) 771-774.
- [98] T. Oberbach, W. Glien, C. Kaddick, *Bioceramics*, Vol 17 284-286 (2005) 995-998.
- [99] V. Saikko, *Proceedings of the Institution of Mechanical Engineers Part H-Journal of Engineering in Medicine* 219 (2005) 437-448.
- [100] P.S. Barbour, M.H. Stone, J. Fisher, *Proc Inst Mech Eng H* 213 (1999) 455-67.
- [101] P.J. Firkins, J.L. Tipper, E. Ingham, M.H. Stone, R. Farrar, J. Fisher, *Journal of biomechanics* 34 (2001) 1291-8.
- [102] J. Fisher, et al., *Journal of materials science. Materials in medicine* 15 (2004) 225-35.
- [103] A. Essner, G. Schmidig, A. Wang, *Wear* 259 (2005) 882-886.
- [104] A. Wang, V.K. Polineni, C. Stark, J.H. Dumbleton, *J Arthroplasty* 13 (1998) 615-20.
- [105] S. Affatato, W. Leardini, A. Jedenmalm, O. Ruggeri, A. Toni, *Clin Orthop Relat Res* 456 (2007) 153-8.
- [106] S. Affatato, R. Torrecillas, P. Taddei, M. Rocchi, C. Fagnano, G. Ciapetti, A. Toni, *Journal of Biomedical Materials Research Part B-Applied Biomaterials* 78B (2006) 76-82.
- [107] H. Oonishi, I.C. Clarke, V. Good, H. Amino, M. Ueno, *J Biomed Mater Res A* 70 (2004) 523-32.
- [108] S. Affatato, M. Frigo, A. Toni, *Journal of Biomedical Materials Research* 53 (2000) 221-226.
- [109] O. Calonijs, V. Saikko, *J Biomech* 35 (2002) 1439-50.
- [110] S.L. Smith, A. Unsworth, *Proceedings of the Institution of Mechanical Engineers Part H-Journal of Engineering in Medicine* 214 (2000) 233-238.
- [111] Y.S. Liao, P.D. Benya, H.A. McKellop, *J Biomed Mater Res* 48 (1999) 465-73.
- [112] H. Saari, S. Santavirta, D. Nordstrom, P. Paavolainen, Y.T. Konttinen, *J Rheumatol* 20 (1993) 87-90.
- [113] J.P. Binette, K. Schmid, *Arthritis Rheum* 8 (1965) 14-28.
- [114] B. Decker, K.B. Mc, G.W. Mc, C.H. Slocumb, *Arthritis Rheum* 2 (1959) 162-77.
- [115] H.W. Fang, M.L. Shih, J.H. Zhao, H.T. Huang, H.Y. Lin, H.L. Liu, C.H. Chang, C.B. Yang, H.C. Liu, *Applied Surface Science* 253 (2007) 6896-6904.
- [116] D. Mazzucco, *Variation of joint fluid composition and its effect on the tribology of replacement joint articulation*, Massachusetts Institute of Technology, 2003.

- [117] T.C. Chang, Effects of select fluids on the friction of metal-on-polyethylene joint replacement surfaces, Massachusetts Institute of Technology, 2005.
- [118] J.Q. Yao, M.P. Laurent, T.S. Johnson, C.R. Blanchard, R.D. Crowninshield, *Wear* 255 (2003) 780-784.
- [119] C.E. Lentner, Geigy Scientific Tables, Ciba-Geigy Ltd, Basle, Switzerland, 1981.
- [120] T. Ahlroos, V. Saikko, *Wear* 211 (1997) 113-119.
- [121] A.P. Harsha, T.J. Joyce, *Proceedings of the Institution of Mechanical Engineers Part H-Journal of Engineering in Medicine* 225 (2011) 948-958.
- [122] T. Kadar, O. Furnes, A. Aamodt, K. Indrekvam, L.I. Havelin, K. Haugan, B. Espehaug, G. Hallan, *J Bone Joint Surg Br* 94 (2012) 302-7.
- [123] J.E. Nevelos, E. Ingham, C. Doyle, J. Fisher, A.B. Nevelos, *Biomaterials* 20 (1999) 1833-40.
- [124] M. Al-Hajjar, I.J. Leslie, J. Tipper, S. Williams, J. Fisher, L.M. Jennings, *J Biomed Mater Res B Appl Biomater* 95 (2010) 263-8.
- [125] T. Stewart, J. Tipper, R. Streicher, E. Ingham, J. Fisher, *J Mater Sci Mater Med* 12 (2001) 1053-6.
- [126] A. Hatton, J.E. Nevelos, A.A. Nevelos, R.E. Banks, J. Fisher, E. Ingham, *Biomaterials* 23 (2002) 3429-40.
- [127] S. Williams, M. Butterfield, T. Stewart, E. Ingham, M. Stone, J. Fisher, *Proc Inst Mech Eng H* 217 (2003) 147-53.
- [128] S. Williams, T.D. Stewart, E. Ingham, M.H. Stone, J. Fisher, *J Biomed Mater Res B Appl Biomater* 70 (2004) 233-9.
- [129] R. De Haan, C. Pattyn, H.S. Gill, D.W. Murray, P.A. Campbell, K. De Smet, *The Journal of bone and joint surgery British volume* 90 (2008) 1291-1297.
- [130] A.J. Hart, P. Buddhdev, P. Winship, N. Faria, J.J. Powell, J.A. Skinner, *Hip International* 18 (2008) 212-219.
- [131] I.J. Leslie, S. Williams, G. Isaac, E. Ingham, J. Fisher, *Clinical orthopaedics and related research* 467 (2009) 2259-65.
- [132] J.G. Kennedy, W.B. Rogers, K.E. Soffe, R.J. Sullivan, D.G. Griffen, L.J. Sheehan, *J Arthroplasty* 13 (1998) 530-4.
- [133] S. Patil, A. Bergula, P.C. Chen, C.W. Colwell, Jr., D.D. D'Lima, *J Bone Joint Surg Am* 85-A Suppl 4 (2003) 56-63.

- [134] M.M. Morlock, N. Bishop, J. Zustin, M. Hahn, W. Ruther, M. Amling, *J Bone Joint Surg Am* 90 Suppl 3 (2008) 89-95.
- [135] A.V. Lombardi, T.H. Mallory, D.A. Dennis, R.D. Komistek, R.A. Fada, E.J. Northcut, *Journal of Arthroplasty* 15 (2000) 702-709.
- [136] D.A. Dennis, R.D. Komistek, E.J. Northcut, J.A. Ochoa, A. Ritchie, *J Biomech* 34 (2001) 623-9.
- [137] R.D. Komistek, D.A. Dennis, J.A. Ochoa, B.D. Haas, C. Hammill, *J Bone Joint Surg Am* 84-A (2002) 1836-41.
- [138] D. Glaser, R.D. Komistek, H.E. Cates, M.R. Mahfouz, *J Bone Joint Surg Am* 90 Suppl 4 (2008) 112-20.
- [139] B. Derbyshire, M.L. Porter, D. Howard, L. Kenney, C. Nester, *The Journal of Arthroplasty* 16 (2001) 1085-1086.
- [140] M. Manaka, I.C. Clarke, K. Yamamoto, T. Shishido, A. Gustafson, A. Imakiire, *J Biomed Mater Res B Appl Biomater* 69 (2004) 149-57.
- [141] W.L. Walter, G.M. Insley, W.K. Walter, M.A. Tuke, *J Arthroplasty* 19 (2004) 402-13.
- [142] J. Nevelos, E. Ingham, C. Doyle, R. Streicher, A. Nevelos, W. Walter, J. Fisher, *J Arthroplasty* 15 (2000) 793-5.
- [143] T.D. Stewart, J.L. Tipper, G. Insley, R.M. Streicher, E. Ingham, J. Fisher, *J Biomed Mater Res B Appl Biomater* 66 (2003) 567-73.
- [144] C. Brown, S. Williams, J.L. Tipper, J. Fisher, E. Ingham, *Journal of materials science. Materials in medicine* 18 (2007) 819-27.
- [145] J.G. Bowsher, P.A. Williams, I.C. Clarke, D.D. Green, T.K. Donaldson, *J Biomed Mater Res B Appl Biomater* 86 (2008) 253-63.
- [146] S. Williams, M. Al-Hajjar, G.H. Isaac, J. Fisher, *J Biomed Mater Res B Appl Biomater* 101 (2013) 770-5.
- [147] N. Fillot, I. Iordanoff, Y. Berthier, *Wear* 262 (2007) 949-957.
- [148] A. Wang, A. Essner, *Wear* 250 (2001) 212-216.
- [149] S. Affatato, G. Bersaglia, I. Foltran, P. Taddei, G. Fini, A. Toni, *Biomaterials* 23 (2002) 4839-4846.
- [150] A. Wang, G. Schmidig, *Wear* 255 (2003) 1057-1063.
- [151] C.R. Bragdon, M. Jasty, O.K. Muratoglu, D.O. O'Connor, W.H. Harris, *J Arthroplasty* 18 (2003) 553-61.

- [152] C.R. Bragdon, M. Jasty, O.K. Muratoglu, W.H. Harris, *J Arthroplasty* 20 (2005) 379-85.
- [153] K. Kubo, I.C. Clarke, T. Sorimachi, P.A. Williams, T.K. Donaldson, K. Yamamoto, *Wear* 267 (2009) 734-742.
- [154] T. Sorimachi, I.C. Clarke, P.A. Williams, A. Gustafson, K. Yamamoto, *Proceedings of the Institution of Mechanical Engineers Part H-Journal of Engineering in Medicine* 223 (2009) 607-623.
- [155] T.D. Brown, H.J. Lundberg, D.R. Pedersen, J.J. Callaghan, *Clin Orthop Relat Res* 467 (2009) 1885-97.
- [156] E.W. Morscher, A. Hefti, U. Aebi, *J Bone Joint Surg Br* 80 (1998) 267-72.
- [157] J.A. Davidson, R.A. Poggie, A.K. Mishra, *Biomed Mater Eng* 4 (1994) 213-29.
- [158] M. Scherge, D. Shakhvorostov, K. Pohlmann, *Wear* 255 (2003) 395-400.
- [159] T.M. Wright, S.B. Goodman, *Implant Wear in Total Joint Replacement: Clinical and Biological Issues, Material and Design Considerations* (2001) 176-185.
- [160] B. Bhushan, *Tribology: Friction, Wear, and Lubrication*, CRC Press, 2000.
- [161] B.J. Hamrock, D. Dowson, *Lubrication* 81692 (1981).
- [162] Z.M. Jin, D. Dowson, J. Fisher, *Thin Films in Tribology* 25 (1993) 545-555.
- [163] Z.M. Jin, D. Dowson, J. Fisher, *Proc Inst Mech Eng H* 211 (1997) 247-56.
- [164] D.D. Auger, D. Dowson, J. Fisher, Z.M. Jin, *Proc Inst Mech Eng H* 207 (1993) 25-33.
- [165] E. Ingham, J. Fisher, *Proc Inst Mech Eng H* 214 (2000) 21-37.
- [166] M.J. Jasty, W.E. Floyd, 3rd, A.L. Schiller, S.R. Goldring, W.H. Harris, *J Bone Joint Surg Am* 68 (1986) 912-9.
- [167] N.A. Johanson, P.G. Bullough, P.D. Wilson, Jr., E.A. Salvati, C.S. Ranawat, *Clin Orthop Relat Res* (1987) 123-35.
- [168] J.M. Mirra, R.A. Marder, H.C. Amstutz, *Clin Orthop Relat Res* (1982) 175-83.
- [169] H.C. Amstutz, P. Campbell, N. Kossovsky, I.C. Clarke, *Clin Orthop Relat Res* (1992) 7-18.
- [170] D.W. Howie, D.R. Haynes, S.D. Rogers, M.A. McGee, M.J. Pearcy, *Orthop Clin North Am* 24 (1993) 571-81.
- [171] S.B. Goodman, V.L. Fornasier, J. Lee, J. Kei, *J Biomed Mater Res* 24 (1990) 517-24.
- [172] W.J. Maloney, M. Jasty, A. Rosenberg, W.H. Harris, *J Bone Joint Surg Br* 72 (1990) 966-70.

- [173] S. Santavirta, V. Hoikka, A. Eskola, Y.T. Konttinen, T. Paavilainen, K. Tallroth, J Bone Joint Surg Br 72 (1990) 980-4.
- [174] K.J. Margevicius, T.W. Bauer, J.T. McMahon, S.A. Brown, K. Merritt, Journal of Bone and Joint Surgery-American Volume 76A (1994) 1664-1675.
- [175] P. Campbell, S. Ma, B. Yeom, H. McKellop, T.P. Schmalzried, H.C. Amstutz, J Biomed Mater Res 29 (1995) 127-31.
- [176] K. Hirakawa, T.W. Bauer, B.N. Stulberg, A.H. Wilde, M. Secic, Journal of Bone and Joint Surgery-American Volume 78A (1996) 1235-1243.
- [177] R.M. Baxter, T.A. Freeman, S.M. Kurtz, M.J. Steinbeck, Clinical Orthopaedics and Related Research 469 (2011) 2308-2317.
- [178] A. Cale, C.P. Christensen, A.S. Greenwald, H. McKellop, Journal of Bone and Joint Surgery-American Volume 89A (2007) 2779-2786.
- [179] L.D. Dorr, Z.N. Wan, C. Shahrddar, L. Sirianni, M. Boutary, A. Yun, Journal of Bone and Joint Surgery-American Volume 87A (2005) 1816-1821.
- [180] C.A. Engh, A.S. Stepniewski, S.D. Ginn, S.E. Beykirch, C.J. Sychterz-Terefenko, R.H. Hopper, C.A. Engh, Journal of Arthroplasty 21 (2006) 17-25.
- [181] C.H. Geerdink, B. Grimm, W. Vencken, I.C. Heyligers, A.J. Tonino, Clinical Orthopaedics and Related Research 467 (2009) 979-984.
- [182] I. Papageorgiou, V. Shadrack, S. Davis, L. Hails, R. Schins, R. Newson, J. Fisher, E. Ingham, C.P. Case, Mutation research 643 (2008) 11-9.
- [183] I. Catelas, J.B. Medley, P.a. Campbell, O.L. Huk, J.D. Bobyn, Journal of biomedical materials research. Part B, Applied biomaterials 70 (2004) 167-78.
- [184] H. Pandit, Glyn-Jones, S., McLardy-Smith, P., Gundle, R., Whitwell, D., Gibbons, C.L.M., Ostlere, S., Athanasou, N., Gill, H.S., Murray, D.W., The Journal of bone and joint surgery British volume 90 (2008) 847-851.
- [185] H.J. Griffiths, J. Burke, F.R.C.S. London, T.A. Bonfiglio, Skeletal Radiology 16 (1987) 146-152.
- [186] Y.-M. Kwon, S.J. Ostlere, P. McLardy-Smith, N.a. Athanasou, H.S. Gill, D.W. Murray, The Journal of arthroplasty 26 (2011) 511-8.
- [187] A.J. Hart, P.D. Quinn, B. Sampson, A. Sandison, K.D. Atkinson, J.a. Skinner, J.J. Powell, J.F.W. Mosselmans, Acta biomaterialia 6 (2010) 4439-46.
- [188] Z. Xia, Y.-M. Kwon, S. Mehmood, C. Downing, K. Jurkschat, D.W. Murray, Nanomedicine : nanotechnology, biology, and medicine 7 (2011) 674-681.

- [189] C.H. Lohmann, J.V. Nuechtern, H.G. Willert, S. Junk-Jantsch, W. Ruether, G. Pflueger, *Orthopedics* 30 (2007) 760-1.
- [190] N. Hallab, K. Merritt, J.J. Jacobs, *J Bone Joint Surg Am* 83-A (2001) 428-36.
- [191] H.G. Willert, G.H. Buchhorn, A. Fayyazi, R. Flury, M. Windler, G. Koster, C.H. Lohmann, *J Bone Joint Surg Am* 87 (2005) 28-36.
- [192] H. Amstutz, *Orthopedics Today Letter to the Editor* (2012).
- [193] M.P. Laurent, T.S. Johnson, R.D. Crowninshield, C.R. Blanchard, S.K. Bhambri, J.Q. Yao, *J Arthroplasty* 23 (2008) 751-61.
- [194] F. Billi, P. Benya, A. Kavanaugh, J. Adams, E. Ebramzadeh, H. McKellop, *Clinical Orthopaedics and Related Research* 470 (2012) 329-338.
- [195] C. Atienza, Jr., W.J. Maloney, *J Surg Orthop Adv* 17 (2008) 27-33.
- [196] J.L. Hailey, E. Ingham, M. Stone, B.M. Wroblewski, J. Fisher, *Proc Inst Mech Eng H* 210 (1996) 3-10.
- [197] A. Wang, A. Essner, C. Stark, J.H. Dumbleton, *Biomaterials* 17 (1996) 865-71.
- [198] S. Affatato, B. Fernandes, A. Tucci, L. Esposito, A. Toni, *Biomaterials* 22 (2001) 2325-31.
- [199] S. Niedzwiecki, C. Klapperich, J. Short, S. Jani, M. Ries, L. Pruitt, *J Biomed Mater Res* 56 (2001) 245-9.
- [200] T.R. Green, J. Fisher, J.B. Matthews, M.H. Stone, E. Ingham, *J Biomed Mater Res* 53 (2000) 490-7.
- [201] I. Catelas, J.D. Bobyn, J.B. Medley, J.J. Krygier, D.J. Zukor, a. Petit, O.L. Huk, *Journal of biomedical materials research* 55 (2001) 320-9.
- [202] I. Catelas, J.D. Bobyn, J.J. Medley, D.J. Zukor, a. Petit, O.L. Huk, *Journal of biomedical materials research* 55 (2001) 330-7.
- [203] F. Billi, P. Benya, A. Kavanaugh, J. Adams, H. McKellop, E. Ebramzadeh, *Clinical orthopaedics and related research* (2011).
- [204] A. Doran, F.C. Law, M.J. Allen, N. Rushton, *Biomaterials* 19 (1998) 751-9.
- [205] M. Germain, A. Hatton, S. Williams, J. Matthews, M. Stone, J. Fisher, E. Ingham, *Biomaterials* 24 (2003) 469-479.
- [206] S. Williams, J.L. Tipper, E. Ingham, M.H. Stone, J. Fisher, *Proceedings of the Institution of Mechanical Engineers. Part H, Journal of engineering in medicine* 217 (2003) 155-63.
- [207] R.E. Andrews, K.M. Shah, J.M. Wilkinson, A. Gartland, *Bone* 49 (2011) 717-23.

- [208] W.P. Zijlstra, S.K. Bulstra, J.J.A.M. van Raay, v.L. B.M., R. Kuijer, *Journal of Orthopaedic Research* (2011) 1-8.
- [209] S.D. Ulrich, et al., *Int Orthop* 32 (2008) 597-604.
- [210] *Hospital Episode System Data*, Department of Health, London, 1996.
- [211] L. Zagra, L. Bianchi, R.B. Ceroni, in, Springer Berlin Heidelberg, 2012, pp. 9-17.

## 3. Analysis of retrieved CoCrMo components

---

### 3.1 Introduction

Fourteen retrieved metal components have been supplied by Biomet throughout this project for surface analysis. All explants were made from CoCrMo and manufactured by Biomet, from either their M2a-Magnum MOM or ReCap Resurfacing systems.

This chapter aims to thoroughly examine the surface features of the retrieved components through zygo non-contacting profilometry and imaging with both optical microscopy and scanning electron microscopy. These three surface characterisation techniques are discussed in chapter sections 3.2.

The results and limitations will then be discussed in sections 3.3 and 3.4 respectively. The aim of the MOM biotribological studies shown in chapter 4 will be to generate physiologically scratched CoCrMo acetabular cups with features similar to that seen in this chapter. Hence, as well as comparing the surface characterisation results with previous literature, methods that have previously been employed to scratch CoCrMo components *in vitro* will be reviewed in the discussion in section 3.5. The results are concluded in section 3.6.

Information about all of the explants is shown in Table 3.1, followed by photos of the components in Figure 3.1 and Figure 3.2. Five modular CoCrMo femoral heads, one resurfacing CoCrMo femoral head and eight CoCrMo acetabular cups have been analysed.

### 3. Analysis of retrieved CoCrMo components

Table 3.1: Available information from all received retrievals.

Reference	Type	Component	Notes Available
<b>FAR 4</b>	M2a	Cup	Metallosis of surrounding tissue, dull highly scratched regions on both head and shell.
<b>FAR 4</b>	M2a	Head	
<b>FAR 33</b>	M2a	Cup	60 year old male, impingement of stem on shell
<b>FAR 33</b>	M2a	Head	
<b>FAR 72</b>	Recap	Head	Failure of recap femoral head via fracture of stem due to bending overload/fatigue
<b>FAR 77</b>	M2a PC	Cup	Significant metallosis in joint, shell fixed in acetabulum
<b>FAR 77</b>	M2a	Head	
<b>FAR 80</b>	Recap	Cup	Bone ingrowth on PPS coating, not significant amount though
<b>FAR 86</b>	Recap	Cup	Revised after around 2 years due to pain
<b>FAR 101</b>	Recap	Cup	Revised after 3 years due to dislocation
<b>FAR 149</b>	M2a	Ringloc	Ring detached, liner rim fracture, high inclination angle
<b>FAR 149</b>	M2a	Head	
<b>FAR 164</b>	M2a	Flared cup	Possible adverse loading
<b>FAR 164</b>	M2a	Head	

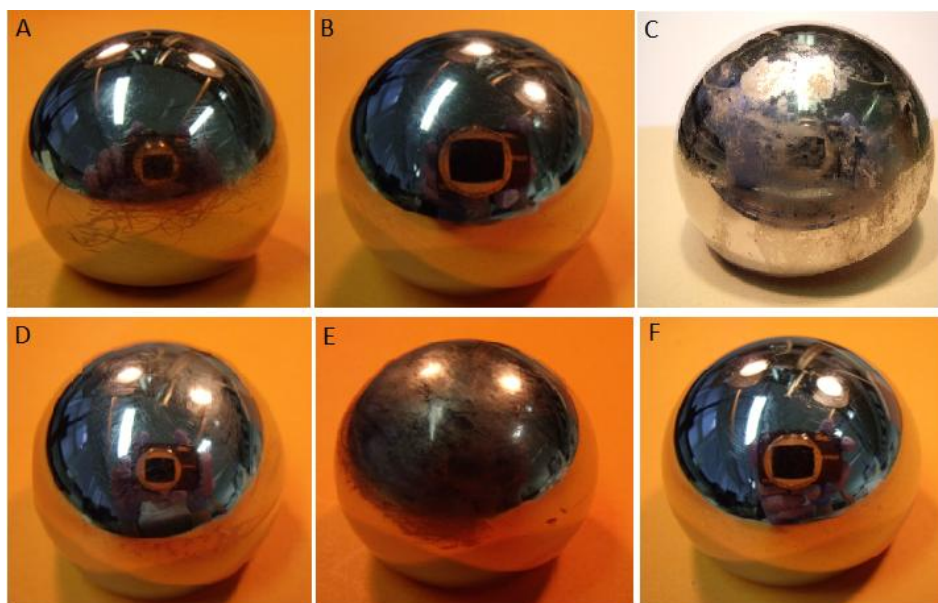


Figure 3.1: Retrieved femoral components, A: FAR 4, B: FAR 33, C: FAR 72, D: FAR 77, E: FAR 149, F: FAR 164.



Figure 3.2: Retrieved acetabular components, A: FAR 4, B: FAR 33, C: FAR 77, D: FAR 80, E: FAR 86, F: FAR 101, G: FAR 149, H: FAR 164.

## 3.2 Surface characterisation techniques

### 1) Zygo non-contacting profilometry

Measurements of the surface topography were taken at ten points across each bearing surface. Three-dimensional surface profiles were created using the Zygo NewView 100 non-contacting 3D profilometer with the 10x Mirau lens and 0.1 nm resolution. This technique is non-contact and is based on scanning white light interferometry whereby a fringe pattern of bright and dark lines result from an optical path difference between an internal reference and a sample beam.

In literature, most authors [1-8] report information about the surface profile of hip bearings in terms of average surface roughness ( $R_a$ ).  $R_a$  is defined as the height deviation taken within the evaluation length or area and is measured from the mean linear surface. The equation for  $R_a$  is given below.

$$R_a = \frac{1}{l_x l_y} \int_0^{l_x} \int_0^{l_y} n(x, y) dx dy$$

Affatato *et al.* [9] have reported the significance of also considering skewness ( $R_{skw}$ ) when discussing surface roughness.  $R_{skw}$  is a measure of symmetry of the surface profile around the mean line. A positive skewness measure denotes asymmetry above the mean line indicating that a surface has a predominance of peaks. A negative skewness measure denotes asymmetry below the mean line indicating a predominance of valleys. It is beneficial for bearing surfaces to have negative skew. The equation for  $R_{skw}$  is given below, where rms is the root mean square roughness-the average of the measured height deviations taken within the evaluation length or area as measured from the mean linear surface.

$$R_{skw} = \frac{1}{rms^3} \int_{-\infty}^{\infty} \int_{-\infty}^{\infty} n^3(x, y) p(n) dx dy$$

Zygo non-contacting profilometry has been used throughout this project not only to look at the retrieved CoCrMo components in this chapter but also to track the change in surface features of the bearings subject to biotribological testing shown later in chapters 4 and 5. The only bearing surface in this project which was unable to be successfully tracked by zygo profilometry was the inner pole of the E1 liners in chapter 5. This was because the lens was too wide to image inside the convex area which would ordinarily press fit onto the 28 mm CoCrMo heads. This surface was only able to be imaged optically.

## 2) Optical microscopy

An Axiotech optical microscope was used to image the worn surfaces of retrieved hip components. The majority of images were taken with the 10x magnification lens. Optical microscopy also allowed the changes on the surface of each component due to biotribological wear testing to be followed and recorded in chapters 4 and 5. Images were taken within the wear patch of the bearing surfaces throughout the hip simulator studies at atleast 0, 0.5, 1.0, 2.5 and 5.0 MC of each 5 MC test. When a test was shorter in duration images were taken more frequently at every 0.5 MC. This is in contrast to the images taken from the retrieved CoCrMo components in this chapter where only the final images after implant removal were possible to obtain.

#### **3) Scanning electron microscopy**

Scanning electron microscopy (SEM) was used to investigate the topography of the retrieved metal cups using a Philips/FEI XL30 ESEM operating at between 20-25kV. The same SEM (in Environmental mode) was used later in chapter 5 to image the wear around the rim of each E1 liner operating at 20kV without coating the samples.

SEM works by generating a focused beam of high energy electrons which is accelerated towards the sample. The accelerated electrons can either pass through the sample without interaction or undergo elastic or inelastic scattering. Elastic and inelastic scattering produce the secondary and backscattered electrons which are commonly used for imaging. Secondary electrons are the electrons responsible for showing morphology and topography at the sample surface. They are attracted towards an electrically biased grid and accelerated towards the detector. The topographical image of the sample surface is dependent on how many secondary electrons reach the detector.

### **3.3 Surface characterisation results**

#### **1) Zygo non-contacting profilometry**

Initial surface roughness values for the articulating surfaces of MOM prostheses have been approximated to lie in the range between 0.005 and 0.025  $\mu\text{m}$   $R_a$  [10]. As a comparison from this study, the seven ReCap resurfacing femoral heads used in MOM Test 1 had an average initial surface roughness value of  $0.009 \pm 0.004 \mu\text{m}$ .

Figure 3.3 shows the average surface roughness  $R_a$  data  $\pm$  standard deviation from ten points across each bearing surface. The average surface roughness across the six explanted CoCrMo heads was  $0.078 \pm 0.09 \mu\text{m}$ . Evidently the roughness values of the bearing surface have increased whilst in the body.

Head sample FAR 149 has the highest surface roughness of the samples investigated ( $0.208 \pm 0.130 \mu\text{m}$   $R_a$ ) with a large variation. This is indicative of the varied wear conditions it has experienced due to the high inclination angle and possible contact with the detached liner rim.

### 3. Analysis of retrieved CoCrMo components

---

Head sample FAR 77 has the lowest surface roughness ( $0.017 \pm 0.008 \mu\text{m R}_a$ ) which is surprising given the significant metallosis around the joint. Zygo analysis of the heads from FAR 4, 33, 72 and 164 were similar in magnitude and range.

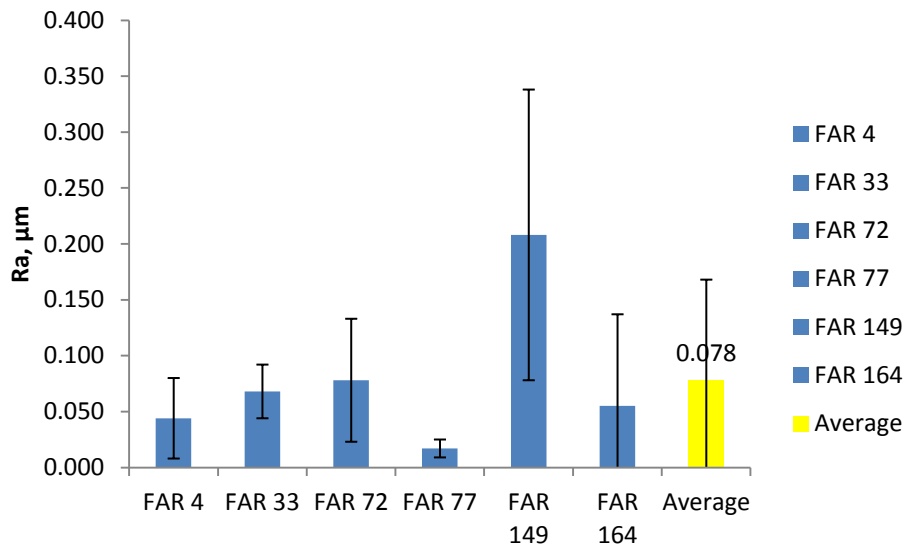


**Figure 3.3: Surface roughness ( $R_a$ ) of retrieved CoCrMo heads.**

Surface skewness is not commonly reported in literature because it can have great range and variation. From the initial data from the seven heads used in MOM Test 1, the average surface skewness was  $-1.910 \pm 6.255 \mu\text{m}$ . Figure 3.4 shows the average surface skewness  $R_{skw}$  data  $\pm$  standard deviation from ten points across each bearing surface. The average surface skewness across the six explanted heads was  $-2.261 \pm 3.051 \mu\text{m}$ . This indicates that the skewness has become more negative whilst in the body.

Interestingly the head from FAR 77 has the lowest skewness value of the samples investigated ( $-4.934 \pm 2.752 \mu\text{m R}_{skw}$ ). This is indicative of material loss from the metal matrix and/or carbide removal which could explain the metallosis around the joint.

Head sample FAR 72 was the only ReCap resurfacing femoral explanted head under investigation in this project and zygo data in terms of both surface roughness and skewness has been comparable to the M2a modular CoCrMo heads.

### 3. Analysis of retrieved CoCrMo components

---

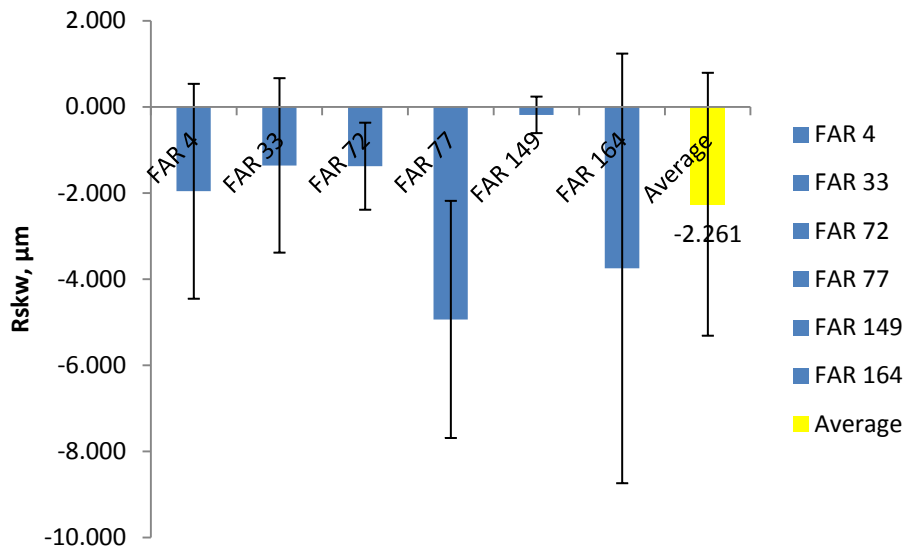


**Figure 3.4: Skewness (Rskw) of retrieved CoCrMo heads.**

An example of the zygo images taken from the explanted heads is shown in Figure 3.5. Deep scratching is clearly visible. In unworn metal bearing surfaces, zygo images normally show carbides as obvious asperities which protrude above the metal matrix. Carbides are not as distinct in the images taken from the explants which indicate that they have been worn away whilst in the body.

### 3. Analysis of retrieved CoCrMo components

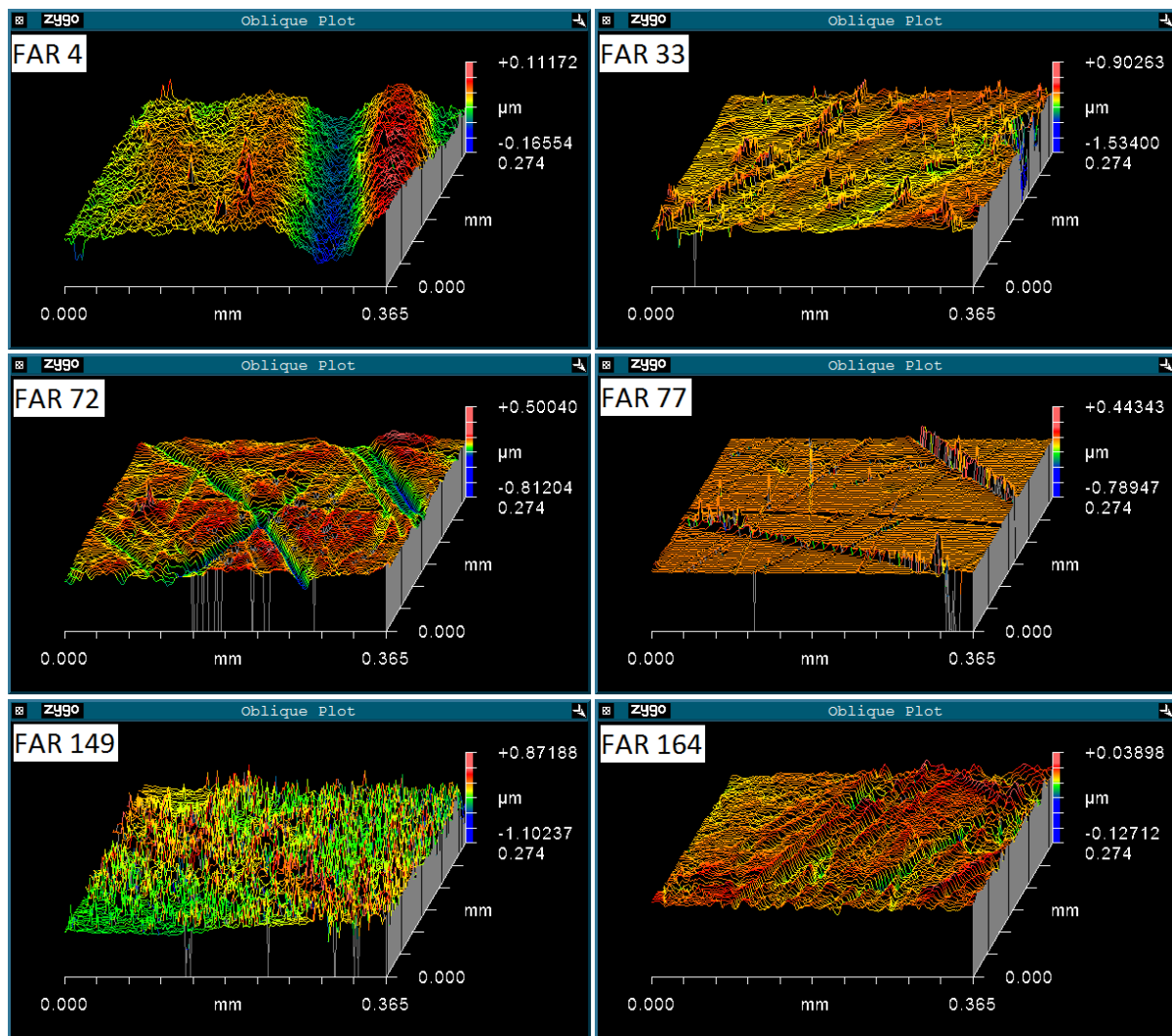


**Figure 3.5: Selection of surface profiles taken from retrieved femoral heads.**

In comparison to the retrieved cups, the seven acetabular CoCrMo cups used in MOM Test 1 had an average initial surface roughness value of  $0.010 \pm 0.004 \mu\text{m} R_a$  with an average surface skewness of  $0.075 \pm 4.446 \mu\text{m}$ .

Zygo analysis of the eight explanted CoCrMo cups showed that the average surface roughness of the bearing surface at the point of revision was  $0.031 \pm 0.03 \mu\text{m}$  with a surface skewness of  $-5.042 \pm 4.682 \mu\text{m}$ . Zygo data for each explant is shown in Figure 3.6 and Figure 3.7 for the surface roughness and skewness respectively.

As with the heads, surface roughness of the cups has increased whilst surface skewness has decreased whilst in the body.

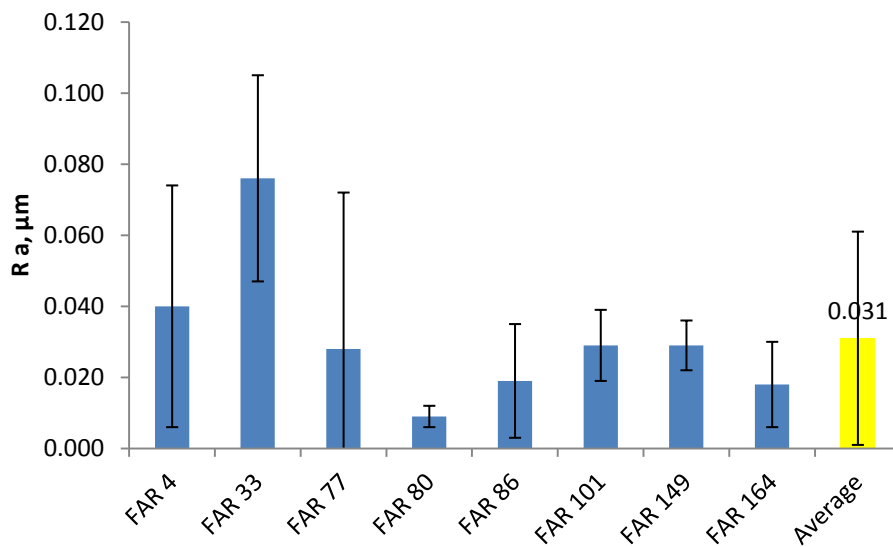


Figure 3.6: Surface roughness (Ra) of retrieved CoCrMo cups

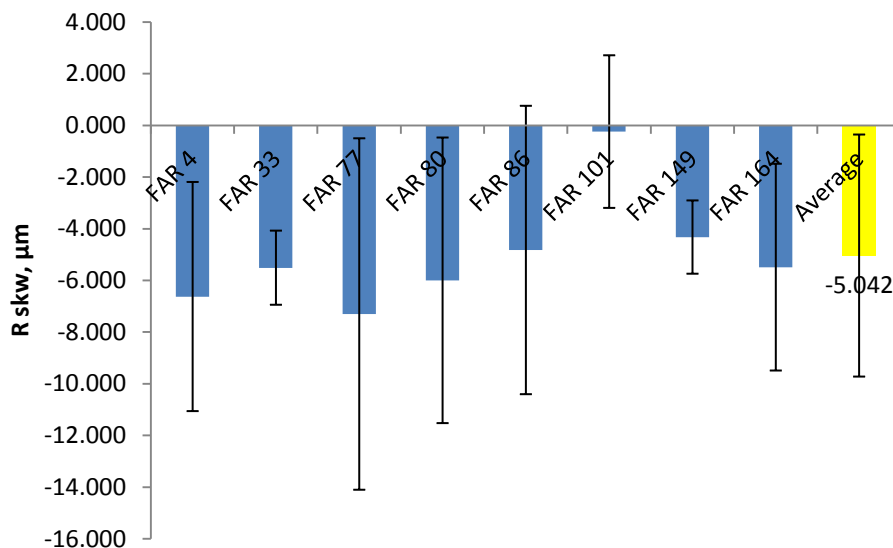


Figure 3.7: Skewness (Rskw) of retrieved CoCrMo cups.

Cup sample FAR 33 had the largest surface roughness, and also has a higher surface roughness than its head counterpart. This is a result of the impingement of the head stem onto the cup bearing surface *in vivo*.

The retrieved CoCrMo cups are similar in terms of surface skewness with the exception of FAR 101 which has a less negative  $R_{skw}$  value ( $-0.246 \pm 2.952 \mu\text{m}$ ).

### 3. Analysis of retrieved CoCrMo components

---

Although the average value of surface roughness across all explanted cups is lower than the average value for the heads, in the instance where both the head and corresponding cup have been available for analysis at the time of revision there is no correlation in terms of surface roughness between the two articulating surfaces.

In samples FAR 33 and 77, the cups have a higher surface roughness than the explanted heads. In samples FAR 4, 149 and 164 the converse statement is true. This will vary patient to patient depending on numerous factors including inclination angle, surgical implant technique, patient activity, age and gender.

Cup samples FAR 80, 86 and 101 were from resurfacing joints. As with the heads, the surface roughness and skewness data was comparable to data from the M2a-Magnum MOM system.

Examples of the zygo images taken at the surface of the retrieved CoCrMo cups can be seen in Figure 3.8. Multidirectional scratching and carbide pull-out is apparent.

### 3. Analysis of retrieved CoCrMo components

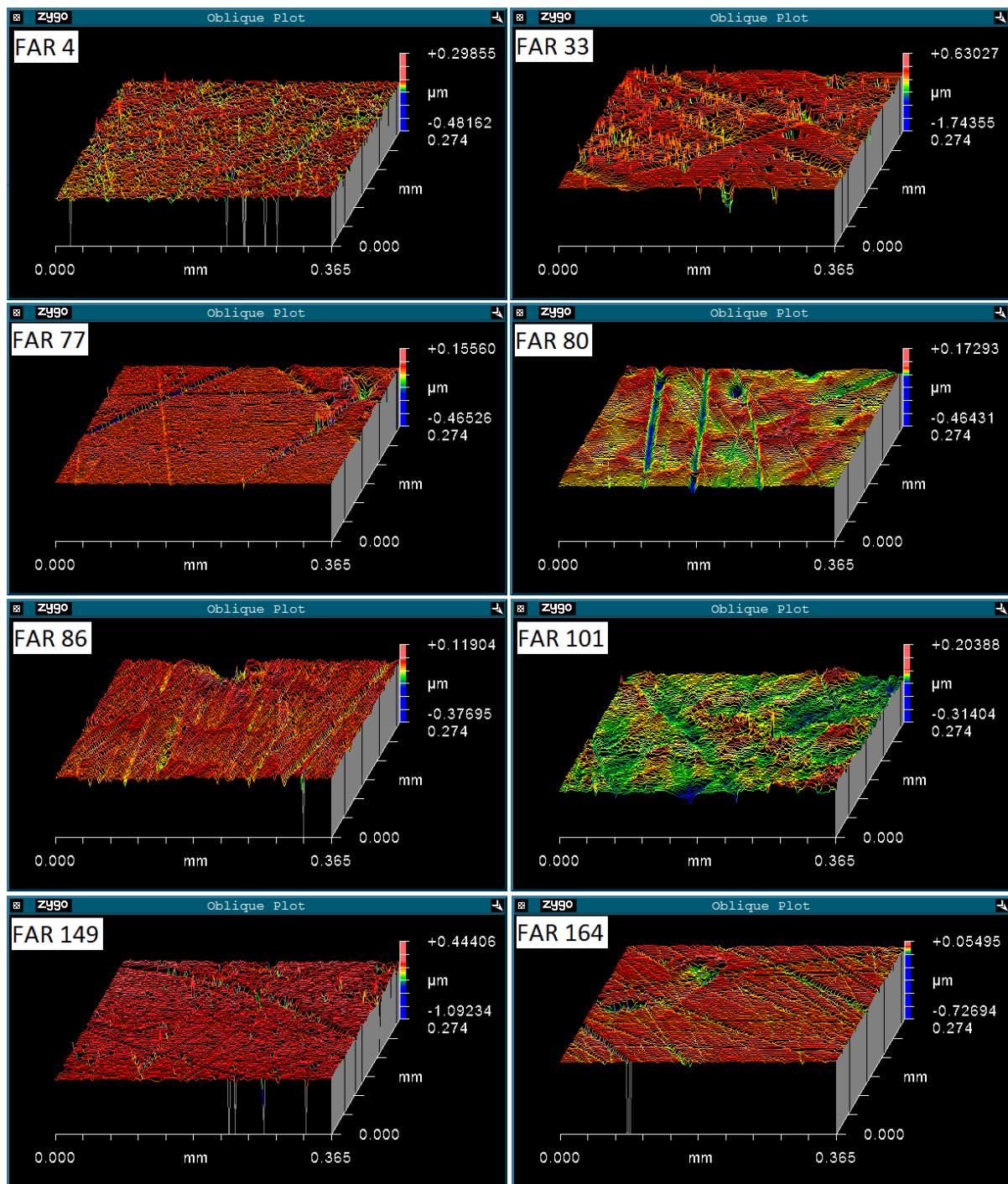


Figure 3.8: Selection of surface profiles taken from retrieved CoCrMo cups.

## 2) Optical microscopy

Optical images taken from the bearing surface of each retrieved implant are presented in Figure 3.9 and Figure 3.10 for the heads and cups respectively.

Head sample FAR 72 was too large to focus on with the optical microscope. The surface was instead imaged using SEM.

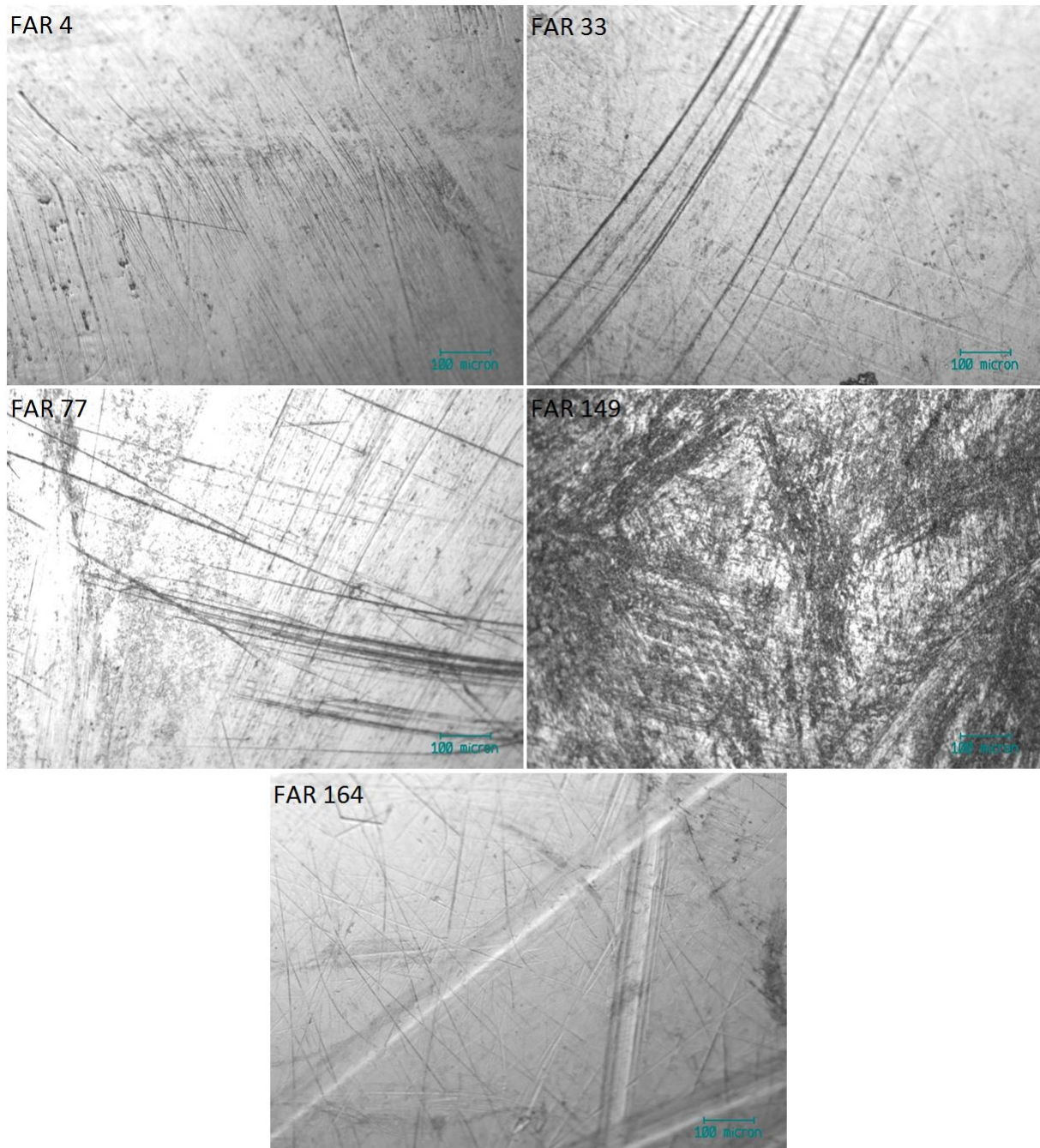


Figure 3.9: Selection of optical images taken from retrieved femoral heads.

### 3. Analysis of retrieved CoCrMo components

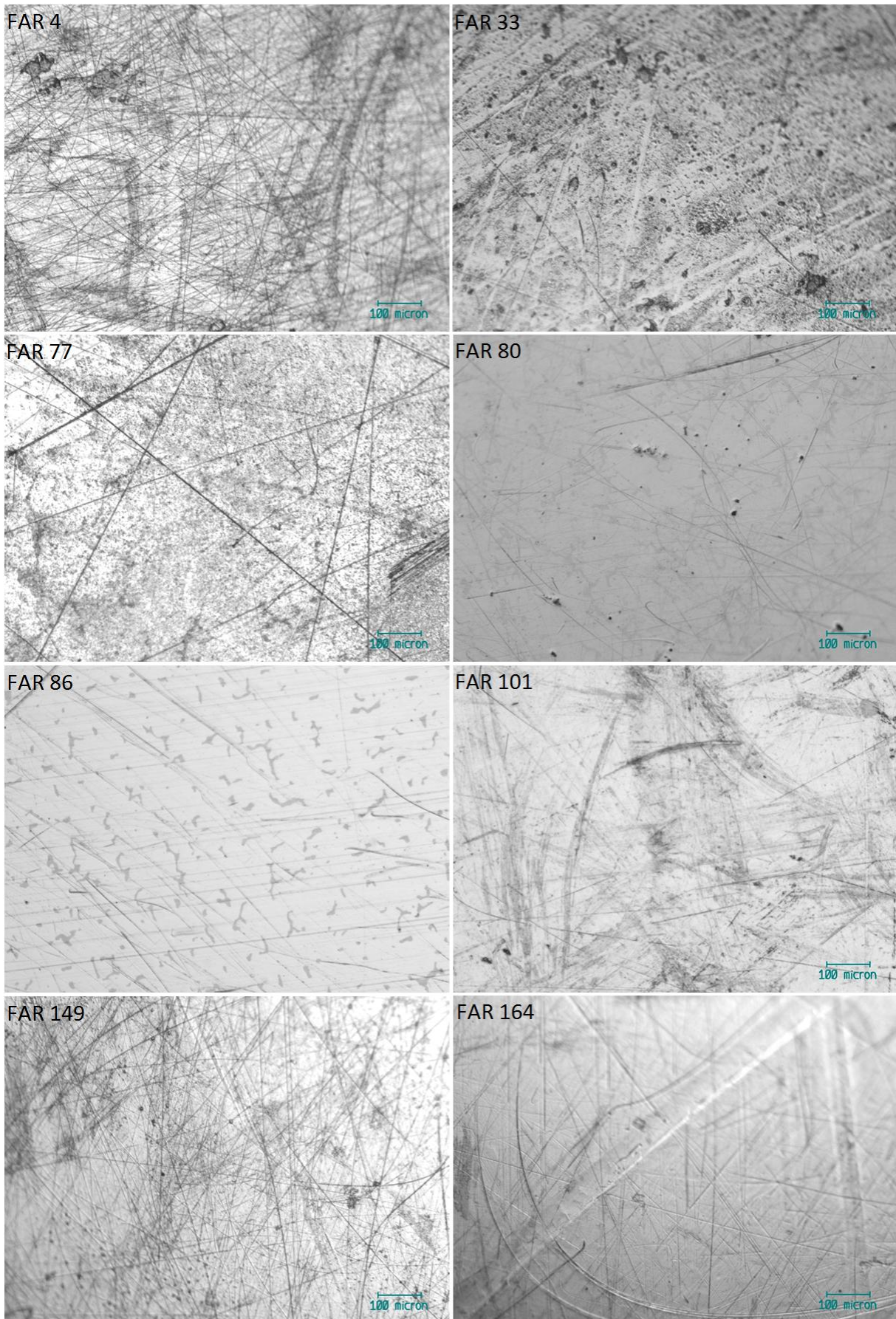


Figure 3.10: Selection of optical images taken from retrieved acetabular cups.

### 3. Analysis of retrieved CoCrMo components

---

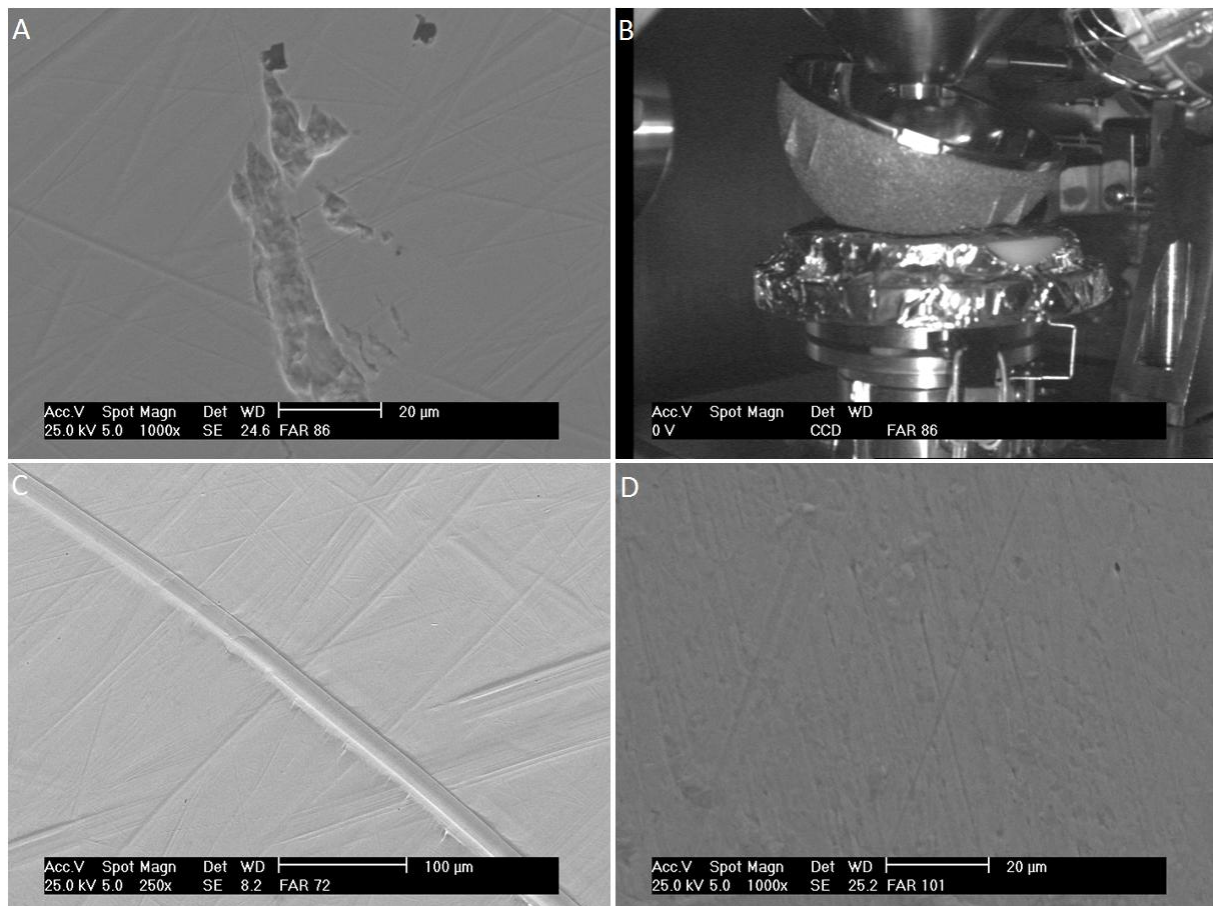
The optical images from the retrievals show a wide range of features including abrasive multidirectional scratching and pitting on the surface. Images from head sample FAR 149, which had the highest surface roughness, highlight the extent of the damage experienced at the bearing surface.

Pitting can be seen most clearly in Figure 3.9 from FAR 4 and Figure 3.10 from cup sample FAR 4 and FAR 33.

#### 3) Scanning electron microscopy

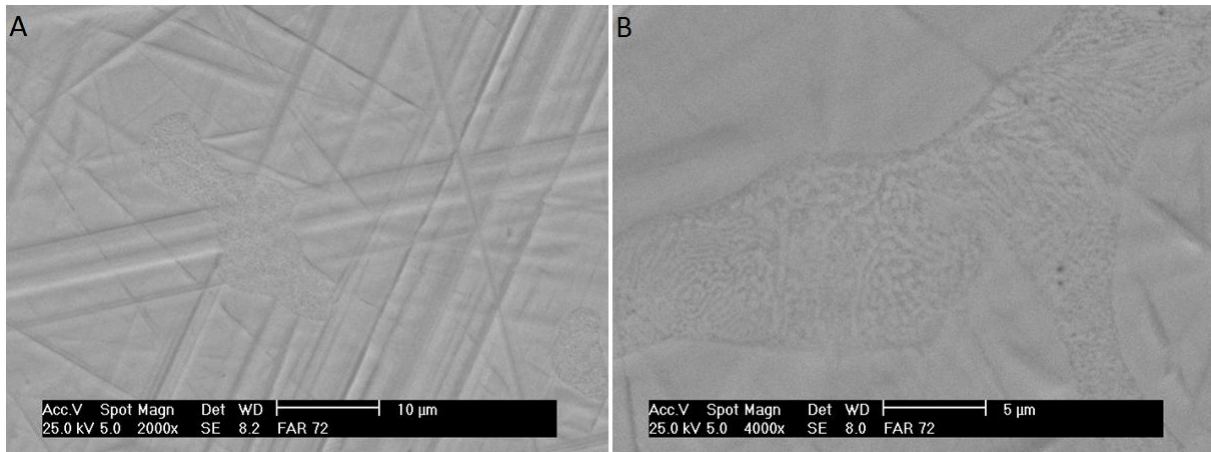
The bearing surface of selected retrievals was additionally analysed using SEM. Figure 3.11 shows a range of images from the ReCap samples FAR 72, 86 and 101. Abrasive scratching and carbide pull-out are shown in images A, C and D.

Image B shows the set up inside the SEM chamber. The normal imaging stage had to be removed first in order to allow adequate room for the joints to be positioned.



**Figure 3.11: Selection of SEM images. A: scratching and metal removal from FAR 86, B: FAR 86 positioned in SEM chamber, C: scratching from FAR 72, D: scratching from FAR 101.**

Figure 3.12 shows two SEM images taken from head sample FAR 72. Image A captures a carbide with abrasive scratching around it. The carbide itself has not been scratched; this indicates how hard the structures are. Image B shows a magnified image of a carbide, highlighting their porous structure.



**Figure 3.12: SEM images of carbides from FAR 72, A: Carbides among scratching, B: Magnified image of carbide.**

### 3.4 Limitations

One aim of this project is to recreate the worn features of a metal resurfacing cup at the stage of revision. Hence characterisation of the surface properties from retrieved CoCrMo cups is vital. The main limitation of the retrieval analysis was that only three explanted ReCap resurfacing cups were available for examination.

Five cups from the M2a-magnum system, made from the same CoCrMo alloy, were also available and since the surface roughness data from zygo analysis was comparable to that from the resurfacing cups it can be assumed that all surface features seen could theoretically have been produced in a resurfacing joint.

Most of the retrievals examined in this work have common features which include multidirectional scratching, pitting and high surface roughness coupled with a decrease in surface skewness.

As fourteen retrievals in total have been analysed, it is important that the zygo data should only be used as a guide when attempting to recreate the wear properties of the CoCrMo cups. The average values may not be representative of a larger collection of retrieved CoCrMo components. Variation in patient lifestyle and initial operating

technique will have a large affect on the wear conditions that the implants are subject to which will result in a wide variety of surface features.

## 3.5 Discussion

In literature, analysis of explanted prostheses has been carried out using coordinate measuring machines, roundness and out of roundness machines in order to assess the wear rate of failed hip joints [11].

Lord *et al.* [12] used a high-precision coordinate measuring machine to show that the mean volumetric wear rate for twenty-two acetabular cups at revision ranged from 0.30 to 63.59 mm<sup>3</sup>/yr. The mean volumetric wear rate for thirty-two femoral heads ranged from 0.21 to 31.91 mm<sup>3</sup>/yr. These wear rates were much higher than anticipated from previous simulator studies which has demonstrated wear rates in the region of 0.03-3.59 mm<sup>3</sup>/MC[13-15].

Joyce *et al.* [16] used MOM surface roughness data to demonstrate the self-polishing effect sometimes seen in metals. This was characterised by a reduction in surface roughness accompanied by a reduction in skewness. Two MOM total hip prostheses were obtained at revision surgery. The surface roughness of head 1 was shown to be  $14.7 \pm 7.4$  nm in the 'unworn' region of explanted head 1 in comparison to  $8.1 \pm 5.8$  nm in the 'worn' region of the same head.

This chapter aims to assess the surface features of failed hip explants with increased wear and discuss the possible causes in order to reproduce cups with similar features.

In 2009 Joyce *et al.* [17] published surface roughness data from a single-surgeon clinical cohort of failed resurfacing hip prosthesis. Data is reported for five explanted heads and two explanted cups with articulating diameters ranging from 42.5 to 50.5 mm. For each component ten roughness measurements were taken and the average of these was calculated and compared to a 'Do Not Implant' (DNI) ASR prosthesis. The surface roughness values are given below.

### 3. Analysis of retrieved CoCrMo components

Table 3.2: Experimental results from explanted resurfacing implants, published by Joyce *et al.* 2009 [17].

Sample/Patient	DNI	Patient 1	Patient 2	Patient 3	Patient 4	Patient 5
<b>Roughness head (<math>\mu\text{m R}_a</math>)</b>	0.010	0.135	0.045	0.047	0.025	0.062
<b>Roughness cup (<math>\mu\text{m R}_a</math>)</b>	0.012	0.058	0.044	-	-	-

All the  $R_a$  values presented in Table 3.2 fall within the range of the surface roughness data collected in this chapter. The average surface roughness ( $\pm$  the standard deviation) for the retrievals analysed in this project is shown in comparison to the data published by Joyce *et al.* [17] It was established that, as in the explants investigated in this project, all components studied had roughened whilst in the body. It is worth noting that no surface skewness data was provided in the publication.

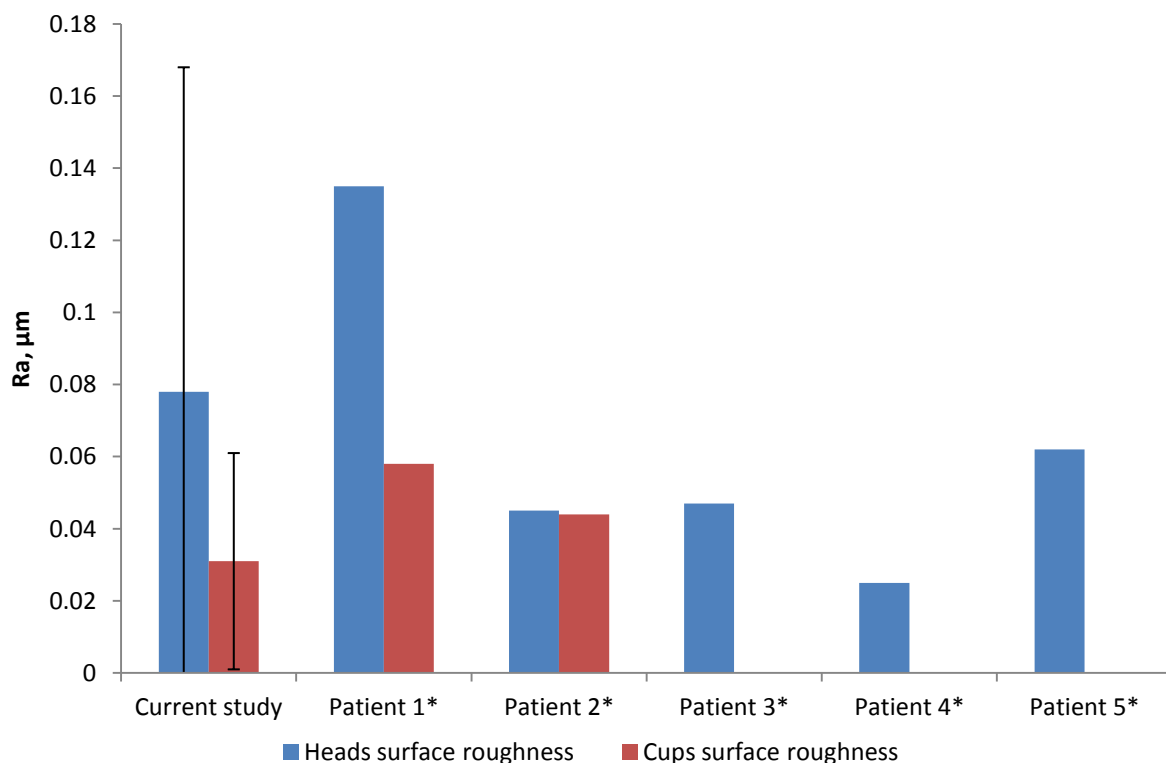


Figure 3.13: Zygo roughness data from the current study compared to (\*) data from Joyce *et al.* 2009 [17].

A zygo image was also shown of the explanted femoral head from patient 1 in the study which shows carbide pull-out and metal loss which has also been seen in the retrievals analysed in this chapter.

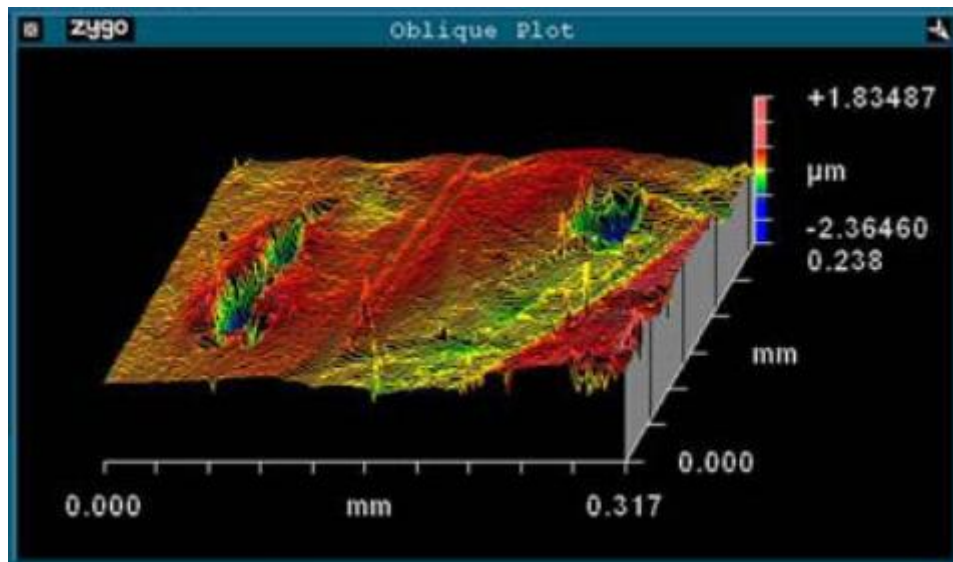


Figure 3.14: Zygo image of explanted femoral head from patient 1 in Joyce *et al.* 2009 [17].

Joyce *et al.* [17] suggested that the explanted prostheses may have operated under boundary lubrication rather than fluid film lubrication.

During fluid film lubrication the two articulating surfaces are completely separate and do not contact whereas in boundary lubrication asperities break through the fluid film layer and hence contact between the two surfaces can occur. This leads to increased friction and wear.

Other factors which are known to cause an increase in wear include joint fracture (seen here in FAR 72 and 149), impingement (seen in FAR 33), high inclination angle (seen in FAR 149), edge loading (possibly seen in FAR 164 as well as in previous literature [18-20]) and the effect of third body particles [21].

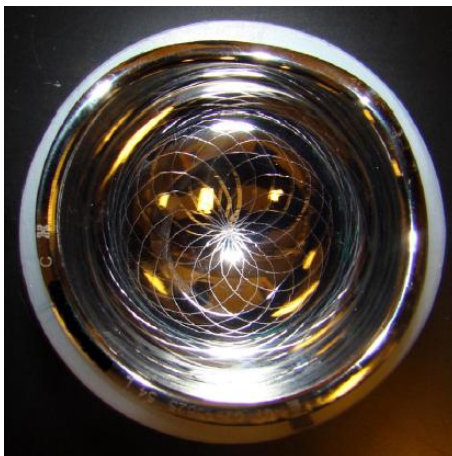


Figure 3.15: Scratched acetabular cup from Loving *et al.* 2013 [22].

In February 2013 work by Loving *et al.* [22] was published that investigated the performance of Stryker UHMWPE dual mobility heads. One of the tests in the study included the use of physiologically worn cups. The cups were scratched prior to testing using a Rockwell C diamond indenter to create a sinusoidal abrasion pattern. An image of the resulting cup is shown in Figure 3.15. No optical images taken from the surface of the cup are

### 3. Analysis of retrieved CoCrMo components

---

provided in the paper so it is not known how the surface of the cup compares to that seen in retrievals.

The method used by Loving *et al.* [22] to scratch the cups was verified by a previous study carried out by Lee *et al.* [23] which aimed to produce metal heads with scratches similar to that seen *in vivo*. This method was justified with comparison to one explanted head. The resultant scratched femoral head can be seen in Figure 3.16.

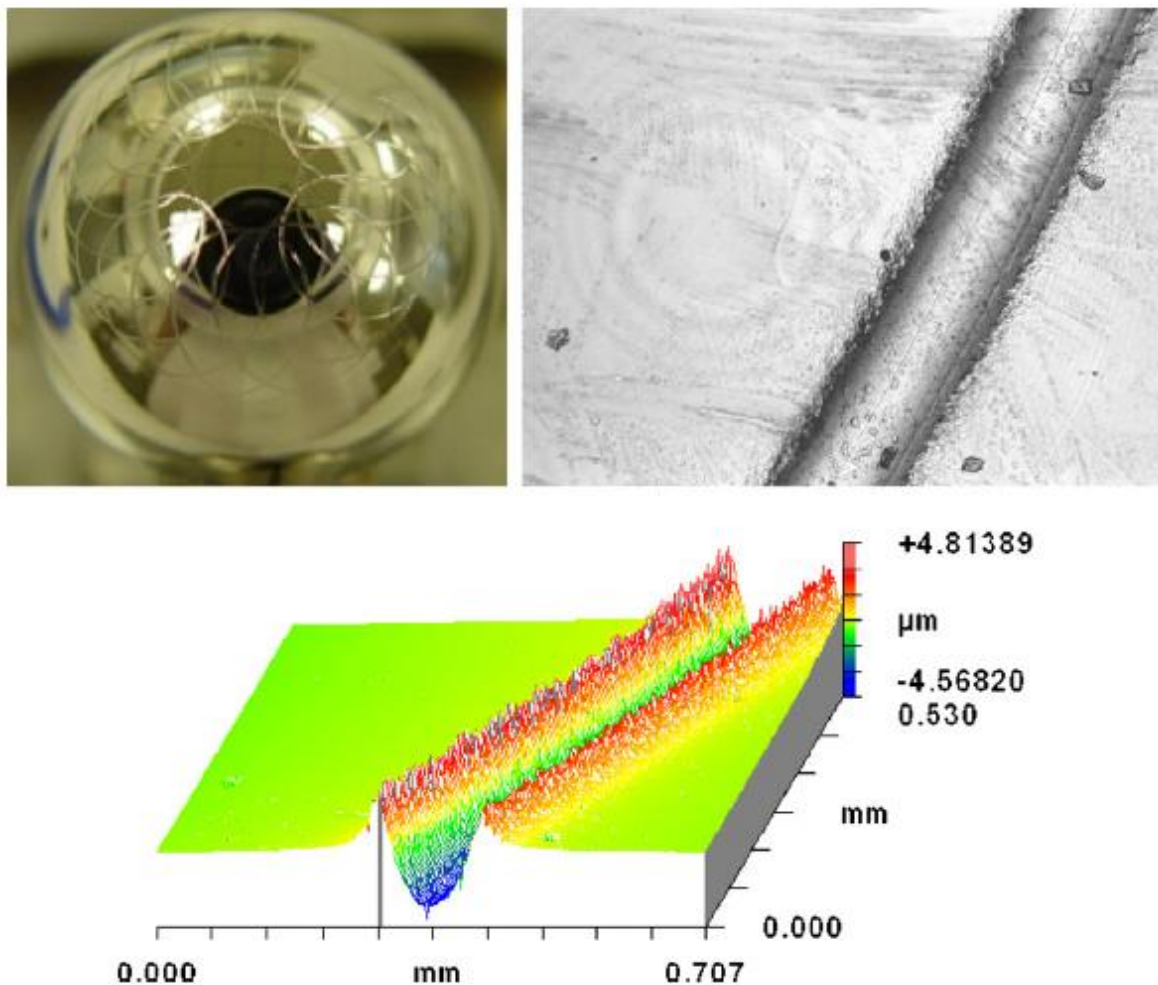


Figure 3.16: Scratched femoral CoCrMo head taken from Lee *et al.* 2009 [23].

The resulting zygo image in Figure 3.16 is similar to that seen in the head from FAR 4 in Figure 3.5 but is not comparable to any of the images produced from the retrieved cups in this study as shown in Figure 3.6. The optical image is also not comparable to those seen in Figure 3.10.

Studying the effects of physiologically scratched CoCrMo femoral heads articulating against UHMWPE has been extensively studied in literature with varied results. Table 3.3 gives a summary of techniques that have been employed previously to scratch femoral heads prior to testing.

As seen above, scratching using a diamond stylus generates deep, narrow scratches with sharp, high peaks whereas for the acetabular retrievals studied in this chapter shallower scratches were more common.

Scratching femoral heads using emery paper has been employed in several studies but there are concerns that third body particles which are not clinically relevant may remain in the metal matrix and affect the subsequent test data.

Simulator studies have been carried out with the addition of third body particles to the test serum in order to generate multidirectional scratches to the femoral component. PMMA is a common choice of third body particle to use, with concentrations ranging from 1 to 10 mg/ml.

There are many sources of third body particles found in the hip joint at revision surgery. As well as PMMA cement debris, there can also be corrosion products from the metal tapers, metal fragments from other fixation devices, bone particles, metal beads or fibres from porous coatings and hydroxyapatite coatings [24].

### 3. Analysis of retrieved CoCrMo components

**Table 3.3: Methods previously employed to scratch femoral heads *in vitro*.**

<b>Author</b>	<b>Year</b>	<b>Components used</b>	<b>Method of wear</b>	<b>Outcome</b>
Wang <i>et al.</i> [25]	1998	32 mm CoCr head	Grinding against various grit SiC paper in random motion	$R_a$ ranged from 0.01 to 0.85 $\mu\text{m}$
Barbour <i>et al.</i> [26]	2000	28 mm CoCr head	Either scratched using a diamond stylus or with a spherical CoCr bead embedded into a UHMWPE pin	$R_a$ for embedded bead was $0.017 \pm 0.004 \mu\text{m}$ , and $0.035 \pm 0.019 \mu\text{m}$ for diamond stylus
Bowsher <i>et al.</i> [27]	2001	28 mm CoCr head	Manually roughened with 400 grit SiC paper	$R_a = 0.38 \pm 0.014 \mu\text{m}$
Wang <i>et al.</i> [28]	2001	32 mm CoCr head	Addition of 10 mg/ml 160 $\mu\text{m}$ PMMA to test serum for 1 MC (CoCr vs. UHMWPE)	Mild CoCr scratches
Saikko <i>et al.</i> [29]	2002	28 mm CoCr head	Manually roughened with emery paper	$R_a$ ranged from 0.017 to 0.057 $\mu\text{m}$
Wang <i>et al.</i> [30]	2003	32 mm CoCr head	Addition of 5 mg/ml 150 $\mu\text{m}$ PMMA to test serum for 2 MC (CoCr vs. UHMWPE)	$R_a = 0.057 \pm 0.049 \mu\text{m}$
Affatato <i>et al.</i> [9]	2006	28 mm CoCr head	Either addition of 10 mg alumina powder for 18000 cycles or addition of PMMA at 1 mg/ml for 2.5 MC. (CoCr vs. UHMWPE)	$R_a$ ranged from 0.017 to 0.057 $\mu\text{m}$
Lee <i>et al.</i> [23]	2009	28 mm CoCr head	Scratched with diamond stylus	Sinusoidal abrasive scratching pattern applied
Sorimachi <i>et al.</i> [31]	2009	32 mm, 44 mm CoCr head	Addition of 10 mg/ml 40 $\mu\text{m}$ PMMA to test serum for 2 MC (CoCr vs. UHMWPE)	$R_a$ (32 mm) = 0.018 $\mu\text{m}$ , $R_a$ (44 mm) = 0.022 $\mu\text{m}$
Jedenmalm <i>et al.</i> [32]	2009	28 mm CoCr head	Manually roughened with P320 grit SiC paper	$R_a = 0.4 \mu\text{m}$

### 3. Analysis of retrieved CoCrMo components

---

This project will look at two alternative ways to recreate the wear features seen in this chapter. Initially, a 5 MC MOM simulator study will be carried out using ReCap resurfacing joints. This is because all the retrievals analysed in this chapter have been subject to MOM wear so it is important that the metal articulation is studied.

A 5 MC simulator study is representative of the implants being in the body for five years, which is a longer duration than some of the joints analysed here have been *in vivo*.

Furthermore, a second MOM simulator study will be carried out which investigates the effect of third body wear particles in the test serum and the resulting effect with respect to both the wear rate and the surface properties of the two articulating surfaces.

The resulting cups from both of these studies will then be analysed in comparison to the retrieved samples and it is hoped that they will have features characteristic of the data shown in this chapter.

#### 3.6 Conclusion

One CoCrMo head and three CoCrMo cups from the ReCap Resurfacing system along with five CoCrMo heads and five CoCrMo cups from the M2a-Magnum system were provided by Biomet for retrieval analysis.

The average surface roughness across the six explanted CoCrMo heads was  $0.078 \pm 0.09$   $\mu\text{m}$  whilst the average surface skewness was  $-2.261 \pm 3.051$   $\mu\text{m}$ .

The average surface roughness across the eight explanted CoCrMo cups was  $0.031 \pm 0.03$   $\mu\text{m}$  with a corresponding surface skewness of  $-5.042 \pm 4.682$   $\mu\text{m}$ .

In comparison to unworn components, the average surface roughness of both the heads and cups has increased whilst the average surface skewness has decreased during implantation in the body. Optical images of the retrievals show a wide range of features including abrasive multidirectional scratching and pitting on the surface. SEM images of the retrievals look at the structure of the carbides present in the metal matrix. Carbide pull out has been imaged as well as carbides which have not been affected by the abrasive scratching in the surrounding area.

Physiological scratching has previously been applied in literature with the use of a diamond stylus. However the resultant surface features were not comparable to the data from the retrieved cups in this study and so the research shown in Chapter 4 will use alternative methods with the aim of creating worn cups comparable to the retrievals.

### 3.7 References

- [1] V. Saikko, O. Calonius, J. Keranen, *J Biomed Mater Res* 57 (2001) 506-12.
- [2] A.P. Elfick, R.M. Hall, I.M. Pinder, A. Unsworth, *J Biomed Mater Res* 48 (1999) 712-8.
- [3] M.T. Raimondi, P. Vena, R. Pietrabissa, *J Biomed Mater Res* 58 (2001) 436-48.
- [4] M.T. Raimondi, R. Pietrabissa, *Biomaterials* 21 (2000) 907-13.
- [5] V. Saikko, T. Ahlroos, O. Calonius, J. Keranen, *Biomaterials* 22 (2001) 1507-1514.
- [6] C. Piconi, M. Labanti, G. Magnani, M. Caporale, G. Maccauro, G. Magliocchetti, *Biomaterials* 20 (1999) 1637-46.
- [7] L. Que, L.D. Topoleski, *J Biomed Mater Res* 48 (1999) 705-11.
- [8] K. Haraguchi, N. Sugano, T. Nishii, T. Sakai, H. Yoshikawa, K. Ohzono, *Int Orthop* 25 (2001) 29-34.
- [9] S. Affatato, G. Bersaglia, Y. Junqiang, F. Traina, A. Toni, M. Viceconti, *Proc Inst Mech Eng H* 220 (2006) 457-64.
- [10] Z.M. Jin, M. Stone, E. Ingham, J. Fisher, *Current Orthopaedics* 20 (2006) 32-40.
- [11] T.J. Joyce, D.J. Langton, A.V.F. Nargol, *Tribology International* 44 (2011) 517-522.
- [12] J.K. Lord, D.J. Langton, A.V.F. Nargol, T.J. Joyce, *Wear* 272 (2011) 79-87.
- [13] K. Vassiliou, A.P.D. Elfick, S.C. Scholes, A. Unsworth, *Proceedings of the Institution of Mechanical Engineers Part H Journal of engineering in medicine* 220 (2006) 269-277.
- [14] C. Heisel, N. Streich, M. Krachler, E. Jakubowitz, J.P. Kretzer, *Journal of Bone and Joint Surgery-American Volume* 90A (2008) 125-133.
- [15] I. Leslie, S. Williams, C. Brown, G. Isaac, Z.M. Jin, E. Ingham, J. Fisher, *Journal of Biomedical Materials Research Part B-Applied Biomaterials* 87B (2008) 163-172.
- [16] T.J. Joyce, H. Grigg, D.J. Langton, A.V.F. Nargol, *Tribology International* 44 (2011) 513-516.

### 3. Analysis of retrieved CoCrMo components

---

- [17] T.J. Joyce, D.J. Langton, S.S. Jameson, A.V.F. Nargol, Proceedings of the Institution of Mechanical Engineers Part J-Journal of Engineering Tribology 223 (2009) 317-323.
- [18] M. Al-Hajjar, J. Fisher, S. Williams, J.L. Tipper, L.M. Jennings, J Biomed Mater Res B Appl Biomater 101 (2013) 213-22.
- [19] I. Leslie, S. Williams, G. Isaac, P. Hatto, E. Ingham, J. Fisher, Proc Inst Mech Eng H 227 (2013) 345-9.
- [20] S. Williams, M. Al-Hajjar, G.H. Isaac, J. Fisher, J Biomed Mater Res B Appl Biomater 101 (2013) 770-5.
- [21] P.E. Sinnett-Jones, J.A. Wharton, R.J.K. Wood, (2005) 898-909.
- [22] L. Loving, R.K. Lee, L. Herrera, A.P. Essner, J.E. Nevelos, Journal of Arthroplasty 28 (2013) 1041-1046.
- [23] R. Lee, A. Essner, A. Wang, W.L. Jaffe, Wear 267 (2009) 1915-1921.
- [24] C.R. Bragdon, M. Jasty, O.K. Muratoglu, D.O. O'Connor, W.H. Harris, J Arthroplasty 18 (2003) 553-61.
- [25] A. Wang, V.K. Polineni, C. Stark, J.H. Dumbleton, J Arthroplasty 13 (1998) 615-20.
- [26] P.S. Barbour, M.H. Stone, J. Fisher, Proceedings of the Institution of Mechanical Engineers Part H Journal of engineering in medicine 214 (2000) 569-576.
- [27] J.G. Bowsher, J.C. Shelton, Wear 250 (2001) 167-179.
- [28] A. Wang, A. Essner, Wear 250 (2001) 212-216.
- [29] V. Saikko, O. Calonijs, J. Keranen, Journal of Biomedical Materials Research 63 (2002) 848-853.
- [30] A. Wang, G. Schmidig, Wear 255 (2003) 1057-1063.
- [31] T. Sorimachi, I.C. Clarke, P.A. Williams, A. Gustafson, K. Yamamoto, Proceedings of the Institution of Mechanical Engineers Part H-Journal of Engineering in Medicine 223 (2009) 607-623.
- [32] A. Jedenmalm, S. Affatato, P. Taddei, W. Leardini, U.W. Gedde, C. Fagnano, M. Viceconti, Journal of Biomedical Materials Research Part A 90A (2009) 1032-1042.

## 4. Generation of physiologically scratched CoCrMo cups

---

### 4.1 Introduction

This chapter details the studies carried out in order to generate physiologically scratched CoCrMo cups similar to the retrievals which were analysed in chapter 3.

The materials and methods used in this chapter are discussed in sections 4.2 – 4.5. Section 4.2 introduces the Durham hip simulator which is used during the two biotribological MOM studies in this chapter in section 4.6 and 4.8.

Section 4.3 introduces the pin-on-plate machine used in the wear screening test for MOM Test 2 that is given in section 4.7.

Section 4.4 and 4.5 explain the lubricant and wear characterisation techniques used throughout the two simulator studies and the pin-on-plate test in this chapter.

The experimental results are discussed in sections 4.6 – 4.8.

Section 4.6 gives the results from an ISO-standard MOM biotribological study testing 60 mm CoCrMo ReCap resurfacing joints.

Section 4.7 gives the results from a MOM pin-on-plate wear screening test designed to investigate and compare the effect of hydroxyapatite and titanium particles on the MOM interface.

Section 4.8 gives the results from an aggressive third-body MOM biotribological study testing the effect of hydroxyapatite and titanium particles on 60 mm CoCrMo ReCap resurfacing joints.

Each experimental section will include a discussion whereby the resulting scratched CoCrMo cups are compared to the retrieved CoCrMo cups from chapter 3.

## 4.2 Durham hip simulator

Both MOM simulations detailed later in this chapter were completed in the Durham hip simulator [1], [2].



**Figure 4.1: Durham hip simulator.**

An AC motor and gearbox drove a crank and connecting rod which provided flexion/extension in the horizontal plane and oscillated the femoral component with an approximate sinusoidal motion through  $+30^\circ$  to  $-15^\circ$  at a frequency of 1 Hz.

Internal/external rotation along the top axis was generated by a second crank and connecting rod which oscillated the acetabular component with an approximate sinusoidal motion of  $\pm 10^\circ$ .

The simulator does not have abduction/adduction so internal/external rotation and flexion/extension were  $90^\circ$  out of phase to produce the figure 8 wear track over the acetabular surface.

A self-aligning gimbal mechanism ensured that the centre of the acetabular cup was in line with the centre of the femoral head. Loading was controlled by three optical switches and a pneumatic proportional valve which ensured load was applied during the stance phase of the walking cycle. The output pressure from the proportional valve was pneumatically amplified using a booster valve and a manifold was used to supply an equal pressure to the pneumatic actuator in each of the six stations.

Of these six stations, five underwent motion as well as loading. Station 6 was subject only to load. During wear testing, the load was set to a maximum of  $2500 \pm 400$  N and a minimum of  $150 \pm 100$  N.

### 4.3 Pin-on-plate machine

The pin-on-plate machine used in section 4.7 consisted of four stations that applied both reciprocation and rotational motion. The cycle frequencies of both motions were set at approximately 1 Hz. The machine can be seen in Figure 4.2 and Figure 4.3.

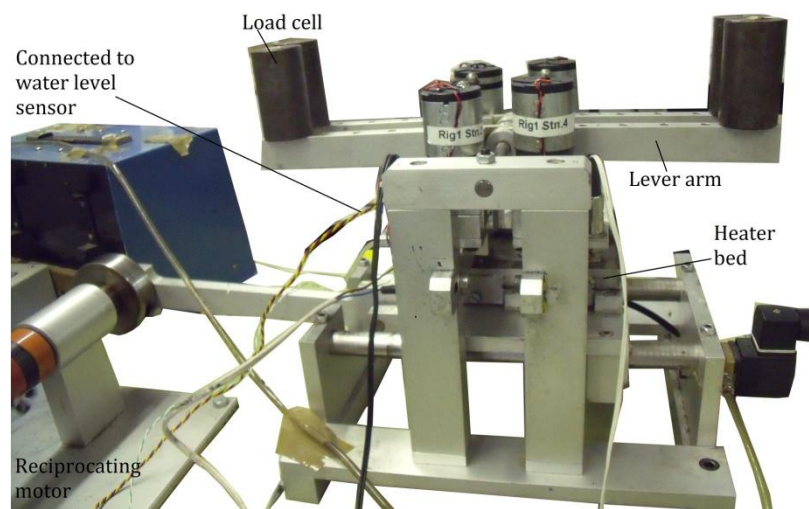


Figure 4.2: Pin-on-plate machine, front view.

Reciprocation was applied by a sledge moving along two fixed parallel hardened steel bars. The sledge was driven by a 150 W DC shunt motor. The speed of the motor was controlled using a variable voltage supply. The heater bed, stainless steel bath and plate holder were positioned on top of this sledge. The test lubricant was heated by resistors positioned within the heater bed controlled by a thermocouple which maintained a constant temperature of  $37^\circ$  throughout the test. Any evaporation from the lubricant was restored by topping up with deionised water using an automatic water level sensor made from platinum wire which was fitted to prevent the rig running without lubricant.

The four loaded pins were held in stainless steel holders and a load of 40 N was applied to each station via a lever arm mechanism.

#### 4. Generation of physiologically scratched CoCrMo cups

---

An electronic counter was connected to the reciprocating sledge to count the number of cycles completed and tests were carried out in 0.25 MC intervals. The stroke length was set to 25 mm, giving a sliding distance of 50 mm per cycle.

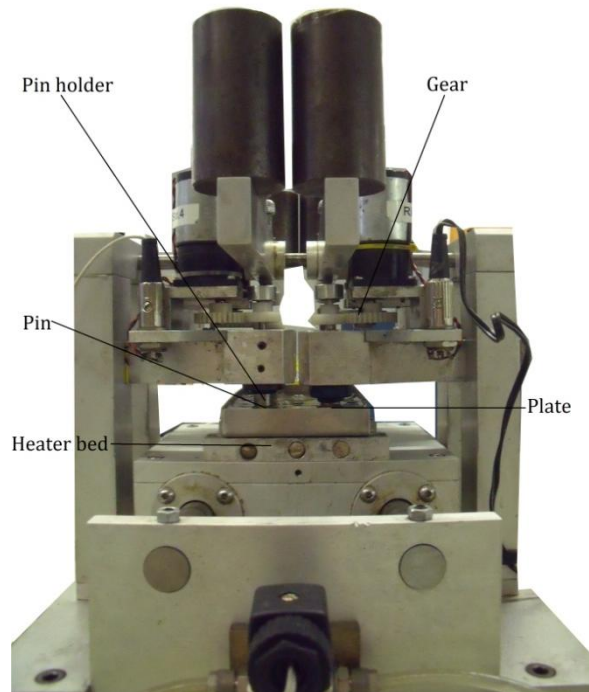


Figure 4.3: Pin-on-plate machine, side view.

Whilst the test was in operation a perspex cover was placed over the entire rig to prevent dust contamination from the atmosphere.

### 4.4 Lubricant

#### 4.4.1 ISO-standard lubricant

The lubricant used in this study was 25% bovine serum diluted with deionised water in accordance with ISO 14242-1. In addition, 8-10 pellets of NaOH, 20 mMol EDTA and 0.2% w/v of sodium azide were added. NaOH creates the desired pH to allow EDTA to dissolve. EDTA stops calcium deposition while sodium azide slows down any bacterial growth in the lubricant. The simulator ran in 0.5 MC intervals for 1.5 MC. After every 0.5 MC, the lubricant was extracted from the set-up and frozen for storage and future digestion.

The newborn calf serum was supplied by PAA (PAA Laboratories Ltd, Somerset, BA22 8YG). The same batch number, B00109-0614, was used consistently for all simulator tests within this study. The test lubricant had a resulting protein content of 17 g/L.

#### 4.4.2 Lubricant with Third-Body Particles

Two third-body particle tests were carried out during this study, both using two types of particles, hydroxyapatite (HA) and titanium (Ti).



**Figure 4.4: Porous titanium coating on the back of CoCrMo acetabular cup.**

Titanium is commonly used on the back of replacement acetabular cups in order to create a rough coating, see Figure 4.4, that aids in short and long term fixation and greatly reduces the risk of osteolysis [1].

Hydroxyapatite is an optional coating available for the acetabular cups in order to accelerate bony ingrowth. It has been demonstrated that HA stimulates osteoblastic activity for optimal initial stability when applied over the top of the Ti backing [2]. Both Ti and HA offer great benefits and hope to increase the longevity of a successful hip resurfacing.

As discussed in the literature review, if a resurfacing fails due to implant loosening then it is possible that particulate debris from the coating on the back of the cup may disintegrate and enter the joint cavity which could then have the ability to accelerate wear [3; 4]. Hence both HA and Ti are discussed here as clinically relevant third-body particles and our objective is to analyse the effect of these particles on metal resurfacing joints.

The first test was a pin-on-plate simulation (section 4.7) to assess any difference in effect on the MOM interface due to the presence of HA or Ti third-body wear particles.

Biomet UK supplied two samples of HA and Ti particles to be used in this project.

Both samples were examined using SEM and characterised from analysis of the images. A summary is shown in Table 4.1. There is a notable difference in morphology and size between the two types of particle. Ti is both sharper in structure and larger in size.

Table 4.1: Summary of morphology and size of third-body particles.

Particle Type	Morphology	Average diameter/ length, $\mu\text{m}$	$\pm$ Standard Deviation
HA	Mostly spherical and globular shapes	57	16
Ti	Irregular with sharp edges	234	73

An example of the SEM images of the particles can be seen in Figure 4.5 and Figure 4.7 for HA and Ti respectively. The size distribution of each sample is given in Figure 4.6 and Figure 4.8.

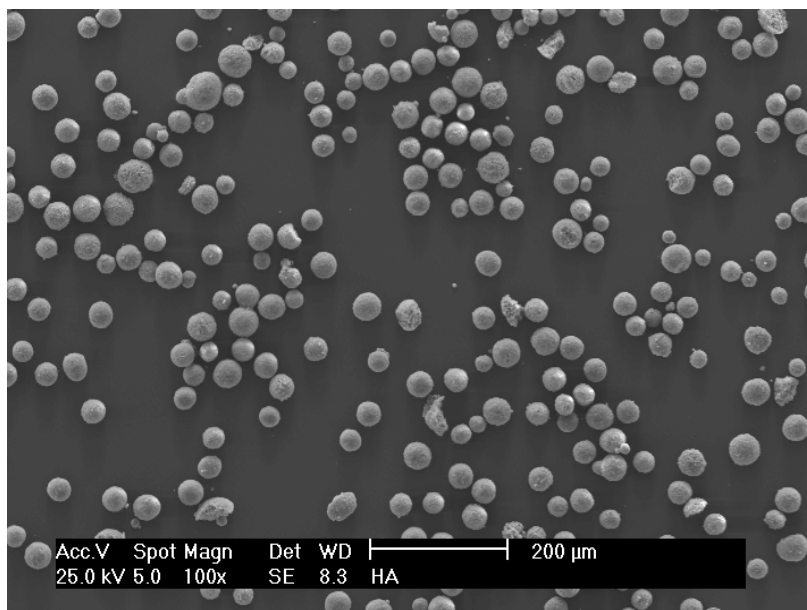


Figure 4.5: SEM image of HA particles.

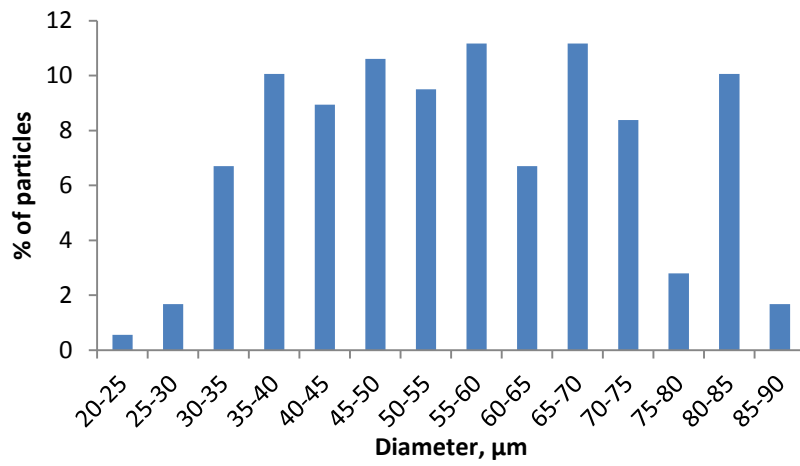


Figure 4.6: Size distribution of HA particles from SEM images.

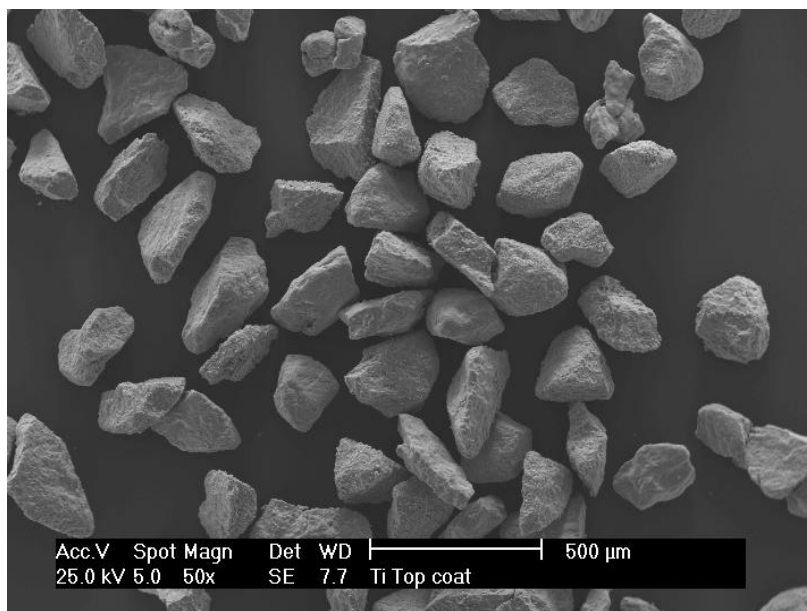


Figure 4.7: SEM image of Ti particles.

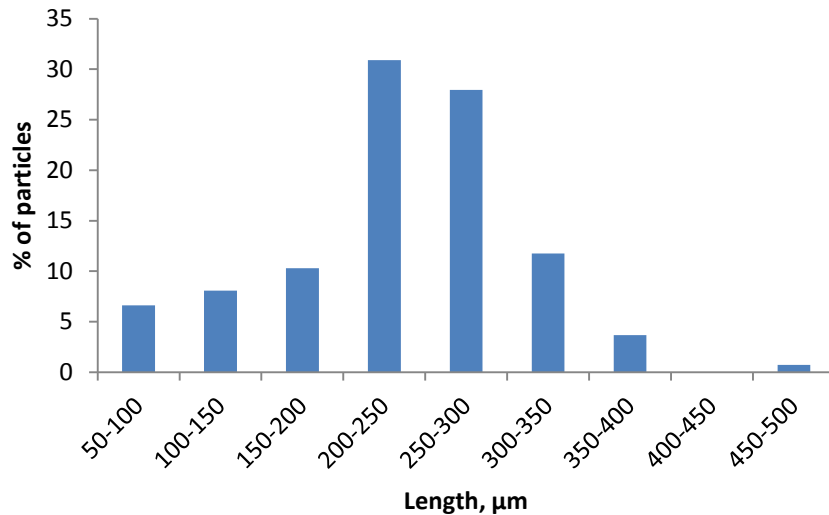


Figure 4.8: Size distribution of Ti particles from SEM images.

The pin-on-plate test was carried out in 0.25 MC intervals. In addition to the standard test lubricant, 5 mg/ml of third-body wear particles (either HA or Ti depending on the stage of the test) were added to the solution. Half of the wear particles were placed directly on to the plates during set up and half of the particles were mixed in the serum for four hours prior to testing, see Figure 4.9.



Figure 4.9: HA stirring in test lubricant for 4 hours prior to pin-on-plate simulation.

The second test was a third-body MOM hip simulation (section 4.8). Again, both HA and Ti particles were used in different stages of testing. Based on the results from the pin-on-plate simulation, the concentration of the third-body wear particles added to the

standard test lubricant for the hip simulation was increased to 10 mg/ml. Half of the wear particles were applied directly to the cups during set up, half of the particles were mixed in the serum overnight prior to testing. It was especially important whilst working with Ti wear particles that the lubricant was swirled whilst pouring into the gaiter during set up to ensure that the majority of the particles entered each station.

### **4.5 Wear characterisation**

#### **4.5.1 Gravimetric method**

Each component was cleaned, dried and weighed in intervals of 0.5 MC for any component undergoing testing in a hip simulator and 0.25 MC for any sample undergoing testing in a pin-on-plate machine, as described in ISO 14242-2. The cleaning protocol is provided in Appendix B.

The weighing balance used in this study for each component is the Mettler Toledo AX205. It is accurate to 0.01 mg and can withstand a maximum weight of 220 g. The balance had a readability of 0.1 mg and repeatability of 0.03 mg. Initially each sample was left to acclimatise next to the balance for thirty minutes prior to weighing. Three consecutive masses within  $\pm 0.1$  mg were recorded for each sample. This accuracy was achieved for all metal components. Volume change was then calculated from the mass data using the density of the material, which for CoCrMo was 8.276 g/cm<sup>3</sup>. After this, volume change was plotted versus number of cycles in Microsoft Excel and the wear rate in mm<sup>3</sup>/MC was calculated using linear regression analysis.

#### **4.5.2 Surface characterisation techniques**

The surface topography of the metal bearings used in this chapter have been analysed throughout each MOM test using zygo non-contacting profilometry as discussed in section 3.2. Images of the worn surfaces have also been taken with optical microscopy (also discussed previously in section 3.2). The only bearings which could not successfully be imaged were the 60 mm CoCrMo resurfacing heads which were too large to focus on. These bearing surfaces were only able to be investigated via zygo profilometry. However the 60 mm CoCrMo cups were imaged successfully and the carbides were clearly defined.

#### 4.6 MOM Test 1: ISO-standard biotribological study

For this test 60mm ReCap CoCrMo resurfacing components were articulating under standard conditions in the Durham hip simulator at 45° (standard inclination angle). There were five active stations, a loaded soak control and a soak control under no loading, left at room temp throughout the test.



Figure 4.10: 60mm ReCap CoCrMo Resurfacing Head and Cup.

##### 4.6.1 Joint replacement clearance

Eight resurfacing CoCrMo femoral heads were paired with CoCrMo acetabular cups. The samples were paired to give a radial clearance that was as close as possible. The mean radial clearance across the active samples was 118  $\mu\text{m}$ . The mean radial clearance across all the samples was 121  $\mu\text{m}$ . Table 4.2 shows the full list of clearances.

It is worth noting that the initial resurfacing head and cup being tested in Station 1 (referenced as Stn 1a) had to be replaced after 1 MC. The reason for this will be explained in the following section. The bearing combination that replaced it is shown in Table 4.2 as Stn 1b.

Table 4.2: Radial clearance of 60mm CoCrMo components.

Test 1	Femoral	Batch, Batch ID	Shell	Batch, Batch ID	Clearance, $\mu\text{m}$
Stn 1a	1	2410669, 1	38	2410665, 2	119
Stn 1b	25	2410694, 1	48	2410667, 2	119
Stn 2	4	2410669, 4	39	2410665, 3	117
Stn 3	9	2410670, 3	43	2410666, 2	119
Stn 4	6	2410669, 6	42	2410666, 1	117
Stn 5	15	2410671, 3	45	2410666, 4	119
Load cntrl	3	2410669, 3	40	2410665, 4	132
Soak cntrl	20	2410672, 2	47	2410667, 1	122

#### 4.6.2 Wear results

The test consisted of five active stations, all under standard conditions. In addition to this, there was a load soak control, and a soak control under no loading. There were problems throughout the test with the quality of the silicon gaiters which led to serum loss and increased wear during leakages from the neck of the gaiters during the stress of internal/external rotation. The main leakage events are summarised in Figure 4.11. After Station 1 had suffered a large serum loss during the first 0.5 MC and ripped again between 0.5-1MC, at the start of 1.5 MC the station began to squeak due to the increased friction between the components as a result of dry wear. The station bearing had also become loose so it is probable that the station oscillation had an additional effect on the wear. The station was tightened and the bearing was replaced with fresh components (represented in the data as Station 1b). The test then ran to 6MC in order to obtain 5 MC of data for this station.

During the test, only Station 1b and 4 did not suffer any leaks at all, so the wear data has been split into those that suffered leaks and those that did not. There is a considerable difference between the two sets of data and the change in lubrication conditions and mode of wear has had a significant effect on the rate of wear.

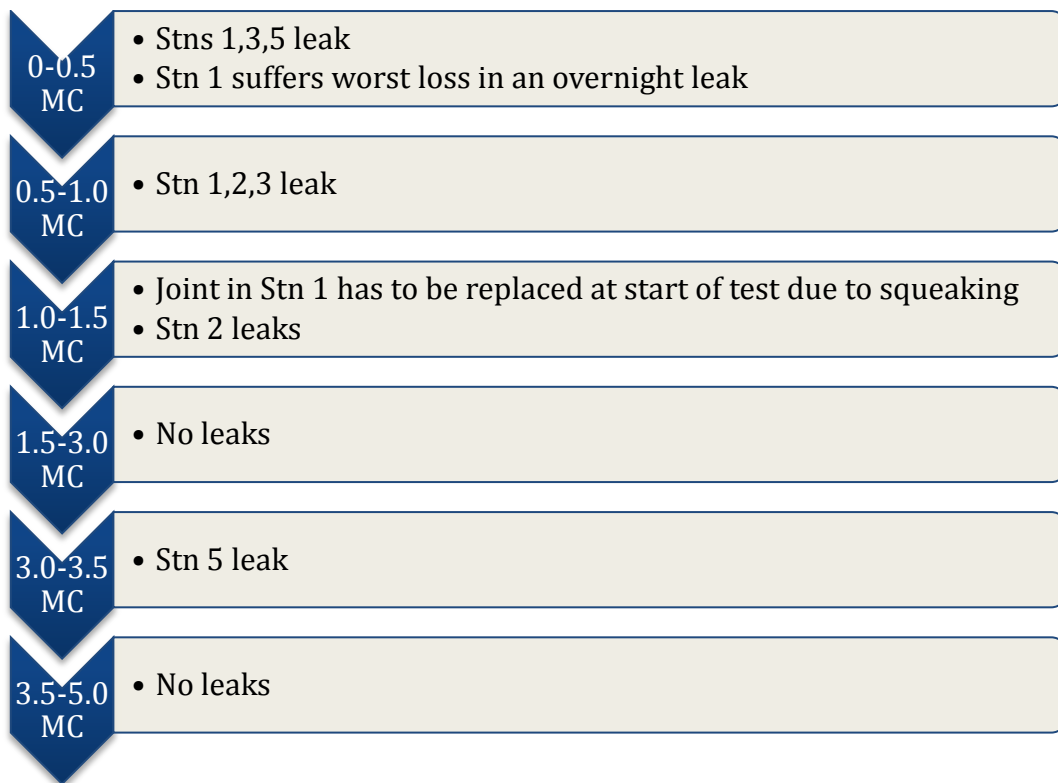


**Figure 4.11: Summary of complications with gaiters throughout 5 MC.**

The mass loss of each component was corrected by the change of the load soak to account for the fluctuations in mass measurements over the test. The cumulative weight loss from the femoral resurfacing heads and acetabular cups in Stations 1b and 4 are shown in Figure 4.12 and Figure 4.13 respectively. The cumulative weight loss from the femoral resurfacing heads and acetabular cups in Stations 2, 3 and 5 are shown in Figure 4.14 and Figure 4.15.

#### 4. Generation of physiologically scratched CoCrMo cups

---

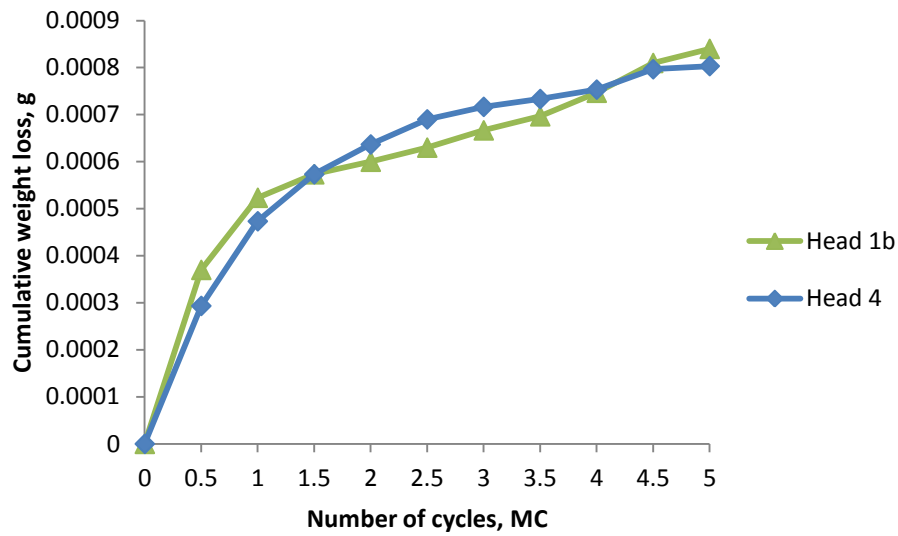


Figure 4.12: Cumulative weight loss of 60mm resurfacing CoCrMo heads from Stn 1b and Stn 4, accounting for the load soak.

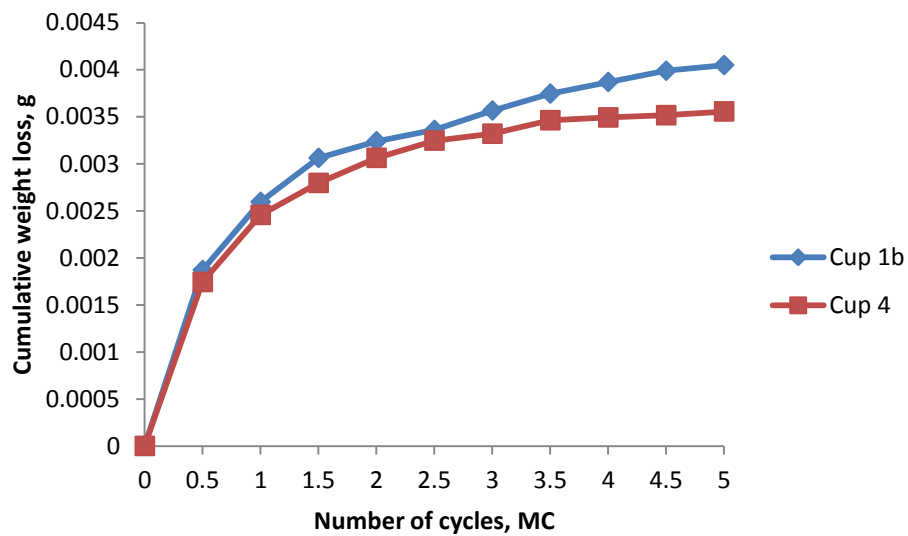


Figure 4.13: Cumulative weight loss of 60mm acetabular CoCrMo cups from Stn 1b and Stn 4, accounting for the load soak.

#### 4. Generation of physiologically scratched CoCrMo cups

---

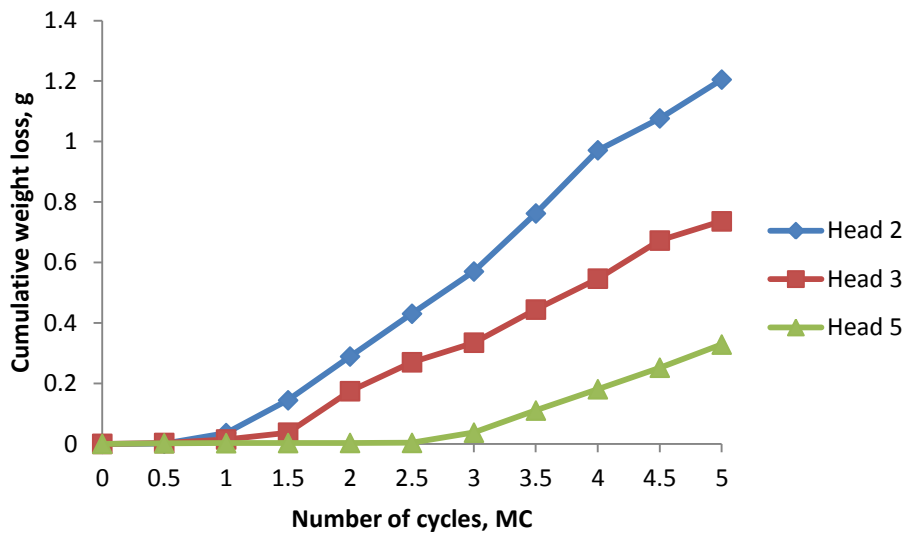


Figure 4.14: Cumulative weight loss of 60mm resurfacing CoCrMo heads from Stns 2,3 and 5, accounting for the load soak.

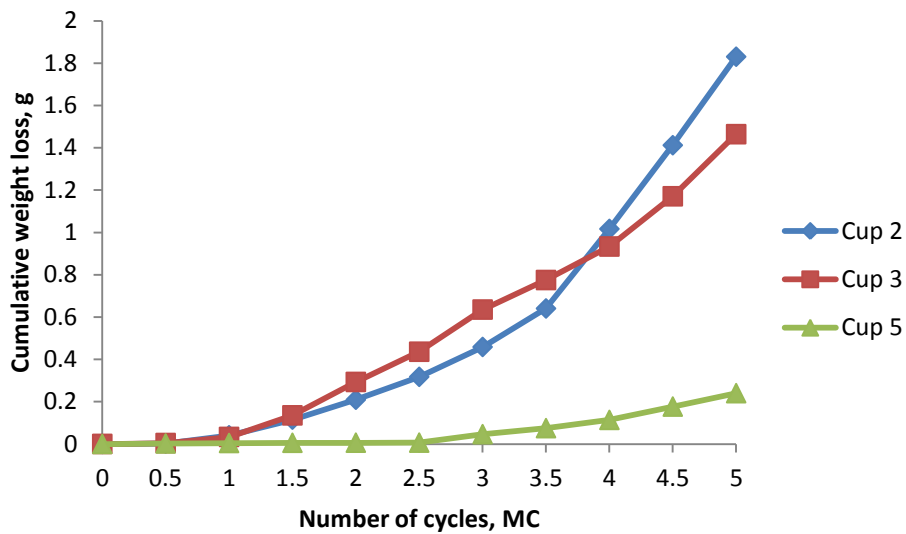


Figure 4.15: Cumulative weight loss of 60mm acetabular CoCrMo cups from Stns 2,3 and 5, accounting for the load soak.

#### 4. Generation of physiologically scratched CoCrMo cups

---

It is clear to see wear in Stations 1b and 4 has been very low, whereas the leakages have had a huge detrimental effect on the wear rates in Stations 2, 3 and 5, creating 'runaway wear'.

Wear rates ( $\text{mm}^3/\text{MC}$ ) have been calculated for each station. For Stations 1b and 4, wear has been divided into run-in wear (0-1 MC) and steady-state wear (1-5 MC). The results are shown in Table 4.3. For the 'runaway' stations which have suffered multiple leaks, the overall (0-5 MC) wear rate is shown in Table 4.4. Station 5 has experienced a lower wear rate than Stations 2 or 3 since it suffered its most major leak further along in the test.

**Table 4.3: Wear rates for 60mm resurfacing CoCrMo heads,  $\text{mm}^3/\text{MC}$ .**

<b>Wear Rates</b>	<b>Run-in</b>	<b>Steady State</b>	<b>Overall</b>
<b>Head 1b</b>	0.069	0.009	-
<b>Head 2</b>	-	-	32.19
<b>Head 3</b>	-	-	19.62
<b>Head 4</b>	0.060	0.009	-
<b>Head 5</b>	-	-	7.53

**Table 4.4: Wear rates for 60mm acetabular CoCrMo cups,  $\text{mm}^3/\text{MC}$ .**

<b>Wear Rates</b>	<b>Run-in</b>	<b>Steady State</b>	<b>Overall</b>
<b>Cup 1b</b>	0.34	0.041	-
<b>Cup 2</b>	-	-	41.78
<b>Cup 3</b>	-	-	35.82
<b>Cup 4</b>	0.32	0.031	-
<b>Cup 5</b>	-	-	5.28

At worst, the wear rates in the 'runaway' stations are over 1000 times greater than those which have not experienced any leaks. This is thought to be due to the increased friction between the articulating surfaces which later decreased the stability of the head stem in the head stem holder causing slight additional wear around the head stem.

With the exception of Station 5, the acetabular components have had a greater wear rate than the femoral components.

### 4.6.3 Surface characterisation

#### 1) Zygo non-contacting profilometry

Ten zygo images were taken at the pole and at 33° around the pole for each component in the five active stations at different stages throughout the test. The load control and soak control were also analysed for comparison.

Wear testing has caused the surface roughness (Ra) to increase slightly in Stations 1b and 4 for both the heads and cups. In Stations 2, 3 and 5, that have leaked, the increase in roughness is much greater for all components. The surface roughness of the load control components have barely changed. Again, data has been collected and averaged over the stations that have not encountered leaks, and those that have. Figure 4.16 and Figure 4.17 show the results; the error bars indicate the standard deviation of the data.

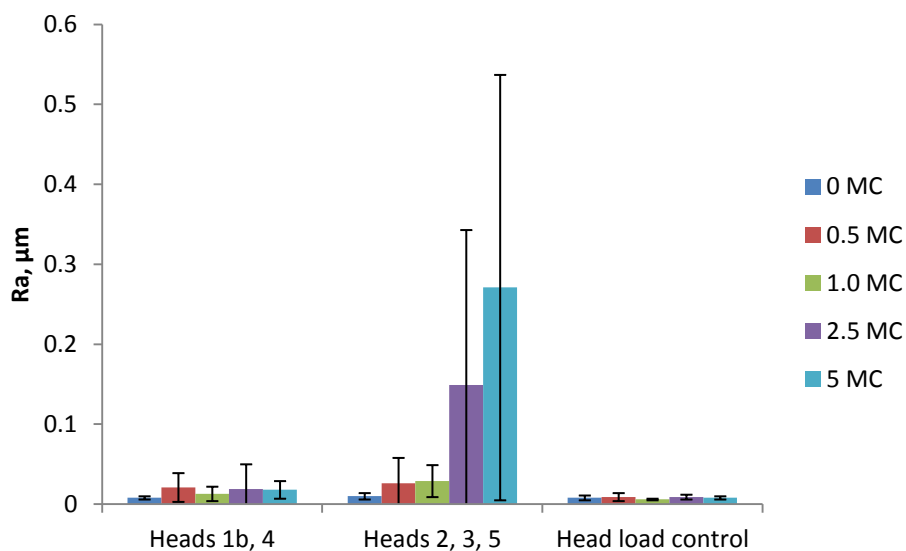


Figure 4.16: Surface roughness of 60mm resurfacing CoCrMo heads during testing.

#### 4. Generation of physiologically scratched CoCrMo cups

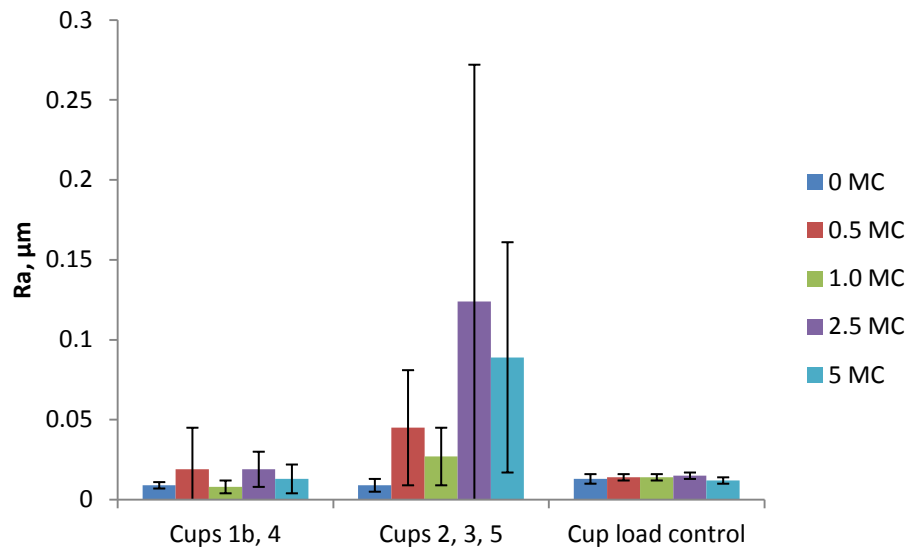


Figure 4.17: Surface roughness of 60mm acetabular CoCrMo cups during testing.

The trend in the changing skewness is much harder to see, especially since any measurement that has a significant positive or negative skewness can affect the mean value. This can be seen in the load control data, where the skewness has decreased throughout the test, but at the same time the standard deviation has increased also. Generally, during the run-in phase of the test, skewness has decreased, which is more favourable for lubrication.

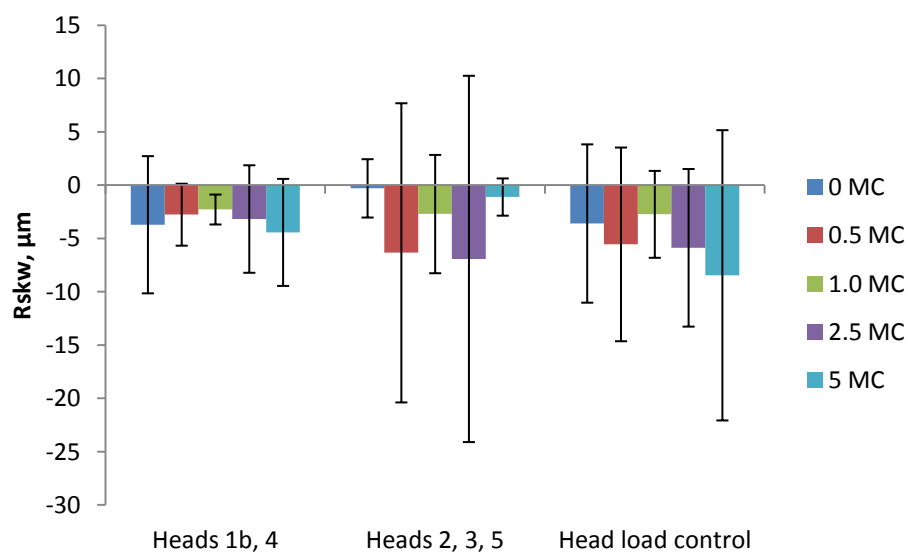
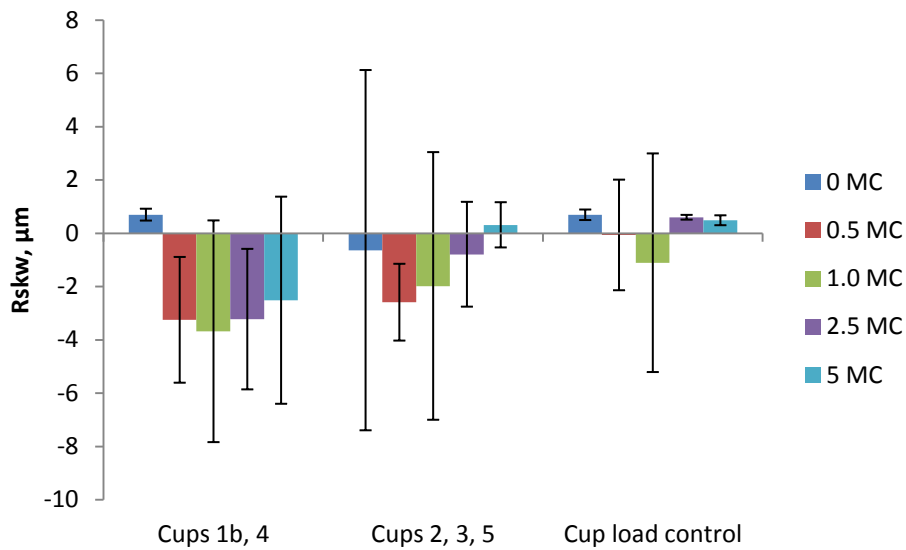


Figure 4.18: Skewness of 60mm resurfacing CoCrMo heads during testing.



**Figure 4.19: Skewness of 60mm acetabular CoCrMo cups during testing.**

Figure 4.20 and Figure 4.21 show a selection of zygo images showing 3D profiles of the surface of the femoral and acetabular components. The first is a typical image taken from the cups at 0 MC. The images that follow are taken after 5 MC from each station. The surface topography from the bearings in Stations 1b and 4, shown in images B and E from both Figure 4.20 and Figure 4.21, is much smoother than from the bearings that experienced leaks.

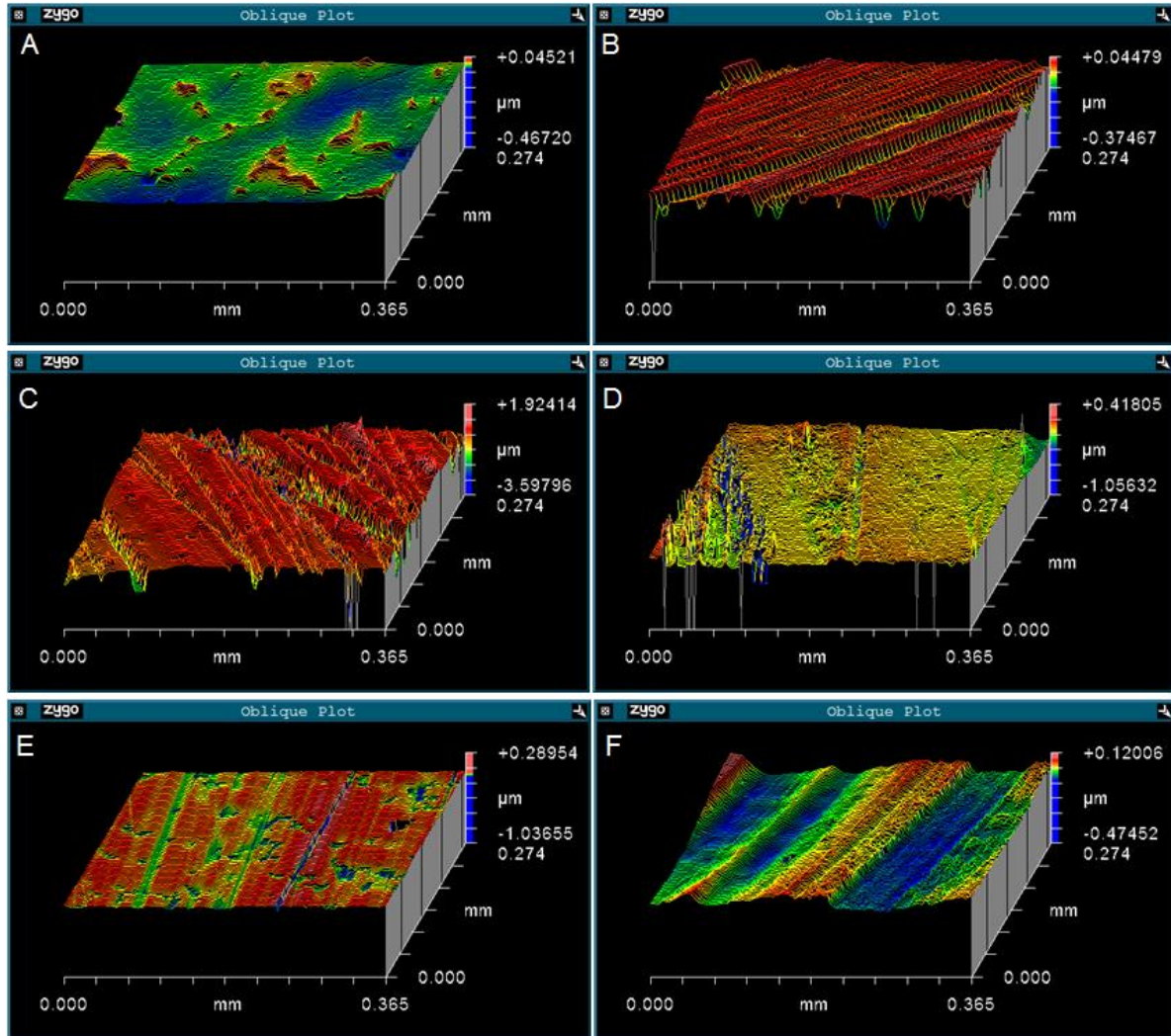


Figure 4.20: Surface profiles of femoral resurfacing heads imaged throughout this test. A: OMC from Station 1b, B: 5 MC from Station 1b, C: 5 MC from Station 2, D: 5 MC from Station 3, E: 5 MC from Station 4, F: 5 MC from Station 5.

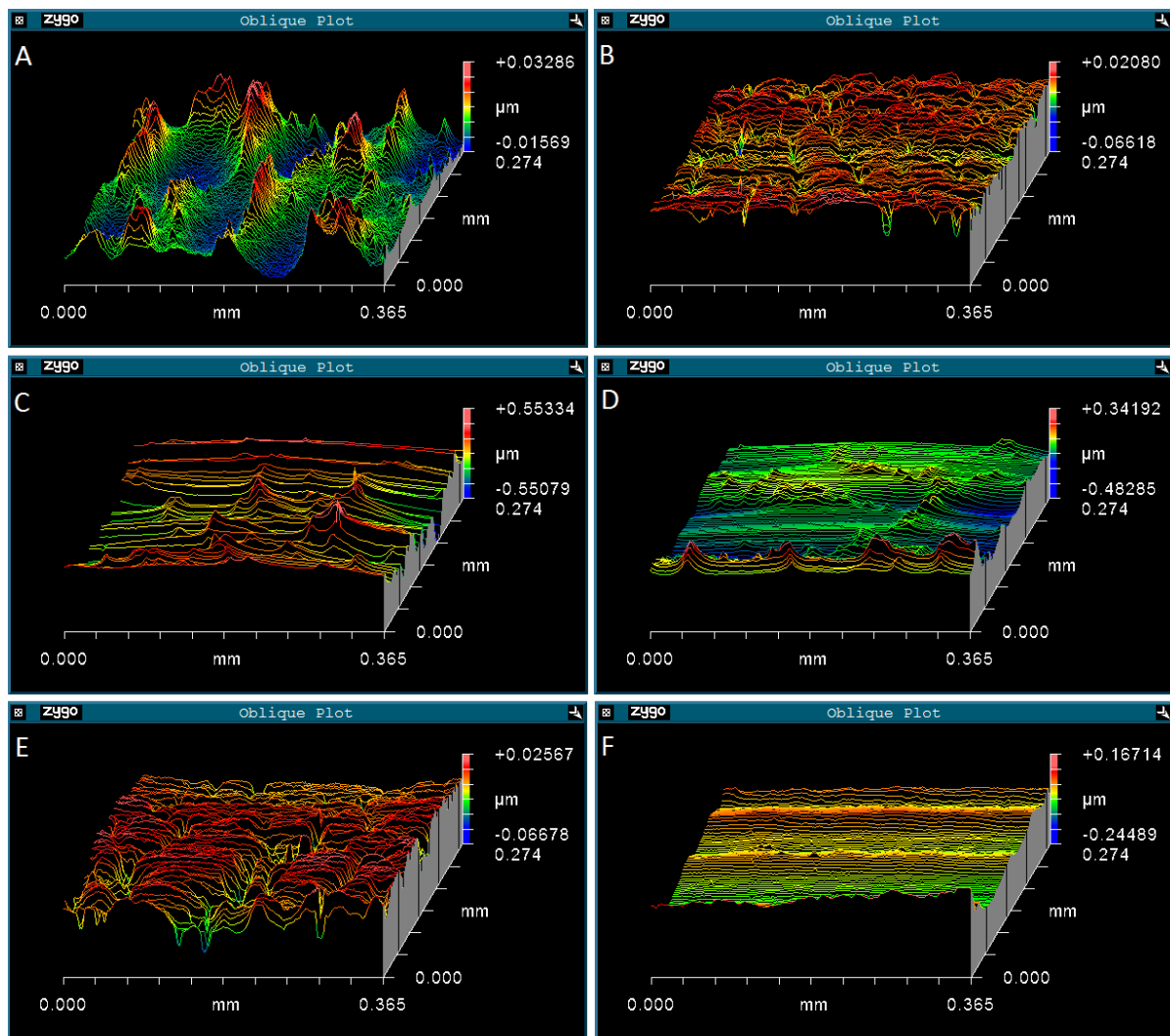


Figure 4.21: Surface profiles of acetabular cups imaged throughout this test. A: OMC from Station 1b, B: 5 MC from Station 1b, C: 5 MC from Station 2, D: 5 MC from Station 3, E: 5 MC from Station 4, F: 5 MC from Station 5.

## 2) Optical microscopy

The following images were taken with an Axiotech optical microscope. Figure 4.22 shows a typical image of the surface of the cups at 0 MC in comparison to those after the very first 0.5 MC, the carbides are clearly visible. Figure 4.23 and Figure 4.24 then show images from the cup surfaces after 2.5 MC and 5 MC respectively, including the load control station.

#### 4. Generation of physiologically scratched CoCrMo cups

---

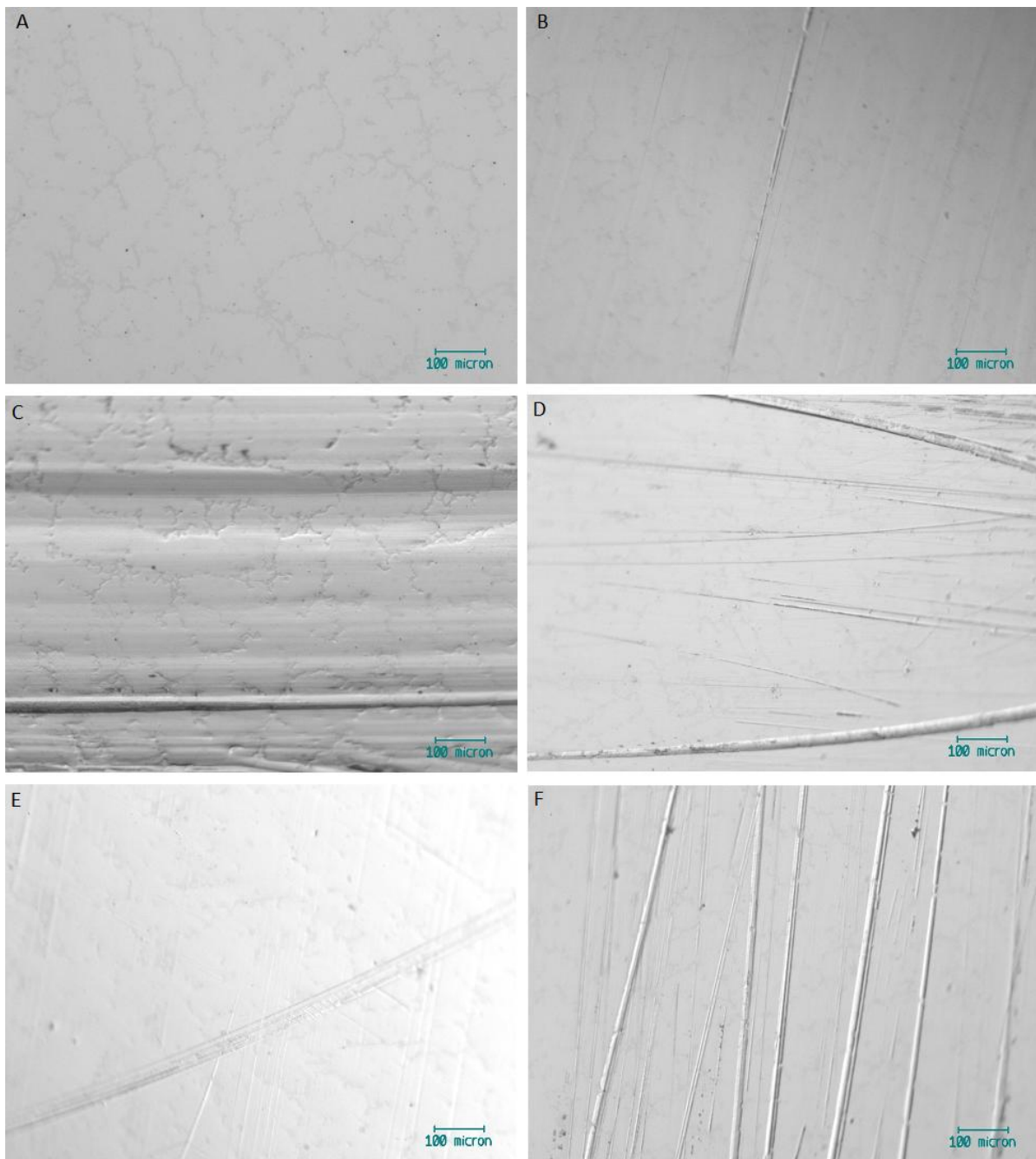


**Figure 4.22: Surface images taken throughout this test. A: OMC from Station 1b, B: 0.5 MC from Station 1b, C: 0.5 MC from Station 2, D: 0.5 MC from Station 3, E: 0.5 MC from Station 4, F: 0.5 MC from Station 5.**

#### 4. Generation of physiologically scratched CoCrMo cups

---

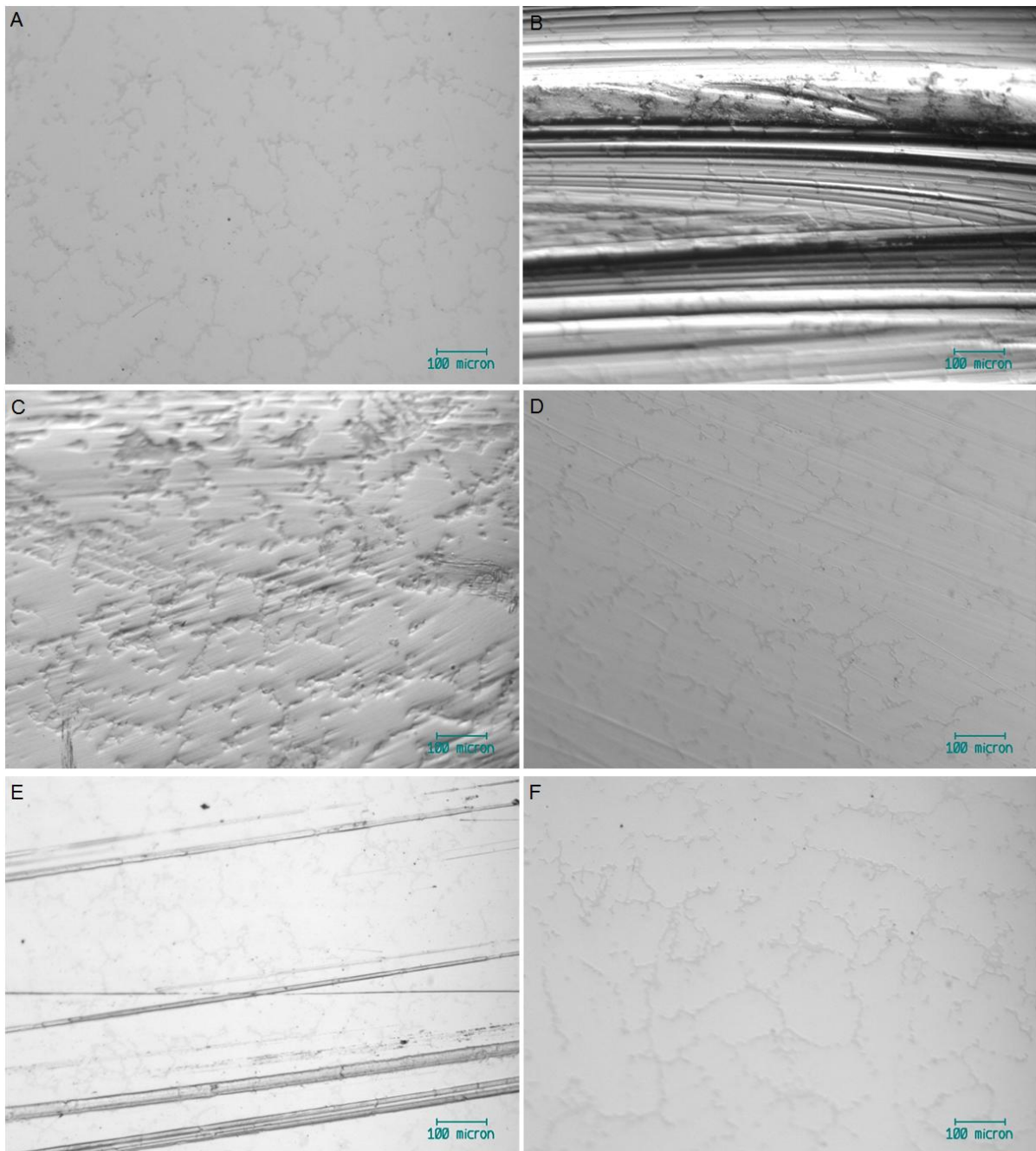


**Figure 4.23: Surface images taken after 2.5 MC of this test. A: Station 1b, B: Station 2, C: Station 3, D: Station 4, E: Station 5, F: the load control station.**

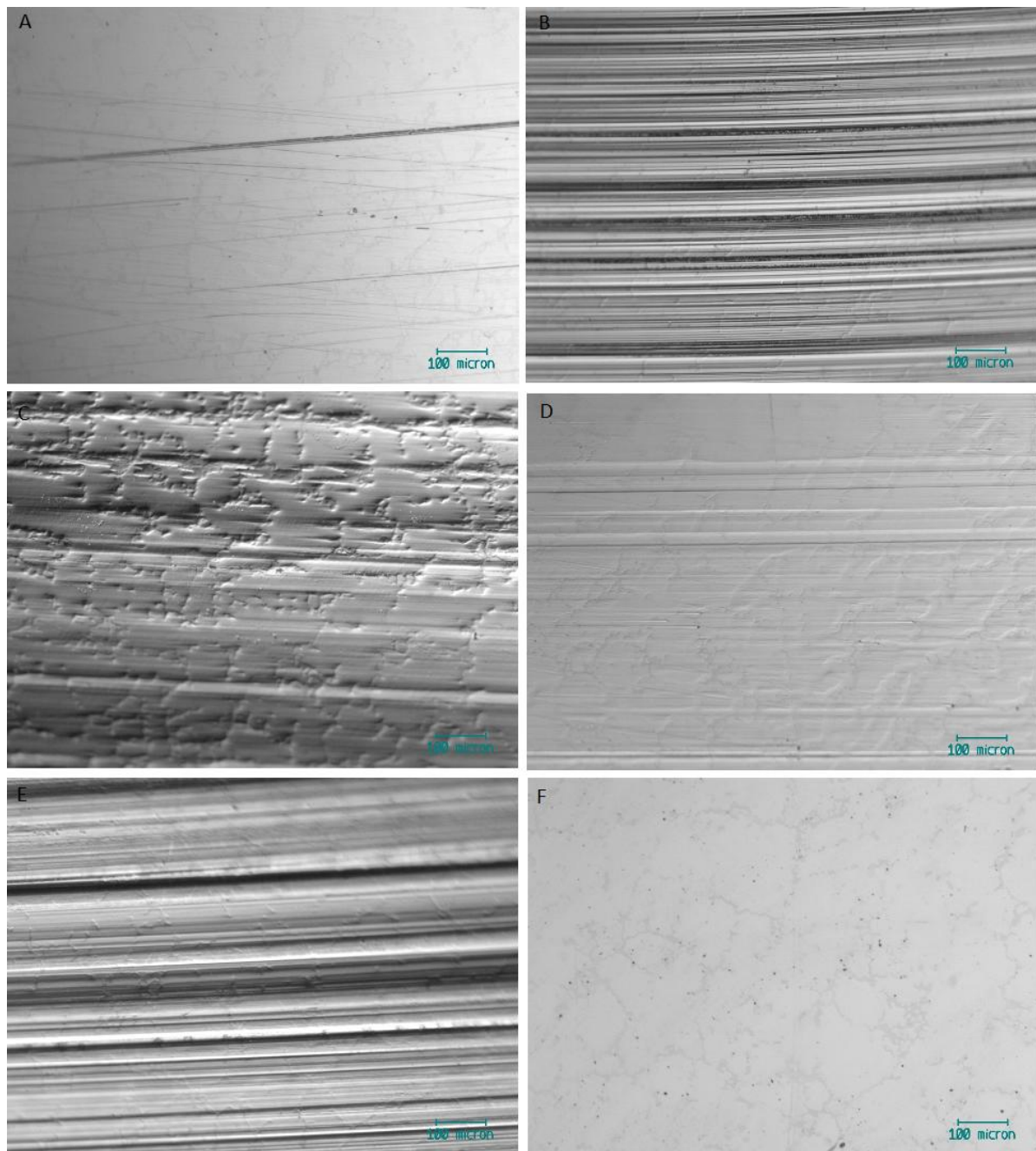


**Figure 4.24: Surface images taken after 5 MC of this test. A: Station 1b, B: Station 2, C: Station 3, D: Station 4, E: Station 5, F: the load control station.**

The difference in the worn areas on the surfaces of the cups from stations that have experienced serum loss through gaiter leaks is clear to see. Stations 1b and 4 were only slightly scratched at the end of the test, but Station 2, 3, 5 are deeply scarred with possible carbide removal.

### 4.6.4 Limitations

The main limitation in this test has been the poor quality of the gaiters, leading to increased loss of serum at certain stages throughout the wear simulation. Alternative gaiters were trialled in the hope of minimising leakages, however the option available, shown in Figure 4.25 below, did not fit the cup holder well, and air bubbles collected in the concertinaed edges. Therefore it was decided to continue with the current style of gaiter, under careful observation, whilst the suppliers looked into the problem. Any leaks that occurred overnight were, sadly, unavoidable.



Figure 4.25: Alternative available gaiter with concertinaed edges (pulled over cup holder and base plate).

### 4.6.5 Discussion

In order to compare the test results seen here, the data will be considered in two parts.

Firstly the data from the stations which did not experience dry wear (one and four) will be compared to previous simulator studies using metal resurfacing bearings.

Secondly the data from the stations which experienced runaway wear (two, three and five) will be compared to data from analysis on retrieved resurfacing bearings.

The data from the 60 mm ReCap resurfacing femoral heads in Stations 1b and 4 has been combined with the data from the acetabular cups in order to compare the total run-in and steady state wear rates with previous studies by Leslie *et al.* [5], Heisel *et al.* [6], Saikko *et al.* [7] and Vassilou *et al.* [8] using a range of resurfacing joints with different diameters. The clearance of the bearings ranged from 0.111  $\mu\text{m}$  to 0.210  $\mu\text{m}$ .

#### 4. Generation of physiologically scratched CoCrMo cups

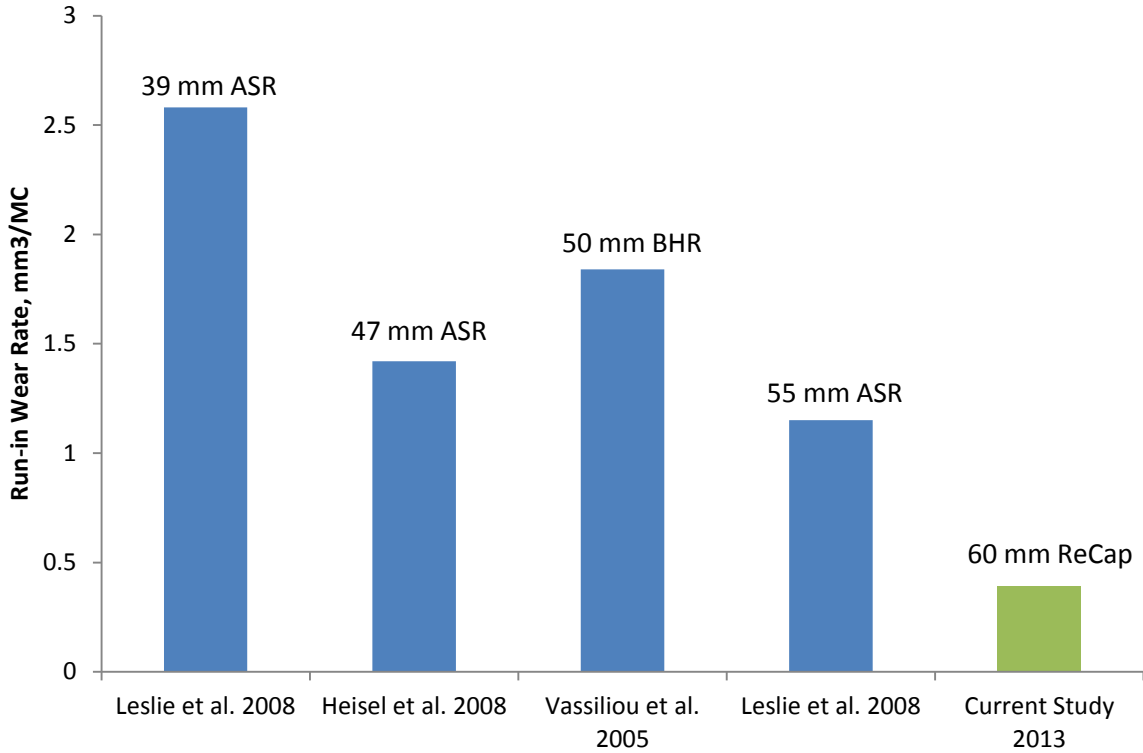


Figure 4.26: Comparison of the run-in wear data from Stns 1b and 4 with previously published simulator studies.

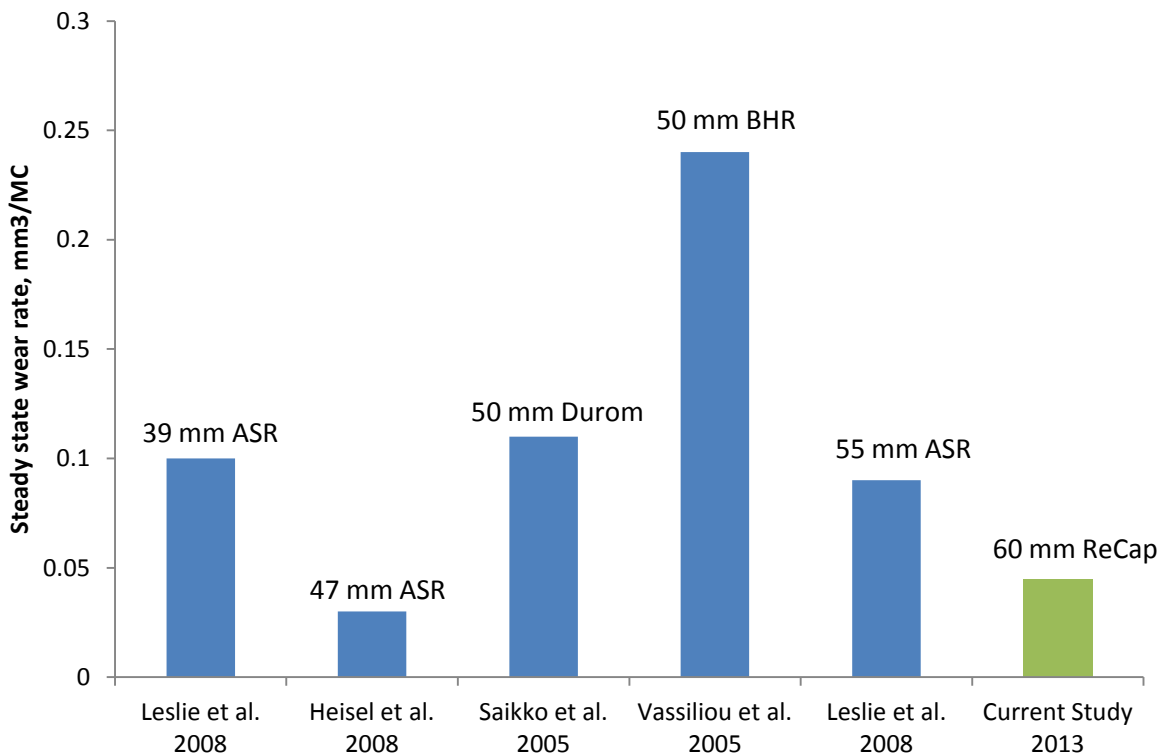


Figure 4.27: Comparison of the steady state wear data from Stns 1b and 4 with previously published simulator studies.

A comparison of the run-in wear rates is given in Figure 4.26 while Figure 4.27 shows the comparison of the steady state wear rates.

The run-in wear rate seen in the well-functioning stations in this study was much lower than those seen in previous studies, whereas the steady state wear rate was more comparable with the previous work.

Sieber *et al.* [9] studied 65 retrieved second-generation MOM heads and 53 retrieved cups. 115 retrievals had a diameter of 28 mm, 3 had a diameter of 32 mm. The average linear wear rate was found to be 0.025 mm for the whole articulation per year in the first year, and then 0.005 mm/year after the third year. The average volumetric wear rate was 0.3 mm<sup>3</sup>/year, this corresponds well to the run-in wear rate seen in bearings in stations 1b and 4 which functioned well, with their wear rates dropping as they continued to steady state.

However, the bearings in this study that suffered leaks had much higher wear rates which were within the range of severe wear rates experienced in failed metal resurfacing joints as determined by Lord *et al.* [10] and can be seen in Figure 4.28.

The additional wear around the stem of the metal resurfacing femoral heads seen in bearings 2, 3 and 5 has also been seen clinically in retrieved implants from patients who have suffered adverse reactions to metal debris and is considered by Takamura *et al.* [11] to be a major concern for large diameter MOM bearings. The study looked at 90 retrieved resurfacing heads produced by several manufacturers.

#### 4. Generation of physiologically scratched CoCrMo cups

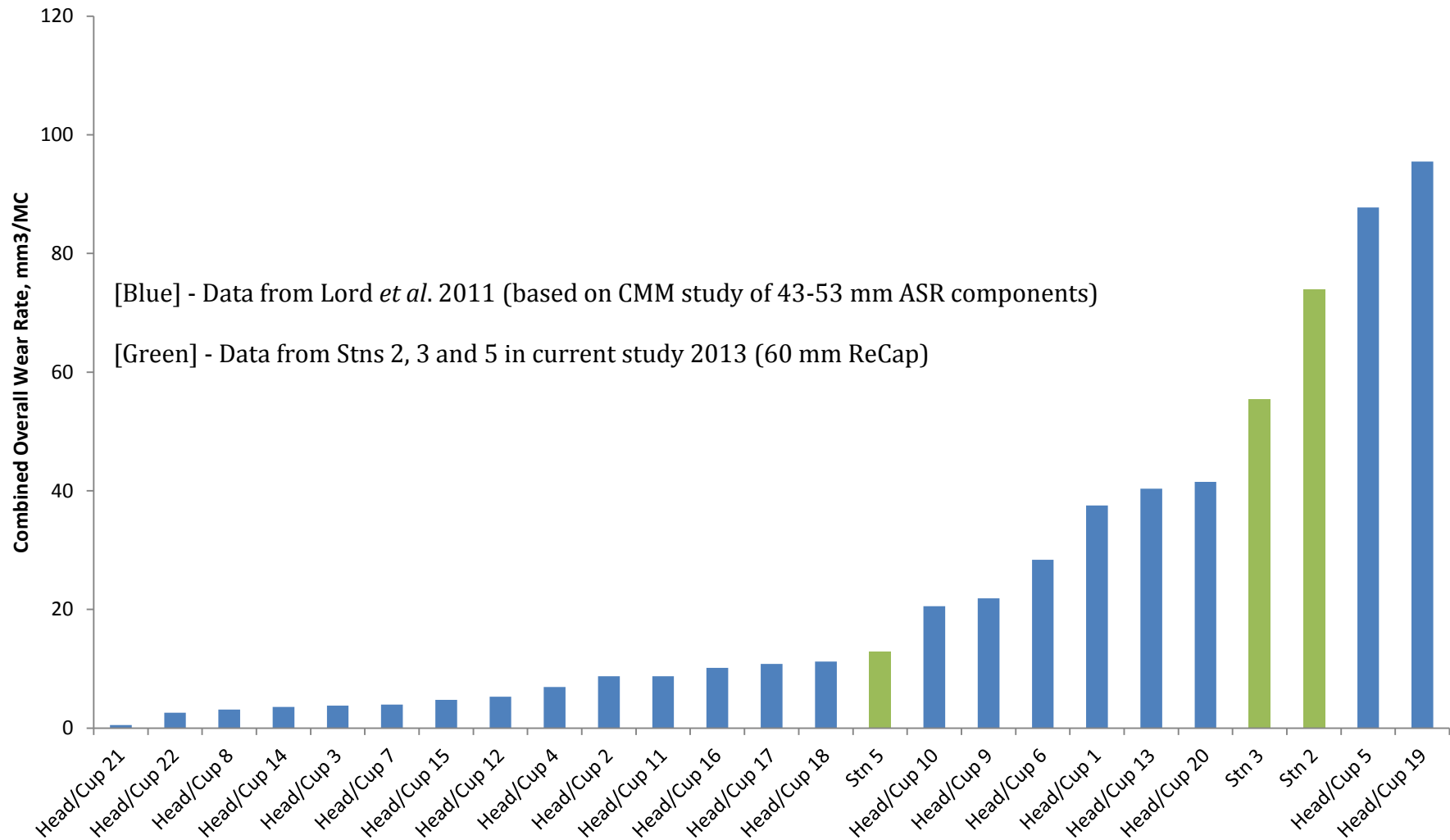


Figure 4.28: Comparison of the wear data from Stns 2, 3 and 5 with retrieval data published by Lord *et al.* [10].

#### 4. Generation of physiologically scratched CoCrMo cups

---

It is important throughout this test to consider that the whole reason behind it is to provide worn cups for the next simulation representing a retrieval operation, replacing the worn femoral component for a new, dual mobility, head.

Initially it was assumed that additional, external wear would be needed to try to make the cups as rough as those extracted during revision procedures. This would have been problematic due to the possible introduction of third-body wear particles from any emery paper, etc used to wear the surface. However, the problems with leaking gaiters have caused such an increase in wear that it has been surprisingly beneficial. Below is a comparison from the zygo data between the test cups and eight retrieval acetabular components that have been studied. The surface roughness of the cups which have experienced leaks is greater than that seen in the retrievals in this project.

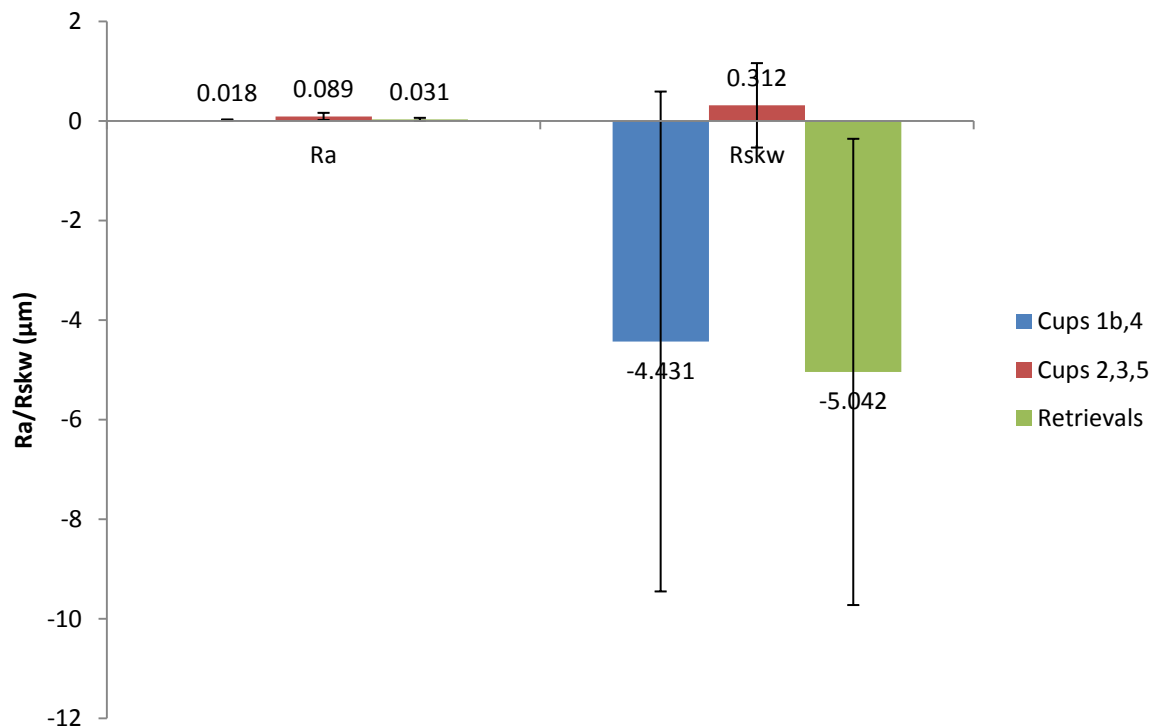
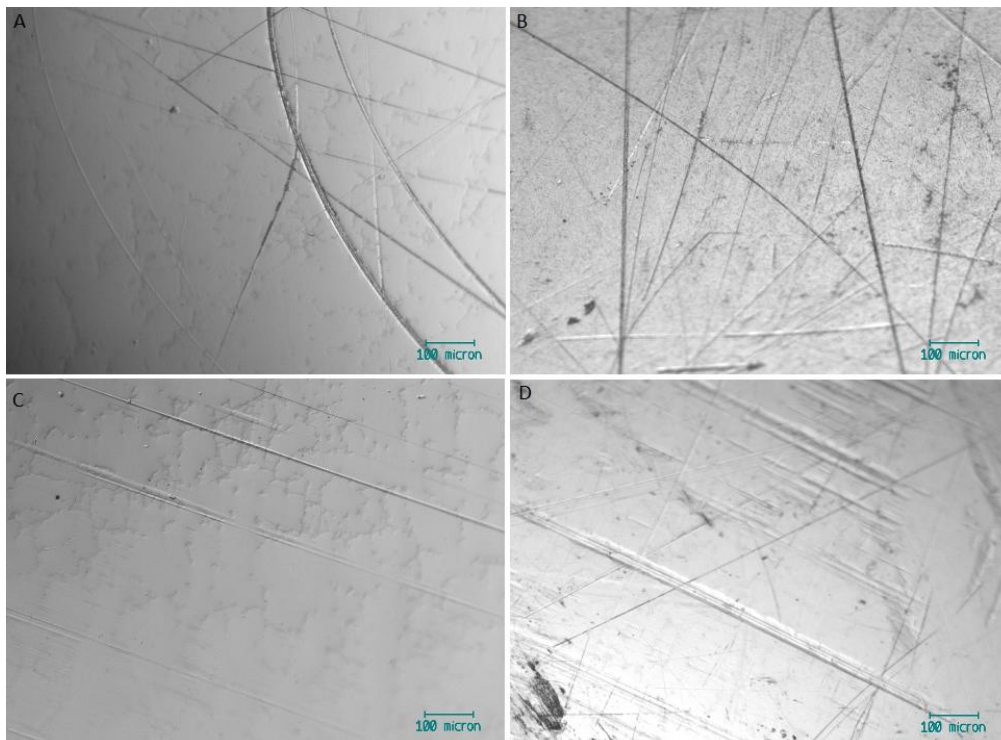


Figure 4.29: Zygo data showing average surface roughness (Ra) and skewness (Rskw) values across all test components in comparison to retrieved acetabular components.

Cups 1b and 4 are smoother than the retrievals but are still relevant since they share some similar features regarding scratching at the surface, this can be seen in Figure 4.30, as well as smoothed carbides at the bearing surface which are shown in the earlier zygo images that are in common with retrieved acetabular cups.

#### 4. Generation of physiologically scratched CoCrMo cups

---



**Figure 4.30: Optical images taken from the surfaces of A: Cup 1b after 5 MC, B: retrieved component FAR 77, C: Cup 4 after 5 MC, D: retrieved component FAR 164.**

The major, expected difference between the test cups and the retrievals is that the retrievals feature a lot more multidirectional scratches, Figure 4.31. Multidirectional scratches are not possible to create in a standard wear test due to the controlled movement of the simulator. However, the wear tracks seen in the ‘runaway’ stations are so deep that if the next test reduces the wear from stations 2, 3, and 5, then it would really be a strong indication that dual mobility heads are a viable solution to a failed hip resurfacing arthroplasty. These three stations have all experienced wear rates within the range seen clinically in retrieved failed metal hip resurfacing joints [10].

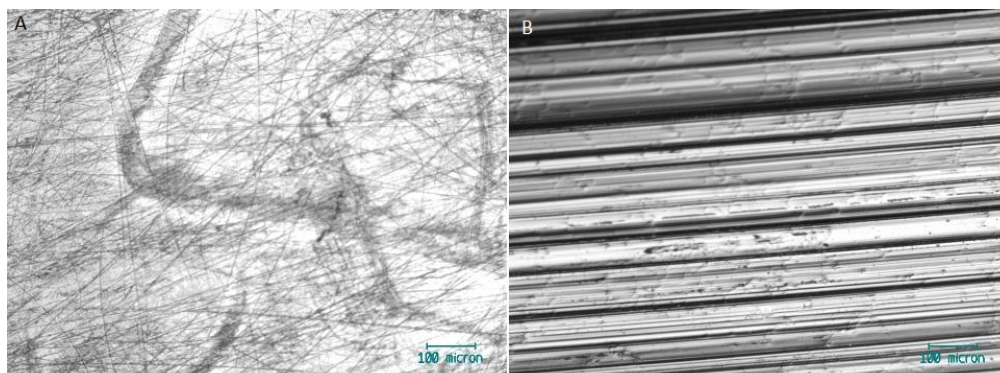


**Figure 4.31: Optical images taken from A: retrieved component FAR 4 (a lot of multidirectional scratches), B: Cup 2 after 5 MC (a lot of deep, unidirectional scratches).**

### 4.6.6 Conclusion

Five resurfacing 60 mm CoCrMo heads have been tested against 60 mm CoCrMo acetabular cups for 5 MC under standard conditions at a standard incline.

Stations 2 and 3 experienced dry wear during the run-in phase, whereas Station 5 experienced dry wear during steady-state, and this led to runaway wear in these stations. The overall wear rates of the CoCrMo resurfacing heads ranged from 7.53 mm<sup>3</sup>/MC to 32.19 mm<sup>3</sup>/MC in these stations. The overall wear rates of the CoCrMo cups ranged from 5.28 mm<sup>3</sup>/MC to 41.78 mm<sup>3</sup>/MC.

Stations 1 and 4 did not experience any leaks. The wear rates of the CoCrMo resurfacing heads ranged from 0.06 – 0.07 mm<sup>3</sup>/MC during run-in wear and was 0.009 mm<sup>3</sup>/MC during steady state. The wear rates of the CoCrMo cups ranged from 0.32 – 0.34 mm<sup>3</sup>/MC during run-in wear and from 0.03 – 0.04 mm<sup>3</sup>/MC during steady state.

Surface roughness generally increased for all components over the course of 5 MC, and was much rougher in the components that had experienced runaway wear. Optical images for these components showed also deep scratches with possible carbide removal.

The wear rates of the CoCrMo cups in the stations which have experienced leaks have been seen clinically in failed MOM THRA hence the complications in this test have provided worn cups for the following dual mobility simulation which represents a retrieval operation *in vitro*.

### 4.7 MOM pin-on-plate wear screening for MOM Test 2: third-body aggressive wear

The purpose of the following pin-on-plate investigation was to establish whether hydroxyapatite (HA) or titanium (Ti) particles have a greater third-body particle effect on the CoCrMo-CoCrMo interface. It was a trial with the aim being to decide the order of third-body particle testing of future hip simulations in order to provide worn cups with similar surface features to those seen *in vivo*. CoCrMo pins with a diameter of 6mm, length 18 mm were tested against CoCrMo plates with dimensions 44 x 24 x 3 mm. The samples had been previously tested. The wear under standard conditions in 25% bovine

#### 4. Generation of physiologically scratched CoCrMo cups

---

serum is not important; it is the comparative wear once the third-body particles have been added that is of interest in this chapter.

Pin-on-plate simulations are carried out in 0.25 MC intervals. For the first 0.5 MC, the pins were worn against the plates under standard conditions in 25% bovine serum. Between 0.5-1.0 MC the test was run in 25% bovine serum plus 5 mg/ml HA particles. Then between 1.0-1.5 MC the pins were worn against the plates under standard conditions again to act as a recovery stage. Between 1.5-2.0 MC the test was run in 25% bovine serum plus 5 mg/ml Ti particles. In each third-body test, half of the particles were mixed in the serum for four hours prior to testing, and the remaining particles were applied directly to the plates during set up. It was hoped that this would ensure particles to be located in the wear track, and also dispersed in the test lubricant.

##### 4.7.1 Wear results

The cumulative weight loss from each pin is shown in Figure 4.32 while Figure 4.33 shows the average mass loss of the four pins and notes the change in lubricant conditions during the 2MC. The mass loss of each pin has been corrected by the change of a soak pin to account for fluctuations in mass measurements during the test. The pins have worn consistently throughout this simulation, despite the change in lubricant conditions.

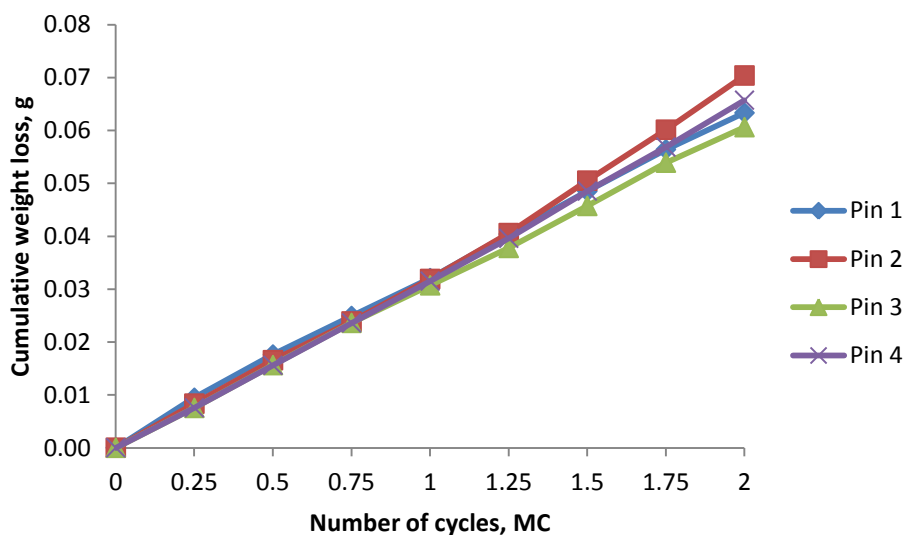
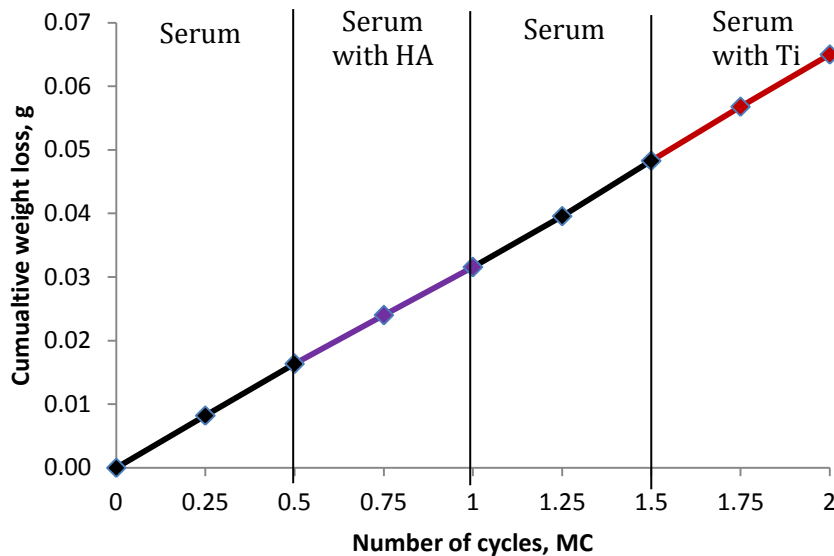


Figure 4.32: Cumulative weight loss of CoCrMo pins, accounting for the soak control.

#### 4. Generation of physiologically scratched CoCrMo cups

---



**Figure 4.33: Cumulative weight loss from an average of the four active pins, noting the different test conditions.**

At the start of 0.5 MC, when HA was first added to the test lubricant, there was a technical problem with the water level sensor. HA particles collected and built up around the sensor and overnight the sensor failed, water evaporated from the serum which was not replaced and this led to dry wear for an unknown amount of time after. This did not affect the wear data for the pins; however the effect is evident in the wear data for the plates. The plates suffered a significant mass loss. Because this was the first test interval where HA particles were added, the extent of wear due to third-body particles or dry wear from the sensor failing was unknown. However during 0.75-1.0 MC when more HA particles were added, and there were no technical issues with the water level sensor, the mass loss from the plates was not significant. This indicates that the mass loss during 0.5-0.75 MC was directly down to dry wear, rather than any third-body particle effect. The cumulative weight loss from each plate is shown in Figure 4.34, and has been corrected by the change in mass of a soak plate. Figure 4.35 shows the average mass loss of the four plates, noting the change in lubricant conditions during the 2MC, as well as the incident of dry wear.

#### 4. Generation of physiologically scratched CoCrMo cups

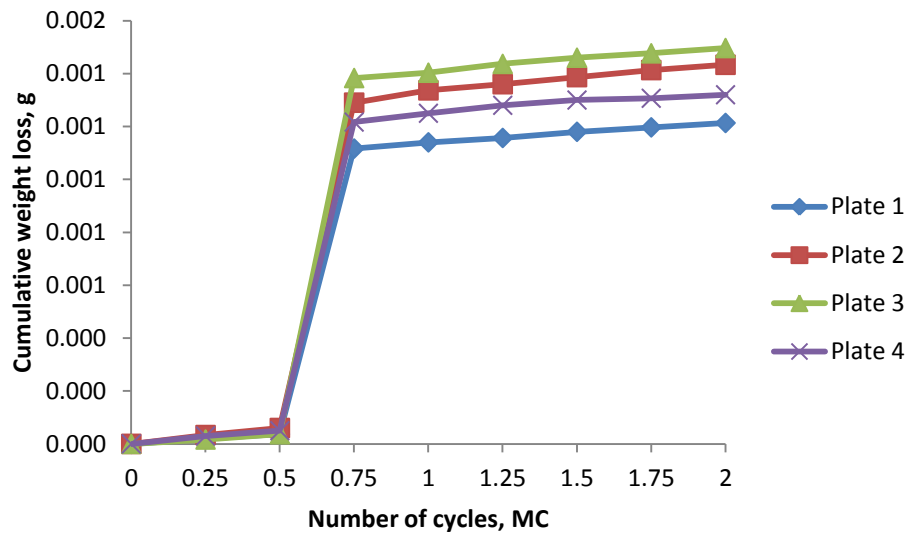


Figure 4.34: Cumulative weight loss of CoCrMo plates, accounting for the soak control.

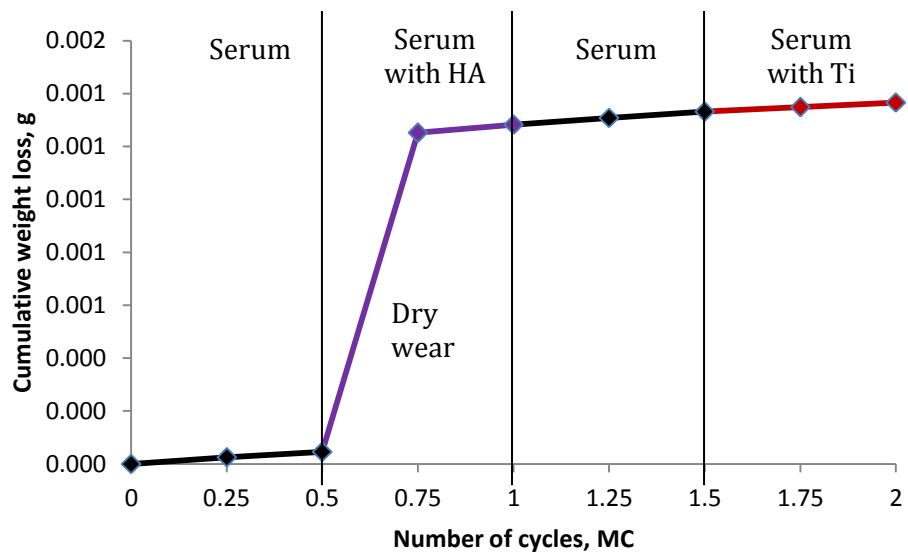


Figure 4.35: Cumulative weight loss from an average of the four active plates, noting the different test conditions.

Using the density of CoCrMo, the volume loss from each test component during each test interval has been calculated from the weight loss. The four sets of values were then averaged and the result is shown in Figure 4.36.

#### 4. Generation of physiologically scratched CoCrMo cups

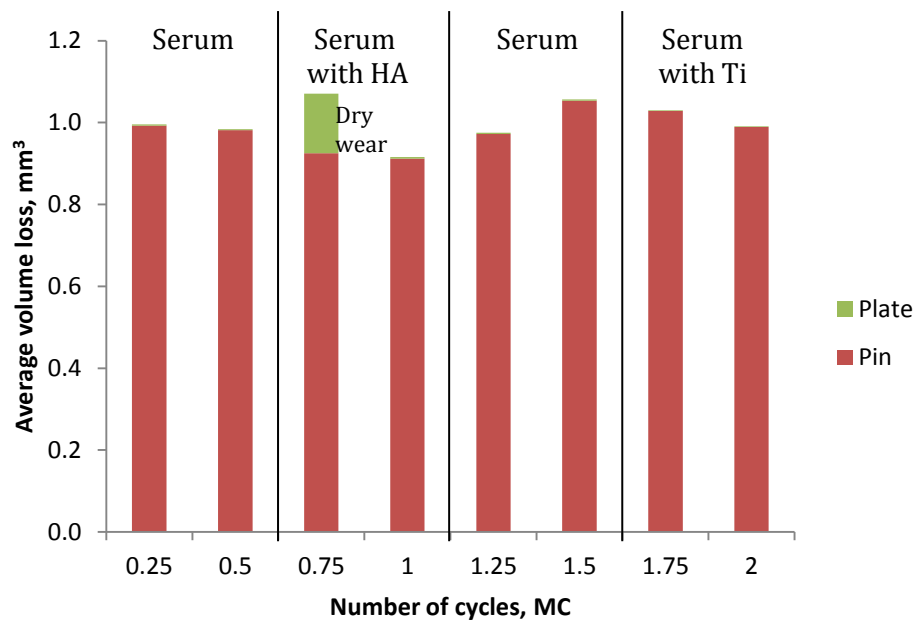


Figure 4.36: Average volume loss from the pins and plates over 2 MC, noting the test conditions.

The total volume loss from each pin and plate in each station has been combined to calculate the total wear rate for each 0.5 MC to separate the different test conditions. The results are shown in Table 4.5. It is clear to see that the change in lubricant, irrespective of the addition of HA or Ti, has had no effect on the wear data.

Table 4.5: Total wear rate at different stages during pin-on-plate test, mm<sup>3</sup>/MC.

Total wear rate, mm <sup>3</sup> /MC	0 – 0.5 MC Serum	0.5 – 1.0 MC Serum with HA	1.0 – 1.5 MC Serum	1.5 – 2.0 MC Serum with Ti
<b>Station 1</b>	4.27	3.76	3.98	3.59
<b>Station 2</b>	4.01	4.02	4.50	4.82
<b>Station 3</b>	3.78	3.98	3.64	3.61
<b>Station 4</b>	3.78	4.14	4.13	4.16
<b>Average</b>	3.96	3.97	4.06	4.04
<b>(± SD)</b>	(± 0.23)	(± 0.16)	(± 0.36)	(± 0.58)

### 4.7.2 Surface characterisation

#### 1) Zygo non-contacting profilometry

Five zygo images were taken within the wear track of each active plate, and three from the soak plate, at each 0.5 MC stage of the pin-on-plate test where the test lubricant conditions changed. The results were combined and shown in Figure 4.37; there is little change in surface roughness over the course of the test.

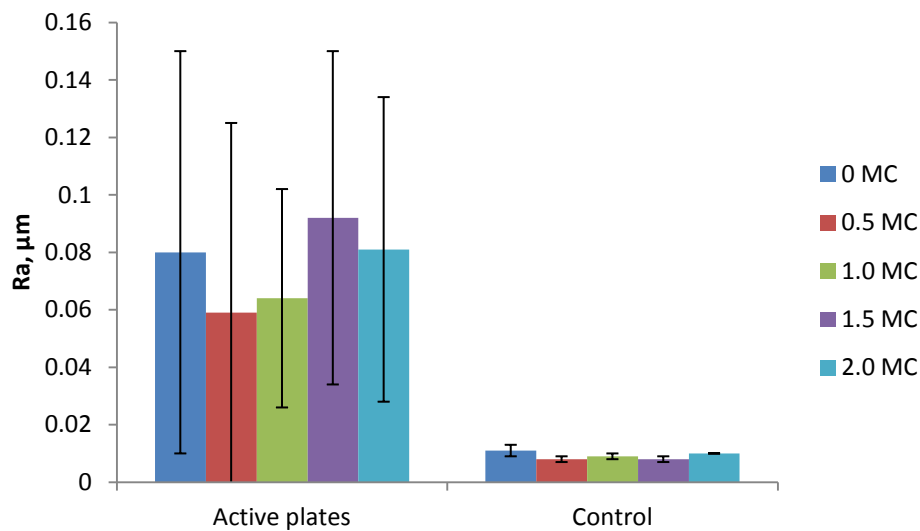


Figure 4.37: Surface roughness of CoCrMo plates during 2.0 MC.

#### 2) Optical microscopy

Images within the wear track, at the edge of the wear track, and outside the wear track were taken for each active plate with an optical microscope throughout the test. Figure 4.38 shows three images taken from plate 2 at the edge of the wear track after each million cycles of testing. There is little change in the features of the wear track, despite the addition of either HA or Ti.

#### 4. Generation of physiologically scratched CoCrMo cups

---

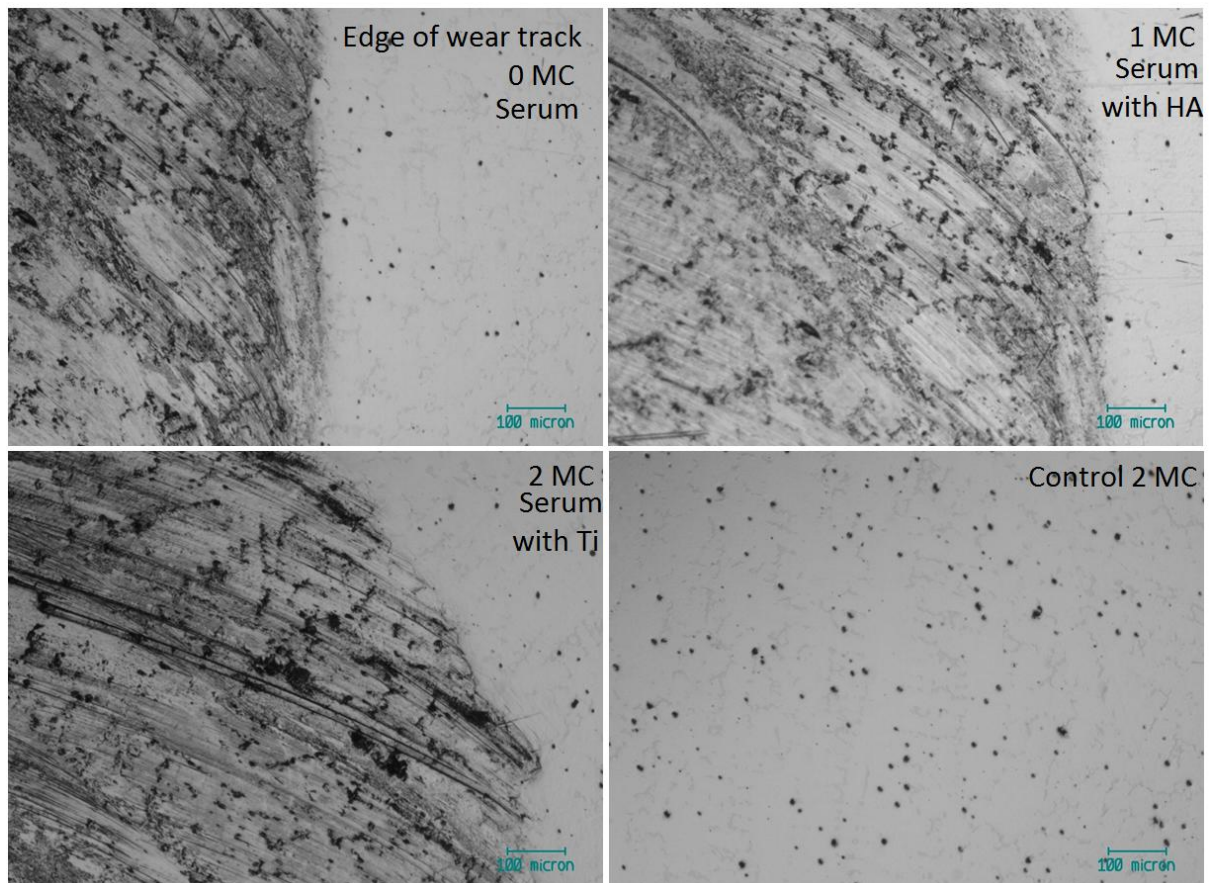


**Figure 4.38: The edge of wear track on plate 2 throughout test in comparison to the soak control.**

The same result is visible in Figure 4.39, which shows the centre of the wear track in plate 1, where again no change is evident. This result is also typical of the images collected for plates 3 and 4.

#### 4. Generation of physiologically scratched CoCrMo cups

---

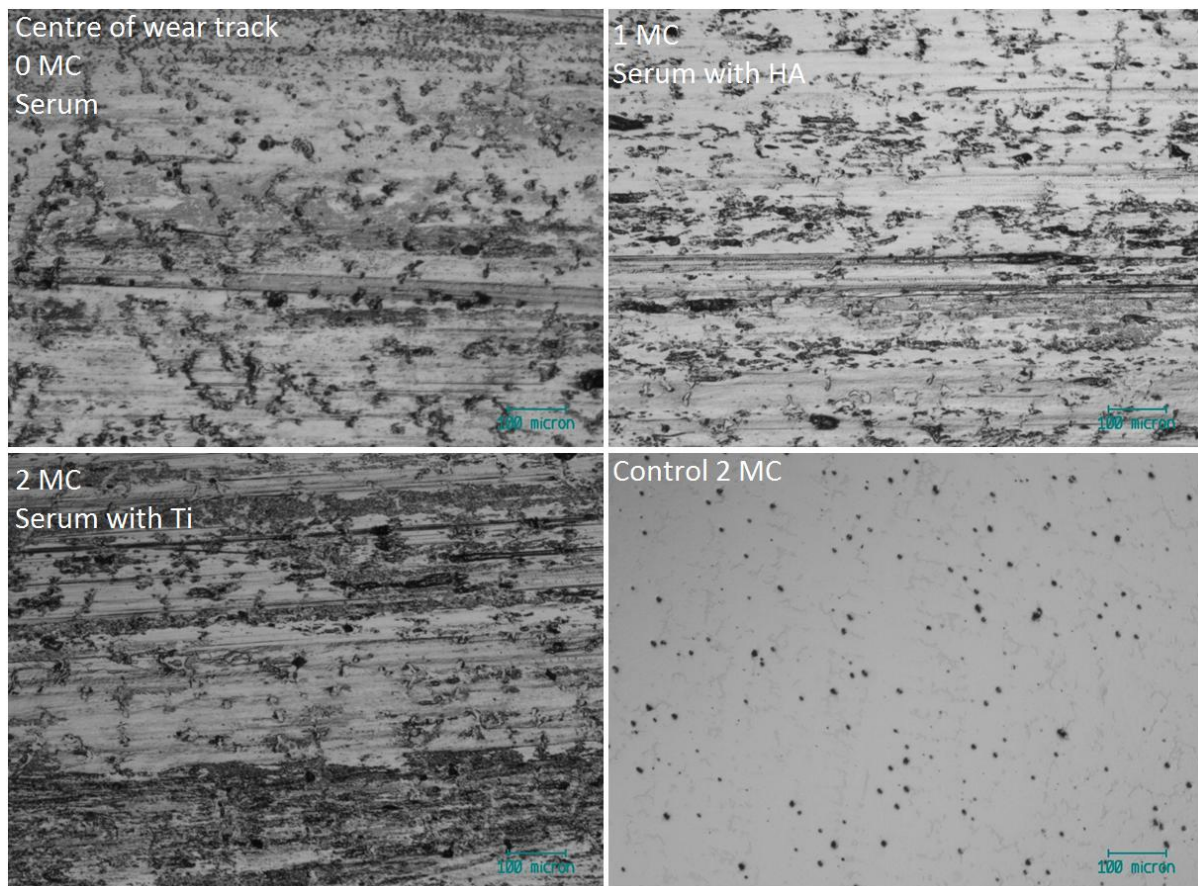


**Figure 4.39: The centre of the wear track on plate 1 throughout test in comparison to the soak control.**

Images were also taken from each pin throughout the test. Figure 4.40 shows how even after 2 MC of testing with the addition of two different types of lubricant with third-body particles, there are little surface features or signs of scratching on the pin head surface.

The optical images support the conclusion from the zygo and wear data that the lubricant with third-body particles has had no real comparative effect on the wear of the pins and plates throughout this study.

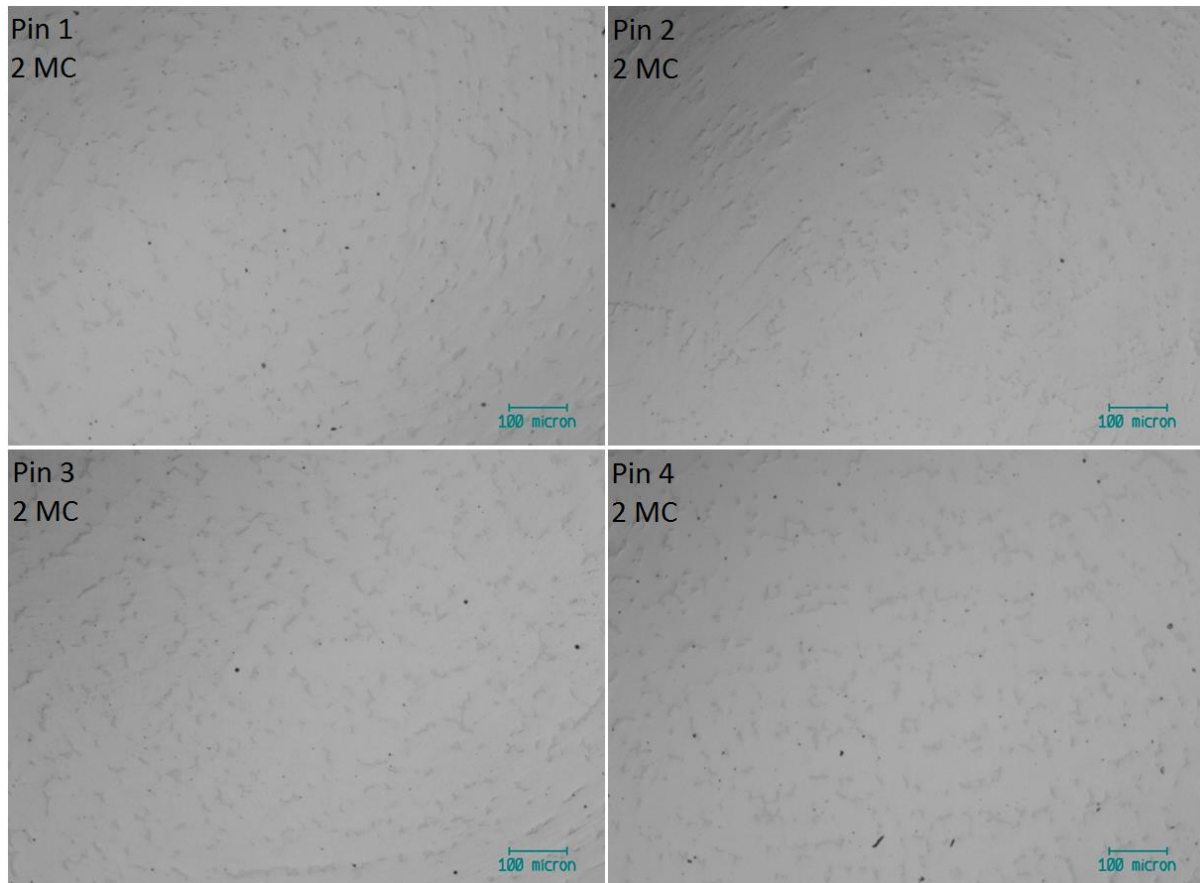


Figure 4.40: Centre of all active pins at 2 MC.

#### 4.7.3 Limitations

The main problem with this pin-on-plate test was that the third-body wear particles visibly moved out of the wear track very quickly so no effect was seen on the CoCrMo-CoCrMo interface. The particles settled on the bottom of the sample tray instead of interfering with the wear track. It is hoped that the motion of a hip simulator would stop this occurring in future hip simulations by 'shaking up' the particles more.

Ti did not seem to mix as well in the serum as HA, and settled quickly in the beaker before being added to the sample tray. For future hip simulations the third-body particles will be spun in the serum overnight prior to testing and it is important to swirl the beaker whilst adding the lubricant with third-body particles to the samples.

The only increase in wear throughout this test occurred when the water level sensor failed, resulting in dry wear. This was a problem caused by the collection of third-body particles around the water sensor. The problem was prevented from happening in further third-body tests by the careful monitoring and regular cleaning of the sensor. It

was important that the test was started early in the day to ensure the sensor was cleaned before leaving it to run overnight.

#### **4.7.4 Discussion**

This pin-on-plate test has been unsuccessful in establishing whether HA or Ti particles have a greater third-body effect on the CoCrMo-CoCrMo interface. There has been very little change in wear, optical or zygo data throughout the test despite the changes in test lubricant. This is believed to be due to the third-body particles not entering the wear track and highlights how difficult it is to know the concentration of third-body particles present in the tribocontact even when the initial total concentration in the test serum is known. For this reason the concentrations of HA and Ti added to the test lubricant for future hip simulations will be increased from 5 mg/ml to 10 mg/ml. This is the upper limit seen in previously published third-body tests (Table 3.3) and will hopefully increase the likelihood that third-body particles will enter the tribocontact, accelerate the wear and produce worn CoCrMo acetabular cups with features similar to that seen *in vivo*.

Both HA and Ti particles could theoretically co-exist within the joint through implant loosening. Since HA is an optional additional coating to the porous Ti coating it is feasible to assume that HA particles count enter the joint cavity primarily which would then expose the Ti coating for further wear. Hence the order of testing for future hip simulations will follow the same order as this test with HA being added to the test lubricant before Ti.

#### **4.7.5 Conclusion**

Previously worn CoCrMo pins have been worn against previously worn CoCrMo plates to try to anticipate the effect of third-body particles on the CoCrMo-CoCrMo interface for future hip simulations.

The pin-on-plate simulation ran for 2 MC. During 0-0.5 MC the test lubricant was 25% bovine serum. Between 0.5-1.0 MC the lubricant was 25% bovine serum plus 5 mg/ml HA particles. Between 1.0-1.5 MC the lubricant returned to 25% bovine serum and in the final 1.5-2.0 MC the lubricant was 25% bovine serum plus 5 mg/ml Ti particles.

Combining and averaging the wear data from all the pins and plates that have undergone wear testing, the wear rate for each 0.5 MC stage of the test ranged from 3.96 mm<sup>3</sup>/MC to 4.06 mm<sup>3</sup>/MC, regardless of the test lubricant. Hence it can be assumed that the change in lubricant with the addition of third-body particles has had no effect on the wear data. Optical images and zygo data also confirm that there was little change in surface features of the samples during the 2 MC. The third-body particles moved out of the wear track very quickly and so no effect was seen on the CoCrMo-CoCrMo interface.

#### **4.8 MOM Test 2: aggressive third-body biotribological study**

For this test 60 mm ReCap CoCrMo resurfacing components, Figure 4.41, were articulating under standard conditions in the Durham hip simulator at 45° (standard inclination angle). The test lubricant was varied during each 0.5 MC interval of the test for the five active stations to assess the effect of third-body particles and produce worn acetabular cups for further testing against dual mobility heads.

Between 0-0.5 MC the test was run in 25% bovine serum plus 10 mg/ml HA particles. Between 0.5-1.0 MC the test was run in standard 25% bovine serum to act as a recovery stage. Between 1.0-1.5 MC the test was run in 25% bovine serum plus 10 mg/ml Ti particles, and then from 1.5-2.0 MC was another recovery stage where the test was run in standard 25% bovine serum. In each third-body test half of the particles were applied directly to the cups during set up whilst the other half of the particles were mixed in the serum overnight prior to testing. There was also a loaded soak control and a soak control under no loading left at room temp throughout the test in 25 % bovine serum.

#### 4. Generation of physiologically scratched CoCrMo cups

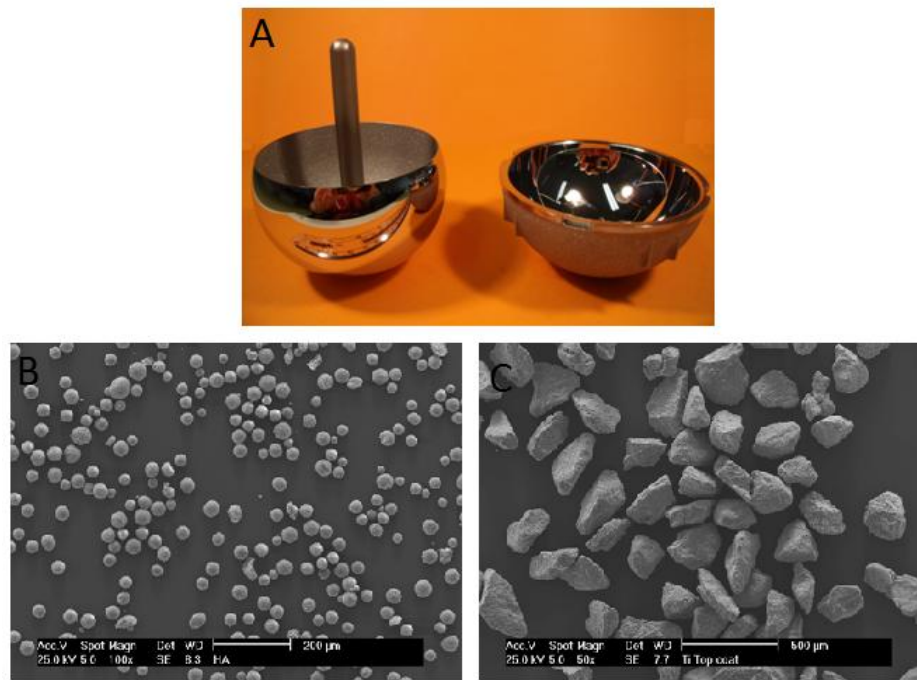


Figure 4.41: A: 60 mm ReCap CoCrMo resurfacing head and cup, B: HA particles, C: Ti particles.

#### 4.8.1 Joint replacement clearance

The acetabular cups from Dual Mobility Test 2 were paired with resurfacing CoCrMo femoral heads. The mean radial clearance across the active samples was 121 µm. Table 4.6 shows the full list of clearances.

Table 4.6: Radial clearance of 60 mm CoCrMo components.

Third-body test	Femoral	Batch, Batch ID	Shell	Batch, Batch ID	Clearance, µm
Stn 1	16	2410671, 4	49	2410667, 3	132
Stn 2	11	2410670, 5	44	2410666, 3	117
Stn 3	23	2410692, 1	50	2410667, 4	119
Stn 4	17	2410671, 5	46	2410666, 5	117
Stn 5	13	2410671, 1	52	2410667, 6	119
Load cntrl	3	2410669, 3	40	2410665, 4	132
Soak cntrl	20	2410672, 2	47	2410667, 1	122

### 4.8.2 Wear results

The test consisted of five active stations all under standard conditions and with either standard lubricant or third-body particle lubricant depending on the stage of testing. There was also a loaded soak control and a soak control under no loading which were both stored in standard lubricant throughout the test.

As before, the mass loss of each component was corrected by the change of the load soak. The cumulative weight loss for each CoCrMo resurfacing head in the changing lubricant conditions are given in Figure 4.42, whilst Figure 4.43 shows the corresponding data for the articulating CoCrMo cups.

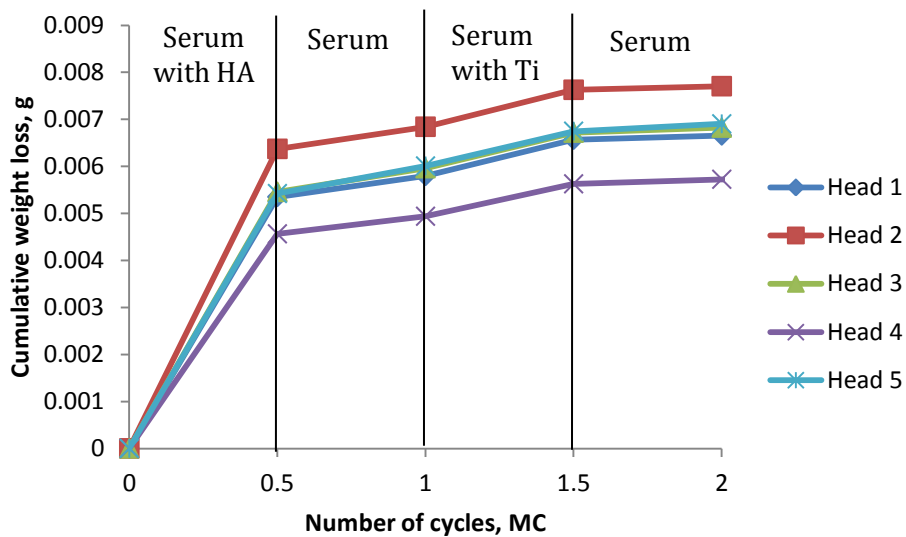


Figure 4.42: Cumulative weight loss of 60 mm resurfacing CoCrMo heads during third-body particle test, accounting for the load soak.

#### 4. Generation of physiologically scratched CoCrMo cups

---

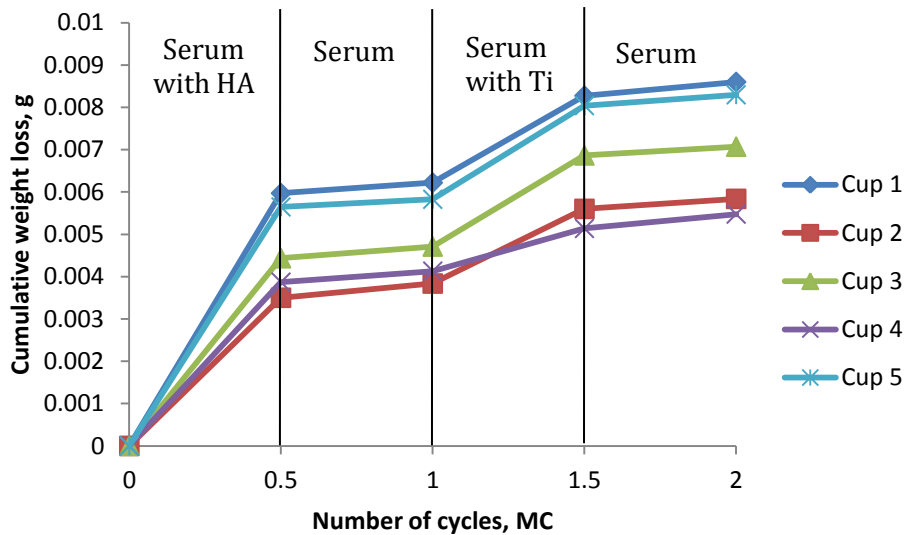


Figure 4.43: Cumulative weight loss of 60 mm acetabular CoCrMo cups during third-body particle test, accounting for the load soak.

The wear rate ( $\text{mm}^3/\text{MC}$ ) for each 0.5 MC interval during the 2.0 MC simulation has been calculated for each station. The results are shown in Table 4.7.

Both HA and Ti have caused an increase in wear for the heads and cups in each active station in this test. The wear rate was greatest when HA was added, though it is possible that this is due to the addition of the particles during the run-in stage of the test, where wear is typically at its maximum.

#### 4. Generation of physiologically scratched CoCrMo cups

---

Table 4.7: Wear rates for each stage of third-body particle test, mm<sup>3</sup>/MC.

Test stage, Lubricant condition	0 – 0.5 MC, 25% BS + 10 mg/ml HA	0.5 – 1.0 MC, 25% BS	1.0 – 1.5 MC, 25% BS + 10 mg/ml Ti	1.5 – 2.0 MC, 25 % BS
Head 1	1.29	0.11	0.19	0.02
Head 2	1.54	0.11	0.19	0.02
Head 3	1.32	0.12	0.18	0.03
Head 4	1.10	0.09	0.17	0.02
Head 5	1.31	0.14	0.18	0.04
Cup 1	1.44	0.06	0.50	0.08
Cup 2	0.85	0.08	0.43	0.06
Cup 3	1.07	0.07	0.52	0.05
Cup 4	0.94	0.06	0.24	0.08
Cup 5	1.36	0.04	0.53	0.06

#### 4.8.3 Surface characterisation

##### 1) Zygo non-contacting profilometry

Ten zygo images were taken at the pole and at 33° around the pole for each component in the five active stations at each 0.5 MC interval of this test. The load control and soak control were also analysed in comparison.

Figure 4.44 and Figure 4.45 shows the zygo data for the CoCrMo resurfacing heads. The wear testing has generally caused an increase in surface roughness and a decrease in skewness throughout the test. The error bars indicate the standard deviation of the data.

#### 4. Generation of physiologically scratched CoCrMo cups

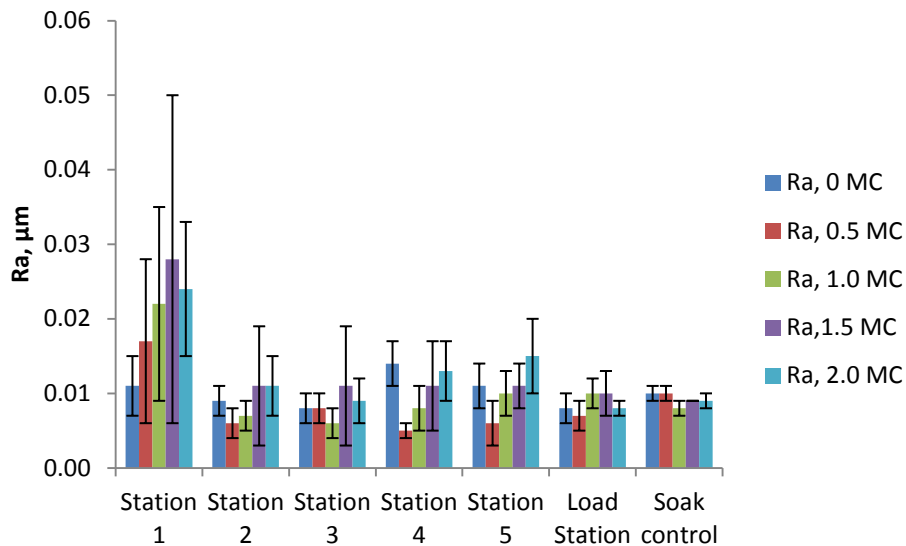


Figure 4.44: Surface roughness of 60 mm CoCrMo resurfacing heads during 2.0 MC third-body test.

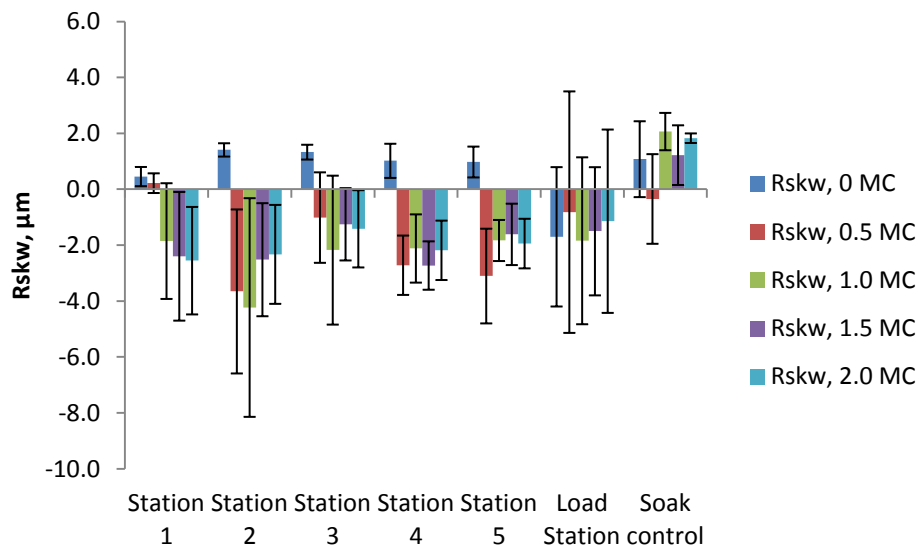


Figure 4.45: Skewness of 60 mm CoCrMo resurfacing heads during 2.0 MC third-body test.

Figure 4.46 shows the surface features near the pole for each active head in this test in comparison to the control which has only experienced loading throughout the test. Scratching is visible on every head that has been tested.

#### 4. Generation of physiologically scratched CoCrMo cups

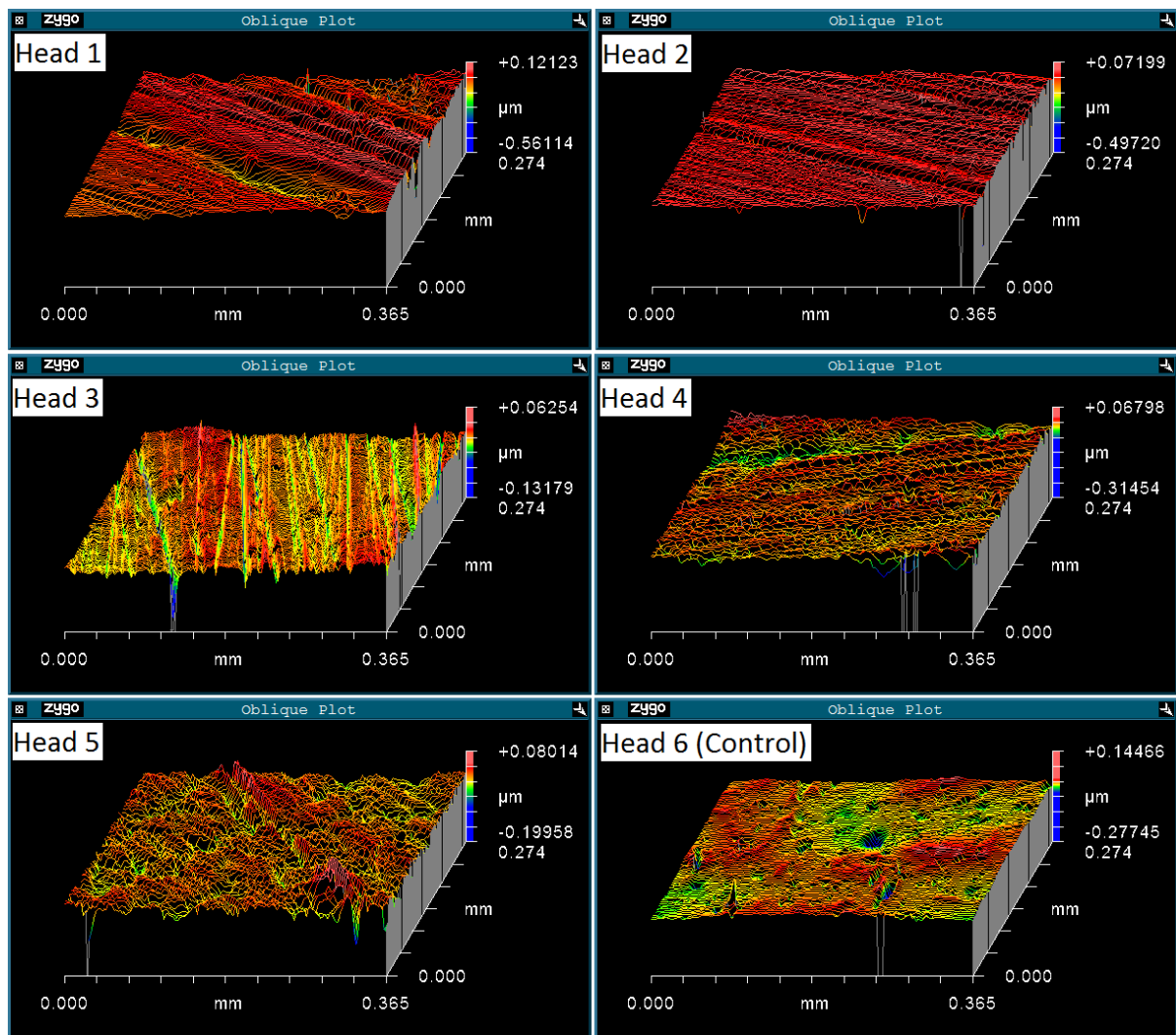


Figure 4.46: Surface profiles of CoCrMo heads after 2 MC of third-body particle test.

Figure 4.47 and Figure 4.48 show the zygo data for the CoCrMo cups. After an initial drop in surface roughness based on the end data from the dual mobility testing, the surface roughness has then increased over the course of the test.

#### 4. Generation of physiologically scratched CoCrMo cups

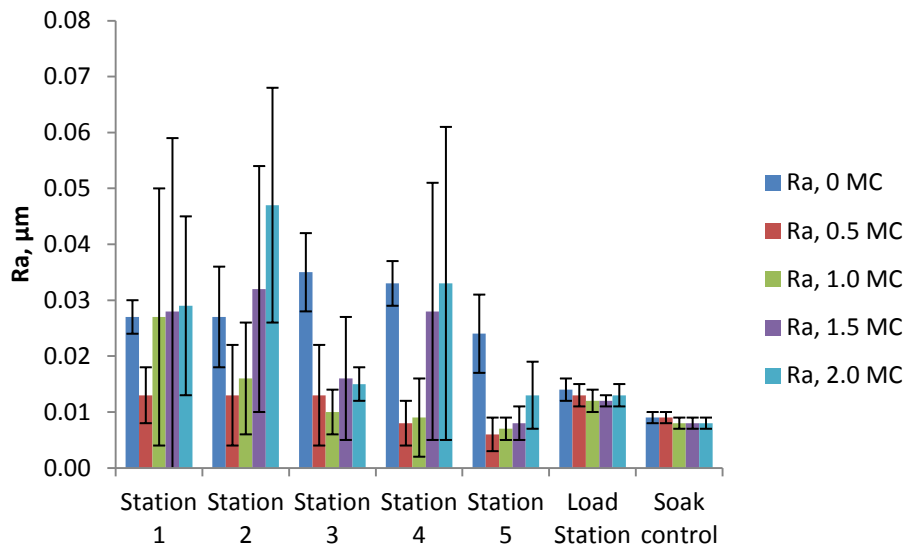


Figure 4.47: Surface roughness of 60 mm CoCrMo acetabular cups during 2.0 MC third-body test.

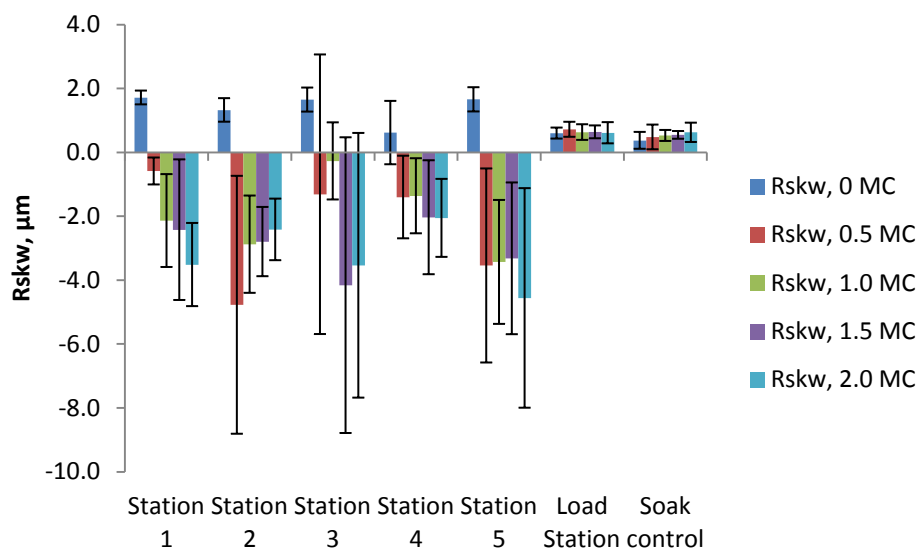


Figure 4.48: Skewness of 60 mm CoCrMo acetabular cups during 2.0 MC third-body test.

The initial drop after 0.5 MC in both the surface roughness and skewness indicates that the protruding carbides which were present at the end of DM Test 2 have been removed straight away.

Figure 4.49 shows that after 0.5 MC the carbide peaks that were previously protruding roughly  $0.2 \mu\text{m}$  from the surface at the end of DM Test 2 have been diminished to less than  $0.02 \mu\text{m}$  which were the original height of the carbides prior to any wear testing.

#### 4. Generation of physiologically scratched CoCrMo cups

As with the heads, the surface roughness has increased and the skewness has then become more negative over the course of the test as scratching has increased.

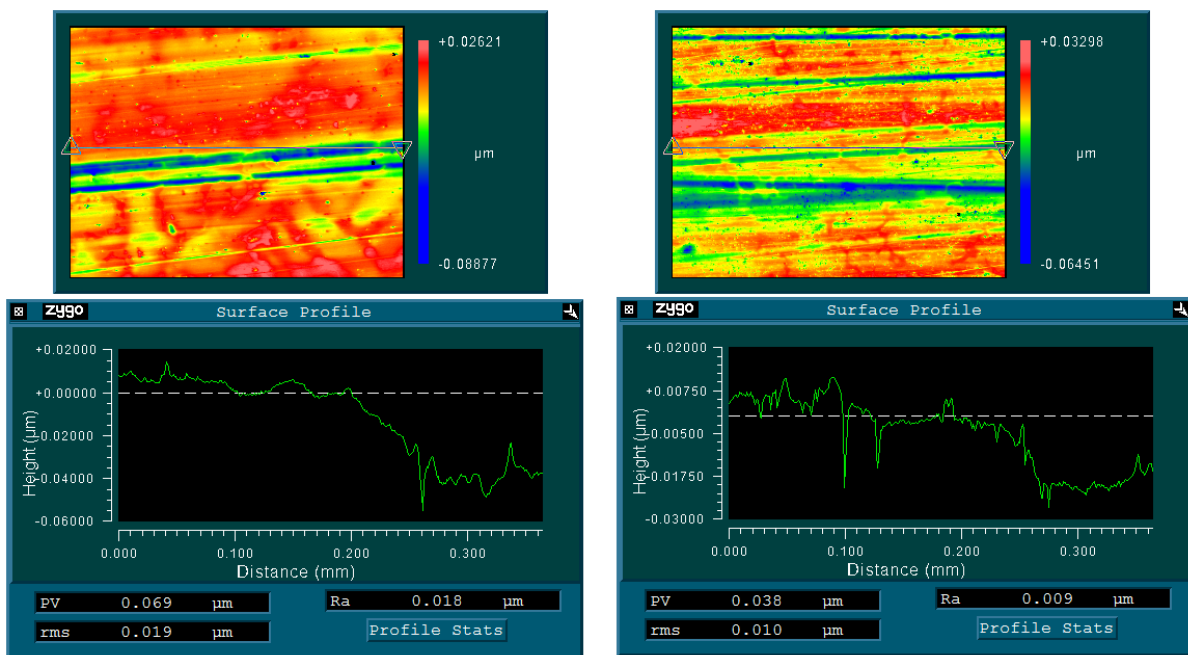


**Figure 4.49:** Zygo data from Cup 1 after 0.5 MC showing the 2D plot and the corresponding line profile of the surface.

Whilst Figure 4.47 shows how the typical  $R_a$  values averaged over each active cup in this test are quite similar to those at the end of the dual mobility test; Figure 4.50 shows that the surface features are very different and the number of scratches and pitting has increased greatly through the third-body particle test.

#### 4. Generation of physiologically scratched CoCrMo cups

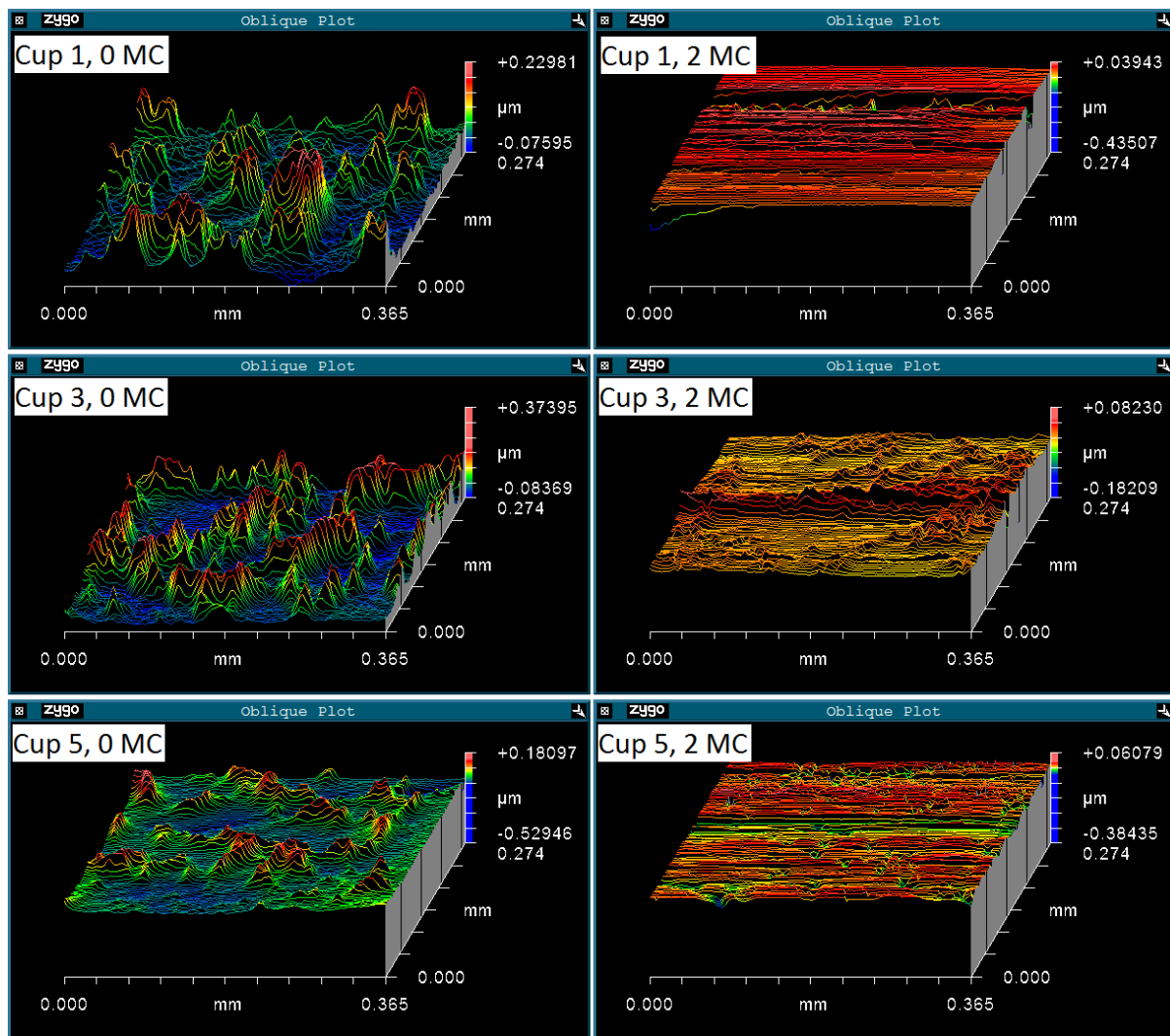
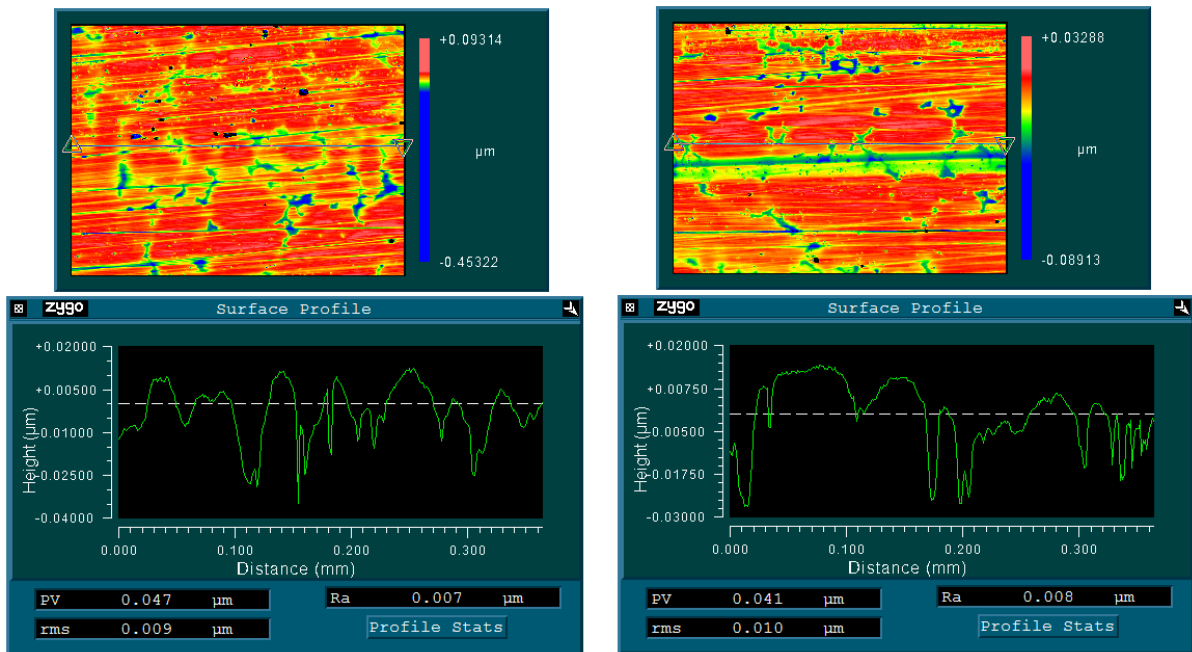


Figure 4.50: Comparison of surface profiles of the CoCrMo cups at the end of the dual mobility test with the resulting surface at the end of the third-body particle test.

The zygo data also shows evidence of carbide pull out. Figure 4.51 shows data from Cup 5 after 1.5 MC. The distinctive carbide shapes which were previously shown in red prior to testing, indicating that they were protruding above the surface, are now shown in blue. The blue represents that the region is now below the surface and indicate that the carbides have been removed due to wear.

#### 4. Generation of physiologically scratched CoCrMo cups

---



**Figure 4.51: Zygo data from Cup 5 after 1.5 MC showing the 2D plot and the corresponding line profile of the surface.**

### 2) Optical microscopy

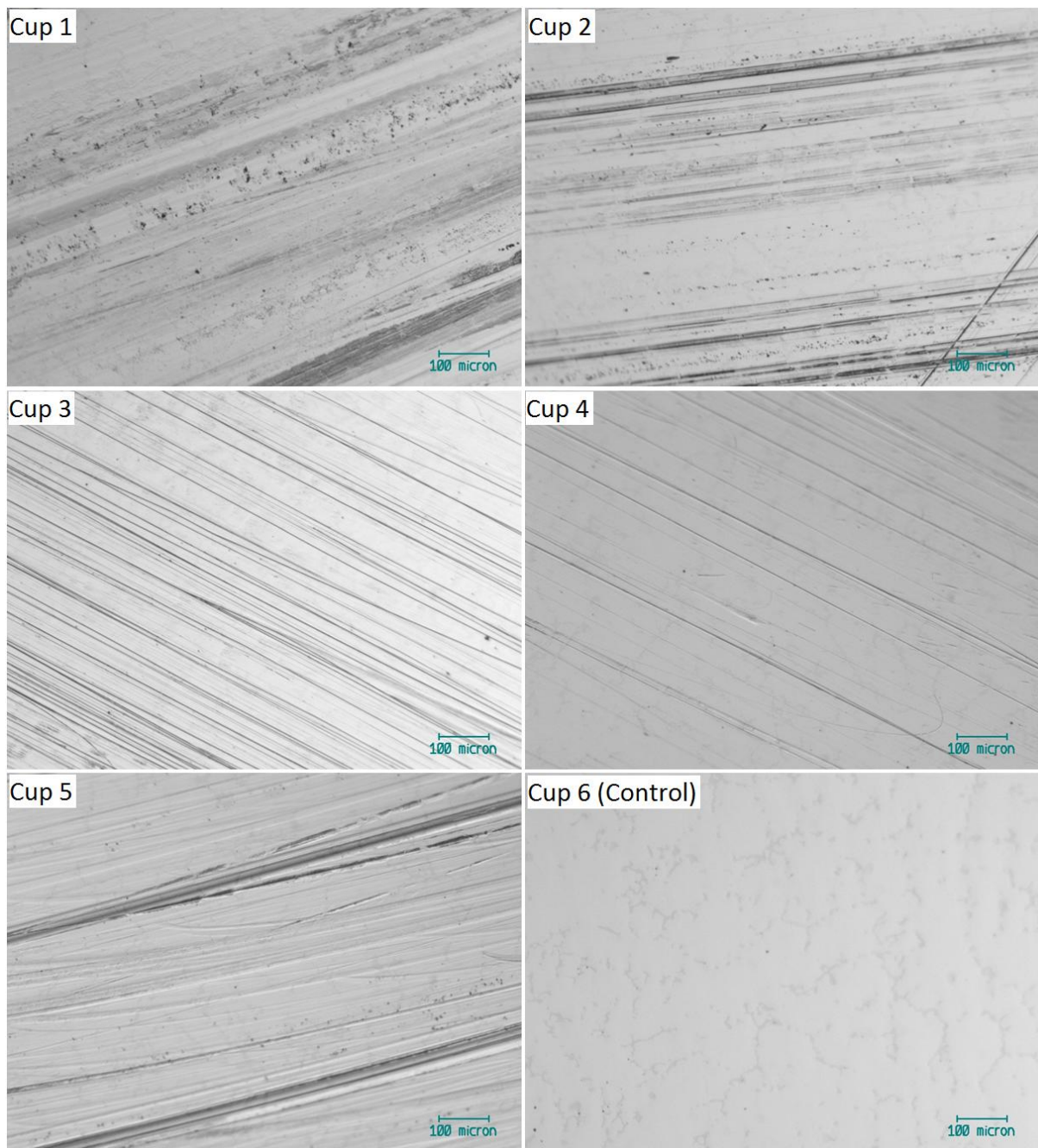
The following images were taken with an Axiotech optical microscope. The images taken of the surface features from the cups prior to the start of the third-body particle test can be seen in Figure 5.60.

Figure 4.52 to Figure 4.55 show the surface features within the wear patch at each stage of the simulation. There is a great difference in surface features in terms of scratching and marking from the end of the dual mobility test.

Optical images of the CoCrMo resurfacing heads were impossible to obtain due to the large nature of the joint which were unable to be focused on. Changes in surface features were tracked using zygo instead.

#### 4. Generation of physiologically scratched CoCrMo cups

---



**Figure 4.52: Optical images taken within the wear patch of 60 mm CoCrMo cups after 0.5 MC (serum with HA).**

#### 4. Generation of physiologically scratched CoCrMo cups

---

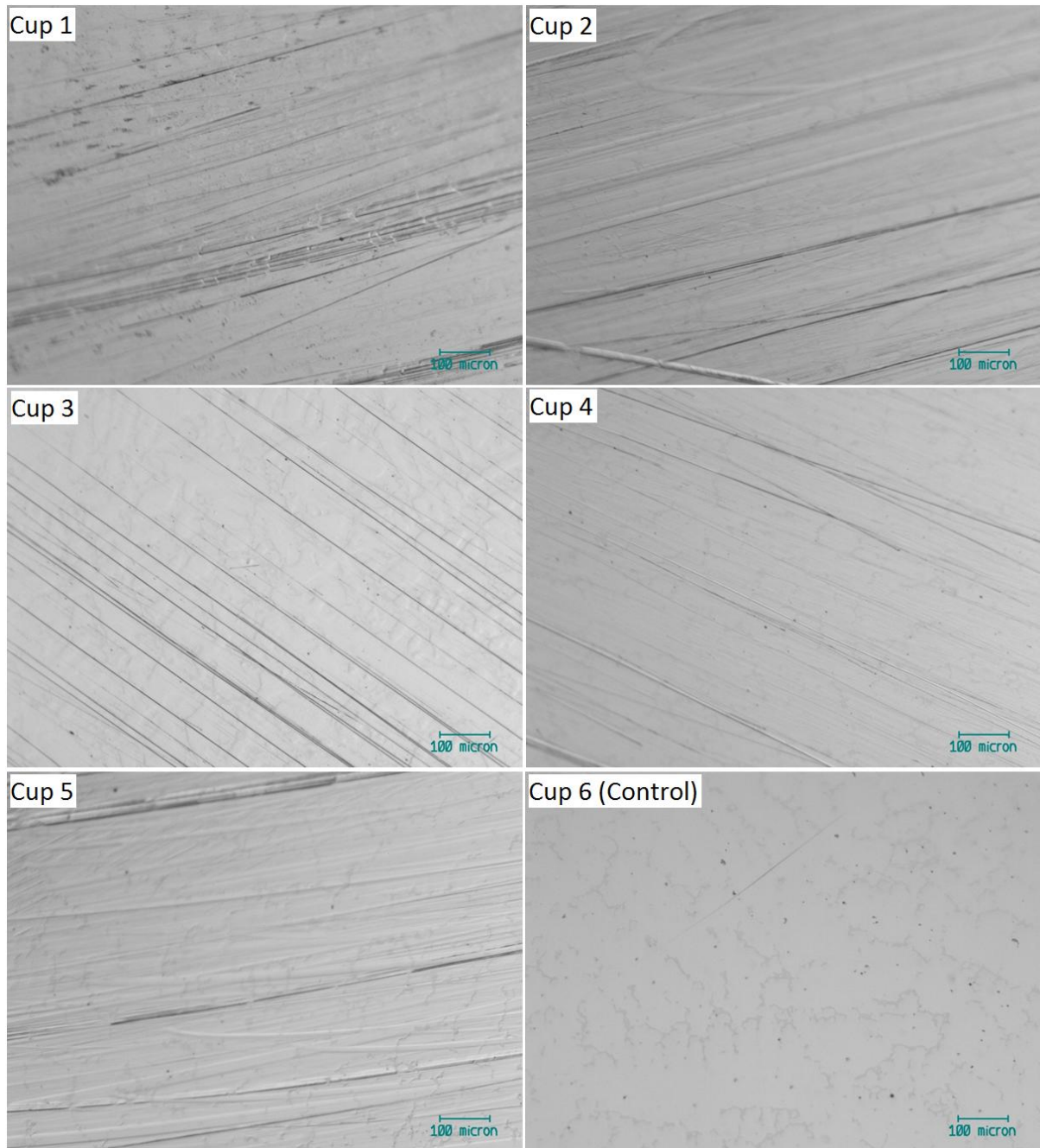


**Figure 4.53: Optical images taken within the wear patch of 60 mm CoCrMo cups after 1.0 MC (serum).**

#### 4. Generation of physiologically scratched CoCrMo cups

---

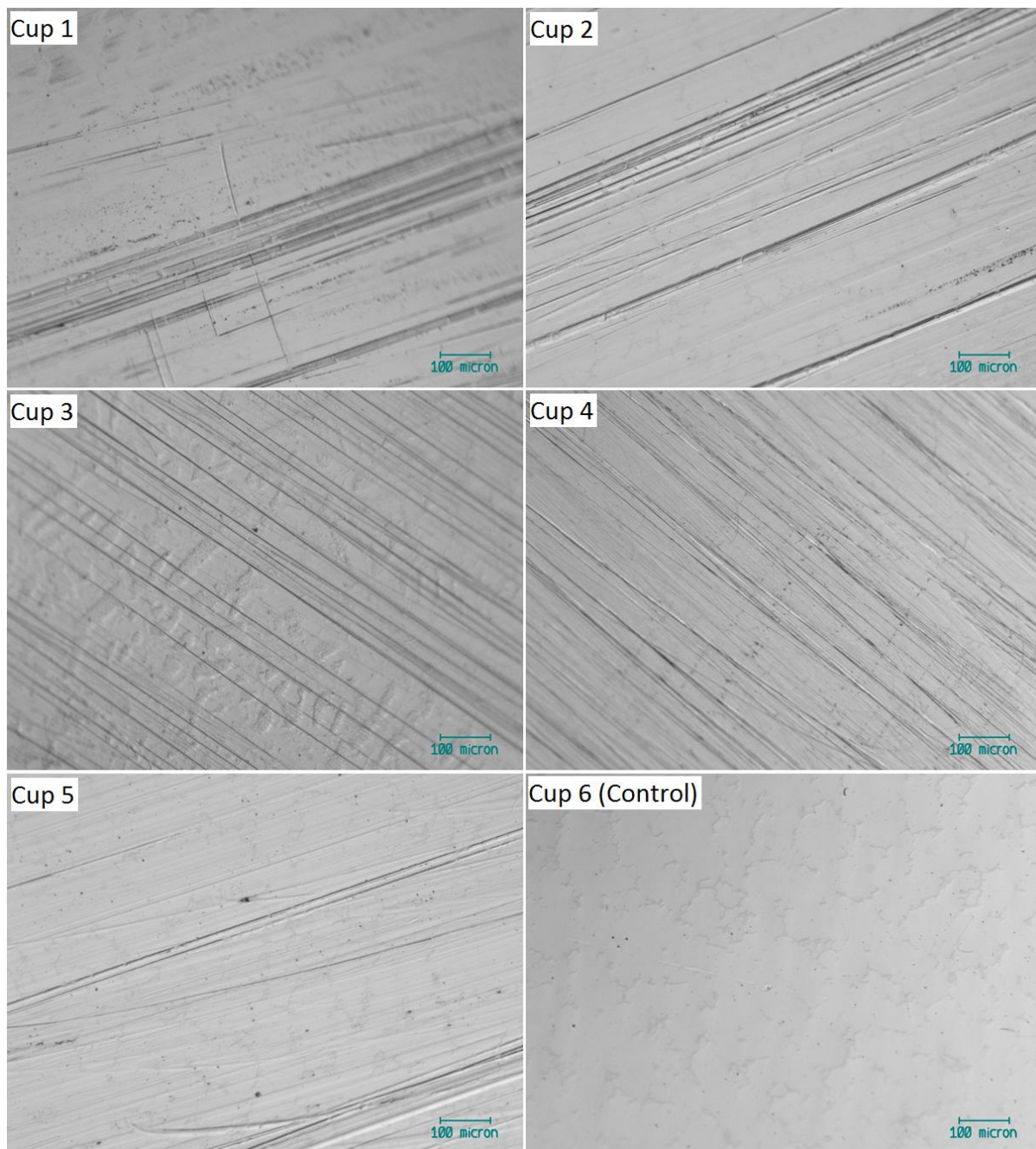


**Figure 4.54: Optical images taken within the wear patch of 60 mm CoCrMo cups after 1.5 MC (serum with Ti).**

#### 4. Generation of physiologically scratched CoCrMo cups

---

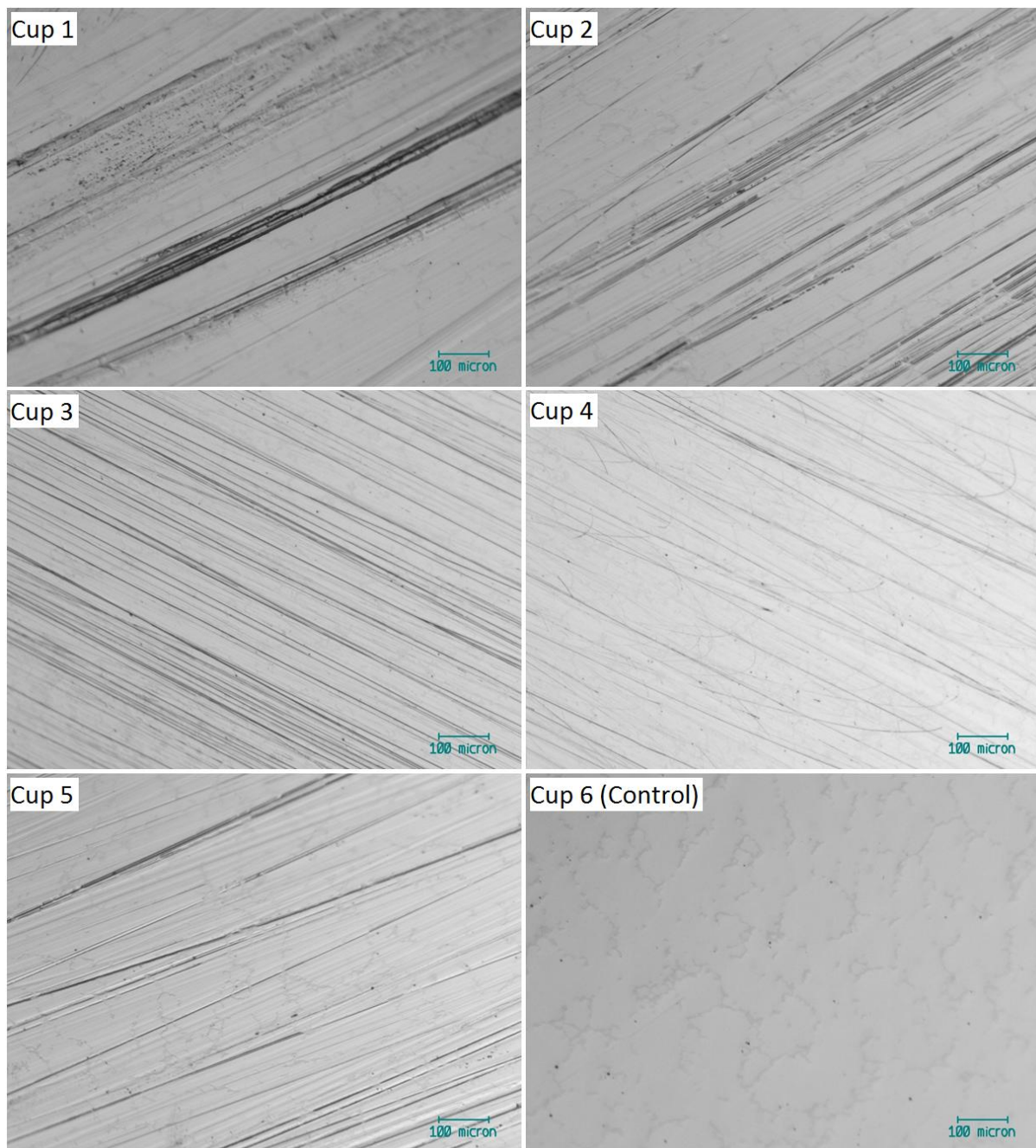


Figure 4.55: Optical images taken within the wear patch of 60 mm CoCrMo cups after 2.0 MC (serum).

#### 4.8.4 Limitations

The main difficulty in this test was trying to ensure a consistent concentration of particles in each active station when using the lubricant with third-body particles. It was impossible to stop some of the particles from settling in the station before the test began. Each station was inverted prior to placing in the simulator but then the particles had the chance to settle again in the time it took to secure each station in place so it is

#### 4. Generation of physiologically scratched CoCrMo cups

---

difficult to know the concentration of particles that have actually affected each MOM interface in this study.

At the end of each test interval using lubricant with third-body particles it was clear when taking apart the station that a lot of the particles has settled on the base of the head platform. Figure 4.56 shows Station 3 after removing the lubricant from the station, where Ti particles are still visible on the base. A similar situation occurred for each active station after the addition of HA particles to the test serum during 0-0.5 MC.

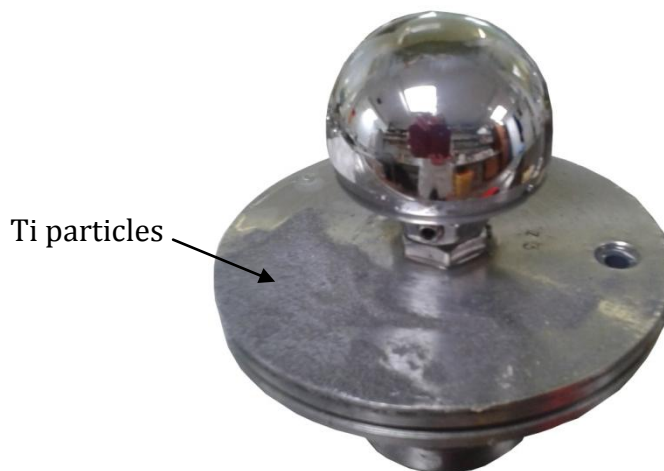


**Figure 4.56: Settled Ti particles on base of platform 3 after 1.5 MC.**

Thorough cleaning of the backing of each CoCrMo cup was essential in this test because the HA and Ti particles stuck to the coating which would have effected wear data if it was not removed properly.

#### **4.8.5 Discussion**

The data from this test has been compared to the data from Station 1b and Station 4 from MOM T1 in section 4.6. Since both of these stations experienced no problems with leaking or dry wear throughout the test, they are a viable baseline for comparison. The addition of both HA and Ti to the test lubricant has resulted in increased wear in every active component. Figure 4.57 shows a plot of the data from the heads in Station 1b and Station 4 averaged over the first 2 MC of MOM T1 in comparison to the average wear data over all five active stations in this third-body test. Figure 4.58 shows the corresponding data for the cups.

#### 4. Generation of physiologically scratched CoCrMo cups

When standard lubricant was used between 0.5 – 1.0 MC and 1.5 – 2.0 MC during the recovery stages of this third-body test, wear rates were similar to those seen in MOM T1. This is shown in Table 4.8 and Table 4.9 for the heads and cups respectively. When lubricant with third-body particles was used between 0 – 0.5 MC and 1.0 – 1.5 MC in MOM T2, the wear rates were higher than those seen in MOM T1.

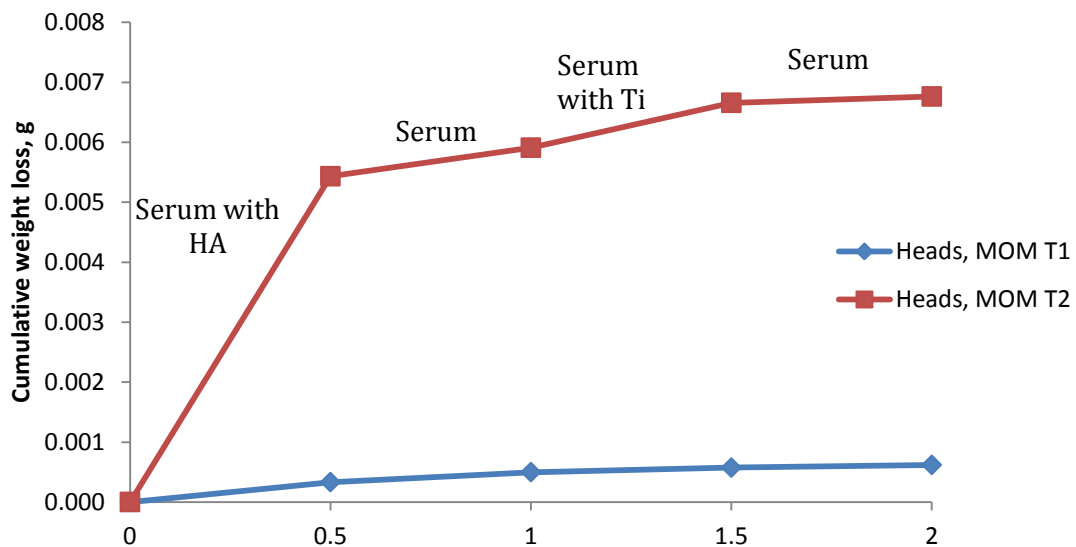


Figure 4.57: Comparison of the average cumulative weight loss of 60 mm resurfacing CoCrMo heads during the third-body particle test (MOM T2) with an average of cumulative weight loss of 60 mm resurfacing CoCrMo heads in MOM test 1 which did not experience dry wear.

Table 4.8: Comparison of wear rates for the heads in MOM T1 with MOM T2, mm<sup>3</sup>/MC.

Test stage	0 – 0.5 MC	0.5 – 1.0 MC	1.0 – 1.5 MC	1.5 – 2.0 MC
Average over Heads 1b & 4 in MOM T1 ± SD	0.08 ± 0.01	0.04 ± 0.00	0.02 ± 0.01	0.01 ± 0.01
Average over Heads 1 – 5 in MOM T2 ± SD	1.31 ± 0.15	0.12 ± 0.02	0.18 ± 0.01	0.03 ± 0.01

#### 4. Generation of physiologically scratched CoCrMo cups

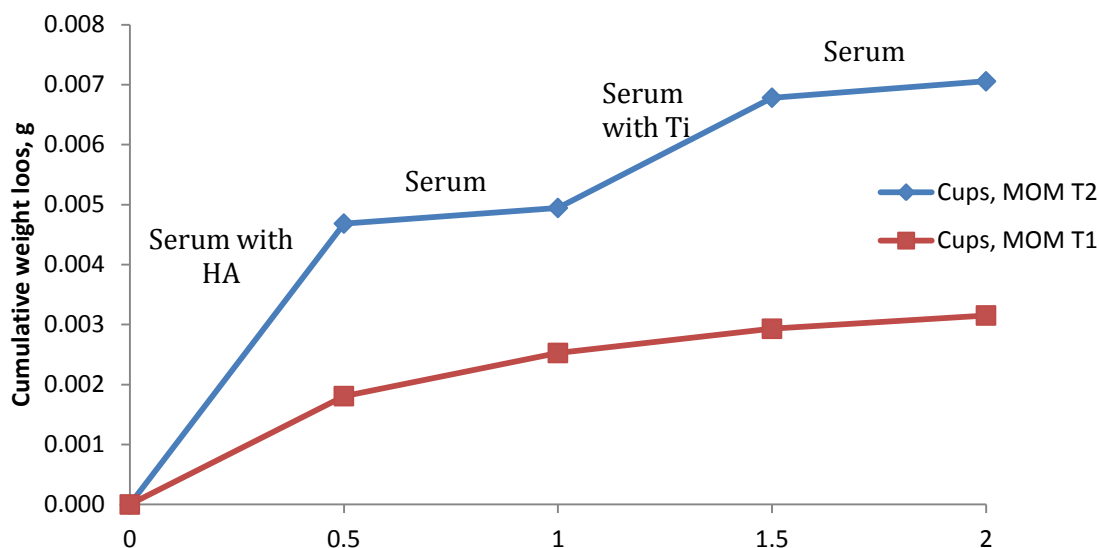


Figure 4.58: Comparison of the average cumulative weight loss of 60 mm acetabular CoCrMo cups during the third-body particle test (MOM T2) with an average of cumulative weight loss of 60 mm acetabular CoCrMo cups in MOM test 1 which did not experience dry wear.

Table 4.9: Comparison of wear rates for the cups in MOM T1 with MOM T2, mm<sup>3</sup>/MC.

Test stage	0 - 0.5 MC	0.5 - 1.0 MC	1.0 - 1.5 MC	1.5 - 2.0 MC
Average over Cups 1b & 4 in MOM T1 ± SD	0.44 ± 0.02	0.17 ± 0.00	0.10 ± 0.02	0.05 ± 0.02
Average over Cups 1 - 5 in MOM T2 ± SD	1.13 ± 0.26	0.06 ± 0.01	0.44 ± 0.12	0.07 ± 0.01

It is important to remember that the aim of this test is to produce worn cups that could be representative of a cup left in the body during revision surgery. From comparing the optical data from the well functioning cups from Stations 1b and 4 after 2.0 MC of MOM T1 to the images taken from the cups in this third-body particle test after 2.0 MC it is clear that the cups in this test show more scratching and signs of wear on the surface. The same is true for the same cups from MOM T1 even after 5.0 MC of testing. Figure 4.59 shows a comparison of optical images taken throughout both MOM simulator studies. From the wear data and surface analysis of the components, it can be concluded that the addition of the third-body particles has helped to accelerate wear.

#### 4. Generation of physiologically scratched CoCrMo cups

---

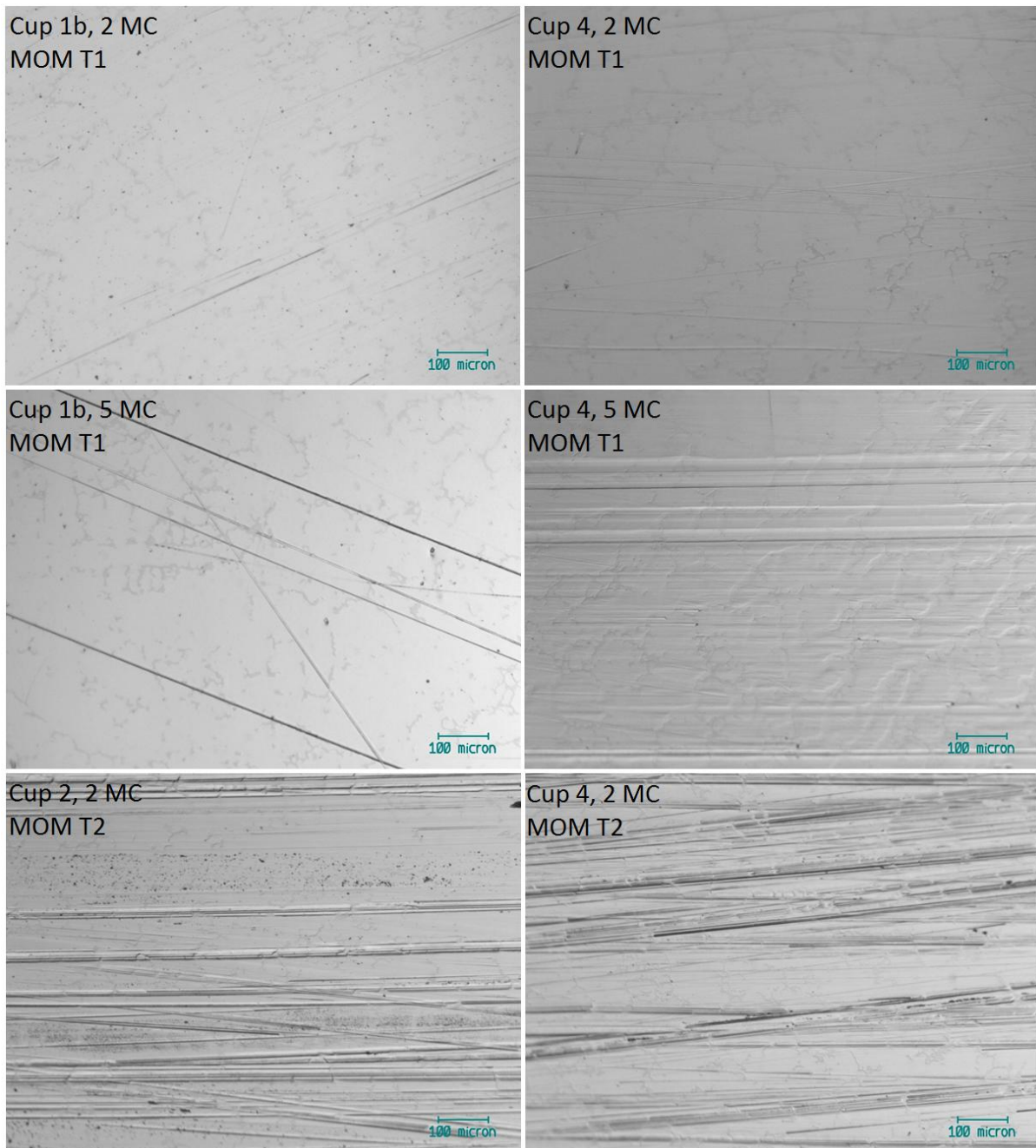


**Figure 4.59: Optical images taken from CoCrMo cups in MOM T1 and MOM T2.**

It is worth noting that the CoCrMo cups in this test have not experienced such great wear as that seen in Cups 2, 3 and 5 in MOM T1 that experienced dry wear.

As well as areas of unidirectional scratching shown in Figure 4.55 there are also areas with multidirectional scratches and surface features which are more comparable to that seen in the retrievals from Chapter 3. This comparison is shown in Figure 4.60.

#### 4. Generation of physiologically scratched CoCrMo cups

---

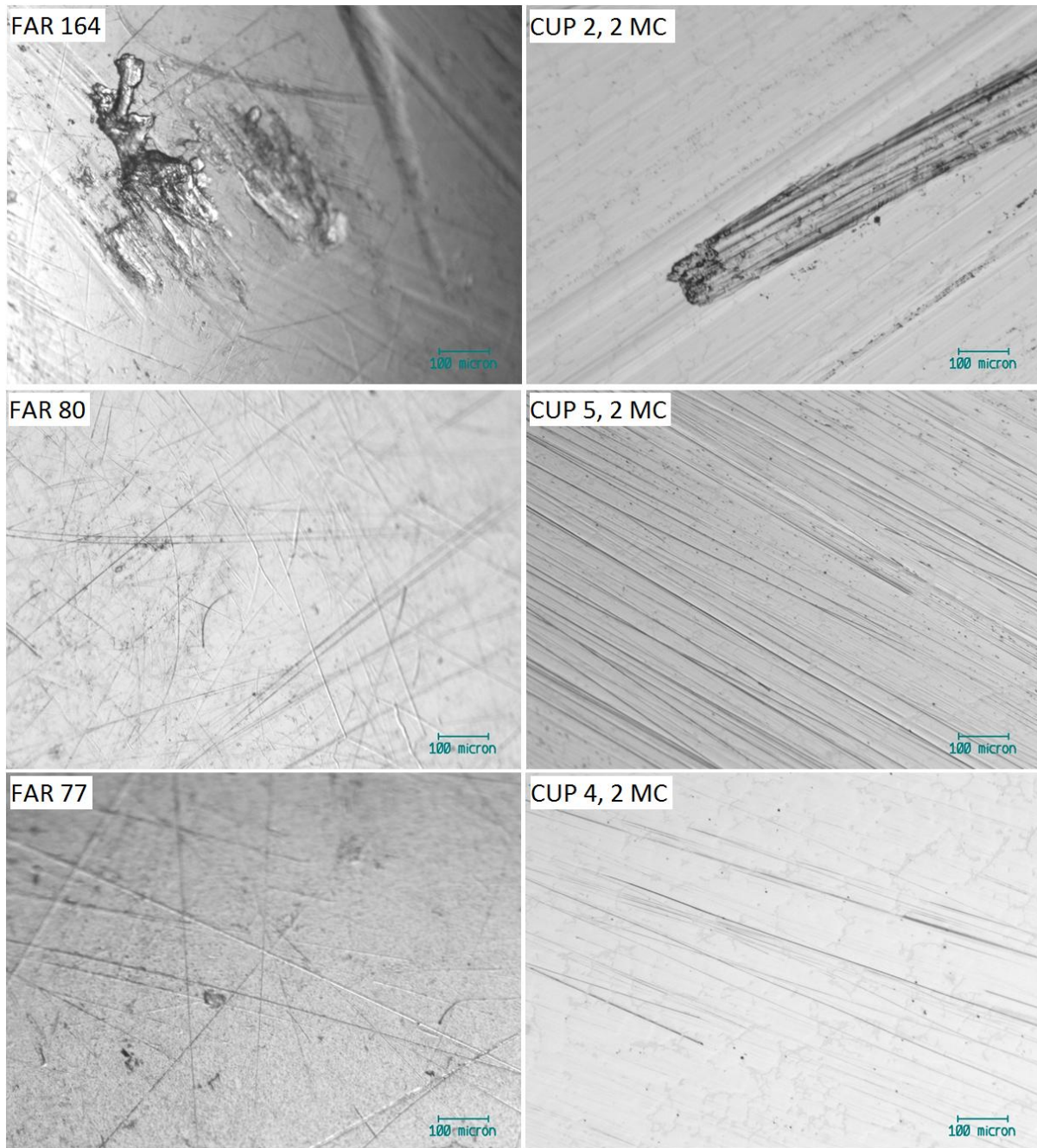


**Figure 4.60: Optical images taken from retrieved CoCrMo cups in comparison to cups from MOM T2.**

The  $R_a$  data from the cups at the end of this test is shown in comparison to the data taken from the retrievals in Figure 4.61. The average surface roughness of the test cups fall within the range of the retrieval data.

The zygo data from this test coupled with the optical data show that MOM Test 2 has been successful in producing cups with similar surface features to that seen in retrievals.

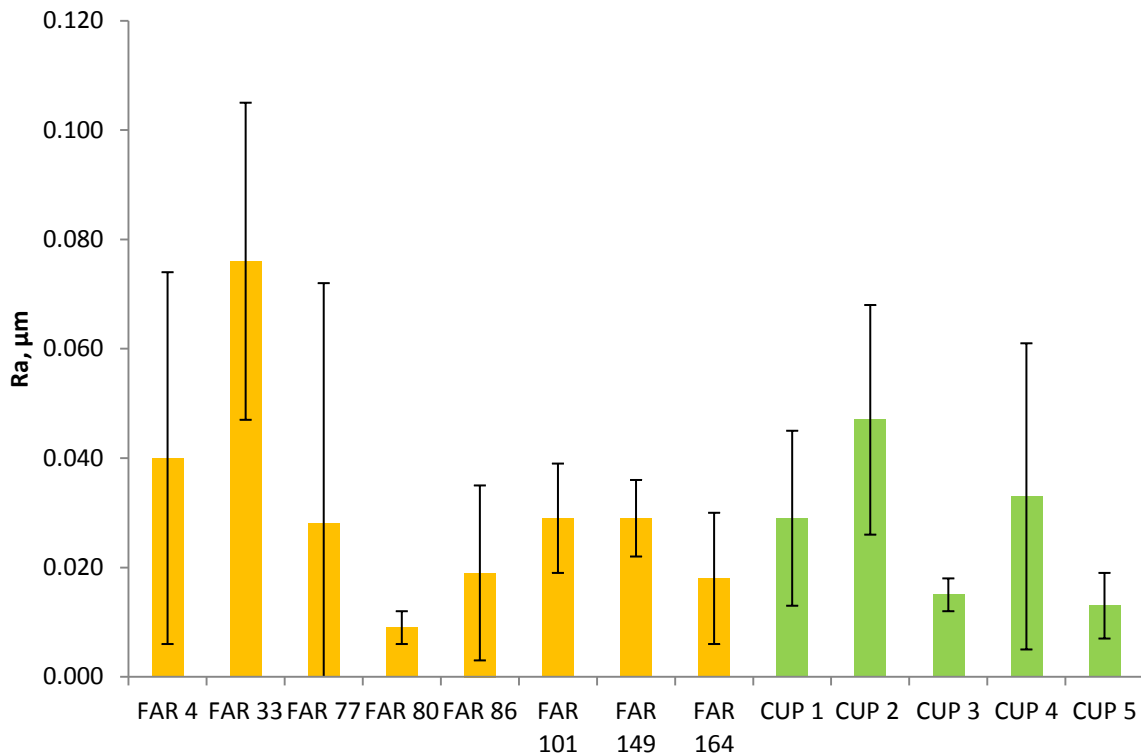


Figure 4.61: Comparison of zygo Ra data from retrieved cups (yellow) to MOM T2 cups (green).

#### 4.8.6 Conclusion

With the addition of 10 mg/ml hydroxyapatite particles to standard test lubricant, during 0 – 0.5 MC, the wear rates of the CoCrMo resurfacing heads ranged from 1.10 mm<sup>3</sup>/MC to 1.54 mm<sup>3</sup>/MC. The wear rates of the CoCrMo acetabular cups ranged from 0.85 mm<sup>3</sup>/MC to 1.44 mm<sup>3</sup>/MC.

With the addition of 10 mg/ml titanium particles to standard test lubricant, during 1.0 – 1.5 MC, the wear rates of the CoCrMo resurfacing heads ranged from 0.17 mm<sup>3</sup>/MC to 0.19 mm<sup>3</sup>/MC. The wear rates of the CoCrMo acetabular cups ranged from 0.24 mm<sup>3</sup>/MC to 0.53 mm<sup>3</sup>/MC.

Surface roughness of the CoCrMo heads has generally increased over the 2 MC test whilst surface skewness has decreased.

After an initial drop in surface roughness based on the end data from DM Test 2 for the CoCrMo cups, the surface roughness has generally increased over the course of testing and surface skewness has decreased.

Comparison of the wear data from this test with the data from Stations 1b and 4 in MOM T1 indicate that the addition of the third-body particles has helped to accelerate wear.

Comparison of the wear, zygo and optical data from MOM T2 with MOM T1 have shown that this test has been successful in producing cups with similar surface features to that seen *in vivo* from a failed hip replacement.

#### 4.9 References

- [1] R.B. Bourne, C.H. Rorabeck, B.C. Burkart, P.G. Kirk, *Clinical Orthopaedics and Related Research* (1994) 37-46.
- [2] M.J. Coathup, G.W. Blunn, N. Flynn, C. Williams, N.P. Thomas, *Journal of Bone and Joint Surgery-British Volume 83B* (2001) 118-123.
- [3] E.W. Morscher, A. Hefti, U. Aebi, *J Bone Joint Surg Br* 80 (1998) 267-72.
- [4] J.A. Davidson, R.A. Poggie, A.K. Mishra, *Biomed Mater Eng* 4 (1994) 213-29.
- [5] I. Leslie, S. Williams, C. Brown, G. Isaac, Z. Jin, E. Ingham, J. Fisher, *Journal of biomedical materials research Part B Applied biomaterials* 87 (2008) 163-172.
- [6] C. Heisel, N. Streich, M. Krachler, E. Jakobowitz, J.P. Kretzer, *Journal of Bone and Joint Surgery-American Volume 90A* (2008) 125-133.
- [7] V. Saikko, *Proceedings of the Institution of Mechanical Engineers Part H-Journal of Engineering in Medicine* 219 (2005) 437-448.
- [8] K. Vassiliou, A.P.D. Elfick, S.C. Scholes, A. Unsworth, *Transactions of the 30th Annual Meeting of the Society for Biomaterials, Memphis, USA* (2005) p. 83.
- [9] H.P. Sieber, C.B. Rieker, P. Köttig, *The Journal of bone and joint surgery British volume* 81 (1999) 46-50.
- [10] J.K. Lord, D.J. Langton, A.V.F. Nargol, T.J. Joyce, *Wear* 272 (2011) 79-87.
- [11] K. Takamura, D. Langton, J. Gandhi, A. Nargol, T. Joyce, J. Lord, R. Sidaginamale, *The Main Issue of Large Diameter MoM Total Hip Arthroplasty: The Taper Junction*, 2012.

# 5. DM biotribological studies including two *in vitro* partial revision simulations

---

## 5.1 Introduction

This chapter details the three dual mobility biotribological studies carried out in order to assess the viability of DM femoral bearings for use in partial revision procedures *in vivo*.

The dual mobility heads used in the following three studies consisted of a 28 mm CoCrMo head and an E1 liner with an inner diameter of 28mm, outer diameter 60 mm. *In vivo*, the 28mm CoCrMo head is designed to press-fit into the E1 liner. Once this has happened, it is extremely difficult to remove. For the benefit of testing, where it is essential that the components are separated, washed and cleaned after every 0.5 MC it was necessary to create a sectioned cut around the head to allow the insertion into, and removal from, the E1 liner.

Four dummy 28 mm heads were trialled, see Figure 5.1. It was decided to section each 28 mm CoCrMo head at 25° to maximise the inner contact area of the head with the liner at the high inclination angle, whilst allowing the repeated insertion and removal from the liner.

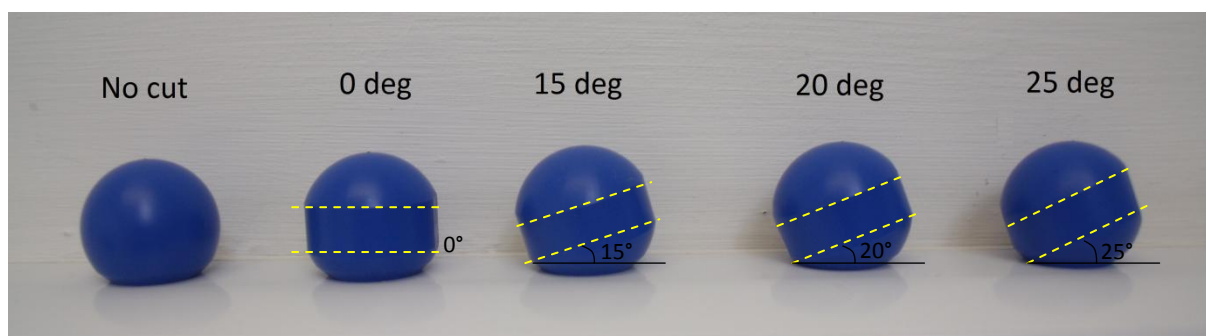


Figure 5.1: Selection of dummy 28 mm heads with sectioned cuts at four different angles: 0°, 15°, 20°, 25°.

The 28mm CoCrMo heads were held in the correct position using a threaded stainless steel taper coated with a thin layer of PMMA, Figure 5.2. The threaded section directly below the PMMA taper had to be smoothed so as to not adversely wear the E1 liners which are freely mobile throughout the entirety of each wear simulation. Markings on the head and liner were used to re-position each component after removal.



**Figure 5.2: Left, PMMA coated stainless steel taper. Right, dual mobility head arrangement held in place with locking nut.**

The sectioning of the 28 mm CoCrMo heads was completed by Tony Lane in Biomet UK while all other cup holders, resurfacing head stem holders and head tapers were made by Arthur Newman in the Durham School of Engineering Mechanical Workshop.

Section 5.2 discusses the Prosim hip simulator that was used during DM Tests 1, 2 and 3. Wear characterisation has been carried out using the same gravimetric methodology and surface characterisation techniques that have already been outlined in section 4.5. For the E1 liners, volume loss has been calculated from the mass data using the density of the material which was  $0.935 \text{ g/cm}^3$ . The inner pole of the E1 liners was the only bearing surface which was unable to be successfully tracked by zygo profilometry. This was because the lens was too wide to image inside the convex area which would ordinarily press fit onto the 28 mm CoCrMo heads. This surface was only able to be imaged optically. Optical microscopy was successful in effectively showing the different rate of removal of the manufacturing streaks from the inner and outer poles of the E1 liners during each test which highlighted the difference between the two articulations and the results are shown in each experimental section.

Section 5.3 gives the results from DM Test 1 which uses the worn CoCrMo cups from MOM Test 1. Section 5.4 gives the results from DM Test 2 which uses unworn CoCrMo cups and provides the cups for MOM Test 2 but also acts as a baseline for comparison against DM Test 1 and DM Test 3. Section 5.5 gives the results from DM Test 3 which uses the worn CoCrMo cups from MOM Test 2.

## 5.2 Prosim hip simulator

The dual mobility simulations were completed in a six-station biomechanical fatigue-loading simulator manufactured by ProSim, Figure 5.3.

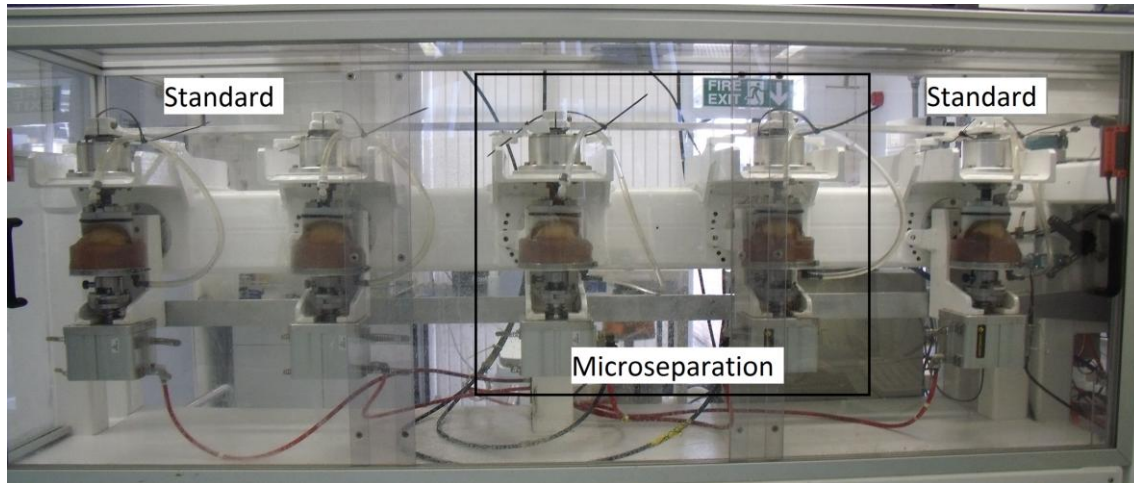


**Figure 5.3: ProSim Hip Simulator.**

Each station has three controlled axes of motion: acetabular rotation (top axis), flexion/extension (side axis) and axial load. Similar to the Durham wear simulator, the ProSim simulator does not have abduction/adduction so again the internal/external rotation and flexion/extension were 90° out of phase to produce the correct figure 8 wear track. A pneumatic load cylinder applies the axial load and the top and side axes are controlled by programmable motor drives. The Eurotherm motor drives used in the hip simulator can position the top and side axes anywhere in a 60° arc at velocities up to 183°/sec and with a repeatability of +/- 0.5°. A digital Sentronic pneumatic valve controls the load applied by the pneumatic load cylinders. One Sentronic valve controls the load on the five active stations. The maximum load is 4 kN and the resolution of the applied load is 15.6 N. The load during each test followed a Paul cycle with a twin peak [3], maximum load 2850 ± 50 N, minimum load 50 N ± 25 N. The load profile aims to follow ISO-14242-1 with reduced max/min load.

Stations 1, 2 and 5 were subject to standard testing conditions. Stations 3 and 4 were subject to testing with microseparation. Station 6 was subject only to load.

Microseparation conditions were enabled in Stations 3 and 4 with the use of movement-limiting screws positioned at the bottom of the front and back of each base plate, as designed by Daniel Giddings during a previous PhD project at Durham University.

During DM Tests 1 – 3 all acetabular cups were positioned at 62° inclination angle. This combination of testing at a high inclination angle, as well as under microseparation conditions in two of the five active stations, has been applied in order to maximise the aggressive nature of the tests and assess the viability of using DM joints during partial revision of a failed MOM THRA *in vivo*.

### 5.3 DM Test 1: aggressive biotribological study with worn CoCrMo cups from MOM Test 1

For this simulation, the worn cups from MOM Test 1 were tested against a dual mobility head consisting of a 28 mm CoCrMo head and an E1 liner with an inner diameter of 28mm, outer diameter 60mm. The test was carried out in the Prosim simulator with five active stations. Three stations were operating under standard conditions; two stations were operating under microseparation conditions. All stations were positioned at 62° (high inclination angle). In addition to the active stations, there was also a loaded soak control and a soak control under no loading, left at room temp throughout the test.



Figure 5.4: 28 mm CoCrMo head, E1 liner, 60 mm CoCrMo cup.

#### 5.3.1 Joint replacement clearance

There are two bearing articulations to consider in this test; the inner articulation, between the 28 mm CoCrMo femoral head and the E1 liner, and the outer articulation, between the E1 liner and the 60 mm CoCrMo cup. Since the CoCrMo cups have already been tested, the combinations of heads and liners were considered primarily and the chosen combinations are shown in Table 5.1. Cups were then assigned to each station based on wear. The mean radial clearance across the active samples was 123  $\mu\text{m}$ . The

radial clearance across the load soak was 128  $\mu\text{m}$  and only the soak had a larger clearance.

**Table 5.1: Radial clearance of dual mobility components.**

	<b>Head</b>	<b>Batch ID</b>	<b>Liner</b>	<b>Batch ID</b>	<b>Clearance, <math>\mu\text{m}</math></b>
<b>Station 1</b>	10	163662	7	P0561E66	122
<b>Station 2</b>	11	163662	4	P0561E66	121
<b>Station 3</b>	12	163662	8	P0561E66	121
<b>Station 4</b>	13	163662	3	P0561E66	125
<b>Station 5</b>	14	163662	5	P0561E66	127
<b>Load Station</b>	5	163662	1	P0561E66	128
<b>Soak control</b>	8	163662	19	P0561E66	224

Two stations (stations 3 and 4) were set up under microseparation conditions. It was decided that one microseparation station would contain the cup from the previous test that has received the worst wear, and the other would have a cup that had experienced little wear. The rest of the worn cups would then be distributed across the standard stations. Table 5.2 details how the cups from MOM Test 1 were assigned.

**Table 5.2: Cup combinations for the dual mobility test.**

	<b>Worn cup from MOM Test 1</b>
<b>Station 1, standard</b>	Cup 1b
<b>Station 2, standard</b>	Cup 3
<b>Station 3, microseparation</b>	Cup 2
<b>Station 4, microseparation</b>	Cup 4
<b>Station 5, standard</b>	Cup 5

### 5.3.2 Soaking data

It was necessary to soak the E1 liners in serum at 37 °C prior to testing due to the nature of the polymer which increases in mass due to fluid adsorption. The E1 liners were repeatedly removed from the soak serum for gravimetric assessment at the same frequency as that used for simulator wear testing. Standard cleaning protocol normally involves leaving the joints to acclimatise for 30 minutes post drying before weighing. However the weight of the large liners fluctuated greatly within this time and stabilisation of three weight data points to within 0.1 mg was not possible. Figure 5.5

shows the weight data for the liners over 5 weeks prior to testing, including error bars showing the standard deviation. Throughout the test the joints were left overnight to acclimatise post drying, and were weighed the following morning, this helped to minimise the range of the weight data. Soaking had little effect on the surface roughness data as shown in Figure 5.6.

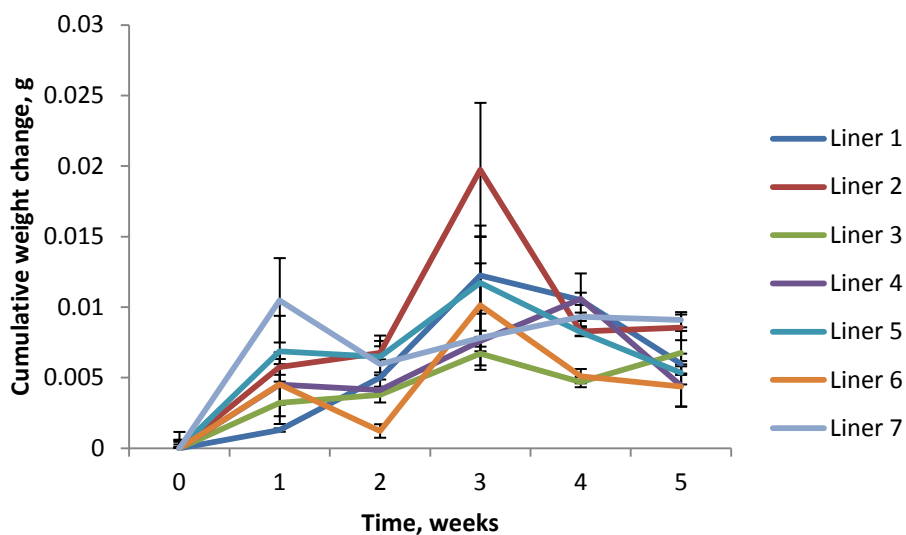


Figure 5.5: Cumulative weight change of E1 liners during soaking over 5 weeks prior to the wear simulation.

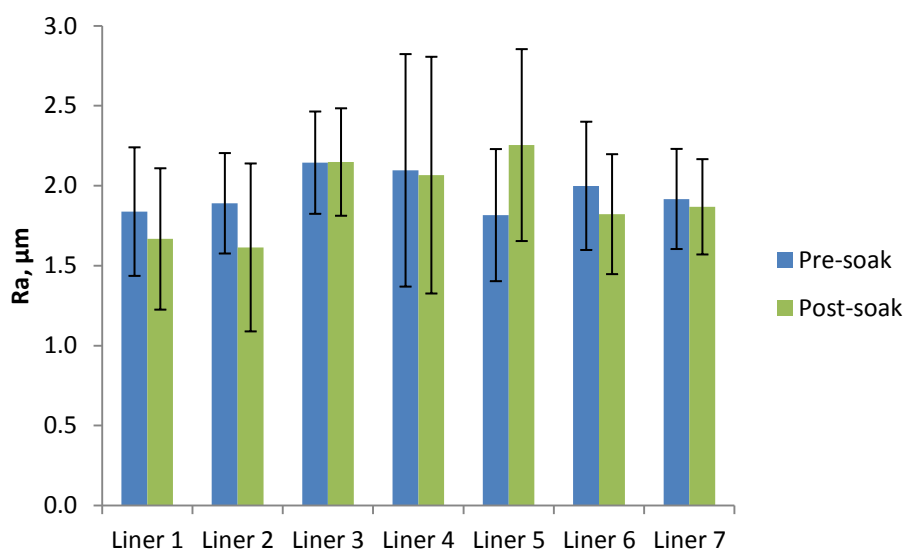


Figure 5.6: Surface roughness of E1 liners prior to test, before and after soaking.

### 5.3.3 Wear results

The test consisted of five active stations, three set up under standard conditions and two under microseparation. In addition to this, there was a loaded soak control, and a

soak control under no loading. There were problems during the first 0.5 MC with the quality of the silicon gaiters which lead to Station 1 losing a third of its serum in an overnight leak. After 0.5 MC the current gaiters were replaced with a new style.

After 2.5 MC of testing, it became clear that station 3 and 4 were producing different wear rates. Whether this was due to a difference in the microseparation conditions or whether it was a result of the difference in worn cups used in the test had to be determined. Between 2.5 and 3.5 MC the joints were switched between the stations (i.e. the joints from station 3 were placed into station 4 and vice versa). However there was no change in the wear data and after 3.5 MC the joints were restored to their original station. Hence it can be assumed that the increased wear seen in station 3 was a result of the initial increased roughness of that cup.

The mass loss of each component was corrected by the change of the load soak to account for fluctuations in mass measurements over the test. The cumulative weight loss after 5 MC from the 28 mm CoCrMo heads, E1 liners and 60 mm CoCrMo cups have been split into those tested under standard conditions, and those under microseparation conditions. The results are shown in Figures 5.7-5.12.

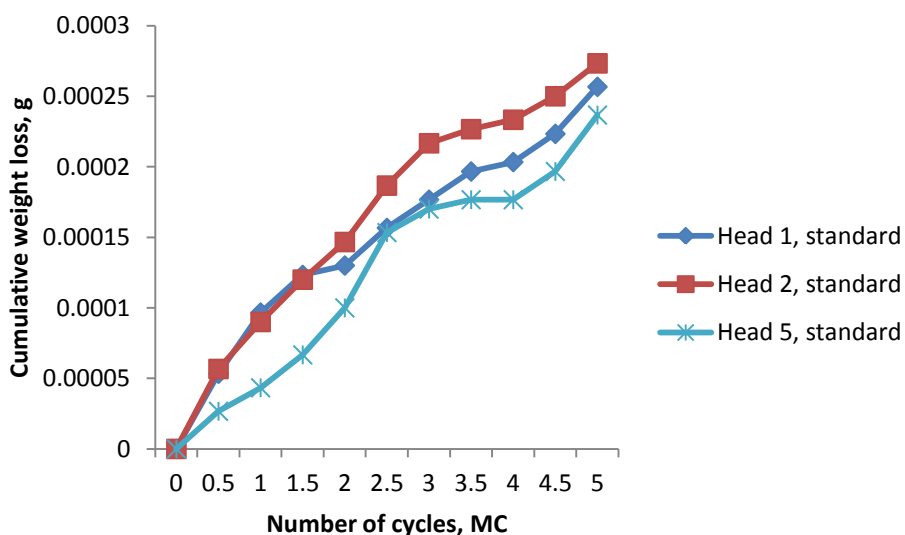


Figure 5.7: Cumulative weight loss of 28 mm CoCrMo heads under standard conditions, accounting for the load soak.

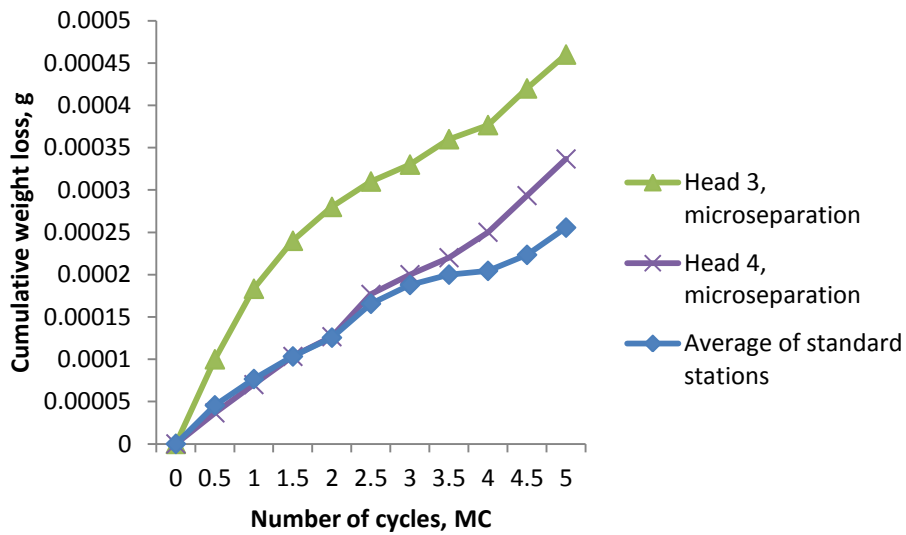


Figure 5.8: Cumulative weight loss of 28 mm CoCrMo heads under microseparation conditions, accounting for the load soak and a comparison with the mean of the corresponding data for standard conditions.

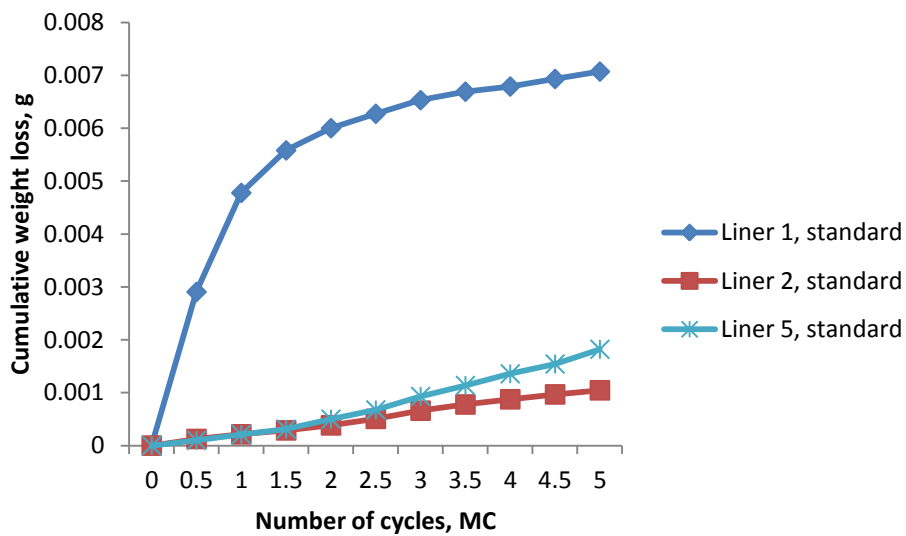


Figure 5.9: Cumulative weight loss from E1 liners under standard conditions, accounting for the load soak. Note that station 1 was affected by serum loss during the first 0.5 MC.

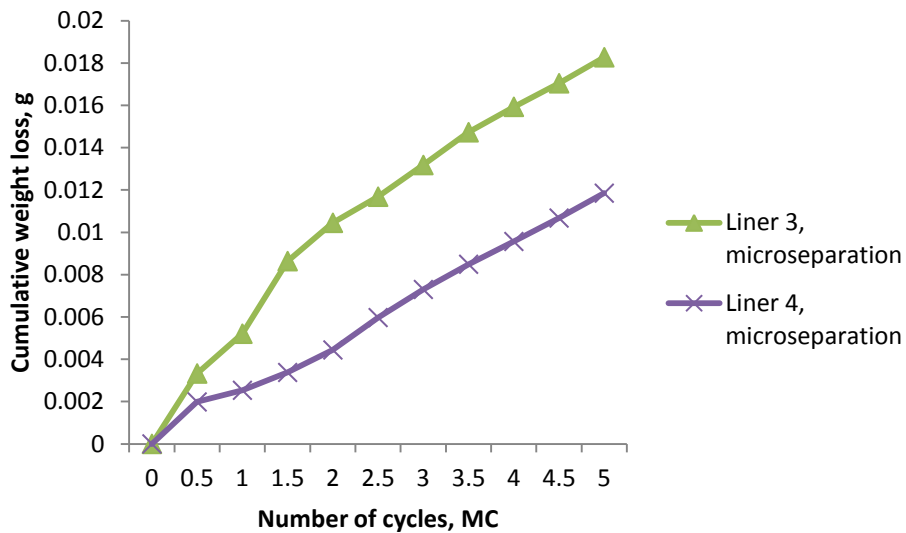


Figure 5.10: Cumulative weight loss from E1 liners under microseparation conditions, accounting for the load soak.

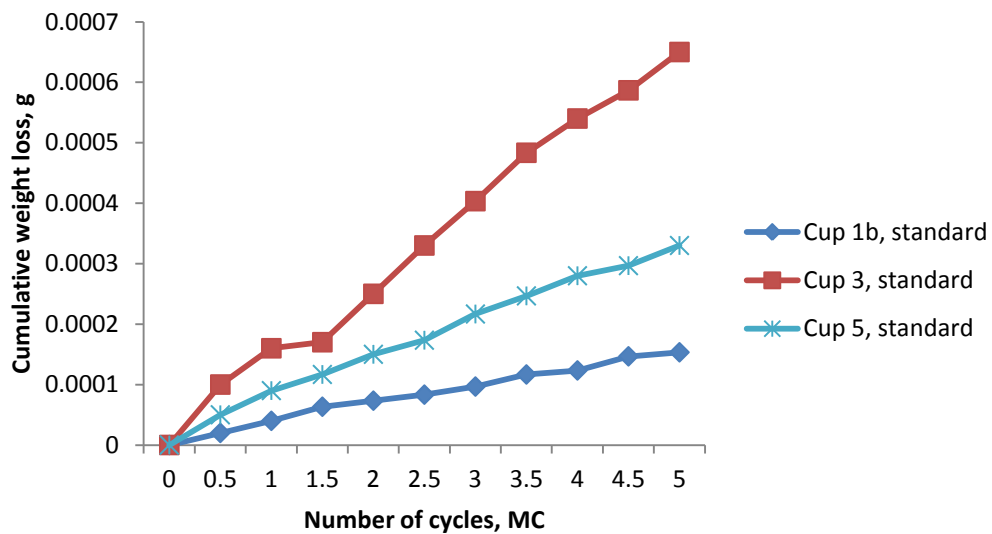


Figure 5.11: Cumulative weight loss of 60 mm CoCrMo cups under standard conditions, accounting for the load soak.

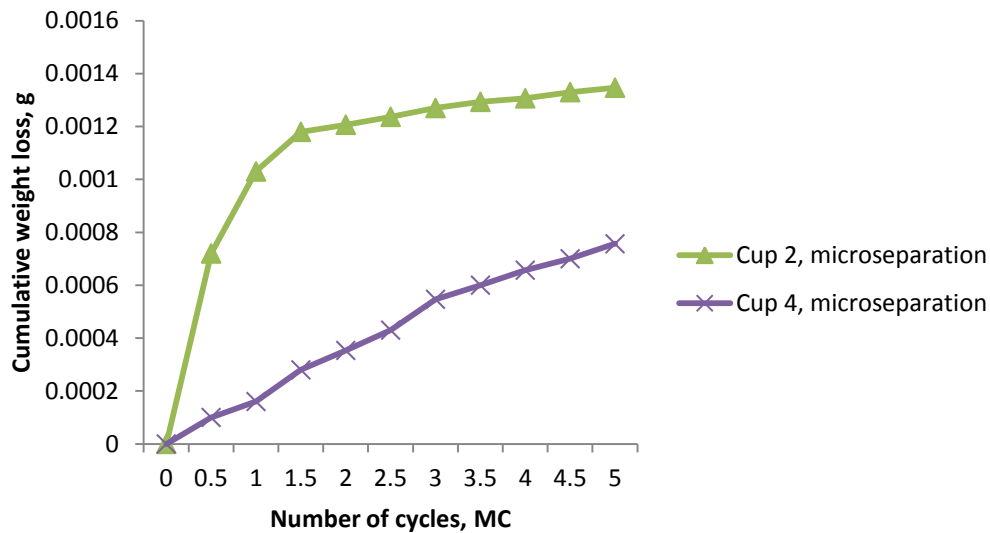


Figure 5.12: Cumulative weight loss of 60 mm CoCrMo cups under microseparation conditions, accounting for the load soak.

The overall wear rate ( $\text{mm}^3/\text{MC}$ ) has been calculated for each station. The results are shown in Table 5.3. Note that the wear rate for the E1 liner in Station 1 has been calculated between 1-5 MC to compensate for the leak at the very start of the test. If this is included, the wear rate between 0-5 MC is  $1.171 \text{ mm}^3/\text{MC}$ . Interestingly the wear has stabilised after the initial leak, unlike in the previous MOM test.

Table 5.3: Wear rates based on overall test, mm<sup>3</sup>/MC. \* Wear rate calculated between 1-5 MC.

Station, Test Condition	28 mm CoCrMo Head	E1 Liner	60 mm CoCrMo Cup
1, Standard	0.005	0.427*	0.004
2, Standard	0.006	0.230	0.016
3, Microseparation	0.010	3.759	0.023
4, Microseparation	0.008	2.493	0.019
5, Standard	0.006	0.397	0.008

All the wear rates for the 28 mm CoCrMo heads were linear ( $R^2 = 0.93 - 0.99$ ).

Only the CoCrMo cup in Station 3 had non-linear regression ( $R^2 = 0.6$ , for the cups in the remaining stations  $R^2 = 0.99$ ). This was the most previously worn cup from MOM Test 1 and it experienced increased wear during 0 – 1 MC.

The E1 liners in stations 2 – 4 all experienced a linear wear rate ( $R^2 = 0.97 - 0.99$ ). Liner 1 had non linear regression ( $R^2 = 0.7$ ) due to the station experiencing a leak between 0 – 0.5 MC which increased the initial wear of the liner. This then stabilised during the remainder of the test.

### 5.3.4 Surface characterisation

#### 1) Zygo non-contacting profilometry

Ten zygo images were taken at and around the pole for each component in the five active stations at 0, 0.5, 1.0, 2.5 and 5.0 MC of the test. The load control and soak control were also analysed for comparison.

Wear testing has caused the surface roughness (Ra) and skewness (Rskw) to decrease across all the liners. The CoCrMo heads and cups have not changed too much in comparison. Figure 5.13 and Figure 5.14 show the zygo data for the worn CoCrMo shells from the previous test. There is little difference in surface roughness and skewness at the end of the test with the values measured before the test. Figure 5.15 and Figure 5.16 show the zygo data for the CoCrMo heads, there is little difference in the data. Figure 5.17 and Figure 5.18 show the zygo data for the E1 liners. The behaviour across all the stations was quite similar so the data across Stations 1, 2 and 5 has been averaged to give the standard result. The data from Stations 3 and 4 has been averaged to give the microseparation result. The error bars indicate the standard deviation of the data.

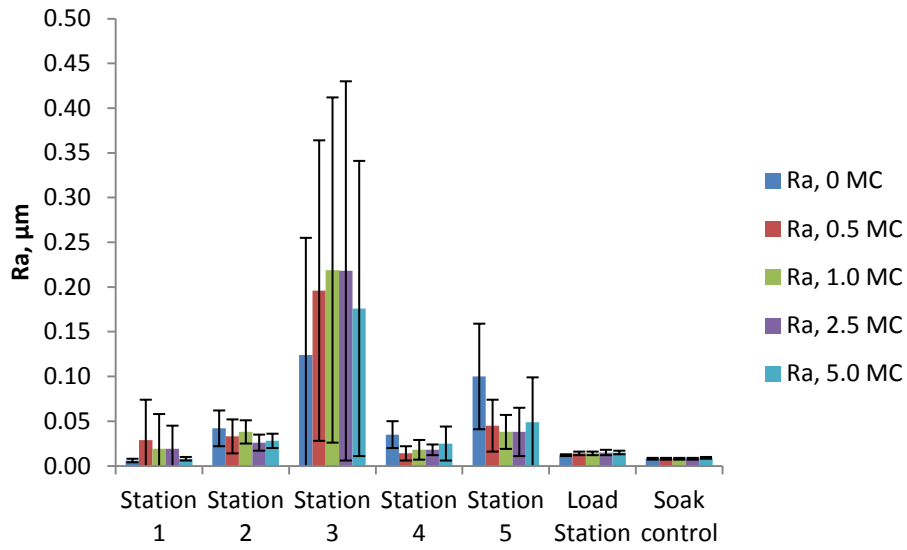


Figure 5.13: Surface roughness of 60 mm CoCrMo cups during 5.0 MC.

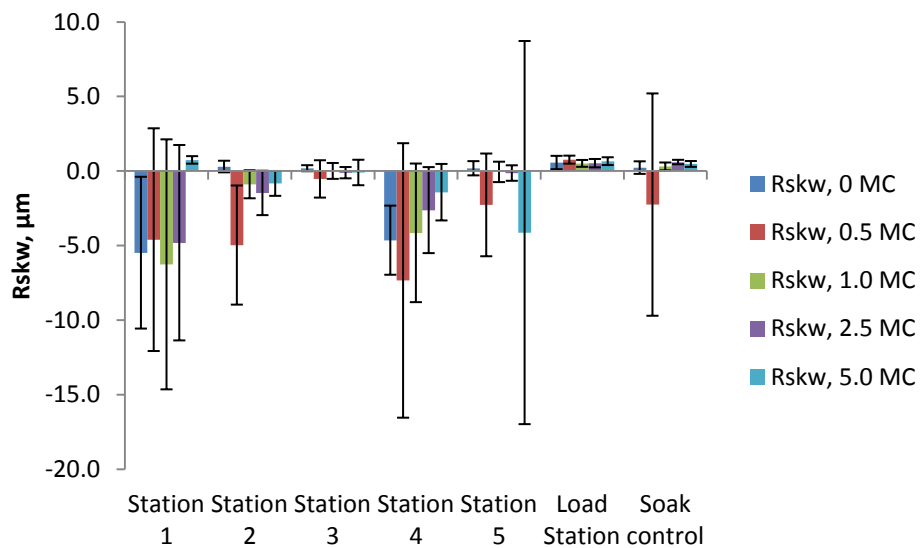


Figure 5.14: Skewness of 60 mm CoCrMo cups during 5.0 MC.

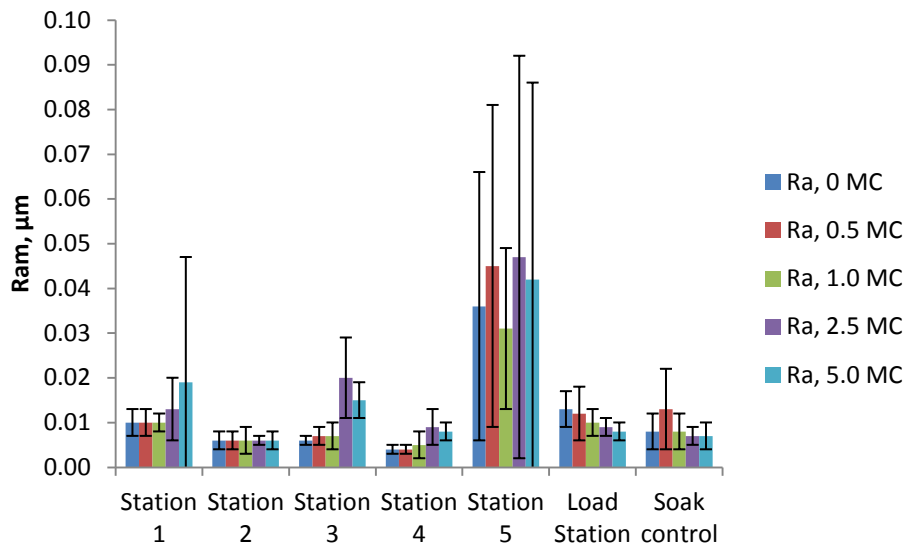


Figure 5.15: Surface roughness of 28 mm CoCrMo heads during 5.0 MC.

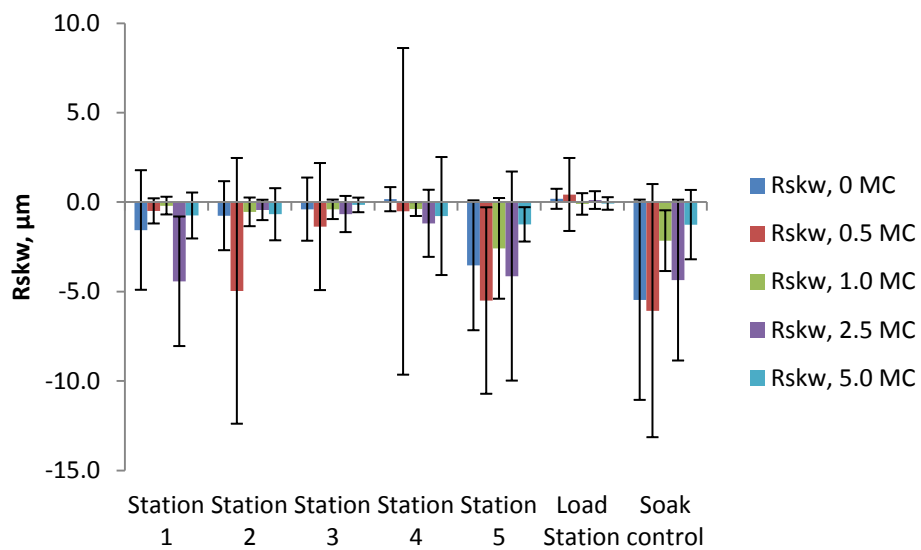


Figure 5.16: Skewness of 28 mm CoCrMo heads during 5.0 MC.

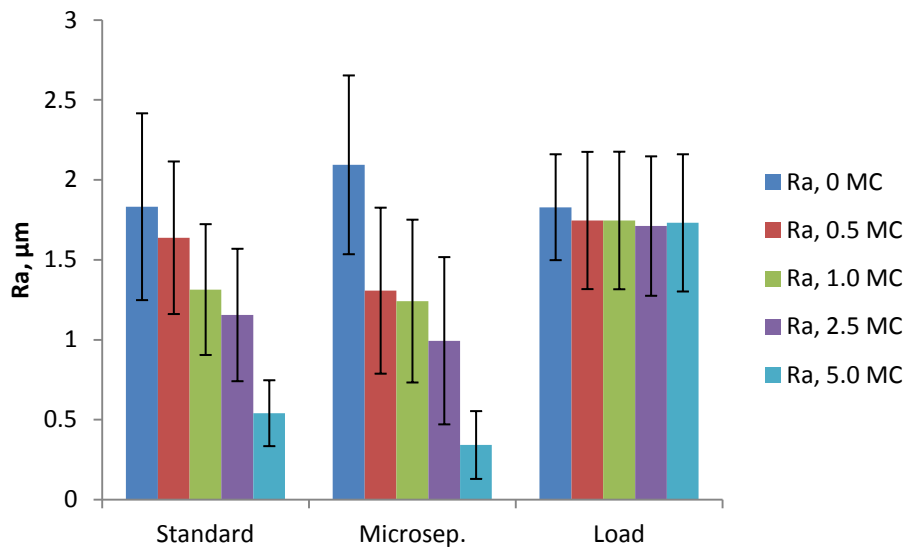


Figure 5.17: Surface roughness of E1 liners during 5.0 MC.

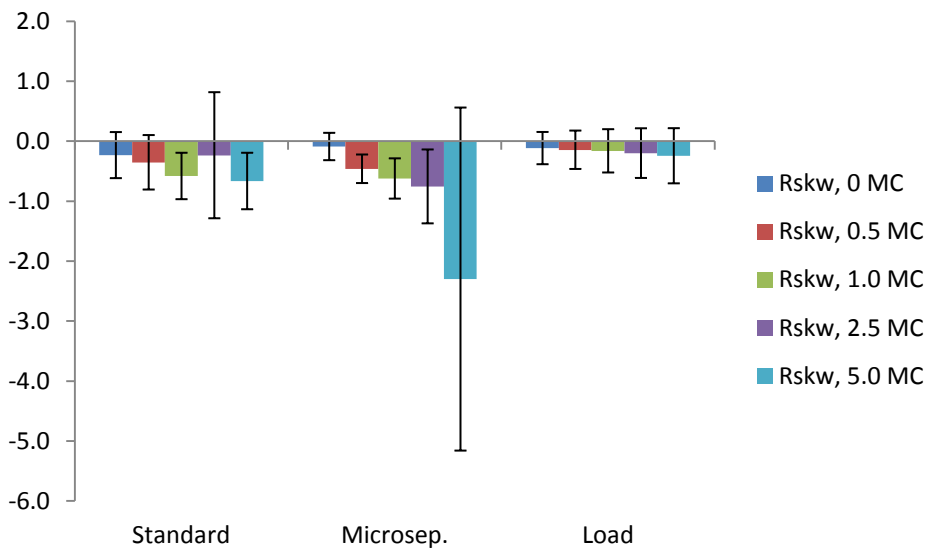


Figure 5.18: Skewness of E1 liners during 5.0 MC.

Eight additional zygo measurements were taken at 45° around the liners after 5 MC, as seen in Figure 5.19. Here the manufacturing streaks, which are most noticeable at the pole, are not as evident.

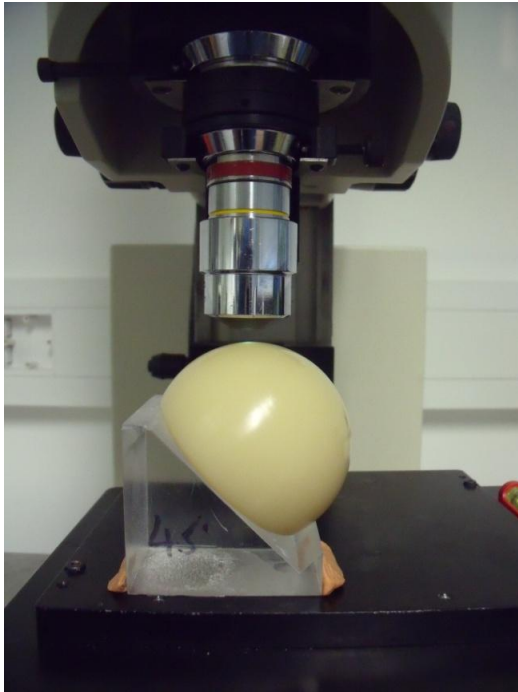


Figure 5.19: Zygo set up at 45° with E1 liner.

The results are shown in Figure 5.20. As before, the data from Stations 1, 2, and 5 were averaged to give the result for the standard stations. The data from Stations 3 and 4 were averaged to give the result for the microseparation stations. The surface roughness of the liners in the microseparation stations have decreased more than those in the standard stations, and the skewness has also become more negative. Figure 5.21 shows the 3D surface profiles of the E1 liners.

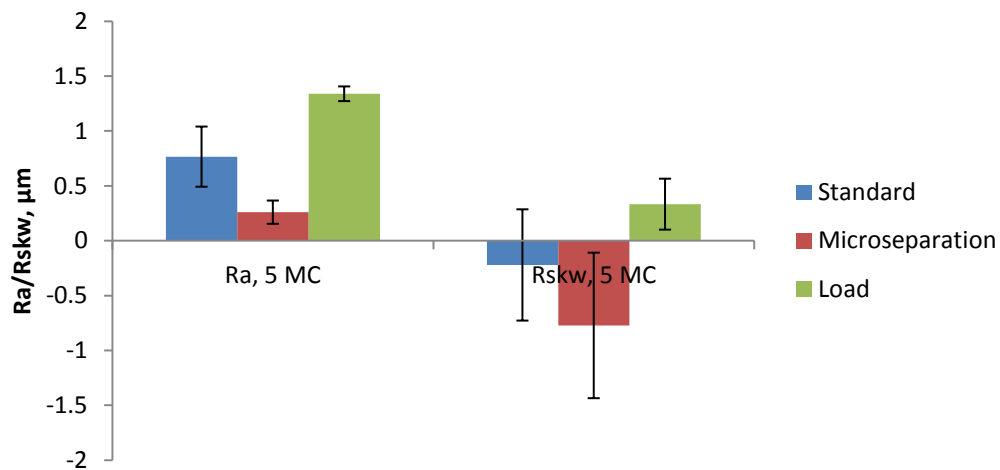


Figure 5.20: Additional data for surface roughness and skewness at 45° around E1 liners.

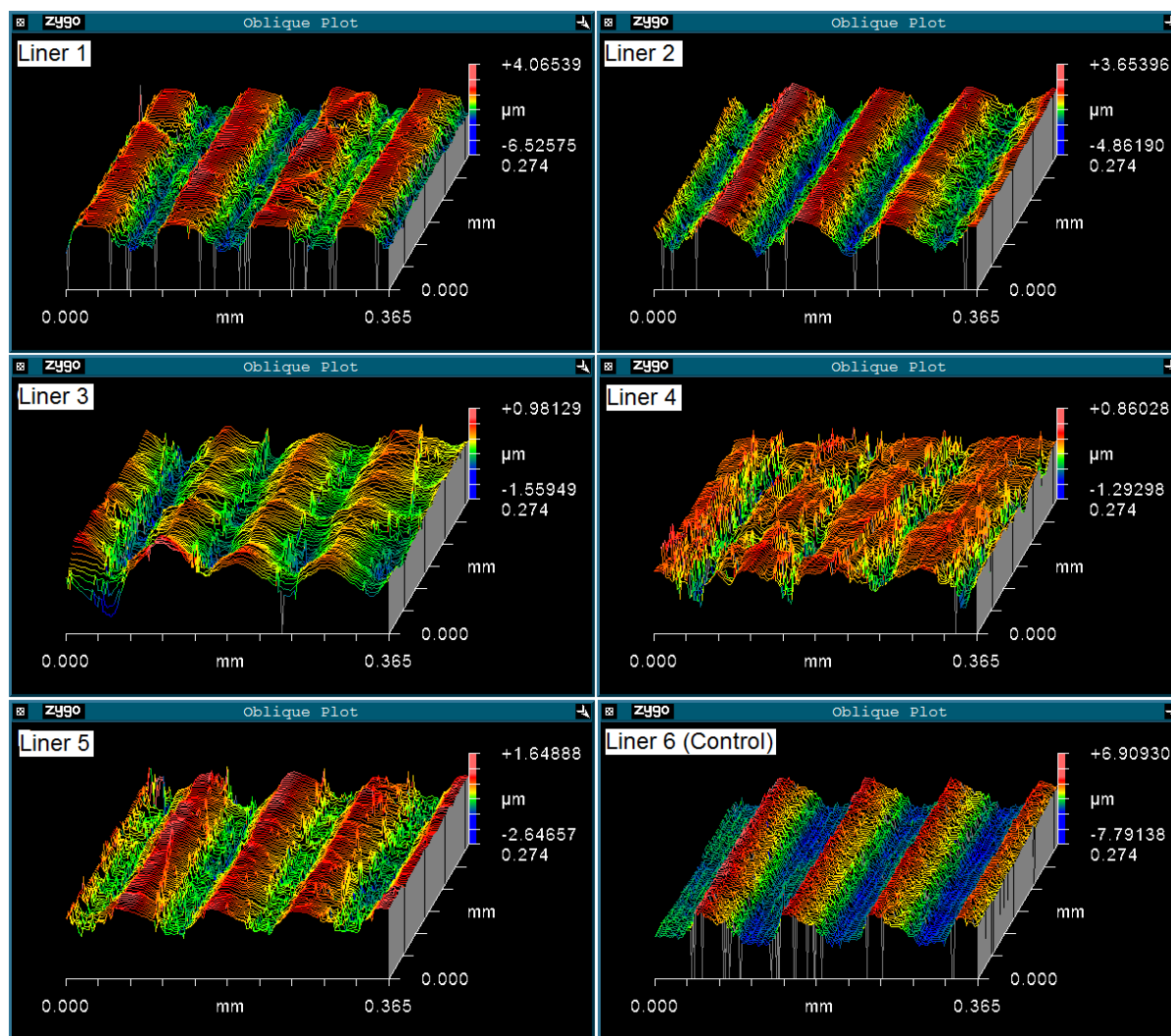
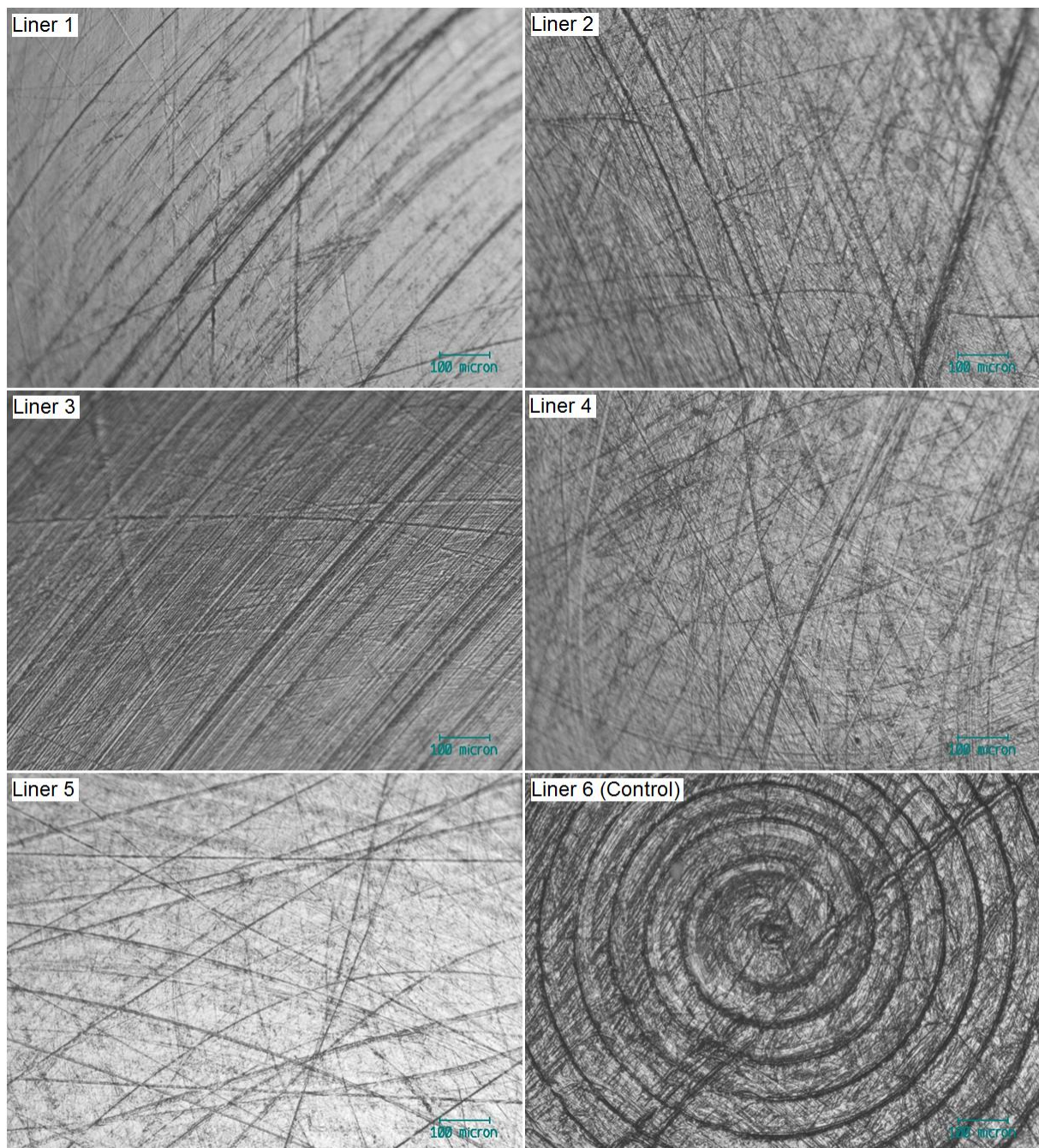


Figure 5.21: Surface profiles of E1 liners imaged after 5 MC at 45 °.

Figure 5.21 shows that the surface topography is smoother in each liner that has undergone testing, and surface roughness is the least in liners 3 and 4 that were subject to testing under microseparation conditions.

## 2) Optical microscopy

The following images were taken with an Axiotech optical microscope. Figure 5.22 shows the inner pole of one E1 liner before the test in comparison to after 0.5 MC for all liners. Figure 5.23 shows corresponding data for the outer pole. The difference between these two figures highlight that the inner articulation experiences greater wear than the outer articulation. Figure 5.23 also indicates that the outer articulation is engaged more during microseparation than under standard testing.



**Figure 5.22: Inner pole of E1 liners after 0.5 MC.**

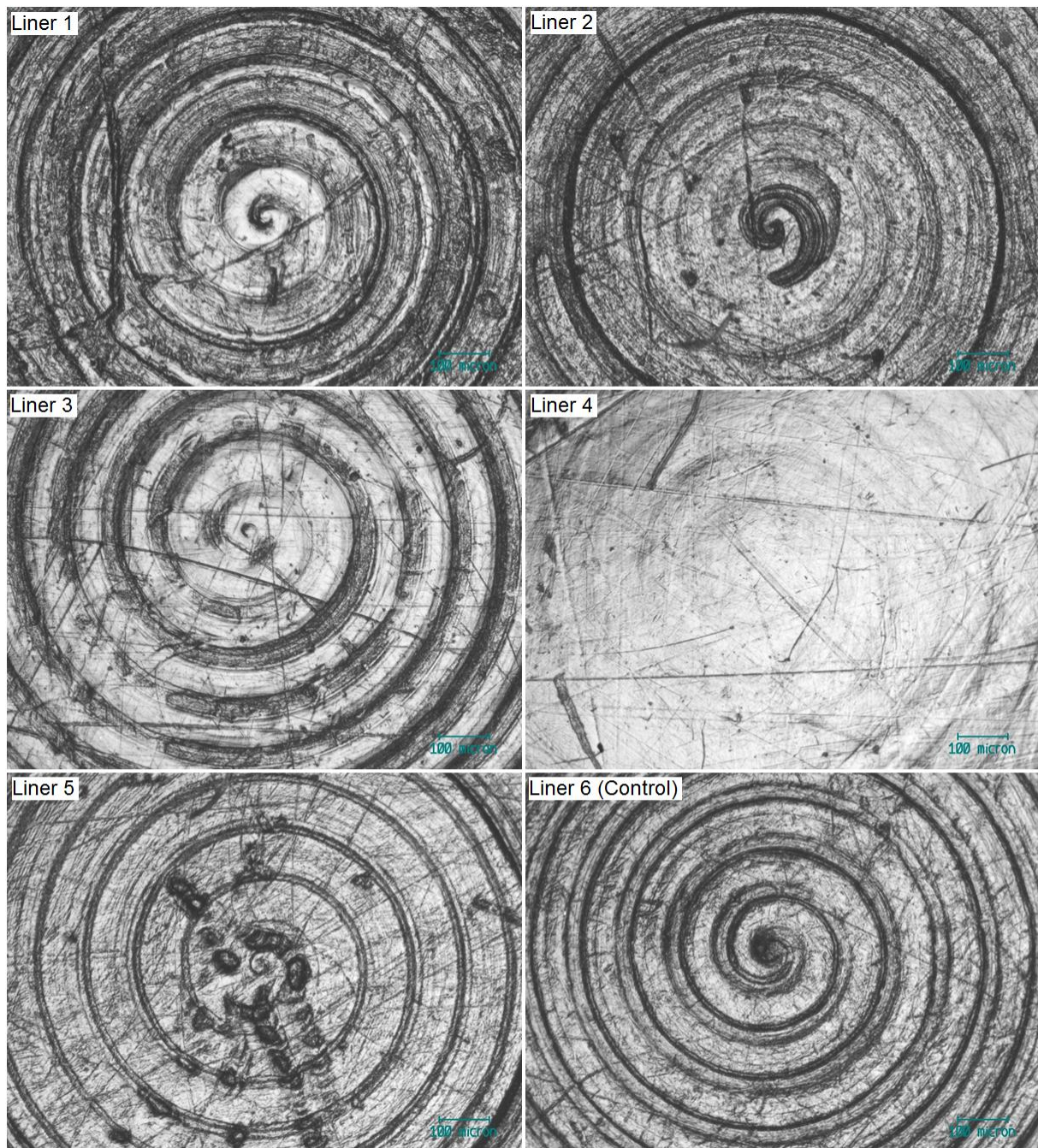


**Figure 5.23: Outer pole of E1 liners after 0.5 MC.**

Figure 5.24 shows the inner pole of the E1 liners after 2.5 MC in comparison to the load soak control, whilst Figure 5.25 shows the outer poles at the same stage of the test. The outer articulation is still much less worn than the inner articulation. Figure 5.26 and Figure 5.27 show the inner and outer poles respectively at the end of the test after 5 MC.

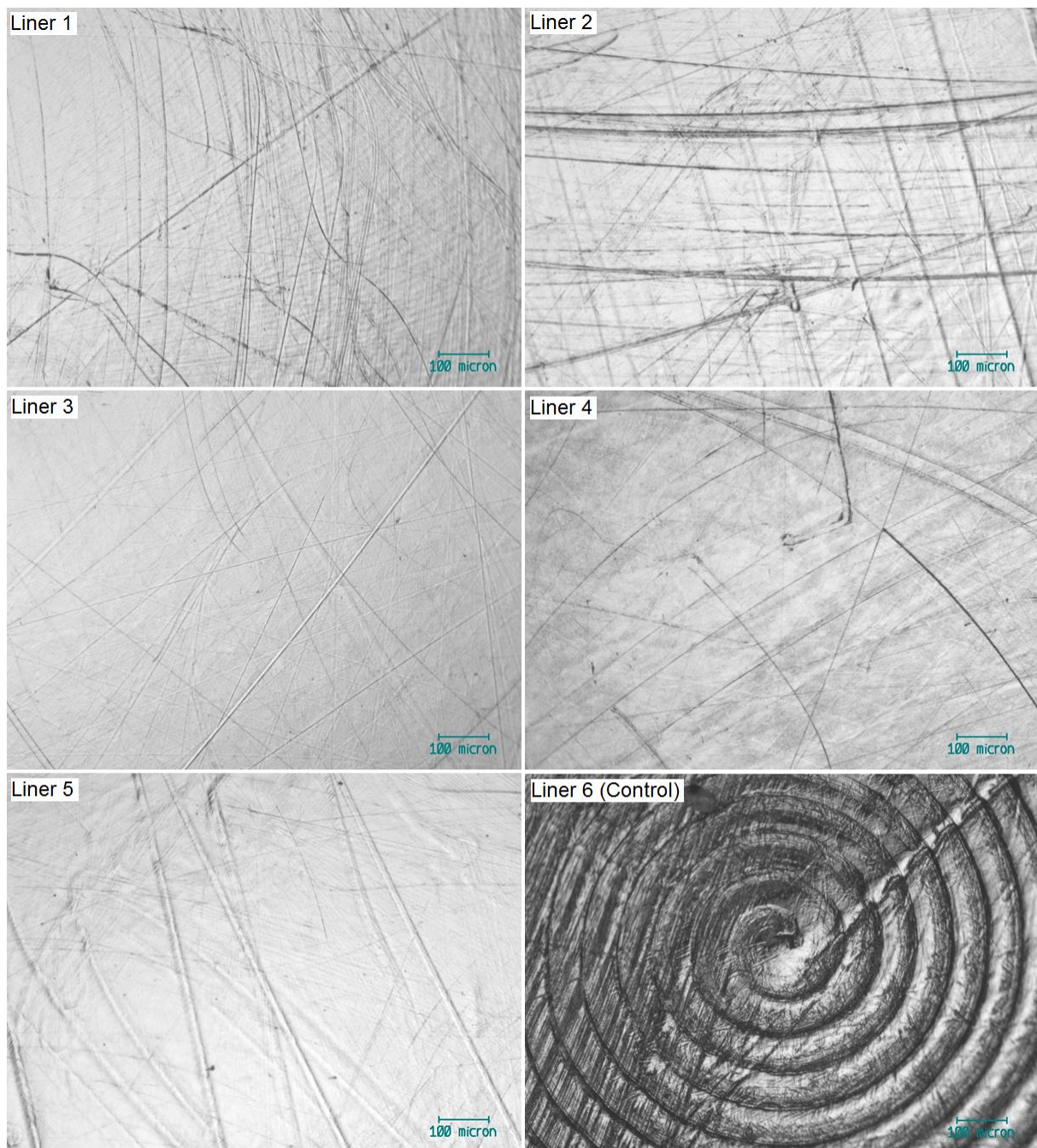


**Figure 5.24: Inner pole of E1 liners after 2.5 MC.**

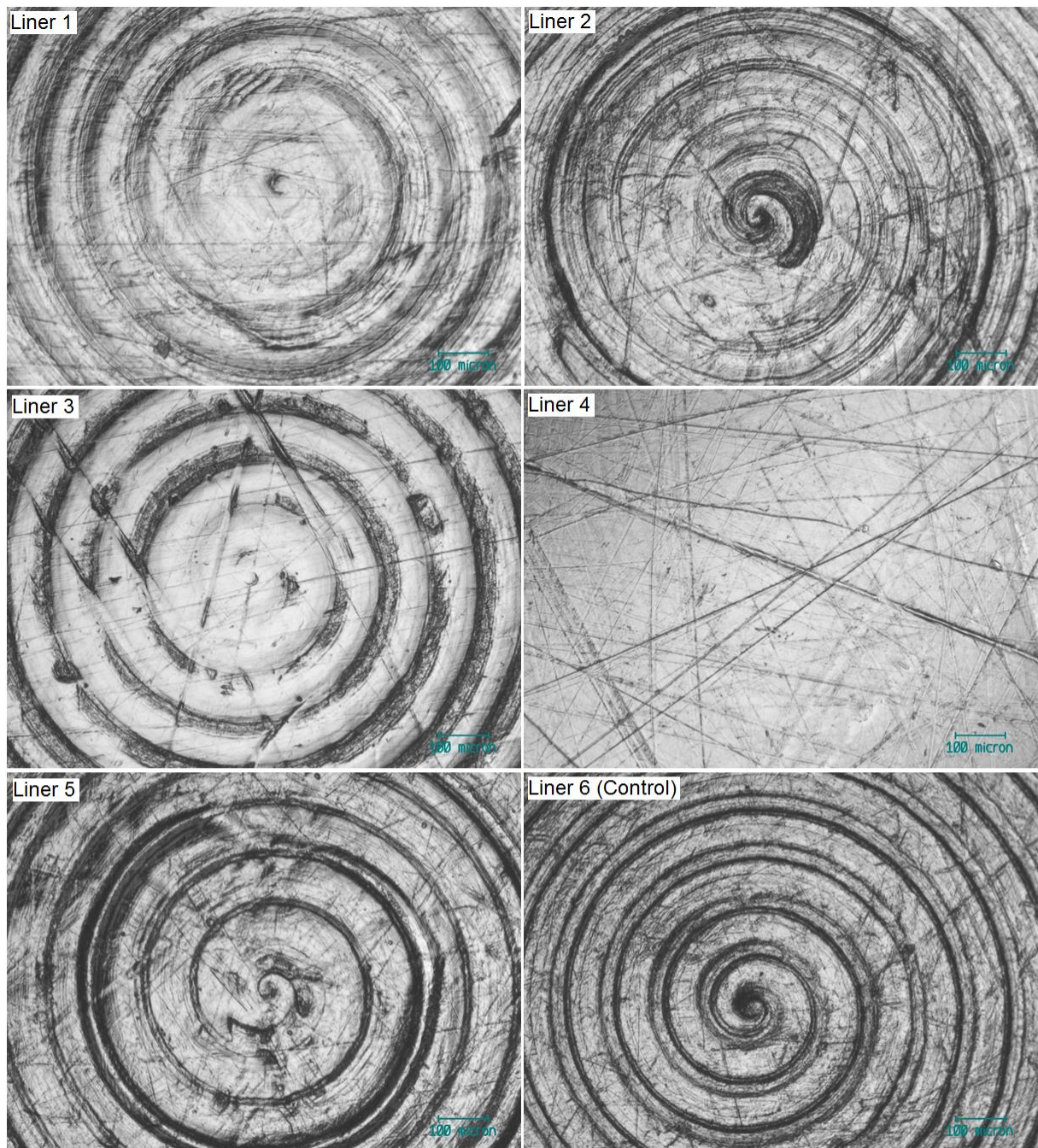


Figure 5.25: Outer pole of E1 liners after 2.5 MC.

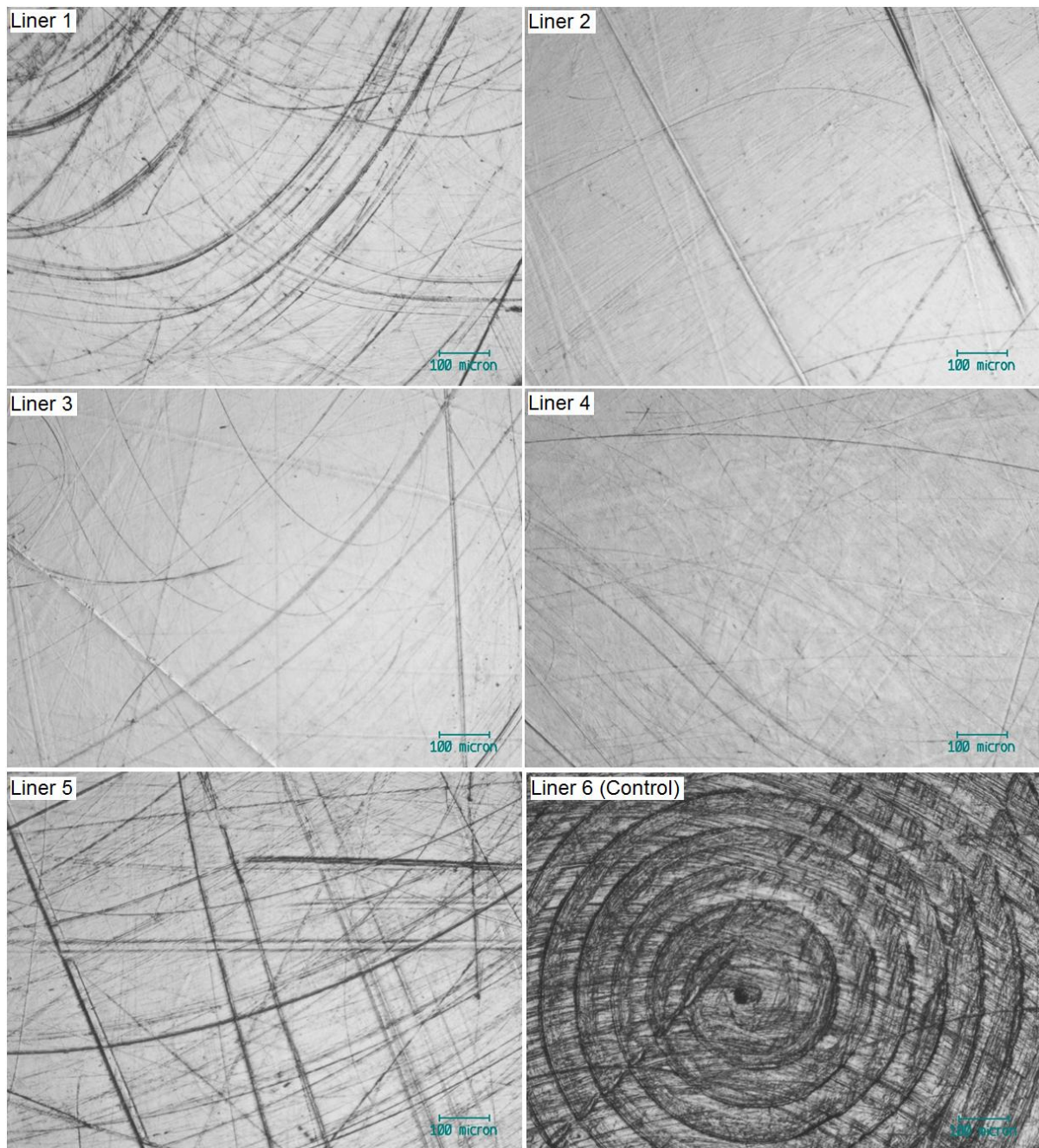
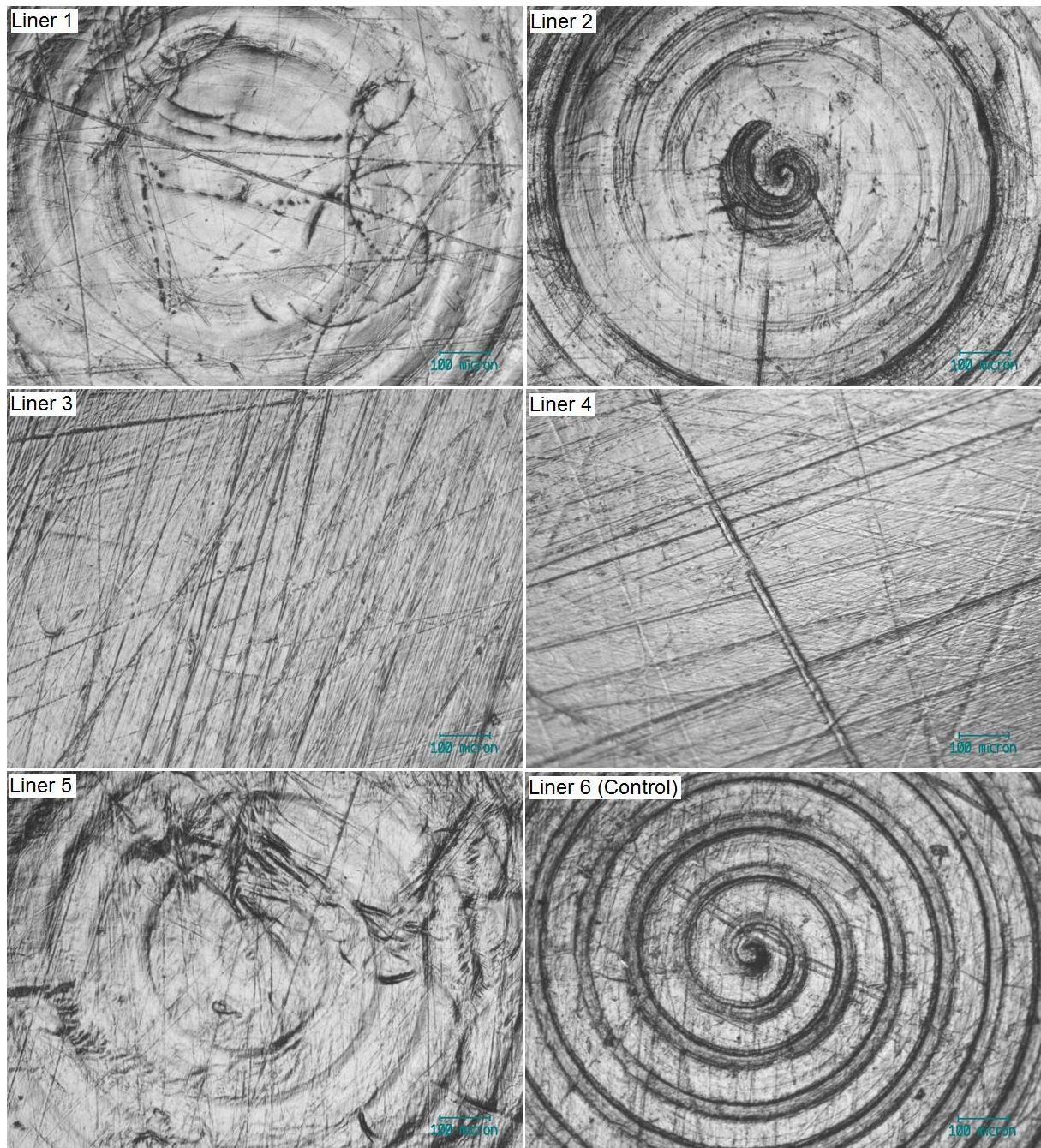


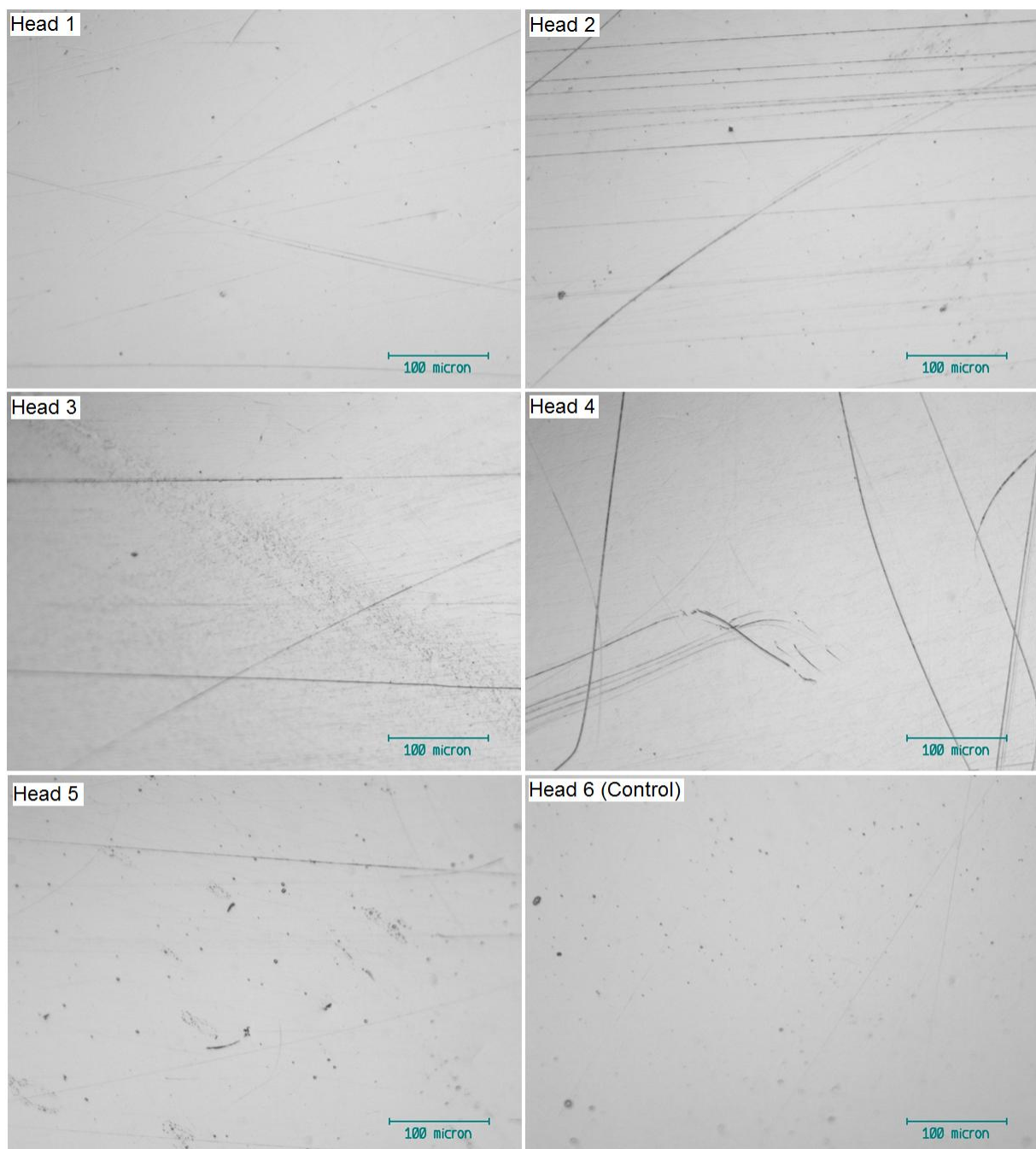
Figure 5.26: Inner pole of E1 liners after 5.0 MC.



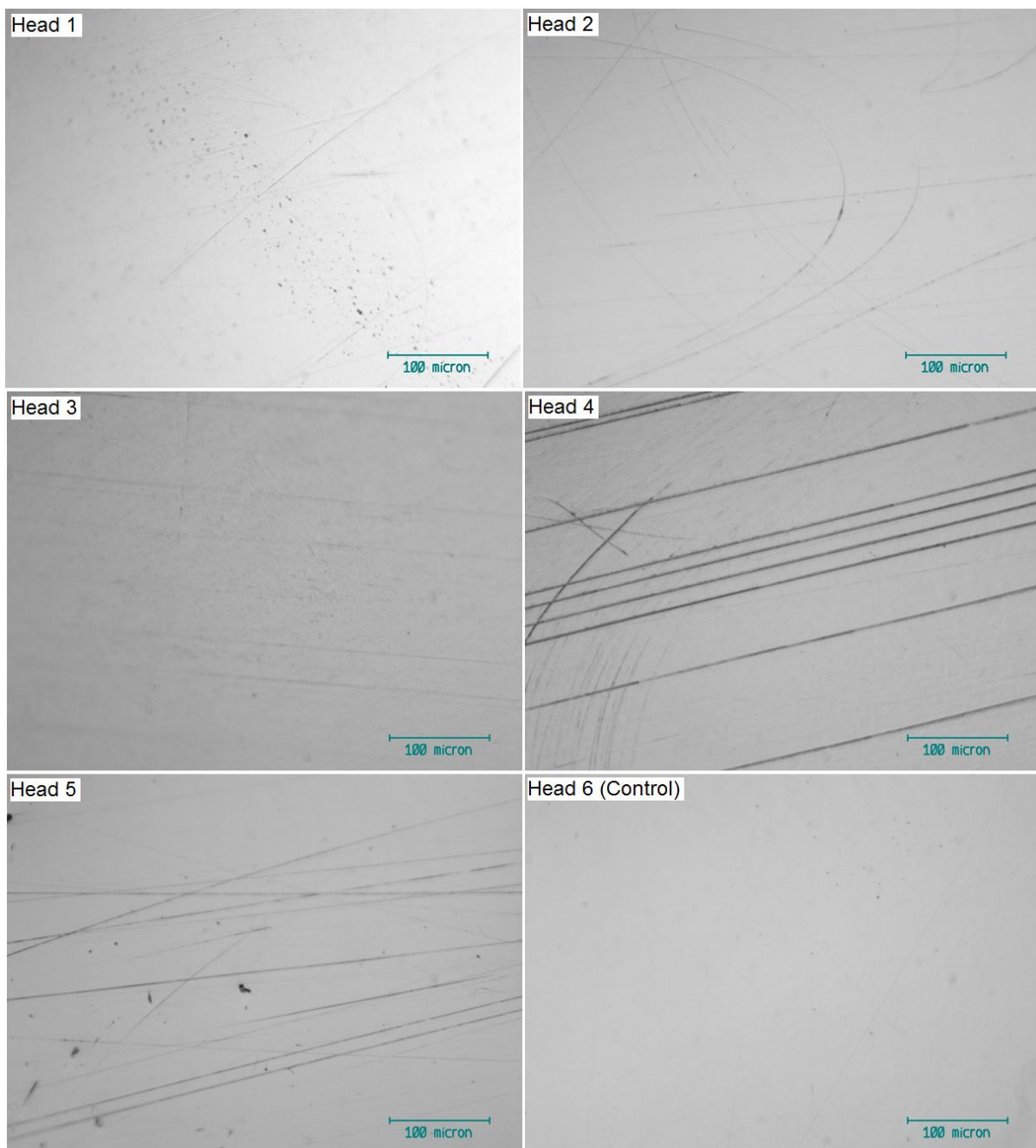
**Figure 5.27: Outer pole of E1 liners after 5.0 MC.**

Figure 5.27 shows that after 5MC, the manufacturing streaks on the outer poles of the liners in the standard stations are still partially visible, though they are subject to some scratches. This is not the case in the microseparation stations which have experienced more wear. This is in great comparison to the manufacturing streaks on the inner poles of the liners which were removed from all liners within 0.5 MC, highlighting the difference between the inner and outer articulations.

Figure 5.28 and Figure 5.29 look at the 28 mm CoCrMo heads after 1.0 MC and 5.0 MC respectively.



**Figure 5.28: Pole of 28 mm CoCrMo heads after 1.0 MC.**



**Figure 5.29: Pole of 28 mm CoCrMo heads after 5.0 MC.**

The optical images show that each metal head has experienced light scratching, and a vast improvement to the optical images seen in MOM Test 1.

Figure 5.30 compares a selection of the CoCrMo cups from the end of the MOM test with the end of the dual mobility test and supports the conclusion from the weight and zygo data that little has changed in the cups throughout the test.

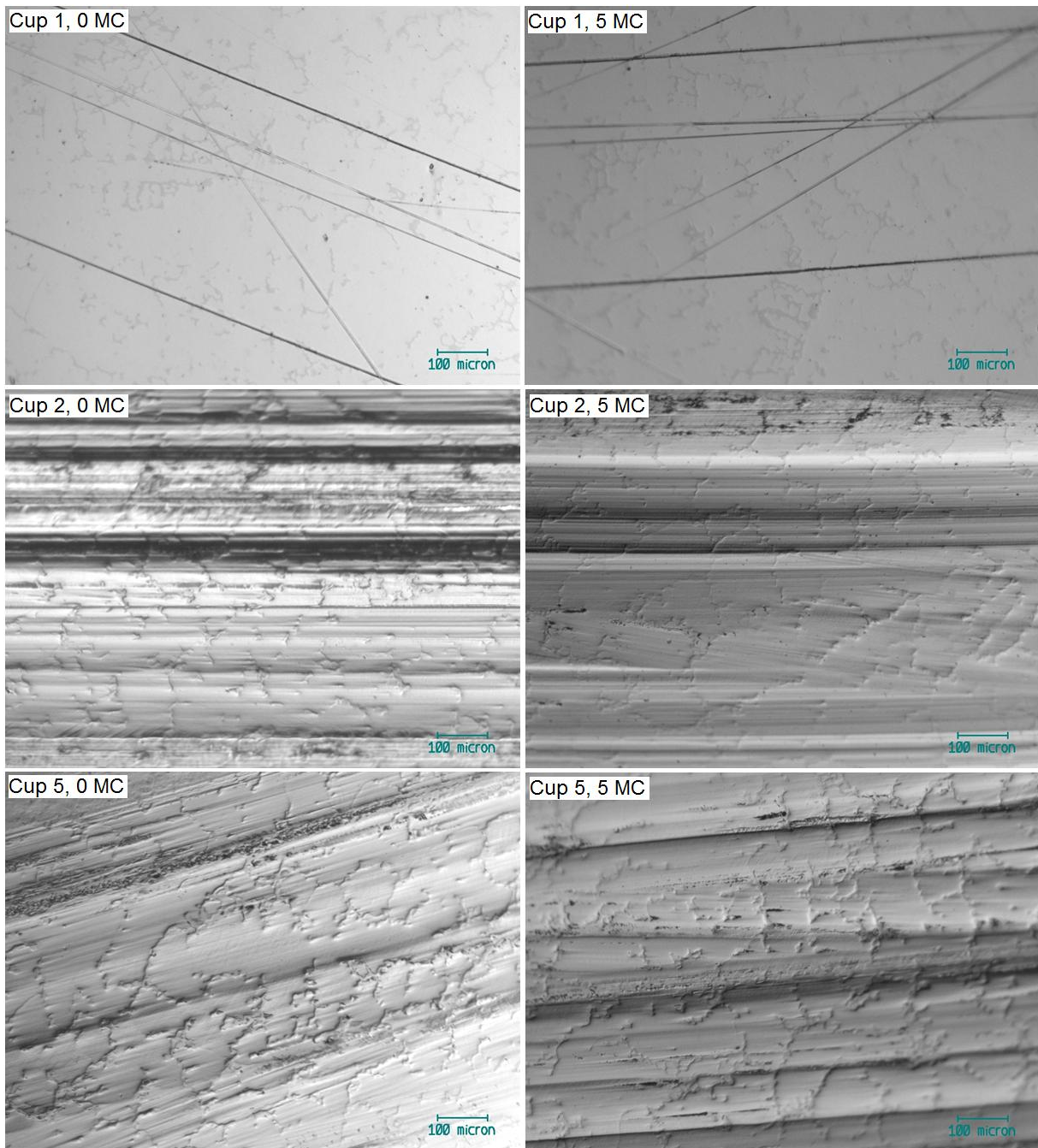


**Figure 5.30: Optical images taken from 60 mm CoCrMo cups from Stations 1, 3 and 5 before and after the dual mobility test.**

### 3) Environment scanning electron microscopy

Photographs were taken to show the change to the rim after 5 MC of wear testing of the liners, see Figure 5.31. Image F shows the load control liner at 5 MC, which is representative of all the liners at 0 MC. All liner rims have experienced wear. The liners numbered 3 and 4 in the microseparation stations have experienced greater wear than those in the standard stations. ESEM images taken at the liner rim after 5 MC can be seen in Figure 5.32.

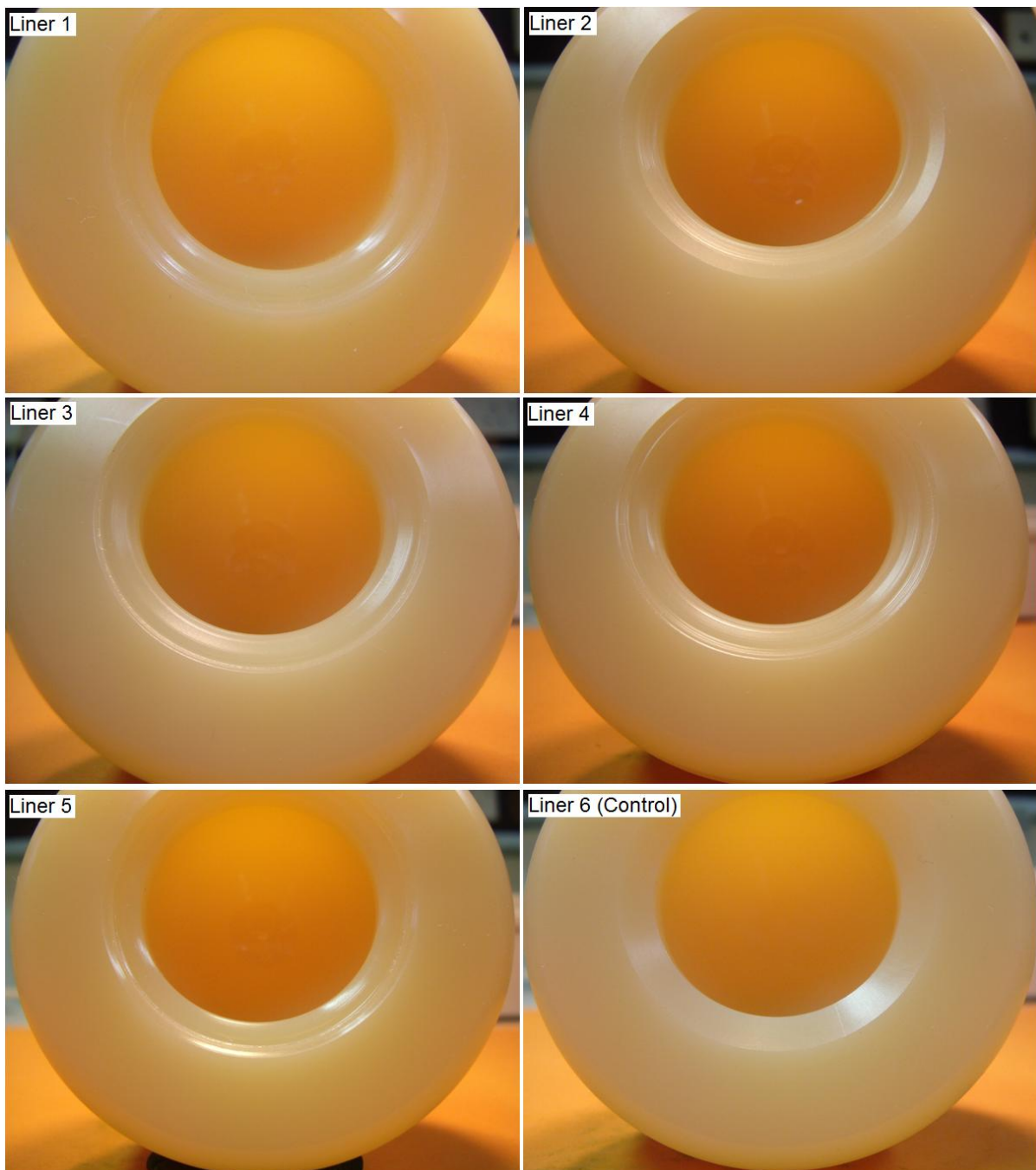


Figure 5.31: Photographs of the E1 liners at 5 MC.

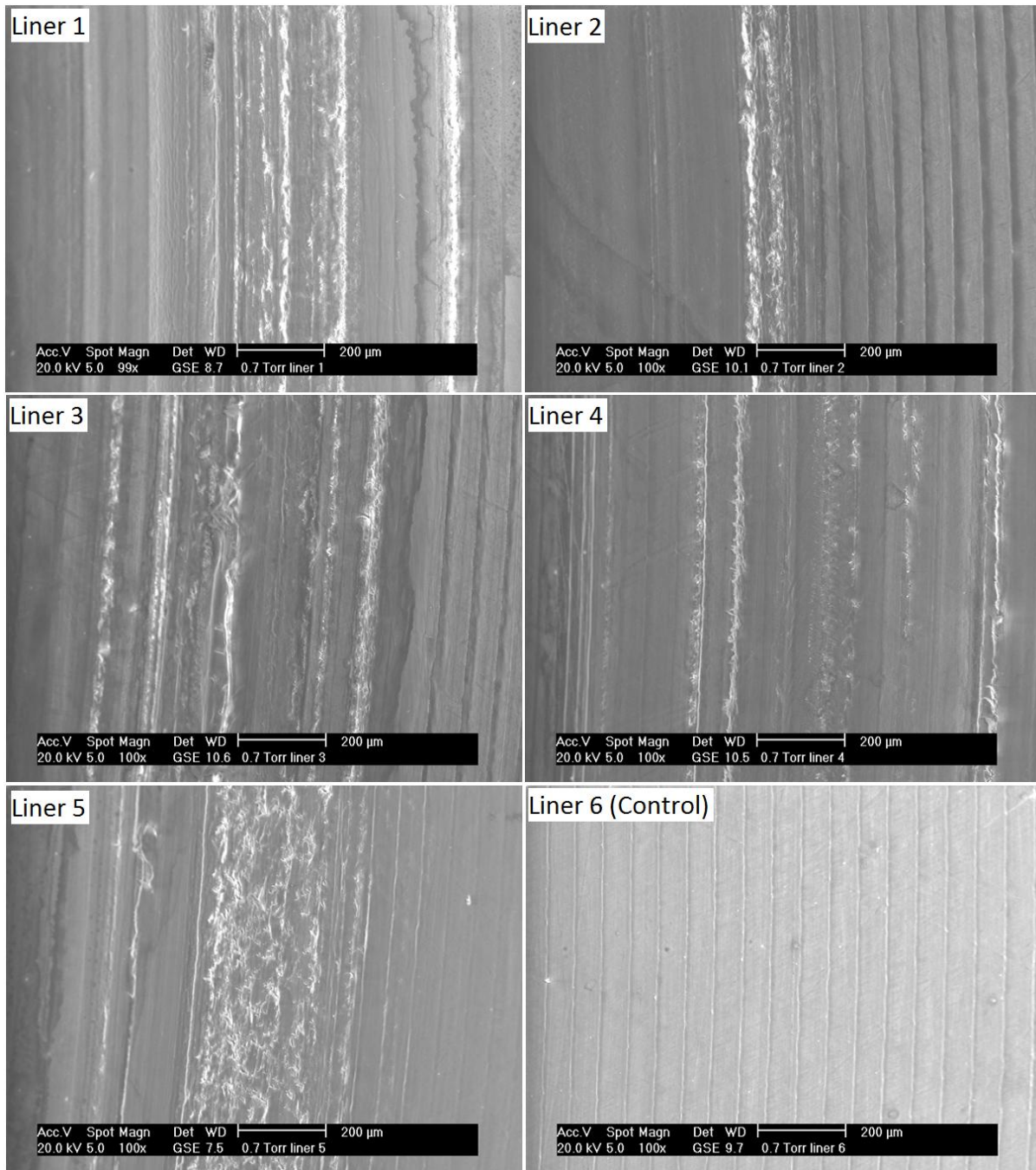


Figure 5.32: ESEM images around the liner rim after 5 MC.

### 5.3.5 Limitations

During the first 0.5 MC, station 1 suffered a leak overnight where it lost a third of the serum. After this test, SimSol terminated the production of the gaiters currently in use. A new manufacturer was found and a new tool was made for a slightly larger gaiter with improved quality. The new style of gaiter required clamping with cable ties rather than O-rings to provide a tighter fit around the cup holder, and they lasted longer in testing without ripping.



**Figure 5.33: Left: 'New' gaiter, Right: 'Old' gaiter.**

The second limitation was that the E1 liners sometimes would not stabilise to give three weight data points within 0.1 mg, even after being left overnight. For this reason, four weight data measurements were recorded at each stage of the test and averaged to give the final result.

The third limitation was that it was impossible to be certain if the E1 liners started in the same position at the start of every 0.5 MC stage of the test. This is due to the mobile nature of the design. The best that could be done was to make sure that the liner was pushed on to the head in the same way every time, but it is unknown whether the liner remained in that position by the time the joint was arranged in the station.

### **5.3.6 Discussion**

In the previous test, MOM Test 1, three stations were experiencing runaway wear. Cup 2, in particular, was wearing at a rate of 41.78 mm<sup>3</sup>/MC. Even though this cup was then subject to wear at a higher inclination angle, and under microseparation conditions, the replacement of the 60 mm resurfacing CoCrMo head by the dual mobility head has decreased its wear to less than 0.1 % of its previous value. This is an incredible result and is a strong indication that replacing failed MOM hip replacements with a dual mobility head should be a success.

Figure 5.34 and Figure 5.35 show the wear data from the least and most worn cups respectively from the initial MOM test combined with the wear data from the complete 5.0 MC of the current dual mobility test. Note that the blue line indicates where the 60 mm resurfacing CoCrMo head was replaced with the dual mobility head after 5 MC.

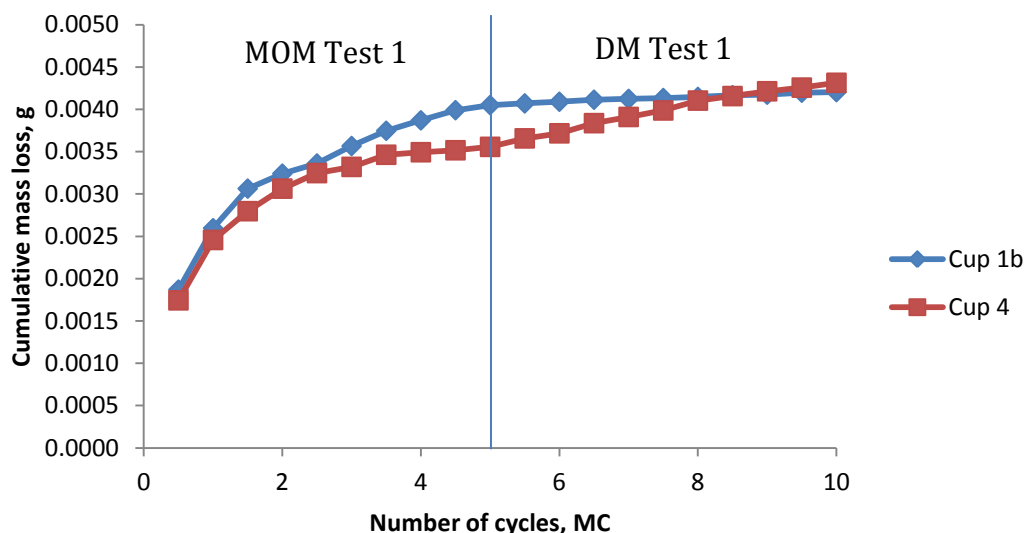


Figure 5.34: Cumulative weight loss of 60 mm CoCrMo cups throughout both tests, accounting for the load soak.

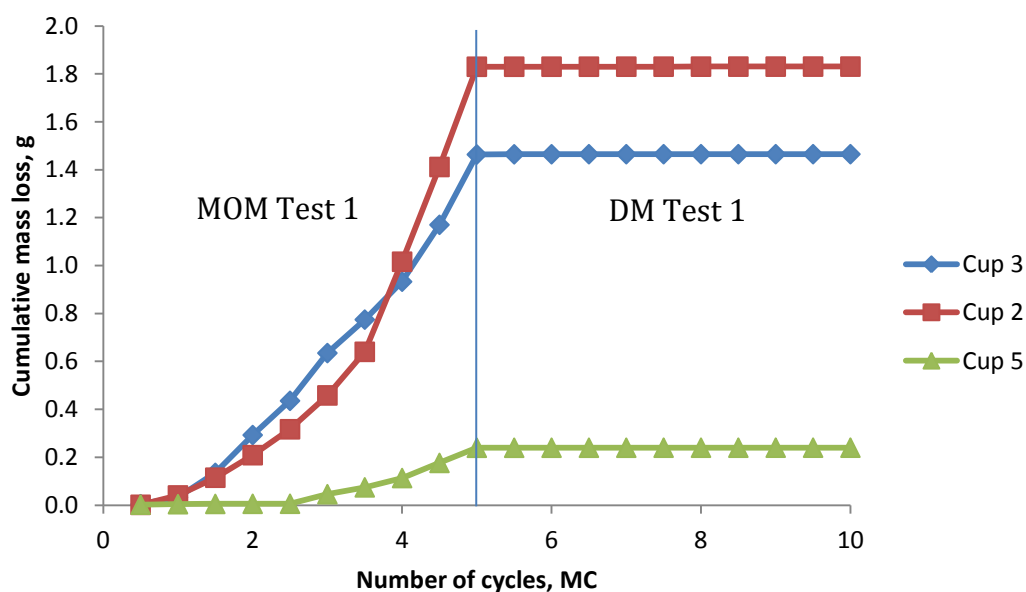


Figure 5.35: Cumulative weight loss of 60 mm CoCrMo cups throughout both tests, accounting for the load soak.

As can be seen in Figure 5.35, replacing the metal femoral heads with the dual mobility heads has really helped to end the runaway wear. Table 5.4 compares the volume loss from each cup in the 2.5 MC prior to the replacement of the metal femoral head with the dual mobility head with the volume loss in the 2.5 MC after the replacement. It can be seen from both Figure 5.34 and Table 5.4 that Cup 4 is the only bearing to experience an

increase in wear, but given that the cup had previously been wearing well and in this current test it had been subject to testing under microseparation at a high incline, this is expected.

**Table 5.4: Volume loss from each cup 2.5 MC prior to the replacement of the femoral head with the dual mobility head compared with the corresponding data after the replacement. 'm' indicates that the cup was subject to microseparation.**

	<b>Volume loss in 2.5 MC prior to change (mm<sup>3</sup>)</b>	<b>Volume loss in 2.5 MC after change (mm<sup>3</sup>)</b>
<b>Cup 1b</b>	0.08	0.01
<b>Cup 2</b>	182.81	0.15 (m)
<b>Cup 3</b>	124.22	0.04
<b>Cup 4</b>	0.04	0.05 (m)
<b>Cup 5</b>	28.24	0.02

Rieker *et al.* [1] have analysed 172 second generation 28 mm CoCrMo retrievals. A linear regression analysis gave a running-in metal wear volume of 1.70 mm<sup>3</sup> for the first year and a steady state wear of 0.44 mm<sup>3</sup>/yr for the whole bearing. In the worst case scenario in this test (station 3; which featured the most worn cup undergoing microseparation at a high incline), the metal wear volume released was 0.15 mm<sup>3</sup> for the first MC and a wear volume of 0.02 mm<sup>3</sup>/MC between 1-5 MC. So the aim to reduce the amount of CoCrMo being released through the use of a dual mobility head has definitely been achieved. It is important to note that on average 3.76 mm<sup>3</sup>/MC of polyethylene particles are also being released from the E1 liner in addition to the CoCrMo particles, but this is much lower than the wear rate reported from conventional polyethylene bearings which lies in the range 38-191 mm<sup>3</sup>/yr [2].

Wear rates of dual mobility total hip arthroplasty has been investigated *in vivo* [3-5]. It is usual for the wear rate to be presented as a linear wear rate showing how far the head has penetrated into the cup liner. It is possible to calculate the volumetric wear rate from this; however the method uses assumptions that produce error [6]. Kusaba *et al.* [5] measured the annual wear rate in 68 dual mobility prostheses, with 22mm inner

head diameter, to be 0.17 mm/yr by taking radiographs of the inner articulation. Osteolysis occurred in 25 hips and there was no difference between the annual wear rate of hips with and without osteolysis. By looking at 19 retrieved dual mobility prostheses, abrasion of the rim was deeper in the hips with osteolysis than those without it. This suggests that wear around the rim can play an important part in the onset of osteolysis.

Homogenous and symmetrical wear around the liner rim similar to that seen in this study has been seen *in vivo* and an image taken from the study by Fessy *et al.* [7] is shown in Figure 5.36. Whilst all liners in this test have experienced wear around the rim, the wear rate has been very low, even in the microseparation stations.

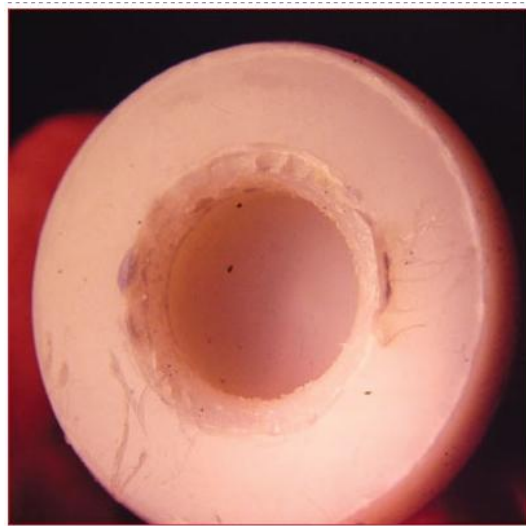


**Figure 5.36: Photo taken from [7] showing homogenous and symmetrical wear around the rim of a retrieved DM liner.**

Adam *et al.* [4] analysed 40 polyethylene liners after a mean implantation time of 8 years which were removed after prosthesis infection or mechanical failure. Every liner had lost their manufacturing streaks on the outer pole of the convex surface, while 40% of the liners showed visible wear of the collar retention. The mean annual wear for the outer pole was 0.009 mm/yr, and 0.073 mm/yr for the inner pole. The volumetric wear in the middle of the tolerance averaged 28.9 mm<sup>3</sup>/yr for the outer pole, and 25.5 mm<sup>3</sup>/yr for the inner pole, so that the annual total volumetric wear rate was 54.3 mm<sup>3</sup>/yr. Adam *et al.* concluded that the dual articulation was not associated with increased wear in comparison with conventional metal-on-polyethylene bearings, with the goal of retention and the advantage of greater stability. In this test, the inner pole

has also experienced greater wear than the outer pole, although after 5 MC in the standard testing stations, the manufacturing streaks were still partially visible on the outer pole. It was only in the stations subject to microseparation conditions that the manufacturing streaks had been removed. The total volumetric wear rate per MC has been much lower in this test than that seen in vivo using standard polyethylene liners, indicating that this combination using vitamin E infused polyethylene liners has greatly improved the wear properties of the dual mobility head, whilst retaining all the stability advantages associated with that of the polyethylene dual mobility set up.

More information about the nature of the polyethylene particles produced throughout this test needs to be established. Green *et al.* [8] have shown that only polyethylene particles between 0.5 to 10  $\mu\text{m}$  can induce secretion of interleukin 6 in macrophages with the subsequent formation of granuloma and hence osteolysis.

### 5.3.7 Conclusion

Five dual mobility heads, consisting of a 28 mm CoCrMo head and an E1 liner with an inner diameter of 28 mm, outer diameter 60 mm have been tested against a range of previously worn 60 mm CoCrMo cups. The 28 mm heads were sectioned to allow removal from the E1 liner for cleaning throughout the test.

Over 5 MC of testing, under either standard or microseparation conditions at a high incline, the wear rates of the 28 mm CoCrMo heads ranged from 0.005 and 0.010  $\text{mm}^3/\text{MC}$ . The wear rates of the E1 liners ranged from 0.230 to 3.759  $\text{mm}^3/\text{MC}$ . Vitamin E has greatly improved the wear properties of the dual mobility head. The wear rates of the 60 mm CoCrMo cups ranged from 0.004 to 0.023  $\text{mm}^3/\text{MC}$ .

For all the CoCrMo heads and cups there was little difference in surface roughness at the end of the test compared with the data recorded at the start.

Surface roughness has decreased across all the liners, and is smoothest in the liners that were subject to testing under microseparation conditions.

Optical images of the outer and inner pole of the E1 liners indicates that the inner articulation experiences greater wear than the outer articulation, and also that the outer articulation is engaged more during microseparation than under standard testing. Circumferential abrasion was experienced in each E1 liner in the test.

The wear, optical and zygo data all indicate low wear rate even under harsh testing conditions and are a strong indication that the partial revision of a failed MOM THRA with a dual mobility head is a viable solution.

### **5.4 DM Test 2: aggressive biotribological study with unworn CoCrMo cups**

During this simulation, unworn 60 mm CoCrMo cups were tested against a dual mobility head consisting of a 28 mm CoCrMo head and an E1 liner with an inner diameter of 28mm, outer diameter 60mm. The test was carried out in the ProSim hip simulator with five active stations, using the same test conditions as in the previous test. Again, each 28mm head was sectioned at 25° prior to testing to allow for removal from the liner throughout the test. Three stations were operating under standard conditions; two stations were operating under microseparation conditions. All stations were positioned at 62° (high inclination angle). In addition to the active stations, there was also a loaded soak control and a soak control under no loading, left at room temp throughout the test.



Figure 5.37: 28 mm CoCrMo head, E1 liner, 60 mm CoCrMo cup.

#### **5.4.1 Joint replacement clearance**

Two articulations are considered in this test; the inner articulation, between the 28 mm CoCrMo femoral head and the E1 liner, and the outer articulation, between the E1 liner and the 60 mm CoCrMo cup. The chosen combinations are shown in Tables 5.5 and 5.6.

Table 5.5: Inner clearance of dual mobility components.

	Head	Batch ID	Liner	Batch ID	Clearance, $\mu\text{m}$
<b>Station 1</b>	2	163662	9	P0561E66	77
<b>Station 2</b>	3	163662	11	P0561E66	78
<b>Station 3</b>	4	163662	2	P0561E66	99
<b>Station 4</b>	7	163662	12	P0561E66	90
<b>Station 5</b>	9	163662	10	P0561E66	80
<b>Load Station</b>	6	163662	6	P0561E66	112
<b>Soak control</b>	8	163662	16	P0561E66	229

Table 5.6: Outer clearance of dual mobility components.

	Cup	Batch, Batch ID	Liner	Batch ID	Clearance, $\mu\text{m}$
<b>Station 1</b>	49	2410667, 3	9	P0561E66	315
<b>Station 2</b>	44	2410666, 3	11	P0561E66	302
<b>Station 3</b>	46	2410666, 5	2	P0561E66	312
<b>Station 4</b>	50	2410667, 4	12	P0561E66	299
<b>Station 5</b>	52	2410667, 6	10	P0561E66	297
<b>Load Station</b>	40	2410665, 4	6	P0561E66	325
<b>Soak control</b>	47	2410667, 1	16	P0561E66	305

The mean inner radial clearance across the active samples was 85  $\mu\text{m}$ . The mean inner radial clearance across the load soak was 112  $\mu\text{m}$  and only the soak had a larger clearance. The mean outer radial clearance across the active samples was 305  $\mu\text{m}$ , and 308  $\mu\text{m}$  across all samples including the load soak and soak control.

#### 5.4.2 Soaking data

The E1 liners were soaked in serum at 37 °C prior to testing to account for an increase in mass due to fluid adsorption. The E1 liners were repeatedly removed from the soak serum for gravimetric assessment at the same frequency as that used for simulator wear testing. Standard cleaning protocol normally involves leaving the joints to acclimatise for 30 minutes post drying before weighing. However the weight of the large liners fluctuated greatly within this time and stabilisation of three weight data points to within 0.1 mg was impossible. To overcome this issue, liners were left overnight to acclimatise and were weighed the following morning. This helped to minimise the range of the weight data. Figure 5.38 shows the weight data for the liners over 5 weeks prior

to testing. Soaking had little effect on the surface roughness data as shown in Figure 5.39.

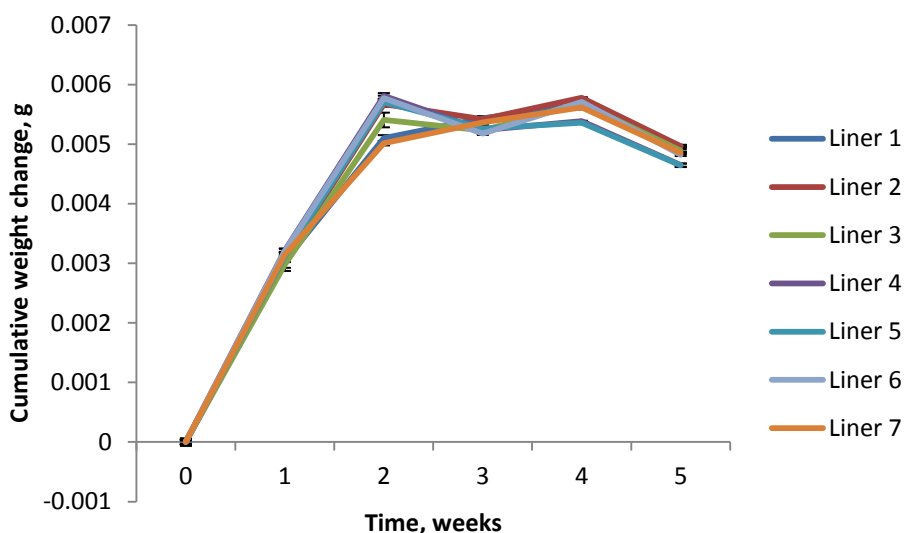


Figure 5.38: Cumulative weight change of E1 liners during soaking over 5 weeks prior to the wear simulation.

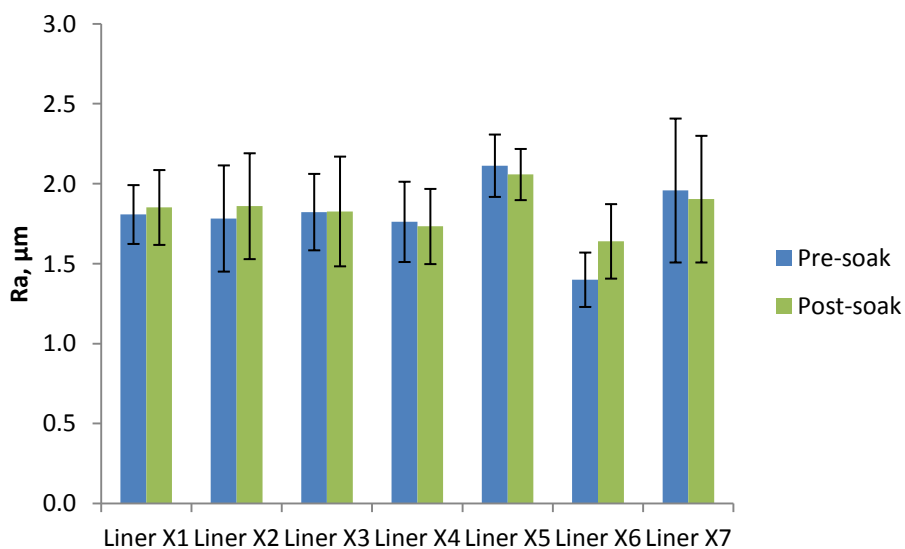


Figure 5.39: Surface roughness of E1 liners prior to test, before and after soaking.

### 5.4.3 Wear results

The test consisted of five active stations, three set up under standard conditions and two under microseparation. In addition to this, there was a loaded soak control, and a soak control under no loading.

The mass loss of each component was corrected by the change of the load soak to account for fluctuations in mass measurements over the test. The cumulative weight loss after 5 MC from the 28 mm CoCrMo heads, E1 liners and 60 mm CoCrMo cups are shown in Figures 5.40-5.42.

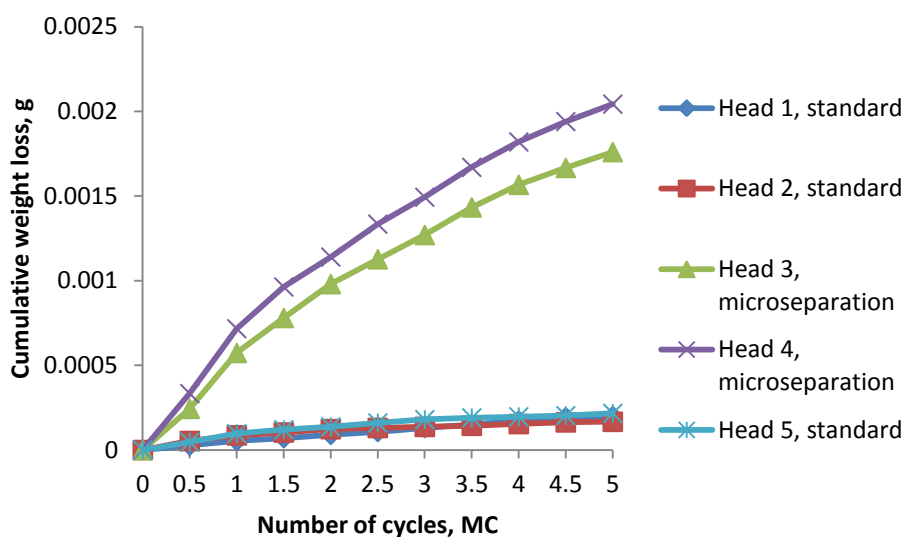


Figure 5.40: Cumulative weight loss of 28 mm CoCrMo heads under standard and microseparation conditions, accounting for the load soak.

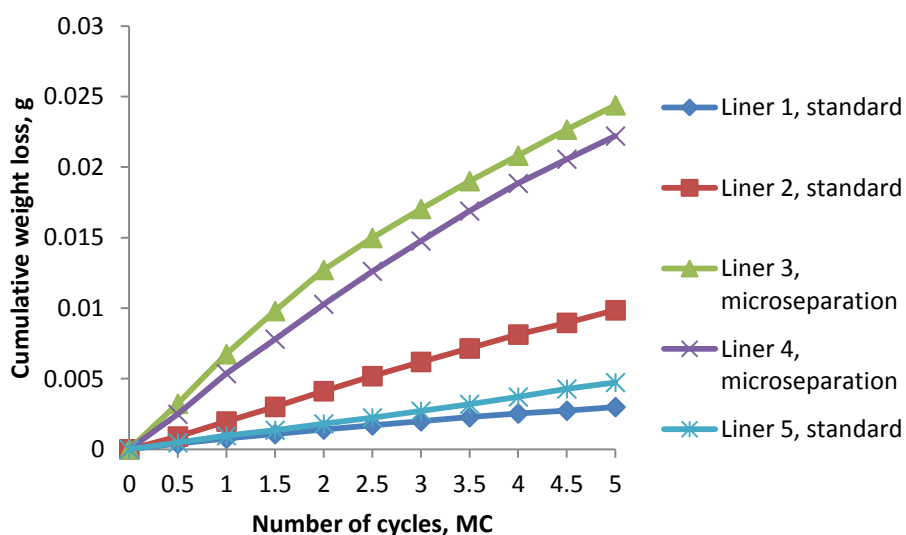


Figure 5.41: Cumulative weight loss from E1 liners under standard and microseparation conditions, accounting for the load soak.

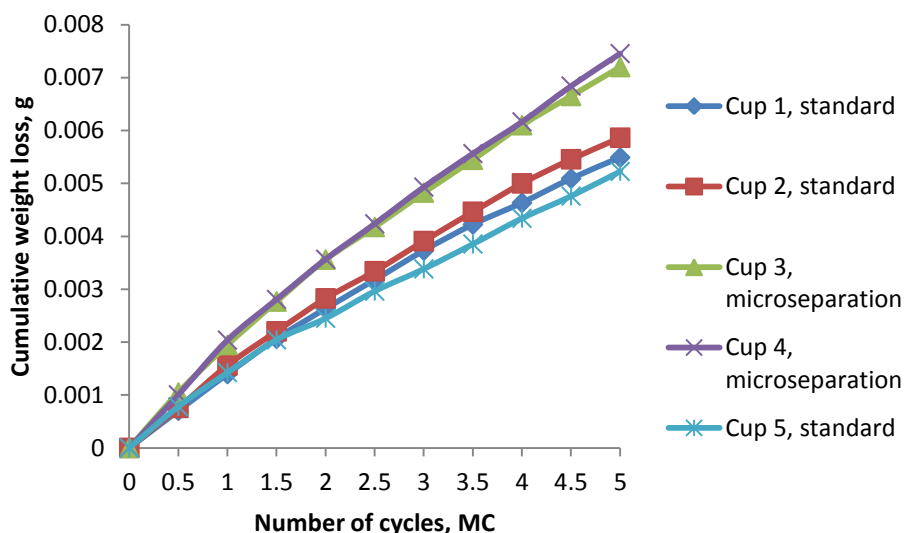


Figure 5.42: Cumulative weight loss of 60 mm CoCrMo cups under standard and microseparation conditions, accounting for the load soak.

The overall wear rate ( $\text{mm}^3/\text{MC}$ ) has been calculated for each station. The results are shown in Table 5.7. Station 2 experienced a slightly higher wear rate for both the liner and cup throughout the test. No increased wear affected the head. After 1.0 MC of testing the simulator was serviced and it was discovered that the bearing in Station 2 had become worn and had to be replaced. It is possible that this may have caused an increase in wear initially that then continued throughout the test.

Table 5.7: Wear rates based on overall test,  $\text{mm}^3/\text{MC}$ .

Station, Test Condition	28 mm CoCrMo Head	E1 Liner	60 mm CoCrMo Cup
1, Standard	0.005	0.635	0.132
2, Standard	0.003	2.146	0.141
3, Microseparation	0.042	5.146	0.170
4, Microseparation	0.048	4.973	0.175
5, Standard	0.005	1.007	0.122

All the wear rates for the 28 mm CoCrMo heads were linear ( $R^2 = 0.86 - 0.99$ ).

All the wear rates for the 60 mm CoCrMo cups were linear ( $R^2 = 0.99$ ).

All the wear rates for the E1 liners were linear ( $R^2 = 0.98 - 0.99$ ).

Student's t-test was performed for each type of component to see whether the data from the standard stations (1, 2 and 5) was statistically significantly different from the data

from the microseparation stations (3 and 4). The two sets of data will be considered to be significantly different if  $p \leq 0.05$ .

The wear data from the CoCrMo heads ( $p = 0.04$ ), E1 liners ( $p = 0.01$ ) and CoCrMo cups ( $p = 0.01$ ) were significantly different between the two test conditions.

#### 5.4.4 Surface characterisation

##### 1) Zygo non-contacting profilometry

Ten zygo images were taken at the pole and at positions  $33^\circ$  from the pole for each component in the five active stations at 0, 0.5, 1.0, 2.5 and 5.0 MC of the test. The load control and soak control were also analysed for comparison. Figure 5.43 and Figure 5.44 show the zygo data for the CoCrMo cups. Wear testing has caused the surface roughness to increase across all samples, with the greatest increase seen in the microseparation stations. The skewness also generally increased for all the cups. The error bars indicate the standard deviation of the data.

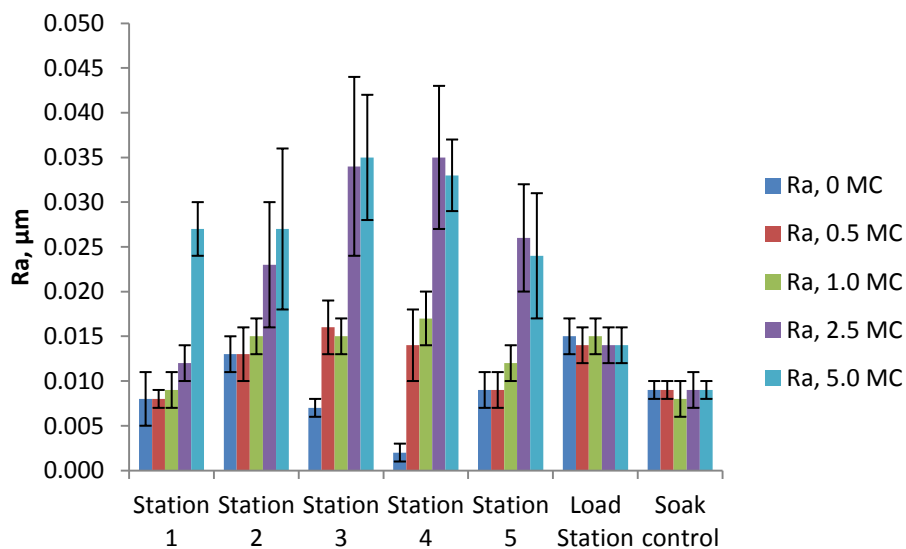


Figure 5.43: Surface roughness of 60 mm CoCrMo cups during 5.0 MC.

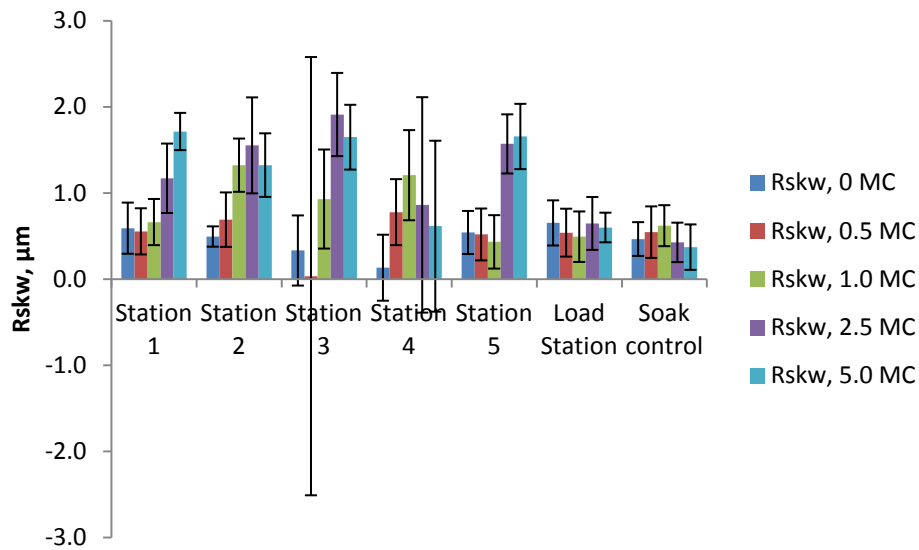


Figure 5.44: Skewness of 60 mm CoCrMo cups during 5.0 MC.

Figure 5.45 and Figure 5.46 show the zygo data for the CoCrMo heads. Surface roughness increased in three stations; station 2, 3 and 4, whilst remaining quite similar in station 5 throughout the test. In station 1 the surface roughness decreased slightly throughout the test, though the initial surface roughness was higher for this head than the others. There was little change in skewness throughout the test.

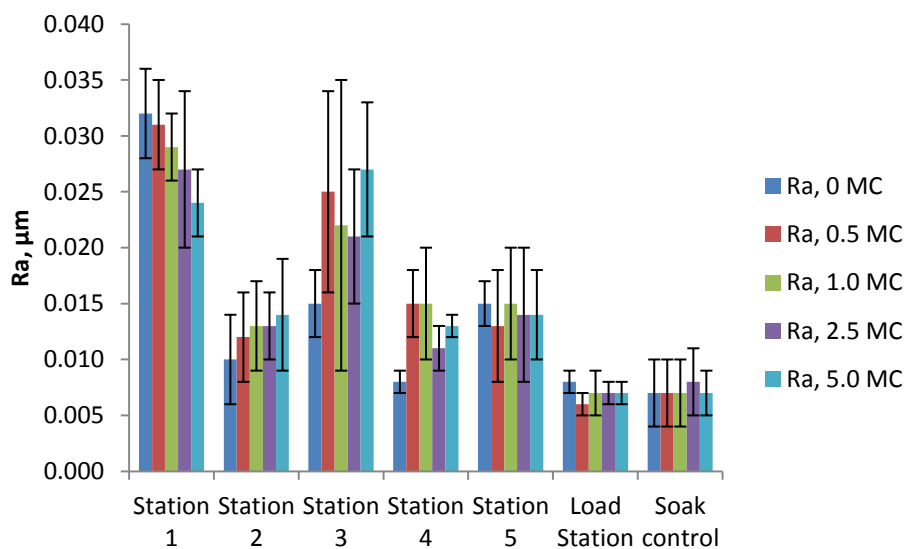


Figure 5.45: Surface roughness of 28 mm CoCrMo heads during 5.0 MC.

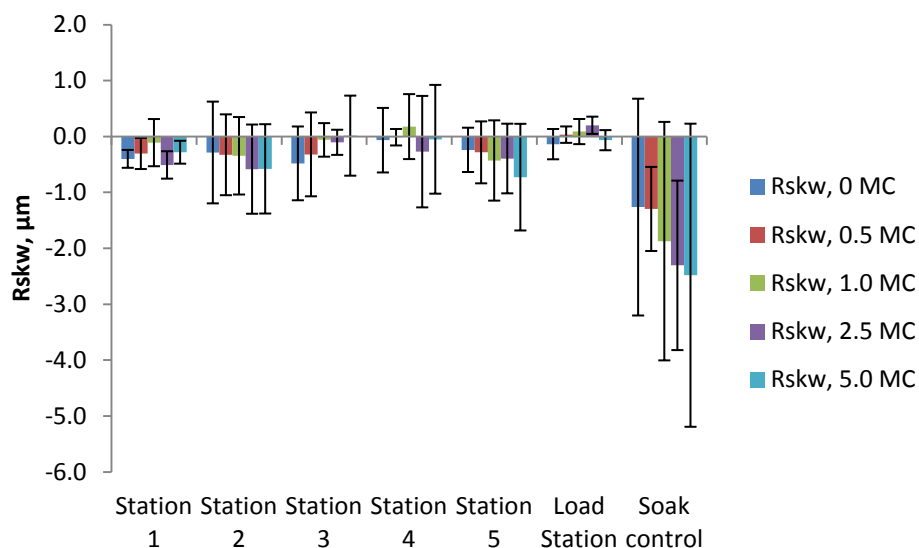


Figure 5.46: Skewness of 28 mm CoCrMo heads during 5.0 MC.

Figure 5.47 and Figure 5.48 show the zygo data for the E1 liners. The data from Stations 1, 2 and 5 has been averaged to give the standard results. The data from Stations 3 and 4 has been averaged to give the microseparation result. Surface roughness has decreased across all the liners, with a greater effect being seen for the microseparation stations. Skewness has also decreased across all liners that have undergone wear testing.

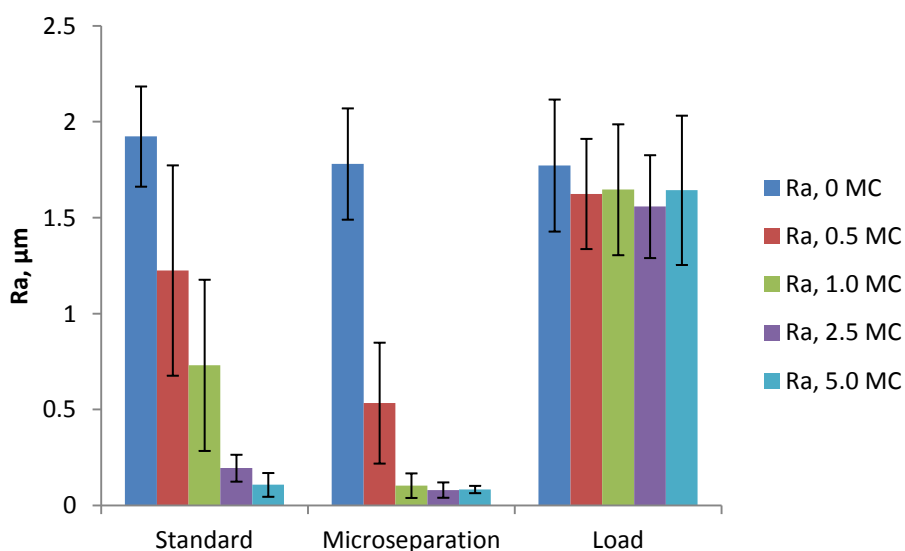


Figure 5.47: Surface roughness of E1 liners during 5.0 MC.

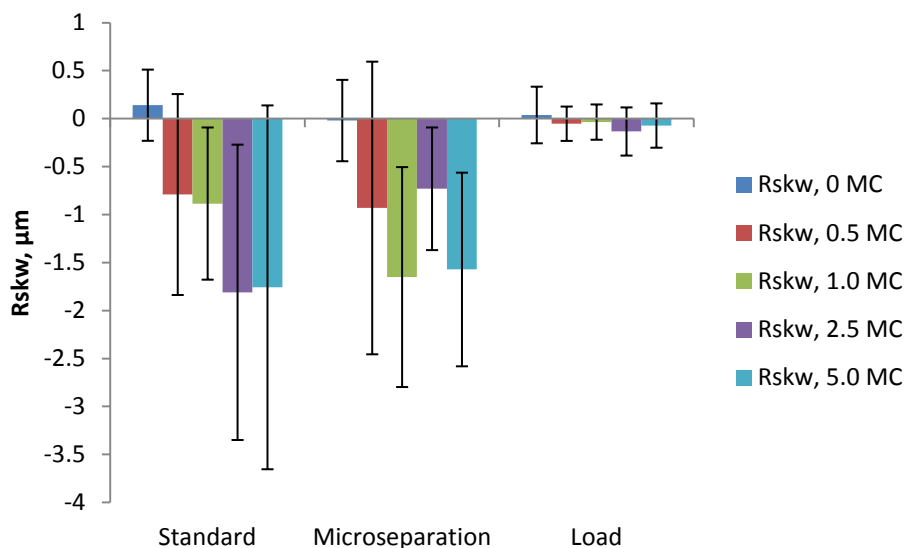


Figure 5.48: Skewness of E1 liners during 5.0 MC.

Eight additional zygo measurements were taken at 45° around the liners after 5 MC. The results are shown in Figure 5.49. As before, the data from Stations 1, 2, and 5 were averaged to give the result for the standard stations. The data from Stations 3 and 4 were averaged to give the result for the microseparation stations. The surface roughness of the liners in the microseparation stations have decreased more than those in the standard stations, and the skewness has also decreased. Figure 5.50 shows the 3D surface profiles of the E1 liners. The surface topography is smoother in each liner that has undergone wear testing, and surface roughness is the least in liners 3 and 4 that were tested under microseparation conditions. For these stations the manufacturing streaks have been removed, whilst they are still visible in the standard stations and the control liner.

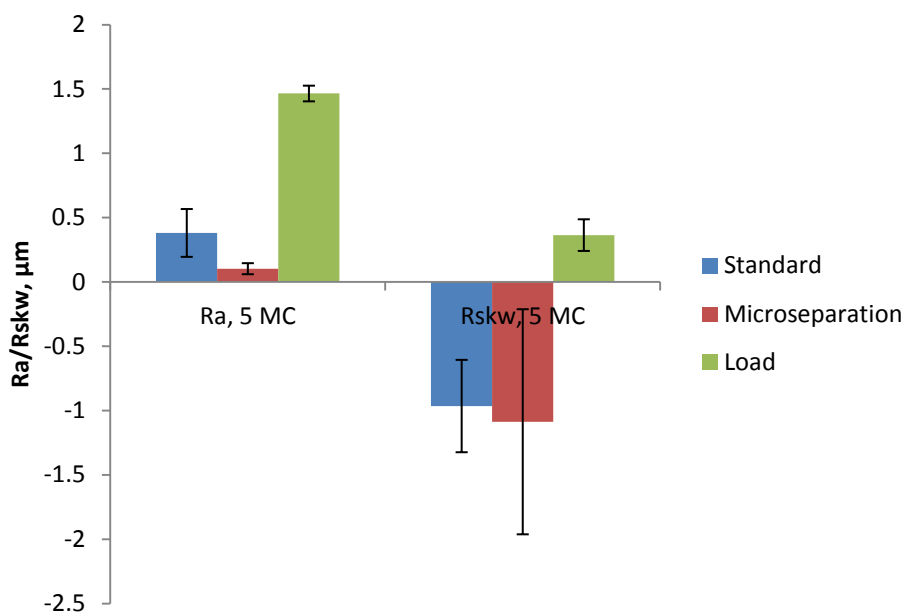


Figure 5.49: Additional data for surface roughness and skewness at 45° around E1 liners.

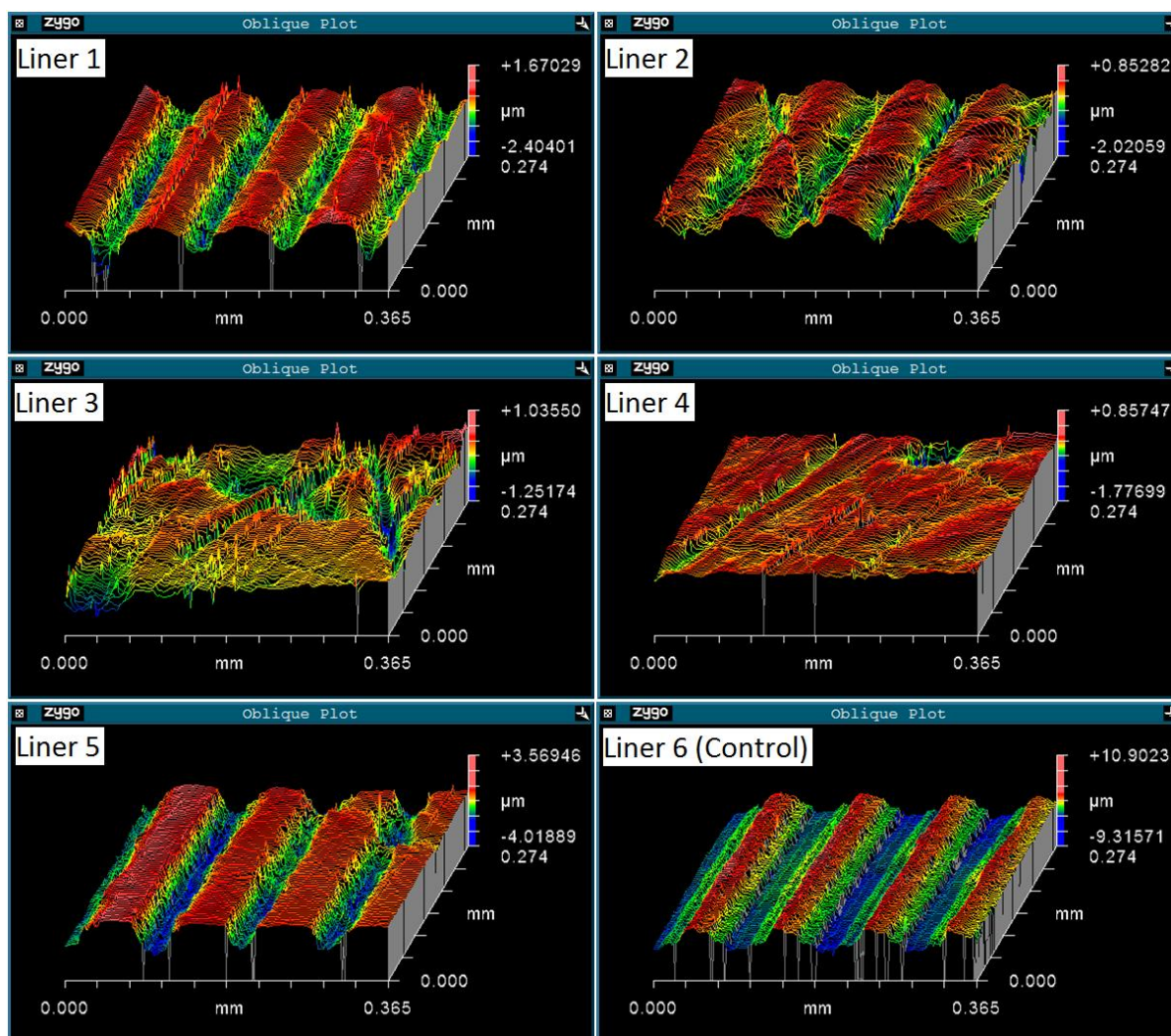


Figure 5.50: Surface profiles of E1 liners imaged after 5 MC at 45 °.

## **2) Optical microscopy**

The following images were taken with an Axiotech optical microscope. Figure 5.51 shows the inner pole of after 0.5 MC for all liners, liner 6 acts as the control because it has only been subject to loading. Figure 5.52 shows corresponding data for the outer pole. The difference between these two figures highlight that the inner articulation experiences greater wear than the outer articulation. In Figure 5.52 it can be seen that only in the microseparation stations were the manufacturing streaks removed. They are partially visible in liner 2, whilst liner 1 and 5 were worn much less, reflecting the wear data for the three standard stations where the cup and liner had worn more in station 2 suggesting that the outer articulation had experienced greater wear.

Figure 5.53 shows the inner pole of the E1 liners after 2.5 MC in comparison to the load soak control, whilst Figure 5.54 shows the outer poles at the same stage of the test. Figure 5.54 shows that after 2.5 MC of wear testing, only in liner 1 are the manufacturing streaks on the outer pole still partially visible. This also correlates with the wear data which showed that liner 1 had the lowest wear rate. Figure 5.55 and Figure 5.56 show the inner and outer poles respectively at the end of the test after 5 MC.

Figure 5.56 shows the outer poles of each liner after 5MC and that the manufacturing streaks have been removed from each liner that has undergone wear testing. From further inspection of all the optical data taken at each 0.5 MC interval throughout the test, the manufacturing streaks were completely removed from the outer pole of the liners in the microseparation stations after 0.5 MC, and removed from the standard stations after 4.0 MC. This shows that the outer articulation is engaged more under microseparation conditions.

In direct comparison, the manufacturing streaks from the inner poles were removed from all liners within 0.5 MC, showing that the inner articulation experiences greater wear than the outer articulation.

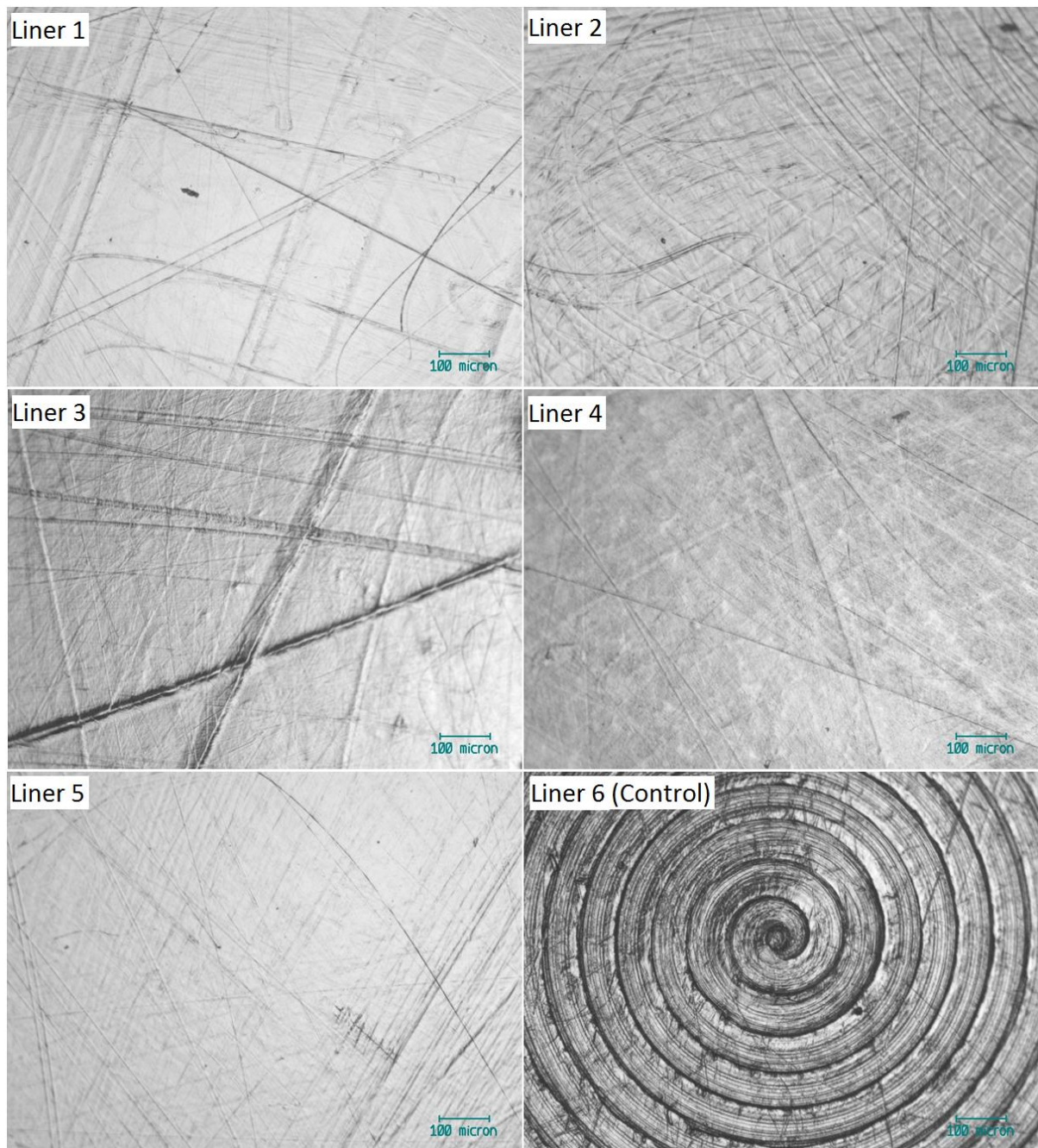


**Figure 5.51: Inner pole of E1 liners after 0.5 MC.**

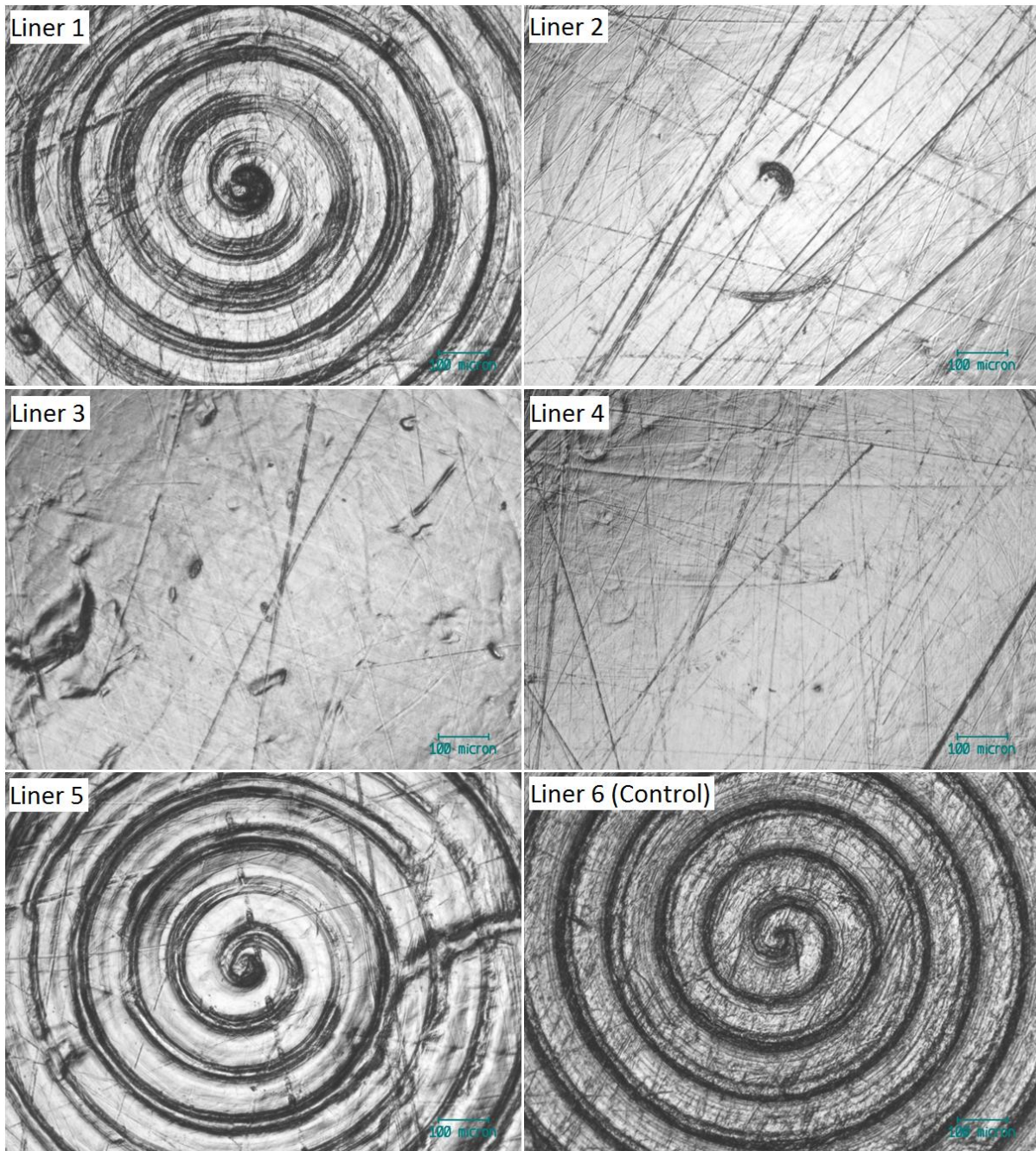
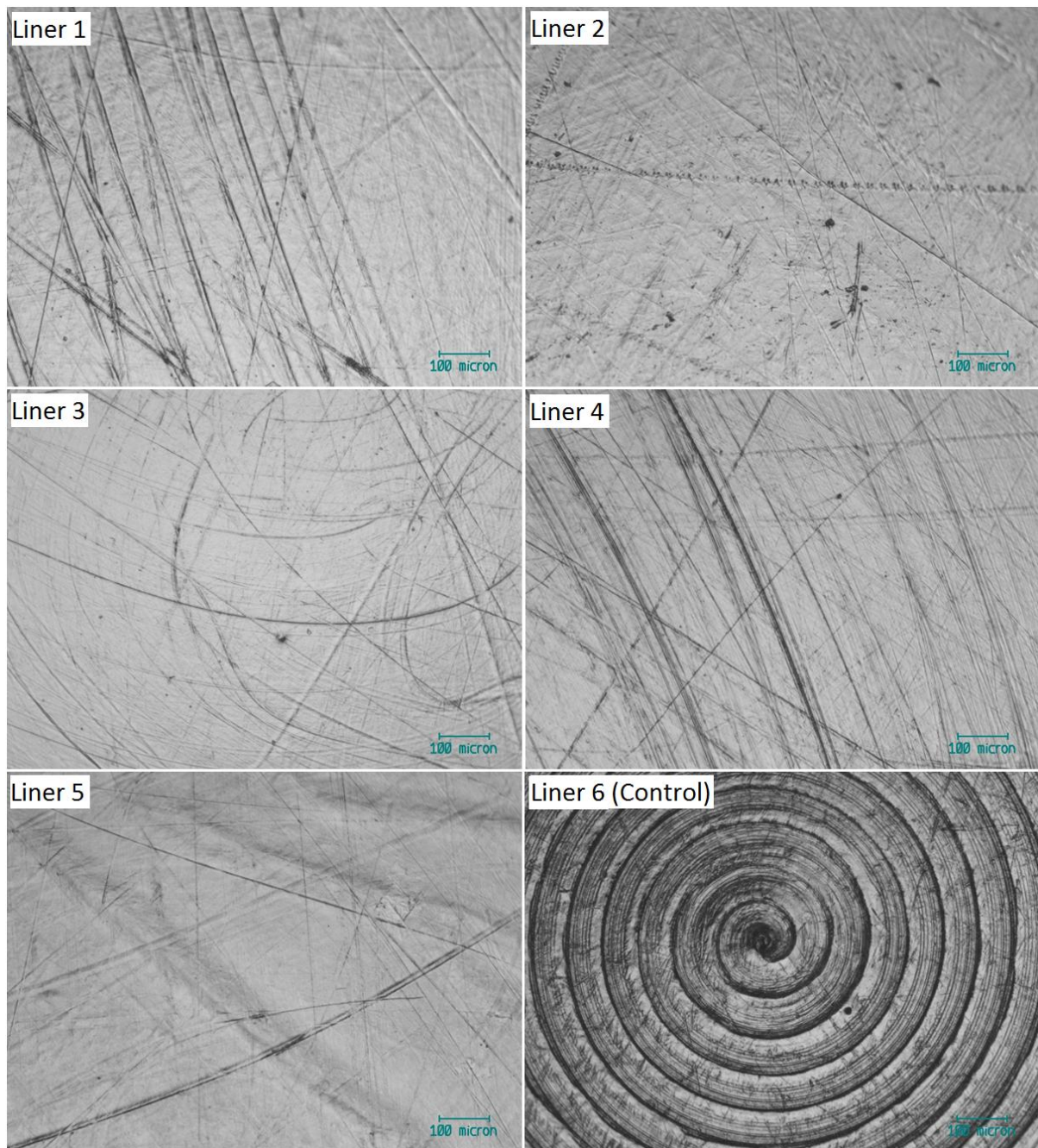


Figure 5.52: Outer pole of E1 liners after 0.5 MC.



**Figure 5.53: Inner pole of E1 liners after 2.5 MC.**

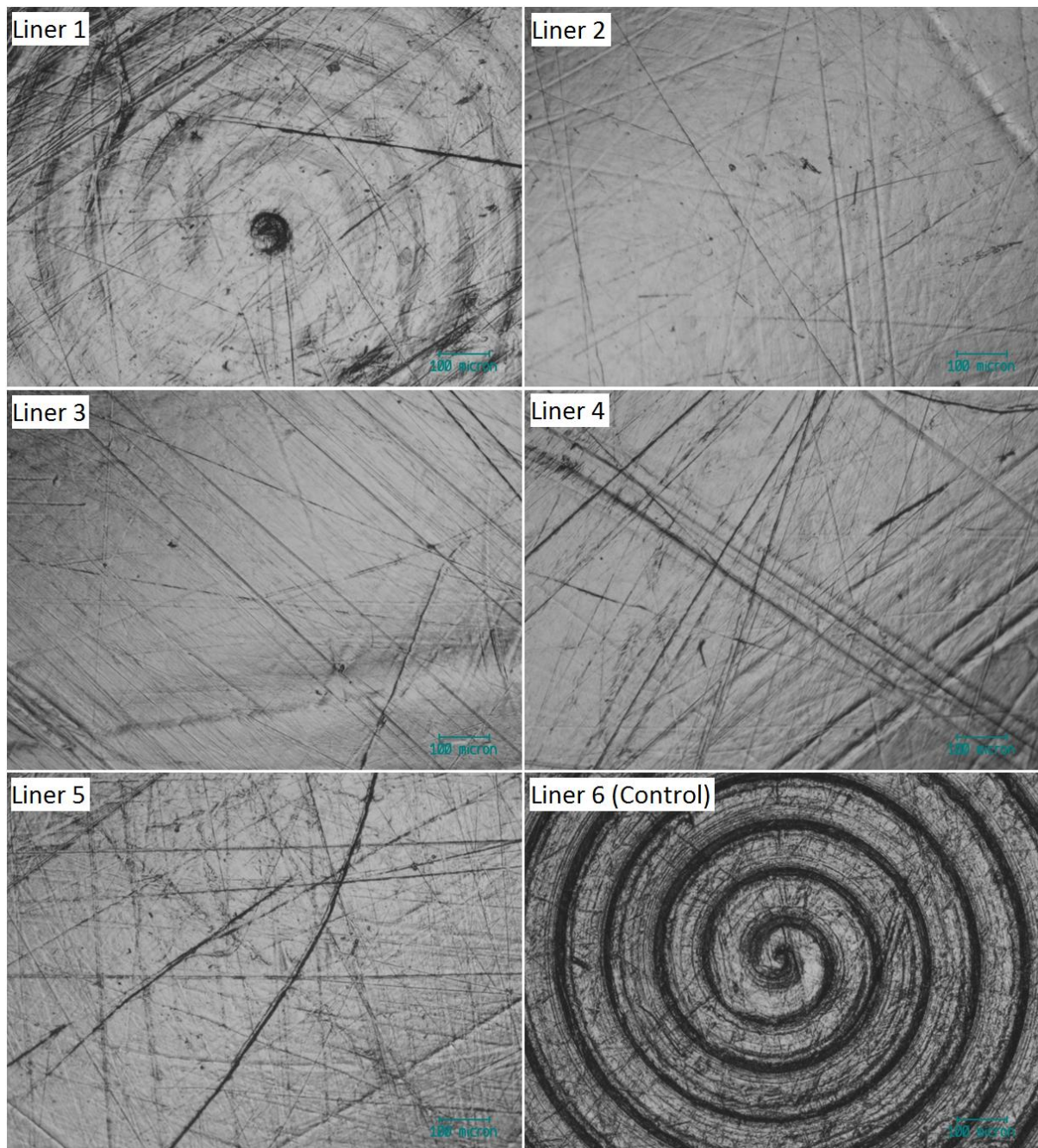
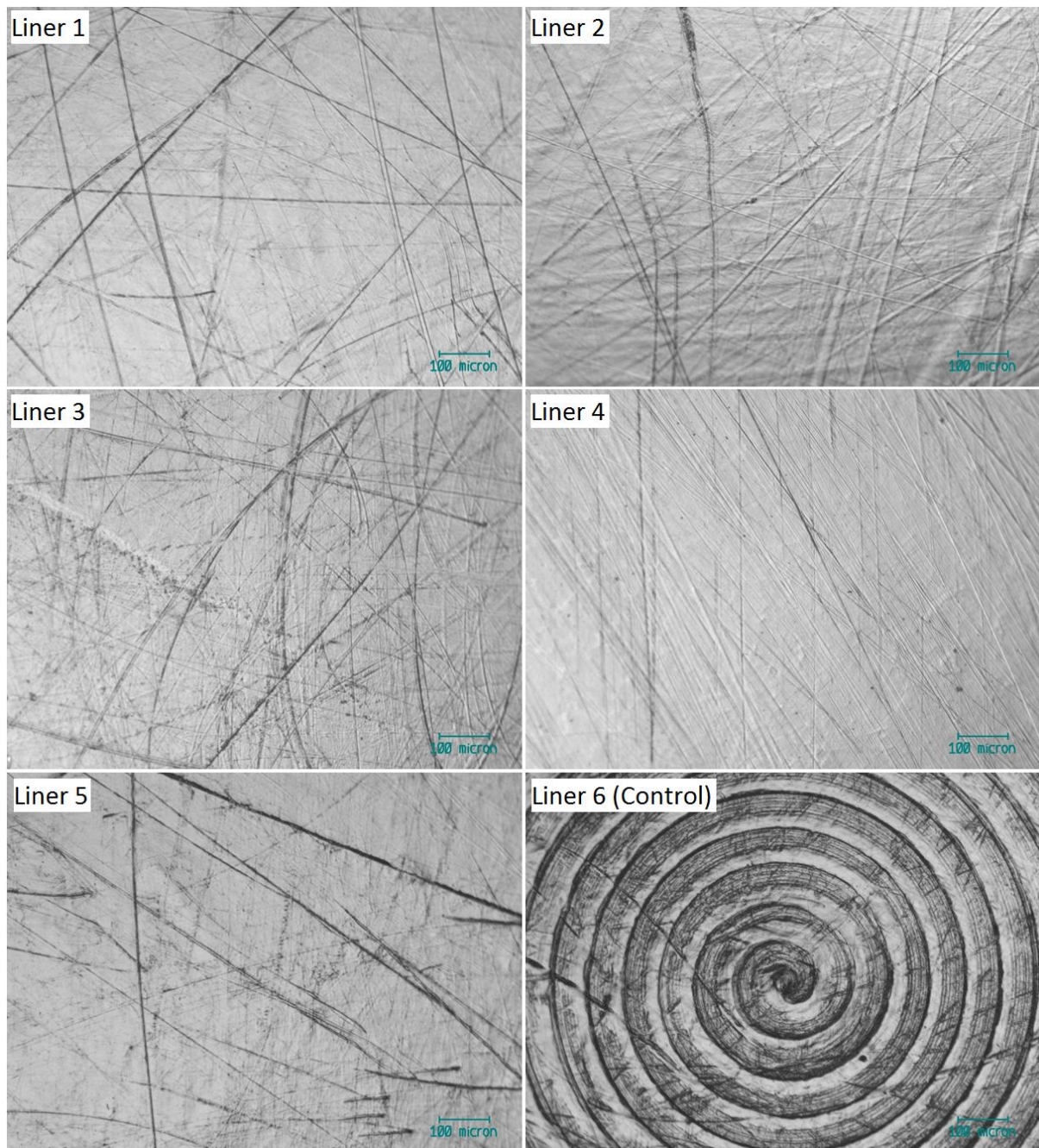
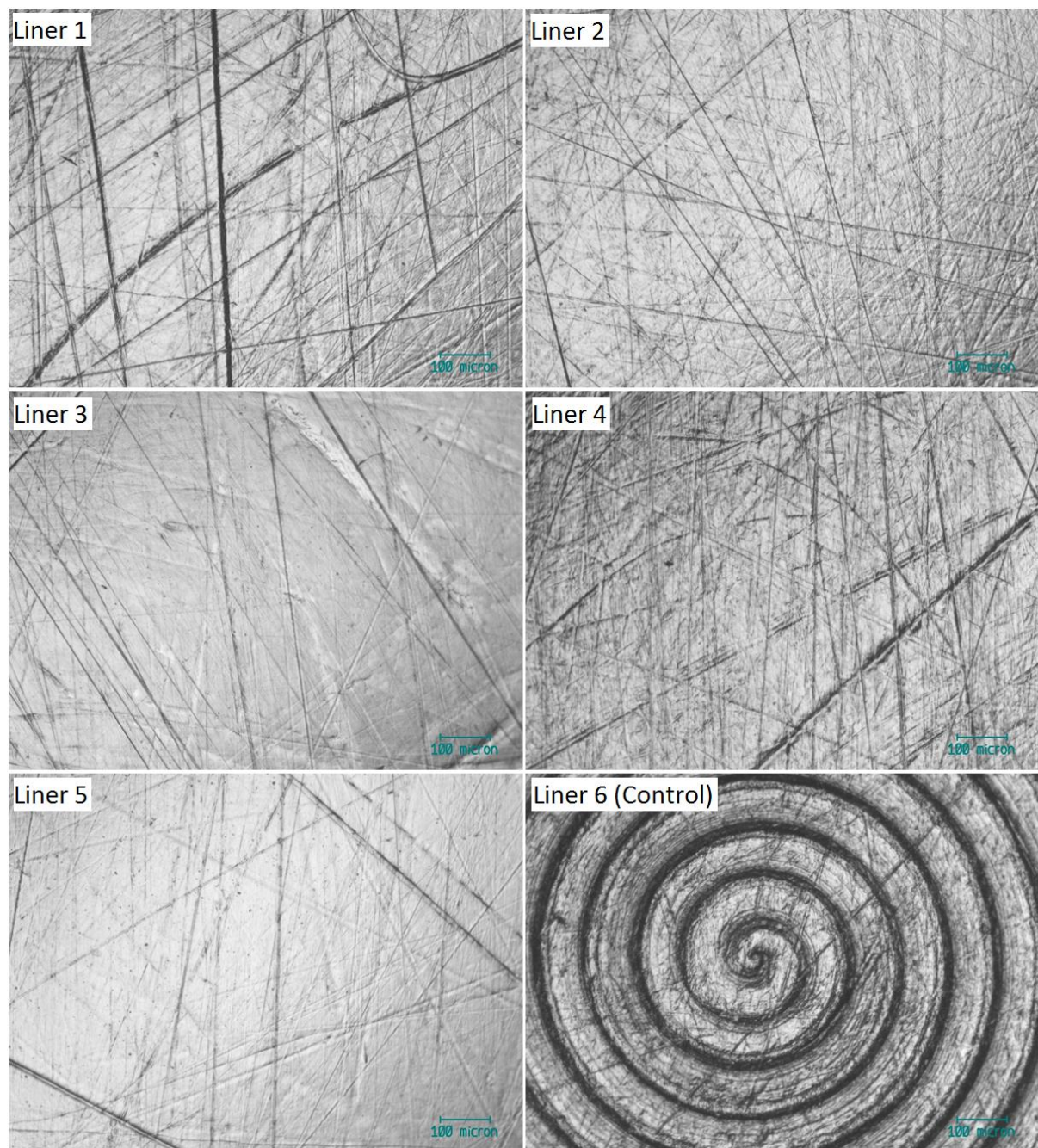


Figure 5.54: Outer pole of E1 liners after 2.5 MC.



**Figure 5.55: Inner pole of E1 liners after 5.0 MC.**



**Figure 5.56: Outer pole of E1 liners after 5.0 MC.**

Figure 5.57 and Figure 5.58 look at the 28 mm CoCrMo heads after 1.0 MC and 5.0 MC respectively.

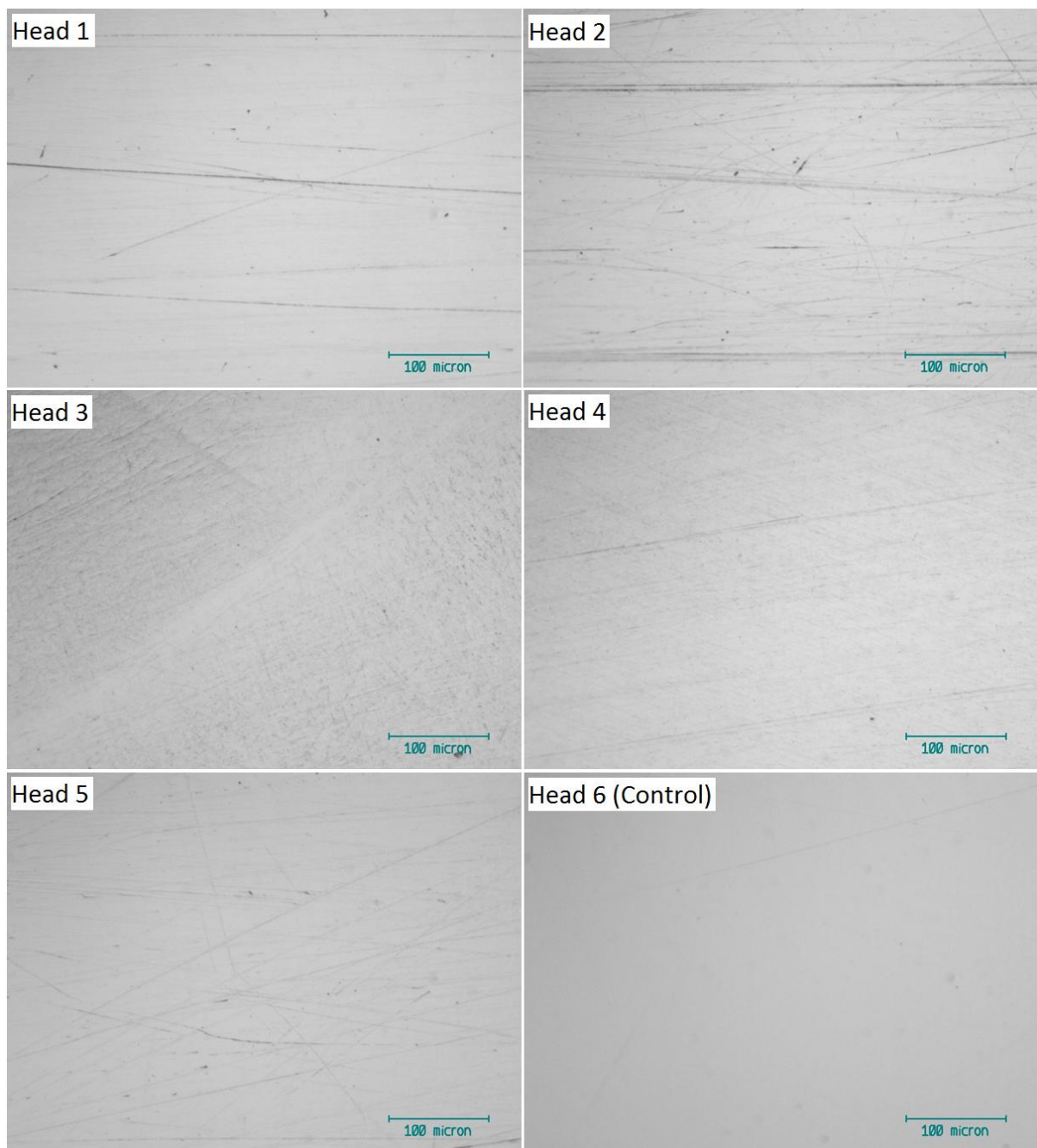
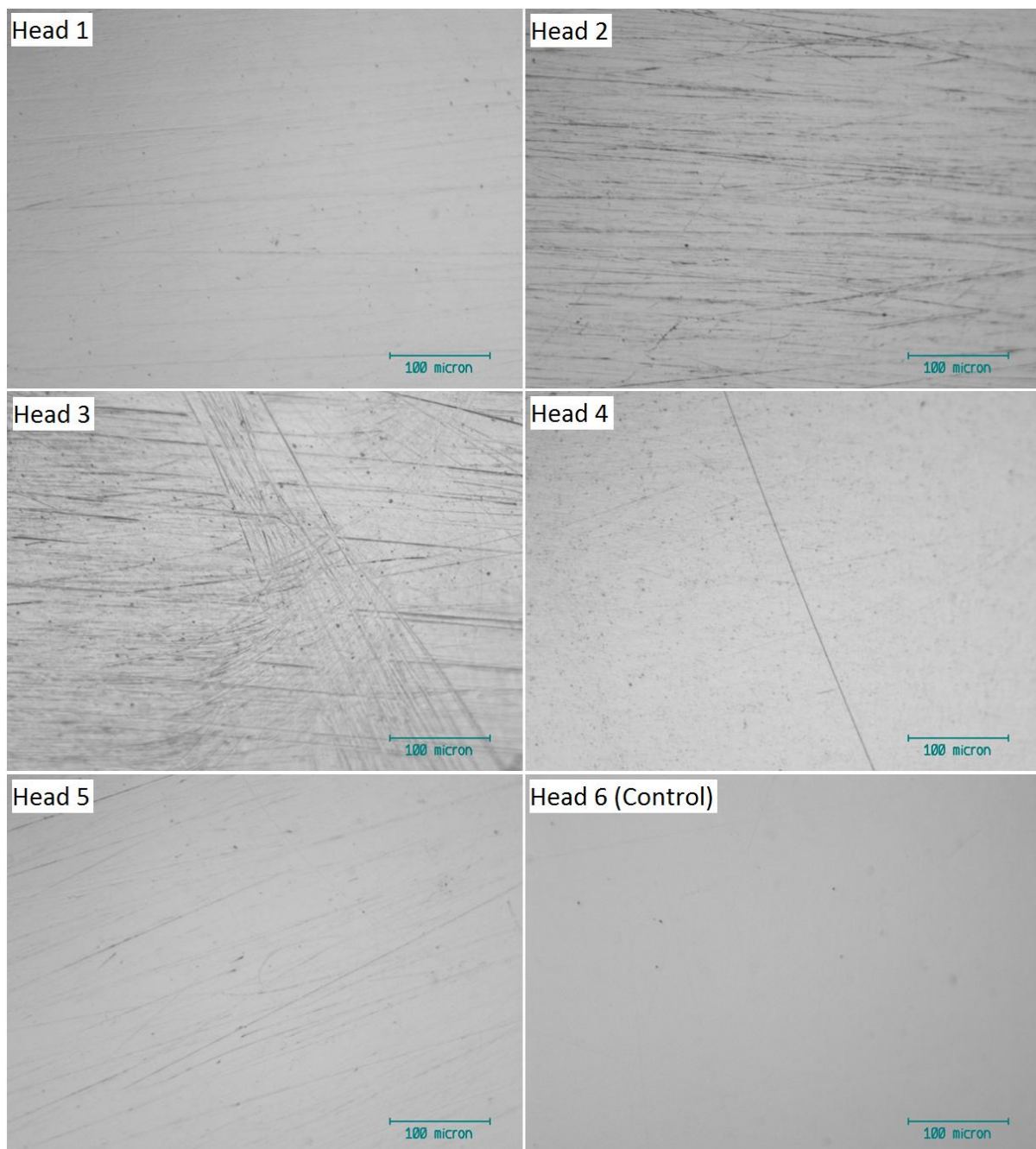
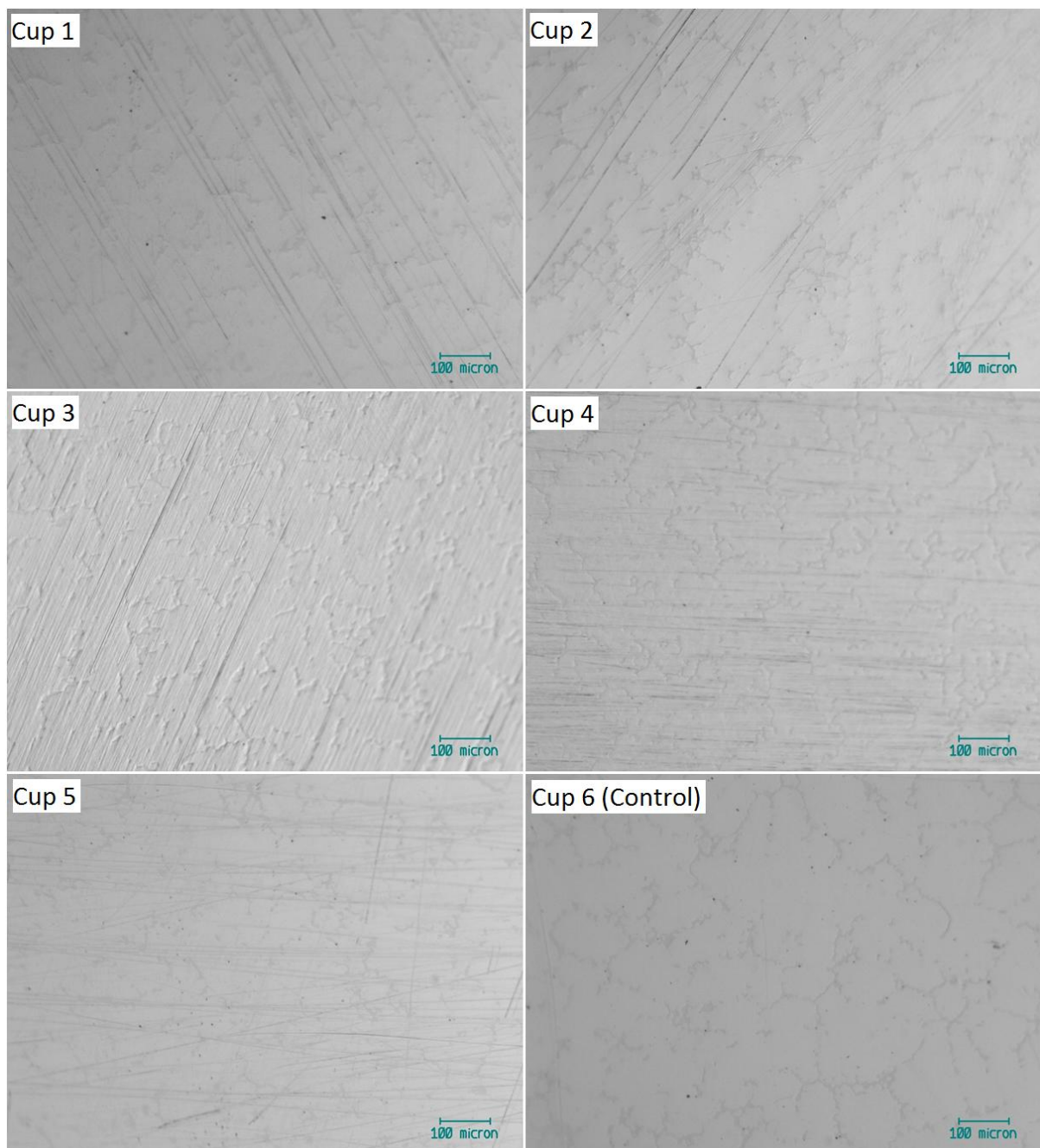


Figure 5.57: Pole of 28 mm CoCrMo heads after 1.0 MC.



**Figure 5.58: Pole of 28 mm CoCrMo heads after 5.0 MC.**

The optical images show that each metal head has experienced light scratching throughout the test. The same was seen in the CoCrMo cups, which also experienced light scratching. Figure 5.59 and Figure 5.60 show images taken within the wear patch of each CoCrMo cup after 1.0 and 5.0 MC respectively.



**Figure 5.59: Optical images taken within the wear patch of 60mm CoCrMo cups after 1.0 MC.**

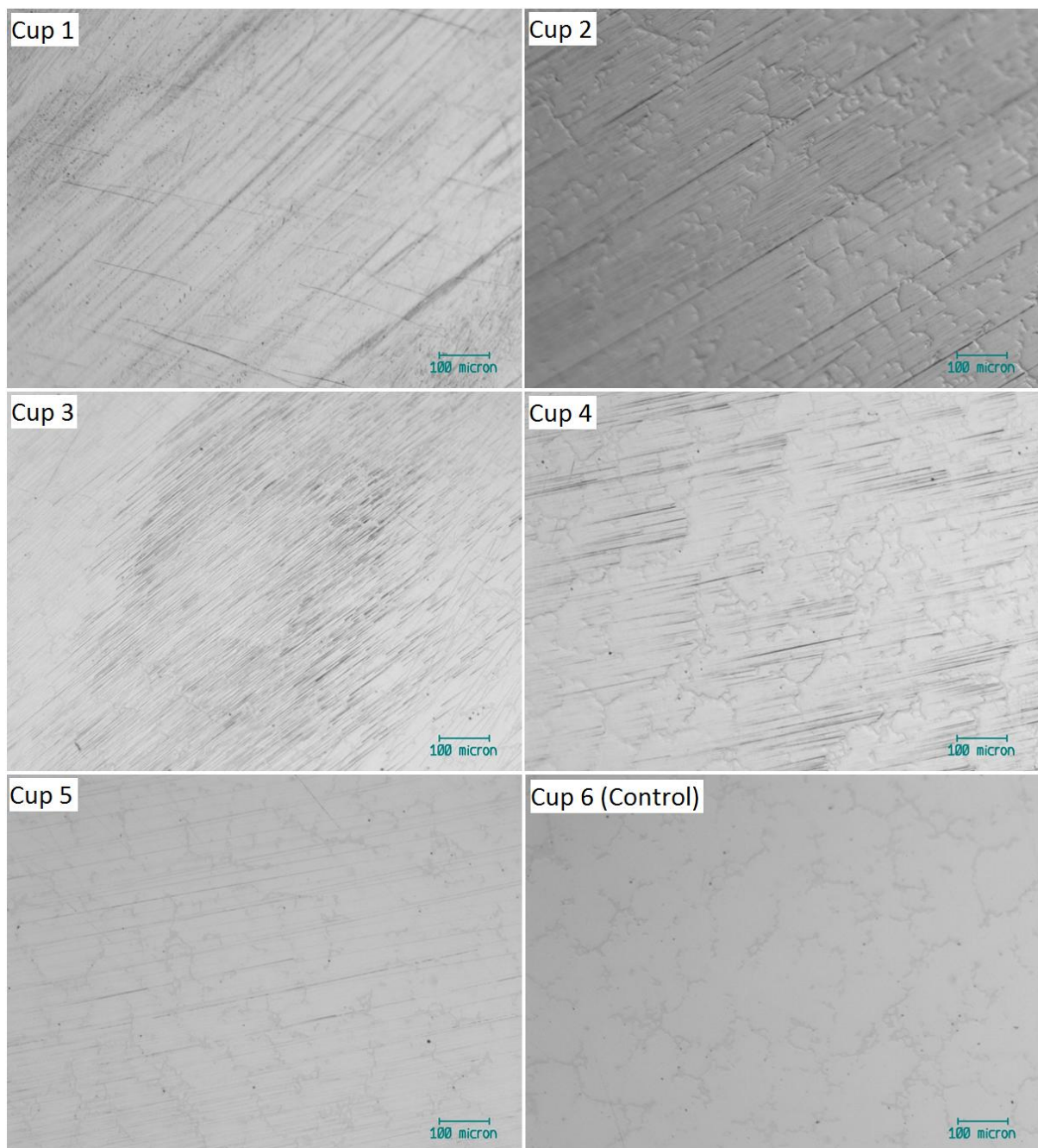


Figure 5.60: Optical images taken within the wear patch of 60mm CoCrMo cups after 5.0 MC.

### 3) Environmental scanning electron microscopy

All liners that have undergone testing have experienced wear around the liner rim. ESEM has been used to track the wear throughout the test. Figure 5.61 shows the wear around the liner rim at 1.0 MC, while Figure 5.62 shows the wear after 5.0 MC.

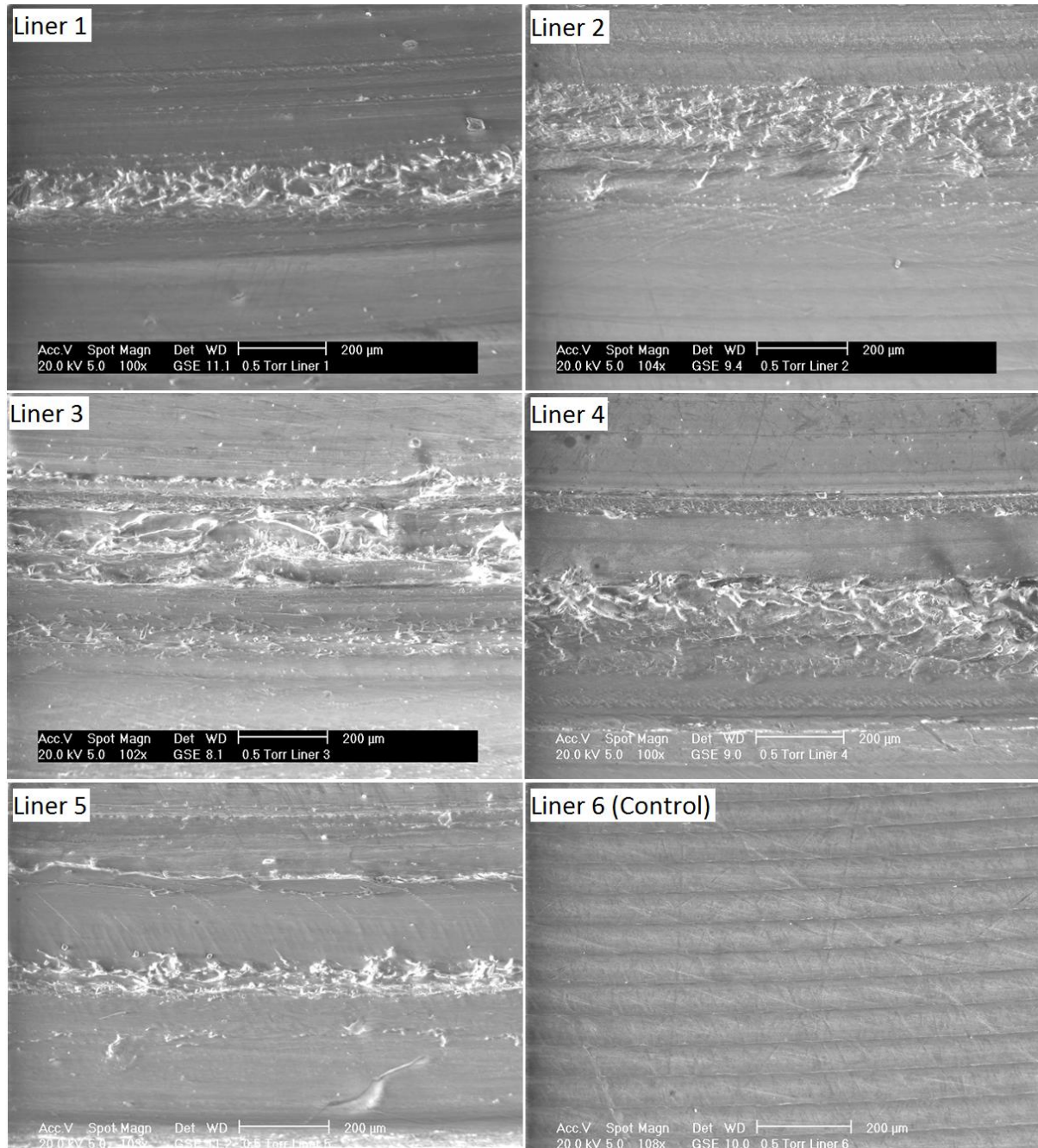


Figure 5.61: ESEM images taken around the E1 liner rim at 1.0 MC.

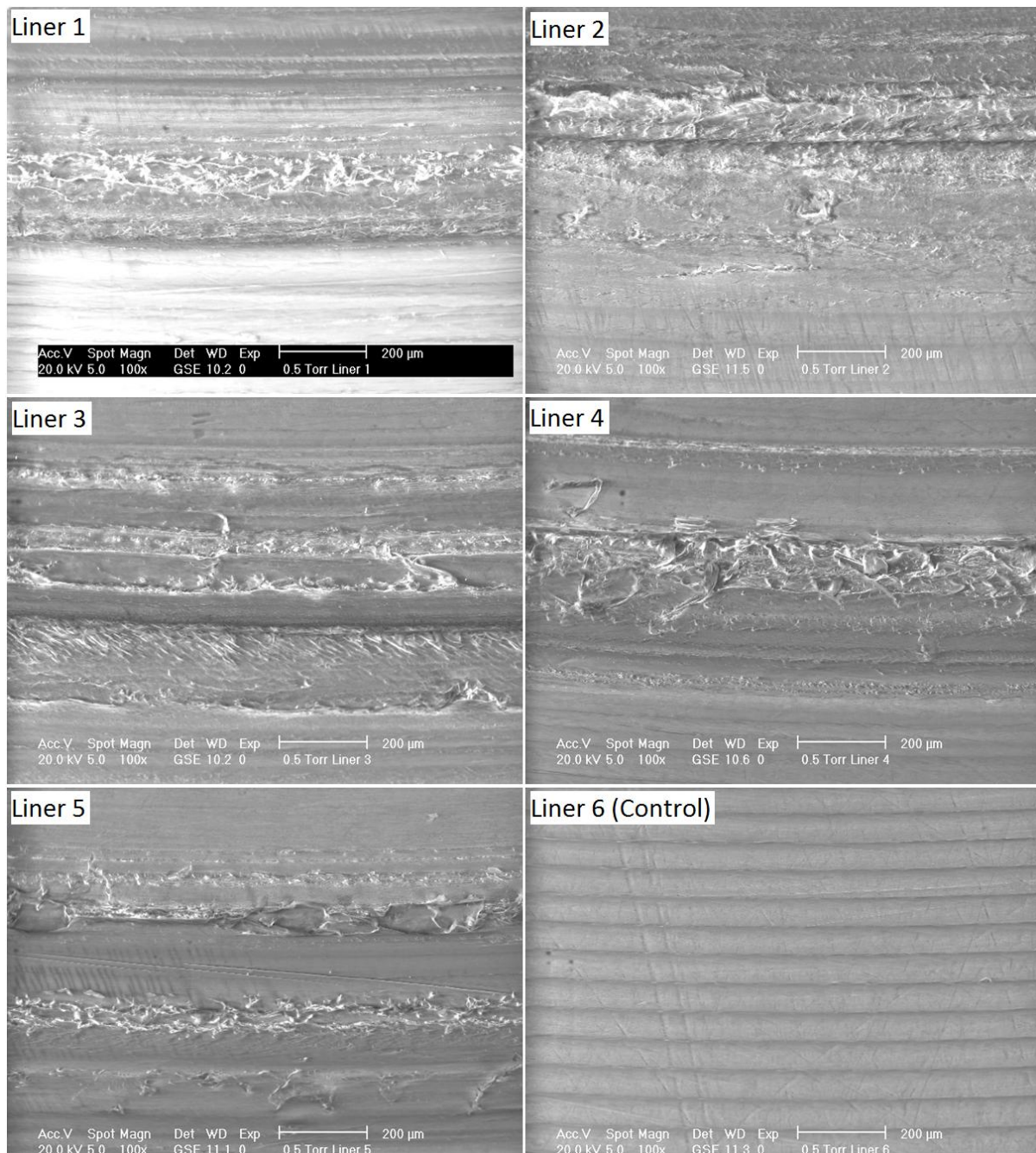


Figure 5.62: ESEM images taken around the E1 liner rim at 5.0 MC.

### 5.4.5 Limitations

The limitations encountered during DM Test 2 are those that are common in testing dual mobility joints. The dual mobility joint provides three potential surfaces for wear debris production:

1. The inner articulation from movement between the CoCrMo head and the inner pole of the E1 liner.

2. The outer articulation from movement between the outer pole of the E1 liner and the CoCrMo cup.
3. The liner rim from interaction between the head stem and the rim of the E1 liner.

It has not been possible during this study to quantify the amount of wear attributed to each articulation, only the total volume loss for each component has been calculated. However the differences between these surfaces during testing have been explored qualitatively as much as possible using zygo, optical and SEM analysis.

The only bearing surface which could not be analysed using zygo profilometry was the inner pole of the E1 liner. This was due to size restrictions.

#### **5.4.6 Discussion**

Perhaps unexpectedly, all components in this test have experienced greater wear than in DM Test 1 despite the fact that the cups used were unworn prior to testing. A notable difference between these two tests is the difference in the zygo and optical data for the CoCrMo cups and E1 liners.

Whereas in DM Test 1 the surface roughness only slightly fluctuated for the cups throughout the test, the cups in this test witnessed an increase in surface roughness. This was accompanied by the E1 liners becoming much smoother. The optical images evidenced that the manufacturing streaks were removed from the pole of the liners in all five active stations after 5 MC, whereas in DM Test 1 the manufacturing stations had been removed from the microseparation stations only.

All zygo data has been thoroughly analysed in order to explain why this has happened.

Initially the zygo data of all cups in DM Test 2 showed the presence of carbides protruding from the surface. As the test continued the zygo data indicated an increase in both surface roughness as well as skewness for the CoCrMo cups.

From further inspection of the line plots across the surface of the cups, it is clear that material from the metal matrix has been removed during wear testing. This has caused the carbides to protrude increasingly higher above the metal surface.

Figure 5.63 shows zygo data about the surface profile from cup 1 prior to testing that is representative of each cup in the test. The carbides can be seen to protrude roughly 0.02  $\mu\text{m}$  from the surface.

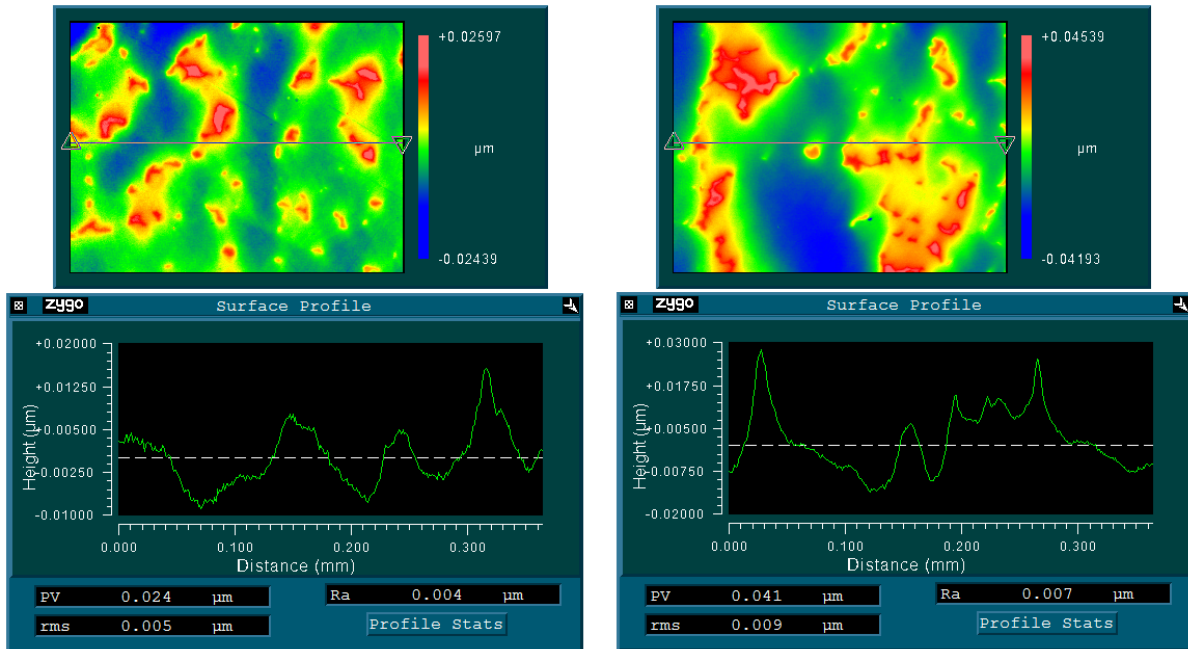


Figure 5.63: Zygo data from Cup 1 at 0 MC showing the 2D plot and the corresponding line profile of the surface.

In comparison, Figure 5.64 shows the profile of cup 1 at the end of the test, where the height of the carbides has increased to approximately 0.15  $\mu\text{m}$ .

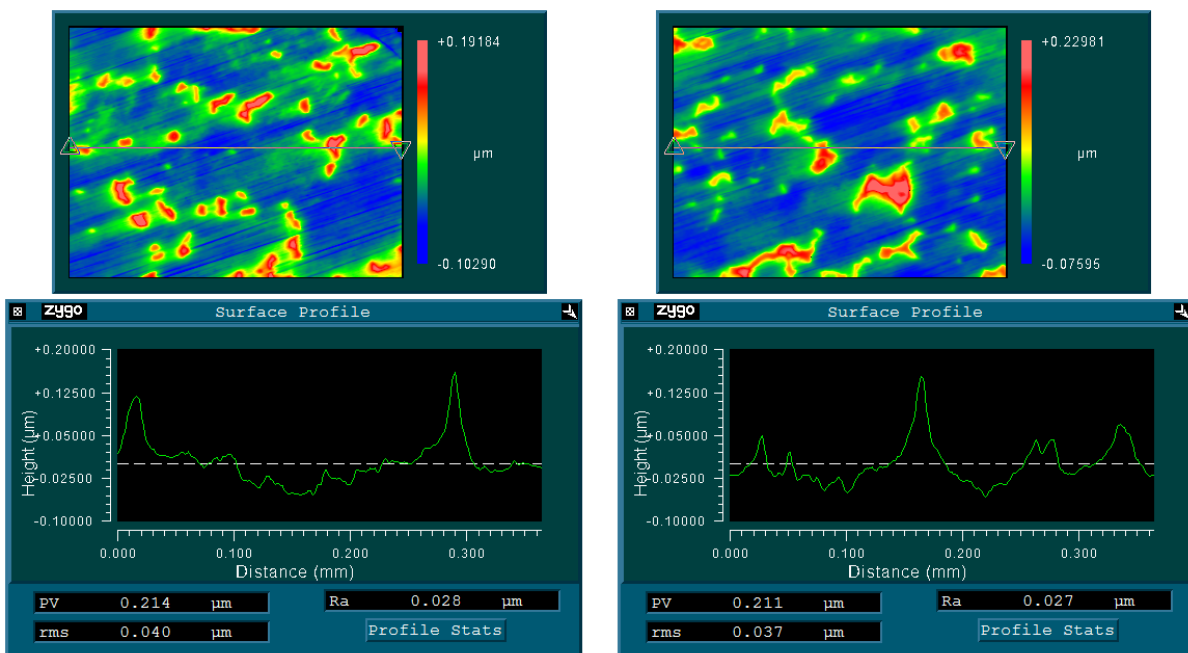


Figure 5.64: Zygo data from Cup 1 after 5 MC showing the 2D plot and corresponding line profile of the surface.

The increased height of the carbide asperities will have caused an increase in wear of the E1 liners and explains why the liners have experienced greater mass loss, removal of manufacturing streaks from the pole and reduction in both surface roughness and skewness during DM Test 2.

This effect was not so apparent in DM Test 1 where the carbides in the worn cups had already been smoothed or removed during MOM Test 1 prior to testing against the dual mobility heads.

### **5.4.7 Conclusion**

Five dual mobility heads, consisting of a 28 mm CoCrMo head and an E1 liner with an inner diameter of 28 mm, outer diameter 60 mm have been tested against unworn 60 mm CoCrMo cups. The 28 mm heads were sectioned to allow removal from the E1 liner for cleaning throughout the test.

Over 5 MC of testing, under either standard or microseparation conditions at a high incline, the wear rates of the 28 mm CoCrMo heads ranged from 0.003 to 0.048 mm<sup>3</sup>/MC. The wear rates of the E1 liners ranged from 0.635 to 5.146 mm<sup>3</sup>/MC. The wear rates of the 60 mm CoCrMo cups ranged from 0.122 to 0.175 mm<sup>3</sup>/MC.

Surface roughness generally increased throughout the test for the CoCrMo heads and CoCrMo cups. Surface roughness has decreased across all the liners, and is smoothest in the liners that were subject to testing under microseparation conditions.

Optical images show slight scratching on the CoCrMo heads and CoCrMo cups during the test. Optical images taken from each E1 liner from the inner and outer pole indicate that the inner articulation experienced greater wear than the outer articulation. They also show that the outer articulation experienced greater wear under microseparation conditions than under standard wear testing conditions. Circumferential abrasion was experienced in each E1 liner in the test.

### 5.5 DM Test 3: aggressive biotribological study with worn CoCrMo cups from MOM Test 2

This simulation articulates the worn cups from the third body simulation in MOM Test 2 against a dual mobility head consisting of the same 28 mm CoCrMo heads that were used in Dual Mobility Test 2, with unworn E1 liners with an inner diameter of 28 mm, outer diameter 60 mm. Three stations operated under standard conditions; two stations under microseparation conditions. All testing was carried out with the cups positioned at 62° (high inclination angle). In addition to this there was also a loaded soak control and a soak control under no loading which was left at room temp throughout the test.



Figure 5.65: 28 mm CoCrMo head, E1 liner, 60 mm CoCrMo cup.

#### 5.5.1 Joint replacement clearance

The two articulations considered in this test are the inner articulation, between the 28 mm CoCrMo femoral head and the E1 liner, and the outer articulation, between the E1 liner and the 60 mm CoCrMo cup. The chosen combinations are shown in Table 5.8 and Table 5.9.

Table 5.8: Inner clearance of dual mobility components.

	Head	Batch ID	Liner	Batch ID	Clearance, $\mu\text{m}$
<b>Station 1</b>	2	163662	13	P0561E66	182
<b>Station 2</b>	3	163662	20	P0561E66	178
<b>Station 3</b>	4	163662	15	P0561E66	184
<b>Station 4</b>	7	163662	14	P0561E66	190
<b>Station 5</b>	9	163662	17	P0561E66	180
<b>Load Station</b>	6	163662	6	P0561E66	112
<b>Soak control</b>	8	163662	16	P0561E66	229

**Table 5.9: Outer clearance of dual mobility components.**

	<b>Cup</b>	<b>Batch, Batch ID</b>	<b>Liner</b>	<b>Batch ID</b>	<b>Clearance, <math>\mu\text{m}</math></b>
<b>Station 1</b>	49	2410667, 3	13	P0561E66	320
<b>Station 2</b>	44	2410666, 3	20	P0561E66	297
<b>Station 3</b>	46	2410666, 5	15	P0561E66	297
<b>Station 4</b>	50	2410667, 4	14	P0561E66	299
<b>Station 5</b>	52	2410667, 6	17	P0561E66	302
<b>Load Station</b>	40	2410665, 4	6	P0561E66	325
<b>Soak control</b>	47	2410667, 1	16	P0561E66	304

The mean inner radial clearance across the active samples was 183  $\mu\text{m}$ . The mean inner radial clearance across the load soak was 112  $\mu\text{m}$  and only the soak had a larger clearance. The mean outer radial clearance across the active samples was 303  $\mu\text{m}$ , and 306  $\mu\text{m}$  across all samples including the load soak and soak control.

### 5.5.2 Soaking data

As in the previous dual mobility tests, the five E1 liners selected for use in the active stations were soaked in serum at 37 °C for five weeks prior to testing. The load control and soak control liners were the same liners that were used in Dual Mobility Test 2. The cleaning and weighing procedures were carried out for the active E1 liners at the same frequency as that used during simulator wear testing. Figure 5.66 shows the weight data for the active E1 liners over 5 weeks prior to testing. Soaking had little effect on the surface roughness data as shown in Figure 5.67.

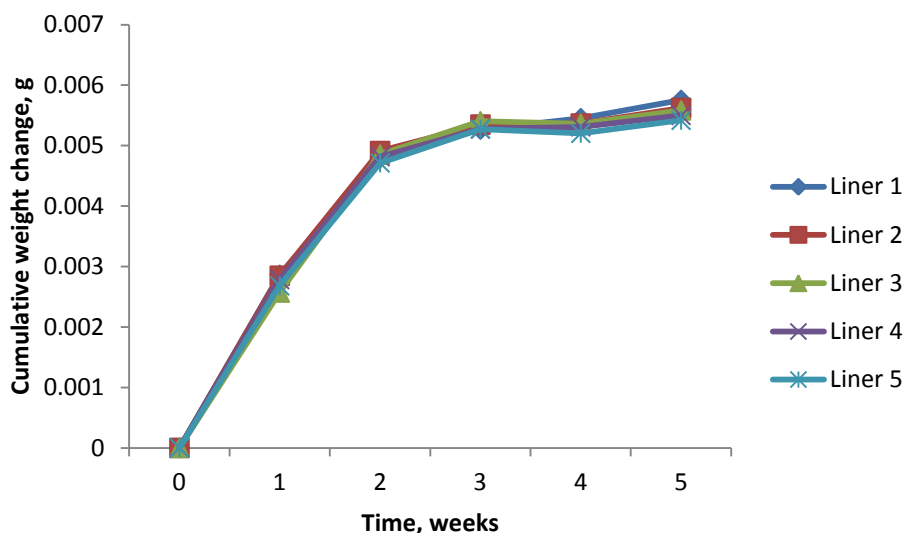


Figure 5.66: Cumulative weight change of E1 liners during soaking over 5 weeks prior to the wear simulation.

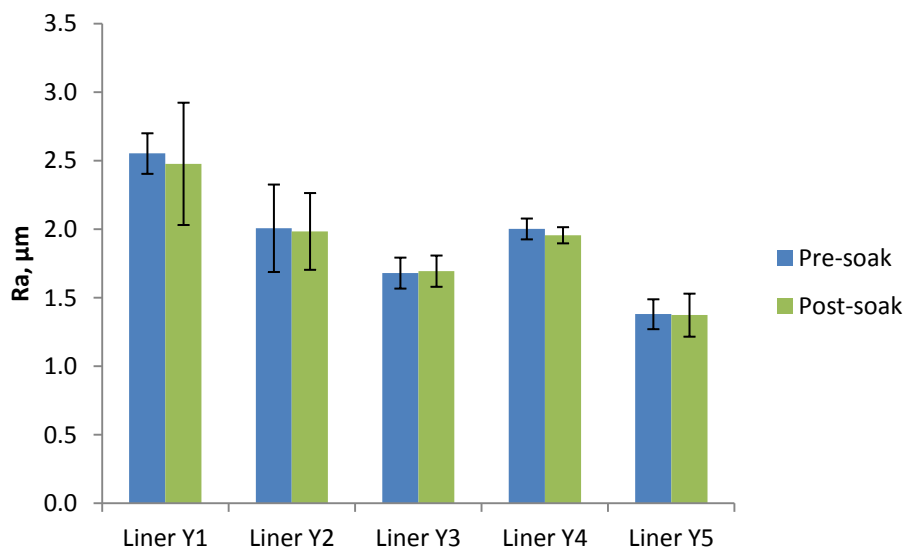


Figure 5.67: Surface roughness of E1 liners prior to test, before and after soaking.

### 5.5.3 Wear results

The test consisted of five active stations, three set up under standard conditions and two under microseparation. In addition to this, there was a loaded soak control, and a soak control under no loading.

The mass loss of each component was corrected by the change of the load soak to account for fluctuations in mass measurements over the test. The cumulative weight

loss after 5 MC from the 28 mm CoCrMo heads, E1 liners and 60 mm CoCrMo cups are shown in Figures 5.68-5.70.

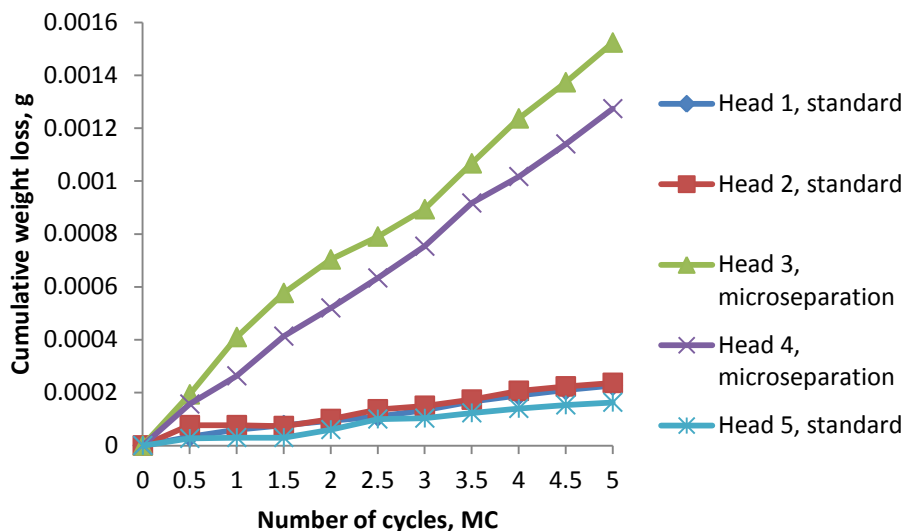


Figure 5.68: Cumulative weight loss of 28 mm CoCrMo heads under standard and microseparation conditions, accounting for the load soak.

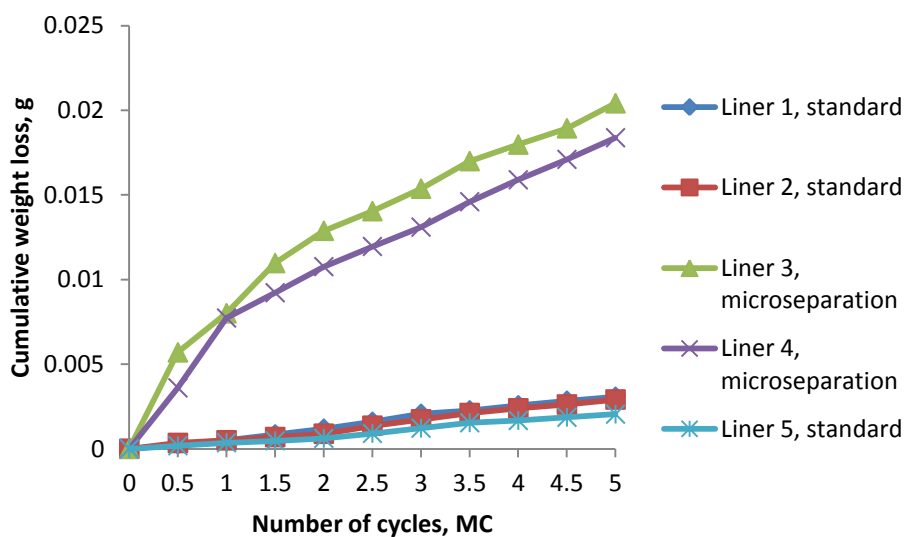


Figure 5.69: Cumulative weight loss from E1 liners under standard and microseparation conditions, accounting for the load soak.

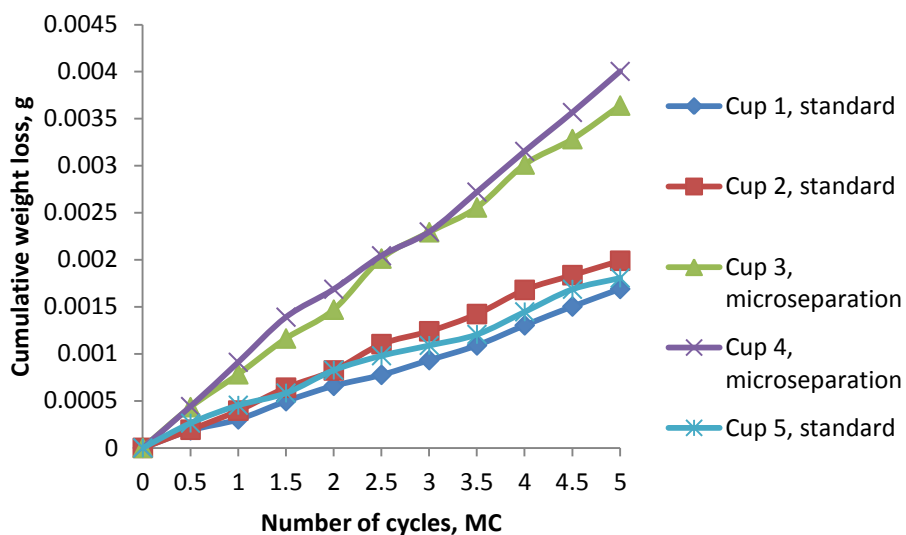


Figure 5.70: Cumulative weight loss of 60 mm CoCrMo cups under standard and microseparation conditions, accounting for the load soak.

The overall wear rate ( $\text{mm}^3/\text{MC}$ ) has been calculated for each station. The results are shown in Table 5.10.

Table 5.10: Wear rates based on overall test,  $\text{mm}^3/\text{MC}$ .

Station, Test Condition	28 mm CoCrMo Head	E1 Liner	60 mm CoCrMo Cup
1, Standard	0.005	0.691	0.040
2, Standard	0.005	0.642	0.049
3, Microseparation	0.035	3.878	0.088
4, Microseparation	0.030	3.567	0.093
5, Standard	0.004	0.459	0.042

All the wear rates for the 28 mm CoCrMo heads were linear ( $R^2 = 0.96 - 0.99$ ).

All the wear rates for the 60 mm CoCrMo cups were linear ( $R^2 = 0.99$ ).

All the wear rates for the E1 liners were linear ( $R^2 = 0.93 - 0.99$ ).

Student's t-test was performed for each type of component to see whether the data from the standard stations (1, 2 and 5) was statistically significantly different from the data from the microseparation stations (3 and 4). The two sets of data will be considered to be significantly different if  $p \leq 0.05$ .

The wear data from the CoCrMo heads ( $p = 0.05$ ), E1 liners ( $p = 0.01$ ) and CoCrMo cups ( $p = 0.003$ ) were significantly different between the two test conditions.

### 5.5.4 Surface characterisation

#### 1) Zygo non-contacting profilometry

Ten zygo images were taken at the pole and at positions 33° from the pole for each component in the five active stations at 0, 0.5, 1.0, 2.5 and 5.0 MC of the test. The load control and soak control were also analysed for comparison. Figure 5.71 and Figure 5.72 show the zygo data for the CoCrMo cups. Wear testing has caused the surface roughness to increase across the cups in the microseparation stations only. The trend in skewness over the course of the test is difficult to see due to the variation in the data.

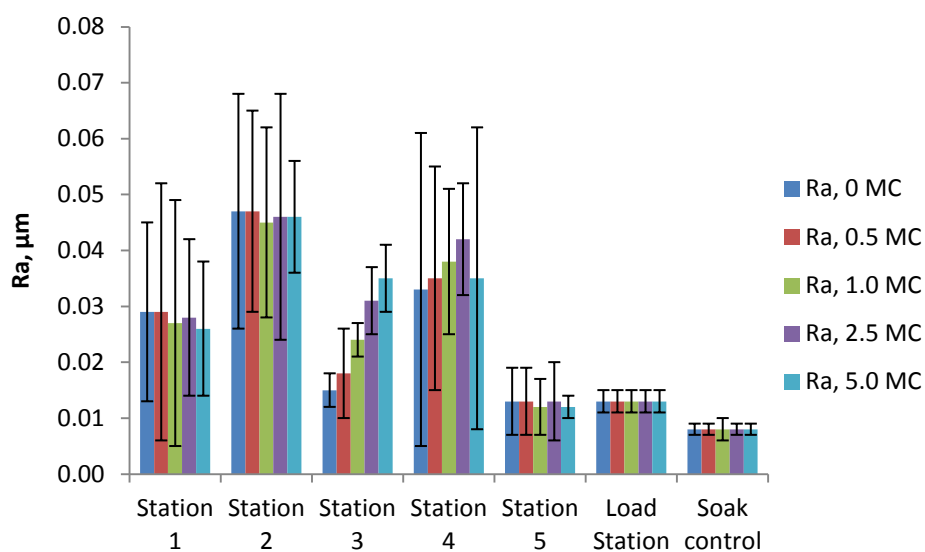


Figure 5.71: Surface roughness of 60 mm CoCrMo cups during 5.0 MC.

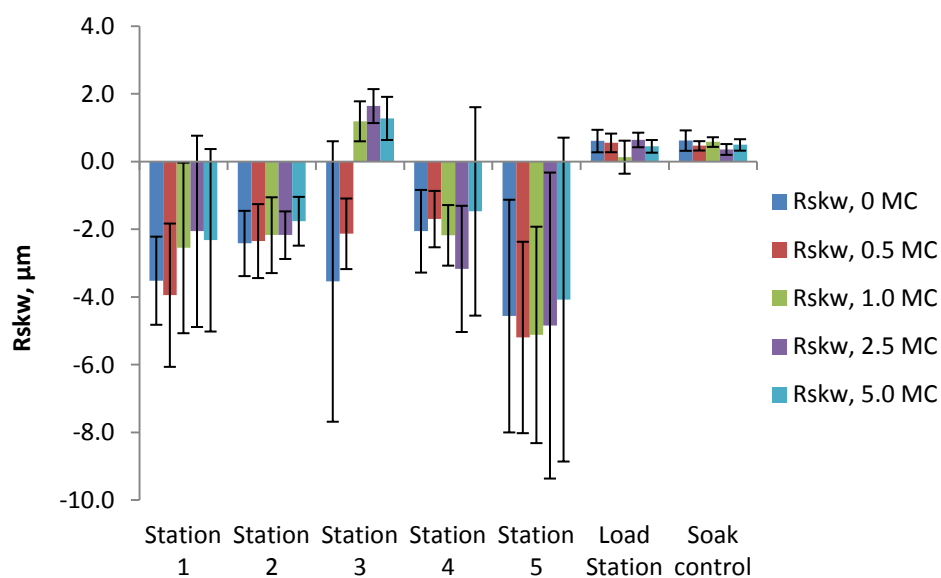


Figure 5.72: Skewness of 60 mm CoCrMo cups during 5.0 MC.

Figure 5.73 and Figure 5.74 show the zygo data for the CoCrMo heads. Surface roughness has increased in the two microseparation stations; stations 3 and 4, whilst remaining quite similar in the standard stations over the 5 MC. There was only slight variation in skewness throughout the test.

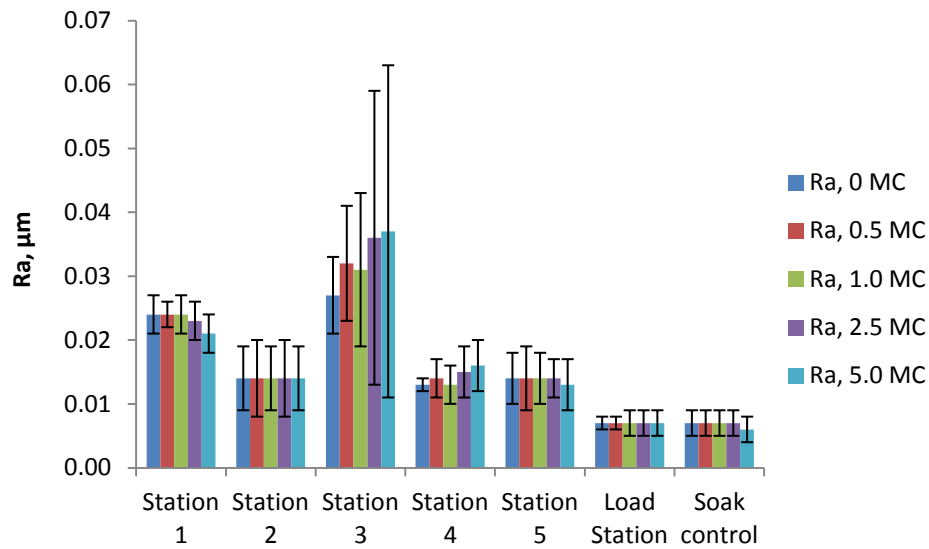


Figure 5.73: Surface roughness of 28 mm CoCrMo heads during 5.0 MC.

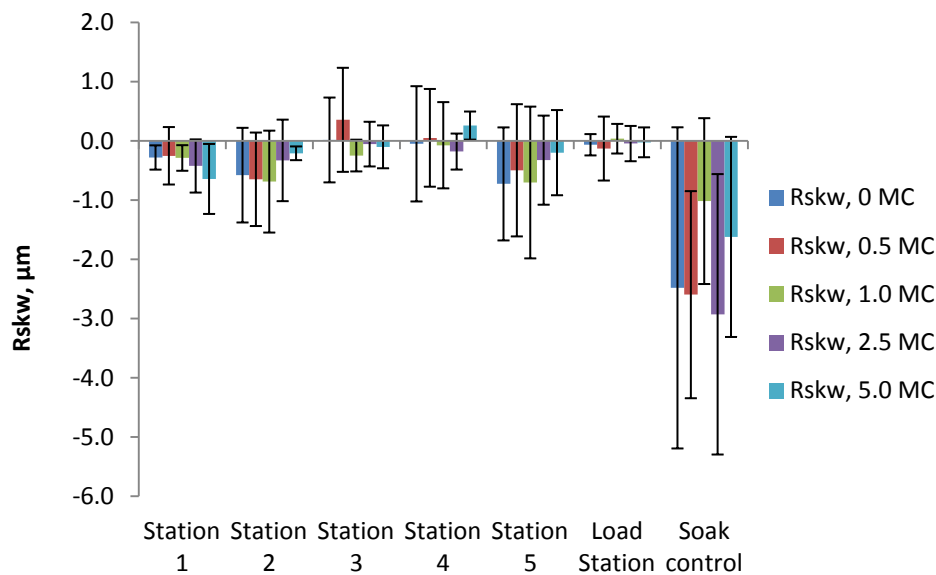


Figure 5.74: Skewness of 28 mm CoCrMo heads during 5.0 MC.

Figure 5.75 and Figure 5.76 show the zygo data for the E1 liners. The data from Stations 1, 2 and 5 has been averaged to give the standard results. The data from Stations 3 and 4 has been averaged to give the microseparation result. Surface roughness has

decreased across all the liners, with a greater effect being seen for the microseparation stations. Skewness has also decreased across all liners that have undergone wear testing, and decreased at a greater rate for the liners which have undergone microseparation.

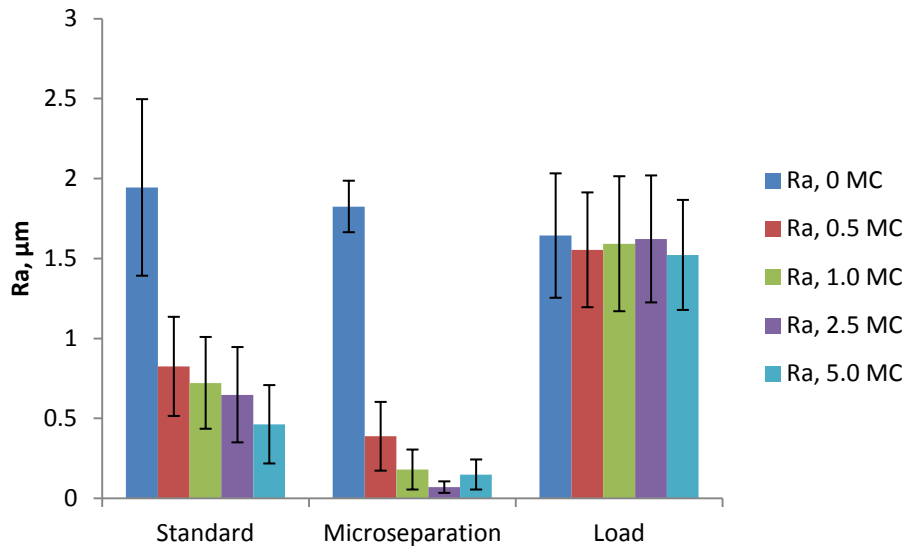


Figure 5.75: Surface roughness of E1 liners during 5.0 MC.

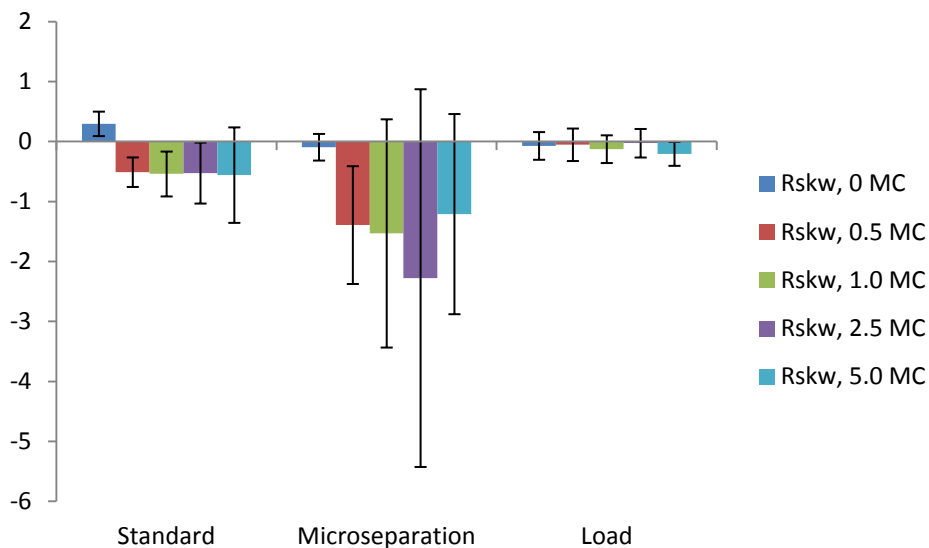


Figure 5.76: Skewness of E1 liners during 5.0 MC.

Eight additional zygo measurements were taken at 45° around the liners after 5 MC. The results are shown in Figure 5.77. As before, the data from Stations 1, 2, and 5 were averaged to give the result for the standard stations. The data from Stations 3 and 4 were averaged to give the result for the microseparation stations. The surface

roughness of the liners in the microseparation stations have decreased more than those in the standard stations, and the skewness has also decreased more. Figure 5.78 shows the 3D surface profiles of the E1 liners. The surface topography is smoother in each liner that has undergone wear testing, and surface roughness is the least in liners 3 and 4 that were tested under microseparation conditions. For these stations the manufacturing streaks have been removed, whilst they are still visible in the standard stations and the control liner.

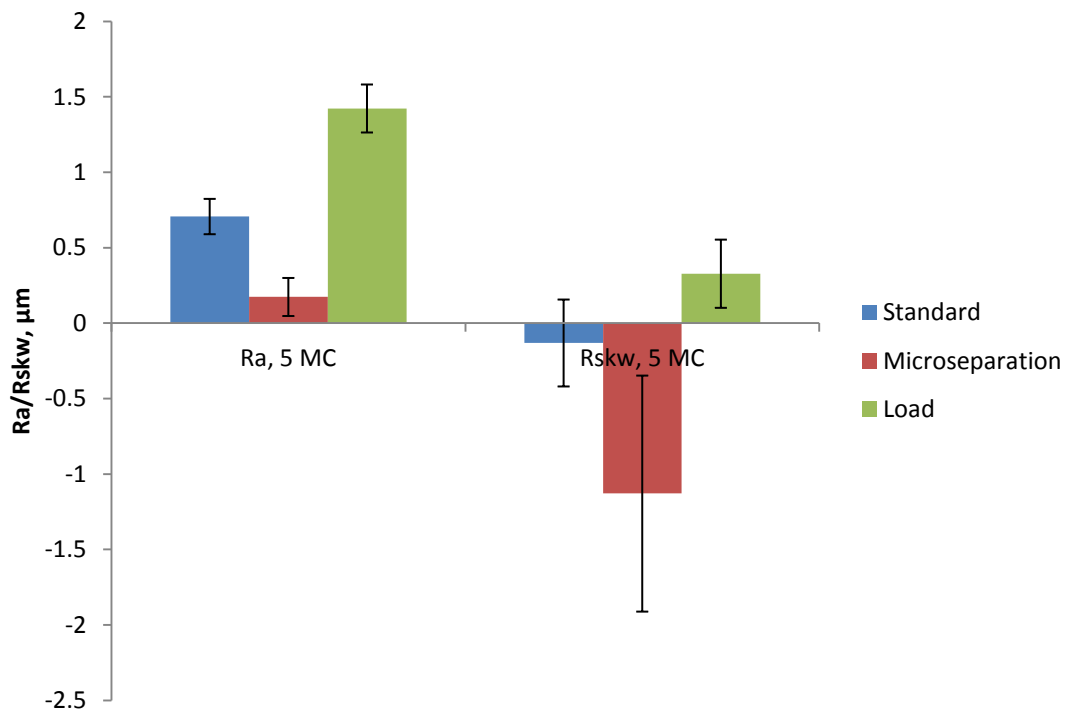


Figure 5.77: Additional data for surface roughness and skewness at 45° around E1 liners.

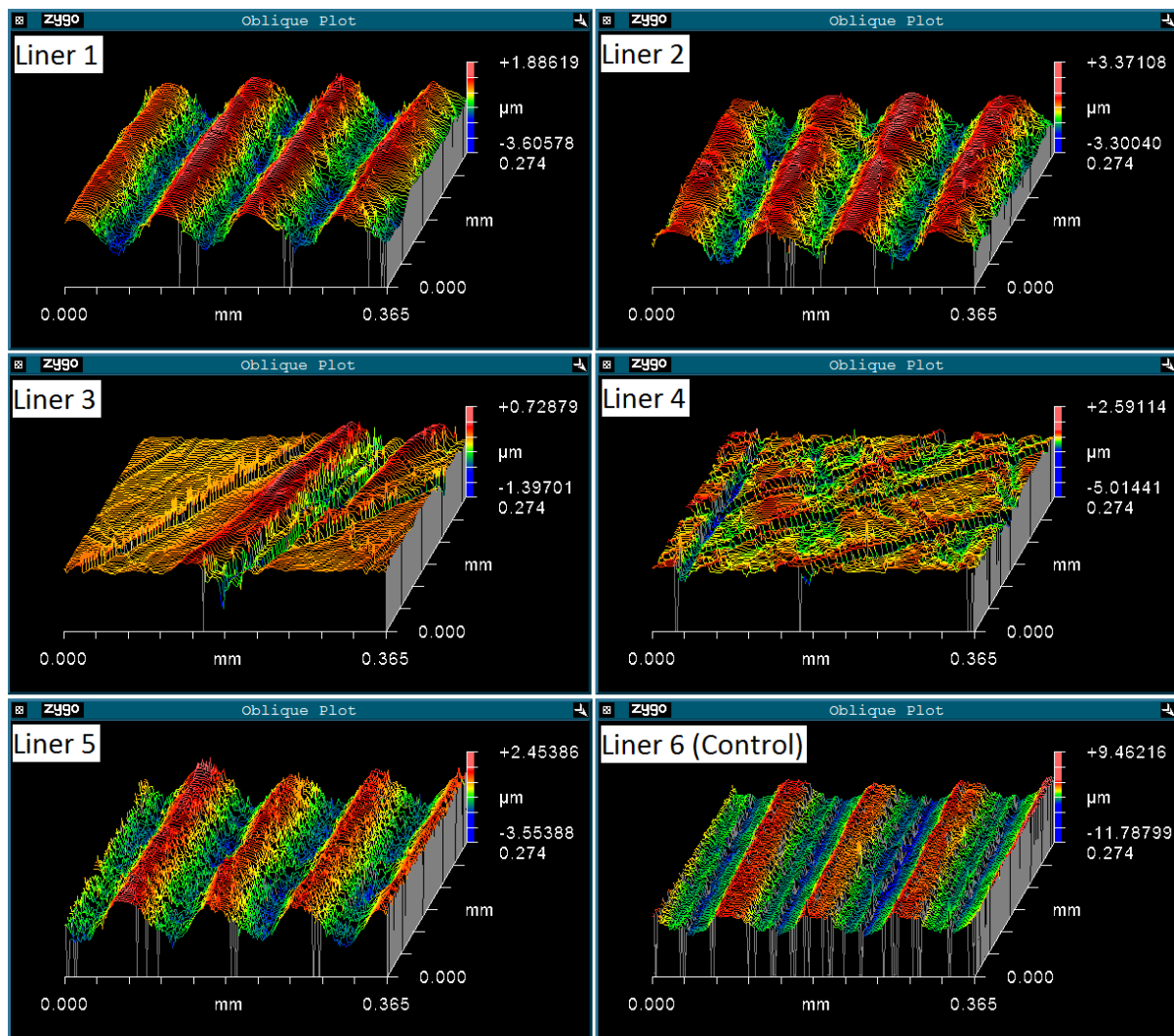
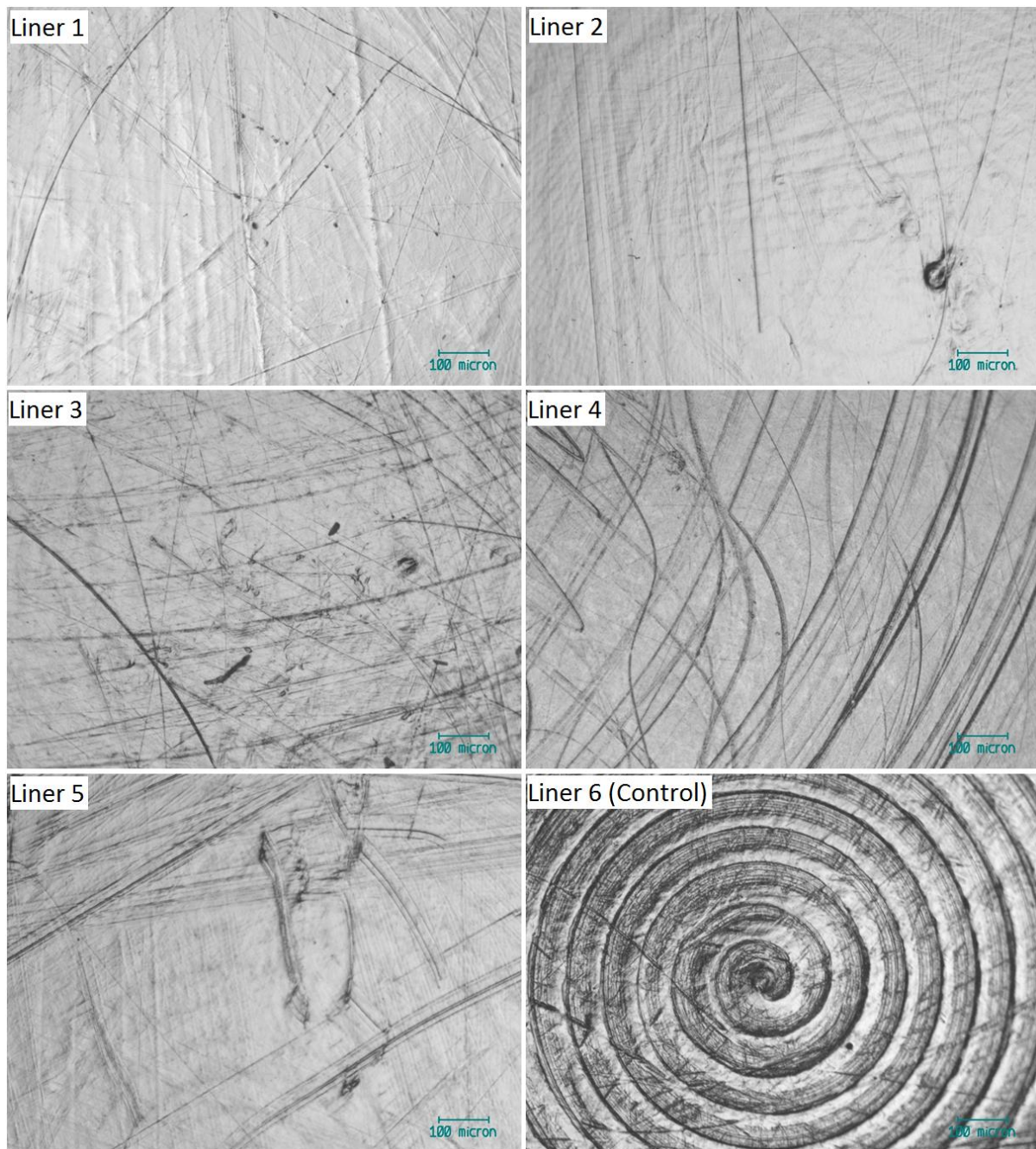


Figure 5.78: Surface profiles of E1 liners imaged after 5 MC at 45 °.

## 2) Optical microscopy

The following images were taken with an Axiotech optical microscope. Figure 5.79 shows the inner pole of all E1 liners after 0.5 MC, including the control liner which has only undergone load and no motion. Figure 5.80 shows corresponding data for the outer pole. The difference between these two figures highlight that the inner articulation experiences greater wear than the outer articulation. In Figure 5.80 it can be seen that only in the microseparation stations were the manufacturing streaks removed.



**Figure 5.79: Inner pole of E1 liners after 0.5 MC.**

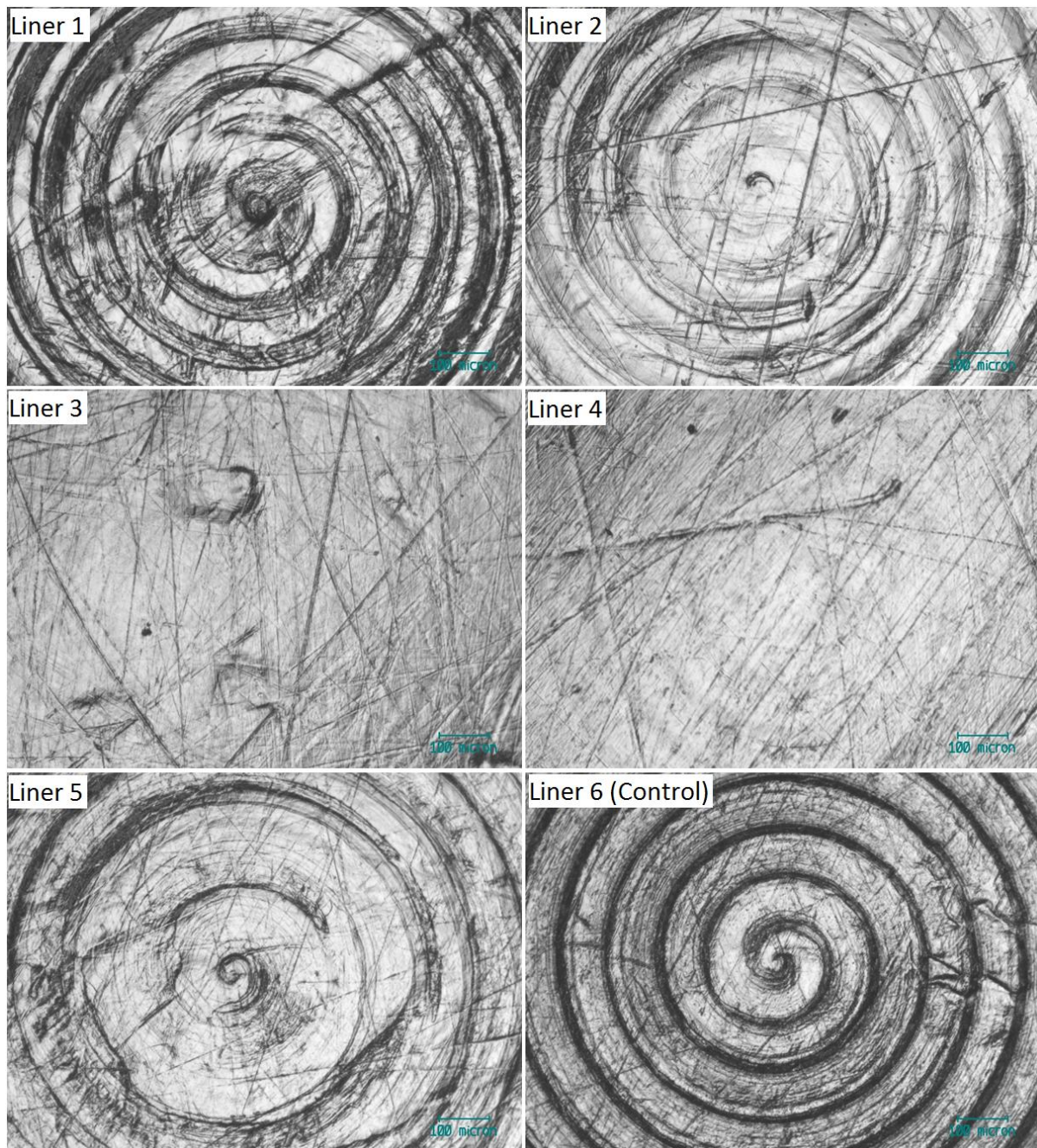


**Figure 5.80: Outer pole of E1 liners after 0.5 MC.**

Figure 5.81 shows the inner pole of the E1 liners after 2.5 MC in comparison to the load soak control, whilst Figure 5.82 shows the outer poles at the same stage of the test. Figure 5.82 shows that after 2.5 MC of wear testing, manufacturing streaks on the outer pole of the liners in the standard stations are still partially visible. Figure 5.83 and Figure 5.84 show the inner and outer poles respectively at the end of the test after 5 MC.

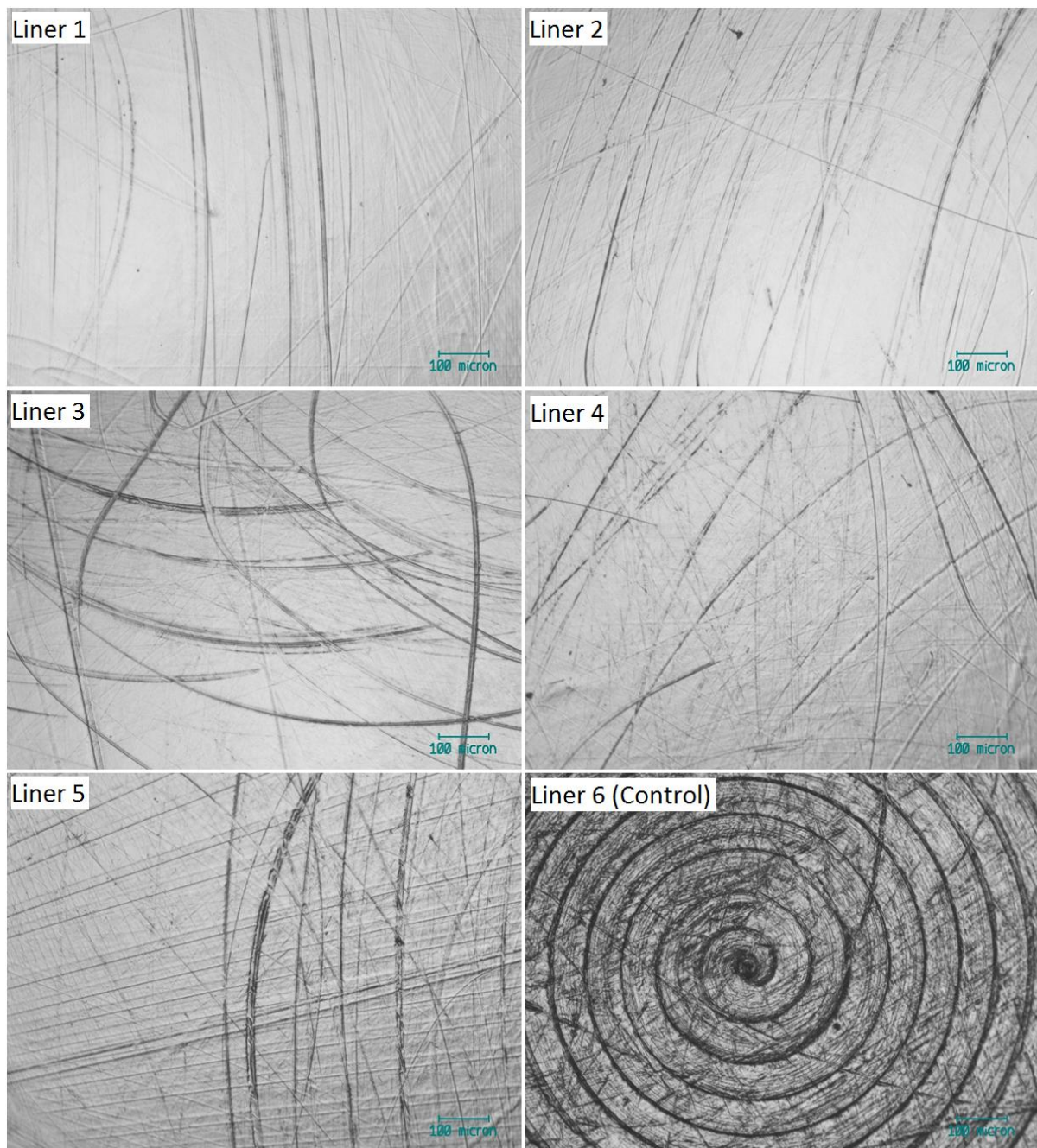


**Figure 5.81: Inner pole of E1 liners after 2.5 MC.**

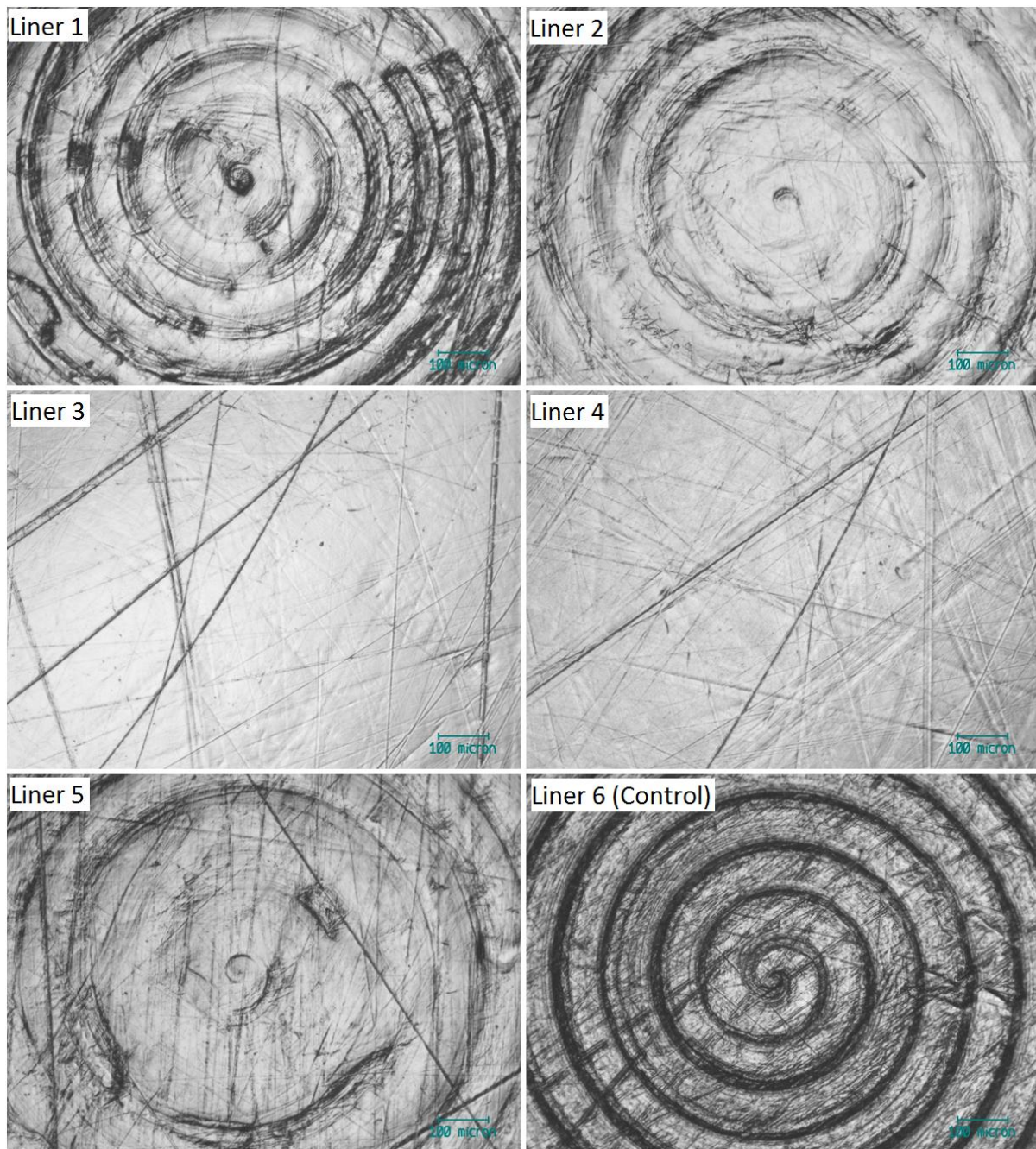
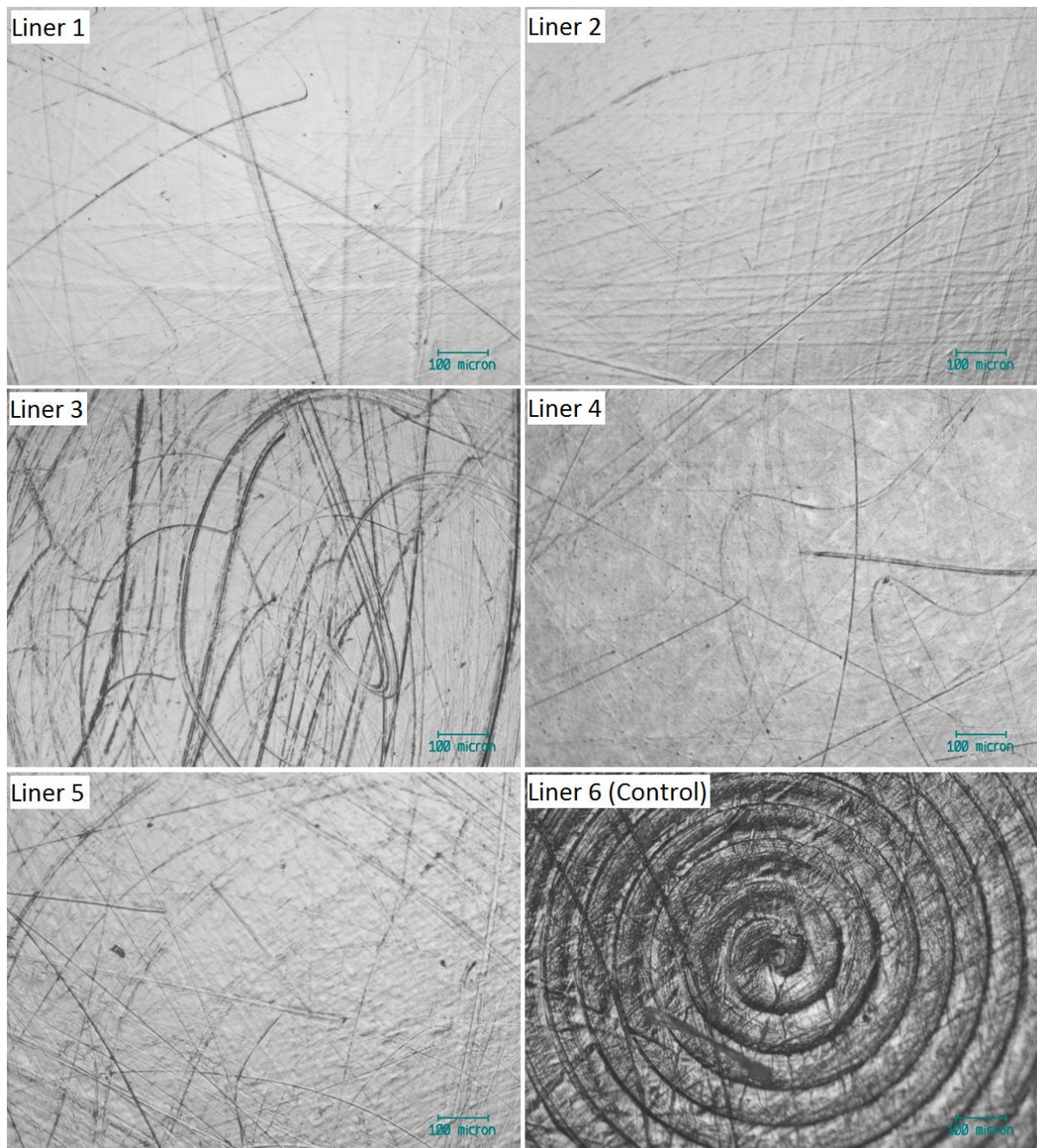
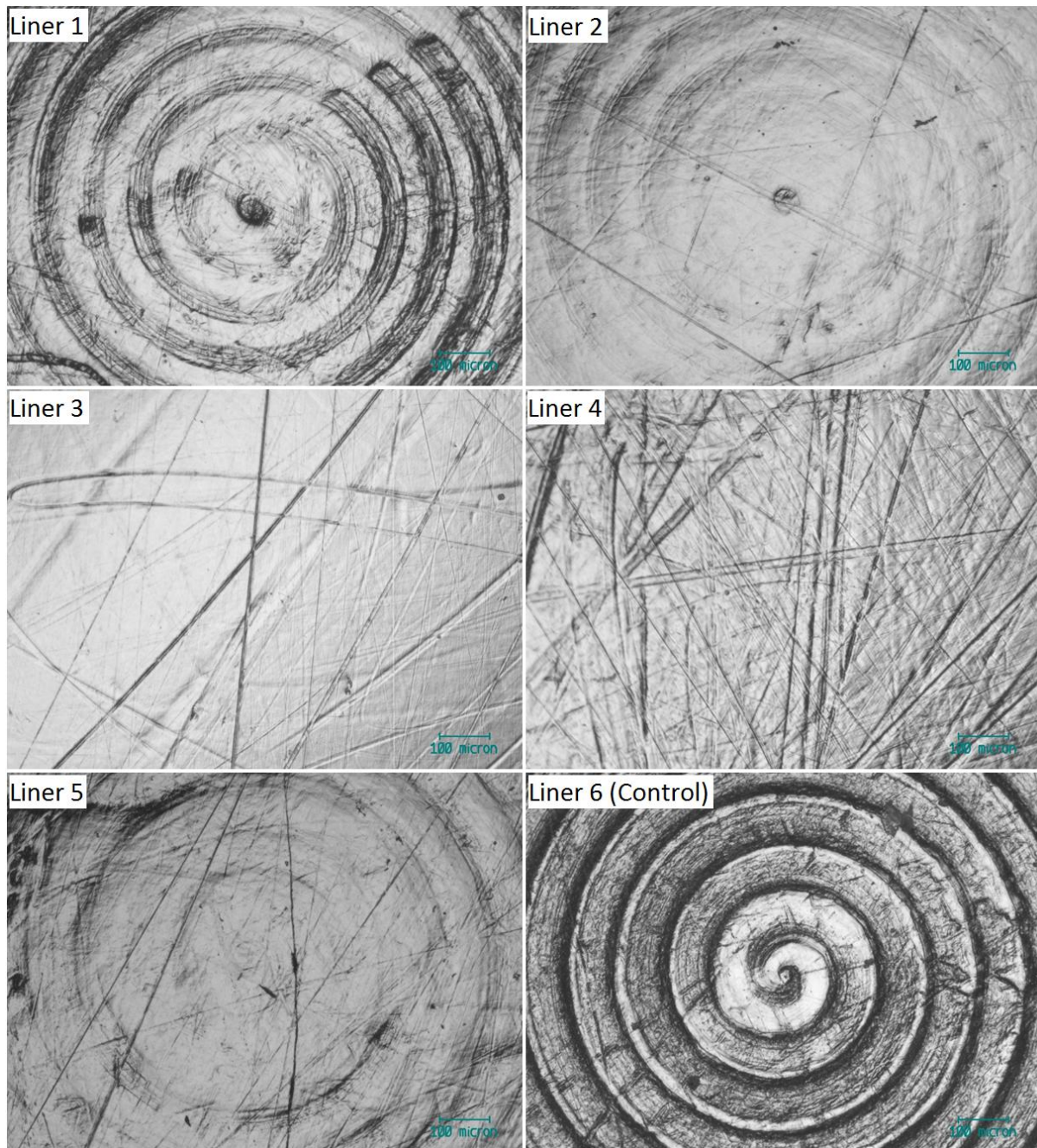


Figure 5.82: Outer pole of E1 liners after 2.5 MC.



**Figure 5.83: Inner pole of E1 liners after 5.0 MC.**



**Figure 5.84: Outer pole of E1 liners after 5.0 MC.**

Figure 5.84 shows that even after 5.0 MC the manufacturing streaks on the outer poles of the liners undergoing standard testing conditions are still partially visible, in contrast to the same stage in DM Test 2 where they had all been removed. The fact that the manufacturing streaks from the outer poles of the liners in the microseparation stations were removed after 0.5 MC, yet the streaks on the outer poles of the liners from the standard stations are still partially visible at 5 MC, highlights that the outer articulation is engaged more under microseparation conditions than standard conditions.

In direct comparison, the manufacturing streaks from the inner poles were removed from all liners within 0.5 MC, showing that the inner articulation experiences greater wear than the outer articulation under standard testing conditions and is the dominant articulation.

Figure 5.85 and Figure 5.86 look at the 28 mm CoCrMo heads after 1.0 MC and 5.0 MC respectively.

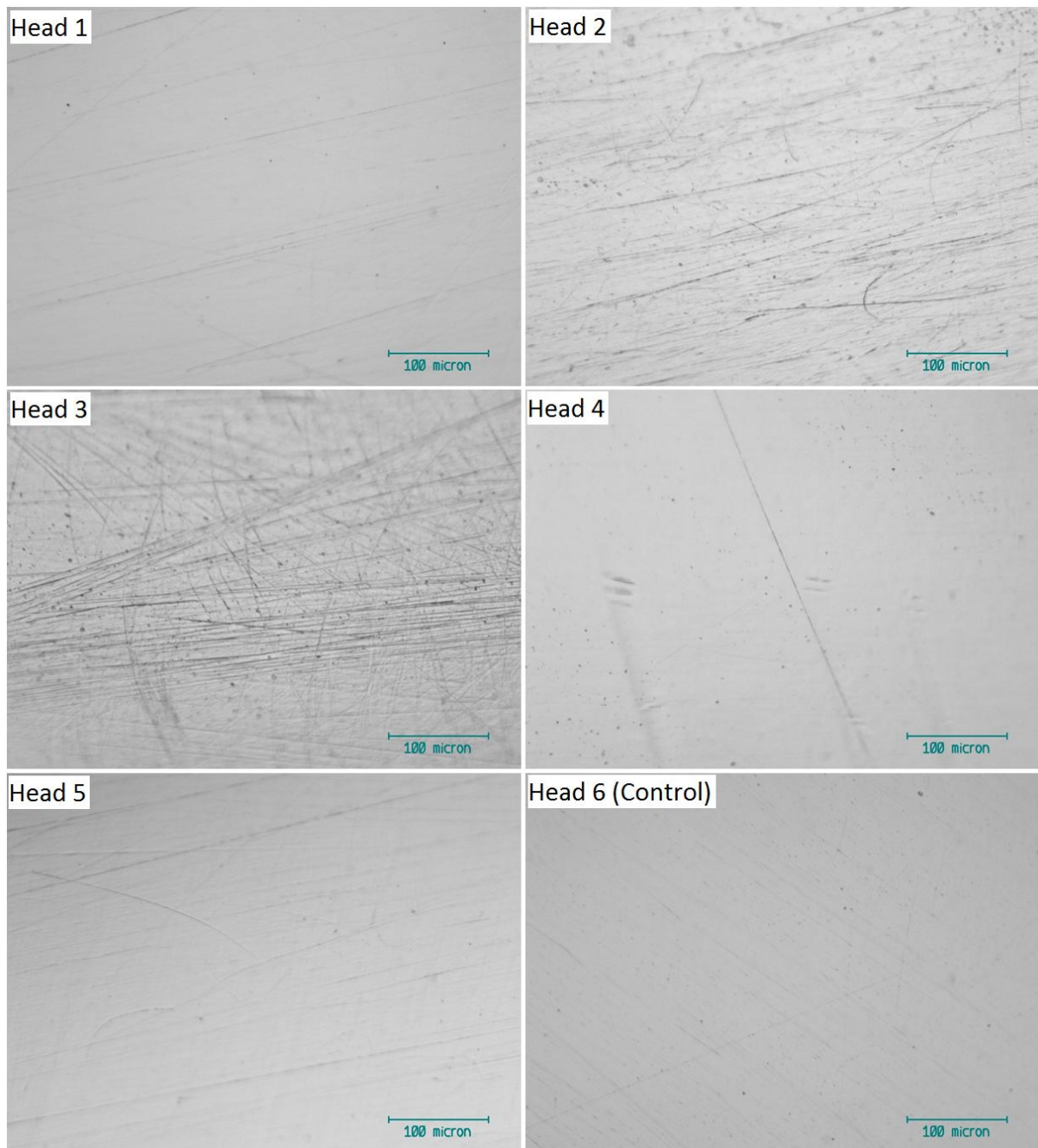


**Figure 5.85: Pole of 28 mm CoCrMo heads after 1.0 MC.**

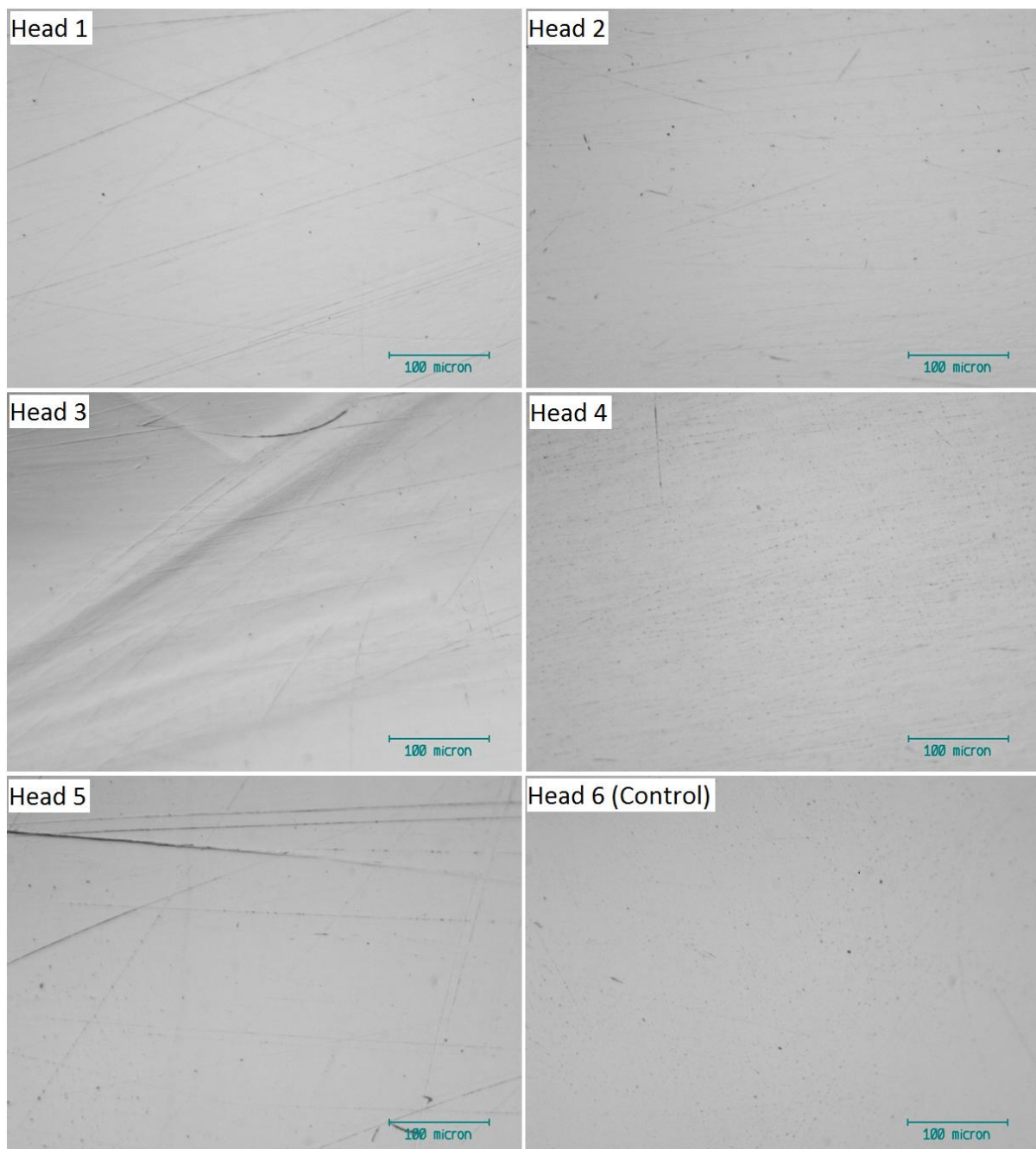


**Figure 5.86: Pole of 28 mm CoCrMo heads after 5.0 MC.**

The optical images show that each metal head has experienced light scratching throughout the test. The same was seen in the CoCrMo cups, which also experienced light scratching. Figure 5.87 and Figure 5.88 show images taken within the wear patch of each CoCrMo cup after 1.0 and 5.0 MC respectively.

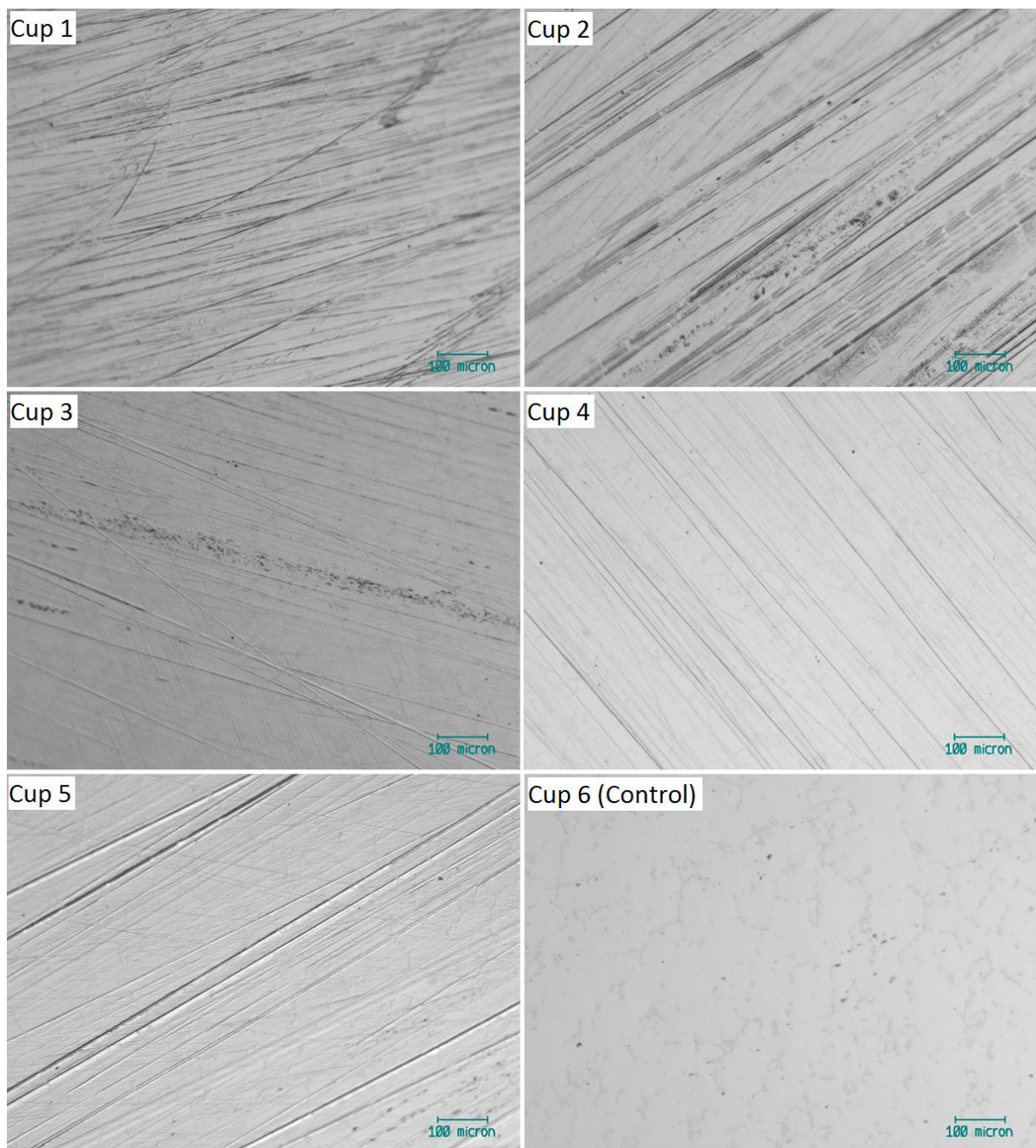


**Figure 5.87: Optical images taken within the wear patch of 60mm CoCrMo cups after 1.0 MC.**

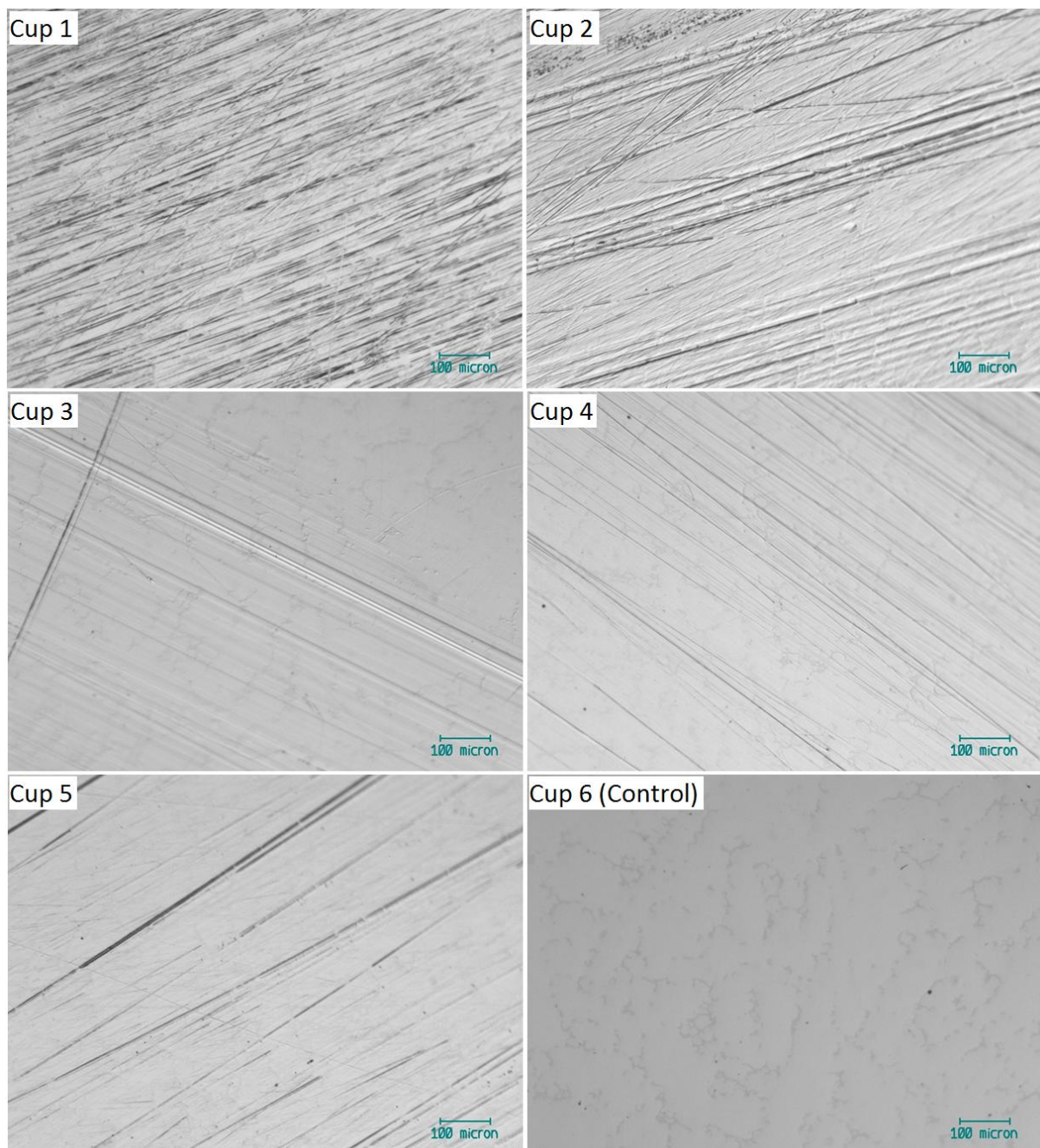


Figure 5.88: Optical images taken within the wear patch of 60mm CoCrMo cups after 5.0 MC.

### 3) Environmental scanning electron microscopy

All liners that have undergone testing have experienced wear. ESEM has been used to track the wear throughout the test. Figure 5.89 shows the wear at 1.0 MC, while Figure 5.90 shows the wear after 5.0 MC.

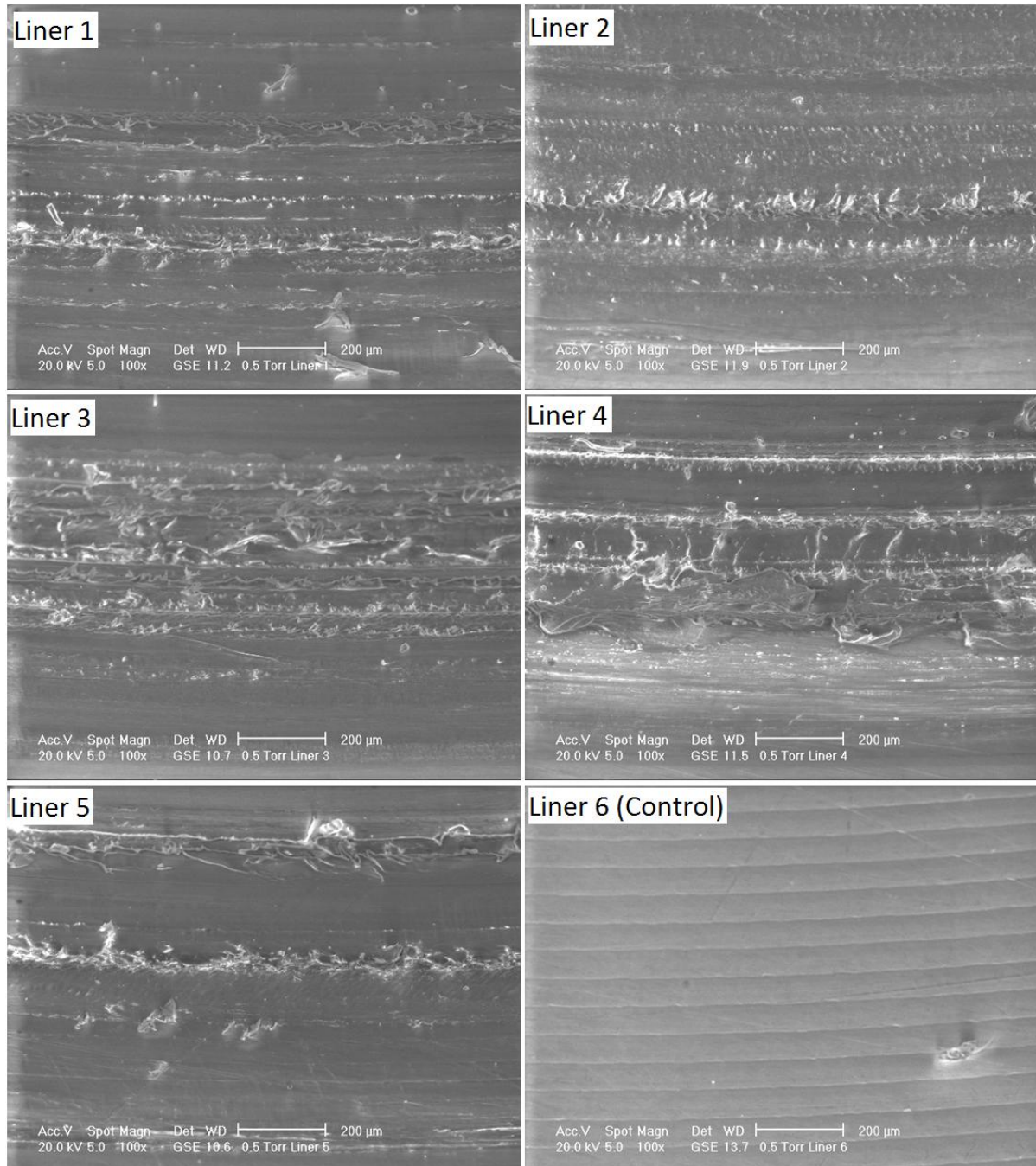


Figure 5.89: ESEM images taken around the E1 liner rim at 1.0 MC.

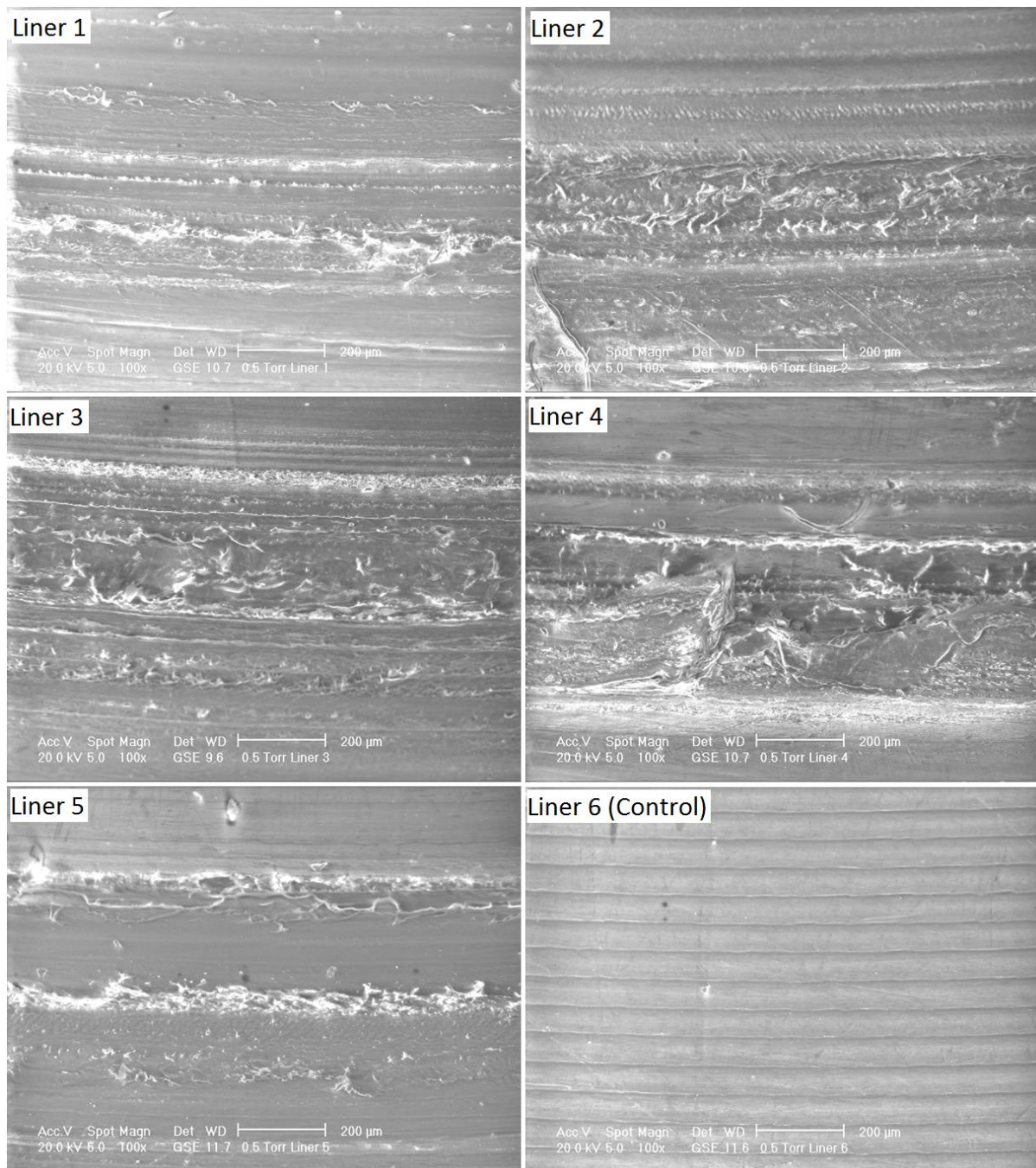


Figure 5.90: ESEM images taken around the E1 liner rim at 5.0 MC.

### 5.5.5 Limitations

The limitations in this study were exactly the same as detailed in section 5.4.5.

### 5.5.6 Discussion

The data for the acetabular cups used in MOM Test 2 and DM Test 3 has been combined and is shown in Figure 5.91.

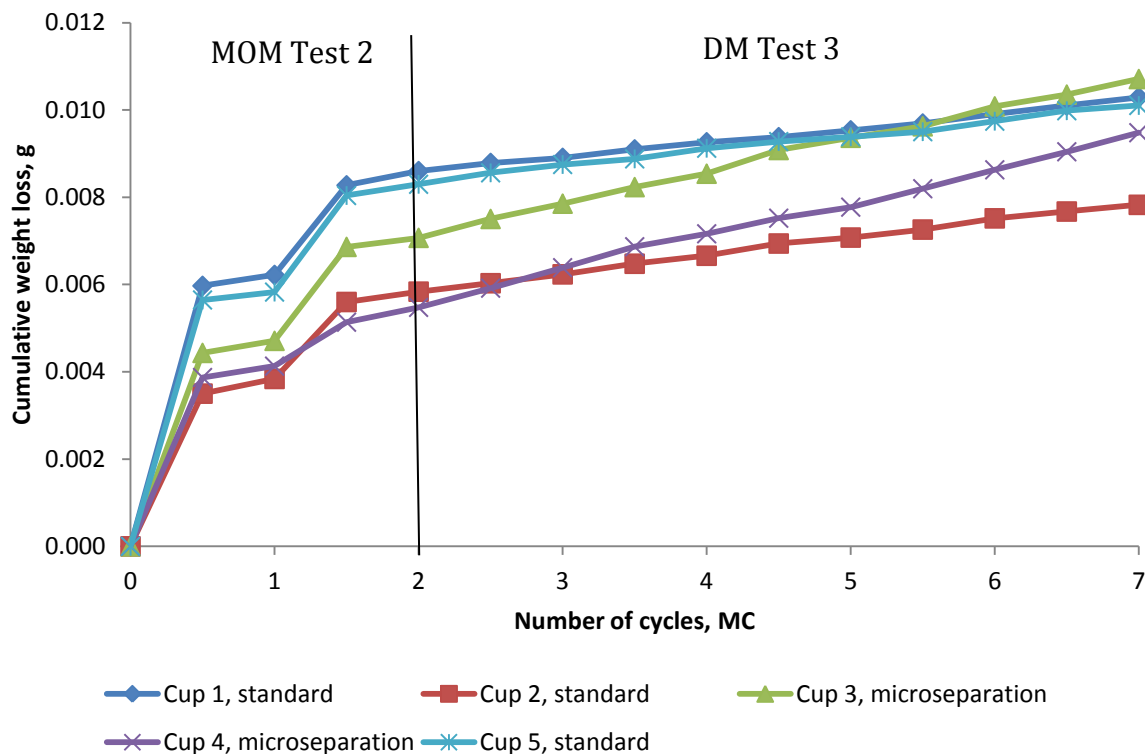


Figure 5.91: Cumulative weight loss of 60 mm CoCrMo cups throughout MOM Test 2 and DM Test 3, accounting for the load soak.

The wear rates experienced by the CoCrMo cups are higher than those in DM Test 1, but still lower than those in DM Test 2. The zygo data has been thoroughly examined in order to explain why this is the case.

Zygo analysis highlights another important difference between the three DM tests; the E1 liners in DM Test 3 have experienced the greatest drop in surface roughness,  $R_a$ , during the first 0.5 MC. This is shown in Table 5.11. The data from the E1 liners in Stns 1, 2 and 5 has been averaged to provide the 'standard' result and the data from Stns 3 and 4 has been averaged to provide the 'microseparation' result.

Table 5.11:  $R_a$  data taken from the E1 liners at 0 and 0.5 MC during the three DM tests.

Stage of Test	Standard E1 liners	Microseparation E1 liners
	$R_a, \mu\text{m}$	$R_a, \mu\text{m}$
DM T1-Initial $R_a$	$1.83 \pm 0.58$	$2.09 \pm 0.56$
DM T1- $R_a$ (0.5 MC)	$1.64 \pm 0.48$	$1.31 \pm 0.52$
DM T2-Initial $R_a$	$1.92 \pm 0.26$	$1.78 \pm 0.29$
DM T2- $R_a$ (0.5 MC)	$1.23 \pm 0.55$	$0.53 \pm 0.32$
DM T3-Initial $R_a$	$1.94 \pm 0.55$	$1.83 \pm 0.16$
DM T3- $R_a$ (0.5 MC)	$0.83 \pm 0.31$	$0.39 \pm 0.22$

This drop in  $R_a$  can be explained by comparing the zygo images taken at the surface of the CoCrMo cups between 0 and 0.5 MC.

Figure 5.92 compares two zygo images taken at 0 and 0.5 MC from DM Test 3 for a cup from a standard station, whereas Figure 5.93 shows corresponding images for a cup from a microseparation station.

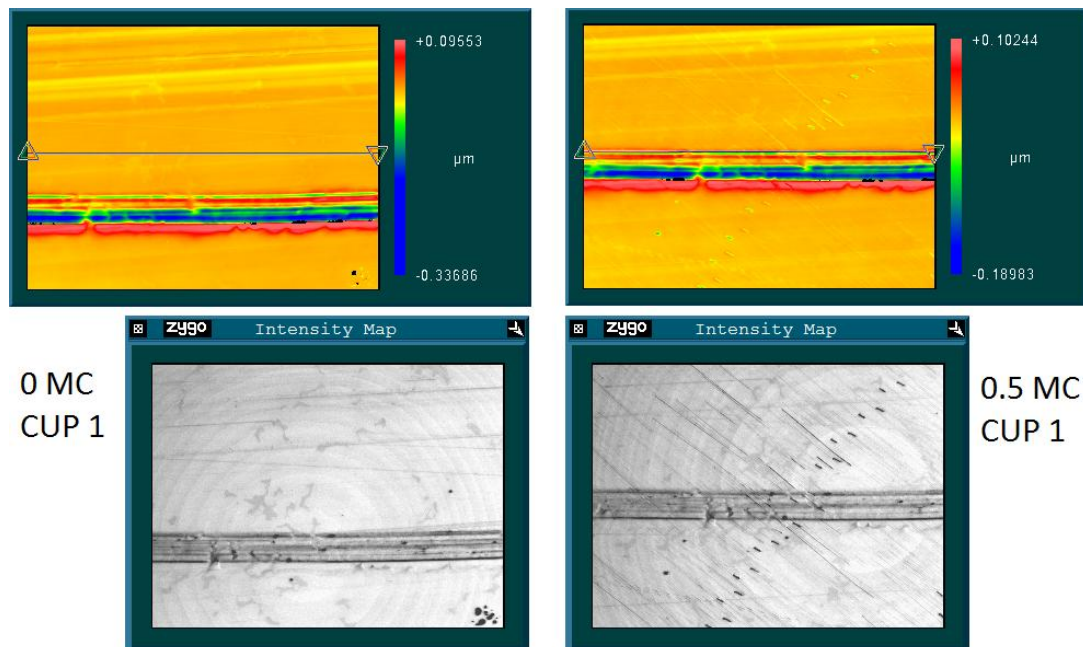


Figure 5.92: Zygo data from Cup 1 at 0 MC (left) and 0.5 MC (right) showing the 2D plot and corresponding image taken at the surface.

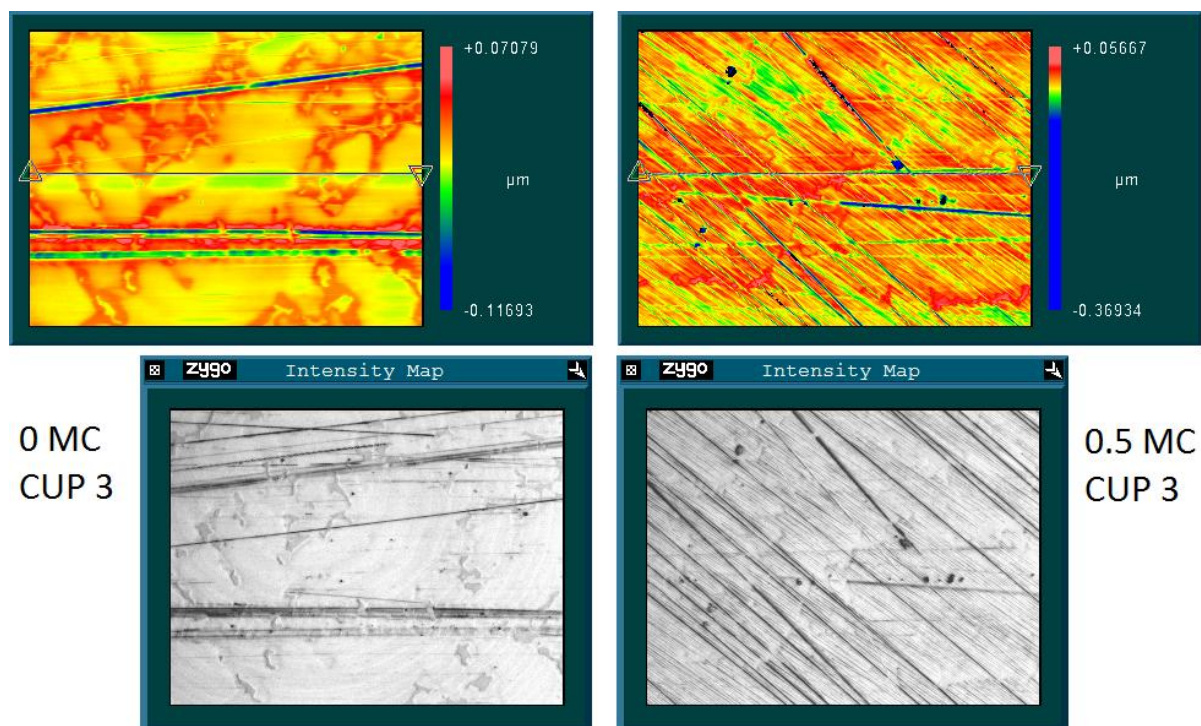


Figure 5.93: Zygo data from Cup 3 at 0 MC (left) and 0.5 MC (right) showing the 2D plot and corresponding image taken at the surface.

The zygo images taken at 0.5 MC show the appearance of ‘comet-tail’ scratching. This effect has not been seen in the CoCrMo cups during the first 0.5 MC of either DM Test 1 or DM Test 2. Figure 5.93 shows that the effect has been greater in the cups in the microseparation stations than in the standard stations due to the outer articulation being engaged more during this test condition.

The scratching is due to the presence of third body particles which have remained embedded in the CoCrMo cups after MOM Test 2 and have scratched through the metal matrix during the initial wear testing in DM Test 3.

This has increased the initial wear rate of the E1 liners, causing them to smooth at a faster rate. As the test has continued, and the test serum has been replaced every 0.5 MC, these particles have been washed out. Hence the E1 liners do not continue to smooth at such a fast rate, see Figure 5.75.

This is an unintended side affect of using third body particles in MOM Test 2 to scratch the CoCrMo cups prior to testing in DM Test 3. It was hoped that the final 0.5 MC ‘recovery stage’ at the end of MOM Test 2 (where the test was ran in standard lubricant) would remove any remaining third body particles.

However since both the HA and Ti particles used in MOM Test 2 are clinically relevant, it is possible that this effect could be seen *in vivo* if a failed resurfacing cup which had been subject to third body wear was left in the body during partial revision surgery.

The positive implication of DM Test 3 is that even if such an occurrence were to happen *in vivo*, then the resulting simulated wear rates with the new E1 dual mobility head were still very low and indicate that replacing a failed metal resurfacing head with a dual mobility head should be a success.

### 5.5.7 Conclusion

Five dual mobility heads, consisting of a 28 mm CoCrMo head and an E1 liner with an inner diameter of 28 mm, outer diameter 60 mm have been tested against worn 60 mm CoCrMo cups from MOM Test 2. The 28 mm heads were sectioned to allow removal from the E1 liner for cleaning throughout the test.

Over 5 MC of testing, under either standard or microseparation conditions at a high incline, the wear rates of the 28 mm CoCrMo heads ranged from 0.004 to 0.035 mm<sup>3</sup>/MC. The wear rates of the E1 liners ranged from 0.459 to 3.878 mm<sup>3</sup>/MC. The wear rates of the 60 mm CoCrMo cups ranged from 0.040 to 0.093 mm<sup>3</sup>/MC.

Surface roughness experienced only small fluctuations throughout the test for the CoCrMo heads and CoCrMo cups in the standard stations. Surface roughness of the CoCrMo cups increased throughout the test in the microseparation stations.

Surface roughness has decreased across all the liners, and is smoothest in the liners that were subject to testing under microseparation conditions.

Zygo analysis showed that third body particles had remained in the metal cups after MOM Test 2 which caused both the initial increase in the wear rate of the E1 liners as well as in the increase in surface roughness of the CoCrMo cups.

Optical images taken from each E1 liner from the inner and outer pole indicate that the inner articulation experienced greater wear than the outer articulation. They also show that the outer articulation experienced greater wear under microseparation conditions than under standard wear testing conditions. Circumferential abrasion was experienced in each E1 liner in the test.

## 5.6 References

- [1] C.B. Rieker, P. Koettig, V. Rieder, M. Shen, Transactions of the 30th Annual Meeting of the Society for Biomaterials, Memphis, USA (2005) p. 84.
- [2] J.H. Dumbleton, M.T. Manley, A.A. Edidin, The Journal of arthroplasty 17 (2002) 649-661.
- [3] C. Lautridou, B. Lebel, G. Burdin, C. Vielpeau, Revue de chirurgie orthopedique et reparatrice de l'appareil moteur 94 (2008) 731-739.
- [4] P. Adam, F. Farizon, M.-H. Fessy, Revue de chirurgie orthopedique et reparatrice de l'appareil moteur 91 (2005) 627-636.
- [5] A. Kusaba, Y. Kuroki, The Journal of arthroplasty 13 (1998) 668-673.
- [6] J.M. Kabo, J.S. Gebhard, G. Loren, H.C. Amstutz, The Journal of bone and joint surgery British volume 75 (1993) 254-258.
- [7] M.-H. Fessy, Maitrise Orthopedique (2006).
- [8] T.R. Green, J. Fisher, M. Stone, B.M. Wroblewski, E. Ingham, Biomaterials 19 (1998) 2297-2302.

## 6. Metal particle analysis

---

### 6.1 Introduction

Test serum from MOM Test 1 and DM Test 1, 2 and 3 has been digested with the aim to isolate and characterise the CoCrMo wear particles generated throughout the wear testing.

The isolation protocol used was based on work by Catelas *et al.* [5] and is described in section 6.2. The resulting solution was then analysed using transmission electron microscopy as explained in section 6.3 and any distinct CoCrMo or Cr particles found were analysed using the Digital Micrograph image analysis software. The chemical composition of any particles found was determined using Energy Dispersive X-Ray (EDX) analysis. Inductively coupled plasma mass spectrometry has also been used in this project to assess the efficiency of the digestion protocol and this process is explained in section 6.4.

Prior to digesting the serum from the simulator studies carried out in this project, test serum from a previous ceramic-on-metal (COM) simulator study carried out by Dr. Qianqian Wang from the Bioengineering group of Durham University was used first as a trial to practice the enzymatic digestion protocol, and the results are provided in section 6.5.

Section 6.6 then shows the results from digesting the serum from MOM Test 1 while section 6.7 shows the results from digesting serum from DM Tests 1, 2 and 3. The findings are compared and discussed at the end of the chapter.

### 6.2 Serum digestion

An isolation protocol based on work by Catelas *et al.* [5] has been used. Each bottle of serum analysed has been allowed to defrost overnight. 125 mL of the CoCrMo particle solution generated by the hip simulator is divided into 40 mL plastic centrifuge tubes and centrifuged at 16,000 x g for 10 min (Beckman Coulter Avanti J-20I). The supernatant was discarded and the particle pellet was resuspended in 3 mL of

## 6. Metal particle analysis

---

remaining serum and split into 2 mL Eppendorf tubes. A photograph of the particle pellet after centrifugation is shown in Figure 6.1.

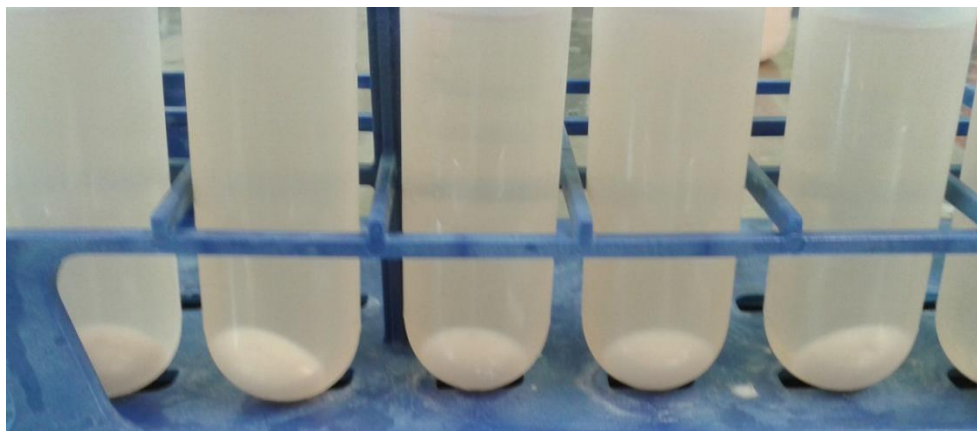


**Figure 6.1: Particle pellet from dual mobility test serum after centrifugation at 16,000 x g.**

Each tube was washed once with 0.5 mL of distilled-deionised water, boiled in 1 mL of distilled deionised water and 150  $\mu$ L of 20% SDS for 10 min, then washed once with 1 mL 80% acetone and three times with 1 mL of 50 mM Tris-HCl, pH 7.6. They were then sonicated and incubated with 1.5U of papain in 1.5 mL of 50 mM Tris HCl, pH 7.6 at 65  $^{\circ}$ C for 24 h.

After incubation, the tubes were cooled at room temp for 10 min before being centrifuged at 16,000 x g for 10 min (Thermo Scientific Heraeus Fresco 17). Next they were boiled in 1 mL of 2.5% SDS for 10 min, then washed twice with 1 mL of 50mM Tris-HCl, pH 7.6 and then sonicated for a few seconds using a mesh. This was then incubated with 400  $\mu$ g of proteinase K in 1 mL of Tris-HCl at 55  $^{\circ}$ C for 24 h.

After incubation, the tubes were allowed to cool at room temp for 10 min and then centrifuged at 16,000 x g for 10 min. They were boiled in 1 mL of 2.5 % SDS for 10 min, and then washed once with 1 mL of 50mM Tris-HCl, pH 7.6, once with 500  $\mu$ L of 80% acetone added to 100  $\mu$ L of 20% SDS, and once with 1 mL of distilled-deionised water. Finally, the particles were stored in 0.5 mL 100% ethanol at 4  $^{\circ}$ C. A brief summary is given in Figure 6.2.

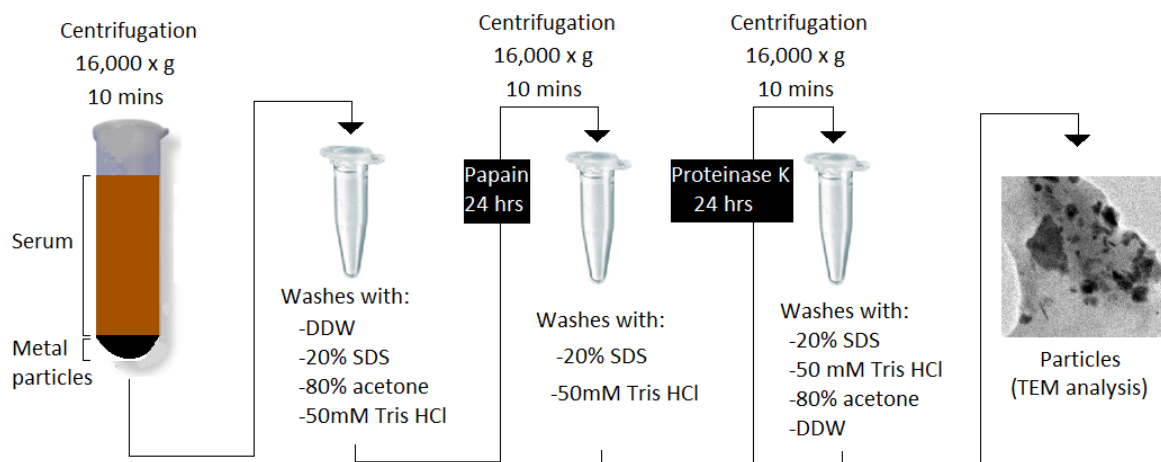


**Figure 6.2: Overview of the digestion protocol.**

The particles were then sonicated to ensure that they were evenly dispersed within the ethanol solution. A few drops were extracted using a pipette and placed onto a holey carbon disc (300 mesh) on a copper grid (supplied by Agar) for examination under a transmission electron microscope (TEM). The image analysis software Digital Micrograph was used to size the particles from the TEM images.

### 6.3 Transmission electron microscopy

During Transmission Electron Microscopy (TEM) a beam of electrons travel through the vacuum in the column of the microscope and are then focused using electromagnetic lenses into a very thin beam. This beam is directed through the sample and the electrons are scattered depending on the density of the material.

The TEM used in this study was the JEOL 2100F FEG TEM, Figure 6.3. This is a high performance TEM which uses a Schottky field emission electron source operating at 200 kV to deliver high long-term stable currents for high performance analysis. It also used a high resolution pole piece giving 2.3 Å point resolution.

With the addition of Energy Dispersive X-Ray (EDX) analysis the TEM can identify elements in areas less than 0.5 µm in diameter. This was used to identify the chemical composition of the wear particles isolated from the test serum.



Figure 6.3: JEOL 2100F FEG TEM used in the Physics Dept. of Durham University.

### 6.4 Inductively coupled plasma mass spectrometry

Inductively Coupled Plasma Mass Spectrometry (ICPMS) is a highly sensitive type of mass spectrometry that can detect metals at a concentration below one part in  $10^{12}$ . The sample to be analysed is placed in a chamber containing argon and transformed into an aerosol of very fine droplets. The aerosol then passes through oxygen plasma at 8,000 – 10,000 °C which is capable of dissociating, atomizing and ionising most elements. A differential vacuum system accelerates the plasma ions towards electrostatic discs that extract the positively charged ions and transport them to the mass filter which selects the ions according to their mass and charge. The process is summarised in Figure 6.4.



Figure 6.4: ICPMS overview.

ICPMS has been used in this project to assess the efficiency of the protocol used to isolate metal wear particles by comparing the concentration of Co, Cr and Mo present before and after the isolation protocol, see Appendix C.

### 6.5 Results from COM study

Zirconia-toughened-alumina (ZTA) ceramic modular femoral heads were tested against 60 mm CoCrMo acetabular cups, as used in this project. An image of the joints tested is shown in Figure 6.5.



Figure 6.5: 60mm ZTA ceramic modular head and 60 mm CoCrMo acetabular cup.

Serum samples from two test conditions in the COM study have been analysed:

**Wear Condition 1, COM:** Combined microseparation and standard inclination angle (45° anatomical angle)

**Wear Condition 2, COM:** Combined microseparation and high inclination angle (62° anatomical angle)

From Wear Condition 1 the TEM images acquired were clear and EDX analysis confirmed the particles to be Chromium, see Figure 6.6.

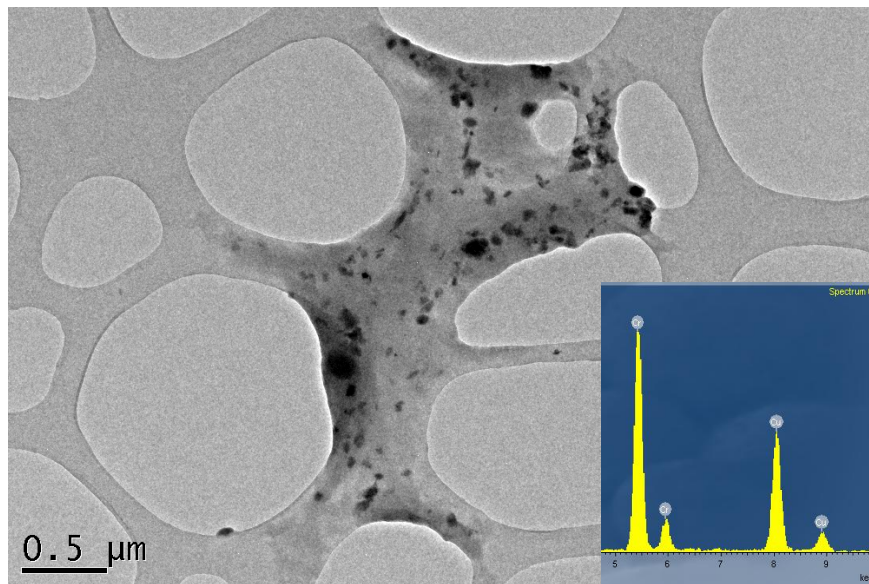


**Figure 6.6: TEM image: Cr particles after 3.8 MC from Wear Condition 1 including EDX spectra.**

All the particles isolated were Chromium, no Cobalt was found. Molybdenum is difficult to detect because its peak coincides with that of Sulphur, which will always be present in a biological system. The presence of Chromium alone is indicative of mild abrasive wear from the continuous generation and removal of the protective layer of the metal surface. The peak showing the presence of copper will be present in all EDX analysis due to the wear particles being displayed on a copper grid.

An adequate number of images were taken in order to be able to size at least one hundred particles using Digital Micrograph software. Particles were either spherical or rod-like in nature. The distribution after 3.8 MC can be seen in Figure 6.7. The average length of the rod-like particles ( $\pm 95\%$  confidence limit) was  $68 \pm 8$  nm, the average width was  $20.5 \pm 3$  nm, and the average diameter of the spherical particles was  $41 \pm 7$  nm.

Another sample, frozen after 5 MC, was then subjected to the same enzymatic protocol. The distribution is shown in Figure 6.8. The distribution has shifted slightly to the left as the average particle size has decreased. The average length of the rod-like particles was  $55 \pm 12$  nm, the average width was  $16.1 \pm 4$  nm, and the average diameter of the spherical particles was  $22 \pm 3$  nm. Again, only Cr particles were detected. This result has also been seen in work by Catelas *et al.* [7]

## 6. Metal particle analysis

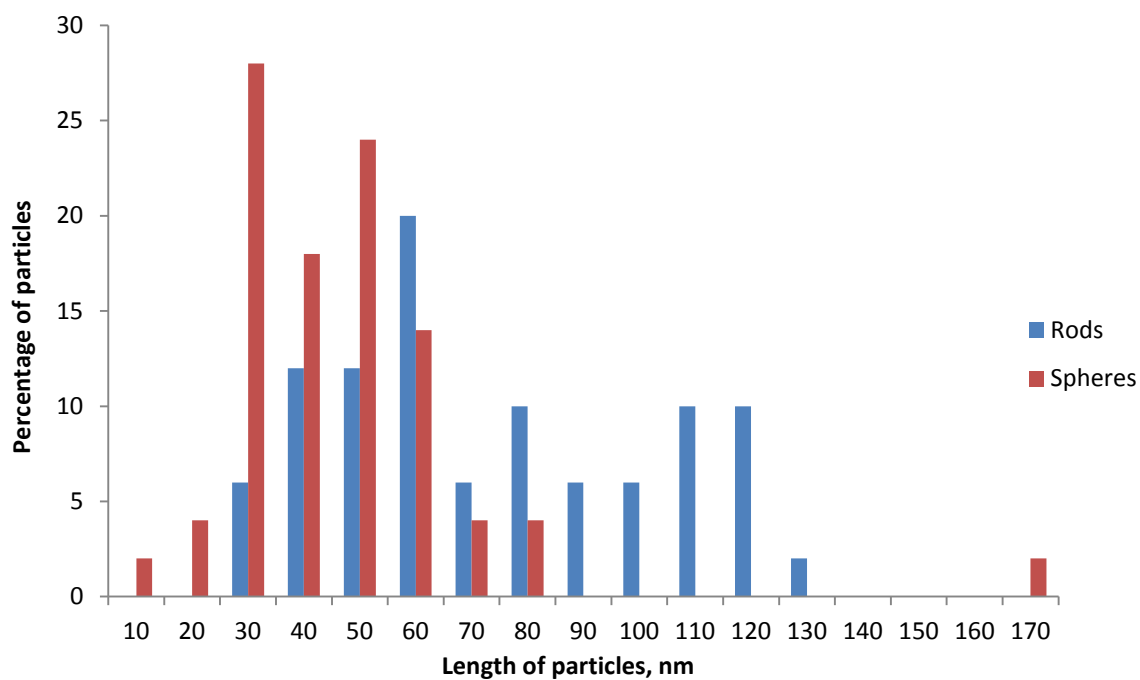


Figure 6.7: Particle distribution after 3.8 MC from Wear Condition 1.

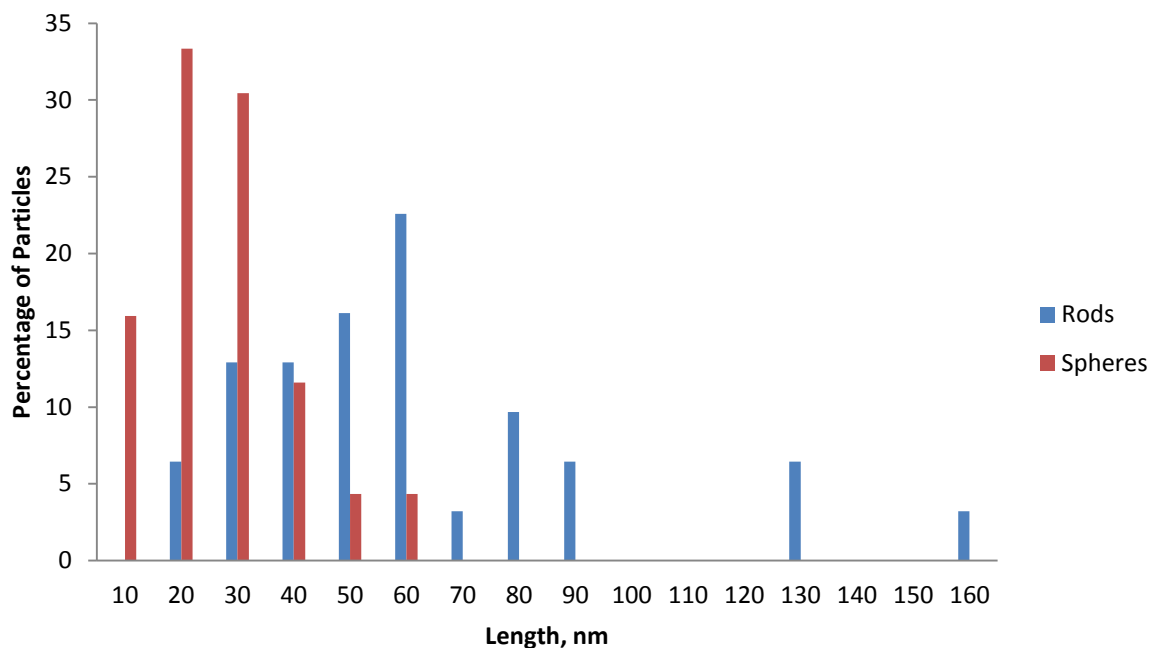
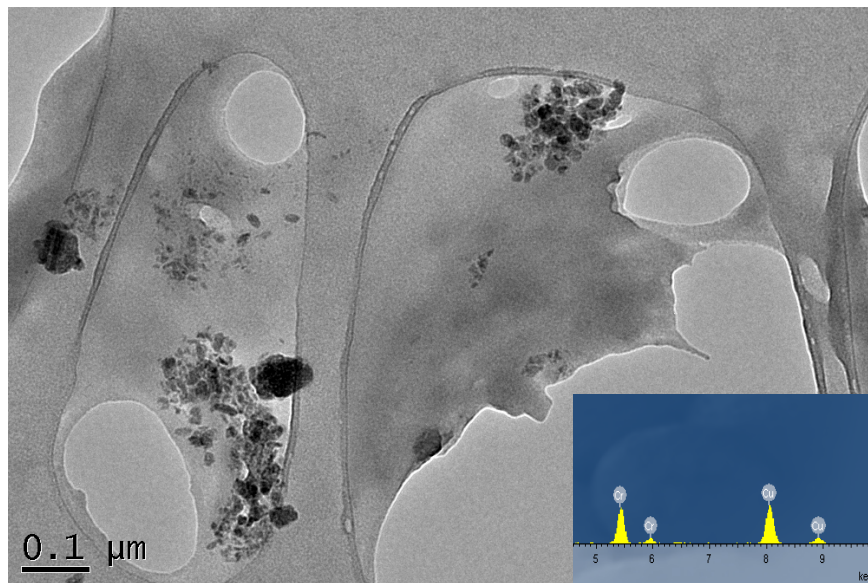


Figure 6.8: Particle distribution after 5 MC from Wear Condition 1.

Two serum samples from Wear Condition 2 of the COM study were also digested and the wear debris has been successfully isolated and analysed. Samples were digested

## 6. Metal particle analysis

after 0.5 and 1.0 MC. Again, only Cr particles were found. An example of the particles imaged is shown in Figure 6.9.



**Figure 6.9: TEM image: Cr particles after 0.5 MC from Wear Condition 2 including EDX spectra.**

There was a significant decrease in particle size at the higher inclination angle. Figure 3.5 shows the particle distribution of the debris isolated after 0.5 MC from Simulation 2. The average length of the rod-like particles was  $17 \pm 6$  nm, the average width was  $2.7 \pm 0.4$  nm, and the average diameter of the spherical particles was  $13 \pm 3$  nm.

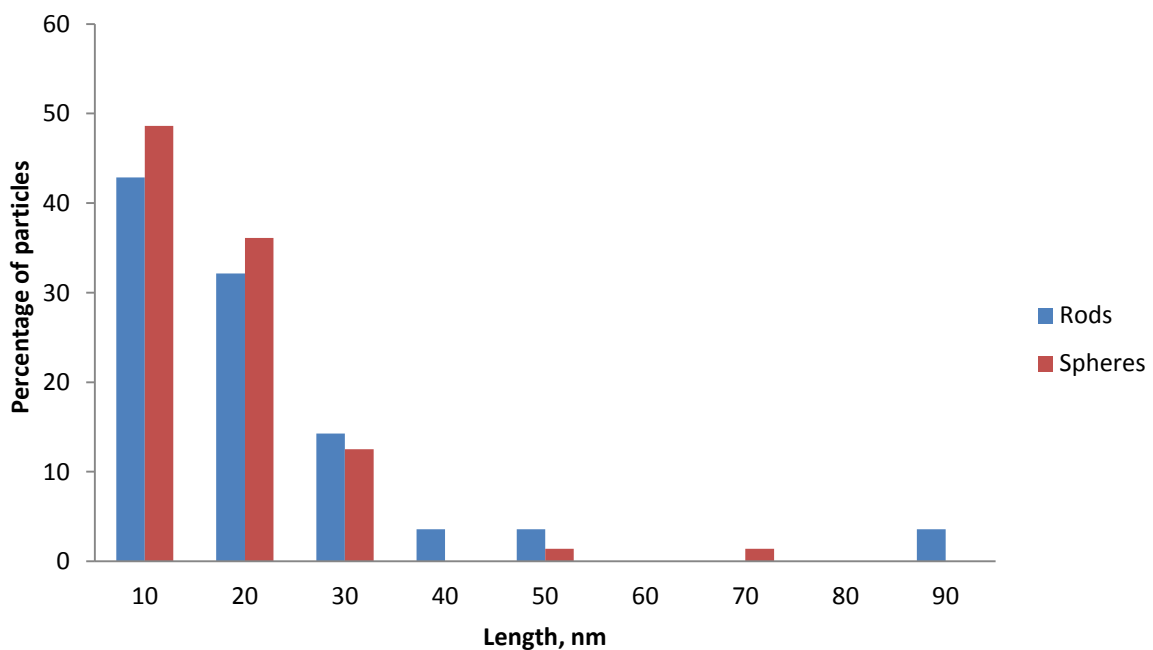


**Figure 6.10: Particle distribution after 0.5 MC from Wear Condition 2.**

## 6. Metal particle analysis

---

After 1 MC, the particles were even smaller and the range also decreased. Figure 3.7 shows their distribution. The average length of the rod-like particles was  $7 \pm 2$  nm, the average width was  $2.5 \pm 0.3$  nm, and the average diameter of the spherical particles was  $3 \pm 1$  nm. Again, only Cr particles were detected.

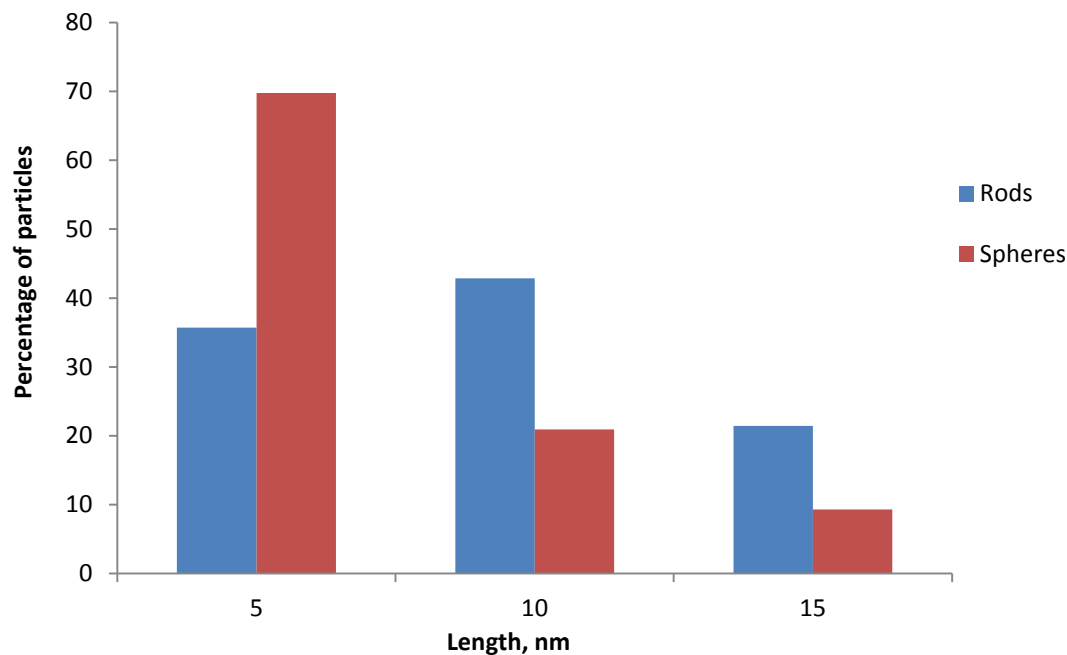


Figure 6.11: Particle distribution after 1 MC from Wear Condition 2.

### 6.6 Results from MOM Test 1

This analysis uses serum that was frozen after the test carried out in section 4.6.

Initially serum taken from Station 2 was digested and analysed. After this station started to suffer from weak gaiters, serum was digested and analysed from Station 4 instead, which did not suffer from any gaiter leaks.

Samples taken after 0.5 and 1.0 MC from Station 2 were analysed, and examples of the particles found can be seen in Figure 6.12. Serum samples taken after 1.0, 2.5, and 5.0 MC from Station 4 were analysed, examples of the particles found are shown in Figure 6.13.

The process to find distinct particles that were not part of agglomerates was very time consuming. After 1.0 MC from Station 4 only small, indistinguishable Cr particles and one larger CoCr particle could be found. This is indicative of only a little wear occurring

## 6. Metal particle analysis

---

at the very surface of the components. From every other sample, CoCr rod-like particles with a polycrystalline structure were seen. At 5MC from Station 4 (where wear was minimal), multiple samples had to be viewed to find even a few CoCr particles.

Statistical analysis of these images is difficult due to the low number of particles imaged (not more than 25 particle images were achievable for any sample in the allocated TEM sessions). Size analysis for the particles that were imaged is given below. NanoSight analysis of the digested serum would be a preferential method in order to give a larger sample analysis and size distribution. However the samples were not purely composed of the CoCr alloy. Silicon particles were a common impurity, which is unable to be differentiated from the CoCr particles within NanoSight. It is likely that silicon has entered the serum due to the silicon gaiters wearing against the cup holder during simulator motion. Also the NanoSight cannot account for agglomerates which were also in the sample.

**Table 6.1: Average particle size of CoCr particles isolated from MOM serum samples, shown with 95% confidence intervals.**

<b>Particle Size</b>	<b>Average Length (nm)</b>	<b>Average Width (nm)</b>
<b>0.5 MC, Stn 2</b>	194 ± 52	44 ± 9
<b>1.0 MC, Stn 2</b>	169 ± 68	53 ± 22
<b>1.0MC, Stn 4</b>	63	31
<b>2.5 MC, Stn 4</b>	107 ± 19	34 ± 11
<b>5.0 Mc, Stn 4</b>	106 ± 35	49 ± 18

## 6. Metal particle analysis

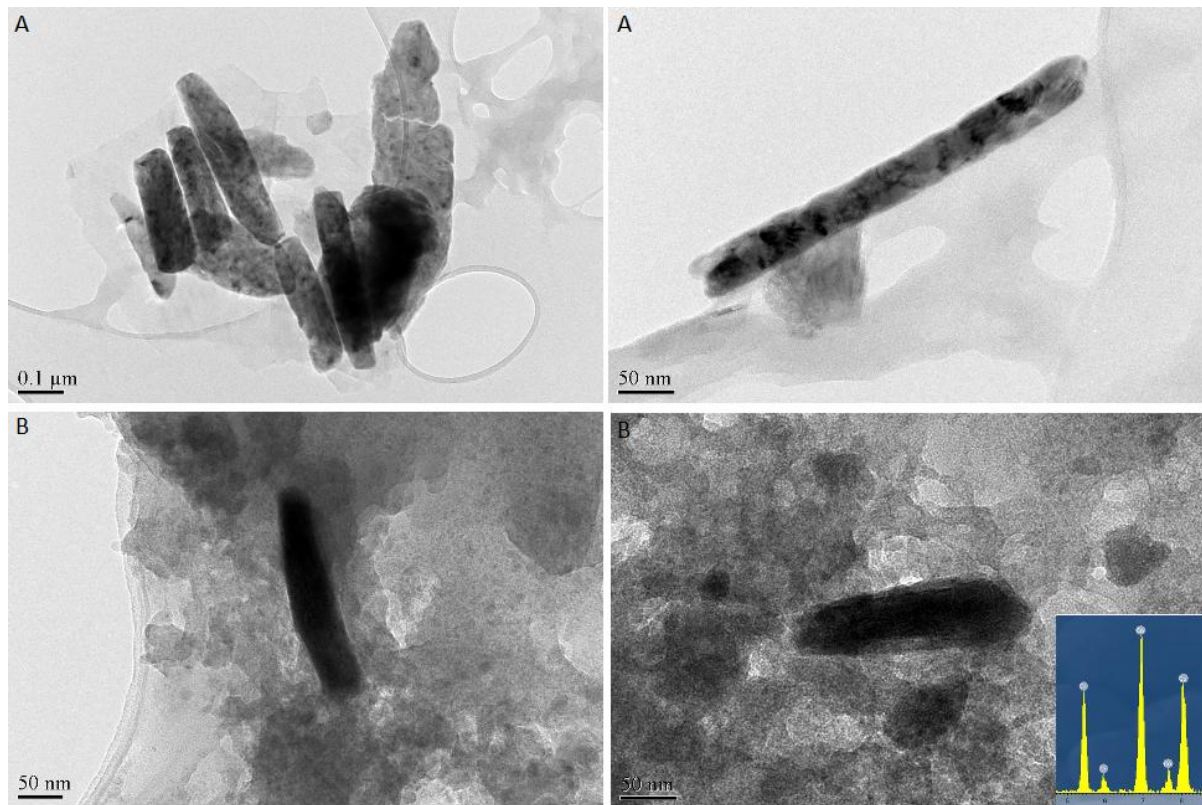


**Figure 6.12: TEM images of CoCr particles seen from Station 2 after A: 0.5 MC, B: 1.0MC. E showing particles to be CoCr at the bottom right.**

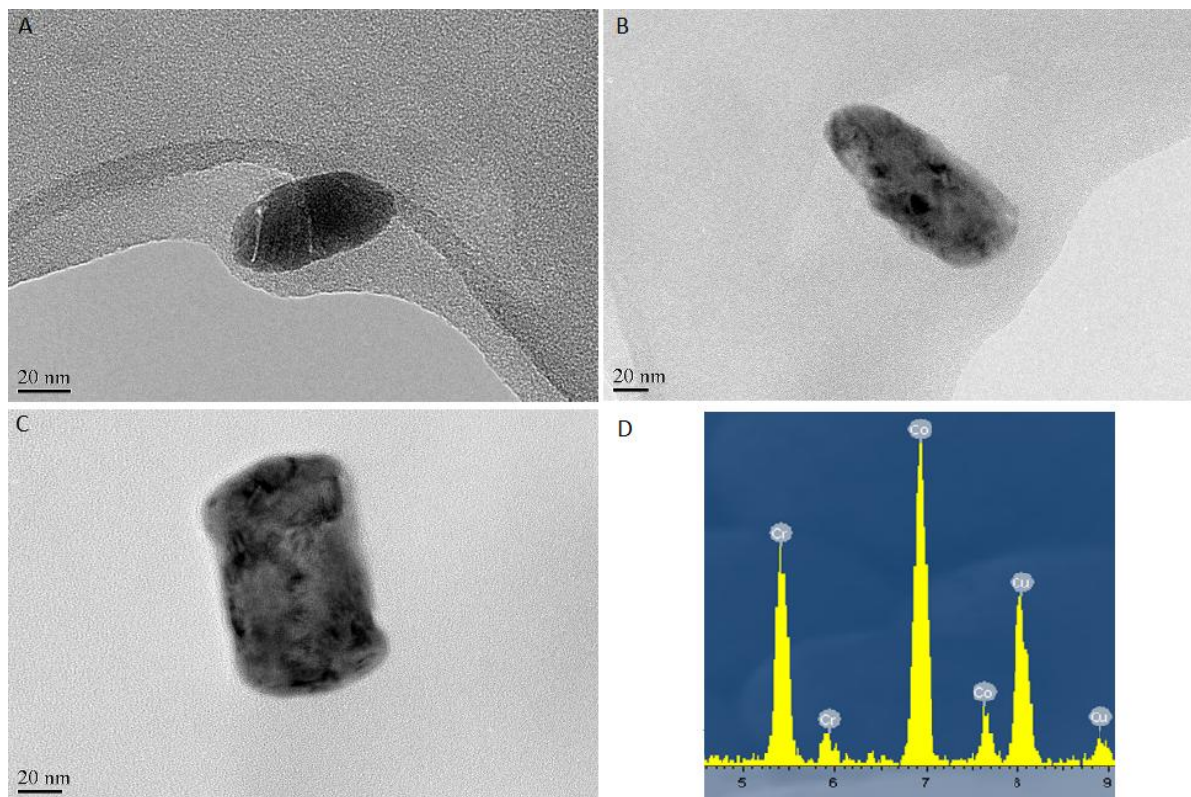


**Figure 6.13: TEM images of CoCr particles seen from Station 4 after A: 1.0 MC, B: 2.5 MC, C: 5.0 MC, D: EDX analysis showing particles confirming CoCr present.**

### 6.7 Results from Dual Mobility Tests 1-3

The test serum from the first 0.5 MC of testing from all three of the dual mobility tests was analysed. For each DM test, one sample of serum frozen after testing in a standard station (1,2 or 5) and one sample of serum frozen after testing in a microseparation station (3 or 4) was analysed. Six serum samples were analysed in total.

Isolation of CoCr or Cr particles proved very challenging due to the presence of stainless steel wear particles that were also present in the serum. Figure 6.14 shows a selection of TEM images from the DM test samples. The EDX analysis confirmed the presence of Chromium, Iron and Nickel, which is indicative of stainless steel wear debris.

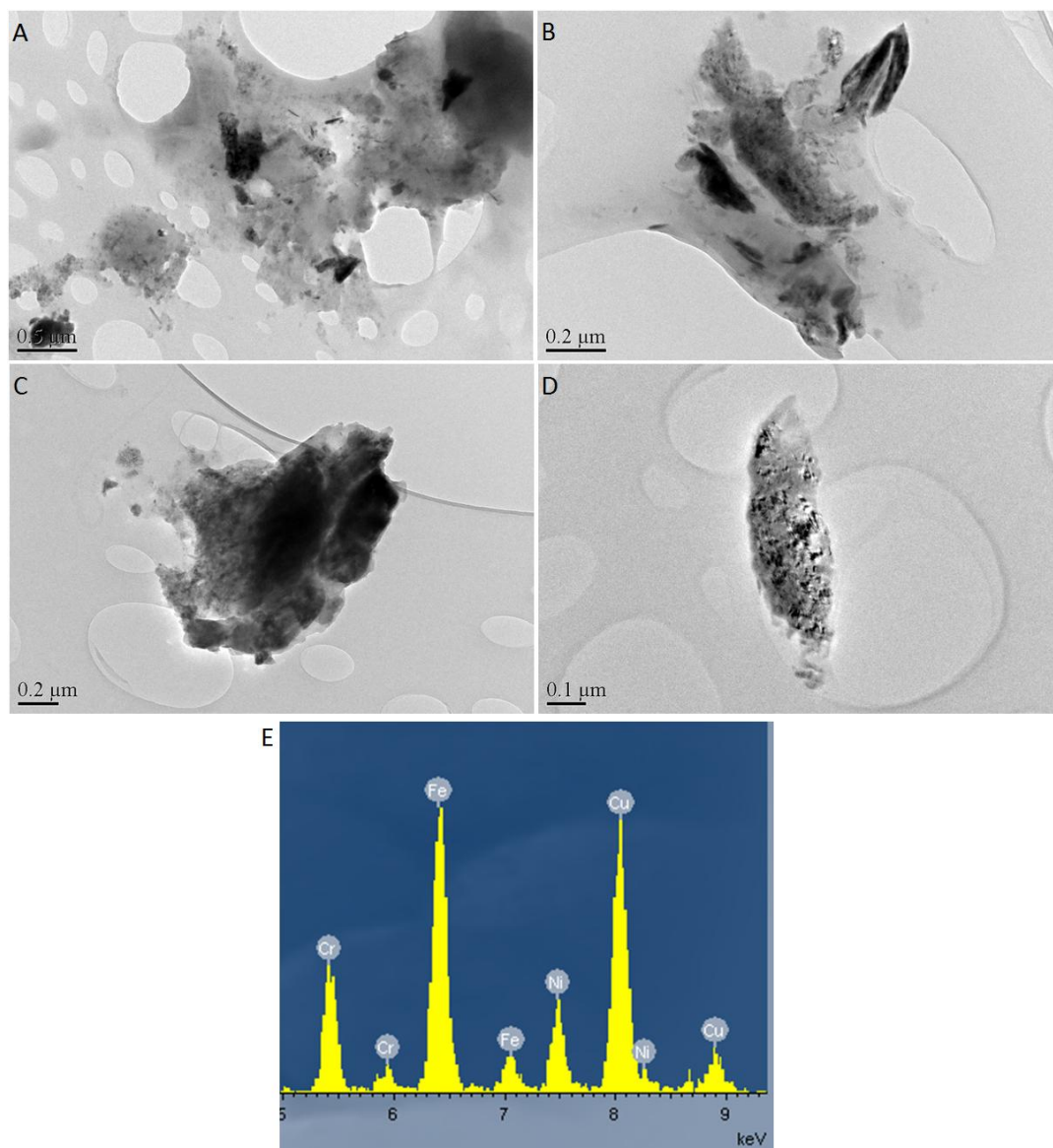


**Figure 6.14: Selection of TEM images taken of stainless steel wear particles present in DM Test samples. A: DM Test 1 (standard), B: DM Test 1 (Microseparation), C: DM Test 2 (standard), D: DM Test 3 (standard), E: EDX spectra confirming presence of Chromium, Iron and Nickel.**

## 6. Metal particle analysis

---

The presence of these stainless steel wear particles confirm that there has been contact between the rim of the E1 liner and the stainless steel head stem. A photograph of the area in question is provided below in Figure 6.15.



**Figure 6.15: Photograph showing the dry set up of the dual mobility joint.**

This contact between the head stem and the E1 liner has been further verified by carrying out zygo analysis on the six head stems used for the dual mobility tests.

Zygo data was recorded at six points taken at 60° increments around the head stem. The results are shown in Figure 6.16. The data from stations 1, 2 and 5 were combined to give the 'standard' result, the 'microseparation' result is an average of the head stem data from stations 3 and 4, and the head stem in the load station acts as the 'control' since it has not undergone any motion and hence will not have contacted the E1 liner.

The results show that both the surface roughness and the skewness of each head stem undergoing wear testing has decreased, indicating that the head stem has become smoother as a result of wear. The effect was greatest in the microseparation stations.

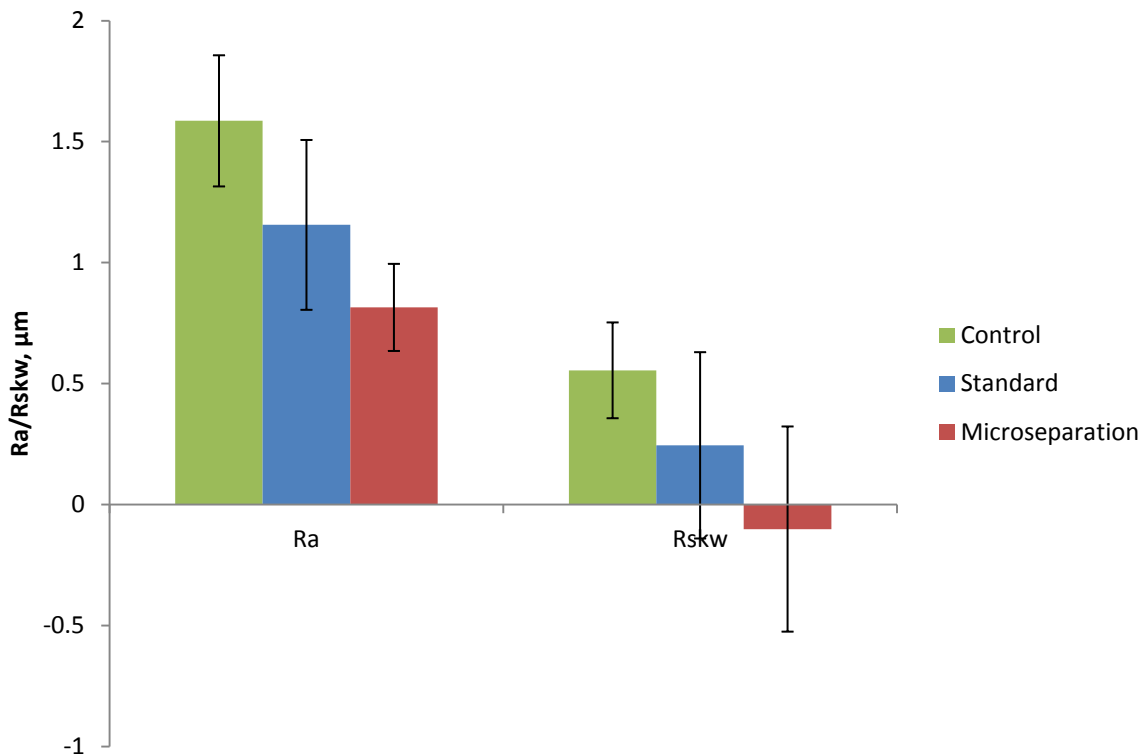


Figure 6.16: Zygo data taken from around the head stems at the end of dual mobility testing.

Only in the test serum from DM Test 2 undergoing microseparation (ie. the test condition which experienced the highest amount of CoCr wear) was it possible to find CoCr particles, but only a handful were found and they were not distinct enough to be able to give any size analysis data. The TEM images are shown in Figure 6.17.

In the microseparation test sample from DM Test 3, Figure 6.18, the EDX analysis confirmed that the stainless steel wear particles and the CoCr wear particles had agglomerated. It is possible that this could have happened either within the serum during testing or during the digestion process.

## 6. Metal particle analysis

---

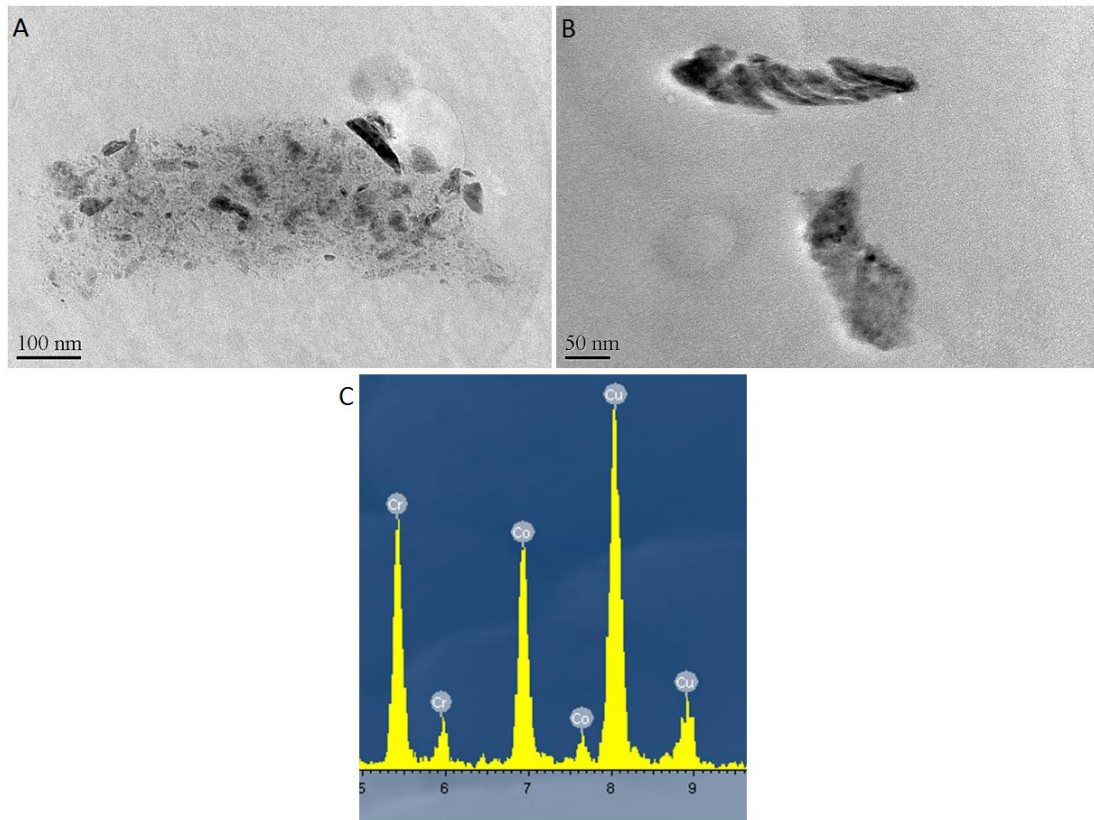


**Figure 6.17: A and B: TEM images of CoCr particles found in serum from DM Test 2 (microseparation) C: EDX spectra confirming presence of CoCr.**

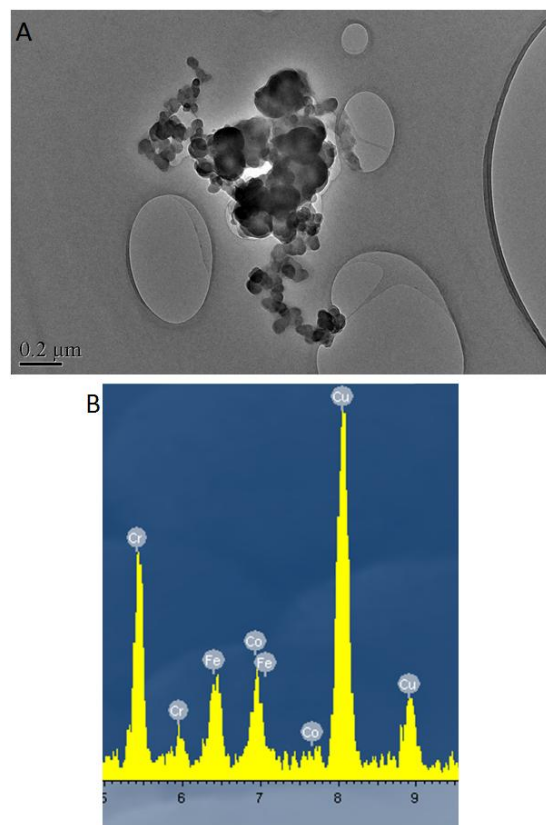


**Figure 6.18: A: TEM image showing agglomeration of CoCr/stainless steel wear debris, B: EDX spectra confirming presence of Co, Cr, Fe.**

## 6. Metal particle analysis

---

On the occasions where the EDX analysis verified the presence of Cr without the presence of either cobalt or iron and nickel, it is not possible to know whether this is Cr from the stainless steel head stem or the CoCrMo bearings.

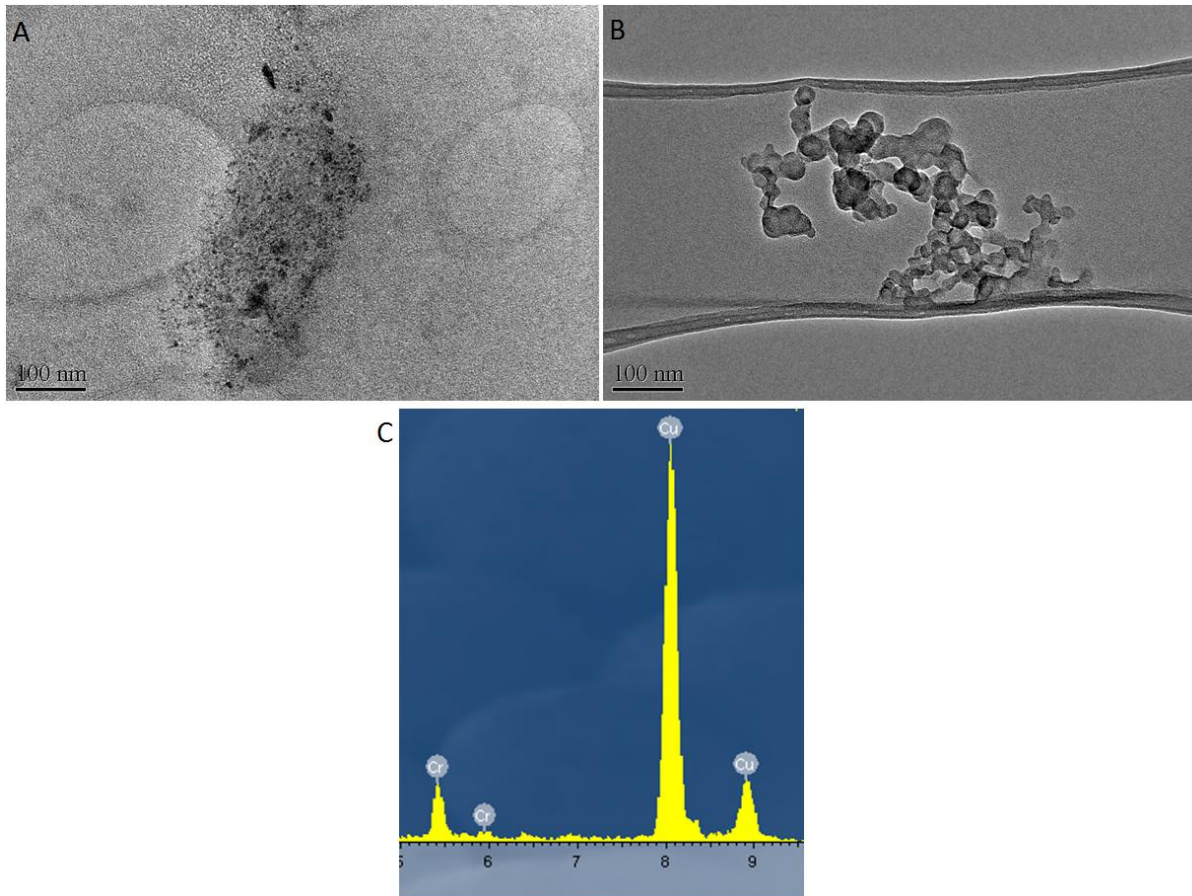


**Figure 6.19: A: TEM image from DM Test 2 (microseparation), B: TEM image from DM Test 3 (microseparation) C: EDX spectra confirming presence of Cr.**

Whilst the presence of stainless steel wear particles has been beneficial in confirming the contact between the head stem and the E1 liner, it has made the isolation and separation of CoCr wear particles a lot more complex and it has not been possible to isolate CoCr wear debris alone from the dual mobility test serum.

### 6.8 Limitations

One limitation of this work was that the experimental protocol used in this study was relatively time consuming. The enzymatic digestion protocol followed here took at least three consecutive days per sample to reach the stage where the particles were isolated. This meant that the protocol could only be followed whilst simulator tests were not in operation due to time constraints.

This was most evident when working with the large dual mobility joints because the procedure between each 0.5 MC stage of testing which included cleaning, weighing and surface analysis, could easily take three continuous days prior to starting the next 0.5 MC stage of the test. It would be extremely beneficial for a protocol to be developed that could be completed alongside simulator work.

As with other published metal particle analysis studies the main limitation of this type of research revolves around the difficulty in isolating a large number of particles from test serum which has a low volume of wear debris. The reactive nature of the metal particles prevents them from being isolated using acids and bases which successfully denature proteins [4; 5; 8] hence enzymatic protocols are favoured. Particle loss and agglomeration are also a common problem [3].

The greatest number of particles imaged in this study was obtained from the COM test serum. From combining the average size of at least 100 particles presented in this project with the volumetric wear data provided by Dr. Wu the results implied that  $10^{12}$  -  $10^{13}$  wear particles were being released every 0.5 MC under Wear Condition 1. This indicates that potentially only 0.0000000001% of the particles have been sized.

In order to address the reason why such a low amount of particles were able to be imaged ICPMS was carried out on the digested COM test serum and found that only 5% of the expected total metal concentrations were present, indicating that metal debris has been lost through the numerous washing and centrifugation steps utilized in the isolation protocol. The ICPMS results are shown in Table 6.2.

## 6. Metal particle analysis

**Table 6.2: ICPMS carried out on digested serum after 1.0 MC from Wear Condition 2. The corrected total weight loss was determined by ICPMS on serum taken from the load control.**

Weight loss determined by ICPMS, mg	Co	Cr	Mo	Total
	0.3308	0.0008	0.0019	0.3335
<b>Corrected total weight loss, mg</b>	0.3297			
<b>Gravimetric weight loss, mg</b>	6.99			
<b>Protocol efficiency, %</b>	4.7			

When only a small percentage of particles are isolated it is not realistic to assume that the distribution is representative of the whole sample. Sizing a larger sample of particles would require extensive TEM sessions and further time spent analysing the images which was not able to be done whilst also carrying out simulator studies.

The number of metal particles analysed in previously published data ranges from 20 to over 1000, see Figure 6.20.

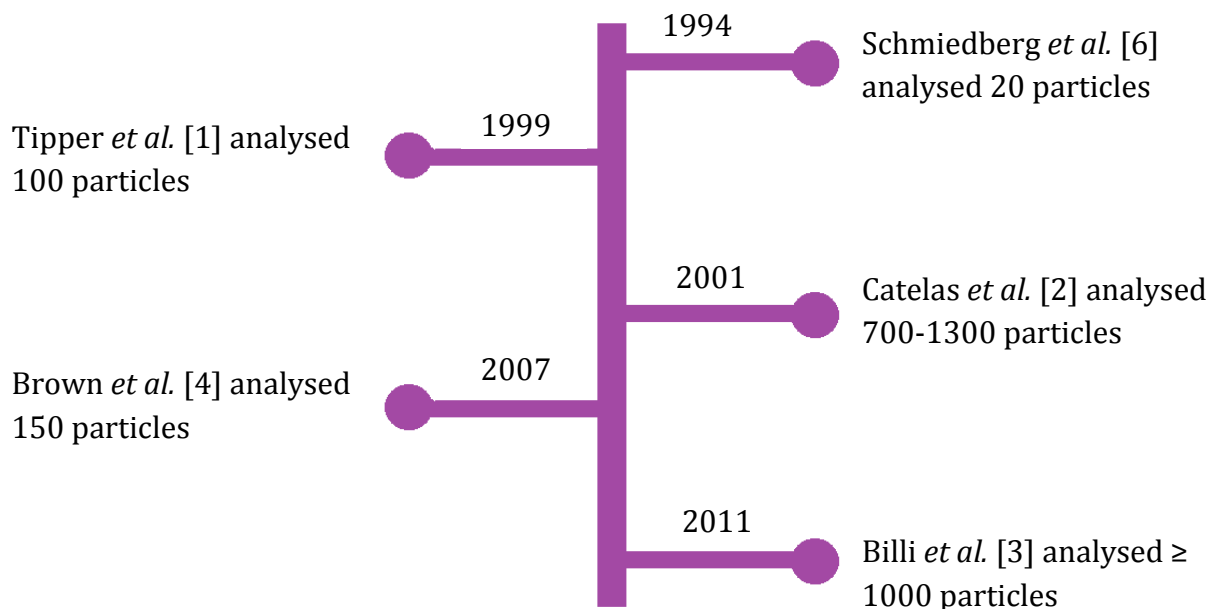


**Figure 6.20: Timeline showing the number of metal wear particles sized in previous studies.**

Even in the metal particle analysis work published by Billi *et al.* [3] which won The John Charnley Award in 2011, the number of particles yielded ranged from 300 to 2,100 particles per sample.

## 6. Metal particle analysis

---

This method took four years to develop and there is no doubt that this is a great achievement. However the exact wear data for the samples analysed is not reported and hence it can be speculated that since the particles under consideration are nanometre in size then even this number of particles may not be enough to provide a size distribution that is relative of the whole sample.

This is an important concern and highlights the time intensive nature of the research that is required for thorough metal particle analysis. The development of a novel method for metal particle isolation capable of being implemented alongside wear testing has not been investigated in this work. Metal particle analysis is worthy of being a stand-alone project.

Another limitation, which is a feature of this project specifically, was that the stainless steel wear particles were not able to be separated from the CoCr wear debris in the dual mobility test serum. Normally if two types of wear debris have different densities they can be separated using density gradient centrifugation. This method has been employed in literature to separate polyethylene particles, which have a density of 0.94 kg/dm<sup>3</sup>, from both test serum [9; 10] and tissues taken from the body during revision surgery [11].

The two metal alloys present in the dual mobility test serum both have very similar and high densities. Stainless steel has a density of 8.0 kg/dm<sup>3</sup> in comparison to the CoCrMo alloy which has a density of 8.27 kg/dm<sup>3</sup>. It is not possible to make liquid density gradients with such a high density capable of separating these two alloys. Hence it is not possible to analyse CoCr wear debris using density gradient centrifugation.

Also there is still the problem when considering the source of wear particles which are confirmed by EDX analysis to be chromium only which could have resulted from either the CoCrMo bearing surface or the stainless steel head stem.

For future work, one solution to this issue is to change the initial test set up and replace the stainless steel head stems. This scenario is considered further in the discussion.

## 6.9 Discussion

Chromium wear particles have been successfully isolated from test serum taken from COM testing subject to two different wear conditions and studied under TEM. The TEM images produced were relatively clear and at least one hundred particles were sized from each sample.

The average particle size of the two samples from Wear Condition 1 corresponds well to data published by Brown *et al.* [4] from another COM simulation study with microseparation at a standard incline. The distribution of particles also corresponds well to that seen *in vivo* in work by Catelas *et al.* [7] where the majority of the particles are distributed around 20-40 nm.

In the COM study when the inclination angle was increased in Wear Condition 2 from 45° to 62° the Cr wear particles decreased in size. The ratio of rods to spheres has also changed with more particles tending to be spherical in shape, with an aspect ratio ranging from 1:1 to approximately 1:9. Only rod-like CoCr wear particles were isolated from MOM Test 1. This can be seen in Figure 6.21.

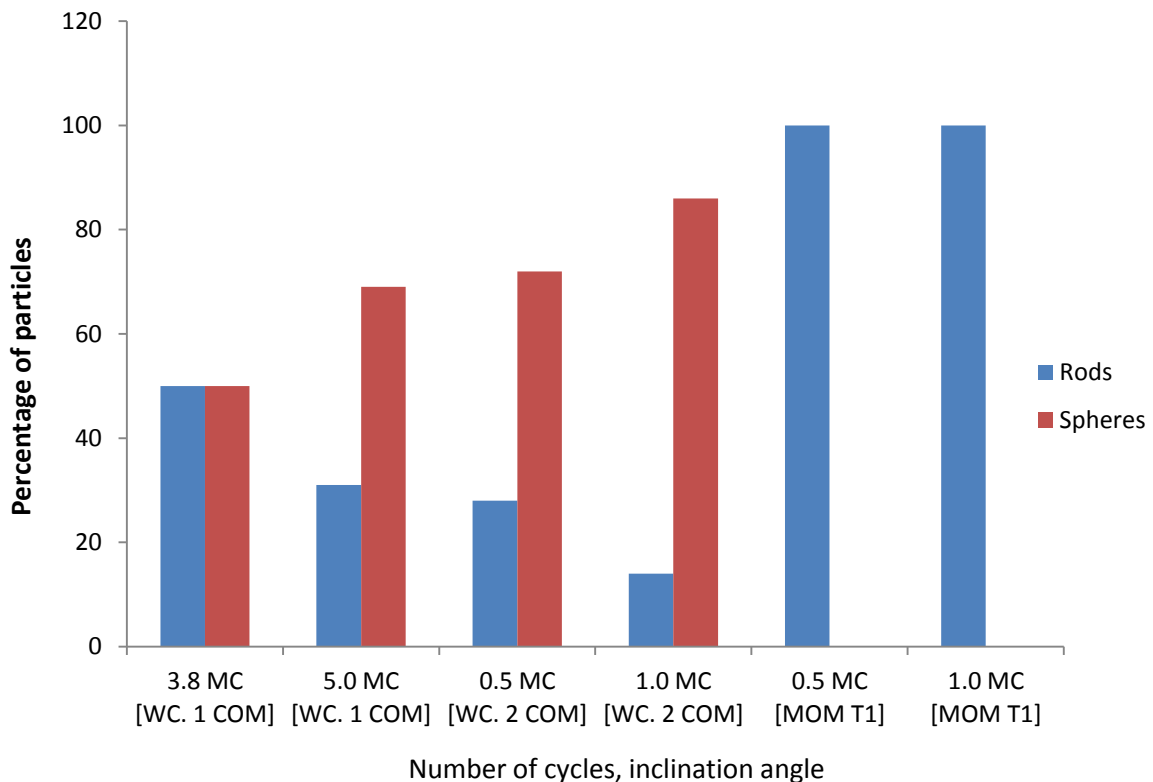


**Figure 6.21: Ratio of rod-like particles to spherical particles in all digested samples from the COM studies and MOM Test 1.**

## 6. Metal particle analysis

---

The comparatively larger, rod-like CoCr wear particles isolated from MOM Test 1 serum indicates that a harsher wear mechanism is operating than for the COM simulations.

The generation of Cr particles is indicative of mild abrasive wear at the surface of the components whereas the production of rod-like CoCr wear particles are more likely to be from abrasive cutting into the bulk mass of the material. This can be seen by comparing optical images of the surface of metal acetabular components between 0 and 1.0 MC from Simulation 3 in Figure 6.22.

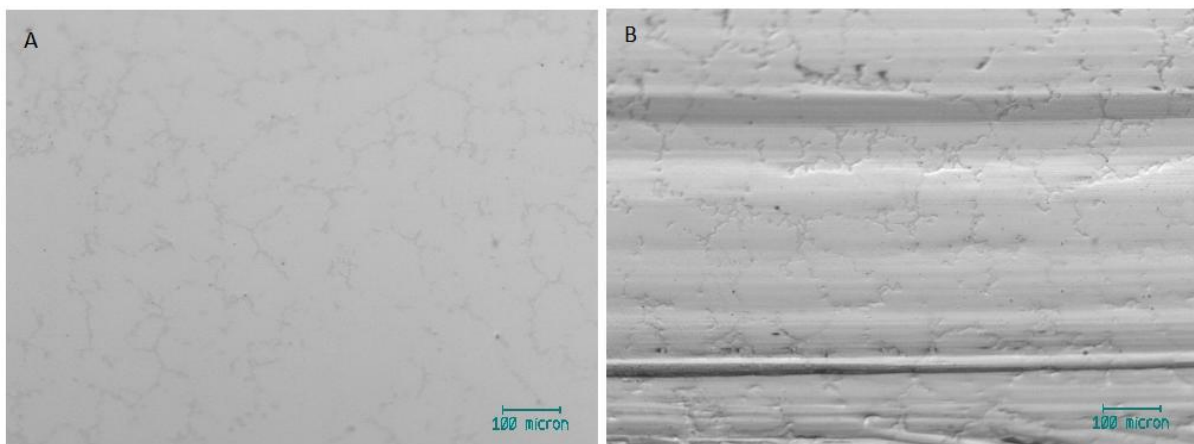


**Figure 6.22: Optical images taken at the surface of a CoCrMo acetabular component from Simulation 3. A: At 0 MC, B: At 1.0 MC.**

It is not possible to compare the wear particles from the dual mobility test serum with those from either the COM studies or MOM Test 1. This is due to the difficulty experienced when trying to isolate the CoCr debris from the stainless steel wear debris that was also present in the test serum.

The stainless steel wear debris has been beneficial in confirming that there has been interaction between the head stem and the liner. No such particles containing chromium, iron and nickel have been found in the previous test serum samples from the COM studies or MOM Test 1.

The interaction between the head stem and the E1 liner has been extremely important in the dual mobility tests. Only when the liner contacts the head stem is the outer articulation engaged.

As this project seeks to understand the effect of leaving a worn metal cup in the body whilst replacing the failed metal resurfacing head with a new dual mobility head it is

essential that the outer surface of the liner articulates against the worn cup during the test simulations.

Under standard conditions the majority of wear occurs within the inner articulation, between the CoCrMo head and the inner pole of the E1 liner. For this reason high inclination, head stem contact and microseparation have all been used within the three dual mobility tests detailed here in order to engage the outer articulation.

This articulation then causes the outer pole of the liner to wear against the previously worn cups which allows the change in wear volume and the change in surface features to be recorded. Hence the worst case wear scenario *in vivo* can be envisaged.

The contact between the head stem and the E1 liner has been essential to this project. However the problem with wear particle analysis for this test set up is that the stainless steel head stems used throughout these tests were not clinically relevant. The presence of stainless steel wear particles in the test serum has meant that finding CoCr wear debris is very difficult. It has also meant that there are two sources of Cr in the test set up and it is not possible to know which of these any lone Cr particles have come from.

In the body, it is estimated that the outer articulation will only be engaged around 20% of the time [12]. Although the interaction between the head stem and the E1 liner will not occur for the majority of the time and so may not produce as much wear debris as that from the inner/outer articulation, it is still an additional source of wear debris that should be considered. Especially since it is not known whether the debris will differ in size and morphology to that produced at the bearing surfaces and so may induce a different reaction *in vivo*.

The commercial head stems currently manufactured for use with the dual mobility joint are typically either polished CoCrMo alloy or Ti alloy. An example of one head stem currently available from Biomet's 'Echo hip system' is shown in Figure 6.23.

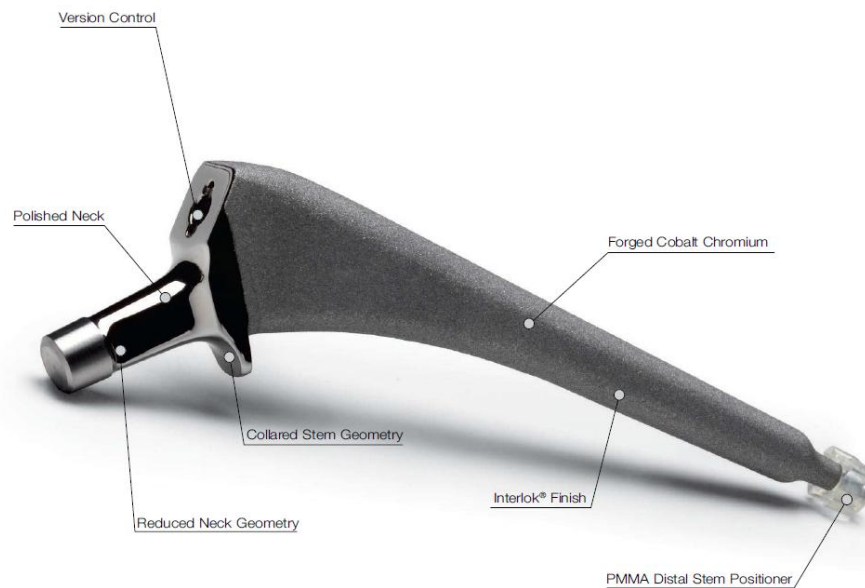


**Figure 6.23: Photograph of the Echo FX Stem taken from the Biomet Echo Hip System product brochure.**

The work presented in this chapter has shown that if the analysis of the wear debris from a dual mobility joint is the main focus of a research project then it is essential that the head stem used in the initial set up is made from the same material with the same polishing and quality control as is manufactured for use in the body. It is worth noting that both CoCrMo and Ti alloy are difficult to machine and a head stem made from either alloy could not have been manufactured within the mechanical workshop at Durham University, which is where the stainless steel head stems were made. This would require extra cost, manufacturing time and collaboration with Biomet prior to testing in order to use head stems that would produce clinically relevant wear debris.

It could be argued that the method devised by Billi *et al.* [3] for metal particle isolation would decrease the time needed for particle analysis since it is a two-step particle isolation method designed to minimise particle loss and improve particle purification. However this method would still not remove the stainless steel wear debris currently present in the dual mobility test serum and hence the initial test conditions need to be addressed first and modified before clinically relevant metal particle analysis studies can be carried out.

### 6.10 Conclusion

Four serum samples taken from Dr Wang's COM study were analysed. All particles isolated were confirmed by EDX analysis to be Cr and either spherical or rod-like in nature. At least 100 particles per sample were isolated and sized.

The average length and width of the rod-like particles produced after 3.8 MC of Wear Condition 1 in the COM study was  $68 \pm 8$  nm and  $20.5 \pm 3$  nm respectively. The average diameter of the spherical particles was  $41 \pm 7$  nm. After 5 MC of testing subject to the same wear condition the average particle size decreased. The average length and width of the rod-like particles was  $55 \pm 12$  nm and  $16.1 \pm 4$  nm respectively. The average diameter of the spherical particles was  $22 \pm 3$  nm.

Increasing the inclination angle from  $45^\circ$  in Wear Condition 1 to  $62^\circ$  in Wear Condition 2 of the COM study decreased the size of the wear debris produced. The average length and width of the rod-like particles produced after 0.5 MC of Wear Condition 2 in the COM study was  $17 \pm 6$  nm and  $2.7 \pm 0.4$  nm respectively. The average diameter of the spherical particles was  $13 \pm 3$  nm. After 1 MC of testing subject to the same wear condition the average particle size decreased. The average length and width of the rod-like particles was  $7 \pm 2$  nm, and  $2.5 \pm 0.3$  nm respectively. The average diameter of the spherical particles was  $3 \pm 1$  nm.

Five serum samples taken from MOM Test 1 were analysed. It was common for particles to agglomerate which meant that they were not suitable for size analysis. Small, indistinguishable Cr particles were seen. CoCr rod-like particles with a polycrystalline structure were imaged. The chemical composition of all particles was confirmed by EDX analysis. Not more than 25 isolated particles were analysed per sample.

Six samples in total were analysed from DM Test 1, 2 and 3. Isolation of CoCr or Cr particles was not achievable due to the presence of wear particles confirmed with EDX analysis to be composed of chromium, iron and nickel. This is indicative of stainless steel wear debris and verifies that there has been contact between the stainless steel head stem and the rim of the E1 liner during simulator motion.

In order to produce clinically relevant wear debris from a dual mobility test the head stems in the current set up have to be modified and a head stem made from the same

material with the same polishing and quality control as is manufactured for use in the body is required.

### 6.11 References

- [1] J.L. Tipper, P.J. Firkins, A.A. Besong, P.S.M. Barbour, J. Nevelos, M.H. Stone, E. Ingham, J. Fisher, *Science* 250 (2001) 120-128.
- [2] I. Catelas, M.a. Wimmer, S. Utzschneider, *Seminars in immunopathology* 33 (2011) 257-71.
- [3] F. Billi, P. Benya, A. Kavanaugh, J. Adams, H. McKellop, E. Ebramzadeh, *Clinical orthopaedics and related research* (2011).
- [4] C. Brown, S. Williams, J.L. Tipper, J. Fisher, E. Ingham, *Journal of materials science. Materials in medicine* 18 (2007) 819-27.
- [5] I. Catelas, J.D. Bobyn, J.B. Medley, J.J. Krygier, D.J. Zukor, a. Petit, O.L. Huk, *Journal of biomedical materials research* 55 (2001) 320-9.
- [6] S.K. Schmiedberg, D.H. Chang, C.G. Frondoza, A.D. Valdevit, J.P. Kostuik, *J Biomed Mater Res* 28 (1994) 1277-88.
- [7] I. Catelas, J.B. Medley, P.a. Campbell, O.L. Huk, J.D. Bobyn, *Journal of biomedical materials research. Part B, Applied biomaterials* 70 (2004) 167-78.
- [8] I. Catelas, J.D. Bobyn, J.J. Medley, D.J. Zukor, a. Petit, O.L. Huk, *Journal of biomedical materials research* 55 (2001) 330-7.
- [9] S. Affatato, D. Emiliani, G. Bersaglia, F. Traina, A. Toni, *Int J Artif Organs* 27 (2004) 424-32.
- [10] F. Billi, P. Benya, A. Kavanaugh, J. Adams, E. Ebramzadeh, H. McKellop, *Clinical Orthopaedics and Related Research* 470 (2012) 329-338.
- [11] P. Campbell, P. Doorn, F. Dorey, H.C. Amstutz, *Proc Inst Mech Eng H* 210 (1996) 167-74.
- [12] [www.medacta.com](http://www.medacta.com), Versafit cup leaflet.

## 7. Discussion and conclusion

---

### 7.1 Discussion

#### 7.1.1 Comparison of retrieved CoCrMo cups with physiologically scratched CoCrMo cups from MOM Test 1 and 2

This section compares the retrieval analysis data from Chapter 3 with the resulting cups from MOM Test 1 and 2 from Chapter 4.

The two simulator studies in Chapter 4 have been carried out with the aim to produce cups with features similar to that seen in retrievals. An overview of the two simulations is given below.

##### **MOM Test 1:**

5 MC standard simulator study with the cups positioned at 45° inclination angle.

##### *Important features of test:*

Stations 2, 3 and 5 experienced leaks leading to runaway wear. This occurred during the running-in stage for Station 2 and 3 and during steady state for Station 5.

##### **MOM Test 2:**

2 MC simulator study with third body particles added to the test lubricant at different stages of the test. All cups were positioned at 45° inclination angle.

##### *Important features of test:*

The test lubricant was varied according to the details below.

0 – 0.5 MC: 25% bovine serum + 10 mg/ml HA

0.5 – 1.0 MC: 25% bovine serum

1.0 – 1.5 MC: 25% bovine serum + 10 mg/ml Ti

1.5 – 2.0 MC: 25% bovine serum

Figure 7.1 and Figure 7.2 compare the surface roughness and skewness data from each of the ten cups at the end of the above simulations in comparison to the retrieved acetabular cups.

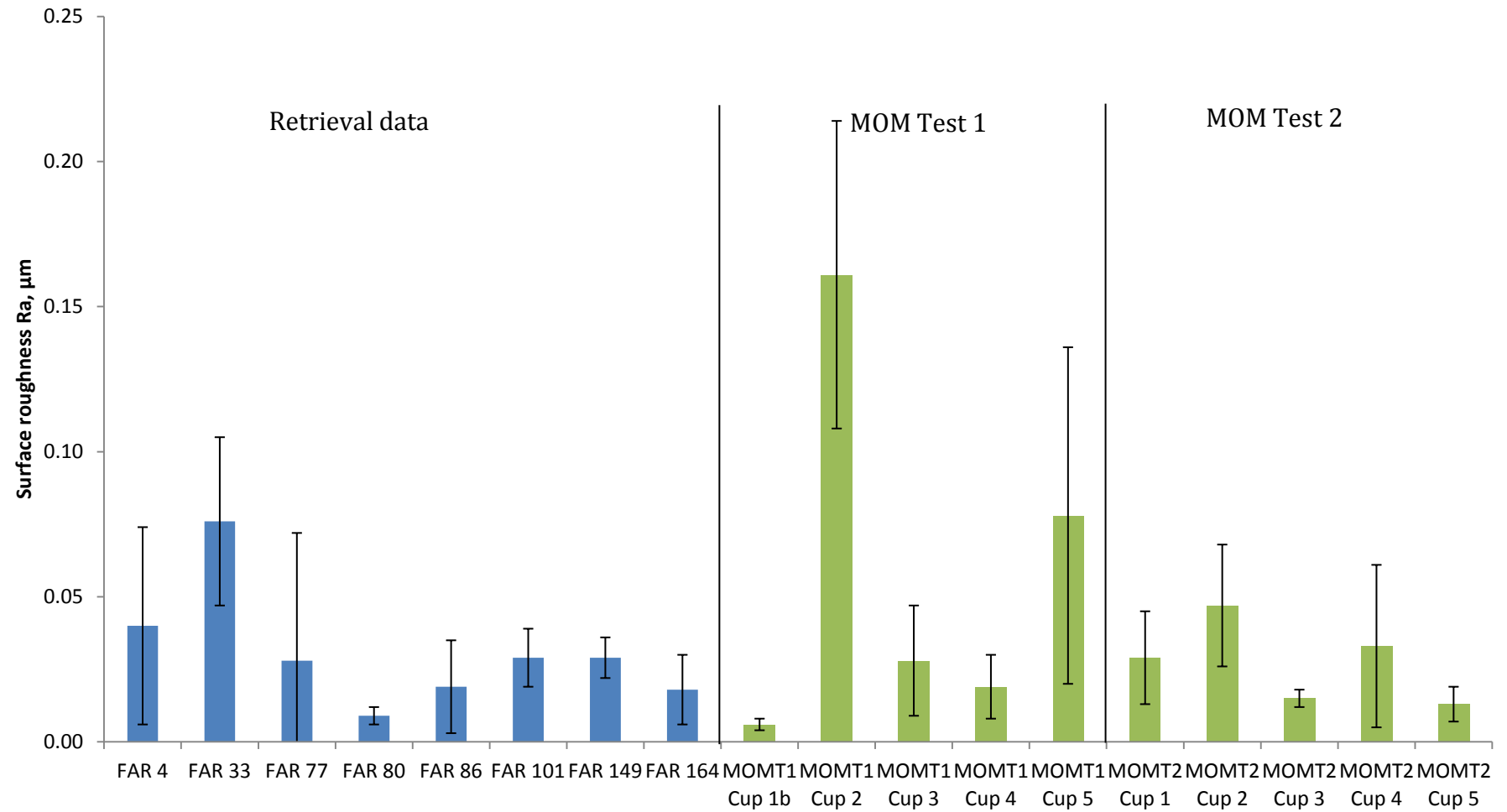


Figure 7.1: Comparison of zygo Ra data from retrieved CoCrMo cups (blue) with CoCrMo cups from MOM T1 and T2 (green).

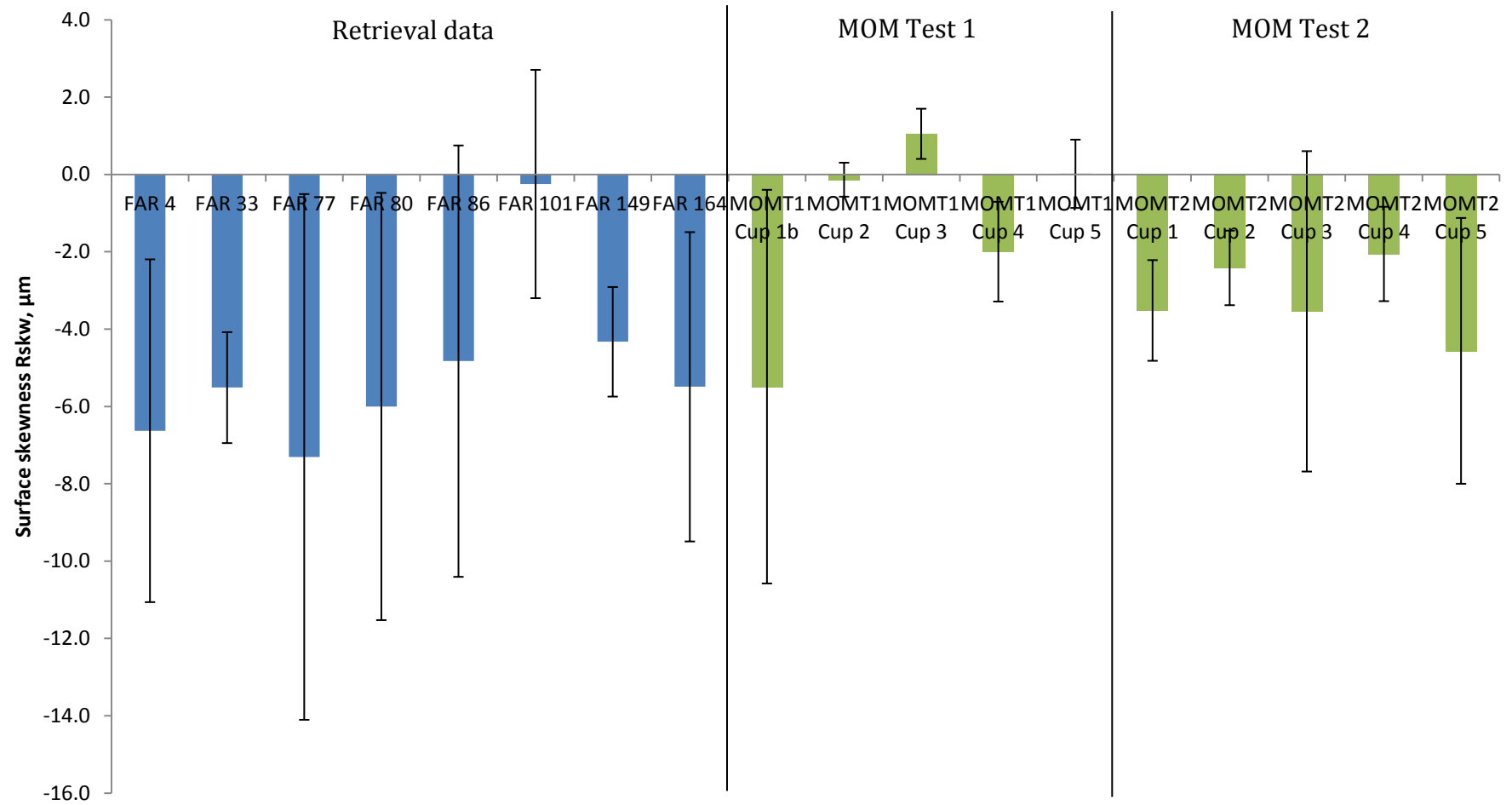


Figure 7.2: Comparison of zygo Rskw data from retrieved CoCrMo cups (blue) with CoCrMo cups from MOM T1 and T2 (green).

MOM Test 1 suffered from dry wear due to the supply of low quality gaiters for testing. Cup 2 in particular suffered a great mass loss and the surface roughness was much greater than in the explants analysed in this study. The wear rate for cup 2 over the 5 MC was 41.78 mm<sup>3</sup>/MC. Wear rates of this magnitude have been seen *in vivo* based on CMM analysis after revision surgery [1]. Cup 3 and 5, both of which experienced leaks, also had high wear rates (35.82 mm<sup>3</sup>/MC and 5.28 mm<sup>3</sup>/MC respectively) as seen *in vivo*. Cups 1 and 4 had low wear rates, with very little change in surface roughness or skewness over the course of the test.

The difference in test conditions due to the occurrence of dry wear led to a variety of surface features and wear rates for each of the cups tested. The components were unable to recover during the test and the results were representative of the unpredictable nature of the MOM articulation which has been seen *in vivo*.

The main difference between the cups from MOM Test 1 and the retrievals was that the test cups had mainly unidirectional scratching. Multidirectional scratches of the type seen in the optical images from retrievals are not easy to create in a simulator study undergoing controlled standard motion. However multidirectional scratches occur easily *in vivo* due to the varied movement and activities carried out by each patient.

MOM Test 2 was carried out with the addition of clinically relevant third body particles to the test serum with the aim to obtain surface features representative of those seen *in vivo*.

From Figure 7.1 and Figure 7.2 it is clear that MOM Test 2 has produced cups with surface roughness values closer to that seen in retrievals as well as the desired negative skewness.

Whilst unidirectional scratches were still a common feature, areas of multidirectional scratching were also present on the surface. The cups from MOM Test 2 were also more uniform with respect to both wear rate and surface features across the five test stations in comparison to MOM Test 1. This is because Simulation Solutions improved the quality of the gaiters supplied and hence dry wear did not affect this test.

The results from MOM Test 2 also indicated that third body particles present in the tribocontact between two CoCrMo components can accelerate wear. HA had a greater effect on the wear rate of both the heads and the cups in MOM Test 2 than Ti.

Figure 7.3 shows a comparison of zygo images from the retrievals and cups from the MOM tests. The retrieval images show that the carbides have been smoothed and, in some places, removed. Scratching of the metal matrix has also occurred. In MOM Test 1, carbides have been smoothed but for those cups subject to dry wear the scratches are much deeper than seen *in vivo* in this study. In MOM Test 2 carbide smoothing, removal and scratching of the matrix are visible and similar to that seen in retrievals.

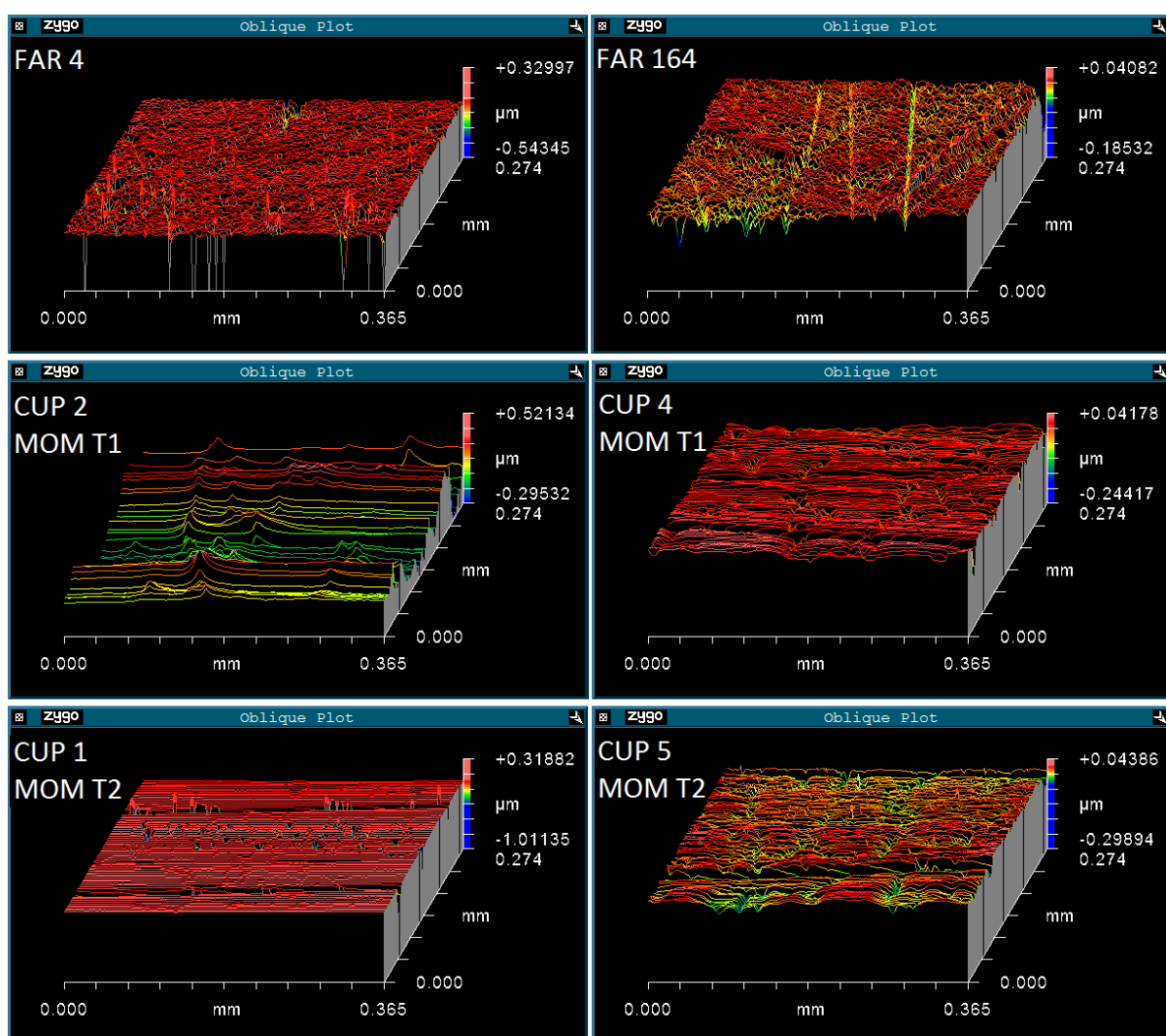
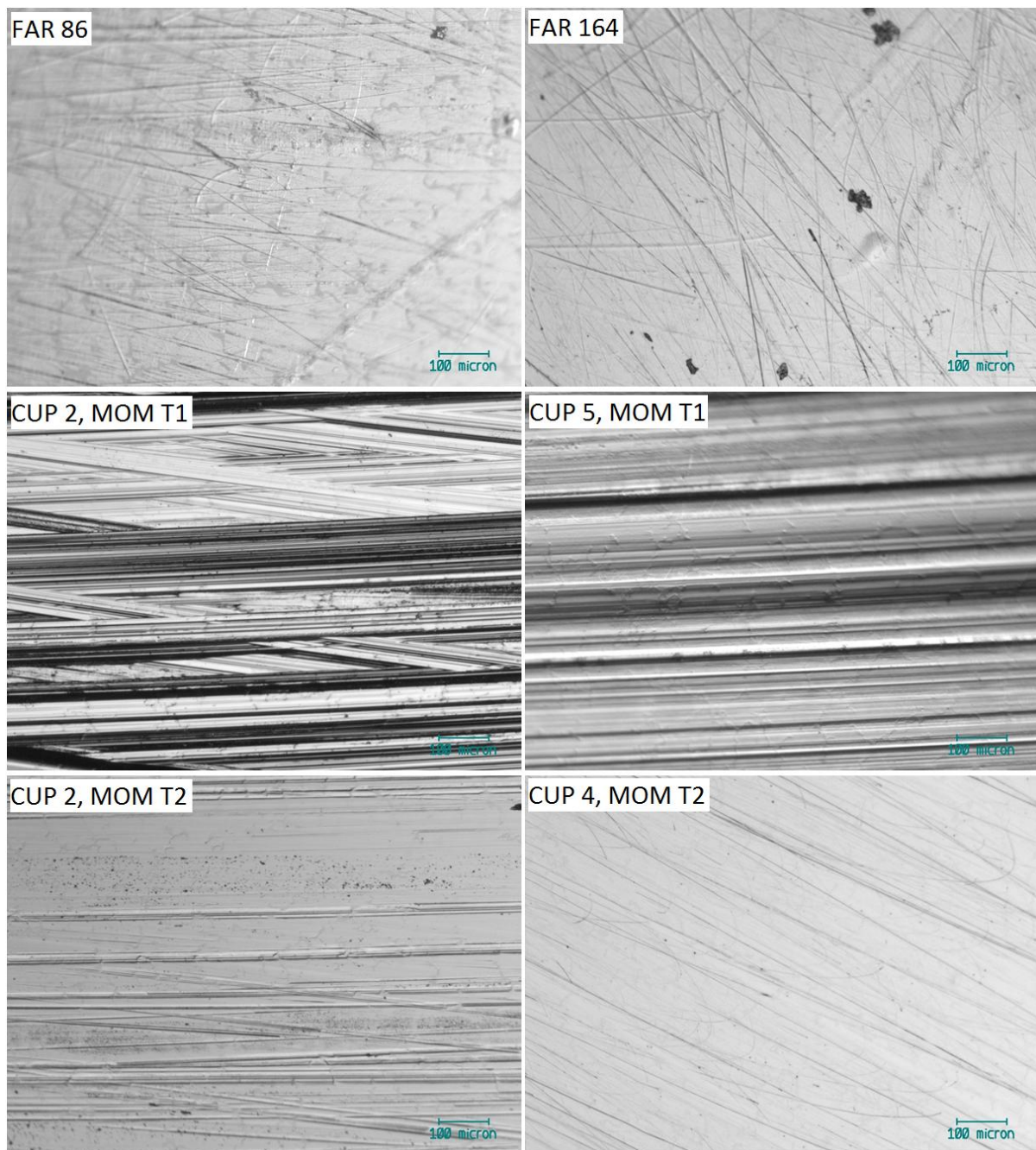


Figure 7.3: Comparison of surface profiles from retrieved CoCrMo cups with the CoCrMo cups at the end of MOM T1 and T2.

The same result can also be seen in the optical images. Figure 7.4 shows a comparison of images taken from the retrievals and the cups from the two tests.



**Figure 7.4: Optical images taken within the wear patch of retrieved CoCrMo cups in comparison to the CoCrMo cups at the end of MOM T1 and T2.**

In conclusion, MOM Test 1 produced a variety of cups with wear rates similar to that seen in failed implants but with unrealistic surface features in some cups due to dry wear causing deep unidirectional scratching. MOM Test 2 had greater success in providing cups with surface features similar to the eight retrieved cups studied in this project.

### 7.1.2 Comparison of results from DM Tests 1-3

This section compares the results from DM Tests 1-3 as detailed in Chapters 5. Three 5 MC DM tests have been carried out in this project and an overview of the test conditions are given below.

**DM Test 1:** DM heads vs. Worn cups from MOM Test 1

**DM Test 2:** DM heads vs. Unworn cups

**DM Test 3:** DM heads vs. Worn cups from MOM Test 2

*Important features of each DM test:*

Stations 1, 2 and 5 were subject to standard testing conditions.

Stations 3 and 4 were subject to microseparation testing conditions.

All cups were positioned at 62° inclination angle.

The wear data from the standard and microseparation testing conditions in each of the three DM tests has been combined and is presented in Figure 7.5 to Figure 7.10. The data for DM Test 2 and DM Test 3 has been analysed using Student's T test to see whether the increased roughness of the cups used in DM Test 3 has made any statistical difference to the data. The corresponding comparison between DM Test 1 and DM Test 2 was not valid due to the large variance in the roughness of the cups in DM Test 1.

Figure 7.5 shows the cumulative volume loss of the CoCrMo heads under standard testing conditions. There has been no statistical difference for the wear rate between the different tests. This shows that under standard conditions when the majority of the wear occurs at the inner articulation, the heads are not affected by the variance in roughness of the cup used in the outer articulation.

Figure 7.6 shows the cumulative volume loss of the CoCrMo heads under microseparation testing conditions. There was no statistical difference between the data from DM Test 2 and DM Test 3 ( $p=0.09$ ) but each head used in DM Test 1 and 3 did experience a lower wear rate than those in DM Test 2.

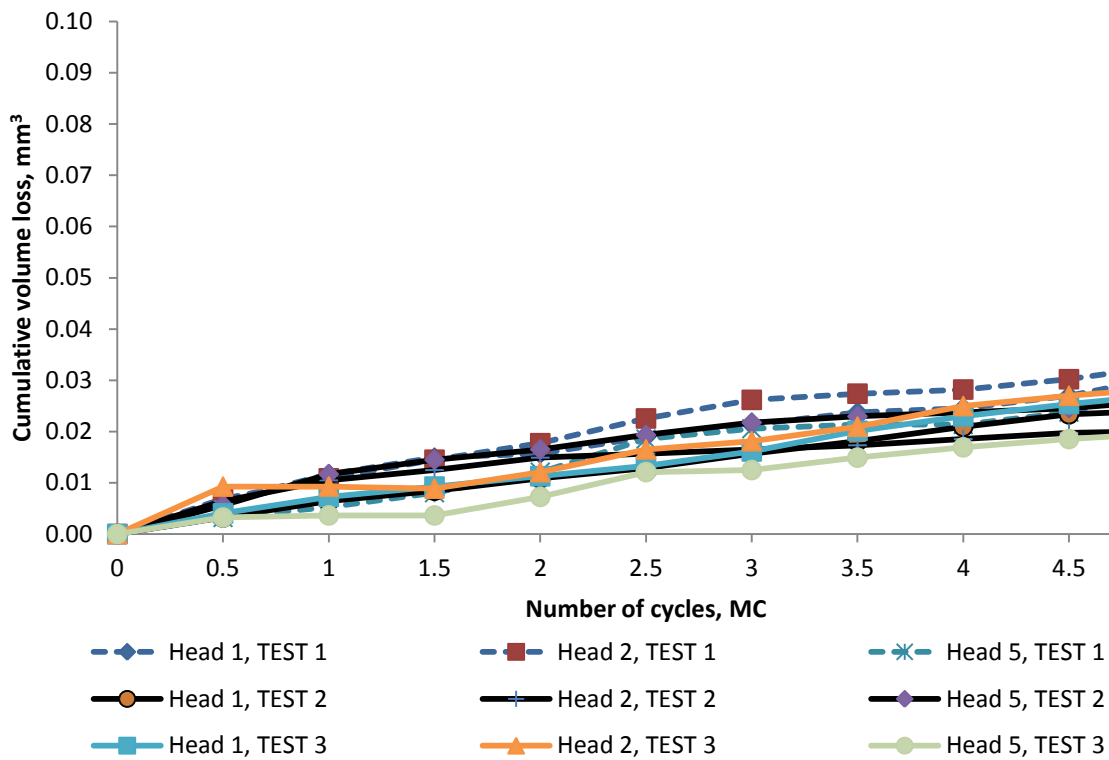


Figure 7.5: Cumulative volume loss of 28 mm CoCrMo heads in all dual mobility tests under standard conditions, accounting for the load soak.

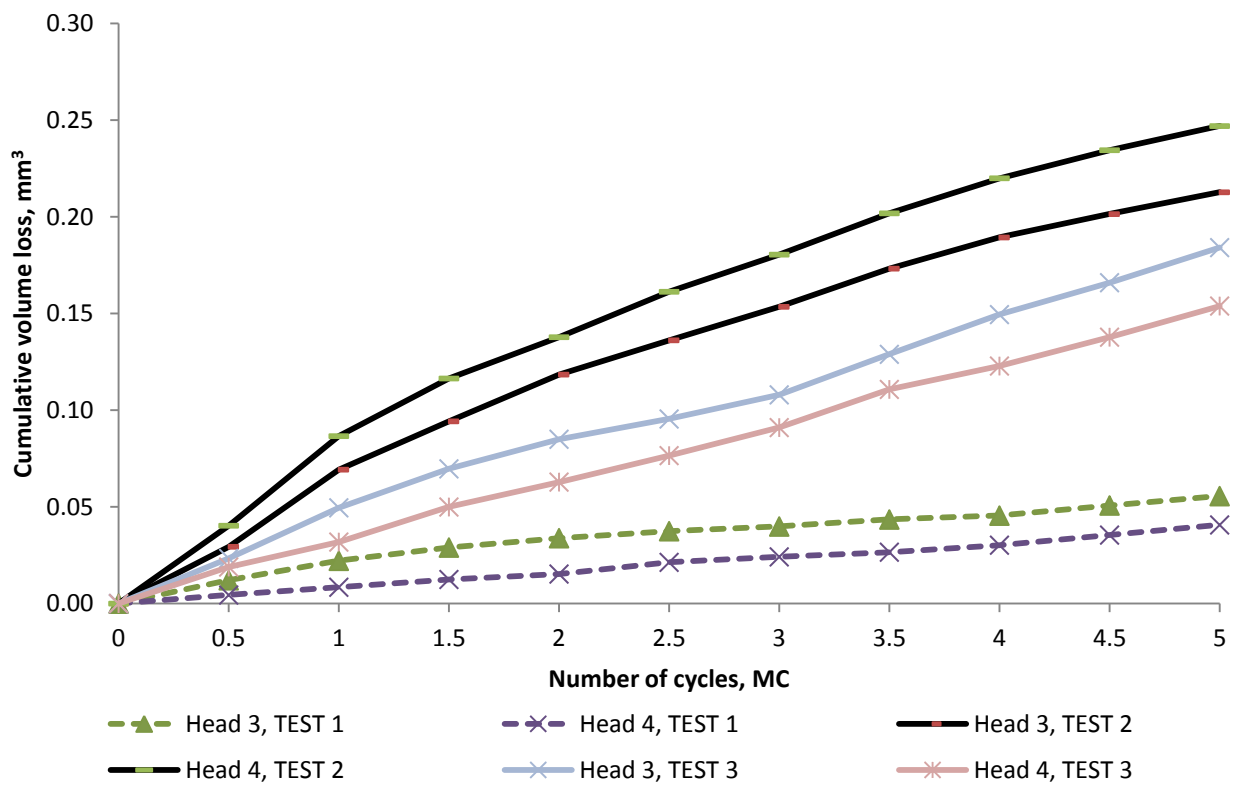


Figure 7.6: Cumulative volume loss of 28 mm CoCrMo heads in all dual mobility tests under microseparation conditions, accounting for the load soak.

Figure 7.7 shows the cumulative volume loss from the E1 liners under standard testing conditions. Liner 1 in DM Test 1 experienced a leak during the initial 0.5 MC of the study which has led to an initial increase in wear which stabilised over the course of the test. The standard liners in DM Test 2 and DM Test 3 have not experienced statistically different results ( $p=0.3$ ) which again concludes that the inner articulation is dominant under standard testing conditions and that it has not been affected by the change in surface roughness of the cups.

Figure 7.8 shows the cumulative volume loss from the E1 liners under microseparation conditions. Initially over the first 1 MC of testing, the liners in DM Test 3 wore more than the liners in DM Test 2. This is due to the presence of third body particles which were present in the metal matrix of the CoCrMo cups at the start of DM Test 3 and shows that the outer articulation is engaged more during microseparation. It is assumed that these particles will have been lost from the test as the serum was replaced at each 0.5 MC interval. Despite this initial increase the liners in DM Test 3 wore statistically less than the liners in DM Test 1 based on analysis of the full 5 MC data.

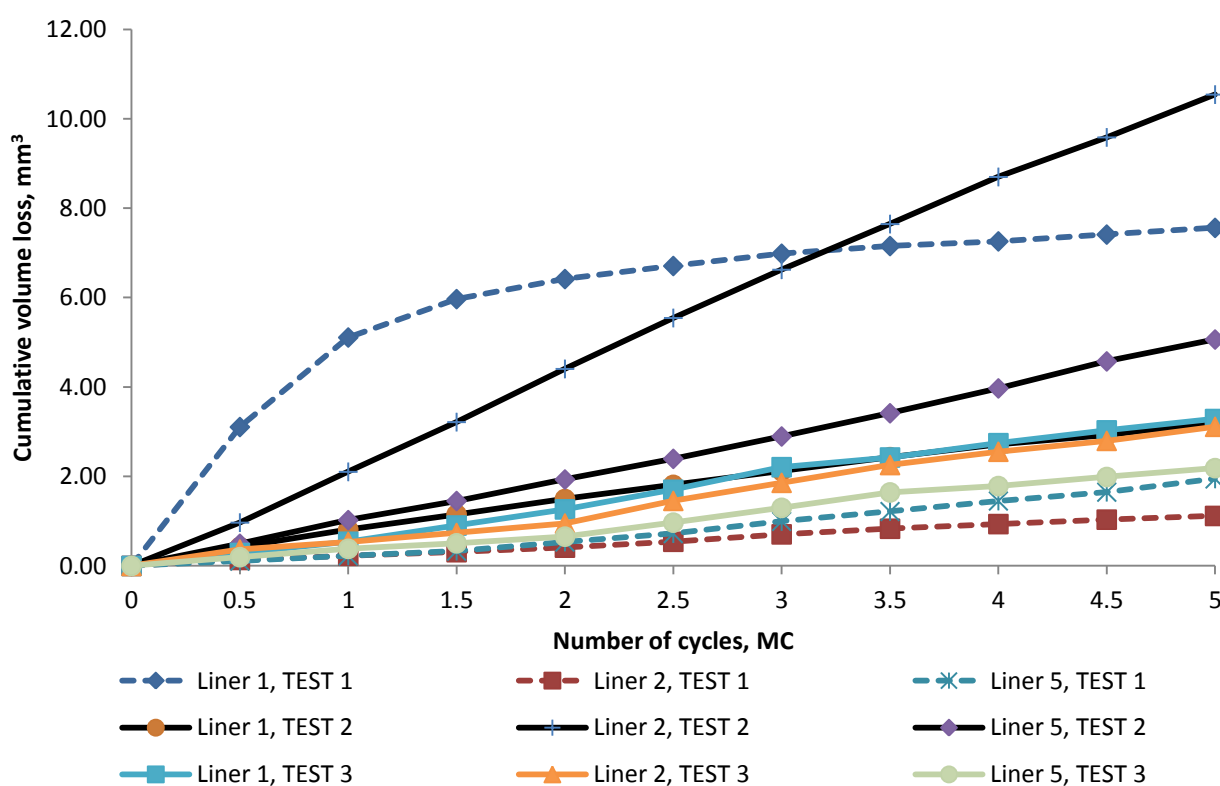
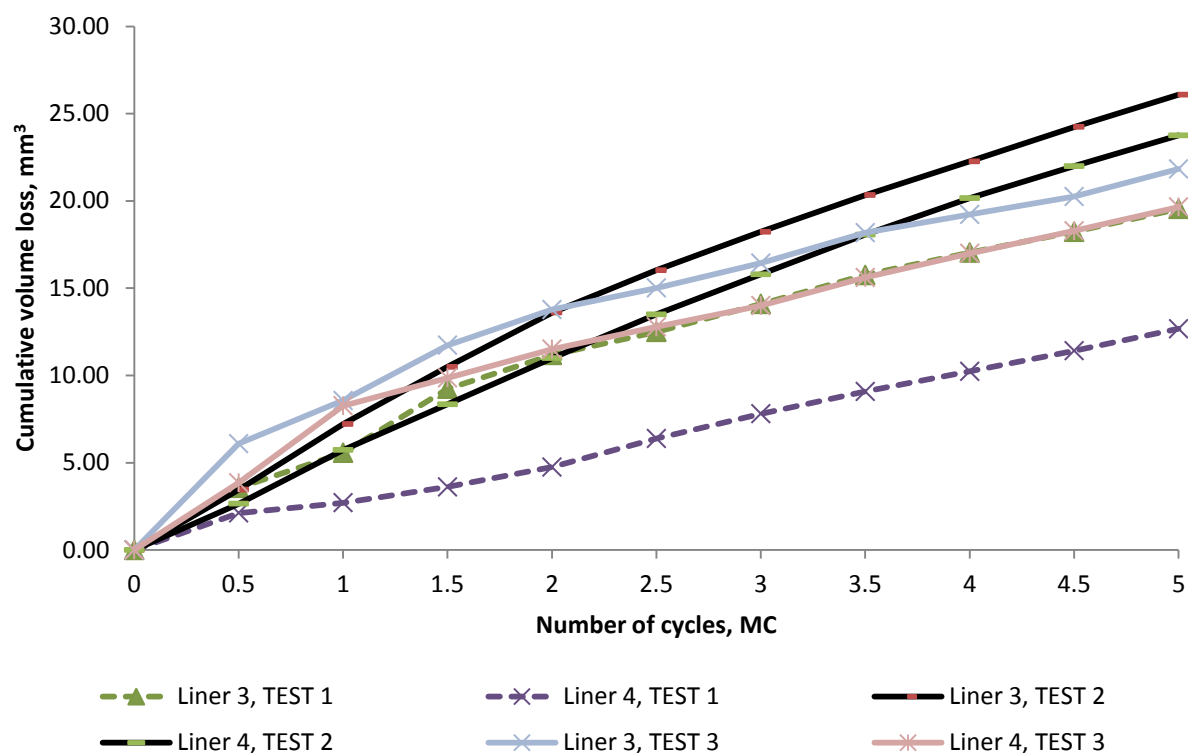


Figure 7.7: Cumulative volume loss from E1 liners in all dual mobility tests under standard conditions, accounting for the load soak.



**Figure 7.8: Cumulative volume loss from E1 liners in all dual mobility tests under microseparation conditions, accounting for the load soak.**

Figure 7.9 shows the cumulative volume loss of the CoCrMo cups under standard testing conditions. The cups in DM Test 3 have worn statistically less than the cups in DM Test 2 ( $p = 0.0008$ ). It is clear from the graph that the cups in DM Test 1 have also worn less than the cups in DM Test 2.

Figure 7.10 shows the cumulative volume loss of the CoCrMo cups under microseparation conditions. The cups in DM Test 3 have worn statistically less than the cups in DM Test 2 ( $p = 0.002$ ) and again it is clear that the cups in DM Test 1 have also worn less than the cups in DM Test 2.

The increase in wear under both standard and microseparation conditions between the CoCrMo cups in DM Test 3 in comparison to those in DM Test 1 may have been a consequence of residual third body particles still present in the CoCrMo cups after MOM Test 2.

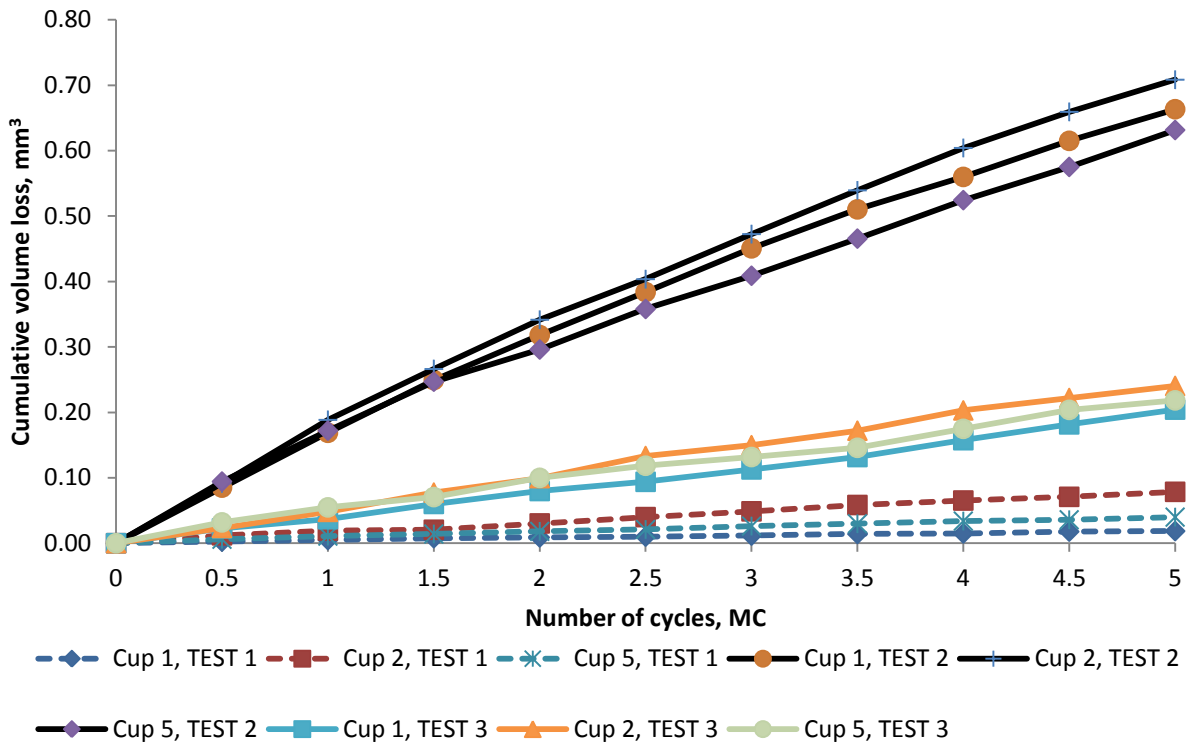


Figure 7.9: Cumulative volume loss of 60 mm CoCrMo cups in all dual mobility tests under standard conditions, accounting for the load soak.

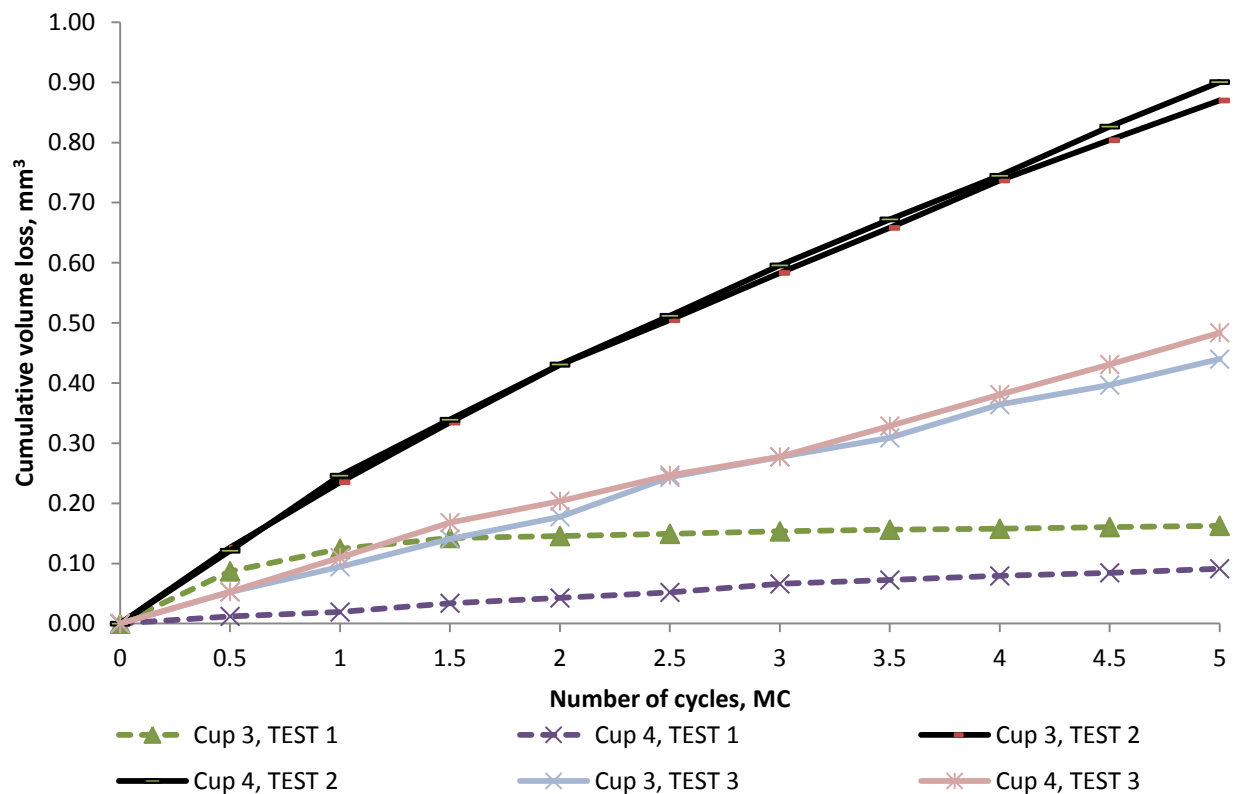


Figure 7.10: Cumulative volume loss of 60 mm CoCrMo cups in all dual mobility tests under microseparation conditions, accounting for the load soak.

## 7. Discussion and conclusion

---

The previously unworn CoCrMo cups used in DM Test 2 have experienced greater wear than the previously worn CoCrMo cups used in both DM Test 1 and 3. The reasons for this will be discussed further with the use of zygo and optical data.

A summary of the wear rates from each component in the three DM tests is given in Table 7.1.

**Table 7.1: Wear rates from each component in each of the three dual mobility tests, mm<sup>3</sup>/MC. Components undergoing microseparation conditions (m) are shown in bold.**

Wear rates, mm <sup>3</sup> /MC (0 – 5 MC)	DM Test 1	DM Test 2	DM Test 3
Head 1	0.005	0.005	0.005
Head 2	0.006	0.003	0.005
<b>Head 3 (m)</b>	<b>0.010</b>	<b>0.042</b>	<b>0.035</b>
<b>Head 4 (m)</b>	<b>0.008</b>	<b>0.048</b>	<b>0.030</b>
Head 5	0.006	0.005	0.004
Liner 1	1.171	0.635	0.691
Liner 2	0.230	2.146	0.642
<b>Liner 3 (m)</b>	<b>3.759</b>	<b>5.146</b>	<b>3.878</b>
<b>Liner 4 (m)</b>	<b>2.493</b>	<b>4.973</b>	<b>3.567</b>
Liner 5	0.397	1.007	0.459
Cup 1	0.004	0.132	0.040
Cup 2	0.016	0.141	0.049
<b>Cup 3 (m)</b>	<b>0.023</b>	<b>0.170</b>	<b>0.088</b>
<b>Cup 4 (m)</b>	<b>0.019</b>	<b>0.175</b>	<b>0.093</b>
Cup 5	0.008	0.122	0.042

Three bearing surfaces were consistently analysed using zygo profilometry and optical microscopy over the course of the three DM tests;

1. The outer bearing surface of the E1 liners
2. The convex bearing surface of the 28 mm CoCrMo heads
3. The concave bearing surface of the 60 mm CoCrMo cups

The inner bearing surface of the E1 liners was too small to allow the zygo lens to fit inside without damaging the liner. This bearing surface was followed by optical microscopy alone.

Zygo profilometry tracked the change in surface roughness,  $R_a$ , and surface skewness,  $R_{skw}$ , throughout each test.

The 28mm CoCrMo heads only experienced small fluctuations in surface roughness and skewness over time in comparison to the CoCrMo cups and E1 liners.

When considering the CoCrMo cups in this project, perhaps the most surprising outcome was that the unworn cups in DM Test 2 experienced greater wear than the previously scratched CoCrMo cups. This was accompanied by both an increase in surface roughness and surface skewness that was not seen in the cups in DM Test 1 or DM Test 3.

As can be seen in Figure 5.64 this is because the metal matrix surrounding the unworn carbides in the CoCrMo cups was removed during testing which caused the carbides to protrude further above the metal surface. This in turn increased the wear rate of the E1 liners.

The general trend in wear rates shows that the components in DM Test 2 wore the most, followed by DM Test 3, and that the components in DM Test 1 wore the least. This difference between DM Test 3 and DM Test 1 was also explained by looking at the zygo data.

The CoCrMo cups used in DM Test 3 had been previously worn using third body particles (HA followed by Ti) in MOM Test 2. This is fully described in Chapter 4. It was hoped that the final 0.5 MC of MOM Test 2 which was performed using standard test lubricant would remove any residual third body particles. However zygo data taken from the cups after the first 0.5 MC of DM Test 3 showed the appearance of comet-tail scratches which had not been seen in the first 0.5 MC of either DM Test 1 or DM Test 2.

The images can be seen in Figures 5.92 and 5.93. The scratches were clearly a consequence of residual third body particles which had remained embedded in the metal matrix. Their presence has also resulted in an increase in the initial wear rate of the E1 liners as well as causing the surface roughness of the liners to decrease at a higher rate in the first 0.5 MC.

Due to the test serum being replaced every 0.5 MC, the third body particles were removed from DM Test 3 set up over time. As a consequence, the wear rate decreased as the test continued and the rate of smoothing in the E1 liners also slowed down.

The optical images taken at the inner and outer pole of the E1 liners highlight important differences between the inner and outer articulations in the three tests using CoCrMo cups of varying roughness. A selection of images taken at 5 MC from the outer pole of one standard E1 liner, one microseparation E1 liner and the control E1 liner from each test is provided for comparison in Figure 7.11 to Figure 7.13.

Under standard testing conditions against the worn cups in DM Test 1 and DM Test 3, the manufacturing streaks on the outer pole of the liners were still partially visible even after 5 MC of testing.

In the microseparation stations in DM Test 1, the manufacturing streaks were removed after approx. 2.5 MC (with some variation between the two stations due to the difference in initial cup roughness) whereas in DM Test 3 the manufacturing streaks were removed within 0.5 MC in the microseparation stations. This is thought to have occurred faster due to the presence of third body particles remaining embedded in the CoCrMo cups after MOM Test 2 which have increased the initial wear rate of the E1 liners.

In DM Test 2 where the liners articulated against unworn cups, the outer pole of the E1 liners were removed from all liners within 4 MC in the standard stations, and within 0.5 MC in the microseparation stations. This observation confirms two points: firstly, that the microseparation testing conditions engage the outer articulation more than standard testing conditions and secondly that even under standard conditions the E1 liners have experienced greater wear against the unworn cups in this study. This is due to the effect of the carbides protruding increasingly higher above the metal surface as the test has continued.

The optical images (Figures 5.22, 5.51 and 5.79) taken at the inner pole of the E1 liners showed that the manufacturing streaks were removed within the first 0.5 MC for all liners under both standard and microseparation testing conditions in each of the DM tests. This verifies that the inner articulation is dominant over the outer articulation.

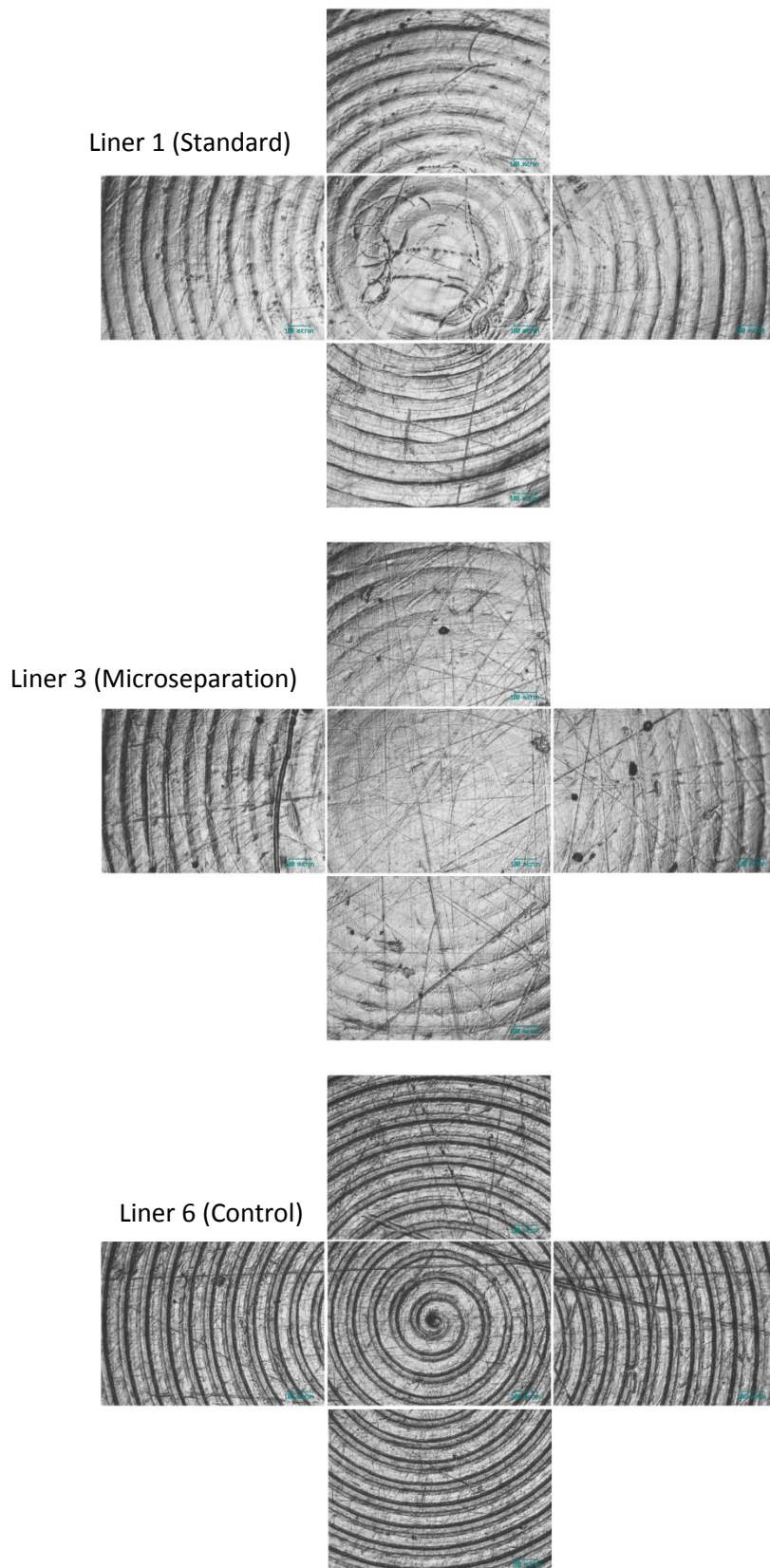


**Figure 7.11: Optical images taken from around the pole of the E1 liners in Dual Mobility Test 1: Worn cups from MOM Test 1 vs. dual mobility heads.**

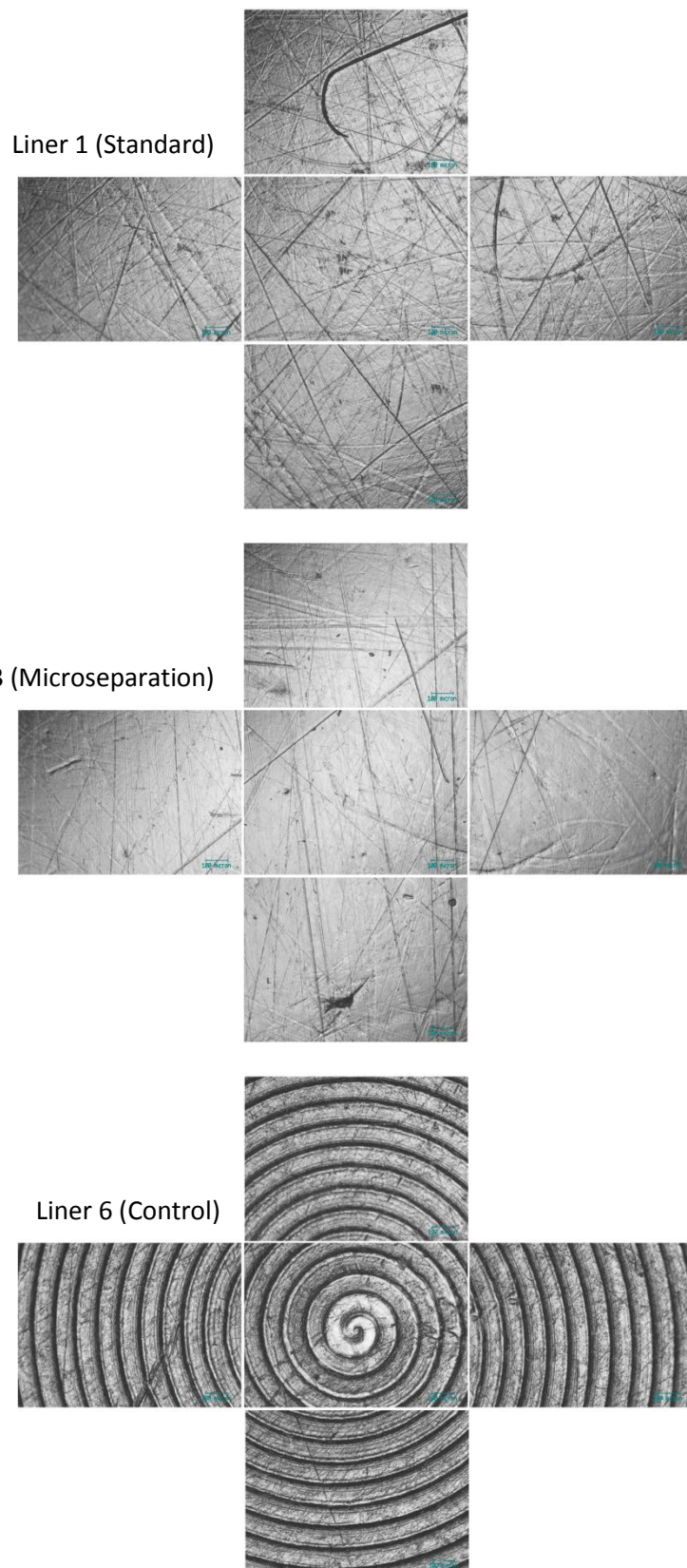


**Figure 7.12: Optical images taken from around the pole of the E1 liners in Dual Mobility Test 2: Unworn cups vs. dual mobility heads.**

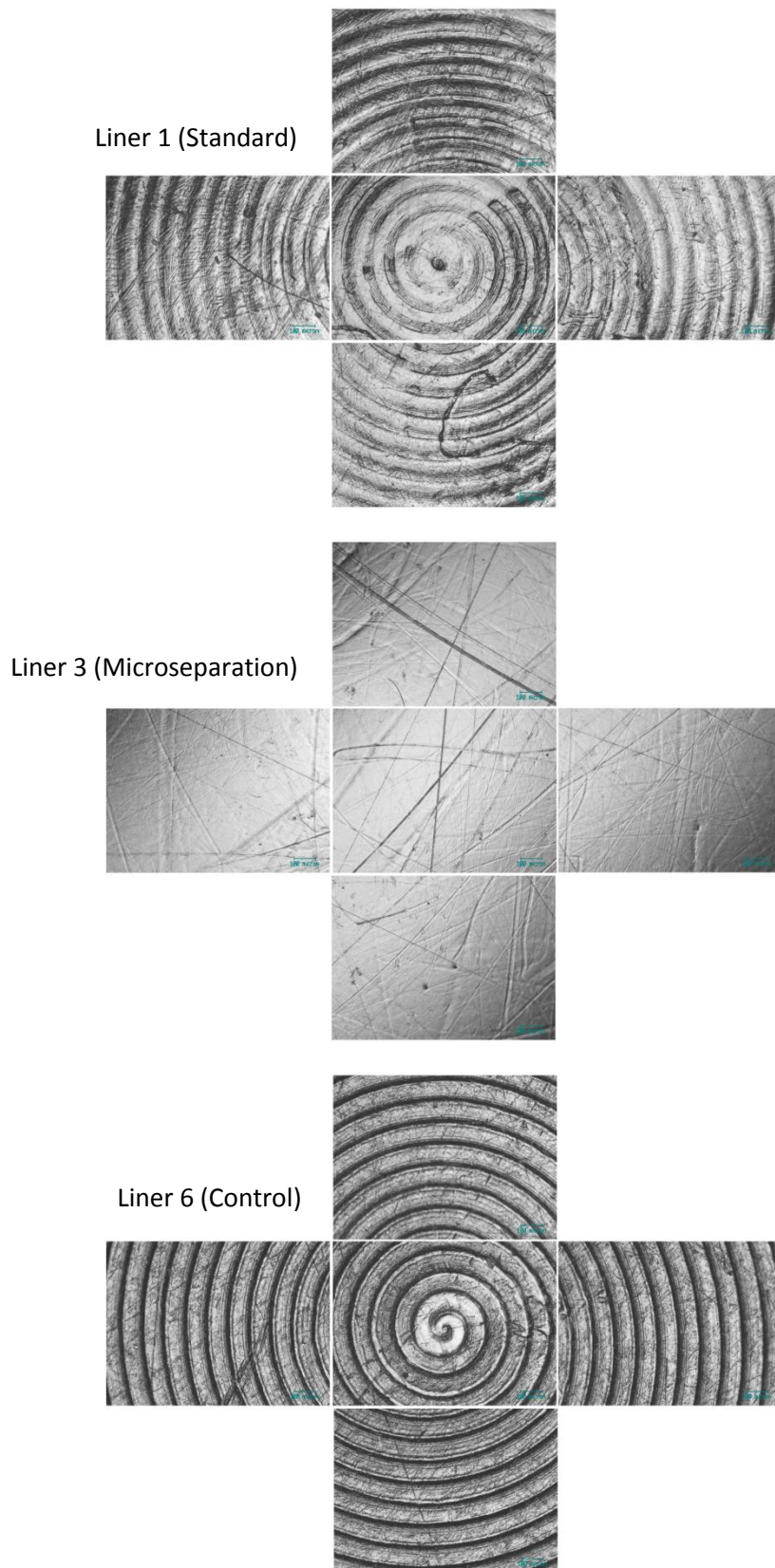


**Figure 7.13: Optical images taken from around the pole of the E1 liners in Dual Mobility Test 3: Worn cups from MOM Test 2 vs. dual mobility heads.**

The difference in the results between DM Test 1 and 3 with DM Test 2 shows that previous carbide removal and smoothing has been beneficial in improving the wear properties of the E1 liners against the CoCrMo cups. Alvarez *et al.* [2] are researching the effect of a novel electropolishing treatment named 'Ultra Polish' in order to reduce the carbide concentration and protrusion at the surface of CoCrMo bearings.

Initial results have shown no improvement in the wear properties of the CoCrMo bearings after the polishing treatment due to the polish not only removing the carbides but significant areas surrounding the carbide as well. However the author still considers the process of carbide removal from metal bearings to be extremely beneficial for future orthopaedic applications, and the results seen in the DM tests in this project support this conclusion.

A previous study by Loving *et al.* [3] which tested dual mobility heads with highly cross-linked UHMWPE liners against CoCrMo cups that had been scratched prior to testing, showed that the scratching caused no statistical difference to the wear of the UHMWPE liner under standard testing conditions.

This study also saw no statistical difference in the wear of the E1 liners under standard testing conditions when using cups of varying roughness. However under microseparation testing conditions, the E1 liners and CoCrMo cups wore statistically less when the CoCrMo cups had been scratched prior to testing.

The volumetric wear of the liners during 2.5 MC in the previous study [3] was within the range of 1.4 – 6.0 mm<sup>3</sup>. No metal wear data was reported in the paper and microseparation was not investigated for the scratched cups.

During the initial 2.5 MC of DM Test 1 and DM Test 3, the volumetric wear of the E1 liners ranged from 0.4 – 6.7 mm<sup>3</sup> including the liner which had a leak during the first 0.5 MC, and from 0.4 – 1.7 mm<sup>3</sup> if this liner was omitted from the data. This lower wear volume is indicative of the improvement the infusion of Vitamin E makes to the wear properties of UHMWPE.

In conclusion the wear, zygo and optical data from the three DM tests have shown that the DM heads with the E1 liners have worn incredibly well against every worn and

unworn cup tested and suggest that they are a viable option for the partial revision of failed resurfacing operations as well as for total hip replacement.

### 7.1.3 Particle analysis

Metal particle analysis has been carried out for a COM study, MOM Test 1 and DM Test 1, 2 and 3. Problems were encountered with size analysis due to the low number of metal particles isolated.

The Cr particles isolated from the COM study were either rod-like or spherical in nature and corresponded well with previously published work from both *in vitro* and *in vivo* studies [4; 5].

The CoCr particles isolated from MOM Test 1 were polycrystalline and rod-like in nature and tended to be within 100-200 nm in length. This was comparable to metal particles isolated from a previous MOM study by Catelas *et al.* [6] where the particles ranged from 12 - 250 nm. In comparison Doorn *et al.* [7] isolated CoCr wear particles from retrieved tissues around MOM implants and found that the particles ranged in size from 51 - 116 nm.

After serum from the DM tests had been digested it became apparent that there was an additional type of metal wear debris present: stainless steel wear particles. This made the isolation of CoCr particles very challenging however it did verify that there had been interaction between the head stem and the rim of the E1 liner. This interaction has further been confirmed by zygo analysis around the head stem which showed that the head stems have become smoother during testing. ESEM images taken around the E1 liner rim also showed signs of wear in the test liners.

Since the interaction between the head stem and the E1 liner rim is a genuine source of wear particles *in vivo*, it is recommended that the initial test set up is modified for future work in order to produce clinically relevant wear debris. The use of a head stem which is made from the same materials with the same polishing and quality control as is manufactured for implantation in the body is recommended.

It must be remembered that metal particles are not the only wear particles of interest in the DM studies. Replacing a metal resurfacing femoral head with a dual mobility head also incurs the introduction of polyethylene wear debris and the risk of osteolysis.

The polyethylene wear debris in the DM test serum has been analysed by Saurabh Lal in the Bioengineering group at Durham University who has specialised in the isolation and size analysis of UHMWPE wear particles during his PhD. The results are discussed fully in his thesis.

From comparison of the results from the current DM studies with previous simulator studies testing 28 mm CoCrMo heads against the 'gold standard' UHMWPE cups, the wear rates of the liners in this study have been very low. Table 7.2 shows a full comparison of test details between the current study and previous work. The corresponding wear rates are shown in Figure 7.15.

The only bearings to have performed as well as the E1 liners seen here were vitamin-E doped UHMWPE cups. Similar low wear rates were also seen by Traynor *et al.* [8] testing 40 mm CoCrMo heads against ECiMa cups as seen in Figure 7.14. This again shows the benefit of adding Vitamin E to cross-linked UHMWPE in order to improve the wear properties.

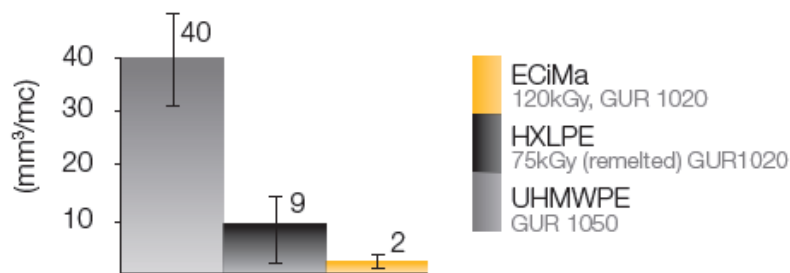


**Figure 7.14: Comparison of wear rate (mm<sup>3</sup>/MC) from the three different materials studied by Traynor *et al.* [8] (after 5 MC for HXLPE and ECiMa, 3 MC for UHMWPE).**

Hence it is hoped that the risk of osteolysis due to polyethylene wear after replacing a failed resurfacing metal head with a DM head will be reduced because the E1 liner releases a smaller volume of wear particles into the test serum in comparison to conventional and highly cross linked UHMWPE.

## 7. Discussion and conclusion

**Table 7.2: Comparison of previous *in vitro* testing of 28 mm CoCrMo heads against single articulation UHMWPE bearings with the current DM study.**

<b>Author</b>	<b>Year</b>	<b>Femoral Component</b>	<b>Acetabular Component</b>	<b>Test Details</b>	<b>Wear Rate</b>
Clarke et al. [9]	2000	28 mm CoCr	UHMWPE (2.5-4 Mrad/N <sub>2</sub> )	10 MC test with 90% Bovine Serum (BS)	13 mm <sup>3</sup> /MC
Saikko et al. [10]	2001	28 mm CoCr	UHMWPE (2.5-4 Mrad)	3 MC test with 50% BS	56.4 ± 13.3 mg/MC
Affatato et al. [11] (a)	2002	28 mm CoCr	UHMWPE (EtO-sterilised, 3 Mrad)	5 MC test with 30% BS	15 mg/MC
Affatato et al. [11] (b)	2002	28 mm CoCr	UHMWPE (gamma-sterilised, 3 Mrad)	5 MC test with 30% BS	13 mg/MC
Galvin et al. [12] (a)	2006	28 mm CoCr	Non cross-linked UHMWPE GUR 1050	5 MC test with 25% BS	45.6 ± 1.35 mm <sup>3</sup> /MC
Galvin et al. [12] (b)	2006	28 mm CoCr	Slightly cross-linked UHMWPE 2.5 Mrad	5 MC test with 25% BS	46.9 ± 9.4 mm <sup>3</sup> /MC
Galvin et al. [12] (c)	2006	28 mm CoCr	Highly cross-linked UHMWPE 7.5 Mrad	5 MC test with 25% BS	15.04 ± 4.28 mm <sup>3</sup> /MC
Galvin et al. [12] (d)	2006	28 mm CoCr	Highly cross-linked UHMWPE 10 Mrad	5 MC test with 25% BS	8.7 ± 3.11 mm <sup>3</sup> /MC
Oral et al. [13] (a)	2006	28 mm CoCr	Conventional gamma-irradiated UHMWPE	5 MC test with 100% BS	9.54 ± 0.73 mg/MC
Oral et al. [13] (b)	2006	28 mm CoCr	Vitamin E-doped UHMWPE	5 MC test with 100% BS	0.78 ± 0.28 mg/MC
Current Study (based on standard stations in DM T2)	2013	28 mm CoCr	E1 dual mobility liner and CoCr cup	5 MC test with 25% BS	1.26 ± 0.79 mm <sup>3</sup> /MC

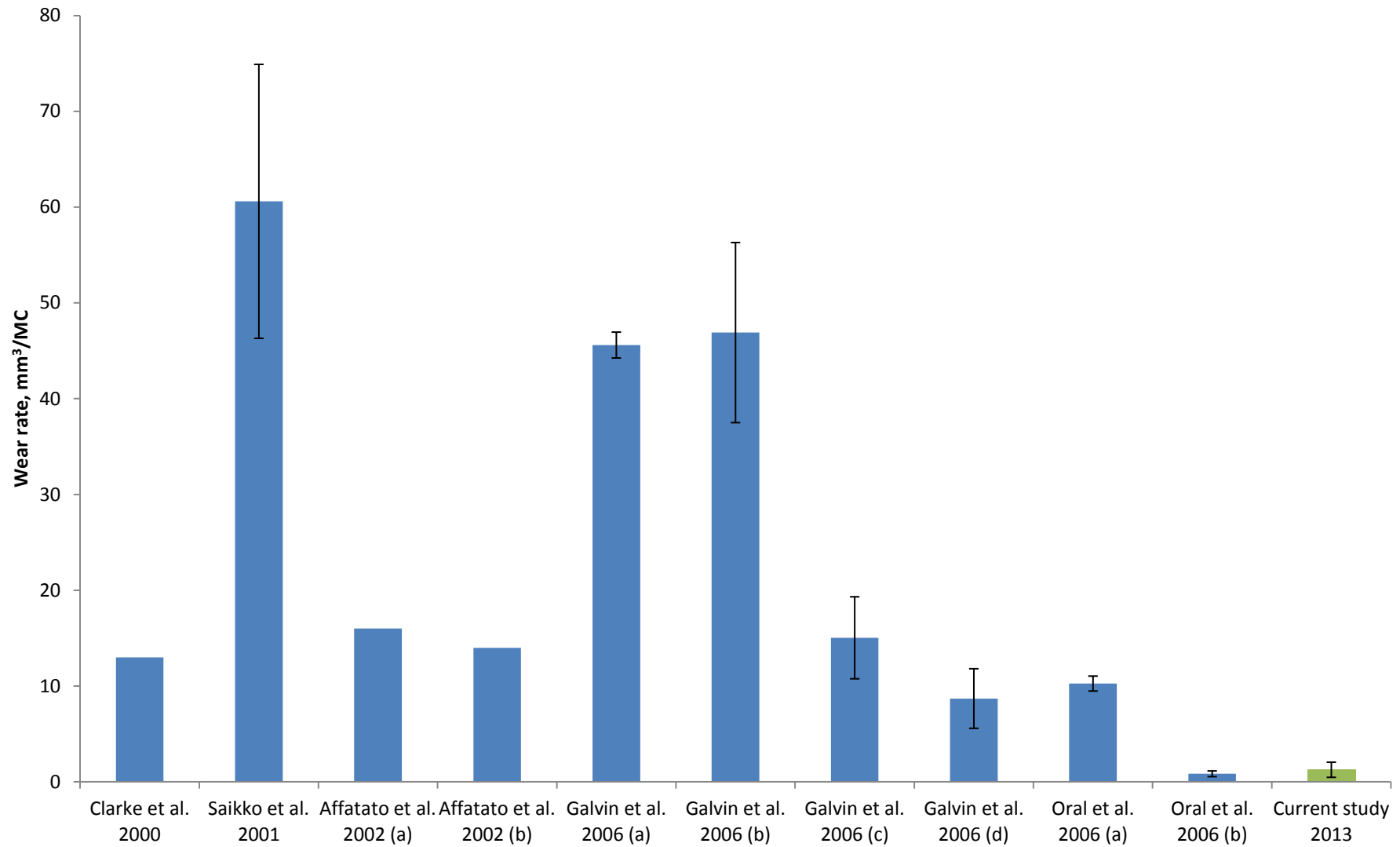


Figure 7.15: Comparison of previous *in vitro* testing of 28 mm CoCrMo heads against single articulation UHMWPE bearings with the current DM study.

### 7.1.4 Options available for partial revision of failed MOM THRA

This project has focused on the viability of replacing a failed metal resurfacing head with a dual mobility bearing. This section will discuss and compare alternative options to the dual mobility bearing for partial revision surgery.

One option is to replace the metal resurfacing femoral head with a modular ceramic head. The reported *in vitro* wear rates for COM joints are very low. Alumina has an ionic structure which creates a hydrophilic surface with higher wettability than metals, thus facilitating lubrication [14].

Williams *et al.* [15] found that the mass loss from ceramic heads articulating against CoCrMo cups to be immeasurable using gravimetric methods. The wear rate of the corresponding CoCrMo cups ranged from  $0.023 \pm 0.005 \text{ mm}^3/\text{MC}$  under standard testing conditions to  $0.623 \pm 0.252 \text{ mm}^3/\text{MC}$  under microseparation testing conditions. Ishida *et al.* [16] determined the overall wear rate for 38 mm COM joints to be  $0.29 \pm 0.19 \text{ mm}^3/\text{MC}$  with a cup wear ratio of  $82 \pm 9 \%$ . Williams *et al.* [17] found that the wear rate for 36 mm COM joints ranged from  $0.02 \pm 0.01 \text{ mm}^3/\text{MC}$  under standard testing to  $0.36 \pm 0.55 \text{ mm}^3/\text{MC}$  under microseparation conditions.

Clinically, Isaac *et al.* [18] have measured whole blood metal ion levels in patients with COM total hip replacements and found that Cr levels were significantly lower in COM bearings than MOM bearings. Co levels were also lower but the difference was not significant.

The clinical data available for metal and polyethylene THR bearings is far more extensive than that available for ceramic joints. Alumina wear particle-induced osteolysis is a very rare phenomenon but has been seen clinically [19].

It is not known how the ceramic wear rate would be affected by the surface roughness of the cup left in the body at revision surgery. Brockett *et al.* [20] tested two explanted COM bearings in a simulator study and found the steady-state wear rate to be comparable with new COM bearings. However there are concerns that ceramic joints can fracture *in vivo* [21-24].

Revision surgery after ceramic fracture shows high rates of early complications due to third body wear after incomplete synovectomy [25; 26]. If the ceramic joint is replaced

## 7. Discussion and conclusion

---

with MOP then ceramic particles can be embedded in the PE cup articulating surface, resulting in severe destruction of the metal femoral head and extensive periprosthetic metallosis [27]. The results of this can be fatal in isolated cases [28].

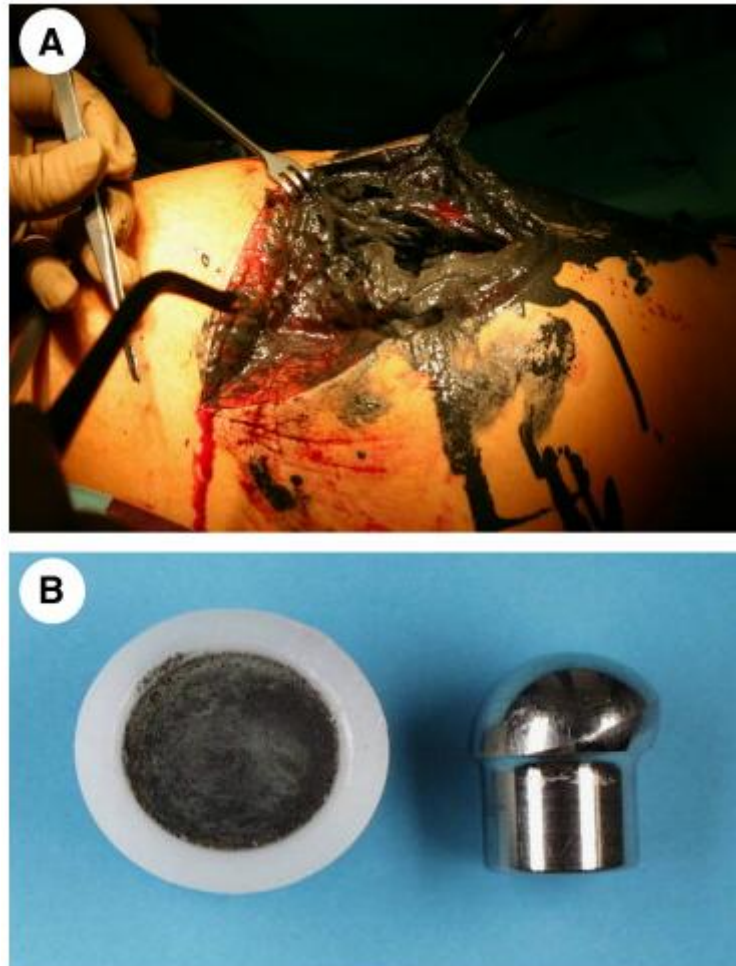


**Figure 7.16: A-Metallosis 1.5 years after treatment with a MOP bearing in the case of a ceramic fracture. [27]**

The use of a metal modular head would not be advised in cases where MOM failure has led to severe metallosis and adverse reaction to metal debris. Potentially the use of modular metal heads with physical vapour deposition (PVD) coatings could be used to remove the MOM interface.

Ortega-Saenz *et al.* [29] have shown that PVD coatings including TiN/CrN, CrN and diamond-like carbon (DLC) protect the metal femoral head and reduce wear up to five times in the case of the DLC coating, and twenty-eight and fifty-five times in the case of the multilayer (TiN/CrN)<sub>3</sub> and CrN respectively compared with standard MOM femoral heads *in vitro*. However, clinical data is limited.

The concern with only replacing the failed metal resurfacing head with a modular head of any material is that with a traditional joint combination the scratched cup may have a great effect on the wear rate. In comparison, the outer articulation of a dual mobility joint is only engaged a small percentage of the time. Whilst the hard bearings discussed above are presented as potential options for partial revision surgery, the author does not consider them to be viable because hard-on-hard bearings generally follow a distinct wear pattern with a run-in and steady state wear phase.

Run-in wear could generate a large number of metal wear particles which could be detrimental to the success of the implant and cause further problems for the patient.

THA is a commonly used option in order to extract the failed MOM articulation completely. The problem with this method is that more bone stock is lost than during partial revision surgery and this may cause problems for younger patients in the future.

Springer *et al.* [30] found that the most common cause of failure after revision surgery is joint instability and accounts for 35% of all failed revision THAs. It is estimated that between 7-20% of revision THAs will dislocate [31; 32].

There are limited articles which address the effect of femoral head size in revision THA but Garbuz *et al.* [33] determined that a large femoral head reduces dislocation rates in patients undergoing revision THA.

Dual mobility heads are proven to reduce the risk of dislocation in THA [34]. It has also been shown that they prevent dislocation following revision THA [35; 36]. In addition to this they provide patients with a large range of motion [37]. Short-term clinical results after six months have been promising [38], and over 5 MC of simulator testing all the DM heads in this study have worn consistently well against scratched CoCrMo cups which have features similar to that seen in retrievals.

However there have also been clinical issues with DM bearings using conventional UHMWPE liners *in vivo*. Rare cases of intraprosthetic dislocation (IPD) where the femoral heads have escaped from inside the DM liners [39-41] have occurred. Cases are isolated and do not yet provide a clear mechanism for failure. Philippot *et al.* [42] have established cup loosening and blockage of the liner due to extrinsic phenomena such as arthrofibrosis and ectopic ossification as contributing to the onset of IPD.

It is worth noting that there have not yet been any reported clinical incidences of IPD in patients with dual mobility bearings with E1liners. At this current moment in time only short-term clinical data is available, it will take at least another ten years to assess the long-term clinical performance of the bearings.

Ultimately, selecting the course of action for a patient who has experienced a failed metal THRA can only be determined after the careful consideration of many factors including patient age, sex, lifestyle and reason for primary THRA failure.

### 7.2 Conclusion

The aims of the project as summarised in section 2.7 are outlined below with the resulting conclusions from this work.

#### **1. Investigate how to recreate surface features seen *in vivo* in CoCrMo acetabular cups from failed MOM THRA.**

Firstly, surface features seen *in vivo* from failed MOM bearing systems were analysed by examining eight retrieved CoCrMo acetabular cups using optical microscopy, SEM and zygo profilometry. The average surface roughness was  $0.031 \pm 0.03 \mu\text{m}$  with a corresponding average surface skewness of  $-5.042 \pm 4.682 \mu\text{m}$ . Optical microscopy and SEM showed a wide range of surface features including abrasive multidirectional scratching, pitting on the surface and carbide removal. Two simulator studies were then completed using MOM ReCap resurfacing joints in order to produce worn CoCrMo cups with surface features similar to that seen in the retrievals.

MOM Test 1 was a standard 5 MC simulator study where three stations experienced leaks and runaway wear. The three CoCrMo cups from these stations had a resulting average surface roughness of  $0.089 \pm 0.072 \mu\text{m}$  and average surface skewness  $0.312 \pm 0.848 \mu\text{m}$ . The two CoCrMo cups which did not experience leaks had a resulting average surface roughness of  $0.013 \pm 0.009 \mu\text{m}$  and average surface skewness  $-2.517 \pm 3.885 \mu\text{m}$ . Whilst the magnitude of the wear rates from the cups which experienced leaks have been seen clinically in failed MOM THRA, the surface features differed from those seen *in vivo* due to the deep unidirectional nature of the scratching.

MOM Test 2 was a 2 MC simulator study completed using MOM ReCap resurfacing joints with the addition of third body particles to the test lubricant. The resulting average surface roughness of the CoCrMo acetabular cups was  $0.027 \pm 0.021 \mu\text{m}$  and average surface skewness  $-3.217 \pm 2.625 \mu\text{m}$ . Whilst unidirectional scratching was still a common feature, areas of multidirectional scratching were also present on the surface of the resulting CoCrMo cups. Carbide smoothing and removal was also visible and similar to that seen in retrievals.

Comparison of the wear, zygo and optical data from the two MOM simulations have shown that MOM Test 2 was more effective than MOM Test 1 in producing cups with similar surface features to that seen *in vivo*. However both simulations have been beneficial in providing a wide variety of CoCrMo cups with different surface features for further testing with DM heads.

### **2. Investigate how the wear rate of a DM head is affected by the initial surface roughness of the mating CoCrMo acetabular cup.**

DM Test 1 used the worn CoCrMo cups from MOM Test 1 with surface roughness and skewness as detailed in the previous section. The corresponding E1 liner wear rate at  $62^\circ$  inclination angle ranged from  $0.23 - 1.17 \text{ mm}^3/\text{MC}$ . Under both high inclination and microseparation the wear rate ranged from  $2.49 - 3.76 \text{ mm}^3/\text{MC}$ .

DM Test 2 used unworn CoCrMo cups with an average initial surface roughness of  $0.008 \pm 0.004 \mu\text{m}$  and surface skewness  $0.419 \pm 0.341 \mu\text{m}$ . The E1 liner wear rate at  $62^\circ$  inclination angle ranged from  $0.64 - 2.15 \text{ mm}^3/\text{MC}$ . Under both high inclination and microseparation the wear rate ranged from  $4.97 - 5.15 \text{ mm}^3/\text{MC}$ .

DM Test 3 used the worn CoCrMo cups from MOM Test 2 with surface roughness and skewness as detailed previously. The corresponding E1 liner wear rate at  $62^\circ$  inclination angle ranged from  $0.46 - 0.69 \text{ mm}^3/\text{MC}$ . Under both high inclination and microseparation the wear rate ranged from  $3.57 - 3.88 \text{ mm}^3/\text{MC}$ .

The E1 liners exhibited lower wear rates when tested against the previously worn CoCrMo acetabular cups from MOM Test 1 and 2. This result was not statistically different under standard testing conditions but was statistically different under microseparation testing conditions when comparing DM Test 2 and DM Test 3.

### **3. Investigate how the wear rate of DM THA is affected by high inclination and microseparation testing conditions.**

In each DM test the combination of both high inclination and microseparation testing conditions increased the wear rate of the E1 liners above that experienced under wear testing at high inclination alone. This result was statistically different for both DM Test 2 and DM Test 3. Optical images taken at the outer pole of the E1 liners also show that the outer articulation has been engaged more under microseparation testing conditions.

### **4. Investigate whether DM THA produces comparable wear rates to traditional MOP THA.**

The E1 wear rates from DM Test 2 using unworn CoCrMo acetabular cups have been compared to previous *in vitro* mechanical testing of 28 mm CoCrMo heads vs. UHMWPE bearings, see Table 7.2. The wear rates from this study are lower than those seen previously using conventional and highly cross-linked UHMWPE bearings and comparable to previous studies using vitamin E doped UHMWPE bearings.

This indicates that DM bearings will not release a higher volume of polyethylene debris into the body than traditional MOP THA despite the additional wear surfaces from the two articulating surfaces as well as the interaction between the head stem and the liner rim.

### **5. Investigate whether the form, size and shape of metallic debris released from MOM THRA vary in comparison to that from DM THA.**

Test serum taken after 0.5, 1.0, 2.5 and 5.0 MC from MOM Test 1 as well as test serum taken after 0.5 MC from both standard and microseparation testing conditions from DM Test 1, 2 and 3 has been digested using an enzymatic protocol. A low number of nanometre sized rod-like CoCr particles with a polycrystalline structure were imaged from the MOM test serum. Although six DM samples were analysed, isolation of either Cr or CoCr particles were not achievable due to the additional presence of stainless steel wear particles in the DM test serum.

The presence of stainless steel wear debris was beneficial in confirming that there had been contact between the stainless steel head stem and the rim of the E1 liner during the DM simulations. However the head stems used in these tests are not representative

of the head stems which would be used *in vivo* and hence the current DM test set up would have to be modified for future work in order to produce clinically relevant wear debris.

### **6. Investigate whether a failed MOM THRA can be converted into a successful THA using a DM head.**

Whilst metal wear particle isolation from the DM tests has been unsuccessful, the wear rates of the CoCrMo heads and cups during the DM tests, using either previously worn or unworn cups, have been consistently low. Hence it is hoped that incidences of adverse reaction to metallic debris post-revision surgery would be low for patients who receive DM THA. Also, MOM Test 1 had three stations which were experiencing runaway wear and after replacement of the metal femoral head with a DM head in DM Test 1 the wear rate of the CoCrMo cups stabilised immediately at a low level.

The wear rates of the E1 liners have also been very low in all tests using previously worn cups therefore it is hoped that incidences of implant loosening due to osteolysis from build up of polyethylene wear debris will be lower than for patients receiving MOP THA with conventional or highly cross-linked UHMWPE bearings.

DM bearings are reported to provide greater stability and reduced risk of dislocation which is hugely beneficial given that the principal cause of failure after revision surgery is joint instability. DM bearings are presented in this work as an option for partial revision surgery because the outer articulation is only engaged a small percentage of the time under standard walking conditions. This project has tested a wide variety of CoCrMo cups with worn features similar to that seen *in vivo* from failed MOM bearings against DM heads and all have worn consistently well. The E1 liners have greatly improved the wear properties of the DM heads whilst retaining all the stability advantages associated with the DM set up.

This project has successfully increased the understanding of DM bearings for application in partial revision procedures and the results indicate that DM heads are indeed a viable solution for the conversion of a failed MOM THRA into a successful THA.

### 7.3 Suggestions for further work

This project has been successful in achieving five of the six aims detailed in section 2.7. The exception was that the form, size and shape of metallic debris released from DM THA were unable to be determined due to the additional presence of stainless steel wear debris in the test serum which was not clinically relevant.

In future work it is suggested that:

- 1) For DM studies, the stainless steel head stems from the current test set up should be replaced with head stems made from the same material (either CoCrMo or Ti alloy) with the same polishing and quality control as is manufactured for use in the body. It must be remembered that the interaction between the head stem and the E1 liner rim will also contribute to the production of polyethylene wear debris as well as metallic wear debris in the test serum. It is not yet known how the size and shape of polyethylene wear debris released from DM THA compares to that from MOP THA. Therefore although the production of clinically relevant head stems for DM wear testing would require extra time, cost and collaboration with Biomet, it is essential in order to produce clinically relevant CoCrMo and polyethylene wear debris for further biological assessment.
- 2) Further metal particle isolation analysis using test serum from MOM pin-on-plate studies should be carried out in order to try and increase the number of metal particles imaged. Pin-on-plate studies will have a high concentration of test particles in a small volume of serum which would allow the digestion protocol to be varied until the particle loss was minimised.
- 3) The duration of DM testing could be extended up to 15 MC per test. Simulations with this duration would not have been viable during the current project due to time constraints. However longer testing would be beneficial in order to assess the long term wear around the liner rim in terms of susceptibility to intra-prosthetic dislocation. This is yet to be seen clinically for E1 bearings but has been seen for a small percentage of patients with conventional DM bearings after around ten years *in vivo*.

## 7.4 References

- [1] J.K. Lord, D.J. Langton, A.V.F. Nargol, T.J. Joyce, *Wear* 272 (2011) 79-87.
- [2] E. Alvarez, J. Vinciguerra, J.D. Des Jardins, *Tribology International* 47 (2012) 204-211.
- [3] L. Loving, R.K. Lee, L. Herrera, A.P. Essner, J.E. Nevelos, *Journal of Arthroplasty* 28 (2013) 1041-1046.
- [4] C. Brown, S. Williams, J.L. Tipper, J. Fisher, E. Ingham, *Journal of materials science. Materials in medicine* 18 (2007) 819-27.
- [5] I. Catelas, J.B. Medley, P.a. Campbell, O.L. Huk, J.D. Bobyn, *Journal of biomedical materials research. Part B, Applied biomaterials* 70 (2004) 167-78.
- [6] I. Catelas, J.D. Bobyn, J.B. Medley, J.J. Krygier, D.J. Zukor, a. Petit, O.L. Huk, *Journal of biomedical materials research* 55 (2001) 320-9.
- [7] P.F. Doorn, P.a. Campbell, J. Worrall, P.D. Benya, H.a. McKellop, H.C. Amstutz, *Journal of biomedical materials research* 42 (1998) 103-11.
- [8] A. Traynor, D. Simpson, S. Collins, *Orthopaedic Product News* October (2011).
- [9] I.C. Clarke, V. Good, P. Williams, D. Schroeder, L. Anissian, A. Stark, H. Oonishi, J. Schuldies, G. Gustafson, *Proc Inst Mech Eng H* 214 (2000) 331-47.
- [10] V. Saikko, T. Ahlroos, O. Caloniun, J. Keranen, *Biomaterials* 22 (2001) 1507-1514.
- [11] S. Affatato, G. Bersaglia, I. Foltran, P. Taddei, G. Fini, A. Toni, *Biomaterials* 23 (2002) 4839-4846.
- [12] A. Galvin, L. Kang, J. Tipper, M. Stone, E. Ingham, Z. Jin, J. Fisher, *J Mater Sci Mater Med* 17 (2006) 235-43.
- [13] E. Oral, S.D. Christensen, A.S. Malhi, K.K. Wannomae, O.K. Muratoglu, *J Arthroplasty* 21 (2006) 580-91.
- [14] M. Slonaker, T. Goswami, *Materials & Design* 25 (2004) 395-405.
- [15] S.R. Williams, J.J. Wu, A. Unsworth, I. Khan, *Proceedings of the Institution of Mechanical Engineers Part H-Journal of Engineering in Medicine* 225 (2011) 783-796.
- [16] T. Ishida, I.C. Clarke, T.K. Donaldson, H. Shirasu, T. Shishido, K. Yamamoto, *J Biomed Mater Res B Appl Biomater* 91 (2009) 887-96.
- [17] S. Williams, M. Al-Hajjar, G.H. Isaac, J. Fisher, *J Biomed Mater Res B Appl Biomater* 101 (2013) 770-5.

- [18] G.H. Isaac, C. Brockett, A. Breckon, D. van der Jagt, S. Williams, C. Hardaker, J. Fisher, A. Schepers, *Journal of Bone and Joint Surgery-British Volume 91B* (2009) 1134-1141.
- [19] K.W. Nam, J.J. Yoo, Y.L. Kim, Y.-M. Kim, M.-H. Lee, H.J. Kim, *The Journal of Bone & Joint Surgery Case Connector* 89 (2007) 2499-2503.
- [20] C. Brockett, A. Breckon, J. Fisher, G. Isaac, A. Schepers, S. Williams, *J Bone Joint Surg Br* 92-B (2010) 511.
- [21] F. Higuchi, N. Shiba, A. Inoue, I. Wakebe, *J Arthroplasty* 10 (1995) 851-4.
- [22] K.H. Koo, Y.C. Ha, W.H. Jung, S.R. Kim, J.J. Yoo, H.J. Kim, *J Bone Joint Surg Am* 90 (2008) 329-36.
- [23] D.P. Rhoads, K.C. Baker, R. Israel, P.W. Greene, *J Arthroplasty* 23 (2008) 1239 e25-30.
- [24] P. Mangione, X. Pascarel, B. Vinciguerra, J.L. Honton, *Int Orthop* 18 (1994) 359-62.
- [25] K.H. Koo, Y.C. Ha, S.Y. Kim, K.S. Yoon, B.W. Min, S.R. Kim, *J Arthroplasty* (2013).
- [26] V. Sharma, A.S. Ranawat, V.J. Rasquinha, J. Weiskopf, H. Howard, C.S. Ranawat, *Journal of Arthroplasty* 25 (2010) 342-347.
- [27] M. Hintner, C. Kaddick, S. Usbeck, L. Scheuber, R.M. Streicher, *Seminars in Arthroplasty* 23 (2012) 241-247.
- [28] M.G. Zywiell, J.M. Brandt, C.B. Overgaard, A.C. Cheung, T.R. Turgeon, K.A. Syed, *Bone Joint J* 95-B (2013) 31-7.
- [29] J.A. Ortega-Saenz, M. Alvarez-Vera, M.A.L. Hernandez-Rodriguez, *Wear* 301 (2013) 234-242.
- [30] B.D. Springer, T.K. Fehring, W.L. Griffin, S.M. Odum, J.L. Masonis, *Clin Orthop Relat Res* 467 (2009) 166-73.
- [31] G.M. Alberton, W.a. High, B.F. Morrey, *The Journal of bone and joint surgery. American volume* 84-A (2002) 1788-92.
- [32] B.F. Morrey, *Orthop Clin North Am* 23 (1992) 237-48.
- [33] D.S. Garbuz, B.A. Masri, C.P. Duncan, N.V. Greidanus, E.R. Bohm, M.J. Petrak, C.J. Della Valle, A.E. Gross, *Clin Orthop Relat Res* 470 (2012) 351-6.
- [34] S. Tarasevicius, M. Busevicius, O. Robertsson, H. Wingstrand, *Bmc Musculoskeletal Disorders* 11 (2010).

- [35] R. Civinini, C. Carulli, F. Matassi, L. Nistri, M. Innocenti, *Clinical Orthopaedics and Related Research* 470 (2012) 3542-3548.
- [36] R. Philippot, P. Adam, M. Reckhaus, F. Delangle, F.X. Verdot, G. Curvale, F. Farizon, *Orthopaedics & Traumatology-Surgery & Research* 95 (2009) 407-413.
- [37] R. Philippot, J.P. Camilleri, B. Boyer, P. Adam, F. Farizon, *International Orthopaedics* 33 (2009) 927-932.
- [38] L.A. Verhelst, H. Van der Bracht, I.S. Vanhegan, B. Van Backle, J. De Schepper, *Journal of Arthroplasty* 27 (2012) 1857-1862.
- [39] P. Massin, V. Orain, R. Philippot, F. Farizon, M.H. Fessy, *Clinical Orthopaedics and Related Research* 470 (2012) 1932-1940.
- [40] R. Philippot, F. Farizon, J.P. Camilleri, B. Boyer, G. Derhi, J. Bonnan, M.H. Fessy, F. Lecuire, *Revue De Chirurgie Orthopedique Et Reparatrice De L Appareil Moteur* 94 (2008) 43-48.
- [41] R. Philippot, P. Adam, F. Farizon, M.H. Fessy, G. Bousquet, *Revue De Chirurgie Orthopedique Et Reparatrice De L Appareil Moteur* 92 (2006) 326-331.
- [42] R. Philippot, B. Boyer, F. Farizon, *Clin Orthop Relat Res* 471 (2013) 965-70.

# Appendix A

---

INTERNATIONAL  
STANDARD

ISO  
14242-1

First edition  
2002-03-01

Licensed copy: Durham University Library, Durham University Library, Version correct as of 21/07/2011 11:43, (c) BSI

---

## Implants for surgery — Wear of total hip-joint prostheses —

### Part 1: Loading and displacement parameters for wear-testing machines and corresponding environmental conditions for test

*Implants chirurgicaux — Usure des prothèses totales de l'articulation de  
la hanche —*

*Partie 1: Paramètres de charge et de déplacement pour machines d'essai  
d'usure et conditions environnementales correspondantes d'essai*



Reference number  
ISO 14242-1:2002(E)

## Implants for surgery — Wear of total hip-joint prostheses —

### Part 1: Loading and displacement parameters for wear-testing machines and corresponding environmental conditions for test

#### 1 Scope

This part of ISO 14242 specifies the relative angular movement between articulating components, the pattern of the applied force, speed and duration of testing, sample configuration and test environment to be used for the wear testing of total hip-joint prostheses.

#### 2 Normative references

The following normative documents contain provisions which, through reference in this text, constitute provisions of this part of ISO 14242. For dated references, subsequent amendments to, or revisions of, any of these publications do not apply. However, parties to agreements based on this part of ISO 14242 are encouraged to investigate the possibility of applying the most recent editions of the normative documents indicated below. For undated references, the latest edition of the normative document referred to applies. Members of ISO and IEC maintain registers of currently valid International Standards.

ISO 3696:1987, *Water for analytical laboratory use — Specification and test methods*

ISO 7206-1:1995, *Implants for surgery — Partial and total hip-joint prostheses — Part 1: Classification and designation of dimensions*

ISO 14242-2:2000, *Implants for surgery — Wear of total hip-joint prostheses — Part 2: Methods of measurement*

#### 3 Terms and definitions

For the purposes of this part of ISO 14242, the terms and definitions given in ISO 7206-1 apply, together with the following.

**3.1**  
**abduction/adduction**  
angular movement shown in Figure 1 a)

**3.2**  
**flexion/extension**  
angular movement shown in Figure 1 b)

**3.3**  
**inward/outward rotation**  
angular movement shown in Figure 1 c)

ISO 14242-1:2002(E)

3.4

**polar axis**

axis of the acetabular component which intersects the centre of the spherical articulating surface and is perpendicular to the plane of the flange, or if no flange is present, perpendicular to the plane of the entry diameter

[ISO 7206-1]

4 Principle

The femoral and acetabular components of a test specimen are placed in position in their normal configuration; the test apparatus transmits a specified time-varying force between the components, together with specified relative angular displacements. A control specimen, if polymers are the object of investigation, is subjected to the same time-varying force to determine the creep of the test specimen and/or the amount of mass change due to fluid transfer. The test takes place in a controlled environment simulating physiological conditions.

5 Reagents and materials

5.1 Fluid test medium, calf serum (25 %  $\pm$  2 %) diluted with deionized water (balance).

Normally the fluid test medium is filtered through a 2  $\mu$ m filter, and has a protein mass concentration of not less than 17 g/l.

To minimize microbial contamination, the fluid test medium should be stored frozen until required for test. An anti-microbial reagent (such as sodium azide) may be added. Such reagents can be potentially hazardous.

Routine monitoring of the pH of the fluid test medium may be undertaken. If it is, the values should be included in the test report [see item 8 e) 5)].

NOTE The use of a fluid test medium of non-biological origin may be considered when performance requirements relating to this test method are being decided.

5.2 Test specimen, femoral head and acetabular components.

The acetabular component shall have the articulating surface attached by its normal immediate backing (for example bone cement or a machined replica of the inner surface of the backing) unless this is impractical due to physical features of the implant system. If the component forming the articulating surface is fixed to the backing by a rim/snap-fit system, the machined replica shall provide the same fixation conditions.

If it is not practical to use the normal backing or cement fixation, due to physical features of the implant system, the support system for the acetabular component should represent normal design features and conditions of use but should allow removal of the component for measurement of wear without destruction.

5.3 Control specimen, identical to test specimen.

6 Apparatus

6.1 Testing machine, capable of producing the angular displacements specified in Figures 1 and 2 in association with the corresponding forces specified in Figures 1 and 3 and operating at a frequency of 1 Hz  $\pm$  0,1 Hz.

6.2 Means of mounting and enclosing the test specimen, using a corrosion-resistant material, capable of holding femoral and tibial acetabular components using attachment methods comparable to the intended anatomical fixation. An enclosure shall be provided which is capable of isolating the test specimen to prevent third-body contamination from the test machine and the atmosphere.

**6.3 Means of aligning and positioning the femoral component of the test specimen** in the inferior position, so that its axis is situated at the centre of the axes of rotation of the test machine and so that the same position and orientation may be reproduced following removal for measurement or cleaning if required.

**6.4 Means of aligning and positioning the acetabular component of the test specimen**, so that its axis is situated at the centre of the axes of rotation of the test machine and so that the same position and orientation may be reproduced following removal for measurement.

**6.5 Motion control system**, capable of generating the angular movements of the femoral component given in Figures 1 and 2 with an accuracy of  $\pm 3^\circ$  at the maxima and minima of the motion and  $\pm 1\%$  of the cycle time for phasing.

**6.6 Force control system**, capable of generating a force whose direction is shown in Figure 1 and which varies as shown in Figure 3, and maintaining the magnitude of the maxima and minima of this force cycle to a tolerance of  $\pm 3\%$  of the maximum force value for the cycle and  $\pm 1\%$  of the cycle time for phasing.

**6.7 Lubrication system**, capable of maintaining the contact surfaces immersed in the fluid test medium.

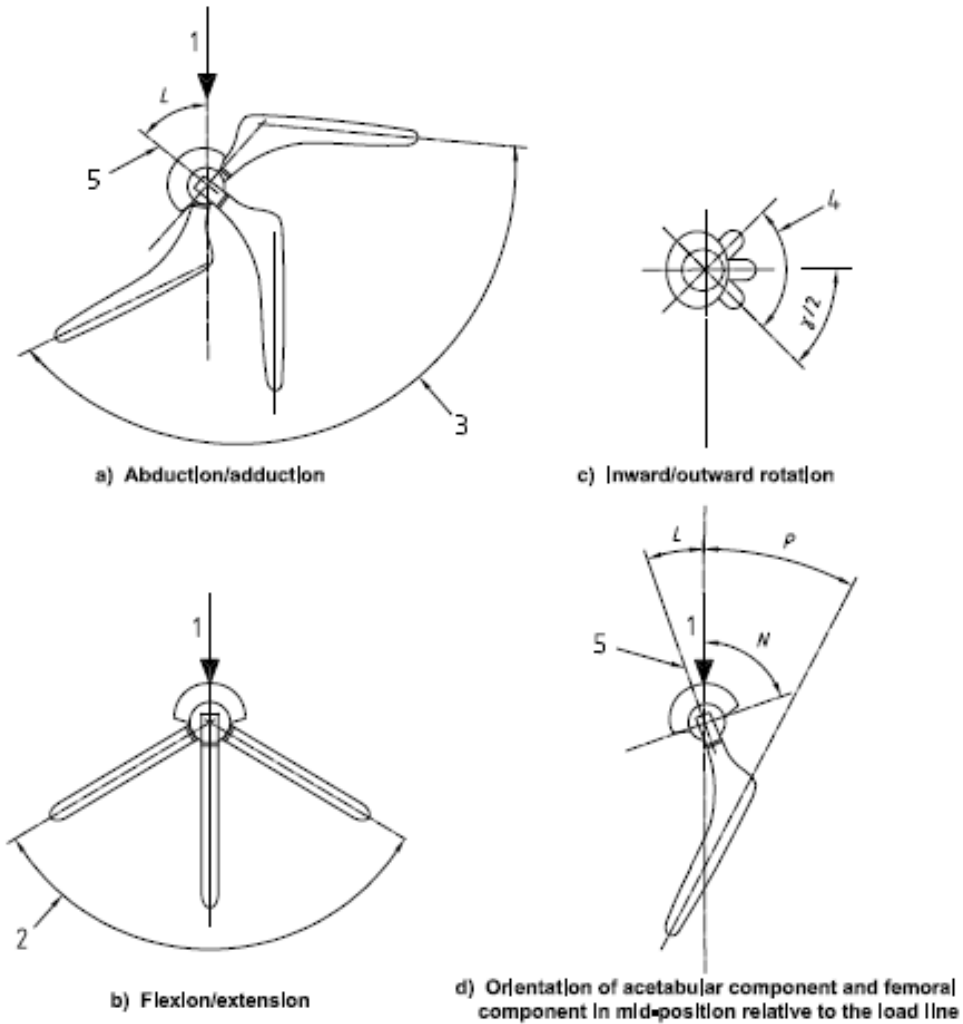
**NOTE** The use of sealed enclosures may prevent evaporation.

**6.8 Temperature control system**, capable of maintaining the temperature of the fluid test medium at (5.1)  $37^\circ\text{C} \pm 2^\circ\text{C}$ .

**6.9 Control station(s)**, capable of applying the loading regime shown in Figures 1 and 3 without the angular displacements shown in Figures 1 and 2 and incorporating the provisions of 6.2, 6.3, 6.4, 6.6, 6.7 and 6.8.

ISO 14242-1:2002(E)

Licensed copy: Durham University Library, Durham University Library, Version correct as of 21/07/2011 11:43, (c) BSI



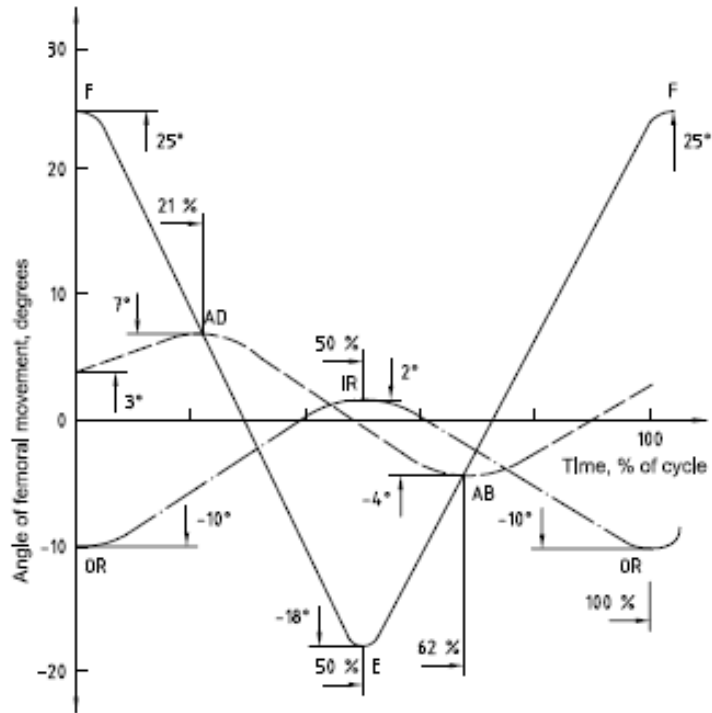
**Key**

- |                                      |  |
|--------------------------------------|--|
| 1 Load axis                          | <i>L</i> Inclination of the polar axis of the acetabular component to the load line                                      |
| 2 Flexion/extension angle            | <i>N</i> Inclination of face of acetabular component equal to $60^\circ \pm 3^\circ$ or as specified by the manufacturer |
| 3 Abduction/adduction angle          | <i>P</i> Inclination of stem axis to load line in mid-position of abduction/adduction range                              |
| 4 Inward/outward rotation angle      |  |
| 5 Polar axis of acetabular component |  |

NOTE Angles *N*, *L* and *P* are specified in 7.3 and 7.4.

**Figure 1 — Angular movement of femoral component and orientation of components relative to the load line**

Licensed copy: Durham University Library, Durham University Library, Version correct as of 21/07/2011 11:43, (c) BSI



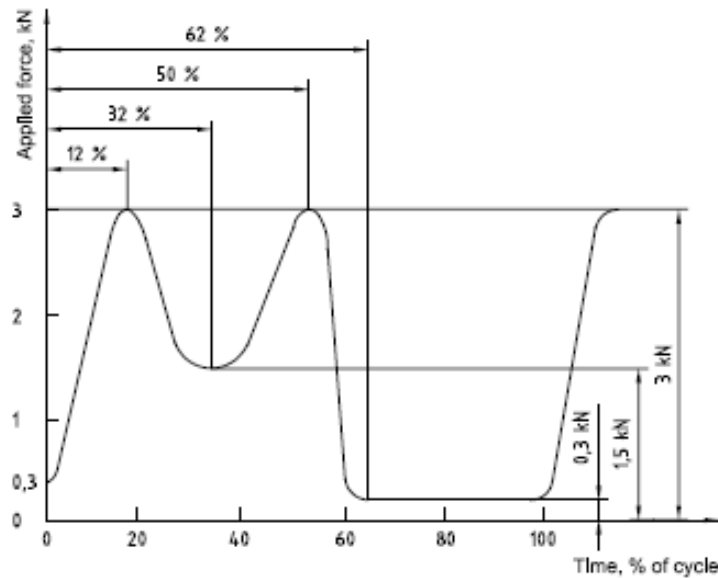
**Key**

- AB - Abduction } -----
- AD - Adduction } -----
- E - Extension } -----
- F - Flexion } -----
- IR - Inward rotation } -----
- OR - Outward rotation } -----

Time, % of cycle $\pm 1\%$	0	21	50	62	100
Angle of flexion (+) or extension (-) $^{\circ} \pm 3^{\circ}$	25		-18		25
Angle of adduction (+) or abduction (-) $\pm 3^{\circ}$	3	7		-4	3
Angle of inward (+) or outward (-) rotation $\pm 3^{\circ}$	-10		2		-10

Figure 2 — Variation with time of angular movement to be applied to the femoral test specimen

ISO 14242-1:2002(E)



Time, % of cycle ( $\pm 3\%$ )	0	12	32	50	62	100
Applied force, kN ( $\pm 90\text{ N}$ )	0,3	3,0	1,5	3,0	0,3	0,3

Figure 3 — Variation with time of the force to be applied along the loading axis

## 7 Procedure

7.1 Make any initial measurements required to determine the subsequent amount of wear and/or creep, and calibrate each test station using a load cell. Undertake this calibration while the load is being developed at other stations, if any, in the test rig.

NOTE Methods of measurement of wear are given in ISO 14242-2.

7.2 Following the initial measurements, clean the test specimen as specified in ISO 14242-2.

7.3 Mount the femoral component of the testing specimen in the test machine in the inferior position with its stem in the abduction/adduction position of  $P = 10^\circ \pm 3^\circ$  as shown in Figure 1 d) and in the inward/outward rotation position  $\gamma/2$  as shown in Figure 1 c).

NOTE For a modular component, the stem of the implant can be replaced by a support which has an identical cone and assures the same positioning of the head in order to leave the test conditions unchanged.

7.4 Mount the acetabular component of the testing specimen in the test machine with the polar axis vertical as illustrated in the view of Figure 1 b) and inclined at an angle  $L$  as shown in Figure 1 a) where  $L$  equals  $30^\circ \pm 3^\circ$  or, if the manufacturer specifies an angle of inclination of the component on surgical implantation to be  $N$  as shown in Figure 1 d), then  $L = (75 - N)^\circ \pm 3^\circ$ .

7.5 Take the control specimen and repeat steps in 7.1, 7.2, 7.3 and 7.4. For implants of a specific design with the same material, shape and dimensions, control data from previous tests may be used.

7.6 Introduce the fluid test medium (5.1) to completely immerse the contact surfaces of the test specimen and the control specimen. Maintain the temperature of the fluid test medium at  $37\text{ °C} \pm 2\text{ °C}$ , taking the measurement at a location representative of the bulk temperature of the fluid.

7.7 Start the testing machine and adjust it so that the loads and displacements specified in Figures 1, 2 and 3 are applied to the test specimen (6.5, 6.6) and the loads specified in Figures 1 and 3 are applied to the control specimen. The curves between the defined maxima and minima in Figures 2 and 3 shall be smooth with no overshoots. Record the displacement and load waveforms at start-up and after each change of fluid test medium.

7.8 Operate the testing machine at a frequency of  $1\text{ Hz} \pm 0,1\text{ Hz}$ .

7.9 Replace the fluid lost by evaporation during the test at least daily, by adding de-ionized water. Replace the fluid test medium completely at least every  $5 \times 10^5$  cycles.

7.10 Stop the test for measurements at at least  $5 \times 10^5$  cycles,  $1 \times 10^6$  cycles and at least every  $1 \times 10^6$  cycles thereafter until the test is terminated (see 7.14).

7.11 Remove the test specimen and control specimen from the testing machine and take wear measurements.

7.12 Following wear measurements, clean the test specimen and control specimen as specified in ISO 14242-2 and reinstall in the testing machine (7.3, 7.4 and 7.5).

7.13 Repeat the steps given in 7.6 to 7.12 until the test is terminated (see 7.14).

7.14 Continue the test until one of the following occurs:

a) completion of  $5 \times 10^6$  cycles;

NOTE At the request of the party submitting the specimen, the test may be continued beyond this limit.

b) break-up or delamination of the articulating surfaces;

c) failure of the testing machine to maintain the force and displacement parameters within the given tolerances (see 6.5, 6.6).

## 8 Test report

The test report shall include the following information:

a) a reference to this part of ISO 14242;

b) the identity of the test specimens, as stated by the party submitting the specimens for test, including size, material, type and manufacturer;

c) a description of the testing machine, including number of stations, type of systems used for generating motions and forces, range of motions and forces, type of systems used for measuring motions and forces, arrangement for mounting specimen (see 5.2), arrangement for lubrication of articulating surfaces, arrangement for temperature control, and arrangement for the exclusion of contaminant particles;

d) whether control specimens were used and, if not, the reference to the tests from which the control data were taken;

e) a statement of results, including:

1) total number of cycles applied;

2) reason for terminating the test if less than  $5 \times 10^6$  cycles were applied;

3) description of all the surfaces of both components at which relative movement has occurred;

**ISO 14242-1:2002(E)**

- 4) description of the condition of the interfaces between subcomponents, if the components are of modular construction;
- 5) pH values, if routine monitoring was undertaken (see 5.1).
- f) details of the method of measurement of wear and the results obtained (ISO 14242-2), namely:
  - 1) method of wear measurement (i.e. gravimetric or dimensional);
  - 2) change in mass for each measurement using the gravimetric method, or change in volume for each measurement using the dimensional method;
  - 3) wear rate (gravimetric or dimensional method).

**9 Disposal of test specimen**

No part of the test specimen or control specimen shall be used for clinical purposes after testing.

# Appendix B

---

## Cleaning, Drying and Weighing Protocol

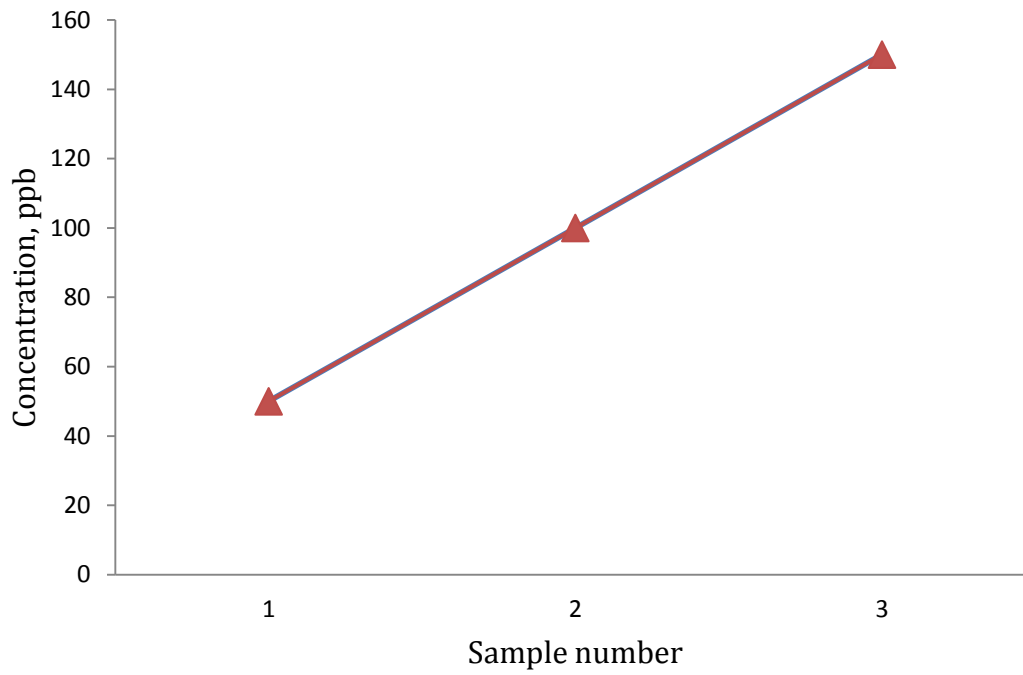
1. Run the ultrasonic bath on degas for 5 minutes.
2. Rinse components and gently clean the backs of the CoCrMo cups with a soft brush to remove any residue.
3. Rinse with deionised water.
4. Put the components into the holding tray and place into ultrasonic bath.
5. Sonicate for 10 mins in deionised water.
6. Remove from bath and rinse with deionised water.
7. Sonicate for 10 mins in a mixture of deionised water with 2 squirts of neutrocon.
8. Remove and rinse in deionised water.
9. Sonicate for 10 mins in deionised water.
10. Remove and rinse in deionised water.
11. Sonicate for 3 mins in deionised water.
12. Dry with lint free tissue.
13. Rinse metal surfaces in isopropanol.
14. Dry with lint free tissue.
15. Dry with a jet of filtered inert gas.
16. Leave all components in the vacuum oven to dry for 30 mins.
17. Leave all components to acclimatise next to weighing balance for 30 mins.
18. Weigh each component to get 3 consecutive results within 0.1 mg.

# Appendix C

---

## ICPMS Protocol

1. Serum frozen after biotribological studies was subject to an enzymatic isolation protocol and stored in an eppendorf tube for analysis. (A blank sample, from applying the isolation protocol to pre-test serum, was also subject to the steps 2-14.)
2. Eppendorf tube was left open in a fume hood (to avoid contamination) at room temp over a weekend to let the ethanol evaporate off and leave the metal residue.
3. Metal residue was transferred to a sample vial and left overnight in 2 ml of conc. HCl to dissolve. (Can weigh sample to prepare CoCrMo predictions to have some concentrations in mind.)
4. Once dissolved, sample was made up to 50 ml with distilled deionised water.
5. Three standards of known concentrations of CoCrMo in 3.5% HNO<sub>3</sub> were made (50 ppb, 100 ppb, 200ppb), along with a blank sample of 50 ml 3.5% HNO<sub>3</sub>.
6. To check ICPMS is working, run a test sample of a known concentration of a mix of analytes six times.
7. Run a wash to flush out the system.
8. Run blank HNO<sub>3</sub>.
9. Run 3 CoCrMo standards to calibrate the machine and check the calibration curves. Should look like:



10. Run two washes to clean out the high metal concentrations.
11. Run serum blank.
12. Run samples.
13. Run wash.
14. Run standard to check it is still correct.